



USING SYSTEM RESPONSE FUNCTIONS OF LIQUID PIPELINES FOR LEAK AND BLOCKAGE DETECTION

Pedro J. Lee



PhD Dissertation

4th February, 2005

FACULTY OF ENGINEERING, COMPUTER AND MATHEMATICAL SCIENCES

School of Civil and Environmental Engineering



ABSTRACT

Two new methods of leak and blockage detection in pipelines using fluid transients are developed in this thesis. Injection of a fluid transient (a pressure variation, the input) and measurement of the subsequent response (the output) provide information concerning the state of a pipeline through the system response function. The system response function exists in two forms, the *impulse response function* in the time domain and the *frequency response function* in the frequency domain. Provided that the system is unchanged, the response function does not change from one test to the next even though the injected transient signals may be different. A procedure that saves many hours over previous methods was developed for extracting frequency response information from experimental data. The procedure was verified both numerically and experimentally. It uses the linear time-invariant system equation. The approximation of linearity was tested by comparing calculations using the linear transfer matrix model to those of the nonlinear method of characteristics.

The system response function allows direct comparisons of the information content of transient traces. Events that create sharp variations in time were shown to have transient signals with the greatest information content. For this reason, transients generated by fast-acting electronic solenoid valves are preferable to slower transients from manual closures or pump trips.

A variety of signals were used to determine their effect on the information content of the system response. This investigation includes the use of step, pulse and pseudo-random binary signals. The use of pseudo-random binary signals was shown to provide the same information as a discrete signal that is many times its magnitude, which is attractive when system damage is of concern or the amplitude of an injected transient is limited for any reason. A specialised solenoid valve was designed and constructed as part of this research to generate pseudo-random binary signals in a laboratory pipe.

Two new methods of leak and blockage detection are developed in this thesis and these methods do not require the use of an accurate simulation model or a leak-free benchmark.

Knowledge of the pipe topology, flow and roughness values, or the role of unsteady friction on the transient event is unnecessary. Leaks and blockages induce a non-uniform pattern on the peaks of the frequency response function and the properties of this pattern allow the accurate location of the problem. In the time domain, leaks and blockages create additional reflections in the impulse response function. The arrival times of these reflections can be used to locate the fault.

Both methods have been validated using numerical and experimental results. The methods were tested under both low and high flow conditions, and a procedure for applying the methods in complex pipeline networks was developed. The time domain method can detect multiple leaks and discrete blockages. The frequency-domain technique provides a higher degree of noise tolerance but is sensitive to system configuration and requires a large bandwidth in the injected signal. In comparison, the time domain technique does not have these limitations and is more versatile; it is usually the better technique. The combination of methods provides an attractive alternative for leak and blockage detection and quantification.

STATEMENT OF ORIGINALITY

This work contains no material that has been accepted for the award of any other degree or diploma in any university or other tertiary institution and, to the best of my knowledge and belief, contains no material previously published or written by another person, except where due reference has been made in the text. All journal publications included in this thesis were planned and written solely by the candidate, with valuable input from the co-authors on a supervisory level. I give consent to this copy of my thesis, when deposited in the University Library, being available for loan and photocopying.

Signed:

Date: 27th May, 2006

Pedro Jose Lee

ACKNOWLEDGEMENTS

I would like to thank a number of people who have made this thesis possible, starting with my supervisors Dr. Martin Lambert and Associate Professor Angus Simpson. Their assistance was vital in the completion of this PhD and their continual support throughout this time is most appreciated. I would also like to thank them for giving me a solid foundation in fluid hydraulics during my undergraduate years and especially to Martin who has stimulated my interest in research early on (and convinced me to take up the PhD in the first place).

Special thanks go to Dr John Vítkovský. Without his knowledge, patience and insightful suggestions this study could not have advanced to its current form. I will miss those afternoon technical discussions that always started out as a short question but inevitably turned into long sagas that take up the whole afternoon. I always leave those discussions feeling a little wiser.

I would like to thank Professor Jim Liggett of Cornell University and Mr Mark Stephens, a fellow PhD candidate, for their invaluable input during this period. Jim's patient instructions on technical writing have made a significant impact on the final form of this thesis and I am most grateful. I have learnt many things from Jim that will have a lasting impact on my career as an academic. Mark is a good friend and colleague and has provided much companionship and advice, along with other fellow post-graduate students in the department over this time.

Lastly (but not least), I would like to thank my family for their support over the years and my fiancée (now my wife) Patricia for her support and encouragement throughout my research.

TABLE OF CONTENTS

CHAPTER 1 – INTRODUCTION

1.1 INTRODUCTION	1
1.2 AIMS OF THE RESEARCH	6
1.3 THESIS OUTLINE	8
1.4 PUBLICATION LIST	9
1.5 SIGNIFICANT CONTRIBUTIONS TO THE FIELD	12

CHAPTER 2 - LITERATURE REVIEW

2.1 INTRODUCTION	13
2.2 NON-HYDRAULIC LEAK DETECTION TECHNIQUES	14
2.3 REMOTE HYDRAULIC METHODS	19
2.3.1 Steady State Methods	19
2.3.2 Unsteady State Methods	21
2.4 SUMMARY	28

CHAPTER 3 - GOVERNING EQUATIONS

3.1 INTRODUCTION	31
3.2 METHOD OF CHARACTERISTICS	32
3.2.1 Incorporation of leak elements	36
3.3 TRANSFER MATRIX EQUATIONS	38
3.3.1 Incorporation of leak elements	42
3.4 UNSTEADY FRICTION	46

CHAPTER 4 - PIPELINE APPARATUS USED FOR NUMERICAL AND EXPERIMENTAL INVESTIGATIONS

4.1 SIMULATION PIPELINE FOR NUMERICAL INVESTIGATIONS	51
4.2 LABORATORY APPARATUS FOR EXPERIMENTAL INVESTIGATIONS	52
4.2 DEVICES FOR TRANSIENT GENERATION	52

CHAPTER 5 - SYSTEMS IDENTIFICATION THEORY FOR TRANSIENT BEHAVIOUR IN PRESSURISED HYDRAULIC SYSTEMS

5.1 INTRODUCTION	59
------------------	----

5.2 SYSTEM IDENTIFICATION THEORY	65
5.2.1 Choice of the input variable	71
5.2.2 System configuration	88
5.2.3 Effect of the injected signal	93
<i>Signal bandwidth</i>	93
<i>Infinite energy signals</i>	97
5.3 EXPERIMENTAL EXTRACTION OF THE SYSTEM RESPONSE FUNCTION	104
5.3.1 Effects of friction on the extracted frequency response function	101
5.3.2 Experimentally injected signals for system response extraction	104
5.3.3 Experimental frequency response function extraction results	107
5.4 CASE STUDY: EXTRACTION OF THE SYSTEM RESPONSE FUNCTION USING PSEUDO RANDOM BINARY SIGNAL	116
5.4.1 Experimental apparatus for the generation of PRBS	117
5.4.2 Experimental extraction of the system response function using PRBS	119
5.5 CONCLUSIONS	125
CHAPTER 6 - LEAK DETECTION USING THE FREQUENCY RESPONSE FUNCTION	
6.1 INTRODUCTION	127
6.2 EFFECT OF LEAKS ON THE FRF OF PIPELINES	130
6.3 NON – ANALYTICAL METHOD OF LEAK DETECTION USING THE FRF	138
6.3.1 Inverse method	138
6.3.2 Peak sequencing method	142
6.4 DEVELOPMENT OF AN ANALYTICAL EXPRESSION DESCRIBING LEAK-INDUCED MODIFICATION ON FRF PEAKS	147
6.4.1 Anti-symmetric boundary conditions	148
<i>Anti-symmetric boundary with in-line valve fully closed</i>	148
<i>Anti-symmetric boundary with in-line valve open</i>	154
6.4.2 Symmetric boundary	157
6.5 ANALYTICAL TECHNIQUE OF LEAK DETECTION	162
6.5.1 Aliasing of leak-induced oscillations	163
6.5.2 Proposed leak detection method	167
6.6 NUMERICAL VALIDATION	169
6.7 APPLICATION OF THE ANALYTICAL LEAK DETECTION TECHNIQUE IN A PHYSICAL SYSTEM	179
6.7.1 Unsteady friction effects on the leak-induced oscillation	179
6.7.2 Effect of signal bandwidth	182
6.7.3 Effect of pipeline irregularities	183
6.7.4 Final leak detection procedure	184
6.8 EXPERIMENTAL VALIDATION	191

6.8.1 Validation of leak detection technique using a side-discharge valve	192
6.8.2 Validation using in-line valve closures	203
6.9 EXTENSION TO MULTIPLE LEAK DETECTION	209
6.9.1 Numerical validation of multiple leak detection	210
6.9.2 Experimental validation of multiple leak detection	212
6.10 EXTENSION INTO DIFFERENT MEASUREMENT / GENERATING POSITIONS	216
6.11 EXTRACTION OF RESPONSE FUNCTION FOR PIPE SEGMENTS CONTAINED IN COMPLEX NETWORKS	220
6.12 DISCRETE BLOCKAGE DETECTION	225
6.12.1 Effect of blockage on the peaks of the FRF	228
6.12.2 Numerical validation of blockage detection technique	232
6.13 LIMITATIONS TO THE FRF TECHNIQUE	236
6.14 CONCLUSIONS	237

CHAPTER 7 - LEAK DETECTION USING THE IMPULSE RESPONSE FUNCTION

7.1 INTRODUCTION	239
7.2 BACKGROUND	240
7.3 ILLUSTRATION OF THE CONVENTIONAL TDR PROCEDURE	242
7.3.1 Detection of reflected signals	245
7.3.2 Location of the leak in the pipeline from arrival time of the reflected signal	251
7.3.3 Experimental verification of improved TDR technique	255
<i>Symmetric boundary configuration</i>	255
<i>Anti-symmetric test</i>	258
7.3.4 Limitations of the conventional TDR technique	260
7.4 IMPULSE RESPONSE FUNCTION FOR THE APPLICATION OF TDR	262
7.4.1 Extraction of the impulse response function (irf)	263
7.4.2 Properties of the impulse response function (irf)	265
7.5 EXPERIMENTAL EXTRACTION OF THE IMPULSE RESPONSE FUNCTION (IRF)	274
7.6 METHOD OF LEAK DETECTION USING THE IMPULSE RESPONSE FUNCTION (IRF)	280
7.6.1 Removal of the need for a leak-free benchmark	280
7.6.2 Refinement of transient reflections	281
7.7 EXPERIMENTAL VALIDATION OF THE IMPROVED TDR PROCEDURE FOR LEAK DETECTION	282
7.7.1 Anti-symmetric System Tests	282
7.7.2 Symmetric boundary conditions	287
7.8 POSSIBLE IMPROVEMENTS TO THE APPLICABILITY OF IRF	290
7.8.1 Extension into discrete blockage detection	290
7.8.2 Detection of multiple faults	292

<i>Presence of higher order reflections</i>	294
7.8.3 IRF for the application of complex signals	296
7.9 CONCLUSIONS	299
CHAPTER 8 - COMPARISON BETWEEN TIME AND FREQUENCY-DOMAIN LEAK DETECTION	
8.1 INTRODUCTION	301
8.2 RELATIONSHIP OF LEAK-INDUCED EFFECTS ON THE FRF AND THE IRF	302
8.3 SENSITIVITY OF TECHNIQUES TO SYSTEM NOISE	308
8.4 SUMMARY OF PROPERTIES OF TIME AND FREQUENCY-DOMAIN TECHNIQUES	313
CHAPTER 9 - CONCLUSIONS	
9.1 SUMMARY AND CONCLUSIONS	317
9.1.1 Summary and conclusions of system response extraction in hydraulic systems	318
9.1.2 Summary and conclusion of leak detection procedures	319
9.2 RECOMMENDATIONS FOR FUTURE WORK	321
REFERENCES	323
APPENDIX A - FORMULATION OF THE TRANSFER MATRIX FOR A TWO-LEAK PIPE SEGMENT	333

FIGURES AND TABLES

Figure 1-1 – Schematic of a single input/output linear system in the context of generated transient disturbances in a pipeline.	4
Figure 1-2 – Measured transient response for a pulse signal in the laboratory system.	4
Figure 1-3 – Measured transient response for a step signal in the laboratory system.	5
Figure 1-4 – Frequency response functions from Figure 1-2 and Figure 1-3	5
Figure 2-1 – Robotic pig-based monitoring system (Source: http://www.Roxar.com).....	15
Figure 2-2 – Operation of leak correlators.....	17
Figure 2-3 – Comparison of transients in intact and leaking pipelines.	22
Figure 2-4 – Illustration of the operation of time-domain reflectometry.	26
Figure 2-5 – Summary of remote hydraulic methods for leak detection.....	29
Figure 3-1 – Graphical representation of the characteristics equations.	34
Figure 3-2 – Effect of increasing the number of nodal points and time steps on the resolution of the MOC analysis.	35
Figure 3-3 – Time marching progression of the MOC solution.....	36
Figure 3-4 – Upstream and downstream discharge for each node.	37
Figure 3-5 – System used for the illustration of the transfer matrix equations.	44
Figure 4-1 – Properties of the smooth numerical pipeline.	52
Figure 4-2 – Schematic of experimental pipeline at the University of Adelaide.	53
Figure 4-3 – Configuration of the wave speed determination test in the laboratory.....	56
Figure 4-4 – Experimental determination of wave speed in experimental apparatus (Data file: C4-1.xls).	57
Figure 5-1 – System layout for numerical simulations.	60
Figure 5-2 – Detection of a leak in the pipeline of Figure 5-1 with a step input signal generated by a 0.266 s closure of the in-line valve from a fully opened position (Data file = C5-1.txt).	60
Figure 5-3 – Detection of a leak in the pipeline of Figure 5-1 with a pulse input signal generated by the rapid perturbation of the initially fully closed valve (Data file = C5-1.txt).....	62
Figure 5-4 – Frequency response functions for the transient events shown in Figure 5-2 and Figure 5-3. Data were generated from an MOC model (Discretisation = 100, analysis time step = 0.0333 seconds) for the pipeline in Figure 5-1.....	63
Figure 5-5 – Structure of the system described in Eqs. (5.1) and (5.2).....	66
Figure 5-6 – Structure of the dependent input system.	69
Figure 5-7 – Procedure for system response extraction using measured input signal.....	72
Figure 5-8 – Pipeline for investigating the influence of the input variable for system response extraction. ...	72
Figure 5-9 – Input and output time series, input from measured valve movement.	73
Figure 5-10 – Nature of the valve opening fluctuation (Data file: C5-2.txt).	73
Figure 5-11 – Correlation functions between input (x) and output (y) functions.	74
Figure 5-12 – Spectrum of correlation functions.	74

Figure 5-13 – Comparison between transfer matrix equations and method of characteristics for $\Delta\tau_{Max}^* = \Delta\tau = 0.001$. The results overlap perfectly (Data file: C5-2.txt).....	75
Figure 5-14 – Comparison between transfer matrix equations and method of characteristics for $\Delta\tau_{Max}^* = \Delta\tau = 0.5$ (Data file: C5-3.txt).....	77
Figure 5-15 – Fourier decomposition of time series transient traces from the method of characteristics for a reservoir-pipe-valve system with no leak and for forcing functions of two different magnitudes (Data file: C5-4.txt).....	78
Figure 5-16 – Percentage error at $\omega/\omega_h = 1.0$ as a function of the magnitude of valve opening variation.	78
Figure 5-17 – Original modelling of the transient generation valve.	79
Figure 5-18 – Identification of induced-head response by the movement of the transient-generating valve for a step input.	80
Figure 5-19 – Identification of induced-head response by the movement of the transient-generating valve for a pulse input.	81
Figure 5-20 – Sequence showing interference from boundary reflection.	82
Figure 5-21 – Procedure for system response extraction using only the measured pressure response.....	84
Figure 5-22 – Comparison between FRF generated from the transfer matrix equations and the proposed technique using time series results from MOC for the anti-symmetric system of Figure 5-8 (Data set: C5-5.txt).....	85
Figure 5-23 – Correction for the perturbation of an initially closed in-line valve.....	85
Figure 5-24 – System configuration for the symmetric test.	86
Figure 5-25 – System configuration for the anti-symmetric test.....	86
Figure 5-26 – Comparison between the FRF generated from the transfer matrix equations and the proposed technique using time series results from MOC for the situation shown in Figure 5-24 (Data file: C5-6.txt).....	87
Figure 5-27 – Comparison between the FRF generated from the transfer matrix equations and the proposed technique using time series results from MOC for the situation shown in Figure 5-25 (Data file: C5-7.txt).....	87
Figure 5-28 – Determination of the position where maximum response is measured for each location of the transient-generating source, x_G^*	91
Figure 5-29 – Average response magnitude for varying measurement and generation positions for an anti-symmetric system.....	92
Figure 5-30 – Average response magnitude for varying measurement and generation position for a symmetric system.	92
Figure 5-31 – Injected signals for the bandwidth investigation (Data file: C5-8.txt).....	94
Figure 5-32 – Spectrum of input signal #1 and the corresponding head response spectrum from the system (Data file: C5-9.txt).....	95
Figure 5-33 – Extracted frequency response function from the system using injected signal #1 (Data file: C5-9.txt).....	95
Figure 5-34 – Spectrum of the input signal #2 and the corresponding head response spectrum from the system (Data file: C5-9.txt).....	96

Figure 5-35 – Extracted frequency response function from the system using injected signal #2 (Data file: C5-9.txt),	97
Figure 5-36 – FRF from the uncorrected discharge input from a full in-line valve closure generated using the MOC model.	99
Figure 5-37 – Correction for step input function.	100
Figure 5-38 – Comparison between MOC generated FRF for an in-line valve closure and an in-line valve perturbation.....	101
Figure 5-39 – FRF from a pipeline with no losses.....	102
Figure 5-40 – Comparison of the FRF for different friction cases.....	103
Figure 5-41 – Variation of peak magnitudes across different frequencies for all friction cases.....	103
Figure 5-42 – Typical discharge perturbation for a solenoid step closure.....	104
Figure 5-43 – Typical resultant discharge perturbation from a solenoid pulse.....	105
Figure 5-44 – Spectrum of input signal generated by the solenoid valve.....	106
Figure 5-45 – Original and corrected step signal from the manual closure.....	107
Figure 5-46 – Spectrum of corrected input signal generated by the in-line ball valve.....	107
Figure 5-47 – Configuration of the laboratory test validating FRF extraction.....	108
Figure 5-48 – Measured transient response for a pulse signal in the laboratory system (Data file: C5-10.txt).	109
Figure 5-49 – Measured transient response for a step signal in the laboratory system (Data file: C5-10.txt).	109
Figure 5-50 – Relationship between the time series of the two transient traces.	110
Figure 5-51 – FRF of the experimental pipeline generated by a step in comparison to that generated by a pulse.	111
Figure 5-52 – Relationship between the FRF generated by a step and a pulse.....	111
Figure 5-53 – System configuration for in-line valve closure test.....	113
Figure 5-54 – Head response from manual closure of the in-line valve (Data file: C5-11.txt).....	113
Figure 5-55 – FRF of the experimental pipeline generated by a step using hand closure of the in-line valve (Data file: C5-11.txt).	114
Figure 5-56 – Comparison between time series from experiment and MOC (Data file: C5-12.txt).	114
Figure 5-57 – Comparison between theoretical and experimental FRF (Data file: C5-12f.txt).....	115
Figure 5-58 – PRBS Signal Generator designed and constructed at the University of Adelaide.....	118
Figure 5-59 – Typical pulses generated by the continuous signal generator.	119
Figure 5-60 – Laboratory configuration for the PRBS test.....	120
Figure 5-61 – Input (a) and output (b) sequences from the PRBS sequence (Data file: C5-13.txt).....	120
Figure 5-62 – Correlation functions from the injection of the PRBS, (a) auto-correlation of the input, (b) auto-correlation of the output and (c) cross-correlation between the two.	121
Figure 5-63 – Input (a) and output (b) spectrums from the injected PRBS.	122
Figure 5-64 – Comparison of PRBS results with theoretical results (Data file: C5-14.txt).	123
Figure 6-1 – Comparison of the results from Mpesha <i>et al.</i> (2001, 2002) with the transfer matrix model for a leak-free system.	129

Figure 6-2 – Comparison of the results from Mpesha <i>et al.</i> (2001, 2002) with the transfer matrix model for a leaking system.....	129
Figure 6-3 – Configuration of the system for test shown in Figure 6-4.....	130
Figure 6-4 – Effect of a leak located at 1400 m from upstream boundary with $C_d A_L = 0.00014 \text{ m}^2$ ($C_d A_L / A = 1.98 \times 10^{-3}$).....	131
Figure 6-5 – System configuration for Figure 6-4.....	132
Figure 6-6 – Effect of a leak located at 1136 m from upstream boundary with $C_d A_L = 0.00014 \text{ m}^2$ ($C_d A_L / A = 1.98 \times 10^{-3}$).....	132
Figure 6-7 – Effect of a leak located at 500 m from upstream boundary with $C_d A_L = 0.00014 \text{ m}^2$ ($C_d A_L / A = 1.98 \times 10^{-3}$).....	133
Figure 6-8 – System configuration for Figure 6-7.....	133
Figure 6-9 – Effect of a leak located at 500 m from upstream boundary with $C_d A_L = 0.00042 \text{ m}^2$ ($C_d A_L / A = 5.94 \times 10^{-3}$).....	134
Figure 6-10 – Procedure of testing the effect of the leak position on the measured response magnitude.....	135
Figure 6-11 – Effect of leak position on the frequency response of the first 3 harmonic peaks.....	135
Figure 6-12 – Effect of leak size on the resonance peak responses.....	136
Figure 6-13 – Effect of leak size on the frequency response of the first 3 harmonic peaks (note all three series overlap).....	136
Figure 6-14 – System configuration for Figure 6-15.....	139
Figure 6-15 – Inverse calibration for the frequency response measured at a location 800 m from the upstream boundary (Data file: C6-1.txt).....	140
Figure 6-16 – System configuration for Figure 6-17.....	141
Figure 6-17 – Inverse calibration for the frequency response measured at the optimum position in the pipeline (Data file: C6-2.txt).....	141
Figure 6-18 – System configuration for Figure 6-20.....	142
Figure 6-19 – System configuration for Figure 6-21.....	143
Figure 6-20 – Leak at 1400 m from upstream reservoir (Data file: C6-3.txt).....	143
Figure 6-21 – Leak at 700 m from upstream reservoir (Data file: C6-3.txt).....	144
Figure 6-22 – Effect of leak position on the frequency response of the first 3 harmonic peaks.....	144
Figure 6-23 – Illustration of the system configuration where a leak exists in the pipeline with a closed downstream valve.....	148
Figure 6-24 – FRF from the pipeline with no losses.....	151
Figure 6-25 – Comparison between Eq. (6.29) and the transfer matrix model.....	154
Figure 6-26 – Comparison between analytical peak magnitudes described by Eq. (6.33) and the transfer matrix model.....	156
Figure 6-27 – Comparison between analytical peak magnitudes described by Eq. (6.35) and the transfer matrix model.....	156
Figure 6-28 – System configuration used for the derivation of the leak-induced modification on a symmetric boundary system.....	157
Figure 6-29 – FRF from a frictionless pipeline in a symmetric configuration.....	159

Figure 6-30 – Comparison between analytical peak magnitudes described by Eq. (6.53) and the transfer matrix model.	161
Figure 6-31 – An illustration of the sampling theorem for an oscillation taking place between three consecutive peak values and the effect of aliasing on high-frequency oscillations.	164
Figure 6-32 – Phase diagram of the different leak positions.	166
Figure 6-33 – Phase zones to identify leak location.	166
Figure 6-34 – System configuration for numerical validation of the first anti-symmetric system.	169
Figure 6-35 – FRF of the pipeline containing a leak at $x_L^* = 0.7559$	170
Figure 6-36 – Inverted peak magnitudes of the FRF of Figure 6-35.	170
Figure 6-37 – Spectral content of Figure 6-36, showing a dominant leak-induced frequency that is associated with two possible leak positions.	171
Figure 6-38 – Phase spectrum of Figure 6-36.	172
Figure 6-39 – Expanded phase spectrum from Figure 6-38.	172
Figure 6-40 – Spectrum of inverted peak oscillations for different leak positions in a static anti-symmetric system.	173
Figure 6-41 – Spectrum of inverted peak oscillations for different leak positions in a flowing anti-symmetric system.	174
Figure 6-42 – System configuration for the numerical symmetric validation.	175
Figure 6-43 – FRF of leaking pipe in a symmetric system with leak located at $x_L^* = 0.634$	175
Figure 6-44 – Variation of the inverted peak magnitudes in the FRF of Figure 6-43.	176
Figure 6-45 – Spectrum of inverted peak oscillations in a symmetric system.	176
Figure 6-46 – Phase spectrum of inverted peak oscillations for symmetric system.	177
Figure 6-47 – Examples of leak detection in the symmetric system.	177
Figure 6-48 – Investigation into the effect of unsteady friction.	180
Figure 6-49 – System configuration for investigation into unsteady friction effects on the leak-induced modification on the FRF.	180
Figure 6-50 – Comparison of the inverted peak magnitudes for a leaking pipeline with and without unsteady friction.	181
Figure 6-51 – Spectrum of inverted peak magnitudes for the case with and without unsteady friction.	181
Figure 6-52 – FRF from the experimental pipeline showing the effect of bandwidth.	183
Figure 6-53 – Comparison between model and experimental FRF for a leak symmetric system.	184
Figure 6-54 – Trend distortion effects on the peak oscillations as a result of unsteady friction.	185
Figure 6-55 – Scale distortion effects on the peak oscillations.	186
Figure 6-56 – The comparison between the trend correction function for laminar and turbulent flow cases.	187
Figure 6-57 – Feasible region for anti-symmetric boundaries.	189
Figure 6-58 – Feasible region for symmetric boundaries.	189
Figure 6-59 – Laboratory configuration for anti-symmetric no-leak test.	192
Figure 6-60 – Experimental transient trace for anti-symmetric system with no leak.	193
Figure 6-61 – FRF for anti-symmetric experimental system with no leak.	193

Figure 6-62 – System configuration for the anti-symmetric leaking test with a 1.0 mm ($C_d A_L / A = 1.69 \times 10^{-3}$) leak at $x_L^* = 0.751$	194
Figure 6-63 – Transient signal for the anti-symmetric leaking test with a 1.0 mm ($C_d A_L / A = 1.69 \times 10^{-3}$) leak at $x_L^* = 0.751$ (Data file: C6-L3.txt).	194
Figure 6-64 – FRF for the anti-symmetric leaking test with a 1.0 mm ($C_d A_L / A = 1.69 \times 10^{-3}$) leak at $x_L^* = 0.751$	195
Figure 6-65 – Dominant frequency and phase extraction for the anti-symmetric leaking test with a 1.0 mm ($C_d A_L / A = 1.69 \times 10^{-3}$) leak at $x_L^* = 0.751$	195
Figure 6-66 – Laboratory configuration for the anti-symmetric leaking test with a 1.5 mm ($C_d A_L / A = 4.17 \times 10^{-3}$) leak at $x_L^* = 0.179$	196
Figure 6-67 – Transient signal for the anti-symmetric leaking test with a 1.5 mm ($C_d A_L / A = 4.17 \times 10^{-3}$) leak at $x_L^* = 0.179$ (Data file: C6-L2.txt).	197
Figure 6-68 – Expanded transient signal for the anti-symmetric leaking test with a 1.5 mm ($C_d A_L / A = 4.17 \times 10^{-3}$) leak at $x_L^* = 0.179$ (Data file: C6-L2.txt).	197
Figure 6-69 – FRF for the anti-symmetric leaking test with a 1.5 mm ($C_d A_L / A = 4.17 \times 10^{-3}$) leak at $x_L^* = 0.179$	198
Figure 6-70 – Dominant frequency and phase extraction for the anti-symmetric leaking test with a 1.5 mm ($C_d A_L / A = 4.17 \times 10^{-3}$) leak at $x_L^* = 0.179$	198
Figure 6-71 – Dominant frequency and phase extraction for the no-leak case in the anti-symmetric system using the solenoid valve as generator.	199
Figure 6-72 – Laboratory configuration for symmetric leaking test with 1.5 mm ($C_d A_L / A = 4.17 \times 10^{-3}$) leak at $x_L^* = 0.179$	200
Figure 6-73 – Transient trace for the symmetric leaking test with a 1.5 mm ($C_d A_L / A = 4.17 \times 10^{-3}$) leak at $x_L^* = 0.179$ (Data file: C6-L5.txt).	201
Figure 6-74 – FRF for the symmetric leaking test with a 1.5 mm ($C_d A_L / A = 4.17 \times 10^{-3}$) leak at $x_L^* = 0.179$	201
Figure 6-75 – Dominant frequency and phase extraction for the symmetric leaking test with a 1.5 mm ($C_d A_L / A = 4.17 \times 10^{-3}$) leak at $x_L^* = 0.179$	202
Figure 6-76 – FRF for symmetric system with no leak using solenoid valve as generator.....	203
Figure 6-77 – System configuration for the in-line valve leak detection tests.	204
Figure 6-78 – In-line manual valve closure in the leak-free laboratory system.	204
Figure 6-79 – Transient trace for the in-line valve closure leaking test with a 1.5 mm ($C_d A_L / A = 4.17 \times 10^{-3}$) leak at $x_L^* = 0.75$ (Data file: C6-L6.txt).	205
Figure 6-80 – Transient trace for the in-line valve closure leaking test with a 1.0 mm ($C_d A_L / A = 1.69 \times 10^{-3}$) leak at $x_L^* = 0.75$ (Data file: C6-L7.txt).	205
Figure 6-81 – FRF from a non-leaking pipeline generated by the manual closure of the in-line valve.	206
Figure 6-82 – FRF from experimental pipeline with a 1.5 mm leak ($C_d A_L / A = 4.17 \times 10^{-3}$, $x_L^* = 0.75$) using in-line valve closure.	206
Figure 6-83 – FRF from experimental pipeline with a 1.0 mm leak ($C_d A_L / A = 1.69 \times 10^{-3}$, $x_L^* = 0.75$) using in-line valve closure.	207

Figure 6-84 – Dominant frequency and phase extraction for leak size $C_d A_L / A = 4.17 \times 10^{-3}$ (1.5 mm) when in-line valve closure is used.....	208
Figure 6-85 – Dominant frequency and phase extraction for leak size $C_d A_L / A = 1.69 \times 10^{-3}$ (1 mm) when in-line valve closure is used.....	208
Figure 6-86 – System configuration for the numerical validation of multiple leak detection.....	211
Figure 6-87 – Spectrum of peak magnitudes when three leaks exists in the pipeline.....	211
Figure 6-88 – System configuration for the experimental multiple leak detection.....	212
Figure 6-89 – Transient trace from a multiple leak situation in the laboratory pipeline (Data file: C6-L8.txt).....	213
Figure 6-90 – FRF for the multiple leak situation.....	213
Figure 6-91 – Dominant frequency and phase extraction for the multiple leak case.....	214
Figure 6-92 – Result of the multiple leak search on a single leak data for anti-symmetric leaking test with 1.5 mm ($C_d A_L / A = 4.17 \times 10^{-3}$) leak at $x_L^* = 0.751$	215
Figure 6-93 – Schematic for the measurement position transfer in an anti-symmetric system with transient generated by in-line valve.....	217
Figure 6-94 – The FRF from different measurement positions.....	218
Figure 6-95 – Results of the FRF from single pipeline when the original FRFs from each measurement point are combined in Eq. (6.79) (the results overlap perfectly).....	219
Figure 6-96 – Illustration of network analysis using the proposed procedure.....	220
Figure 6-97 – Configuration of pipeline section.....	221
Figure 6-98 – Typical numerical results from an arbitrary network shown in Figure 6-96.....	222
Figure 6-99 – Extension of the first half period data in Figure 6-97.....	223
Figure 6-100 – Synthetically extended data for the extraction of the pipe FRF.....	223
Figure 6-101 – Approximate FRF of pipeline using half-period extension procedure.....	224
Figure 6-102 – FRF of the pipeline existing as a separate pipeline.....	224
Figure 6-103 – System configuration of the blockage example.....	226
Figure 6-104 – Illustration of the resonant peaks shift as a result of a 5 m blockage in the numerical pipeline with a reduced flow diameter of 0.05 m.....	226
Figure 6-105 – Illustration of the resonant peaks shift as a result of a 3 m blockage in the numerical pipeline with a reduced flow diameter of 0.05 m.....	227
Figure 6-106 – Illustration of the resonant peaks shift as a result of a 0.5 m blockage in the numerical pipeline with a reduced flow diameter of 0.05 m.....	227
Figure 6-107 – Pipeline under consideration.....	228
Figure 6-108 – FRF of the blocked and unblocked numerical pipeline.....	229
Figure 6-109 – Phase relationship with the block location.....	232
Figure 6-110 – Spectrum of the inverted peaks magnitudes for three different blockage conditions.....	233
Figure 6-111 – System configuration for multiple block test.....	234
Figure 6-112 – Spectrum of the inverted peaks magnitudes for multiple blockages.....	235
Figure 7-1 – Operation mechanism for a conventional radar system.....	240
Figure 7-2 – Operation mechanism of TDR in pipelines.....	241

Figure 7-3 – Schematic of pipeline for illustrating the generation of leak-reflected signals in a transient trace.	242
Figure 7-4 – Numerical comparison of transient traces from leaking and intact pipes (Data file: C7-1.txt).	243
Figure 7-5 – Transient propagation at $t = 0$ s.	243
Figure 7-6 – Transient propagation at $t = L / (2a)$ s.	244
Figure 7-7 – Transient propagation at $t = L/as$	244
Figure 7-8 – Illustration of the operation of the negative CUSUM.	247
Figure 7-9 – System configuration for determination of the threshold value in the CUSUM algorithm in the laboratory.	248
Figure 7-10 – Smallest detectable leak reflection in the experimental system.	248
Figure 7-11 – Expanded view of the leak reflection.	249
Figure 7-12 – Configuration of the anti-symmetric system for the determination of model accuracy.	250
Figure 7-13 – Comparison between experimental results and method of characteristics prediction with Zielke (1968) unsteady friction model for a no-leak situation (Data file: C7-3.txt).	250
Figure 7-14 – Illustration of the operation of time-domain reflectometry.	251
Figure 7-15 – Operation mechanism of TDR in pipelines under non-optimum configuration.	252
Figure 7-16 – Configuration of the system used for mathematical derivation of the relationship between occurrence time and leakage location.	252
Figure 7-17 – Scenario #1 for generating a leak-induced disturbance in the transient trace measured at the transducer.	253
Figure 7-18 – Scenario #2 for generating a leak-induced disturbance in the transient trace measured at the transducer.	253
Figure 7-19 – System layout for the symmetric test.	256
Figure 7-20 – Transient trace at the measuring station 18.82 m from upstream reservoir for symmetric system test (Transducer 1) – (Data file: C7-L1.txt).	257
Figure 7-21 – Transient trace measured 0.345 m from the downstream reservoir for symmetric system test (Transducer 2) – (Data file: C7-L1.txt).	257
Figure 7-22 – System layout for the anti-symmetric test.	258
Figure 7-23 – Transient trace measured 18.71 m from upstream reservoir for the anti-symmetric system test (Transducer 1) – (Data file: C7-L2.txt).	259
Figure 7-24 – Transient trace measured at the transient source (0.16 m from closed valve) for anti-symmetric system test (Transducer 2) – (Data file: C7-L2.txt).	259
Figure 7-25 – Possible start points of the transient signal in Figure 7-24.	261
Figure 7-26 – Possible arrival points of the reflected signal in Figure 7-24.	261
Figure 7-27 – Impulse response function from a system.	265
Figure 7-28 – The overall response from the system when a complex single is applied at the input.	266
Figure 7-29 – System configuration for numerical extraction of the impulse response function.	267
Figure 7-30 – Input to the leak-free numerical system (Data file: C7-I1.txt).	267
Figure 7-31 – Output from the leak-free numerical system (Data file: C7-I1.txt).	268
Figure 7-32 – FRF from the symmetric leak-free pipeline.	268

Figure 7-33 – Impulse response extracted from the input and output pair.....	269
Figure 7-34 - Configuration for numerical extraction of the impulse response function in a leaking system.....	269
Figure 7-35 – Output from the leaking system with a leak 1500 m from upstream boundary, $C_d A_L / A = 3.96 \times 10^{-3}$ (Data file: C7-IL2.txt).	270
Figure 7-36 – Impulse response from the leaking system with a leak 1500 m from upstream boundary, $C_d A_L / A = 3.96 \times 10^{-3}$	270
Figure 7-37 – Refinement of leak-reflected pulse using the impulse response function.	271
Figure 7-38 – Output from the same leaking system using a step closure of the valve as the injected signal.	272
Figure 7-39 – Comparison of the impulse response function using the two different injected signals in Figure 7-35 and Figure 7-38 (the series overlap perfectly).	272
Figure 7-40 – System configuration for the experimental extraction of the IRF.	274
Figure 7-41 – Transient trace from the experimental system (Data file: L7-I3.txt).	275
Figure 7-42 – Unsmoothed IRF from leak-free experimental pipeline.	275
Figure 7-43 – Bandwidth-related high-frequency noise in FRF.	276
Figure 7-44 – Shape of the (a) Hamming and (b) Blackman filter.	277
Figure 7-45 – Filtered FRF result using the Blackman filter.	277
Figure 7-46 – Effect of each filter on the form of the IRF, with (a) the unfiltered IRF, (b) the filtered IRF using Hamming and (c) the filtered IRF using Blackman.	278
Figure 7-47 – Comparison of reflection shapes between the original signal and the filtered IRF	278
Figure 7-48 – Procedure for extracting the impulse response function from the pipeline	279
Figure 7-49 – Regions for leak detection in the IRF.....	280
Figure 7-50 – Estimation of the arrival time of leak-reflected signals using the IRF.	281
Figure 7-51 – System layout for the anti-symmetric test #1 using the improved TDR procedure.....	282
Figure 7-52 – Original transient trace for the anti-symmetric example for transducer #1 (Data file: C7-IL1.txt).	283
Figure 7-53 – Improvement of the reflection form using the IRF for transducer #1.	284
Figure 7-54 – CUSUM results of anti-symmetric example for transducer #1.	284
Figure 7-55 – Estimation of the arrival time from the transient trace from estimated start times of the signals for transducer #1.....	285
Figure 7-56 – Estimation of the arrival time from the transient trace from signal peaks for transducer #1...	285
Figure 7-57 – IRF measured from transducer #2 in the anti-symmetric system (Data file: C7-IL1b.txt).....	286
Figure 7-58 – Configuration of the second anti-symmetric example.....	286
Figure 7-59 – CUSUM result for 1.5mm leak at the mid point of a pipe with anti-symmetric boundaries (Data file: C7-IL2.txt).	287
Figure 7-60 – Configuration of the first symmetric test example.	288
Figure 7-61 – Symmetric test example 1 (Data file: C7-IL3.txt).....	288
Figure 7-62 – Configuration of the second symmetric test.	289
Figure 7-63 – Results of the second symmetric test (Data file: C7-IL4.txt).	289

Figure 7-64 – Impulse response function comparing the reflection from a leak and from a discrete blockage.....	291
Figure 7-65 – System configuration for results shown in Vítkovský <i>et al.</i> (2003a).....	291
Figure 7-66 – Multiple leak detection in an anti-symmetric system.	292
Figure 7-67 – System configuration for experimental multiple leak detection.	293
Figure 7-68 – Original transient signal for the multiple leak case shown in Figure 7-67 (Data file: C6-L8.txt).	293
Figure 7-69 – Leak detection using the IRF for system shown in Figure 7-67.	294
Figure 7-70 – Diagram showing higher order reflections from the leak.	294
Figure 7-71 – Expanded impulse response for the first $2L/a$ seconds for transducer #1 system shown in Figure 7-72.	295
Figure 7-72 – System layout for the illustration of the effect of higher order reflections.	296
Figure 7-73 – Numerical simulation of PRBS analysis using IRF.....	297
Figure 7-74 – Input and output sequences for PRBS signal.....	298
Figure 7-75 – Comparison between raw transient trace and IRF.....	298
Figure 8-1 – System configuration for investigation.....	303
Figure 8-2 – Input discharge perturbation at the side-discharge valve.....	303
Figure 8-3 – Transient response from the leaking pipeline measured upstream of the in-line valve.	304
Figure 8-4 – FRF of the transient event.	304
Figure 8-5 – Modified transient response with leak reflections removed.	305
Figure 8-6 – FRF of transient trace with leak reflections removed.....	305
Figure 8-7 – Corrected transient trace with the first reflection from the leak removed.	306
Figure 8-8 – IRF for the modified transient signal with the first reflection removed.....	307
Figure 8-9 – FRF of transient signal with first reflection removed.....	307
Figure 8-10 – System configuration for testing the effect of noise in data	308
Figure 8-11 – Original transient signal (Data file: C6-L5.txt).	309
Figure 8-12 – Contaminated transient signal.	309
Figure 8-13 – Comparison between the FRF of contaminated and original signals.....	310
Figure 8-14 – Comparison between the IRF of contaminated and original signals.	310
Figure 8-15 – Contaminated transient signal with a sinusoidal function.	311
Figure 8-16 – FRF of sine-function contaminated transient data.....	312
Figure 8-17 – IRF of a sine-contaminated transient data.	312

LIST OF PLATES

Plate 4-1 – Photos of the experimental pipeline at the University of Adelaide with (a) view of a pressurised boundary tank and (b) view of pipeline with wall mounted supports.	54
Plate 4-2 – Photos of pipe components (a) Whitney 65TF16 smooth in-line one-quarter turn ball valve (b) Druck PDCR 810 pressure transducers.....	55
Plate 4-3 – Photo of brass block with leak unit attached.	55
Plate 4-4 – Solenoid valves used in the investigation (a) Commercial brass solenoid valve (b) Custom designed solenoid valve.....	58

LIST OF TABLES

Table 6-1 – Peak ranking sequence and corresponding leak position.	146
Table 6-2 – Possible leak positions using the frequency of the oscillation alone.	168
Table 6-3 – Possible leak positions using both phase and frequency of the oscillation.	168
Table 6-4 – Summary of leak detection in a static anti-symmetric system.	173
Table 6-5 – Summary of leak detection in a flowing anti-symmetric system.	173
Table 6-6 – Summary of leak detection in the symmetric system.	178
Table 6-7 – Number of peaks available for leak detection in the experimental pipeline for different transient source.	183
Table 6-8 – Summary of test configurations.	191
Table 6-9 – Results for anti-symmetric test with solenoid generator.	199
Table 6-10 – Results for symmetric tests with solenoid generator.	203
Table 6-11 – Summary for Experimental Tests.	207
Table 6-12 – Comparison of prediction accuracy of multiple leaks.	211
Table 6-13 – Summary of results for the experimental multiple leaks test.	214
Table 6-14 – Summary of multiple leak detection with single leak data.	214
Table 6-15 – Results of single blockage detection.	233
Table 6-16 – Results of multiple blockage detection.	235
Table 7-1 – The complete set of leak location equations.	255
Table 8-1 – Properties of FRF and IRF procedures for leak detection.	315

NOTATION

Roman Letters

A	=	pipe cross-sectional area
a	=	wave speed
A_L	=	the area of the leak orifice
A_V	=	the area of the valve orifice
C	=	Cepstrum of the signal
C^*	=	the shear decay coefficient
C_d	=	discharge coefficient
$C_d A_L$	=	lumped leak discharge coefficient
$C_d A_V$	=	lumped valve discharge coefficient
C_V	=	valve head loss coefficient
D	=	pipe diameter
d	=	time lag used in the correction of the infinite energy signal
E	=	objective function value or the magnitude of the sine fitting function
erf	=	is the complex error function
f	=	Darcy-Weisbach friction factor
F	=	frequency response function
f_s	=	steady friction factor
f_u	=	unsteady friction factor
g	=	gravitational acceleration or the cumulative sum in CUSUM change detection
H	=	head
h	=	head oscillation magnitude about the steady conditions
h^*	=	head perturbations about the steady conditions
H_0	=	steady state or initial (prior to transient) head
H_L	=	the head at the leak
h_L^*	=	head perturbations about the steady conditions at the leak
H_{L0}	=	the steady state or initial (prior to transient) head at the leak
i	=	$\sqrt{-1}$
I	=	impulse response function
l	=	length of a pipe section
L	=	total length of the pipeline
M	=	number of measurement points in inverse resonance procedure
m	=	peak number in the frequency response function
n_p	=	number of available peaks
Q	=	discharge

q	=	discharge oscillation magnitude about the steady conditions
q^*	=	discharge perturbations about the steady conditions
Q_0	=	steady state or initial (prior to transient) discharge through the pipe
Q_{B0}	=	the steady state or initial (prior to transient) discharge through the blockage
Q_{in}	=	measured inflow to the system
q_L	=	magnitude of leak discharge oscillation about the steady conditions
Q_L	=	discharge at the leak
q_L^*	=	leak discharge perturbations about the steady conditions
Q_{L0}	=	the steady state or initial (prior to transient) discharge at the leak
Q_{out}	=	measured outflow from the system
Q_V	=	discharge through the valve
Q_{V0}	=	discharge through the valve at steady state (prior to transient)
r	=	correlation function (time domain)
R	=	resistance factor
Re	=	Reynolds number = (VD/ν)
R_s	=	friction resistance factor (steady)
R_u	=	friction resistance factor (unsteady)
S	=	correlation function (frequency domain)
s	=	residual error
S	=	scale correction function
t	=	time
T	=	trend correction function, or entries of pipe transfer matrix between 2 measurement points
t^*	=	time lag
T_A	=	analysis time for CUSUM leak detection
T_O	=	time of occurrence of leak reflection
U	=	overall system transfer matrix
V	=	flow velocity
W	=	Weighting function (unsteady friction) or window function (filter)
x	=	distance along the pipe or input to the system (time domain)
X	=	input to the system (frequency domain) or fitting parameters
x_B	=	dimensionless blockage position, x_B/L
x_D	=	minimum value of x_L^* that can be detected
x_L	=	distance of the leak from upstream boundary
x_L^*	=	dimensionless leak position, x_L/L
Y	=	output from the system (frequency domain)
y	=	output from the system (time domain)
Z	=	characteristic impedance for the pipe
Z_B	=	impedance of the blockage = $2\Delta H_{B0}/Q_{B0}$
z_L	=	elevation at the leak
Z_V	=	impedance of the boundary in-line valve = $2\Delta H_{V0}/Q_{V0}$

Greek Symbols

α	=	reflectivity coefficient
ΔH	=	induced-head perturbation at the transient-generating valve
ΔH_{B0}	=	head loss across the blockage at steady state (prior to transient)
ΔH_v	=	head loss across the valve
ΔH_{v0}	=	head loss across the valve at steady state (prior to transient)
ΔQ	=	induced discharge perturbation at the transient-generating valve
$\Delta \tau$	=	oscillatory component of the valve perturbation for a particular frequency
$\Delta \tau^*$	=	valve opening perturbation about the steady state (prior to transient)
ϕ	=	phase
ν	=	kinematic viscosity or expected variation in the data
μ	=	propagation constant
τ	=	orifice opening coefficient = $C_d A_L / (C_d A_L)_{REF}$
τ_0	=	orifice opening coefficient at steady state = $(C_d A_L)_0 / (C_d A_L)_{REF}$
ω	=	frequency
ω_{th}	=	fundamental frequency of system

CHAPTER 1

INTRODUCTION

1.1 BACKGROUND

The problem of leaks in water distribution pipelines has generated interest due to its associated cost to industry and health concerns about providing entry points for contaminants (Colombo and Karney, 2002). Many pipelines are over 100 years old and are poorly maintained, resulting in increased occurrences of leaks and blockages (Tafari, 2000). An estimated 75,000 breaks occur in mains annually in the United States and most existing pipelines longer than two kilometres develop leaks on an annual basis (Tafari 2000, Alaskan Department of Environmental Conservation 2001). These leaks may arise in pipes for various reasons, including natural ageing, operation beyond design limits, soil movement, poor workmanship and unintentional or intentional damage (Furness and van Reet, 1998). Water industries in Australia lose up to 40% of the total flow from leaks and other unaccounted means (Eiswirth and Burn, 2001), which is comparable to estimated values from around the world, ranging from 8% in Singapore to 62% in Bangladesh (Rao and Sridharan 1996, Wang 2002). The loss of water from Australia amounts to an annual cost of \$A180 million (Eiswirth and Burn, 2001).

In recent years, such economic costs and concern over public health have led to the introduction of stricter penalties on water authorities for leakage loss and have given the necessary incentives for investing in better leak detection technology. Since 1997, the Office of Water Services (OFWAT) in the UK has mandated targets for water industries to control leakage rates, which has resulted in a 37% reduction in leakage loss from the peak levels of 1994-1995 (OFWAT, 2001). This trend is set to continue through a strict target-setting procedure and the promotion of low-cost leak detection services for consumers.

A range of leak detection techniques, starting with physical inspection of pipelines through use of acoustic sound emitted from a leak to determine its location, is currently used. Acoustic methods that rely on detection of high-frequency noise emitted from water jetting out through a leak are popular (Fuchs and Riehle 1991, Tafuri 2000). Other techniques such as ground penetrating radar—which detects points of low electric impedance along the pipe, indicative of a collection of water (Eiswirth and Burn, 2001)—or electromagnetic techniques that find breaks in metallic pipes (Atherton *et al.*, 2000) are increasingly popular. These methods are able to detect and locate problems in short lengths (2 to 300 m) of pipeline (Tafuri, 2000).

Many methods are hampered by their short operation range. For example, acoustic methods use leak-induced signatures that attenuate quickly with distance, becoming undetectable beyond 250 m from the leak (Tafuri, 2000). Ground penetrating radar, electromagnetic procedures, sensor and visual inspections have operational ranges that are limited to the immediate vicinity of the detection equipment (Eiswirth and Burn, 2001). The use of these techniques for detecting leaks in a transmission main, typically many kilometres long, requires a section-by-section testing of the pipeline or many monitoring units. This limitation leads to the situation where leak detection procedures are only applied when the damage caused by the leak has become noticeable, often too late to minimize damage (Black, 1992).

An alternative approach to leak detection is to utilise the fact that a leak causes a noticeable change in hydraulic behaviour such as imbalance between inflow and outflow, change in frictional losses between different sections or change in the unsteady behaviour of the system (Furness and van Reet 1998, Black 1992). These changes can be detected at large distances from the leak and can be used as a means of system monitoring. Hydraulic techniques currently form the basis of the computational pipeline monitoring systems (CPM) for existing oil and gas pipelines as required by the U.S. Department of Transportation Office of Pipeline Safety (DOT-OPS) regulation 49 CFR 195 (Scott 1999a, 1999b).

An especially attractive hydraulic method of leak detection operates through injection of a transient pressure signal and analysis of subsequent pressure responses. These pressure signals are known as *fluid transients* and their behaviour is similar to propagation of sound

waves in air. A leak in a pipeline changes the measured pressure response of an injected signal. The nature of such changes provides clues as to the state of the system and can be used as a tool for detecting and locating a leak. Examples of publications on this topic include Jönsson and Larson (1992), Liggett and Chen (1994), Nash and Karney (1999), Vítkovský *et al.* (1999), Brunone (1999), Covas and Ramos (1999), Wang *et al.* (2002), Covas *et al.* (2003) and Kapelan *et al.* (2003).

Many of these hydraulic techniques require an accurate numerical model of the pipeline or the existence of a leak-free benchmark to ascertain its nominal behaviour when no leak exists. This approach is successful in controlled situations but can encounter difficulties in cases where the system properties or the leak-free behaviour are unknown. In reality, the hydraulic behavior of the system is usually uncertain and it is this lack of information that has led to the development of fault detection procedures in the first place. Alternative approaches that can detect problems without a detailed knowledge of the system are necessary.

Injection of fluid transients as a probe for detecting leaks bears similarities to system identification procedures in integrity testing of materials, biological components and electrical circuits (Poussart and Ganguly 1977, Brekke 1984, Ogawa *et al.* 1994, Li *et al.* 1994, Hwang and Kim 2004). In all these cases, a controlled signal is introduced and the subsequent response measured. Using the known applied signal (input) and the measured response (output), functions are developed that illustrate how the system modifies the introduced signal as it propagates through the system (Deutsch 1969). The nature of this modification is an indication of system properties. The developed functions between input and output are *system response functions*. The application of system response functions allows detection of faults without extensive knowledge of the system components (Poussart and Ganguly 1977, Lampton 1978, Niederdränk 1997, Dallabetta 1996).

System response functions provide insight into system behaviour by simplifying measured output to a form that is solely dependent on the physical nature of the system (Deutsch, 1969) and independent of the input signal. Any change from one day to the next—for example, the development of a problem—is detected as a change in the system response function even though the injected signal on those two days may not be identical.

This type of methodology is clearly advantageous when it comes to detection and location of faults in pipelines using injected pressure transients, as the object of interest in these situations is the state of the system itself and not the raw measured response. The schematic of a system's approach is shown in Figure 1-1. The input is the injected transient signal and the output is the measured pressure response. System response functions can be derived from the interrelationship between the two.



Figure 1-1 – Schematic of a single input/output linear system in the context of generated transient disturbances in a pipeline.

Experimental transient traces from the same pipeline using two different injected signals, one generated by a pulse perturbation of a side-discharge valve and the other by sharp closure of this valve, are shown in Figure 1-2 and Figure 1-3.

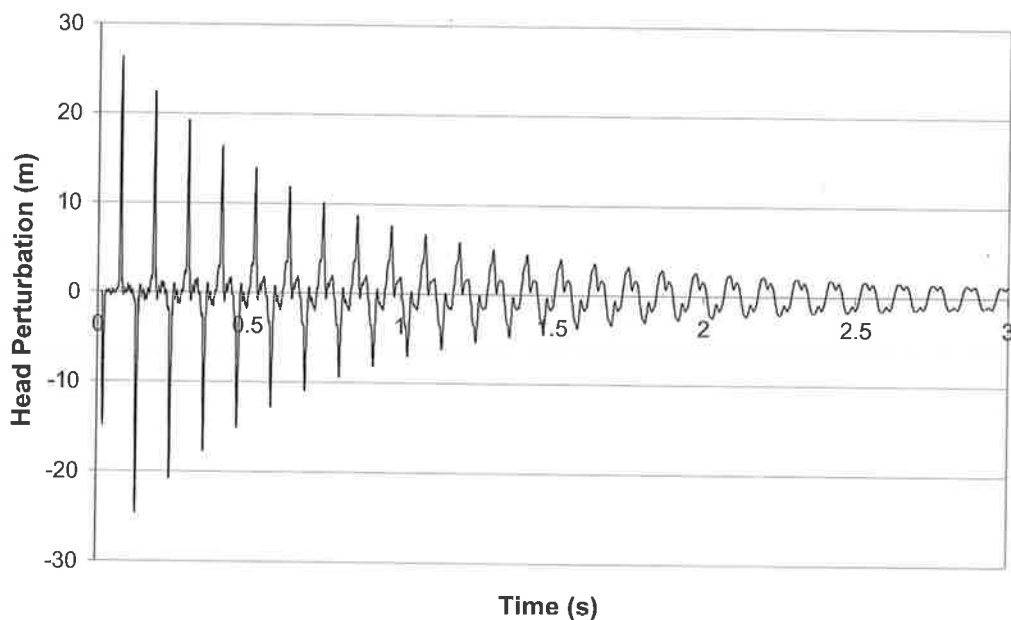


Figure 1-2 – Measured transient response for a pulse signal in the laboratory system.

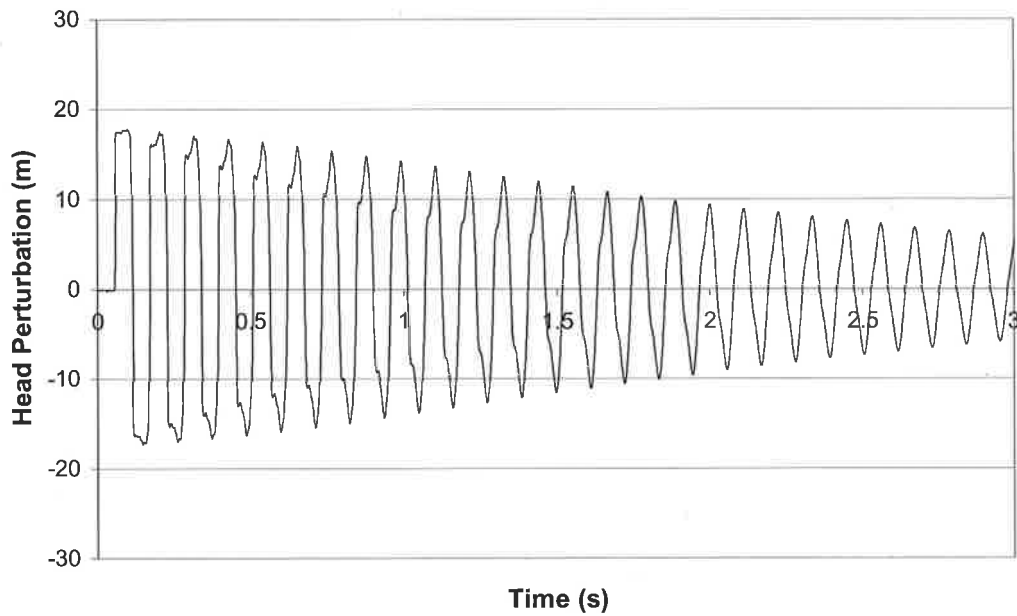


Figure 1-3 – Measured transient response for a step signal in the laboratory system.

The system response functions, shown in Figure 1-4, are very similar despite applying two different injected transients, thus illustrating the way these functions can determine underlying behaviour from a measured pressure response. In the same fashion, the integrity of a pipeline can be determined from the system’s response diagram.

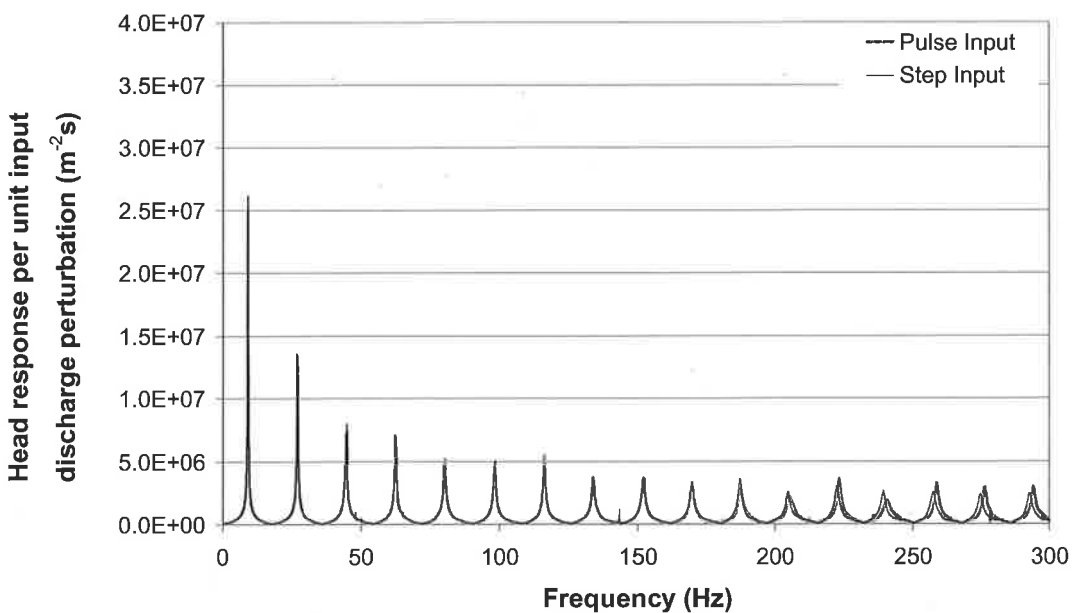


Figure 1-4 – Frequency response functions from Figure 1-2 and Figure 1-3

1.2 AIMS OF THE RESEARCH

The major aim of this research is to investigate procedures for leak detection using injected transient signals. In particular, this thesis focuses on the development of techniques that do not rely on use of an accurate numerical model. This dissertation has the following specific aims.

1. To determine a procedure for extracting system response functions without using oscillatory signals.
2. To quantify the effect of a leak on the response of the system in the *frequency* domain and develop a method of leak detection based on an analytical understanding of leak-induced behaviour.
3. To quantify the effect of a leak on the response of the system in the *time* domain and enhance existing reflectometry techniques using the system response function.
4. To compare leak detection approaches in the frequency domain and the time domain and determine situations where each is more appropriate.
5. To validate the proposed leak detection procedures using numerical and experimental results.

These objectives are met in this dissertation through application of the systems identification approach. As discussed in the introduction, extracted system response functions provide insight into the effect of a leak and the effect of different injected signals in the time and frequency domains. The system response function in the frequency domain is of particular interest as it identifies the harmonic frequencies of a pipe and is important for design of pipelines and stability of associated turbomachinery (Brekke, 1984).

In the past, system response functions were extracted through the use of sinusoidal oscillations of specially designed valves (Zielke *et al.* 1969, Brekke 1984, Svingen 1996). This approach is time consuming as the pipeline needs to be sequentially excited at many frequencies, which can take many hours depending on the size of the system and the resolution required in the response functions. Alternatively, this thesis uses conventional transient signals such as sharp closures of valves. The time required for the extraction of

the response function in this fashion is equal to the duration of a single transient event. The bounds of validity of this approach, including the selection of the input variable to avoid system non-linearities were investigated.

Analysis of a transient signal in the frequency domain has gained attention in recent years as an alternative to conventional time-domain approaches, for example, in Covas and Ramos (1999), Mpesha *et al.* (2001, 2002) and Ferrante *et al.* (2001). However, these papers present conflicting theories concerning the effect of a leak on the frequency response of a pipeline, and the leak detection methods in these papers have yet to be experimentally verified. This thesis establishes the true frequency response of a leaking pipeline and develops a leak detection procedure based on this behaviour. This procedure is verified numerically and experimentally to confirm its applicability.

When an injected transient signal impinges upon a leak, part of its energy is reflected to form a separate signal. Detection of this reflected signal in the time series pressure trace and determination of its arrival time give the leak location. This technique is known as time-domain reflectometry (Maloney 1973, Harding 1974). The system response function in the time domain, known as the *impulse response function*, can improve existing time-domain reflectometry procedures.

Care was taken to address many of the issues that would be encountered in a field pipeline system. These issues include the application of the technique on pipelines systems with complex topologies (branch, networks), the effect of steady and unsteady friction, the effect of a shift in measurement position, the effect of multiple faults of different characteristics (leaks and blockages) and the effect of random and harmonic noise contamination. While this list of issues is not intended to cover the range of complexities in a full field trial, these investigations allow the logical progression of the work into real system in future research.

This dissertation provides a critical comparison between leak detection procedures in the time and frequency domains. Through this investigation, the advantages and disadvantages of each procedure are determined.

1.3 THESIS OUTLINE

The first three chapters of this thesis provide background to the study. Chapter 2 is the literature review and contains a summary of the current leak detection techniques. Chapter 3 presents the fundamental equations of unsteady flow in a pipeline with both the time- and frequency-domain solutions to the equations. Using these governing equations, two numerical models were developed in Fortran 90, one in the time domain and the other in the frequency domain. Chapter 4 presents the experimental and numerical pipelines used in this dissertation.

In Chapter 5, a procedure for extracting the system response function is presented and experimentally verified. The bounds imposed by the linearity assumption are investigated in this chapter. Original work in this chapter includes determination of the best input signal, of the optimum system configuration and of the effect of different injected signals on the response extraction process. Chapter 5 presents a procedure where infinite energy signals (signals that do not return to the original level, e.g. a step) can be modified so that conventional Fourier analysis can take place. This modification is vital for the accurate extraction of system response functions using these signals.

Chapters 6 and 7 show how system response functions can be used to locate leaks. In particular, Chapter 6 presents a set of derived analytical expressions that describes the effect of a leak on the frequency response function for different boundary conditions. These expressions were incorporated into a leak detection method and were experimentally validated. The leak detection procedure can be applied to complex pipeline networks, detection of multiple leaks and detection of discrete blockages. Chapter 7 introduces the time-domain method of leak detection, known as time-domain reflectometry, and shows how the conventional methodology may be improved through the impulse response function. Chapter 8 compares procedures for fault detection in the time domain compared to the frequency domain and describes situations when each approach is more appropriate. Finally, the conclusions of the thesis are summarised in Chapter 9. The transient data presented in this thesis are included in an attached CD-ROM. The file name for each data set is stated in the captions of the figures.

1.4 PUBLICATION LIST

The following is the list of publications produced during this research.

Journal Publications:

1. Lee P.J., Simpson A.R., Lambert M.F., Vítkovský J.P., Misiunas, D. "Leak detection in pipelines using transient reflection." Submitted to *Journal of Hydraulic Engineering*, ASCE, Nov 2003. *Under Review*.
2. Lee P.J., Vítkovský J.P., Lambert M.F., Simpson A.R., Liggett J.A. (2003). "Detecting pipeline leaks using the frequency response diagram." *Journal of Hydraulic Engineering*, ASCE. *In print*.
3. Lee P.J., Vítkovský J.P., Lambert M.F., Simpson A.R., Liggett J.A. (2003). "Pattern-damping of the system frequency response function for the location of leaks in single pipelines." *Journal of Sound and Vibration*. *In print*.
4. Lee P.J., Vítkovský J.P., Lambert M.F., Simpson A.R., Liggett J.A. (2003). "Detection of discrete blockages in fluid pipelines using the frequency response function." Submitted to *Journal of Hydraulic Engineering*, ASCE, Nov 2003. *Under review*.
5. Lee P.J., Lambert M.F., Simpson A.R. (2002). "Critical depth prediction in straight compound channels." *Journal of Water and Maritime Engineering*, Proceedings of the Institution of Civil Engineers, **154**(4), December, pp. 317 - 332.
6. Lee P.J., Lambert M.F., Simpson A.R., Vítkovský J.P., Liggett J.A. "Experimental verification of leak detection in pipelines using linear transfer functions." Submitted to *IAHR, Journal of Hydraulic Research.*, May 2004. *Under review*.
7. Lee P.J., Vítkovský J.P., Lambert M.F., Simpson A.R. "Experimental extraction of frequency response function in hydraulic systems using PRBS." Submitted to *Journal of Fluids*, May 2004, *under review*.

-
8. Lee P.J., Vítkovský J.P., Lambert M.F., Simpson A.R. "Leak location in pipelines using the impulse response function." *In Process*.

Journal Discussions / Closures

1. Lee P.J., Vítkovský J.P., Lambert M.F., Simpson A.R., Liggett J.A. (2003). Discussion of "Leak detection in pipes by frequency response method using a step excitation by Witness Mpesha, M. Hanif Chaudhry and Sarah L. Gassman. 2002, 40(1), 55-62." *Journal of Hydraulic Research*. IAHR, 41(2), 221-223.
2. Lee P.J., Lambert M.F., Simpson A.R. (2003). Closure to "Critical Depth Prediction in Straight Compound Channels. *Journal of Water and Maritime Engineering*, Proceedings of the Institution of Civil Engineers, *In Print*

Conference Papers

1. Lee P.J., Vítkovský J.P., Lambert M.F., Simpson A.R. and Liggett J.A. (2004). "Experimental validation of frequency response coding for the location of leaks in single pipeline systems." *The practical application of surge analysis for design and operation, 9th international conference on pressure surges*, BHR Group. Chester, UK, 24 – 26 March 2004, pp. 239 – 253.
2. Lee P.J., Vítkovský J.P., Lambert M.F., Simpson A.R. and Liggett J.A. (2003). "Frequency response coding for the location of leaks in single pipeline systems." *Pumps, Electromechanical Devices and Systems Applied to Urban Water Management*, IAHR – IWA, 22-25 April, Valencia, Spain.
3. Lee P.J., Vítkovský J.P., Lambert M.F., Simpson A.R., Liggett J.A. (2002) "Leak detection in pipelines using an inverse resonance method." *Environmental and Water Resources Systems Analysis (EWRSA) symposium*. May 19-22, Roanoke, Virginia, USA

-
4. Lee P.J., Lambert M.F., Simpson A.R. (2001). "Predicting critical depth in straight compound channels." *6th International Conference on Hydraulics in Civil Engineering*. The Institution of Engineers, Australia. 28th – 30th November 2001, Hobart, Australia.
 5. Vítkovský J.P., Lee P.J., Stephens M.L., Lambert M.F., Simpson A.R. and Liggett J.A. (2003). "Leak and blockage detection in pipelines via an impulse response method." *Pumps, Electromechanical Devices and Systems Applied to Urban Water Management*, IAHR – IWA, 22-25 April, Valencia, Spain.
 6. Lambert M.F., Simpson A.R., Vítkovský J.P., Wang X.J. and Lee P.J. (2003). "A Review of leading-edge leak detection techniques for water distribution systems." *Ozwater Convention Exhibition – AWA 20th Convention*, 6-10 April, Perth, Australia.
 7. Vítkovský J.P., Stephens M.L., Lee P.J., Simpson A.R., Lambert M.F. (2003) "The detection and location of leakage, blockage and air pockets using radar-based techniques." *Australian Water Association SA Branch Regional Conference*, 6 August, Adelaide, Australia.
 8. Lambert M.F., Simpson A.R., Vítkovský J.P., Wang X.J. and Lee P.J. (2002). "A Review of leading-edge leak detection techniques for water distribution systems." *Australian Water Association SA Branch Regional Conference*, 5 July, Adelaide, Australia.

1.5 SIGNIFICANT CONTRIBUTIONS TO THE FIELD

The main contributions from this research are:

- The development of a procedure for extracting frequency response functions without using oscillatory signals. This procedure operates within the bounds of the linearity approximation. This procedure can be beneficial for the study of frequency dependence behaviour such as unsteady friction, fluid-structure interaction and stability analysis of turbomachinery in pipelines.
- The determination of injected signal properties that provide maximum information. Related to this outcome is the determination of the range of useful frequencies in any measured transient signal. This result allows the optimum design of filters for removal of high-frequency contamination in transient data.
- The quantification of the effect of leaks and blockages on the frequency response of a pipeline and comparison between time and frequency-domain techniques for leak and blockage detection.

CHAPTER 2

LITERATURE REVIEW

2.1 INTRODUCTION

Existing leak detection methods can be grouped under two categories, non-hydraulic and hydraulic methods. Non-hydraulic methods detect a leak based on external clues: noise emission; a point of high electric conductivity, signifying a collection of fluid; non-uniformity in pipe material; or simply a point in the ground where water appears to be originating. Techniques that utilise this type of information range from visual inspection of a pipeline (Black, 1992) through the use of liquid-sensing cables (ADEC, 2000), robotic pigs (Furness and van Reet, 1998), ground penetrating radar (Eiswirth and Burn, 2001) and acoustic correlators (Fuchs and Riehle 1991, Tafuri 2000). These techniques are short ranged and can only detect a leak at close proximity (< 250 m).

On the other hand, hydraulic techniques detect a leak based on its effect on flow behaviour and have a greater detection range. There are two main branches of hydraulic techniques: those that operate under steady state flow and those that operate under unsteady flow. Steady flow occurs when the flow and head conditions at any point do not change with time, whereas in unsteady flow, flow conditions change. Flows in water distribution systems are often unsteady due to fluctuations in demands and boundary conditions. For this reason, unsteady state methods are better suited to this situation. Examples of steady state methods include mass balance (ADEC, 2000) or hydraulic grade line measurements (Covas and Ramos, 1999), whereas unsteady state leak detection requires use of fluid transients (pressure changes). These techniques are discussed in this chapter to identify the advantages in applying fluid transients for detection of leaks.

2.2 NON-HYDRAULIC LEAK DETECTION TECHNIQUES

Non-hydraulic detection procedures range from simple techniques such as visual inspection to acoustic methods. These techniques detect a leak based on its external manifestations, which include:

- A break in pipe material
- Release of water
- Generation of a characteristic hissing noise

The most rudimentary of all is visual inspection. It requires one or more inspectors to be on site looking for visible cracks or leaks. Vegetation change, often associated with an increase in soil moisture, is indicative of a leak. An alternative is to inject odorants (such as mercaptans and trimethylamine) into pipelines and use odour detectors to find positions where material is leaking. Dyes and radioisotopes can also be used in this fashion (Pregelj *et al.*, 1997). This technique requires the pipe to be off-line to ensure the complete removal of these materials.

These basic methods require clear access to suspected leak areas. In some cases, visual inspection of pipes is impossible, for example, if the pipes are located in sensitive areas, buried underground or submerged. The use of odour detectors is dependent on weather conditions (Furness and van Reet 1998, Black 1992). In the United States of America, a landowner-awareness program has been implemented (Scott 1999a, 1999b) whereby landowners are employed by companies to inspect pipes regularly that traverse their own land. This program, however, was found to be inadequate, as small defects can remain unnoticed to untrained eyes.

Another group of non-hydraulic leak detection methods uses special detectors mounted at regular intervals along the pipeline. These devices, while being capital-intensive, provide an alternative to manual inspection. Sensors can be used to detect spillage or non-conformity in a pipe wall. An example is liquid sensing cables. These cables are buried beneath pipes and are designed to detect changes in soil moisture using a continuously transmitted electric pulse (ADEC, 2000). In the presence of a leak, the cable becomes

saturated and the impedance of the wire increases in the region, thus registering a leak in the system. A recent improvement uses fibre optic cables surrounded by a material that swells when exposed to liquid, compressing the attached optical fibre cable. This compression creates a localised loss in transmission that can be detected (MacLean *et al.*, 2001). The exposure of a sensor to fluid can typically be found within 30 seconds to an accuracy within ± 2 m. However, as this cable is required to run beneath the entire pipeline, the installation cost is extremely high. Typical cost of the cable is between \$A30 to \$A100 per metre and the cost of the associated software can range up to \$A100,000 (ADEC, 2000).

The use of a mobile robotic unit, known as a robotic pig, located in a pipe is another maintenance method. Robotic pigs (see Figure 2-1) can carry a vast array of surveillance and acoustic equipment to monitor the internal conditions of pipelines.

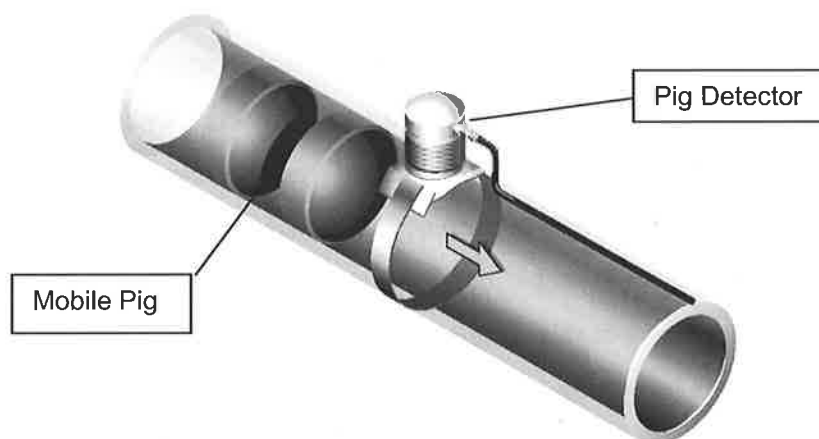


Figure 2-1 – Robotic pig-based monitoring system (Source: <http://www.Roxar.com>).

Pigs require tracking, as their movements are often impeded by debris and junctions (Furness and Van Reet, 1998). Pig-based monitoring, while effective, is subject to limitations imposed by the size and internal environment of the pipeline. High flows, pipe junctions, bends and valves can hinder the applicability of this expensive device (Scott 1999a, 1999b). The use of a robotic pig to detect leakage in an extensive water distribution network is limited.

Another non-hydraulic method of leak detection is the ground penetrating radar. This method injects an electromagnetic pulse into the ground and through the reflection profile picked up by receivers on the surface, the integrity of the pipe is determined. These radars detect a leak in two ways: by detecting soil cavities formed by the erosive effect of a leaking jet and by detecting regions of higher conductivity around the pipe, indicating a localised increase in moisture content (Eiswirth and Burn, 2001). This technique relies on a homogenous soil structure surrounding the pipeline. The presence of existing non-uniformities can be falsely detected as areas of concern.

Amongst the non-hydraulic leak detection methods, acoustic methods are most popular. Fluid jetting out of a leak generates high frequency vibrations in the pipe wall and transducers can be clamped onto pipes to collect the vibration data (AWWA, 1987). The transducers are shifted along the pipe until the maximum leak-induced signal is detected, identifying the location of the problem.

An advanced form of a single acoustic detector is a leak correlator, which uses a pair of transducers clamped upstream and downstream of a suspected leak position. For a leak at any non-central position between the two transducers, the same noise generated by the leak takes a different time to arrive at each of the transducers (see Figure 2-2). The cross-correlation between these two synchronised signals streams shows a maximum correlation at the time lag corresponding to this difference in travel time. By using this time lag, along with the known wave propagation speed and the relative strengths of the signals detected at each transducer, the position of the leak can be determined.

One of the main problems with using acoustic waves for leak detection is that acoustic signals attenuate quickly with distance. For steel pipes, the maximum range is 250 m away from the source (Tafari, 2000). In addition, the presence of elbows, junctions and system irregularities between leak correlators can lead to false detection.

Unlike other techniques, acoustic methods are most applicable in the case of small leaks as larger leaks produce less noise in the characteristic high-frequency range. Furthermore, the composition of the ground, the characteristics of the surface and the material of the pipe play important roles in the results.

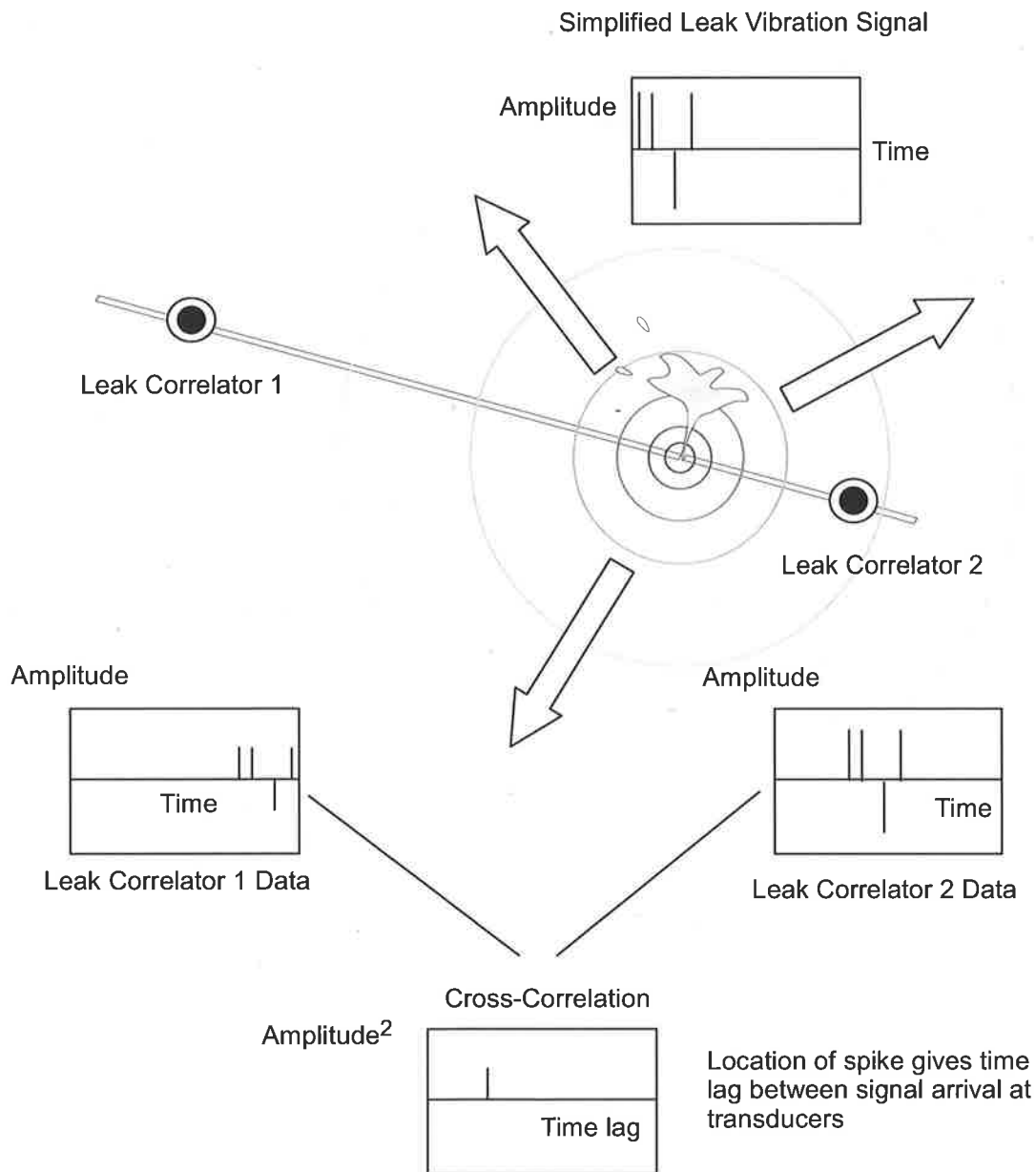


Figure 2-2 – Operation of leak correlators.

For steel or prestressed concrete pipes, the conductivity of the pipe wall can provide the means for detecting breaks (Atherton *et al.*, 2000). This technique requires insertion of an exciter coil and a detector, spaced two meters apart, in the pipeline. A low frequency AC current is passed through the exciter coil, generating a magnetic field. This field propagates along the pipe and is picked up by the detector. The strength of the detected magnetic field gives an indication of the integrity of the pipeline between the exciter and the detector. This technique can detect single or multiple breakages within a short-range (< 2 m). At best, it can test several kilometres in a full day and its range can quickly become prohibiting as the length of the pipeline increases (Atherton *et al.* 2000).

Each non-hydraulic method of leak detection suffers from a low operational range that hampers its application in large-scale pipelines. Typically, leaks can only be detected if the unit is less than 2 m from the leak for electromagnetic techniques and up to 250 m for acoustic methods. For ground penetrating radar, liquid sensing cables and visual inspection, the unit/operator must be in the immediate vicinity of the fault. This shortfall poses a problem for the application of these techniques in transmission mains that are kilometres in length, limiting testing to a section-by-section basis. Furthermore, the use of these techniques in a continuous monitoring system requires a large number of units placed at close intervals and the cost can become prohibitive as the length of the pipe increases. Consequently, such methods are usually applied on an individual basis, when the problem of the leak has become noticeable (which is often too late). For these reasons, techniques that have a range of operation similar to the scale of the system are desirable.

2.3 REMOTE HYDRAULIC METHODS

Hydraulic methods utilise the effect of a leak on flow behaviour in a pipeline for detecting and locating the problem. These effects can be detected at great distances from the leak, giving an operational range that cannot be matched using other methods. As water is continuously being lost from a leak, it causes a difference between inflow and outflow, a change in slope of the hydraulic grade line and a change in unsteady behaviour (Furness and van Reet 1998, Black 1992). Hydraulic techniques currently form the basis of computational pipeline monitoring systems (CPM) for existing large scale oil and gas pipelines as required by the U.S. Department of Transportation Office of Pipeline Safety (DOT-OPS) regulation 49 CFR 195 (Scott 1999a, 1999b).

Two broad categories exist for the classification of hydraulic methods of leak detection. These include steady state and unsteady state techniques. Steady state techniques are used in situations where flow fluctuations at any point in the system can be assumed small, whereas unsteady state techniques apply to a broader range of flow conditions.

2.3.1 Steady State Methods

Mass balance is the most commonly used steady state leak detection method due to its simplicity. The basic principle is that the total volume entering a pipeline must be equal to the total volume exiting (within a certain tolerance). If there is a deficit, then a leak exists. This relationship is stated as

$$|Q_{in} - Q_{out}| \geq \partial Q_m + \frac{\partial V_s}{\Delta t} \quad (2.1)$$

where Q_{in} = measured inflow to the system, Q_{out} = measured outflow from the system, ∂Q_m = bound of uncertainty in flow measurement and ∂V_s = bound of uncertainty in fluid compression over the time interval Δt (ADEC, 2000). While the mass balance procedure is useful in detecting leaks, it cannot find their locations. For a leak to be located, the network must be broken down into subsections, each supplied by a single supply main. A

mass audit is performed for each subsection and a stepwise elimination method is used to gradually remove the subsections that are free from leaks. This method can be time consuming as a volumetric system balance must be performed over a significant period of time to minimise errors (AWWA, 1987). A full water audit may take a number of months to successfully isolate a problem to a single pipe or pipe section (Wang, 2002). In addition, the accuracy of this method hinges on the accuracy of the measuring instrument and size of the leak.

Line pressure measurements are often used in conjunction with the mass balance method. A leak reduces flow downstream and changes the slope of the hydraulic grade line. Predicted hydraulic grade lines from flow measurements can be compared to pressure measurements taken at particular points along the system. Discrepancies between the two are indicative of leaks (Furness and van Reet, 1998).

Using a similar approach, Baghdadi and Mansy (1988), and Covas and Ramos (1999) developed algorithms to determine leak size and location under steady state conditions. The properties of a leak are determined based on the continuity equation, the friction loss along each pipe section and the orifice equation.

Mukherjee and Narasimhan (1996) and Poulakis *et al.* (2003) presented alternative procedures where the steady state head and discharge measurements are incorporated in a statistical maximum likelihood method to identify the leaking pipe in a network. The procedure correctly predicted the leaking pipe in only 70% of the single leak tests. For multiple leaks, the correct leaking pipes were identified 50% of the time.

Pudar and Liggett (1992) proposed an inverse calibration process where the measured steady state head and flow in the pipeline were used to determine the position of leaks in the system. The leak position in a numerical model is varied (through a Levenberg-Marquardt algorithm) until a good match is found with the measured responses. However, flow in steady state was found to supply insufficient data for the sizing and location of leaks using this technique. The application of this technique in unsteady flow removes this problem and is described later in this chapter.

While steady state approaches are successful in controlled situations, nevertheless, the application of these techniques to operating pipelines has proved difficult. The primary problem with these techniques is that each measurement station under steady state flow results only in a single data point. A high number of measurement stations and several experiments under different conditions are required to produce sufficient data for analysis. Sensitivity to discharge readings, presence of system noise and transient disturbances have given low confidence to steady state methods (Covas and Ramos, 1999). Furthermore, steady state condition is a special case of transient flow and rarely occurs in reality (Liggett and Chen 1994). Models based on unsteady conditions are more applicable to real systems.

2.3.2 Unsteady State Hydraulic Methods

Unsteady flows are caused by changes in demands, operation of pumps, adjustment of control valves and accidental events. These changes propagate along a pipeline as transient waves at speeds over 1,000 m/s (Wylie and Streeter, 1993). Fluid transients can persist over many kilometres (Tafari 2000, Silva *et al.* 1996) and each measurement station can produce a very large number of data points for analysis.

A simple technique using transients for leak detection is known as rarefaction wave detection. This technique detects the low-pressure surge generated by pipe rupture (Silva *et al.* 1996, ADEC 2000, Misiunas *et al.* 2003, 2004). The arrival time of this negative wave at each measurement transducer and knowledge of the wave speed gives the leak location. This technique is promising and can be easily incorporated into a real-time fault monitoring system. However, it requires accurate detection of a small pressure signal of an unknown shape. Existing background noise can mask this signal if the leak is small. Further research needs to be conducted in this area to determine the failure mechanism of pipelines, the shape of natural burst signals and the practical implementation of this procedure given the large amount of generated data.

An alternative approach to transient leak detection can be taken if customised pressure signals are *injected* into a pipeline and the subsequent behaviour of the transient analysed. During its travel, a signal acquires properties that relate to the configuration and integrity

of a system. The analysis of this signal can detect and locate leaks in a pipeline. These injected transients are designed to be small and can be used on a regular basis as a system monitoring technique. Using this method, operators are concerned solely with the behaviour of this injected signal, which is distinct from background noise and pressure fluctuations .

A leak changes measured flow and head response from the expected behaviour of a transient event. An illustration of the types of leak-induced modification is shown in the numerical results of Figure 2-3. In the figure both damping rate and the shape of the transient trace have changed in the leaking case.

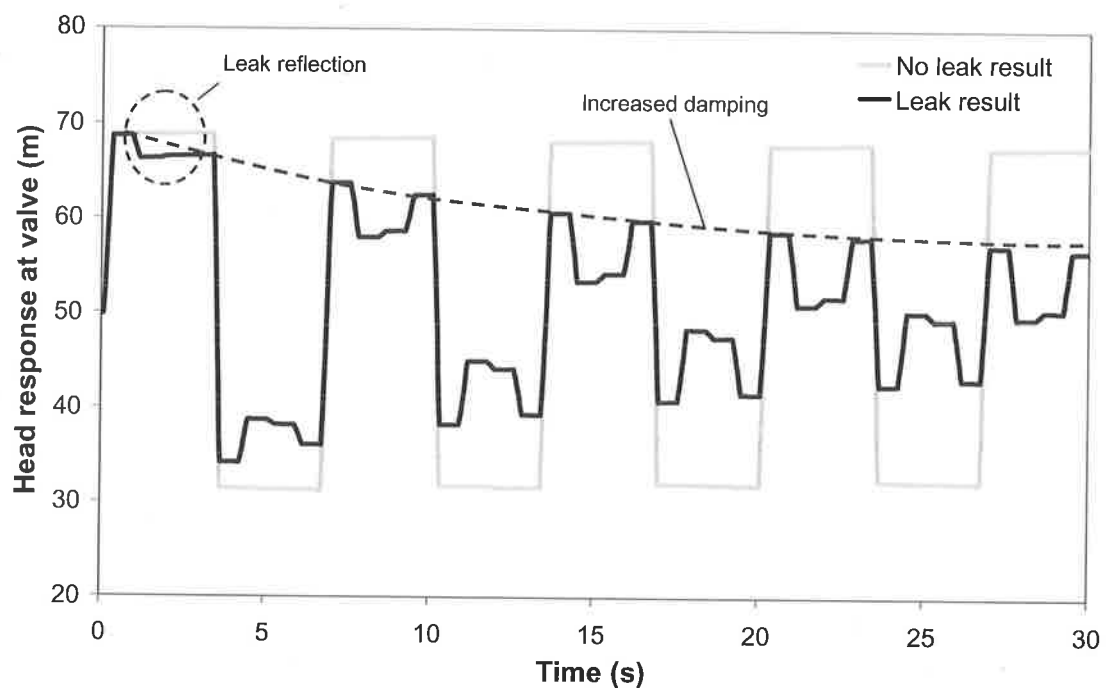


Figure 2-3 – Comparison of transients in intact and leaking pipelines.

Liou and Tian (1995) applied this discrepancy between leak and no-leak transient behaviour for leak detection. A method of characteristics model was used to predict the response given certain initial conditions. Deviation of measured results from predicted transient response indicates a leak. Other developments by Liggett and Chen (1994), Vítkovský and Simpson (1997), Vítkovský *et al.* (1999), Vítkovský *et al.* (2000), Simpson *et al.* (2000) moved leak transient analysis into an area that involves inverse parameter estimation based on a comparison of the observed pressure trace with the predicted trace from a numerical model. Leak size and location are varied through the Levenberg-

Marquardt algorithm (Liggett and Chen 1994), genetic algorithm (Simpson *et al.* 2000) or shuffled complex evolution (SCE) to achieve a least squares fit of the numerical data to the measured data. If the model is an accurate depiction of real system behaviour, the best match is obtained when correct values of leak size and position are selected. The advantage of inverse transient analysis is that detailed flow properties can be determined.

Liggett and Chen (1994), Vítkovský and Simpson (1997) and Vítkovský *et al.* (1999) show this inverse calibration technique (commonly known as inverse transient analysis) to be successful at both numerical and laboratory levels. Covas *et al.* (2004) and Stephens *et al.* (2004a, 2004b) have applied this procedure in the field with promising outcomes. However, there are drawbacks to this type of approach, including the large computational effort that can delay the reaction time of operators to faults in a pipeline. Each iteration of the optimisation algorithm requires a full solution of the transient response in the system and inverse runs with highly discretised numerical models can take hours to converge to the solution using current high-end desktop computers (Pentium IV processors). In addition, the technique relies on the accuracy of the numerical model and detailed inspection of pipeline components is needed before the leak detection process can take place. While the greatest advantage to the inverse transient method is its attention to detail, in a field hydraulic system the existing physical complexities can become overwhelming. Alternative approaches that do not require accurate predictions of the transient trace are attractive.

The effects of a leak on a transient signal can be used as a means for detecting a problem and they are as follows.

- Leaks in a pipeline increase the damping rate of a transient trace (a recording of pressure changes to an injected transient) (Wang *et al.* 2002, Wang 2002).
- Leaks in a pipeline produce reflected signals in a transient trace (Jönsson and Larson 1992, Covas and Ramos 1999).

These specific leak-induced modifications can be identified through knowledge of system behaviour when no leak exists, for example, the rate of damping or the shape of the transient signal. Any detectable difference from the norm is indicative of a leak and can

provide information concerning its location and size. A leak can be located once the analytical relationship between the leak position and the observed leak effect is derived.

The effect of a leak on the damping rate of the transient trace was derived in Wang *et al.* (2002). The energy of the wave front is gradually dissipated through steady and the unsteady friction losses (Zielke 1968, Vardy and Brown 1995) and, as illustrated in Figure 2-3, a leak increases this damping rate of the signal. Once the decay rate of a transient is found under a no-leak condition, any significant deviation from this decay rate indicates a leak. Wang *et al.* (2002) developed an analytical solution describing the decay of harmonic components in a transient trace as

$$h^*(x^*, t^*) = \sum_{n=1}^{\infty} \left\{ e^{-(R+R_{nL})t^*} \left[A_n \cos(n\pi t^*) + B_n \sin(n\pi t^*) \right] \sin(n\pi x^*) \right\} \quad (2.2)$$

where $x^* = x/L$, $t^* = t/(L/a)$, $h^* = (H-H_0)/H_1$ with H_0 = initial head prior to the transient, H_1 = a reference head at a tank. $R = \frac{fLQ_0}{2aDA}$ and R_{nL} = leak-induced damping of each Fourier component given as

$$R_{nL} = \frac{C_d A_L}{A} \frac{a}{\sqrt{2gH_{L0}}} \sin^2(n\pi x_L^*) \quad (2.3)$$

where $x_L^* = x_L/L$, x_L = distance of the leak from upstream boundary, $C_d A_L$ = the lumped leak discharge coefficient, H_{L0} = the head at the leak prior to the transient event, A = pipe area. A_n , B_n for each harmonic number, n , are given by

$$A_n = 2 \int_0^1 f(x^*) \sin(n\pi x^*) dx^* \quad (2.4)$$

$$B_n = \frac{2}{n\pi} \int_0^1 g(x^*) \sin(n\pi x^*) dx^* + \frac{(R+R_{nL})A_n}{n\pi} \quad (2.5)$$

From Eq. (2.3), the leak-induced damping depends on the harmonic number, n . This relationship suggests that the effect of a leak on the transient signal is frequency-dependent. Wang *et al.* (2002) calculated the leak location from the ratio between the leak-induced damping for two harmonic components n_1 and n_2 ,

$$\frac{R_{n_2L}}{R_{n_1L}} = \frac{\sin^2(n_2\pi x_L^*)}{\sin^2(n_1\pi x_L^*)} \quad (2.6)$$

where the magnitude of the leak-induced damping is the difference between the damping from the leaking and intact pipeline. Once x_L^* is known, the size of the leak is found from Eq. (2.3).

The transient damping method does not depend on an accurate numerical model to the same extent as the inverse transient method; however, it requires knowledge of friction damping in the leak-free pipe. The magnitude of the friction losses can be estimated using a numerical model or a known leak-free benchmark.

When a propagating transient signal arrives at a leak, part of the energy in the main transient is diverted to form a new reflected signal. Detection of this reflected signal and measurement of its arrival time can be used to locate the leak. The arrival time of the reflected signal at the transducers is the time needed for the signal to travel from the transient source, reflect off the leak and travel to the measurement station. Given a known wave speed, the location of the fault can be determined from this arrival time. The application of this procedure, known as time-domain reflectometry (TDR), requires knowledge of the shape of the leak-free transient trace to identify leak reflections. The operation of this TDR procedure is illustrated in Figure 2-4.

This technique was used in Jönsson and Larson (1992), Brunone (1999), Covas and Ramos (1999), Jönsson (2001) and Ferrante and Brunone (2001) as a means of leak location. Chapter 7 of this thesis provides an improvement to the TDR approach using system response functions. Although formulations were given in Covas and Ramos (1999), Brunone (1999), Jönsson (2001) for finding leak size from the magnitude of the leak-reflections, these were based on the assumption of negligible friction. In pipes where

losses are dominant, these equations are inaccurate and can only be used as a rough estimate of the leak size. In Brunone (1999), the error was 17% of the true value under laboratory conditions. It is only through a good knowledge of losses that a valid prediction of leak size can be made.

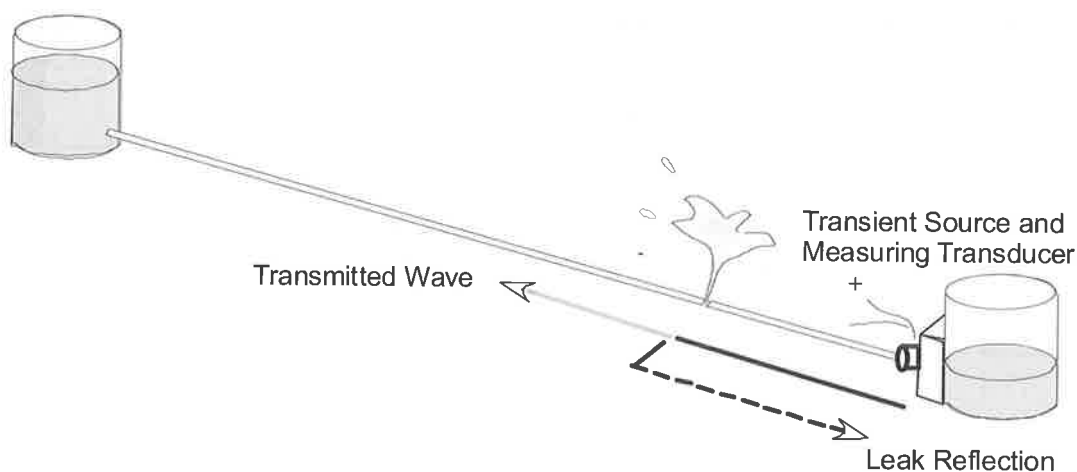


Figure 2-4 – Illustration of the operation of time-domain reflectometry.

The concept of TDR hinges on detection and location of leak-reflected disturbances in the transient trace. In Brunone (1999), these signals were detected through a visual comparison between the leak-free transient response and the observed trace. While simple to apply, an experienced technician is required. Pipeline vibrations, background transients and instrument noise can create pressure traces where leak-reflected signals cannot be easily identified. Slow, smooth transients produce reflections that are difficult to detect, whereas sharp signals create reflections that are more distinguishable (Jönsson and Larson, 1992). An explanation for this observation is given in Chapter 5 of the thesis in terms of signal bandwidth.

Jönsson and Larson (1992) and Covas and Ramos (1999) proposed spectral analysis as a means for detecting leak reflections, postulating that the leak-reflected signal produces a “leak-induced frequency spike” in the frequency domain. This argument was perpetuated in Mpesha *et al.* (2001, 2002) where a frequency-domain leak detection method was presented based on the existence of additional spikes in the spectrum. Chapter 6 of this thesis presents results (from two independent formulations of the governing equations) that are not consistent with this idea, showing that leaks have a detectable effect only at

fundamental frequencies of the pipeline. This finding is supported in Wang *et al.* (2002), Ferrante *et al.* (2001) and with experimental results in Lee *et al.* (2004).

There are recent developments by Ferrante and Brunone (2001) and Ivetić and Savić (2002) that use discrete wavelet transform to detect leak reflections in the transient trace. The wavelet transform involves a time convolution of the data trace with localised mathematical functions and was designed to highlight discontinuities (i.e. sharp edges). These localised mathematical functions can be dilated or contracted in time to produce the time convolution result at different scales. It was suggested that the decomposition of the signal in this way could allow for the detection of a leak-reflected signal in the data. The wavelet transform is best suited for detecting discontinuities in a data trace and is affected by the shape of the injected transient and the rate of sampling (Young 1995). The detection of a leak reflection is difficult when the injected transient signal deviates from a perfect step / impulse. An alternate application of the wavelet transform is presented in Young (1995); it uses the system response functions investigated in this dissertation. This prevailing problem of reflection detection in TDR techniques and its strong dependence on the nature of the injected signal is presented in greater detail in Chapter 7.

2.4 SUMMARY

This chapter provides an outline of various leak detection techniques, including both hydraulic and non-hydraulic based methods. A summary of the hydraulic leak detection methods presented in this section is shown in Figure 2-5. A leak detection method should have a long detection range, allowing its application to a large-scale field pipeline. In this respect, the use of fluid transients is a promising research field as they naturally persist over long distances in pipelines (Silva *et al.* 1996).

A method of leak detection using transients operates through an inverse procedure where the measured result is fitted with the output from an accurate numerical model. The leak location and size are used as fitting variables and the best fit is produced when the correct location and size of the leaks are selected. This procedure is known as the inverse transient method (Liggett and Chen 1994, Vítkovský *et al.* 1999, Vítkovský and Simpson 1997, Simpson *et al.* 2000).

This approach, however, requires a large computational effort and an accurate numerical model. In a complex system, the establishment of this model requires a detailed understanding of the behaviour and location of each existing hydraulic element and a detailed survey is often necessary.

Alternatively, a leak can be detected in the pipeline through some knowledge of the expected leak-induced modifications on a transient response. For a measured transient trace, these leak-induced modifications are an increased damping rate and the presence of leak-reflected signals. This focus on the specific leak-induced modifications can allow the properties of the leak to be extracted from the transient trace without a clear understanding of the hydraulic behaviour of a pipeline.

This thesis investigates approaches that focus on leak-induced modifications on system response functions in both time and frequency domains (i.e. time-domain reflectometry and frequency-domain detection in Figure 2-5).

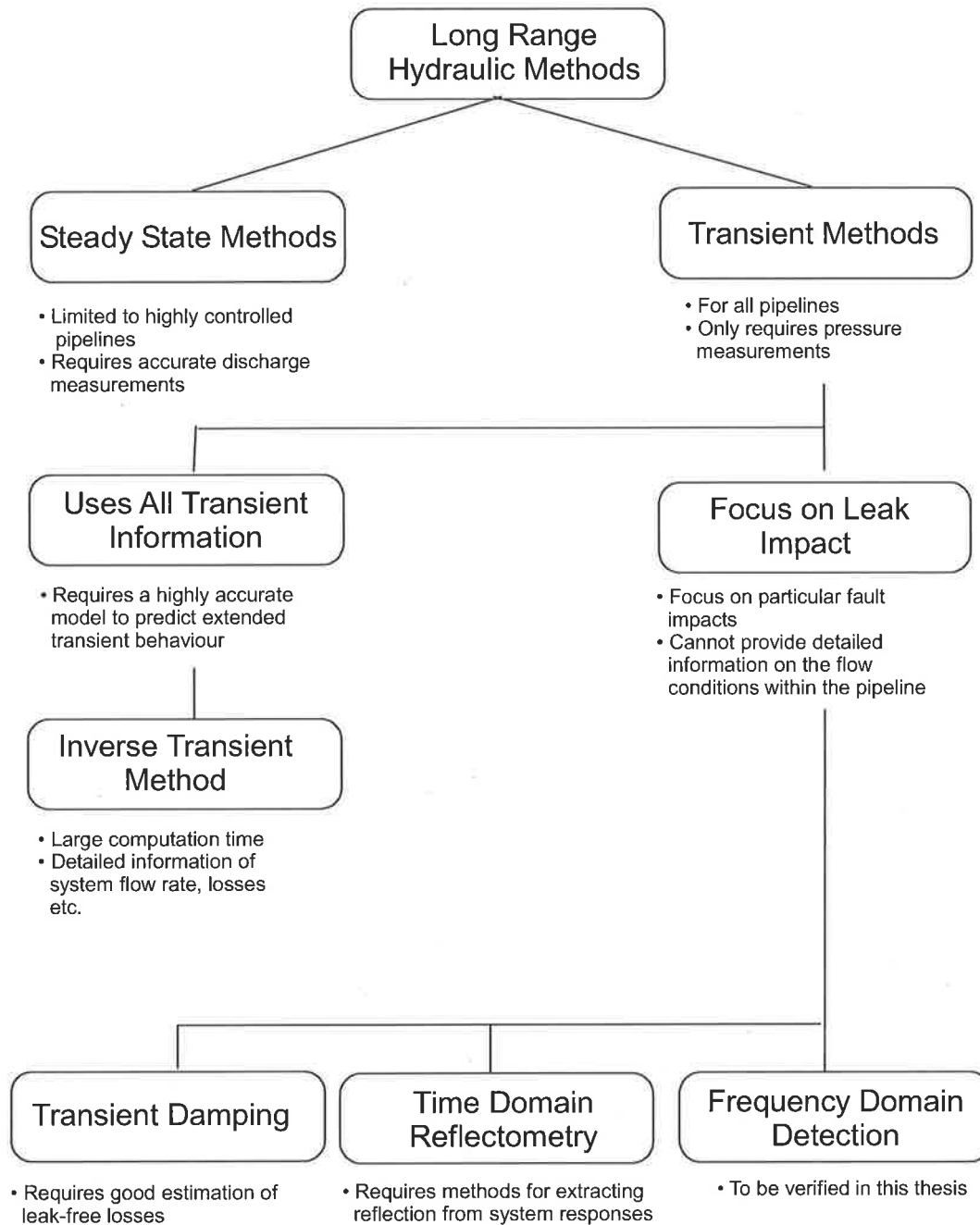


Figure 2-5 – Summary of remote hydraulic methods for leak detection.

CHAPTER 3

GOVERNING EQUATIONS

3.1 INTRODUCTION

The governing equations for unsteady pipe flow represent conservation of mass and linear momentum,

$$\frac{gA}{a^2} \frac{\partial H}{\partial t} + \frac{\partial Q}{\partial x} = 0 \quad (3.1)$$

$$\frac{1}{gA} \frac{\partial Q}{\partial t} + \frac{\partial H}{\partial x} + \frac{fQ|Q|}{2gDA^2} = 0 \quad (3.2)$$

where Q and H = discharge and head in a pipe, g = acceleration due to gravity, D = pipe diameter, A = pipe cross-sectional area, a = wave speed, f = Darcy-Weisbach friction factor, x = distance along the pipe and t = time (Wylie and Streeter, 1993). These equations assume that both the fluid and the pipe deform in a linear elastic fashion. This set of two hyperbolic differential equations can be solved in the time and space domain using a numerical scheme known as the *method of characteristics*, or alternatively, these equations can be linearised and solved in the frequency domain using a procedure known as the *transfer matrix method* (Chaudhry 1987, Wylie and Streeter 1993).

3.2 METHOD OF CHARACTERISTICS

The method of characteristics solution to Eq. (3.1) and (3.2) begins with a linear combination of the two equations. This linear combination allows the partial derivatives to be reformulated into directional (total) derivatives using the chain rule. The head and discharge at each point in a pipe can then be found by integrating the resultant equations (Wylie and Streeter, 1993).

Multiplying the unsteady continuity equation [Eq. (3.1)] by a factor λ and adding this to the momentum equation [Eq. (3.2)] give

$$\lambda \left(\frac{gA}{a^2} \frac{\partial H}{\partial t} + \frac{\partial Q}{\partial x} \right) + \frac{1}{gA} \frac{\partial Q}{\partial t} + \frac{\partial H}{\partial x} + \frac{f|Q|Q}{2gDA^2} = 0 \quad (3.3)$$

Grouping the partial derivatives of head and flow results in

$$\lambda \frac{gA}{a^2} \left(\frac{\partial H}{\partial t} + \frac{1}{\lambda} \frac{a^2}{gA} \frac{\partial H}{\partial x} \right) + \frac{1}{gA} \left(\frac{\partial Q}{\partial t} + \lambda gA \frac{\partial Q}{\partial x} \right) + \frac{f|Q|Q}{2gDA^2} = 0 \quad (3.4)$$

From the chain rule, the directional derivatives (denoted as 'd') of the head and discharge within the pipe can be given as a combination of its partial derivatives ('∂') by

$$\frac{dH}{dt} = \frac{\partial H}{\partial t} + \frac{\partial H}{\partial x} \frac{dx}{dt} \quad (3.5)$$

$$\frac{dQ}{dt} = \frac{\partial Q}{\partial t} + \frac{\partial Q}{\partial x} \frac{dx}{dt} \quad (3.6)$$

Comparing Eq. (3.5) to the expression contained within the first (left-most) parentheses of Eq. (3.4), the value of $\frac{dx}{dt}$ to convert the partial derivatives into a directional derivative is

$$\frac{dx}{dt} = \frac{1}{\lambda} \frac{a^2}{gA} \quad (3.7)$$

Following the same procedure for the second (right-most) parentheses of Eq. (3.4) results in

$$\frac{dx}{dt} = \lambda gA \quad (3.8)$$

Combining Eq. (3.7) and (3.8) gives the value of λ as

$$\lambda = \pm \frac{a}{gA} \quad (3.9)$$

for $\frac{dx}{dt} = \pm a$. When $\frac{dx}{dt} = a$, Eq. (3.4) becomes

$$\frac{1}{gA} \frac{dQ}{dt} + \frac{1}{a} \frac{dH}{dt} + \frac{fQ|Q|}{2gDA^2} = 0 \quad (3.10)$$

and when $\frac{dx}{dt} = -a$, Eq. (3.4) becomes

$$\frac{1}{gA} \frac{dQ}{dt} - \frac{1}{a} \frac{dH}{dt} + \frac{fQ|Q|}{2gDA^2} = 0 \quad (3.11)$$

These resultant equations [Eq. (3.10) and (3.11)] are known as the positive and negative *characteristic equations* and are valid only along the lines $\frac{dx}{dt} = +a$ and $\frac{dx}{dt} = -a$, respectively. These equations can be integrated to give expressions for the head and discharge in a pipe. For the positive characteristic (C^+), the integration is taken between two points ("A" and "P") on a characteristic line with an inverse slope $\frac{dx}{dt} = +a$ (refer to

Figure 3-1). In the same way, the limit of the integration for the negative characteristic (C⁻) is from “B” to “P” and is taken along the characteristic line of slope $\frac{dx}{dt} = -a$.

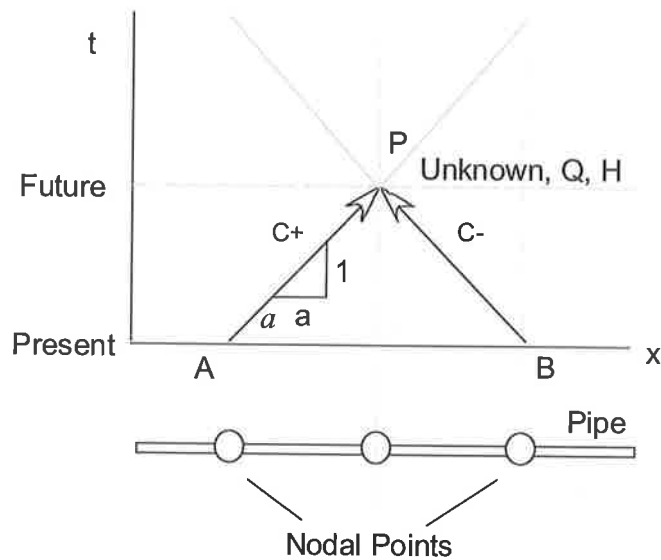


Figure 3-1 – Graphical representation of the characteristics equations.

The integrations along the positive and negative characteristics are shown in Eqs. (3.12) and (3.13)

$$\frac{1}{gA} \int_A^P dQ + \frac{1}{a} \int_A^P dH + \frac{f}{2gDA^2} \int_A^P Q|Q| dt = 0 \quad (3.12)$$

$$\frac{1}{gA} \int_B^P dQ - \frac{1}{a} \int_B^P dH + \frac{f}{2gDA^2} \int_B^P Q|Q| dt = 0 \quad (3.13)$$

The equations are integrated using a finite difference approximation for the friction term (the last term), which restricts results to a small increment in time and space (Jaeger, 1977). The integrated characteristic equations are

$$\frac{1}{gA} (Q_P - Q_A) + \frac{1}{a} (H_P - H_A) + \frac{f Q_A |Q_A| \Delta t}{2gDA^2} = 0 \quad (3.14)$$

$$\frac{1}{gA}(Q_P - Q_B) - \frac{1}{a}(H_P - H_B) + \frac{fQ_B|Q_B|\Delta t}{2gDA^2} = 0 \quad (3.15)$$

The integration of the flow in the friction term may be taken as $Q_P|Q_A|$ and $Q_P|Q_B|$ (Streeter and Wylie, 1983). The two characteristic equations form a set of simultaneous equations with two unknowns and can only be solved at the intersection points of the two characteristics. The head and discharge at an unknown point “P” can be found if conditions at a previous time step “A” and “B” are known (refer to Figure 3-1).

The behaviour of flow in a pipeline in time can, therefore, be modelled using a mesh of such intersecting characteristics, where the solution at each intersection (a *nodal point*) gives the head and discharge at that point for a particular instant in time. The number of nodal points in the pipe (representing the resolution of the analysis in space) can be increased by increasing the number of characteristics, as shown in Figure 3-2.

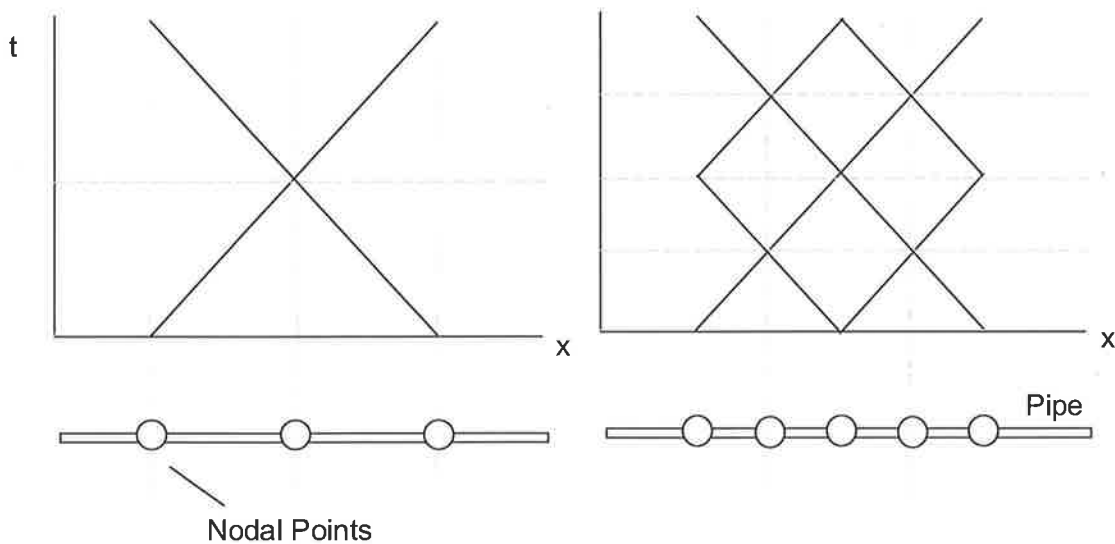


Figure 3-2 – Effect of increasing the number of nodal points and time steps on the resolution of the MOC analysis.

The behaviour of the flow at a future time step can be determined from a set of known head and discharge conditions at the nodal points. This procedure can continue indefinitely given that the conditions at the boundaries (i.e., the extremities of the pipe) are known at each time step. A boundary condition must be given at each end of the pipe and can be a specification of either of the unknowns (discharge or head) or a relationship

between them (e.g. the orifice equation). This time marching process is illustrated in Figure 3-3. More details concerning the method of characteristics (MOC) can be found in Wylie and Streeter (1993) and Chaudhry (1987).

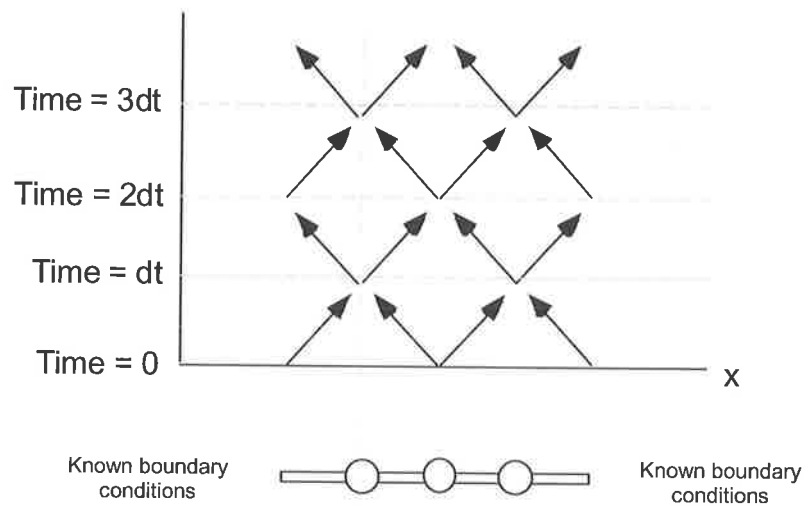


Figure 3-3 – Time marching progression of the MOC solution.

3.2.1 Incorporation of leak elements

A leak in a pipe can be represented in the MOC by a discontinuity in discharge across a node. For a leak the relationship between the flow upstream (Q_{PU}) and downstream (Q_{PD}) of a node is given by

$$Q_{PU} = Q_{PD} + Q_L \quad (3.16)$$

where, Q_L = flow out of the leak. Approximating the leak as an orifice discharging into atmospheric pressure changes Eq. (3.16) to

$$Q_{PU} = Q_{PD} + C_d A_L \sqrt{2g(H_{PU} - z_L)} \quad (3.17)$$

where, $C_d A_L$ = the lumped leak parameter with C_d = discharge coefficient, z_L = elevation of the leak and A_L = the area of the leak orifice. For small leaks, the head upstream of the leak (H_{PU}) can be approximated as equal to the downstream head (H_{PD}),

$$H_{PU} = H_{PD} \quad (3.18)$$

The unknowns at a leaking node are determined using the characteristic equations [Eqs. (3.14), (3.15)] and the relationships between the heads and discharges on either side of the leak [Eq. (3.17), (3.18)]. The variables at a leak orifice are shown in Figure 3-4.

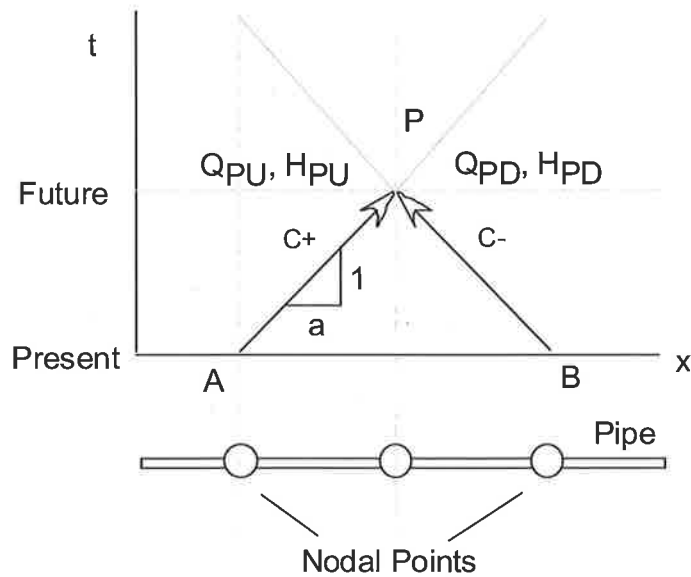


Figure 3-4 – Upstream and downstream discharge for each node.

The MOC scheme provides an efficient way to produce the transient response in the time domain. An alternative numerical scheme, using the linearised unsteady momentum and continuity equations can be used to determine the transient response in the frequency domain.

3.3 TRANSFER MATRIX EQUATIONS

Any injected transient event in a pipeline travels back and forth along the pipe through a series of regular boundary reflections. As a result, all transient signals appear as a periodic perturbation about the base conditions (conditions prior to the transient). The discharge and head in the pipe during a transient event can be written as

$$Q = Q_0 + q^* \quad (3.19)$$

$$H = H_0 + h^* \quad (3.20)$$

where the “0” subscript denotes the base value about which the transient occurs. The terms, q^* , h^* are the discharge and head perturbations about base values.

Substitution of Eqs. (3.19) and (3.20) into the unsteady continuity and momentum equations gives

$$\frac{gA}{a^2} \left(\frac{\partial H_0}{\partial t} + \frac{\partial h^*}{\partial t} \right) + \frac{\partial Q_0}{\partial x} + \frac{\partial q^*}{\partial x} = 0 \quad (3.21)$$

$$\frac{1}{gA} \left(\frac{\partial Q_0}{\partial t} + \frac{\partial q^*}{\partial t} \right) + \frac{\partial H_0}{\partial x} + \frac{\partial h^*}{\partial x} + \frac{f(Q_0 + q^*)|Q_0 + q^*|}{2gDA^2} = 0 \quad (3.22)$$

For a length of intact pipe where the base head and discharge do not change during the transient event and where the flow along the pipe is the same, the equations become

$$\frac{gA}{a^2} \left(\frac{\partial h^*}{\partial t} \right) + \frac{\partial q^*}{\partial x} = 0 \quad (3.23)$$

$$\frac{1}{gA} \frac{\partial q^*}{\partial t} + \frac{\partial H_0}{\partial x} + \frac{\partial h^*}{\partial x} + \frac{f(Q_0 + q^*)|Q_0 + q^*|}{2gDA^2} = 0 \quad (3.24)$$

Using a Taylor series expansion to first-order accuracy, where

$$(Q_0 + q^*)^2 = Q_0^2 + 2Q_0q^* \quad (3.25)$$

the equations now become

$$\frac{gA}{a^2} \left(\frac{\partial h^*}{\partial t} \right) + \frac{\partial q^*}{\partial x} = 0 \quad (3.26)$$

$$\frac{1}{gA} \frac{\partial q^*}{\partial t} + \frac{\partial H_0}{\partial x} + \frac{\partial h^*}{\partial x} + \frac{f(Q_0 + 2Q_0q^*)}{2gDA^2} = 0 \quad (3.27)$$

Knowing that the partial derivative of the base head with respect to distance along the pipe is equal to the rate of steady friction loss along the pipe,

$$\frac{\partial H_0}{\partial x} = -\frac{fQ_0}{2gDA^2} \quad (3.28)$$

and performing a Fourier transform on Eqs. (3.26), (3.27) (Oldenburger and Goodson, 1964) give the set of linearised unsteady continuity and momentum equations in the frequency domain as

$$\frac{\partial q}{\partial x} + \frac{i\omega gAh}{a^2} = 0 \quad (3.29)$$

$$\frac{\partial h}{\partial x} + \frac{i\omega q}{gA} + \frac{qfQ_0}{gDA^2} = 0 \quad (3.30)$$

where q , h are the magnitudes of the discharge and head oscillation at each frequency, ω , denoted by the removal of “*” above the terms and $i = \sqrt{-1}$. The word “oscillation” is defined in this thesis as a sinusoidal variation of a particular frequency, whereas “perturbation” implies a variation of any other form. Differentiating Eq. (3.29) with respect to x and multiplying Eq. (3.30) by $-i\omega gA / a^2$ and adding the results give

$$\frac{\partial^2 q}{\partial x^2} - \left(-\frac{\omega^2}{a^2} + \frac{i\omega gAR}{a^2} \right) q = 0 \quad (3.31)$$

where R = the frictional resistance term, equal to $(fQ_0)/(gDA^2)$ for turbulent flows or $(32\nu)/(gAD^2)$ for laminar flows, with ν as the kinematic viscosity. The expression in Eq. (3.31) is in the typical form of a second order partial differential equations with the general solution

$$q = c_1 \sinh(\mu x) + c_2 \cosh(\mu x) \quad (3.32)$$

where $\mu = \frac{1}{a} \sqrt{-\omega^2 + igA\omega R}$ and is known as the propagation function and c_1, c_2 are unknown coefficients. Substituting Eq. (3.32) into Eq. (3.29) gives the expression for the oscillatory head as

$$h = -\frac{a^2 \mu}{igA\omega} [c_1 \cosh(\mu x) + c_2 \sinh(\mu x)] \quad (3.33)$$

By substituting the known conditions at $x = 0$ as $q = q_n, h = h_n$ where the subscript “ n ” denotes the start of the pipe section under consideration, the coefficients c_1 and c_2 are determined to be

$$c_1 = -\frac{igA\omega}{a^2 \mu} h_n \quad (3.34)$$

$$c_2 = q_n \quad (3.35)$$

Using these values of the coefficients, the discharge and head variations measured at a distance “ x_m ” downstream from point “ n ” in the pipe is

$$q^{n+1} = (\cosh(\mu x_m)) q^n - \left(\frac{1}{Z} \sinh(\mu x_m) \right) h^n \quad (3.36)$$

$$h^{n+1} = (-Z \sinh(\mu x_m))q^n + (\cosh(\mu x_m))h^n \quad (3.37)$$

where $Z = \frac{\mu a^2}{i\omega g A}$ and is known as the characteristic impedance for the pipe section and the superscript “n+1” denotes the downstream point (D’Souza and Oldenburger 1964, Akiyama 1986, Chaudhry 1987). The solutions can now be expressed in matrix form,

$$\begin{Bmatrix} q \\ h \end{Bmatrix}^{n+1} = \begin{bmatrix} \cosh(\mu x_m) & -\frac{1}{Z} \sinh(\mu x_m) \\ -Z \sinh(\mu x_m) & \cosh(\mu x_m) \end{bmatrix} \begin{Bmatrix} q \\ h \end{Bmatrix}^n \quad (3.38)$$

Once the magnitude of the responses at the upstream end (at position n) is known, the response at any other point in the pipe can be determined using Eq. (3.38). The response magnitudes at the required downstream position can be produced by substituting different distances from the upstream boundary (x_m) into Eq. (3.38).

A common misconception regarding the transfer matrix solution is that it is limited to the analysis of oscillatory flow conditions in pipes. In reality, as every transient signal (for example a valve closure or pump trip) can be Fourier decomposed into a linear summation of oscillation frequencies, the transfer matrix can be used to describe how each of these frequencies propagates through the system. The results from the transfer matrix can then be inverse Fourier transformed back into the time domain to provide the equivalent transient trace (Tsang *et al.* 1985, Suo and Wylie 1989).

An advantage of the transfer matrix solution is a continuous representation of the pipe that is not restricted to a time-space discretised solution grid as in the method of characteristics when using finite difference approximations. In addition, in modelling unsteady friction and viscoelastic behaviour in pipelines, the analysis in the frequency domain can lead to a substantial increase in computational speed (Suo and Wylie, 1989). A detailed comparison of the results between the transfer matrix solution and the method of characteristics is shown in Chapter 5 where identical results were achieved using the two procedures.

3.3.1 Incorporation of leak elements

A leak that discharges into atmospheric pressure can be described by the orifice equation

$$Q_L = C_d A_L \sqrt{2g(H_L - z_L)} \quad (3.39)$$

where Q_L , H_L are the discharge and the head at the orifice, respectively, with z_L as the elevation at the orifice. Dividing Eq. (3.39) by the initial flow through the orifice (Q_{L0}) transforms Eq. (3.39) into

$$\frac{Q_L}{Q_{L0}} = \frac{C_d A_L \sqrt{(H_L - z_L)}}{(C_d A_L)_0 \sqrt{(H_{L0} - z_L)}} \quad (3.40)$$

Writing the discharge and head as perturbations about the initial condition and dividing both the nominator and the denominator of the right hand side by a reference orifice opening $(C_d A_L)_{REF}$ give

$$\frac{Q_{L0} + q_L^*}{Q_{L0}} = \frac{\tau}{\tau_0} \sqrt{\frac{H_{L0} + h_L^* - z_L}{H_{L0} - z_L}} \quad (3.41)$$

where, τ is the orifice opening coefficient = $C_d A_L / (C_d A_L)_{REF}$ and $\tau_0 = (C_d A_L)_0 / (C_d A_L)_{REF}$. By approximating the square root by a first-order Taylor series expansion and substituting $\tau = \tau_0 + \Delta\tau^*$ gives

$$\frac{q_L^*}{Q_{L0}} = \frac{\Delta\tau^*}{\tau_0} + \frac{h_L^*}{2(H_{L0} - z_L)} + \frac{h_L^*}{2(H_{L0} - z_L)} \frac{\Delta\tau^*}{\tau_0} \quad (3.42)$$

To convert the results into the frequency domain, the equation is Fourier transformed. In addition, assuming head continuity across the small orifice ($h_n = h_{n+1} = h_L$) and that the multiplication of two perturbations is negligible give

$$q_L = \frac{Q_{L0}\Delta\tau}{\tau_0} + \frac{Q_{L0}h_n}{2(H_{L0} - z_L)} \quad (3.43)$$

The Fourier transform changed all perturbation variables q^* , h^* into oscillatory variables, q and h . Using the mass balance across the orifice, where

$$q_n = q_{n+1} + q_L \quad (3.44)$$

and combining this with Eq. (3.43) give

$$q_{n+1} = q_n - \frac{Q_{L0}\Delta\tau}{\tau_0} - \frac{Q_{L0}h_n}{2(H_{L0} - z_L)} \quad (3.45)$$

By setting the size of the orifice opening as a constant ($\Delta\tau = 0$), the transfer matrix for a leak is

$$\begin{Bmatrix} q \\ h \end{Bmatrix}^{n+1} = \begin{bmatrix} 1 & -\frac{Q_{L0}}{2(H_{L0} - z_L)} \\ 0 & 1 \end{bmatrix} \begin{Bmatrix} q \\ h \end{Bmatrix}^n \quad (3.46)$$

Alternatively, the size of the orifice opening may be allowed to change (as in the case of a side-discharge valve). In this case, the $\Delta\tau$ term is retained and the transfer matrix becomes

$$\begin{Bmatrix} q \\ h \end{Bmatrix}^{n+1} = \begin{bmatrix} 1 & -\frac{Q_{L0}}{2(H_{L0} - z_L)} \\ 0 & 1 \end{bmatrix} \begin{Bmatrix} q \\ h \end{Bmatrix}^n + \begin{bmatrix} -\frac{Q_{L0}\Delta\tau}{\tau_0} \\ 0 \end{bmatrix} \quad (3.47)$$

Eq. (3.47) is used to model the behaviour of a side-discharge valve whereas Eq. (3.46) is limited to a static orifice such as a leak. Each transfer matrix determines the value of the head and discharge response downstream ($n+1$) by drawing on the upstream information (n). These transfer matrices can be combined by multiplication to form an overall transfer matrix for the entire pipe. This procedure is illustrated in the following example. Consider the pipe of Figure 3-5 that contains a leak and two horizontal ($z_L = 0$) pipe segments adjacent to the leak.

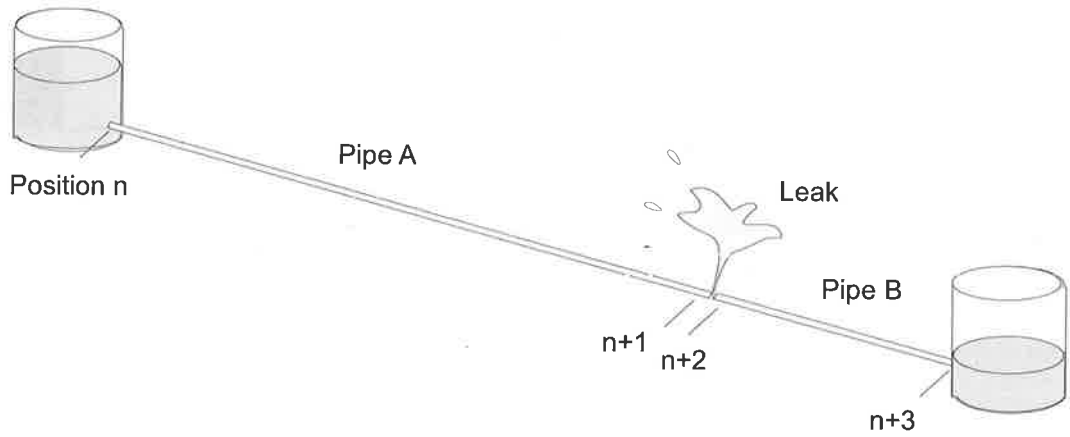


Figure 3-5 – System used for the illustration of the transfer matrix equations.

Beginning at the downstream pipe segment labelled “B,” the transfer matrix of this pipe relates the oscillations in head and discharge between positions n+2 and n+3,

$$\begin{Bmatrix} q \\ h \end{Bmatrix}^{n+3} = \begin{bmatrix} \cosh(\mu_b x_b) & -\frac{1}{Z_b} \sinh(\mu_b x_b) \\ -Z_b \sinh(\mu_b x_b) & \cosh(\mu_b x_b) \end{bmatrix} \begin{Bmatrix} q \\ h \end{Bmatrix}^{n+2} \quad (3.48)$$

The subscript “b” denotes the property of this pipe element and x_b is the total length of pipe “b.” Now, substituting the conditions at n+2 as a function of the transfer matrix of the leak and the conditions upstream of the leak gives

$$\begin{Bmatrix} q \\ h \end{Bmatrix}^{n+3} = \begin{bmatrix} \cosh(\mu_b x_b) & -\frac{1}{Z_b} \sinh(\mu_b x_b) \\ -Z_b \sinh(\mu_b x_b) & \cosh(\mu_b x_b) \end{bmatrix} \begin{bmatrix} 1 & -\frac{Q_{L0}}{2H_{L0}} \\ 0 & 1 \end{bmatrix} \begin{Bmatrix} q \\ h \end{Bmatrix}^{n+1} \quad (3.49)$$

Continuing with the same process, the head and discharge oscillations upstream of the leak can be written as a function of the transfer matrix of the pipe element “a” and the conditions upstream of this pipe,

$$\begin{Bmatrix} q \\ h \end{Bmatrix}^{n+3} = \begin{bmatrix} \cosh(\mu_b x_b) & -\frac{1}{Z_b} \sinh(\mu_b x_b) \\ -Z_b \sinh(\mu_b x_b) & \cosh(\mu_b x_b) \end{bmatrix} \begin{bmatrix} 1 & -\frac{Q_{L0}}{2H_{L0}} \\ 0 & 1 \end{bmatrix} \begin{bmatrix} \cosh(\mu_a x_a) & -\frac{1}{Z_a} \sinh(\mu_a x_a) \\ -Z_a \sinh(\mu_a x_a) & \cosh(\mu_a x_a) \end{bmatrix} \begin{Bmatrix} q \\ h \end{Bmatrix}^n \quad (3.50)$$

The results indicate that the multiplication of the individual unit matrices starting from the downstream boundary will produce an overall transfer matrix for the system that relates the head and discharge oscillations from the upper extremity of the system (n) to the lower extremity ($n+3$). Multiplying all the 2×2 matrices in Eq. (3.50) together gives an overall system transfer matrix U that relates the conditions at the upstream and downstream extremities of the pipeline,

$$\begin{Bmatrix} q \\ h \end{Bmatrix}^{n+3} = \begin{bmatrix} U_{11} & U_{12} \\ U_{21} & U_{22} \end{bmatrix} \begin{Bmatrix} q \\ h \end{Bmatrix}^n \quad (3.51)$$

To account for possible variations in orifice opening size, the equation can be expanded to a 3×3 matrix (Chaudhry, 1987)

$$\begin{Bmatrix} q \\ h \\ 1 \end{Bmatrix}^{n+3} = \begin{bmatrix} U_{11} & U_{12} & U_{13} \\ U_{21} & U_{22} & U_{23} \\ U_{31} & U_{32} & U_{33} \end{bmatrix} \begin{Bmatrix} q \\ h \\ 1 \end{Bmatrix}^n \quad (3.52)$$

where the additional “1” in the column matrix allows the addition of terms that are not coefficients of q or h to the equation. The system can be solved once the number of unknowns is reduced to two using known boundary conditions (Chaudhry, 1987). Due to the linearised nature of the transfer matrix equations, care must be taken so that the magnitude of the response at each frequency does not exceed linear approximations. Chapter 5 presents a procedure where errors due to nonlinear behaviour in a pipe can be minimised. The solutions to the unsteady momentum and continuity equations presented thus far assume that the steady friction dominates losses in the system. While this friction model is adequate for describing steady state losses in a pipe, it does not capture the frequency-dependent losses during unsteady flow, known as *unsteady friction*.

3.4 UNSTEADY FRICTION

Unsteady friction is a well-documented phenomenon that occurs in pipes and is a result of additional shear stresses incurred during accelerating/decelerating flow. These additional shear stresses create frequency-dependent losses that are ignored in the one-dimensional unsteady dynamic equations. There have been a number of developments in the field of 1-D unsteady friction models and details concerning these models can be found in Vítkovský (2001).

Amongst all the proposed 1-D unsteady friction models, the convolution models (which relate losses to the weighted flow history at a point) have a unique advantage when analysis are carried out in the frequency domain. The convolution integral is replaced by a simple multiplication, allowing the fast evaluation of the unsteady friction behaviour (Suo and Wylie 1989, Vítkovský *et al.* 2003a). For this reason, unsteady friction is modelled in this dissertation using these convolution (weighting function) models, specifically the models presented in Zielke (1968) for laminar flows and Vardy and Brown (1995) for smooth-pipe turbulent flows.

The unsteady momentum equation that takes into account unsteady friction effects is given in Zielke (1968) as

$$\frac{1}{gA} \frac{\partial Q}{\partial t} + \frac{\partial H}{\partial x} + \frac{f|Q|Q}{2gDA^2} + \frac{16\nu}{gD^2 A} \int_{-\infty}^t \frac{\partial Q}{\partial t}(t^*) W(t-t^*) dt^* = 0 \quad (3.53)$$

where W is the weighting function, ν is the kinematic viscosity and t^* is the time lag used in the convolution. Eq. (3.54) can be incorporated into the method of characteristics through a change in the friction factor in the characteristics equation of Eq. (3.14) and (3.15). The friction factor, f , can be written as the sum of two terms, f_s and f_u corresponding to the steady and unsteady friction factors, respectively. The steady friction factor is determined using the Swamee and Jain (1976) equation, whereas the unsteady friction factor is found through a discrete time convolution of the past velocities at a point (denoted by “i”) in the pipeline and the weighting function, W ,

$$f_U = \frac{32\nu}{D^2 V_{i,k}^2} \sum_{j=1}^{k-1} (V_{i,j+1} - V_{i,j-1}) W[(k-j)\Delta t] \quad (3.54)$$

where k denotes the time step under consideration and j is the time step counter starting from 1 leading up to $k-1$. The form of the weighting function for laminar flow is given by Zielke (1968) as consisting of two parts. When $\xi > 0.02$, where

$$\xi = \frac{4\nu}{D^2} (k-j)\Delta t \quad (3.55)$$

the weighting function takes the form

$$W(\xi) = \sum_{n=1}^5 e^{-n_i \xi} \quad (3.56)$$

with $(n_i, i = 1 \dots 5) = (-26.3744, -70.8493, -135.0198, -218.9216, -322.5544)$. When $\xi \leq 0.02$

$$W(\xi) = \sum_{n=1}^6 m_i \xi^{(i-2)/2} \quad (3.57)$$

where $(m_i, i = 1 \dots 6) = (0.282095, -1.25, 1.057855, 0.937500, 0.396696, -0.351563)$.

Vardy and Brown (1995) derived an alternative weighting function for smooth-pipe turbulent flows given by

$$W(\xi) = \frac{1}{2\sqrt{\pi\xi}} e^{\left(-\frac{1}{C^*}\xi\right)} \quad (3.58)$$

where, C^* is the shear decay coefficient

$$C^* = \frac{7.41}{\text{Re}^\kappa} \quad (3.59)$$

and where \mathbf{Re} is the Reynolds number = (VD/ν) and

$$\kappa = \log_{10} \left(\frac{14.3}{\mathbf{Re}^{0.05}} \right) \quad (3.60)$$

Both Zielke (1968) and Vardy and Brown (1995) weighting functions are used to model unsteady friction behaviour in this dissertation.

Vítkovský *et al.* (2003b) reformulated these unsteady friction models for the transfer matrices. The unsteady friction effects were incorporated into the transfer matrix solution by setting the frictional resistance, R (located in the propagation function, μ , in the pipe matrix), as a sum of steady and unsteady components, R_s and R_u , respectively. For the Zielke (1968) weighting function, Vítkovský *et al.* (2003b) found the unsteady friction resistance, R_u , to be

$$R_U = \sum_{j=1}^6 R_{U1,j} + \sum_{j=1}^5 R_{U2,j} \quad (3.61)$$

where

$$R_{U1,1} = \frac{4i\omega}{gA} m_1 K \quad (3.62)$$

$$R_{U1,2} = \frac{4i\omega}{gA} \frac{m_2}{b} (1 - e^{-0.02b}) \quad (3.63)$$

$$R_{U1,3} = \frac{4i\omega}{gA} \frac{m_3}{b} \left(\frac{K}{2} - \sqrt{0.02} e^{-0.02b} \right) \quad (3.64)$$

$$R_{U1,4} = \frac{4i\omega}{gA} \frac{m_4}{b^2} (1 - e^{-0.02b} (0.02b + 1)) \quad (3.65)$$

$$R_{U1,5} = \frac{4i\omega}{gA} \frac{m_5}{b^2} \left(\frac{3K}{4} - \sqrt{0.02} e^{-0.02b} \left(0.02b + \frac{3}{2} \right) \right) \quad (3.66)$$

$$R_{U1,6} = \frac{4i\omega}{gA} \frac{m_6}{b^3} (2 - e^{-0.02b} (0.0004b^2 + 0.04b + 2)) \quad (3.67)$$

$$R_{U2,j} = \frac{4i\omega}{gA} \left(\frac{e^{-0.02(b+n_j)b}}{b+n_j} \right) \quad (3.68)$$

and $K = \sqrt{\frac{\pi}{b}} \operatorname{erf}(\sqrt{0.02b})$, with erf = complex error function. In a similar fashion, the formulation of the unsteady friction resistance for Vardy and Brown (1995) unsteady friction model is given in Vítkovský *et al.* (2003b) as

$$R_U = \frac{2i\omega}{gA} \left(\frac{1}{C^*} + \frac{i\omega D^2}{4\nu} \right)^{\frac{1}{2}} \quad (3.69)$$

The unsteady friction models presented in this section were used to provide comparisons with the experimental pipeline at the University of Adelaide in both time and frequency domains. As part of this dissertation, two numerical models, one in the time domain using the method of characteristics and one in the frequency domain using the transfer matrices, were developed. These numerical models were used to model a set of pipelines, the properties of which are presented in the following chapter.

CHAPTER 4

PIPELINE APPARATUS USED FOR NUMERICAL AND EXPERIMENTAL INVESTIGATIONS

The development of the system response extraction procedure and the fault detection techniques are validated in both a simulated (numerical) and a laboratory pipe. The simulation of pipeline behaviour provides a high degree of flexibility in the system configuration and allows the effects of leaks, injected signal, measurement and generator position to be studied in detail. Complex transient signals, such as pseudo-random binary signals were tested numerically prior to the design and construction of a customised valve for its generation. Analytical expressions for the leak impact on the system response function were initially validated using this numerical model, without steady and unsteady friction effects. Such detailed numerical investigations provide the framework for the laboratory experiments required in this study.

4.1 Simulation Pipeline for numerical investigations

The numerical pipeline is 2000 m long bounded by reservoirs at each end. The roughness height of the pipe is small (0.05 mm), its wave speed is 1200 ms^{-1} , its diameter is 0.3 m and the material is steel. The heads at each end are 50 m and 20 m and the pipe is horizontal. A diagram of the simulation system is shown in Figure 4-1. Transients are generated through the sudden opening/closure of a side-discharge or an in-line valve, or the single frequency oscillation of such devices.

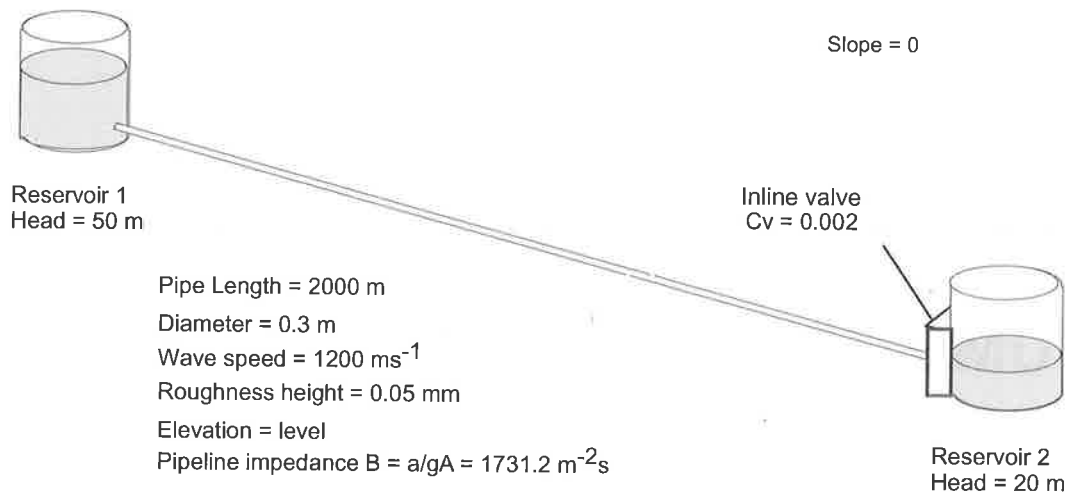


Figure 4-1 – Properties of the smooth numerical pipeline.

In some examples, a static in-line valve is placed at the downstream boundary with a head loss coefficient, C_V , of $0.002 \text{ m}^{5/2}\text{s}^{-1}$ when fully opened. The relationship between C_V , head loss across the valve (ΔH_V) and the flow through the valve (Q_V) is given by

$$Q_V = C_V \tau \sqrt{\Delta H_V} \quad (4.1)$$

The value of $C_V = 0.002 \text{ m}^{5/2}\text{s}^{-1}$ for the in-line valve means that even when the valve is fully opened, the valve boundary behaves like a dead end. This behaviour of the valve is discussed later in the thesis. When the valve is present and fully open, the steady state velocity through the pipe is 0.22 ms^{-1} and the Reynolds number is 65,540, placing the flow in the smooth turbulent flow regime. When the valve is removed from the system, the flow velocity through the pipe is 2.6 ms^{-1} , with a Reynolds number of 780,000. These two configurations of the numerical pipeline allow the development of the techniques under both low and high flow conditions.

4.2 Laboratory apparatus for experimental investigations

The experimental apparatus is located in the Robin hydraulics laboratory in the School of Civil and Environmental Engineering at the University of Adelaide. A schematic of the pipeline is shown in Figure 4-2.

The apparatus comprises a straight 37.53 m length of copper pipe, 22.1 mm internal diameter and 1.6 mm wall thickness and roughness height of 0.0015 mm. The pipe slope is constant throughout with a vertical to horizontal ratio of 1V:18.5H. The elevation difference between the two ends of the pipe is 2 metres. To ensure fluid homogeneity and prevent corrosion of pipeline components, deionised water is used in the system. A photo of the system is in Plate 4-1.

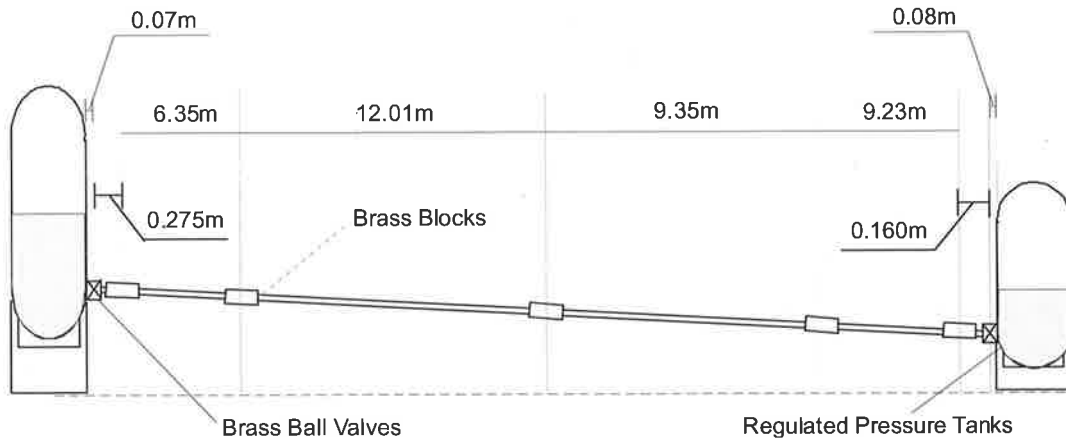


Figure 4-2 – Schematic of experimental pipeline at the University of Adelaide.

The pipe connects two electronically regulated pressure tanks with in-line ball valves (Whitney 65TF16, internal diameter 22.2 mm) located at the boundaries for flow control (Refer to Plate 4-2a). The tanks are pressurised through an air compressor that maintains the set pressures at the tanks during the transient test. Electronic pressure relief valves are at the top of the tanks to allow manual reduction of pressures at the reservoirs. The tanks have a maximum pressure capacity of 70 m.

Pressure signals are measured using Druck PDCR 810 flush-faced pressure transducers with an absolute pressure range of 0 to 600 kPa. The flush fitted face prevents fluid resonance between the pipeline and the transducers. The pressure transducers have a rise time of 5×10^{-6} s and the measurement uncertainty is rated at 0.1% of the full measurement span. The data acquisition card (PCI – 20428W –1) has a maximum single channel sampling rate of 100 kHz and can gather data in as many as 16 channels. The data acquisition is controlled using Visual Designer software installed on a Pentium 150 MHz computer. The pressures are sampled at a frequency of 2000 Hz. To minimise electronic

noise, the pressure transducers are driven by 24 V DC batteries. A photo of the pressure transducer is shown in Plate 4-2b.

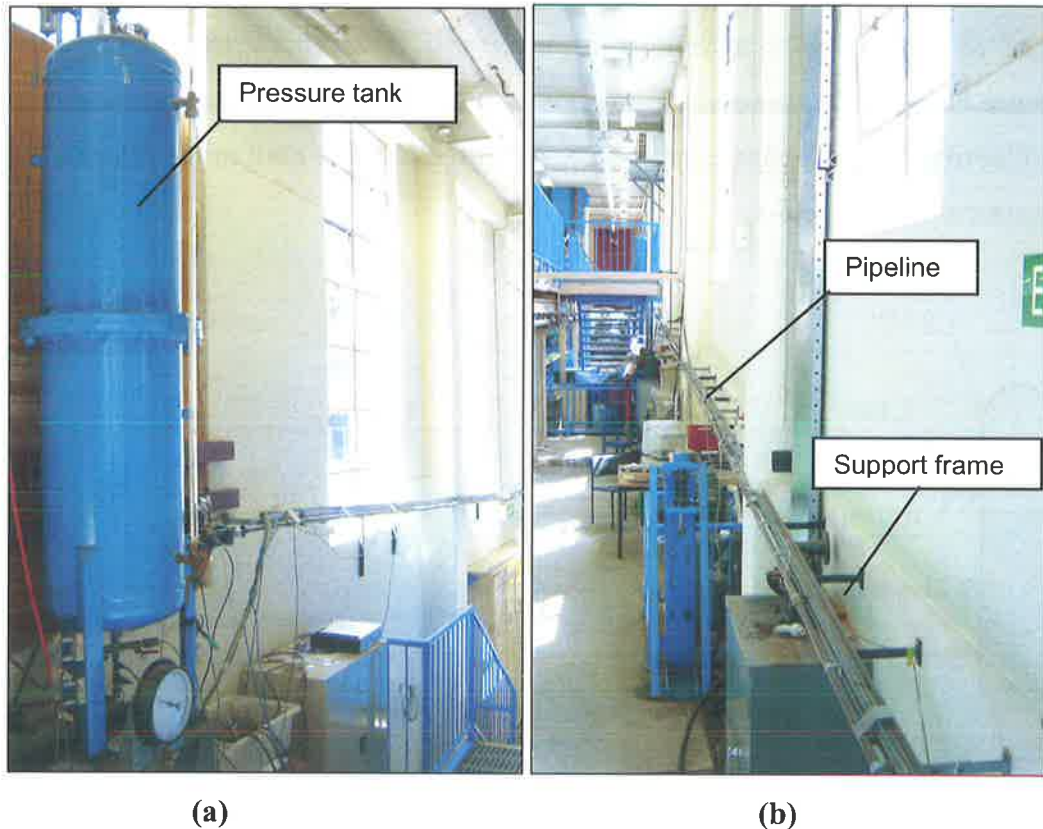


Plate 4-1 – Photos of the experimental pipeline at the University of Adelaide with (a) view of a pressurised boundary tank and (b) view of pipeline with wall mounted supports.

Brass blocks for the connection of pressure transducers, leak units and side-discharge solenoid valves are located at five locations along the pipe as indicated in Figure 4-2 and one of these blocks is shown in Plate 4-3. The internal diameter of the brass block is designed to align smoothly with the adjacent pipes. The blocks are connected to the pipeline with zero tolerance barrel unions to allow easy removal and replacements.

To simulate leaks in the system, side-discharge orifices of varying diameters are connected at brass block locations. In this dissertation, 1 mm and 1.5 mm orifices were used. The leak unit is shown in Plate 4-3. For a driving head of 40 m at the leak the lumped leak coefficient, $C_d A_L$, is $1.60 \times 10^{-6} \text{ m}^2$ for the 1.5 mm orifice and $0.65 \times 10^{-6} \text{ m}^2$ for the 1 mm orifice. The lumped leak coefficients were determined by measuring both the

discharge out of the leak (Q_L) and the driving pressure head at the leak ($H_L - z_L$) during each experimental test and substituting the results into the leak orifice equation,

$$C_d A_L = \frac{Q_L}{\sqrt{2g(H_L - z_L)}} \quad (4.2)$$

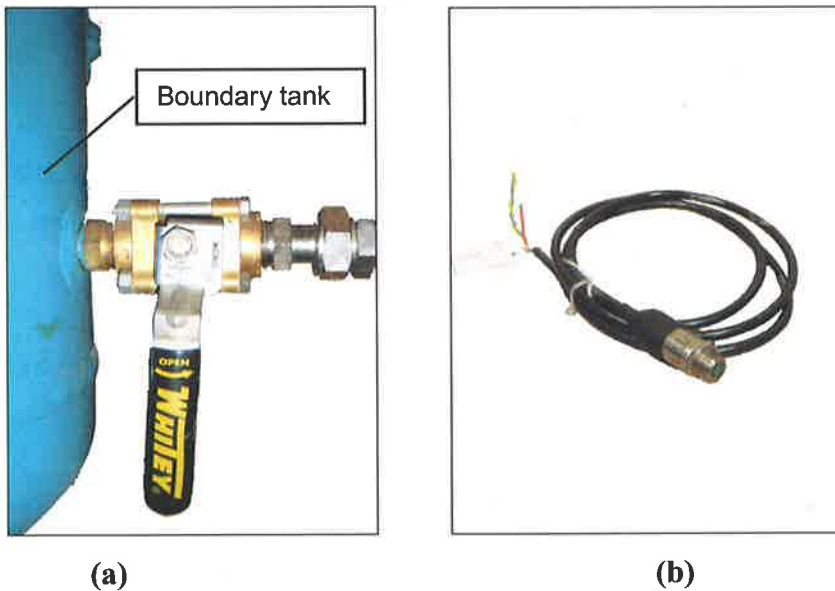


Plate 4-2 – Photos of pipe components (a) Whitney 65TF16 smooth in-line one-quarter turn ball valve (b) Druck PDCR 810 pressure transducers.

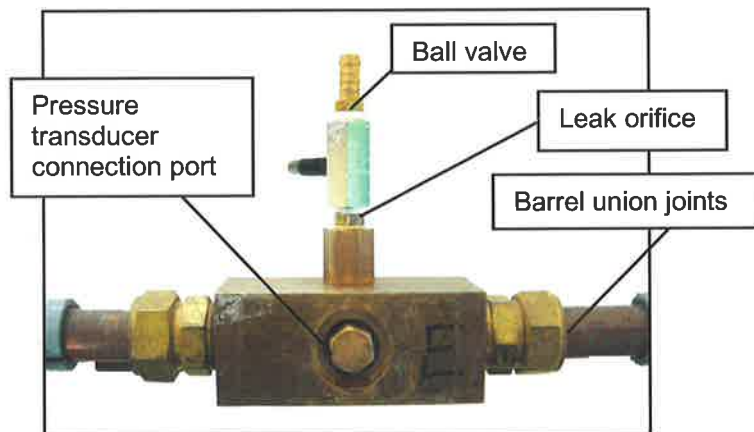


Plate 4-3 – Photo of brass block with leak unit attached.

The steady state flow in the pipeline is measured using the rate of water level change in the tanks. This relationship was calibrated to be

$$V_0 = \frac{\Delta Z}{t_{\Delta Z} C} \quad (4.3)$$

where V_0 is the steady state velocity in the pipe, ΔZ is the observed change in water level, $t_{\Delta Z}$ is the time over which this change occurs and C is the calibrated constant for the tank (Bergant and Simpson, 1995). As the tanks are of different sizes, the upper tank has a calibration value of 2.104×10^{-3} whereas the lower tank has the value of 1.540×10^{-3} .

The wave speed of the pipeline was determined experimentally using the test configuration shown in Figure 4-3. The measured transient traces are shown in Figure 4-4.

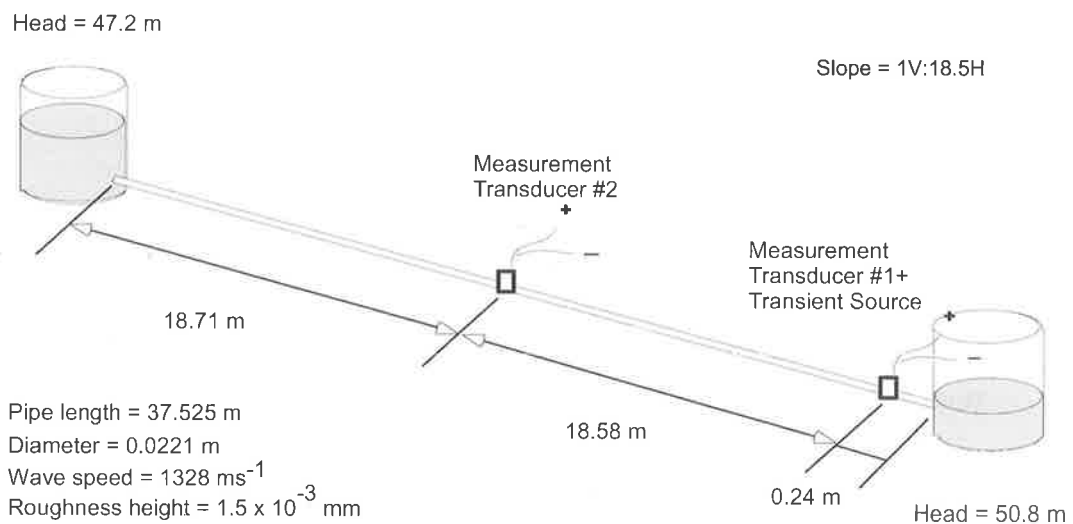
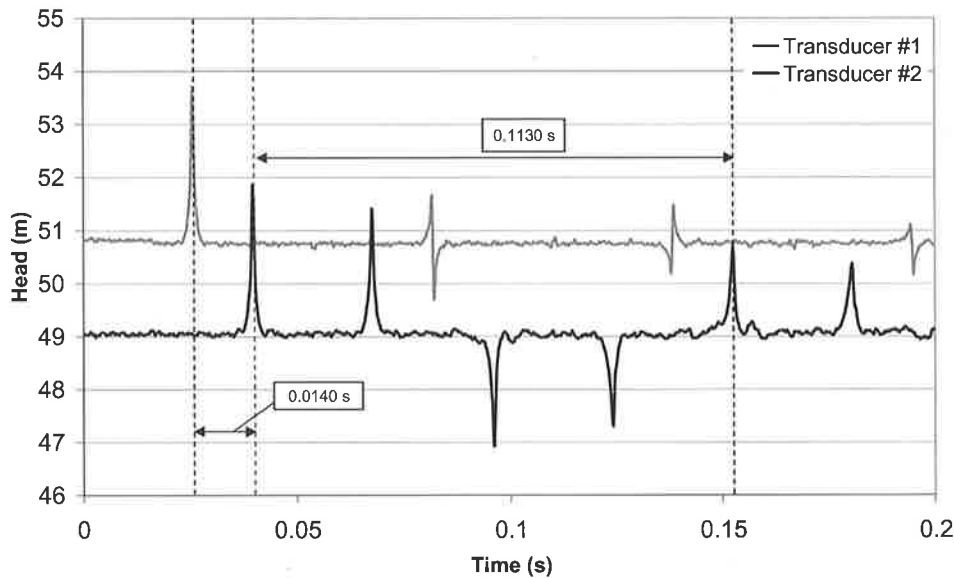


Figure 4-3 – Configuration of the wave speed determination test in the laboratory.

The transient was generated 0.24 m away from an open tank through the closure of an initially open side-discharge valve. The transient is measured at the transient source (transducer #1 in Figure 4-3) and at the midpoint of the pipeline (transducer #2 in Figure 4-3). For increased accuracy, the sampling frequency for this test was 6,000 Hz. The time it takes for the wave to travel from the source to the midpoint transducer is 0.0140 seconds, which gives a wave speed of 1327.1 ms^{-1} . Further confirmation was performed using the period of the transient signal in the pipe ($= 4L/a$). The measured period of the transient signal indicates a wave speed 1328.3 ms^{-1} . The final wave speed is the rounded

average of the two results, taken as 1328 ms^{-1} . This wave speed is used for the remainder of the thesis.



**Figure 4-4 – Experimental determination of wave speed in experimental apparatus
(Data file: C4-1.xls).**

4.3 Devices for transient generation

In previous papers (Bergant and Simpson 1995, Bergant *et al.* 1999, Vítkovský 2001), the fast closures of in-line valves were used as the primary method of generating transients. Such transients are easy to produce and can be generated on all existing pipelines without specialised apparatus. An in-line valve on the experimental pipeline is shown in Plate 4-2a.

Side-discharge solenoid valves are another attractive method for generating transients. These valves have fast operation time and can generate low amplitude (5 to 10 m) transient signals (Wang *et al.* 2002). The movement of the valve can be customised by controlling the electrical current into the valve, allowing the injection of different signals. A commercial brass solenoid valve (Plate 4-4a) and a custom designed solenoid valve constructed at the University of Adelaide were used as part of this research (Plate 4-4b).

Both valves are driven by 24 V AC power and can move from fully opened to fully closed in 4 ms, compared to 10 ms for the manual closure of an in-line valve. The lumped orifice

coefficients (C_dA_V) were determined during each test using Eq. (4.2); they are $1.8 \times 10^{-6} \text{ m}^2$ for the commercial valve and $0.45 \times 10^{-6} \text{ m}^2$ for the customised valve when fully opened under a head of 40 m. The movement of the customised solenoid can be measured directly through a displacement transducer (Duncan 9615 linear motion position sensor). The advantages provided by this direct measurement of the valve operation, along with the detailed design of the customised valve, are discussed in Chapter 5.

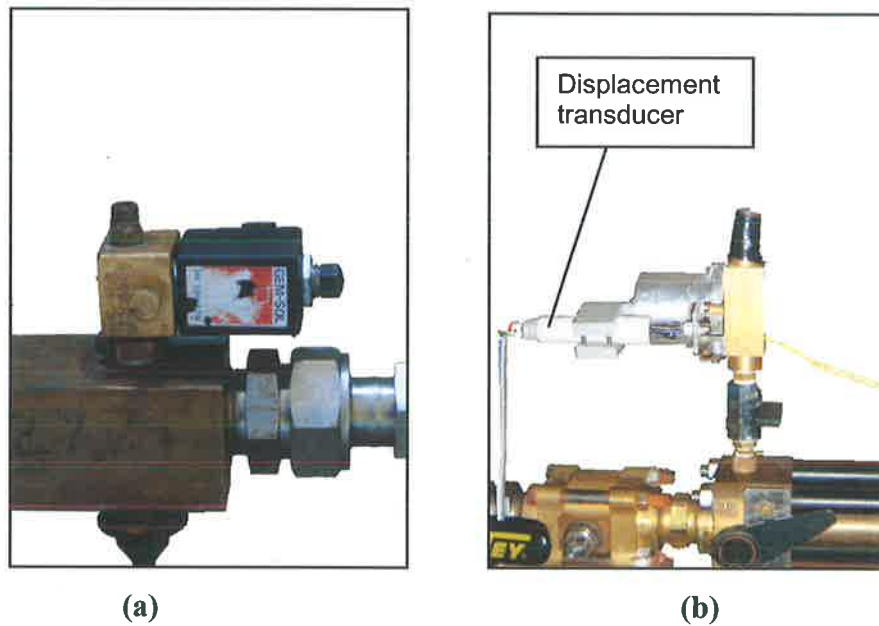


Plate 4-4 – Solenoid valves used in the investigation (a) Commercial brass solenoid valve (b) Custom designed solenoid valve.

CHAPTER 5

SYSTEMS IDENTIFICATION THEORY IN PRESSURISED HYDRAULIC SYSTEMS

5.1 INTRODUCTION

The presence of a leak in a pipeline changes the response of a system to an injected transient signal and the nature of this change can lead to the location of the problem. In Chapter 2, the modification of a measured transient by a leak consists of (1) generation of additional leak-reflected signals and (2) increase in the damping rate of a transient. Techniques that focus on the nature of these leak modifications permit detection and location of a fault without a detailed understanding of the entire transient signal. Leak detection techniques that utilise these specific leak-induced modifications are presented in Chapter 2.

To illustrate the operation of an existing leak detection method, consider the pipeline of Figure 5-1, consisting of a 2,000 m length, 0.3 m internal diameter pipeline where a leak of a lumped discharge coefficient $C_d A_L$ equal to $2.8 \times 10^{-4} \text{ m}^2$ ($C_d A_L / A = 3.96 \times 10^{-3}$) is located 1500 m from the upstream reservoir. The transient is generated by closure of a downstream in-line valve from an initially opened state and the transient is measured at the upstream face of this valve. The transient event is simulated using the method of characteristics model, a discretised numerical scheme for solving unsteady flow in pipelines. Details concerning the method of characteristics model can be found in Chapter 3.

Reservoir 1 Head = 50 m

Slope = 0

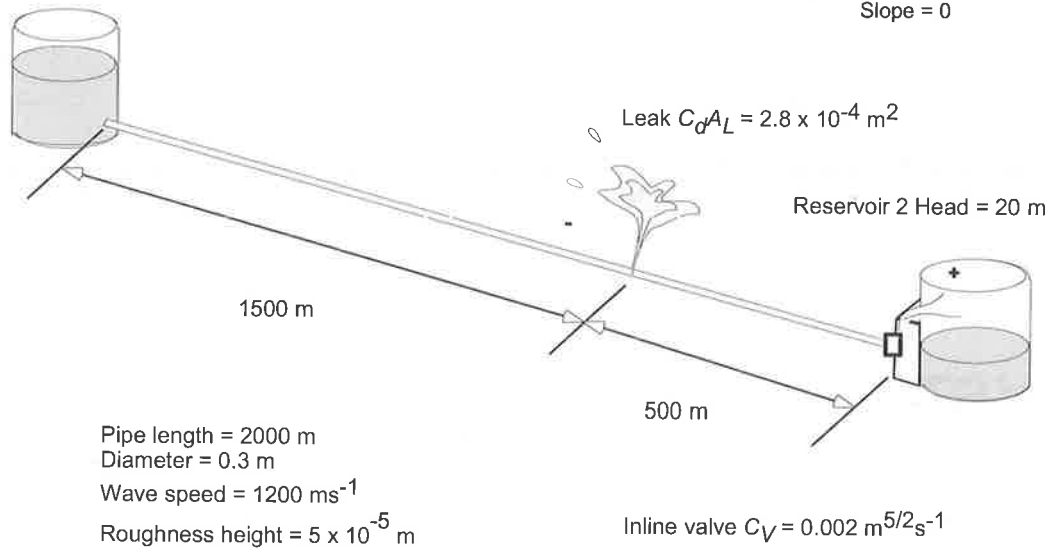


Figure 5-1 – System layout for numerical simulations.

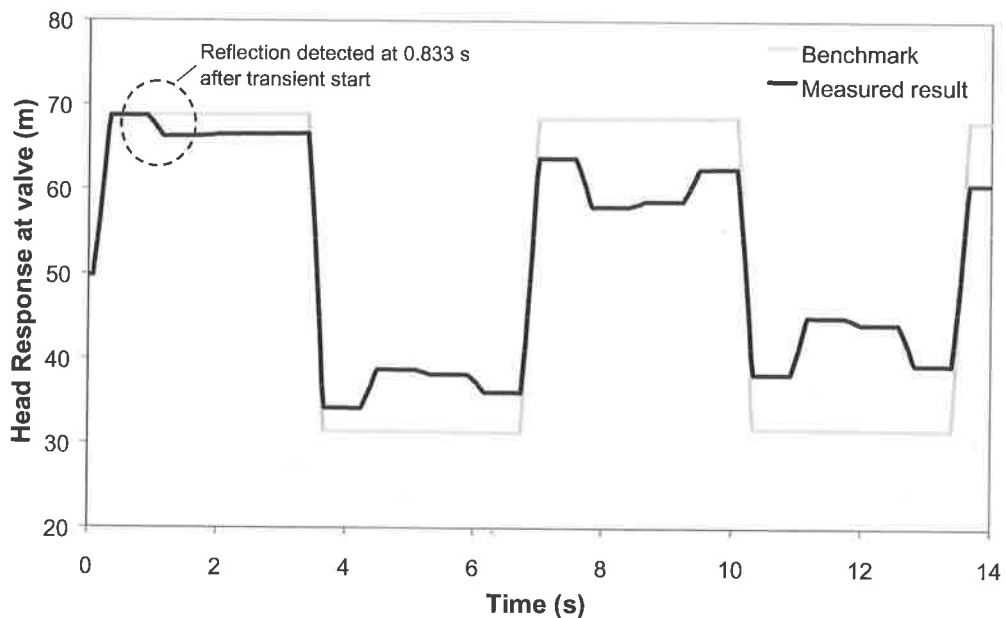


Figure 5-2 – Detection of a leak in the pipeline of Figure 5-1 with a step input signal generated by a 0.266 s closure of the in-line valve from a fully opened position (Data file = C5-1.txt).

The valve was closed in the time of 0.266 s in the method of characteristic model, which discretised the pipeline into 100 reaches, with a computational time step of 0.0333 s. The valve closure profile results in a linear reduction in flow with time. As discussed in

Section 2.3.2., the shape of any transient signal provides clues as to the position of a fault in a pipeline by identifying the arrival time of leak-reflected signals. In Figure 5-2, a comparison of the transient trace with the expected transient behaviour in a leak-free case indicates the presence of leak-reflected signals in the trace, with the first reflection positioned at 0.833 s from the start of the transient. By utilising the known wave speed of the system ($a = 1200 \text{ ms}^{-1}$), the leak is correctly calculated to be 500 m upstream of the in-line valve. In Figure 5-2 the steady HGLs of the graphs were adjusted so that the base lines of the transient in the two tests are at the same level.

Consider another scenario where leak and pipeline properties remain unchanged. In this case, however, the transient is generated not from a closure of the valve, but by a perturbation of the valve (fully closed – partially opened – fully closed). The magnitude of the in-line valve perturbation, $\Delta\tau$, is 0.6 and the duration of the manoeuvre is 0.266 s. The result is shown in Figure 5-3. Again, when the observed transient trace is compared with the response of the leak-free system to this event, reflected echoes are detected at the same position as in Figure 5-2.

While both scenarios result in the accurate positioning of the leak, problems arise when the operator wishes to determine whether the state of the system has changed *between* the two tests, that is, from the time the test in Figure 5-2 was conducted to Figure 5-3. The two measured transient events are of such different shapes that direct comparisons of the results are not possible. Instead, existing reflection-based approaches rely on the existence of an accurate leak-free benchmark that indicates the behaviour of the *same* transient in the pipeline if no leak exists. The benchmark may be generated experimentally when the pipeline is known to be in good condition. The transient generated in the leak-free benchmark must be identical to a subsequent transient for a valid comparison. A change in the mechanics of the transient-generating device some time in the future can lead to a loss in accuracy of the fault detection process. Alternatively, the leak-free benchmark can be generated using a numerical model, but the prediction of the leak-free pipeline behaviour in this way will require a detailed knowledge of the pipeline properties, which is often not available.

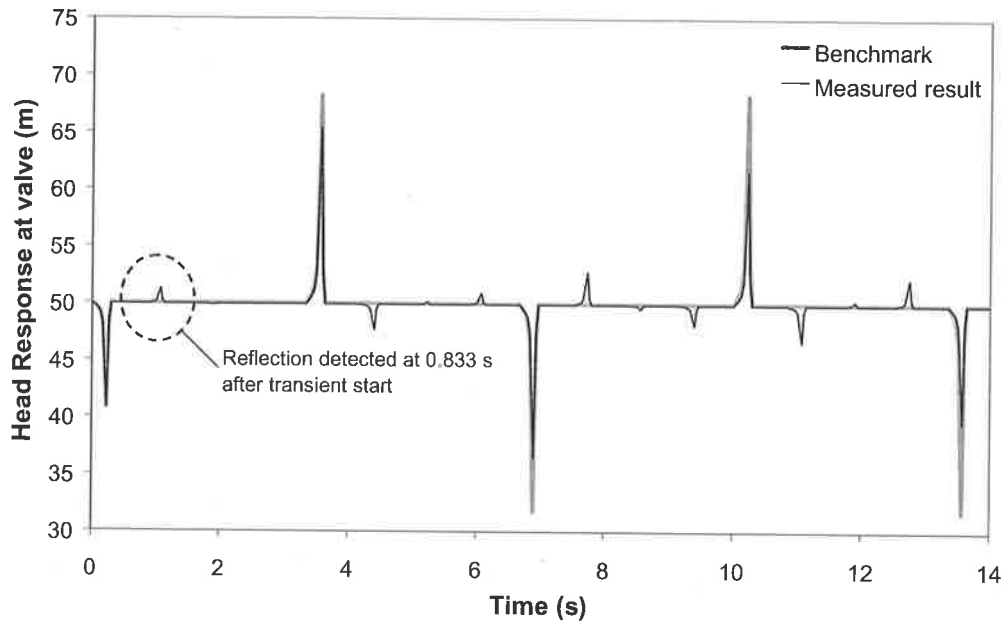


Figure 5-3 – Detection of a leak in the pipeline of Figure 5-1 with a pulse input signal generated by the rapid perturbation of the initially fully closed valve (Data file = C5-1.txt);

Given that the aim of a leak detection procedure is for the determination of the integrity of a pipeline, the information provided by such a procedure should be solely indicative of the state of a system itself and not dependent on the shape of the induced transient. The operator should be able to extract important information about the pipeline from the raw transient response to provide an accurate assessment of the state of a system without having to compare to a benchmark experiment. In reality, if the state of a system remains unchanged, then system integrity information extracted from a pipeline should indicate that fact, regardless of the shape of the injected signal.

This extraction procedure lies within a well-established field of system identification that is commonly used in a range of applications from testing of structural members and mechanical devices to electric components (Poussart and Ganguly 1977, Brekke 1984, Ogawa *et al.* 1994, Li *et al.* 1994, Hwang and Kim 2004). In all these cases, a controlled signal is introduced into a system and the subsequent response measured. For example, for the detection of cracks in materials, a shock wave is introduced at one end of an object in the form of an impact and the vibration of the material is measured at the impact source. Using the known applied signal (input) and the measured response (output), functions are

developed that illustrate how the system modifies the introduced signal as it propagates through the system (Deutsch 1969). The functions that relate input and the output of a system are known as *system response functions* and can be written in either the time or frequency domain where they are known as the *impulse response function* (IRF) and the *frequency response function* (FRF), respectively. These functions summarise the pipeline behaviour and can be used to determine the integrity of the system.

The frequency response function for the two scenarios in Figure 5-2 and Figure 5-3 are shown in Figure 5-4, with the detailed procedure of its extraction discussed later in this chapter. Figure 5-4 indicates that the underlying system responses for the two scenarios are identical although the nature of the injected signal and the subsequently measured responses are completely different. This demonstration highlights the advantage of using such an approach for leak detection in pipelines. Given the system can be described linearly, the extracted system response function using different signals will be the same.

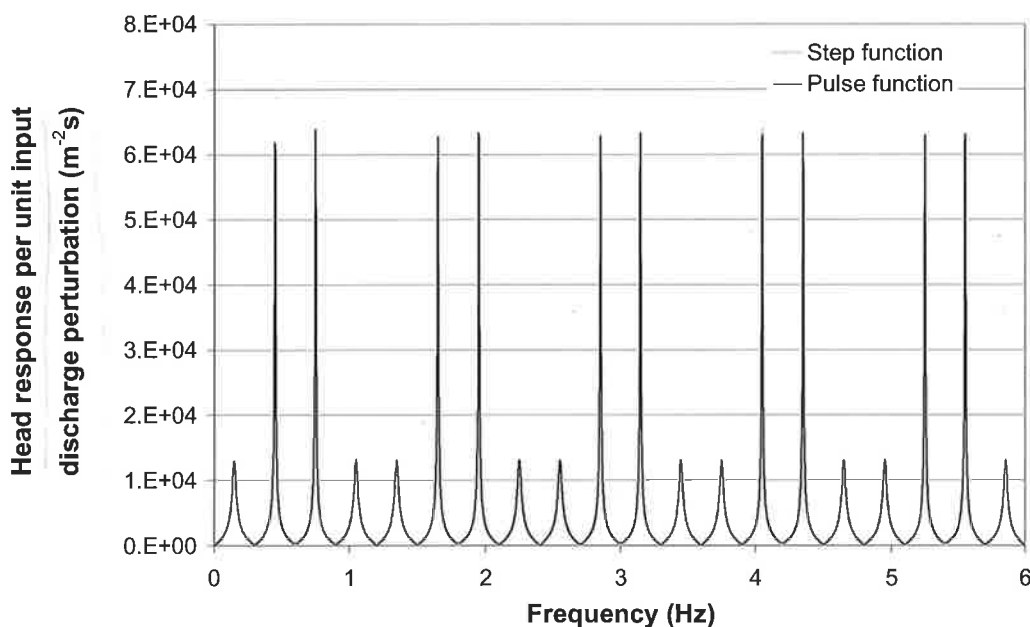


Figure 5-4 – Frequency response functions for the transient events shown in Figure 5-2 and Figure 5-3. Data were generated from an MOC model (Discretisation = 100, analysis time step = 0.0333 seconds) for the pipeline in Figure 5-1.

The remainder of the thesis investigates the use of these response functions for the purpose of leak detection in a pipeline; including the method of extracting these functions from

measured data, the study of leak-induced changes to these functions in both the time and frequency domains and the development of methods that focus on these leak-induced modifications to allow a leak to be located. The scope of this study is broad and is separated into the following three chapters.

The current chapter investigates how the system response functions can be extracted from a pipeline using non-oscillatory signals. The validity of this systems approach for summarising transient behaviour, which includes an assumption of linearity, is discussed. The additional complexities that arise in an experimental situation (as opposed to the case where data are generated artificially as illustrated above) for the extraction of system response functions are discussed with particular focus on how bandwidth of the injected transient and the configuration of the system affect the leak detection process. Although the extraction of the system response function allows accurate determination of the same system response regardless of the nature of the injected signal, certain input signal—such as signals that result in a step change in the pressure—require special attention prior to their use in the extraction process. As part of this study, properties of the optimum injected signal—one that allows the most accurate extraction of the system response functions—are investigated.

Later chapters, Chapter 6 and Chapter 7, investigate the use of these system response functions for the detection of a leak in the frequency and time domain, respectively. The changes caused by a leak in the response functions in both domains are presented and techniques for using these changes for locating a leak are developed.

5.2 SYSTEM IDENTIFICATION THEORY

For any system, the equations governing the extraction of the system response functions depend largely on the system behaviour itself. For a pipeline, the short duration of a typical transient signal means that the measured response can be considered as a “snapshot” in time of the pipeline behaviour (Young 1995) and for a small transient perturbation, the transient response of a pipeline can be approximated linearly (Suo and Wylie 1989). In such systems, the relationship between the injected transient signal (x) and the measured head response (y) is given by

$$y(t) = \int_{-\infty}^{\infty} x(t^*) I(t - t^*) dt^* \quad (5.1)$$

where I is the impulse response function for the system and the injected signal, x , is a variable that describes the nature of the event generating the transient. The Fourier transform of Eq. (5.1) into the frequency domain using the time-convolution theorem gives

$$Y(\omega) = X(\omega) F(\omega) \quad (5.2)$$

where F = frequency response function, X = Fourier transform of the input, Y = Fourier transform of the output and ω = angular frequency (Lynn 1982). The determination of I and F , using the known injected signal (x) and measured transient (y) of the system, is a process known as *system identification* and Eqs. (5.1) and (5.2) are the *linear time-invariant system equations*. The assumption of linearity implies that each injected signal can be broken down into its frequency components and each component acts independently during its propagation through the system (i.e. there is no energy transfer between frequencies). These equations describe the relationship between the input and output of an *open-loop* system—one where the output of the system does not affect the nature of the injected signal. An example of an open-loop system event is the impact of a hammer on a metal plate, where the input is the force applied on the plate and the output is the measured sound level. In this case, the resultant sound level (output) cannot affect the

magnitude of the applied force (input). An illustration of the structure of such a system is shown in Figure 5-5.



Figure 5-5 – Structure of the system described in Eqs. (5.1) and (5.2).

As mentioned in the introduction of this chapter, the system response functions contain all the information pertaining to the integrity of a pipeline. For example, the impulse response function in Eq. (5.1) describes the response of a system in the time domain when a sharp pulse of zero width and infinite magnitude (an *impulse*) is introduced into a pipeline. This function contains a map of the reflections from the system. On the other hand, as the Fourier transform of an impulse has a unit magnitude spectrum across all frequencies, the frequency response function describes the magnitude of the response at each frequency when a unit oscillation of that frequency is imposed on the system.

The equations for the system response functions can be further improved by incorporating a *matched filter*. A matched filter improves the measured output signal such that components that are in response to an injected input signal are emphasised. This process is commonly used in radar systems for detection of reflected signals hidden amongst background chatter (Lynn 1982). The matched filter is essentially a cross-correlation procedure between input and measured output, resulting in additional weighting given to sections of the output that correspond to the shape of the injected signal. The system response relationship in the time domain incorporating this matched filter is given in Lynn (1982) as

$$r_{xy}(t) = \int_{-\infty}^{\infty} r_{xx}(t^*) I(t - t^*) dt^* \quad (5.3)$$

where r_{xy} = the cross-correlation function between x and y , defined as

$$r_{xy}(t^*) = \lim_{T_0 \rightarrow \infty} \int_{-T_0/2}^{T_0/2} x(t) y(t + t^*) dt \quad (5.4)$$

and t = time, t^* = time lag between the two signal, r_{xx} = auto-correlation function of the input. Comparing Eq. (5.3) to Eq. (5.1), the matched-filtered form of the system equation replaced the output series with the cross-correlation between the input and output and the input series is replaced by the auto-correlation of the input. The expression in the frequency domain is

$$S_{XY}(\omega) = S_{XX}(\omega)F(\omega) \quad (5.5)$$

where, S_{XX} = Fourier transform of the auto-correlation of the input signal and S_{XY} is the Fourier transform of the cross-correlation between the input and the output (Schoukens *et al.* 1993).

Use of a frequency response function has been made in the past for the study of frequency-dependent behaviour in pipelines, for example, the study of mode shapes for the placement of surge protection devices (Ogawa *et al.* 1994), unsteady friction (Zielke *et al.* 1968, Brekke 1984), viscoelastic behaviour (Suo and Wylie 1990), fluid-structure interaction (Norton and Greenhalgh 1986, Fan 1989, Zhang *et al.* 1995, Svingen 1996) and resonance behaviour of systems (Brekke 1984). While the theoretical development of these areas is extensive, the validation of the techniques experimentally in the frequency domain has been largely limited by the inefficiency of current procedures for extracting response functions from hydraulic systems.

One of the most common approaches for extracting system response functions involves the sinusoidal variation of certain hydraulic elements in a pipeline in a process known as *frequency-sweeping* (Zielke *et al.* 1968, Zielke and Hack 1972, Muto and Kanei 1980, Fanelli *et al.* 1983, Chaudhry 1987, Mpesha *et al.* 2001, 2002, Brekke 1984). In this procedure, a sinusoidal signal of a single frequency is injected into a system by oscillating a hydraulic device, ranging from specially designed oscillatory valves (Chaudhry 1987, Svingen 1996, Mpesha *et al.* 2001, 2002) to pistons connected to rotating crank shafts (Foster and Parker 1964, Zielke *et al.* 1969, Muto and Kanei 1980). Once a steady oscillation is achieved in the system, the corresponding magnitude of the oscillation is measured providing a single point on the frequency response function. This process is then repeated for sinusoidal signals of different frequencies until the desired resolution of the

frequency response function is derived. The frequency-sweeping procedure is theoretically simple and can extract the frequency response accurately from a pipeline (Zielke *et al.* 1969, Muto and Kanei 1980). The corresponding impulse response function in the time domain can be found through an inverse Fourier transform of the frequency response once it is successfully extracted (described in Chapter 7). However, the application of this approach in reality requires the design and installation of a custom oscillatory apparatus (often involving a motor) and is cumbersome and the task of achieving steady oscillatory flow for each injected sinusoidal signal can be time consuming, especially in large systems. The full process of system response extraction using this approach can take many hours, during which time the boundary and flow conditions of the pipeline must remain constant.

A more attractive alternative is to consider every injected transient in a pipeline as a combination of individual frequencies and apply Eqs. (5.2) or (5.5) for the derivation of the frequency response function. This approach allows the entire frequency response function to be efficiently extracted from a single transient test. It was applied in Suo and Wylie (1989) and later repeated in Ferrante and Brunone (2001). These papers proposed a formulation of the frequency response function in the form of an impedance ratio, where the input and output of the system is set as measured discharge and head response, respectively, at one point of the pipeline. This procedure produces valid results under both numerical and experimental conditions in the case of fast, in-line valve closures. However, care must be taken in its application in relation to the choice of input variable.

In Ferrante *et al.* (2001) and Wylie and Streeter (1993), the input function was set to be the discharge perturbation at a valve throughout the duration of the transient. As a result, the application of this approach is limited to cases where the actual discharge perturbation at the valve is measured or can be assumed to be a result of the valve manoeuvre alone. For example, in cases where an in-line valve was not fully closed after the manoeuvre, a point upstream of the valve will have discharge perturbations throughout the duration of the transient (due to pressure fluctuations) and these perturbations need to be taken into account. In the special case when the in-line valve is fully closed after the manoeuvre, the subsequent arrival of transient signals at the valve after closure does not induce additional flow perturbation as the closed valve itself constitutes a zero-flow boundary. The approximation of discharge as a function of valve movement is, therefore, valid only for

the case of complete closure. In addition, the use of measured discharge perturbation during an entire transient signal as input to a system is incompatible with the system structure assumed in the extraction of system response functions using Eqs. (5.1), (5.2), (5.3) and (5.5). If the valve is not fully closed after generation of a transient, the discharge perturbation at the valve is a function of the measured head response and a feedback loop is established in the system. This feedback process is not accounted for in Eqs. (5.1), (5.2), (5.3) and (5.5). The structure of such a system is described in Figure 5-6.

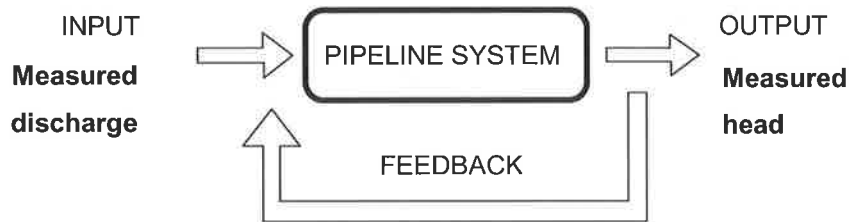


Figure 5-6 – Structure of the dependent input system.

Watanabe and Himmelblau (1986) and Watanabe and Koyama (1990) applied a similar approach where the input and output of a system were defined as two separate measurements of pressure head located at the boundaries of a pipeline. While Watanabe and Himmelblau (1986), Watanabe and Koyama (1990), Wylie and Streeter (1993) and Ferrante *et al.* (2001) have shown that the use of such dependent inputs in Eq. (5.2) can lead to the extraction of certain system behavioural properties, the derived function cannot be described as a “system response function” unless the exact nature of the interaction between the input and output is accounted for. In this respect, the application of *closed-loop* system identification procedures, which incorporates the additional feedback process, would be more accurate in describing the relationship and hence allow accurate extraction of the underlying system behaviour. Such procedures often involve an iterative process to produce the response function.

Further complications arise as a result of the step nature of the valve closure manoeuvre used in Ferrante and Brunone (2001). Being a signal that is unbounded in time, the traditional Fourier transform of a step function is not valid (Lynn, 1982). To overcome this issue, Ferrante and Brunone (2001) approximated all valve closure profiles of duration shorter than 10% of the return time of a transient signal ($t = 2L/a$) as instantaneous closure, with a spectrum defined by the Fourier transform of a Heaviside function. This

approximation means that the actual spectral content of an injected signal is not taken into account during extraction of a frequency response function and depending on the closure profile, may lead to inaccuracies in the result. The problem associated with step closures of a valve is addressed in this chapter where a correction procedure allows the proper extraction of the system response functions (impulse response function or frequency response function) using these signals.

In contrast with the use of discrete signals for extraction of system response functions, Liou (1998) proposed the use of pseudo-random binary signals. Pseudo-random binary signals are composed of a series of pulses that are spaced at random intervals and the sequence of random pulses is set to repeat periodically. The minimum period of a pulse sequence is set at the time needed for a single injected pulse to attenuate to zero (Sharp, 1996) and the extraction of the system behaviour is carried out in a single period of this sequence. Liou (1998) stated that the advantage of the pseudo-random signal is, given that the duration of individual pulses is sharp, a substantial reduction in the level of contamination from background noise while maintaining the same properties as the injection of an impulse (Dunn and Hawksford. 1993, Poussart and Ganguly 1977). The use of this signal is investigated in greater detail later in this chapter through the operation of a customised solenoid valve that was designed and constructed as part of this research.

The above overview of the application of system response extraction procedures has indicated that the extraction process varies greatly in both the definition of the system response function and the procedure taken in the extraction. The variations between publications can be summarised under the following headings:

- the selection of the input variable,
- the location of the transient source / measurement station,
- and the selection of injected signals for the extraction process.

To achieve an optimum procedure for extraction of system response functions from a pipeline, these issues are considered. As the impulse and frequency response functions are a Fourier pair, the analysis of the extraction process on either of these functions is equally valid. The remainder of this chapter focuses on the extraction of frequency response

functions from a pipeline. The impulse response function (time domain) is discussed in Chapter 7.

5.2.1 Choice of the input variable

The choice of input and output variables for the extraction of system response functions not only affects the accuracy of extracted functions but also the amount of useful insight into the system behaviour contained in these functions. For an accurate evaluation of system behaviour using open-loop system equations in Eq. (5.3) and (5.5), the output response from a system should not be allowed to affect the variable used as input (Deutsch 1969).

In this respect, the output can be defined as the measured pressure signal in a system while the input variable can be any variable that describes the operation that generates the transient event. In the case where a transient is generated by the operation of an in-line or side-discharge valve, input can be related to the magnitude of the physical valve perturbation in terms of a dimensionless coefficient, τ (Mpesha *et al.* 2001, 2002) that specifies the percent of valve opening. As the valve opening cannot be affected by pressure in the pipeline, this selection of input variable conforms to the open-loop system configuration as required in Eq. (5.3) and (5.5).

The procedure for the extraction of a system response function from a pipeline is given by Figure 5-7. For a situation where both input and output is measured, the system response is given by the spectrum of their cross-correlation divided by the auto-correlation of the input.

This procedure is illustrated by the following example. The input and output time series of a transient event generated by perturbation of the initially fully opened in-line valve for the leak-free system of Figure 5-8 is given in Figure 5-9. The input function is described as the tau perturbation of the valve and is shown in detail in Figure 5-10, whereas the output is the measured transient trace from a pressure transducer. The correlation functions between input and output are shown in Figure 5-11 and are of a similar form to the original input and output signals. The spectrums of these correlation functions are

shown in Figure 5-12. They are substituted into Eq. (5.5) to determine the frequency response function from the system as illustrated in Figure 5-7. The result is in Figure 5-13.

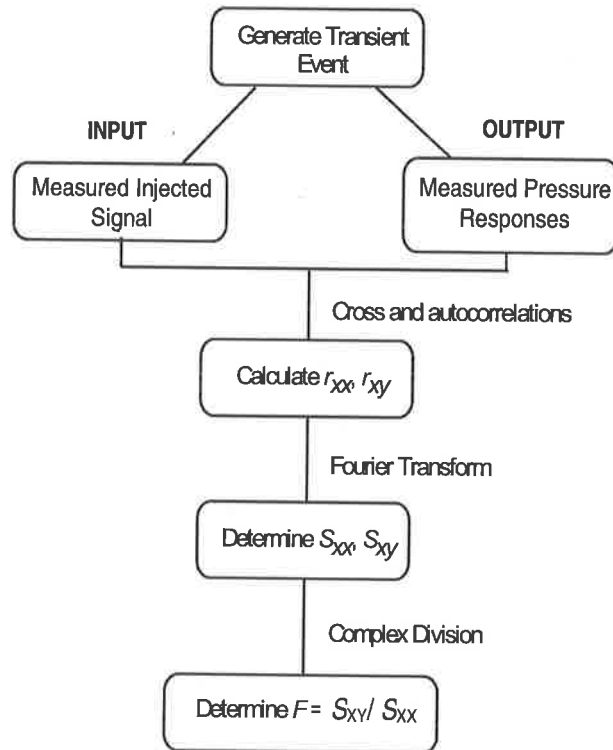


Figure 5-7 – Procedure for system response extraction using measured input signal.

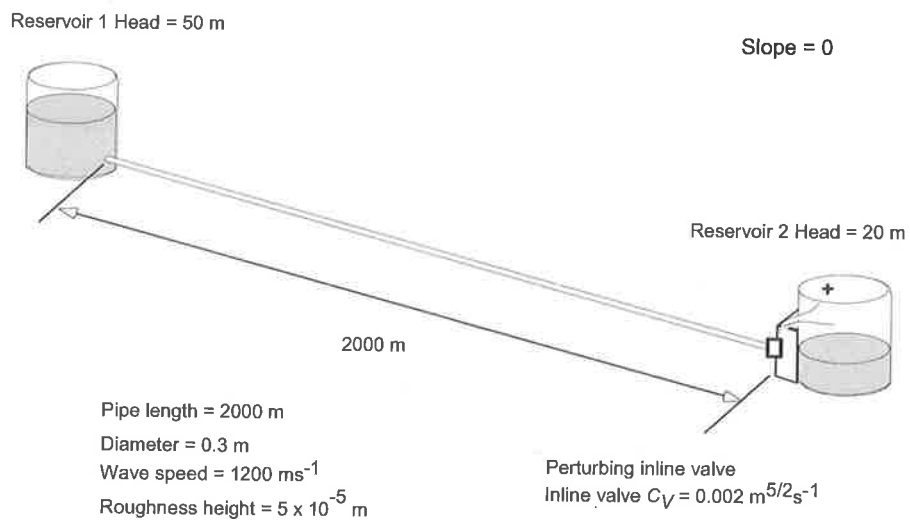


Figure 5-8 – Pipeline for investigating the influence of the input variable.

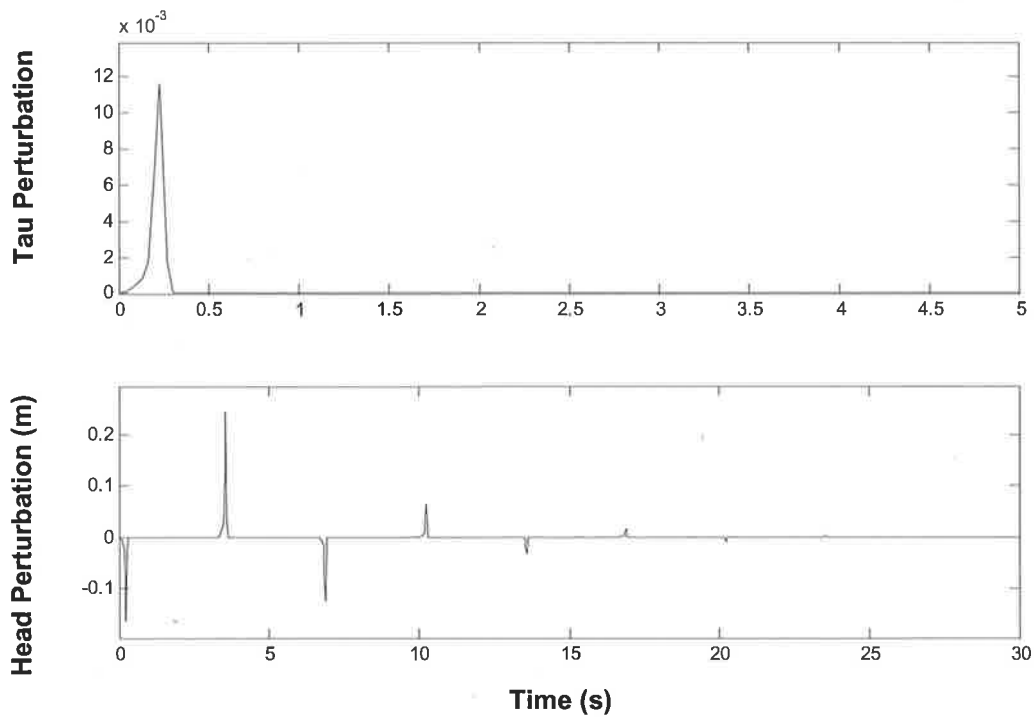


Figure 5-9 – Input and output time series, input from measured valve movement.

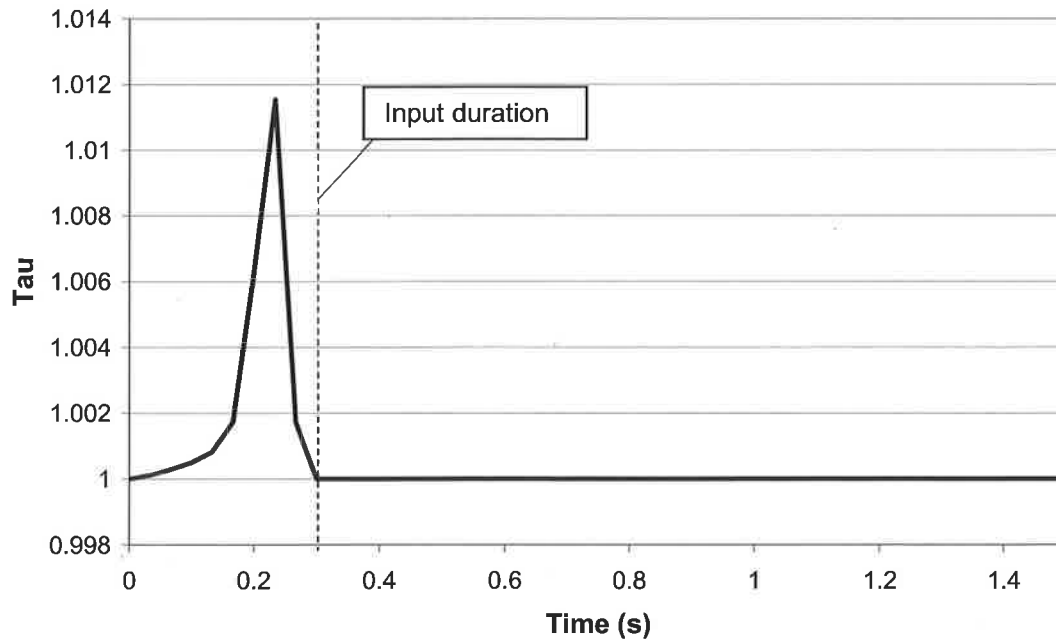


Figure 5-10 – Nature of the valve opening fluctuation (Data file: C5-2.txt).

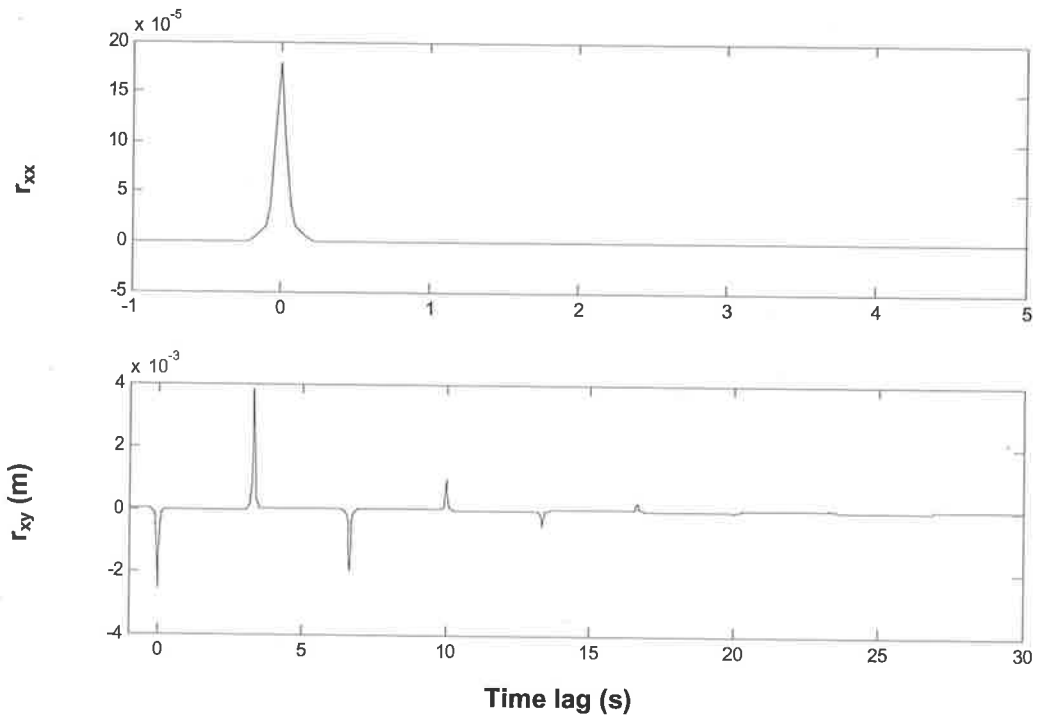


Figure 5-11 – Correlation functions between input (x) and output (y) functions.

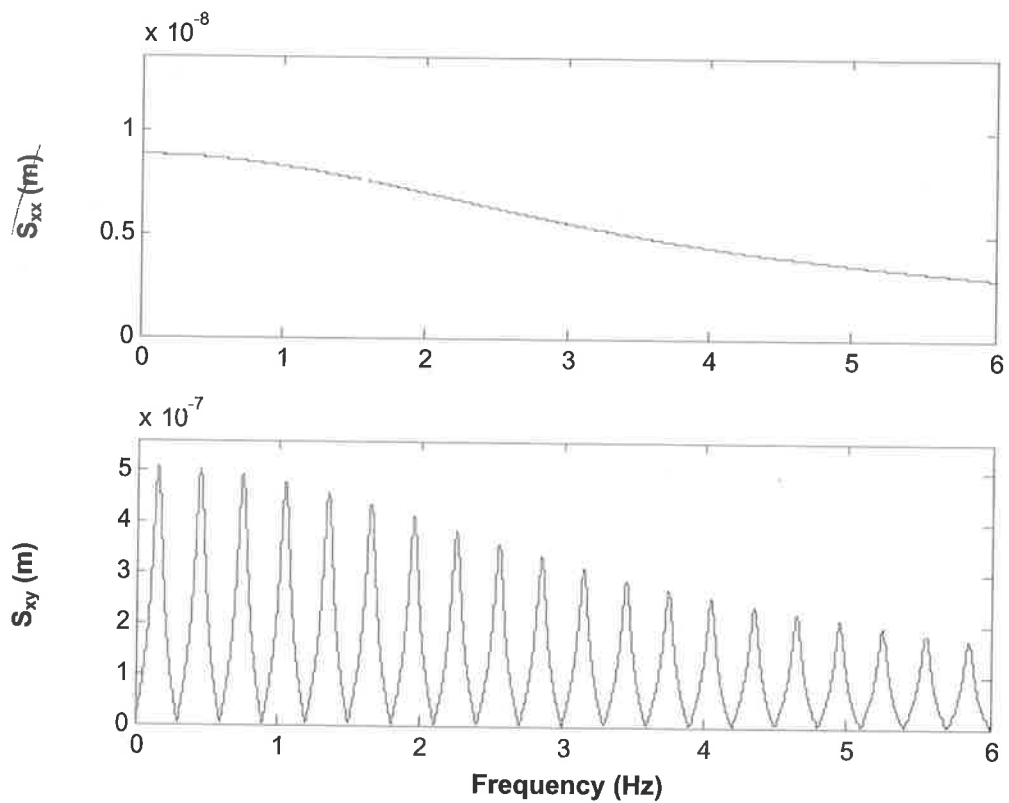


Figure 5-12 – Spectrum of correlation functions.

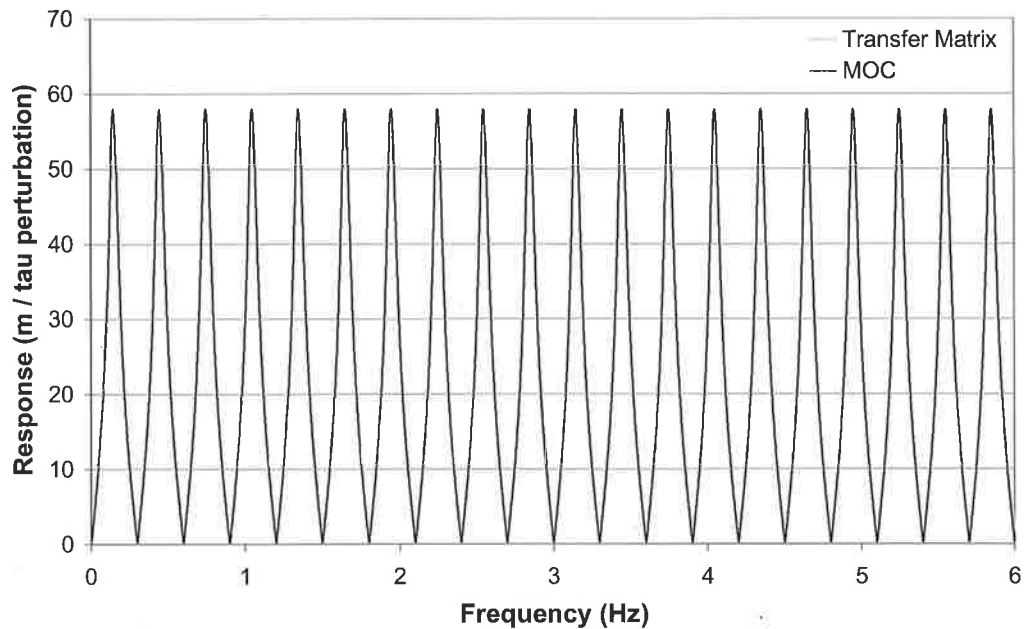


Figure 5-13 – Comparison between transfer matrix equations and method of characteristics for $\Delta\tau_{\text{Max}}^* = \Delta\tau = 0.001$. The results overlap perfectly (Data file: C5-2.txt).

Frequency response is presented in terms of head response at each frequency per unit oscillation of the valve opening, $\Delta\tau$. The frequency response function was derived using both the method of characteristics and the transfer matrix equations. In the transfer matrix, $\Delta\tau$ was set as 0.001 of the τ value at the fully opened state, whereas the method of characteristics results were generated using a pulse perturbation of the valve with the maximum perturbation equal to $\Delta\tau_{\text{Max}}^*$. Note that $\Delta\tau^*$ denotes the perturbation of the valve in a non-oscillatory sense and can be converted to $\Delta\tau$ through a Fourier transform. The resultant magnitude at each of the frequencies contained in the pulse signal is governed by the spectrum of the pulse itself.

From Figure 5-13, there is a good match between the linear transfer matrix and the nonlinear method of characteristics model, indicating that the system is behaving in a linear manner for the small valve perturbation that was selected. The extraction of the system response function using Eq. (5.3) and (5.5) is, therefore, valid under this condition. The frequency response functions were derived for steady friction only and consist of a

series of equally spaced peaks along the frequency axis. The peaks are located at the odd multiples of the system fundamental frequency, ω_{th} , defined in Hertz as

$$\omega_{th} = \sum_{k=1}^{n_{pipe}} \frac{a}{4L} \quad (5.6)$$

for a system bounded by a hydraulic device that has a greater impedance than the pipeline itself (for example, an in-line valve) and

$$\omega_{th} = \sum_{k=1}^{n_{pipe}} \frac{a}{2L} \quad (5.7)$$

when the system is bounded by low impedance units at both ends (Wylie and Streeter 1993). Note that n_{pipe} = number of pipe sections in the system.

For the purpose of nomenclature, systems with a fundamental frequency defined by Eq. (5.6) are referred to as *anti-symmetric* systems for the remainder of the thesis, whereas those with fundamental frequencies of Eq. (5.7) are *symmetric* systems. The frequencies at the peaks of the frequency response function are known as *resonant frequencies* and are of particular importance in the design of hydraulic systems (Ogawa *et al* 1994).

Consider the situation where the maximum magnitude of the valve perturbation is increased from 0.001 to 0.5 in both the transfer matrix equation ($\Delta\tau$) and the method of characteristics model ($\Delta\tau_{Max}^*$) while keeping the number of reaches in the MOC calculations at 100 with a computational time step of 0.0333 s. The comparison of the resultant frequency response functions from the two models is given in Figure 5-14. Unlike Figure 5-13, Figure 5-14 indicates that the transfer matrix model is not an accurate prediction of the frequency response in the pipeline as it over predicts the magnitude of the responses. This inaccuracy appears to be related to the size of valve perturbation.

To illustrate the nature of this discrepancy, a separate comparison between small and large valve perturbation is used. The method of characteristics (with 125 reaches and computational time step of 0.0133 s) was used to generate data for the system configuration in Figure 5-14 for a single frequency. The in-line valve was forced to

oscillate with a fixed frequency of 0.533 Hz, corresponding to $1.875 \omega_{th}$ and the head response at the upstream face of the valve was recorded for two different magnitudes, $\Delta\tau$, of the valve oscillation, 0.001 and 0.3. The resulting time traces for the oscillatory flows are then Fourier decomposed and the results are shown in Figure 5-15. The time spacing of the method of characteristics model and the frequency of the injected signal were carefully selected to prevent frequency leakage. The period of the injected sinusoidal signal is equal to a perfect multiple of the time spacing ($=40\Delta t$) and this signal can be accurately represented in the model.

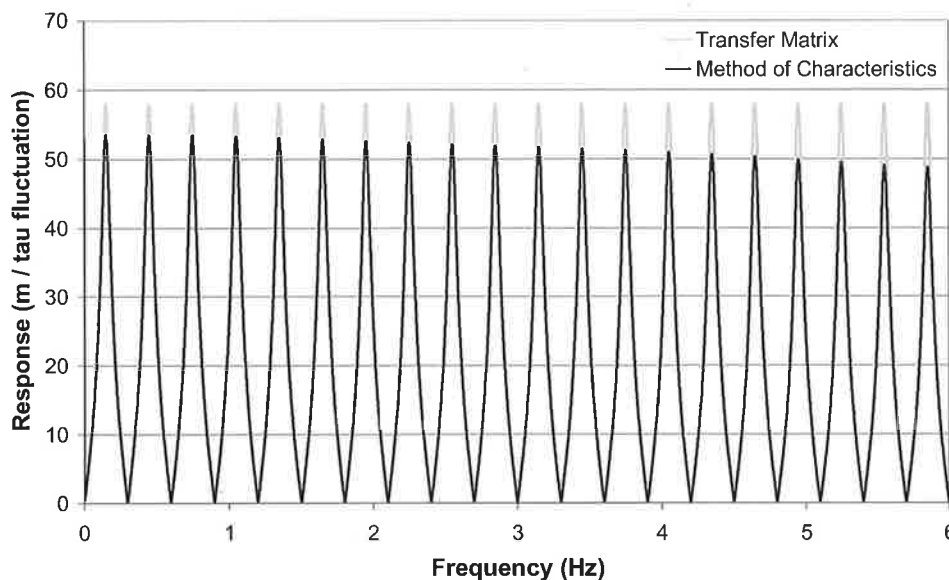


Figure 5-14 – Comparison between transfer matrix equations and method of characteristics for $\Delta\tau_{Max}^* = \Delta\tau = 0.5$ (Data file: C5-3.txt).

The figure indicates that a valve perturbation magnitude of 0.10% of the original valve opening size, τ_0 , results in an oscillation that appears to contain only a single frequency, equal to the driving frequency at the valve. In comparison, when $\Delta\tau = 30\%$ of the original valve opening (using the same numerical model and oscillation frequency), the measured output contains more than one frequency although the system was driven at a single frequency. The presence of additional frequencies suggests that the system exhibits nonlinear behaviour in which energy travels between frequencies. To summarise the relationship between the magnitude of the valve perturbation and the extent of this induced nonlinear error, the oscillation magnitude of the valve was increased from 0.001 to 1 (0.1% to 100% of the initial valve opening size) at the pipe fundamental frequency and the error in the magnitude of the driving frequency component was measured and is

shown in Figure 5-16. The figure indicates that the nonlinear error grows exponentially and reaches a value of 1% at a $\Delta\tau/\tau_0$ of 0.15. The value of $\Delta\tau/\tau_0 = 0.3$ used in Figure 5-15 gives an error of 4.3%. Given the above example, the effects of nonlinear components in the pipeline should be minimised to ensure that the assumption of system linearity is not violated.

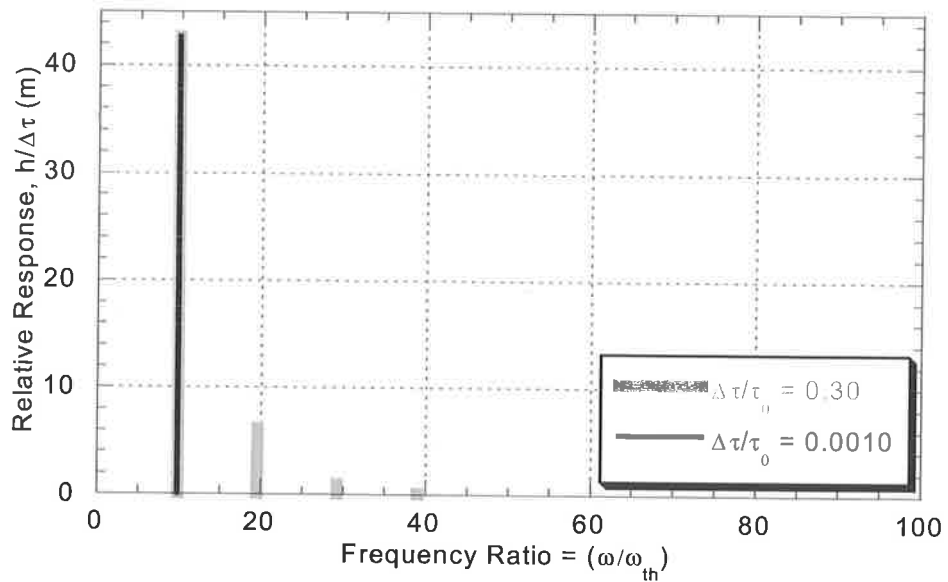


Figure 5-15 – Fourier decomposition of time series transient traces from the method of characteristics for a reservoir-pipe-valve system with no leak and for forcing functions of two different magnitudes (Data file: C5-4.txt).

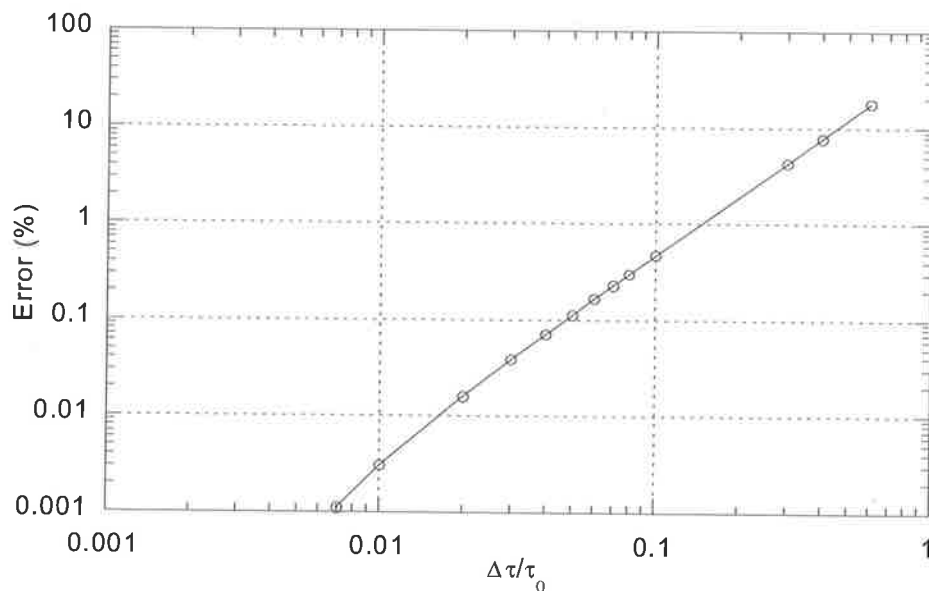


Figure 5-16 – Percentage error at $\omega/\omega_h = 1.0$ as a function of the magnitude of valve opening variation.

From Chapter 3, the modelling of transient behaviour in pipelines contains nonlinear components in two areas: the steady-state friction equation and the orifice equation. While steady-state friction is an intrinsic property of pipeline behaviour and cannot be removed, the nonlinear effect of the orifice equations (at in-line and side-discharge transient-generating valves) can be minimised by changing the input variable to the induced discharge perturbation (Tsang *et al.* 1985, Suo and Wylie, 1989).

Figure 5-17 shows a configuration of the pipeline where the transient-generating valve (located at the midpoint of the pipeline) is modelled using the orifice equation. The variation in the τ value of the valve during the generation of the transient is converted into an implied discharge variation at the valve through the nonlinear orifice equation. The use of the τ perturbation as the input to the system, therefore, requires a transfer through this nonlinear element before a hydraulic response is felt in the pipeline. A more direct approach would be to use the induced discharge perturbation at the valve as the input to the system, thus removing the initial nonlinear transfer through the orifice equation. This approach assumes the induced discharge perturbation as a result of the valve movement alone.

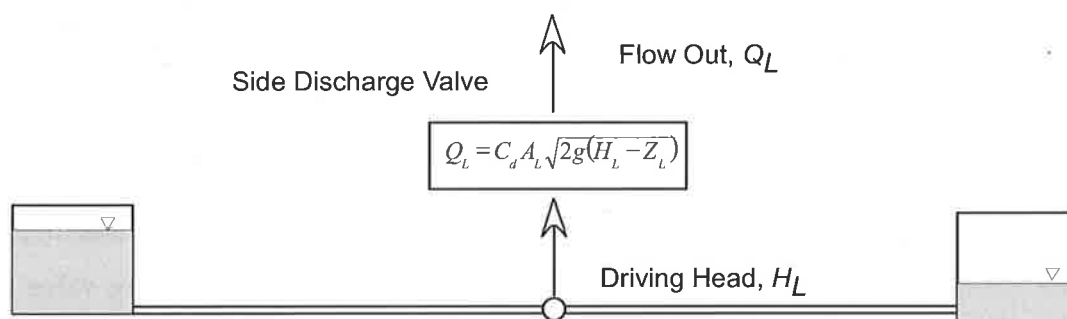


Figure 5-17 – Original modelling of the transient generation valve.

The use of the induced discharge perturbation as the input to the system requires a knowledge of the discharge variation profile as direct measurement of this discharge is not possible using existing devices under the sampling interval needed for fluid transients. Alternatively, in the case where the nature of the injected signal is short, the induced discharge perturbation can be determined indirectly through measurement of the head

response imposed by valve movement and with the use of the Joukowsky equation. This approach requires the isolation of the section of the transient trace that is directly related to the valve movement. For fast manoeuvres, the beginning of this section corresponds with the start of the transient and the end can often be identified by the point where the initial variation in pressure has ceased. The identification of this region is shown in Figure 5-18 for a step signal (repeat of the leaking trace of Figure 5-2).

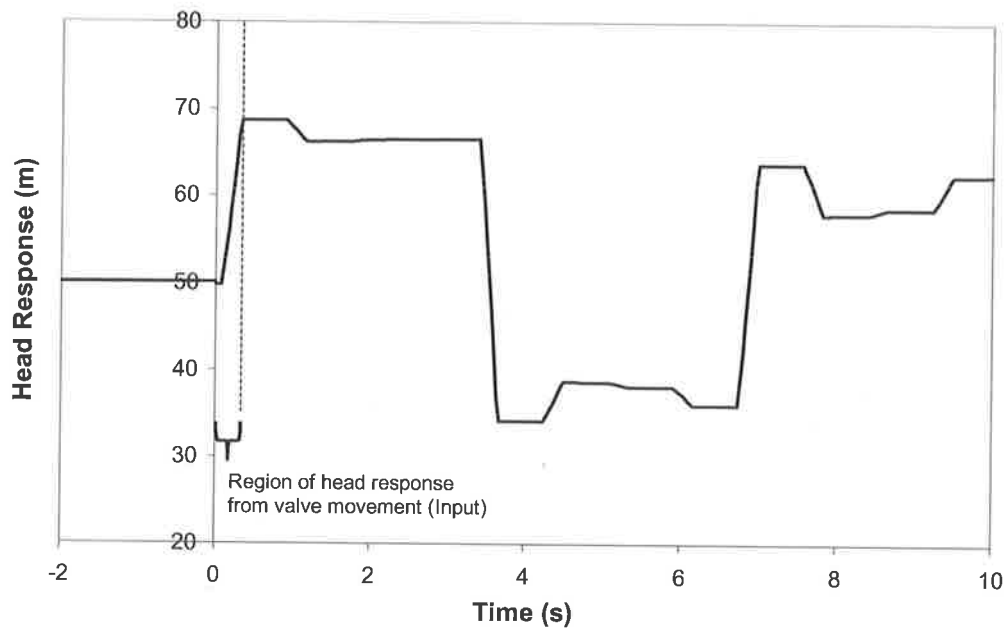


Figure 5-18 – Identification of induced-head response by the movement of the transient-generating valve for a step input.

In the case of a pulse signal injected into the system, the initial head perturbation created by the valve movement can be identified by the first observed pulse in the trace (refer to Figure 5-19). The identification of the region where the transient-generating valve has a direct effect on the head response measured at the generator gives the induced-head perturbation by the valve movement. The corresponding flow associated with this perturbation in a length of pipeline is given by the Joukowsky equation for an in-line valve as

$$\Delta Q = -\frac{gA\Delta H}{a} \quad (5.8)$$

and for a side-discharge valve as

$$\Delta Q = -\frac{2gA\Delta H}{a} \quad (5.9)$$

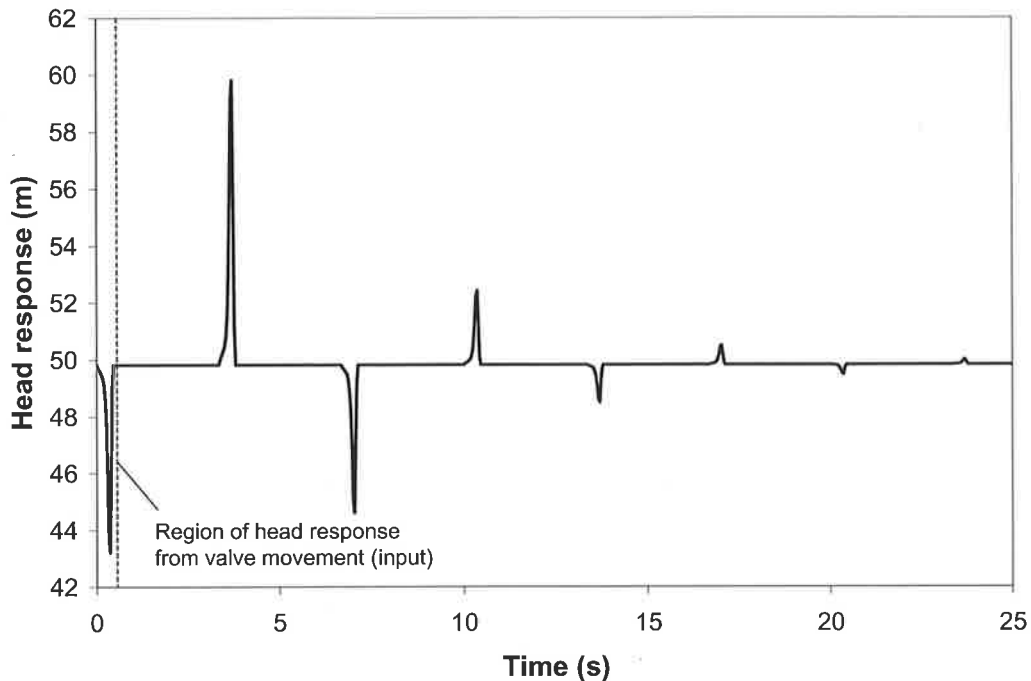


Figure 5-19 – Identification of induced-head response by the movement of the transient-generating valve for a pulse input.

The derivation of the induced discharge perturbation requires the speed of the valve manoeuvre to be fast enough such that the head response at the start of the transient can be assumed to be a result of the valve movement alone and is not contaminated by reflections from the system. The movement of the valve should, therefore, cease prior to the arrival of any reflection arriving at the measurement station. The effect of such contamination from system reflections imposes a change in the magnitude of the discharge perturbation derived through Eq. (5.9) and is not part of the real imposed discharge by the valve. The magnitude of this error is given by the following analysis. Consider a step transient being generated in the system using a side-discharge valve that increases the head by ΔH , as shown in Figure 5-20.

When the wave front reflects off an object in the system (in this case a system boundary), the reflected signal will have a magnitude of $\alpha\Delta H$ where α is the reflectivity coefficient of the object. The reflectivity coefficient is a property of the object and is given by the ratio of the reflected and incident wave magnitudes. When the reflected wave returns to the

transient source, the magnitude of the head at this point is given by $(1+\alpha)\Delta H$ and the determination of the induced discharge perturbation using Eqs. (5.8) and (5.9) leads to errors. In the case where reflections from the system are unavoidable—when the transient generation valve is located next to a system boundary—a correction factor of $(1+\alpha)$ should be applied to the discharge perturbation magnitude determined through Eq. (5.9).

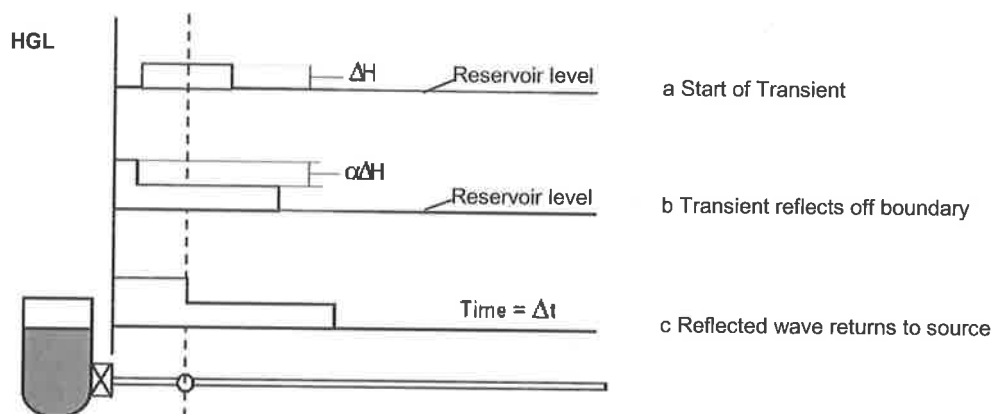


Figure 5-20 – Sequence showing interference from boundary reflection.

The corrected discharge from the system for an in-line valve generation taking into account the presence of reflection contamination is given by

$$\Delta Q = -\frac{gA\Delta H}{a(1+\alpha)} \quad (5.10)$$

and for a side-discharge valve generation as

$$\Delta Q = -\frac{2gA\Delta H}{a(1+\alpha)} \quad (5.11)$$

In the case of a dead-end boundary, the reflection coefficient is 1.0. The use of the correction coefficient only applies to cases where the reflections off the object can be assumed to be in effect during the *entire* valve manoeuvre. For this reason, the transient source should either be placed adjacent to any strongly reflecting object (i.e. $|\alpha| > 0.1$) such that Eq. (5.11) can be applied, or be placed far away such that its reflection does not arrive during the transient generation. A transient source placed adjacent to a reservoir

boundary (i.e. $\alpha \approx -1$) results in an undefined discharge perturbation using Eq. (5.11) as the head perturbation measured at the source is assumed to be close to zero at all times. The procedure for system response extraction when the input function is derived from the initial section of the measured pressure response is given in Figure 5-21.

The advantage of the shift in the input variable from $\Delta\tau^*$ to the discharge perturbation is shown in Figure 5-22 with a comparison of the frequency response function from both the method of characteristics and the transfer matrix equation. In this example, the in-line valve (located at the downstream boundary) in the system of Figure 5-8 is perturbed from a fully closed position. The MOC model is discretised into 100 reaches with a computation time step of 0.0333 s. The valve is fully opened then returned to its closed state ($\Delta\tau_{\text{Max}}^* = 1.0$). This situation constitutes the largest perturbation of the valve possible. If the dimensionless valve opening is used as the system input, then nonlinear errors of up to 20% can be expected in the resultant response function (refer to Figure 5-16, with a $\Delta\tau > 0.6$). In contrast, the shift to the discharge perturbation for this case produced a match between the nonlinear and linear models with an error less than 1% in the peak magnitudes, indicating that the original error has been largely removed through this change in the input variable.

To model the perturbation of the in-line valve as a discharge perturbation in the transfer matrix, a unit magnitude discharge oscillation was placed at the upstream face of the closed in-line valve. This approach provides the head response from the system in terms of the unit input discharge variation at the valve. This discharge oscillation has the transfer matrix of

$$\begin{Bmatrix} q \\ h \end{Bmatrix}^{n+1} = \begin{bmatrix} 1 & 0 \\ 0 & 1 \end{bmatrix} \begin{Bmatrix} q \\ h \end{Bmatrix}^n + \begin{bmatrix} 1 \\ 0 \end{bmatrix} \quad (5.12)$$

where $n+1$ is at the upstream face of the in-line valve. This approximation of the physical nature of the situation is necessary to incorporate the use of discharge perturbation as input to the system in the transfer matrix model (refer to Figure 5-23). Due to the nature of the in-line valve equations in the transfer matrix model, the simultaneous presence of the head loss generated by the valve in addition to a discharge perturbation at this point is not

possible. For this reason, the transfer matrix model should not be used to predict the frequency response function when the transient is generated by the perturbation of an open in-line valve (e.g. open-closed-open), or for events generated by the opening of closed in-line valves.

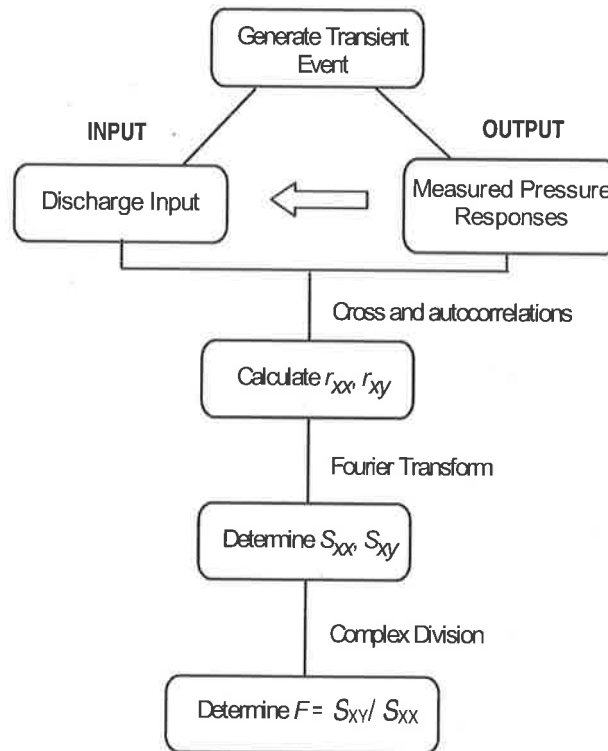


Figure 5-21 – Procedure for system response extraction using only the measured pressure response.

For this situation, if no flow exists in the system at steady state, the friction losses in the system are zero and the magnitudes of the resonance peaks in the frequency response function are infinity, making comparisons between the two models impossible. To remedy this problem, a side-discharge orifice of $C_d A_L = 0.00014 \text{ m}^2$ ($C_d A_L / A = 1.98 \times 10^{-3}$) was placed at the midpoint of the pipeline to create an initial flow in this system.

Further confirmation using a side-discharge valve for the transient generation process is shown in the system of Figure 5-24 and Figure 5-25 (results in Figure 5-26 and Figure

5-27). In both cases, an initially closed side-discharge valve in the pipeline was fully opened and subsequently shut.

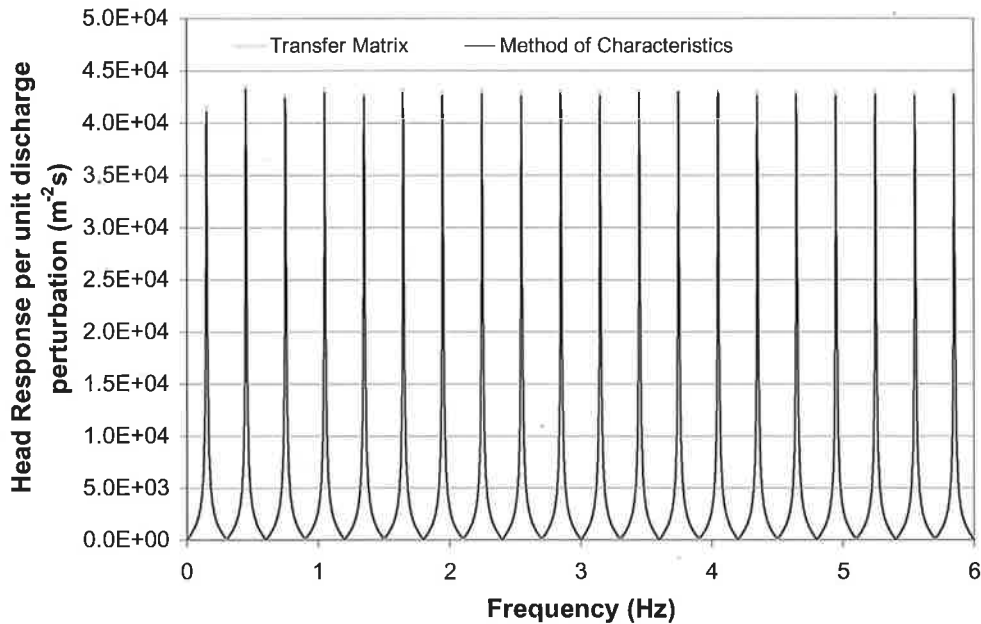


Figure 5-22 – Comparison between FRF generated from the transfer matrix equations and the proposed technique using time series results from MOC for the anti-symmetric system of Figure 5-8 (Data set: C5-5.txt).

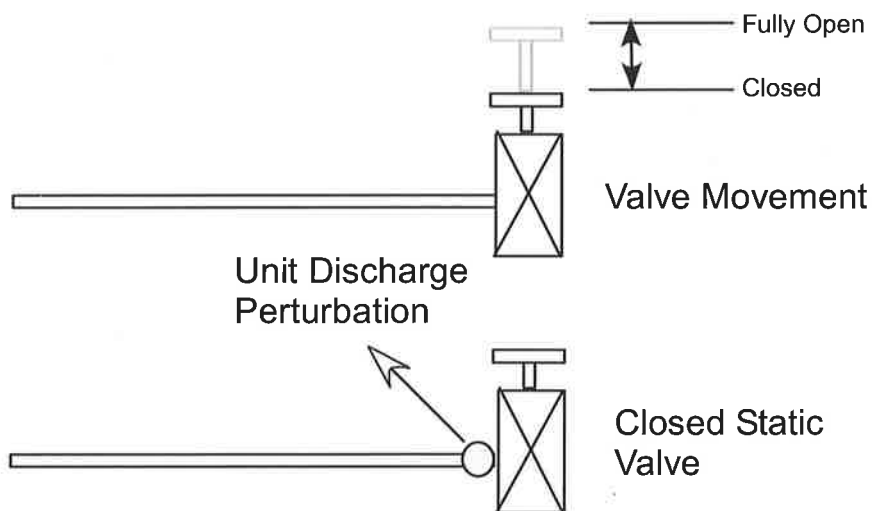


Figure 5-23 – Correction for the perturbation of an initially closed in-line valve.

Reservoir 1 Head = 50 m

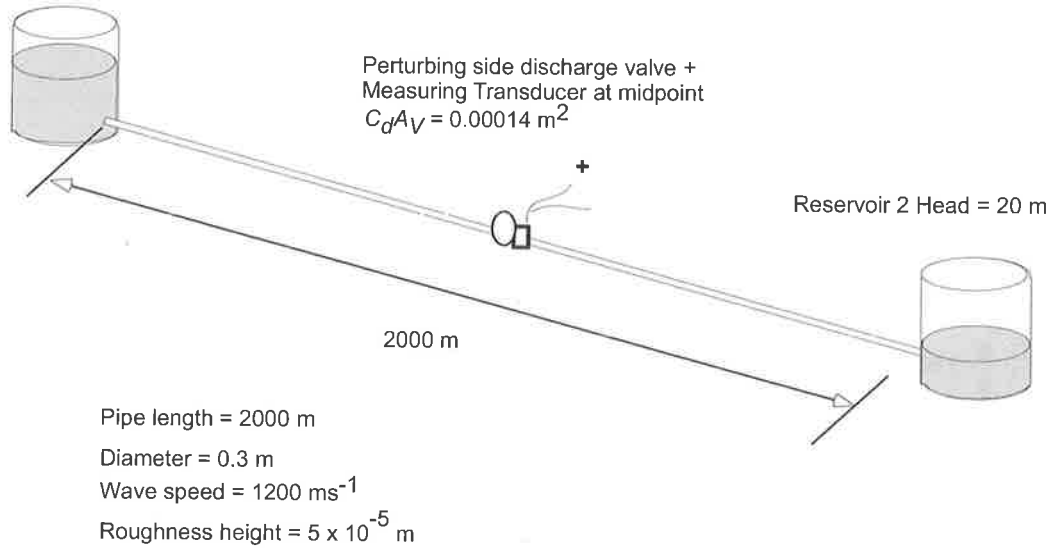


Figure 5-24 – System configuration for the symmetric test.

Reservoir 1 Head = 50 m

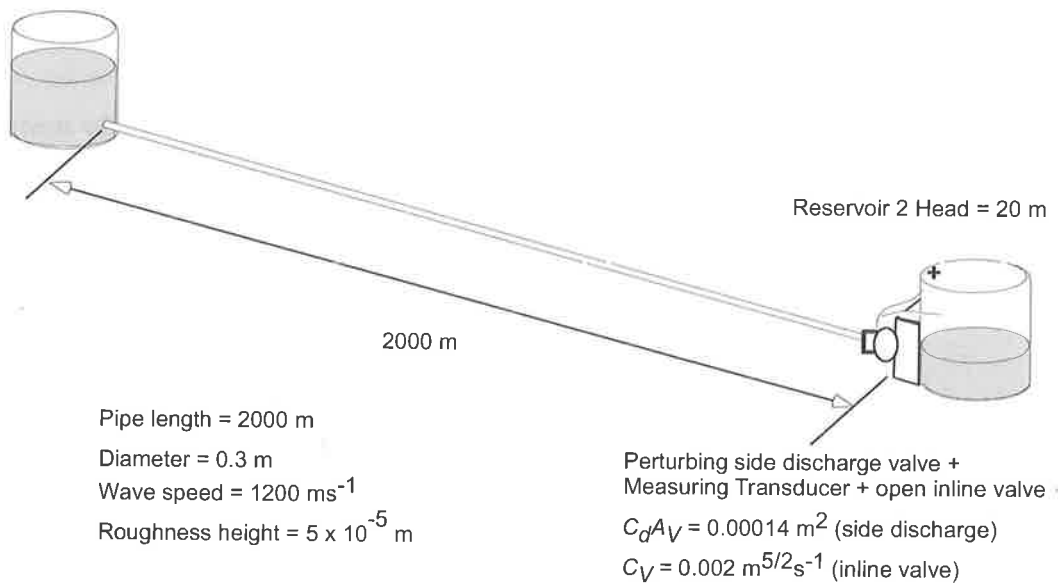


Figure 5-25 – System configuration for the anti-symmetric test.

As in the in-line valve example, the transient-generating side-discharge valve is modelled by a unit discharge oscillation in the transfer matrices given by Eq. (5.12). The discretisation—1000 reaches with a computational time step of 0.00333s—for these examples was made finer to determine any possible effect from the size of the time steps in MOC. Good matches result once again between the linear and nonlinear models and

validate the removal of the nonlinear errors when the discharge perturbation is used as input to the system.

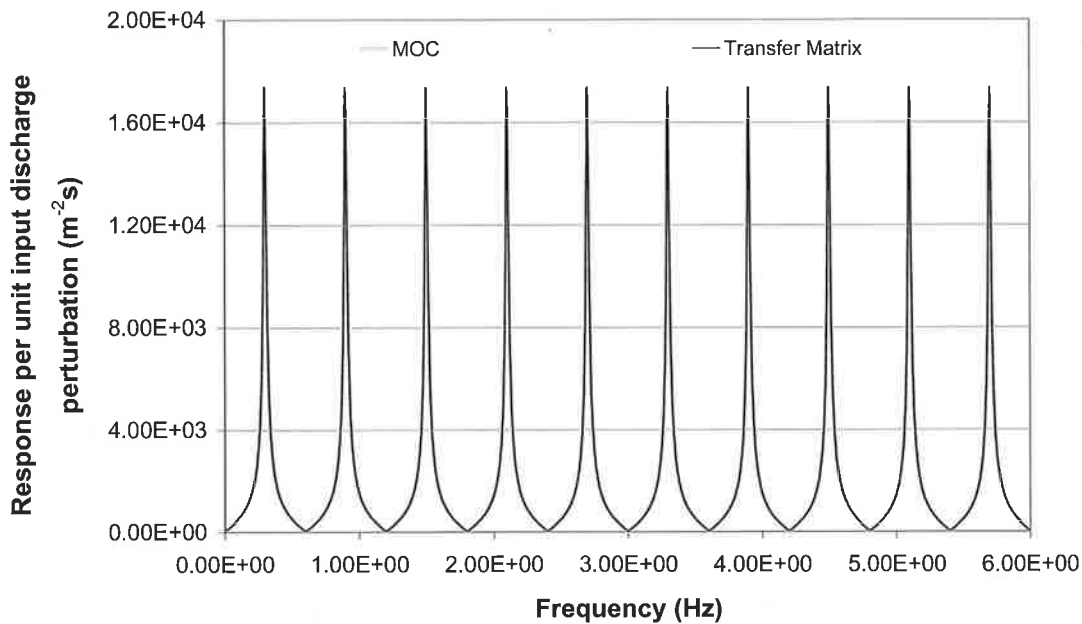


Figure 5-26 – Comparison between the FRF generated from the transfer matrix equations and the proposed technique using time series results from MOC for the situation shown in Figure 5-24 (Data file: C5-6.txt).

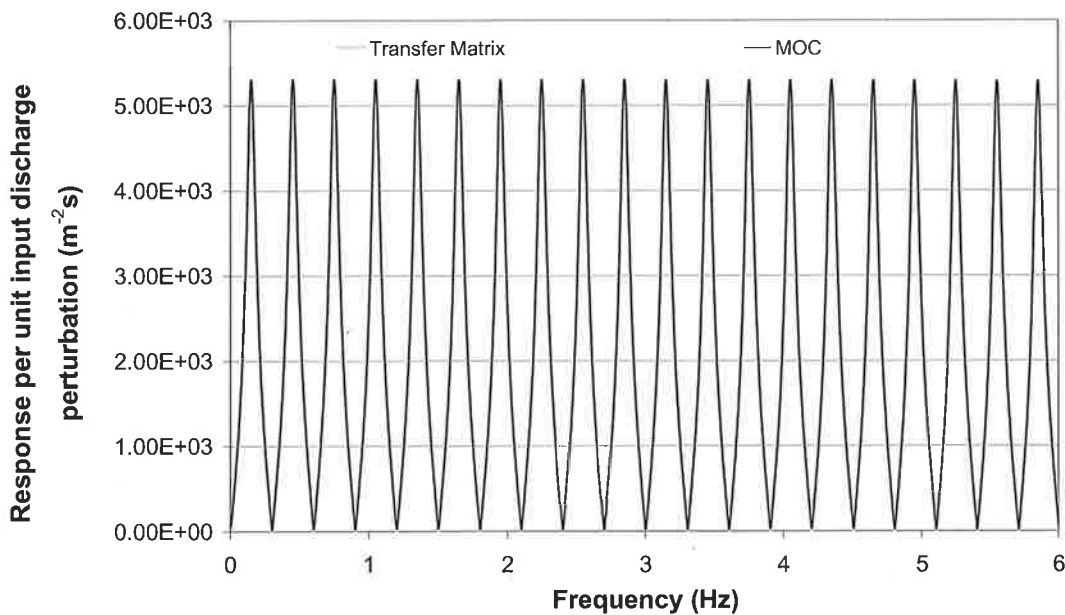


Figure 5-27 – Comparison between the FRF generated from the transfer matrix equations and the proposed technique using time series results from MOC for the situation shown in Figure 5-25 (Data file: C5-7.txt).

The level of discretisation in the MOC model has increased the accuracy to the approach. An agreement with negligible error is now observed compared to the previous example where the peaks from the two models have a 1% error (refer to Figure 5-22).

In the case where the generated transient signal is continuous (for example, a pseudo-random binary signal), however, this indirect determination of the valve-induced discharge is no longer possible as the induced-head change at the valve cannot be separated from system reflections. In such cases, the system response functions must be derived using the measured $\Delta\tau$ as input to the system with due care taken that the magnitude of the perturbation does not result in excessive errors, as indicated in Figure 5-16.

In conclusion, the extraction of the frequency response function (FRF) using both the change in the dimensionless valve opening ($\Delta\tau$) or the induced discharge perturbation during the transient-generating manoeuvre of pipeline valves has been considered. The results indicate that unless the valve movement from its initial state is small, the system behaves nonlinearly when $\Delta\tau$ is used as the input, violating the linearity assumption of the system response extraction process. In contrast, the shift in the input variable to the induced discharge perturbation was found to remove the nonlinear response in cases where the perturbation is generated by a side-discharge or in-line valve. This improvement was observed for all magnitudes of the valve movement.

5.2.2 System configuration

The examples in the previous section have shown that the frequency response function can be extracted from the system under two different arrangements of the transient-generating valve and the measurement transducer. Figure 5-22 and Figure 5-27 show the frequency response function when transient generation is conducted at the end of a pipeline—at or adjacent to a downstream in-line valve—whereas Figure 5-26 shows the case where generation occurs at the mid point of a pipeline. In all these cases, the transient is measured at the generation point (i.e. the input and output are at the same position). However, there are no constraints on the physical location of the input and output to a system and a system response function can be extracted for all locations of the transient source (input) and the measuring transducer (output). Given that the input is independent

of the output signal, a valid response function can be extracted even when the transient source is positioned at one end of a pipe with the measurement at the other end. The resultant response function describes the way in which an induced transient event at the transient source affects the measured head response.

This section investigates the effect of the generating and measurement locations on the strength of the system response function. As discussed previously, the boundary conditions of the system affect the value of the fundamental frequency and hence the position of resonant peaks in the frequency response function (Pejović *et al.* 1983, Wylie and Streeter 1993). This behaviour is shown in Figure 5-26 and Figure 5-27 where the spacing and location of the resonant peaks in the frequency response function are changed as a result of the boundary conditions. As the behaviour of the system boundaries result in a dramatic change in system response functions, the optimum locations of the transient source and measuring station need to be determined for each case.

The tests conducted in this dissertation can be grouped under two different boundary configurations, anti-symmetric and symmetric boundaries. The two different configurations result in a change in the periodic behaviour of the transient response and are defined in Wylie and Streeter (1993). For a frictionless pipe, the characteristic impedance is given by

$$Z = \frac{a}{gA} \quad (5.13)$$

and the impedance of the in-line valve at the system boundary is

$$Z_v = \frac{2\Delta H_{v0}}{Q_{v0}} \quad (5.14)$$

where, ΔH_{v0} and Q_{v0} are the steady-state (initial) head loss and discharge across the valve, respectively. When $Z_v \geq Z$, Wylie and Streeter (1993) defined the fundamental frequency of a system (in radians) as

$$\omega_{th} = 2\pi \frac{a}{4L} \quad (5.15)$$

The system is defined as *anti-symmetric* where the resonant peaks in the system occur at odd multiples of this fundamental frequency. This type of boundary condition can be achieved by placing a fully closed or throttled valve at a boundary. For the simulation system, when the in-line valve of $C_V = 0.002 \text{ m}^{5/2}\text{s}^{-1}$ exists at a boundary (either fully opened or fully closed), the conditions across this valve results in a Z_V that is greater than Z and the system behaves anti-symmetrically. In this case, the reflective boundary at the valve is similar to a dead end (Wylie and Streeter, 1993). Such boundary conditions translate to reality in testing carried out under a reduced or no-flow condition.

When $Z_V \leq Z$, the fundamental frequency of the system is (Wylie and Streeter, 1993)

$$\omega_{th} = 2\pi \frac{a}{2L} \quad (5.16)$$

where the resonant peaks are at the odd multiples of this frequency. Testing carried out under this condition is aimed to simulate application of the procedure when the pipeline is in operation with no high impedance element located at the boundaries of the system. Such reflective conditions at the boundaries are similar to that of a reservoir. Further information concerning this shift in boundary behaviour as a result of Z_V can be found in Wylie and Streeter (1993).

The optimum arrangement of measurement and generating positions for both configurations is illustrated in the following example with the anti-symmetric case considered first. A side-discharge valve with a $C_d A_V = 0.00014 \text{ m}^2$ is placed at a point 1700 m from the reservoir boundary in the numerical pipeline. A fully opened in-line valve of a $C_V = 0.002 \text{ m}^{5/2}\text{s}^{-1}$ is located at the downstream boundary (refer to Figure 5-28). The measurement station is initially placed at the upstream boundary. The frequency response function is extracted using the induced discharge perturbation (ΔQ) at the side-discharge valve as the input to the system and using the transfer matrix model. To obtain an indication of the magnitude of the extracted frequency response function, the values at the first 250 resonant peaks are averaged and this process is then repeated for the same

location of the side-discharge valve but for a different position of the measuring station. An illustration of the procedure is shown in Figure 5-28. The averaged response magnitudes for each location of the measurement station (given a particular location of the transient source) provide a method of determining the combination that gives a maximum recorded system response from the pipeline.

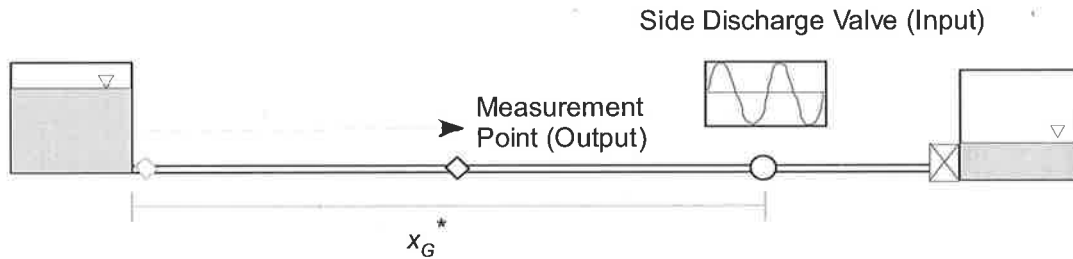


Figure 5-28 – Determination of the position where maximum response is measured for each location of the transient-generating source, x_G^* .

The result of this analysis for different locations of the transient generation source is shown in Figure 5-29. For the anti-symmetric system, the maximum response occurs when measurements are taken adjacent to the downstream valve for all positions of the transient source. However, locating the source at the valve gives the overall maximum response for all the combinations of the transient source and measuring transducer location. In an anti-symmetric system, therefore, the optimum configuration of the system—providing the highest signal-to-noise ratio in the extraction of the response function—is where both the source and the measurement are conducted next to the high impedance boundary.

Following the same procedure, the optimum locations for both the generation and measurement in the symmetric pipeline are determined with the average response shown in Figure 5-30. The result indicates that for a symmetric system the optimum configuration of the transient source and the measurement station is where both are located at the midpoint of the pipeline. The selection of the input variable and the optimum system configuration for the extraction of the system response function from a pipeline is, therefore, established. A final topic—the effect of the nature of the injected signal—needs to be investigated prior to experimental verification of the procedure.

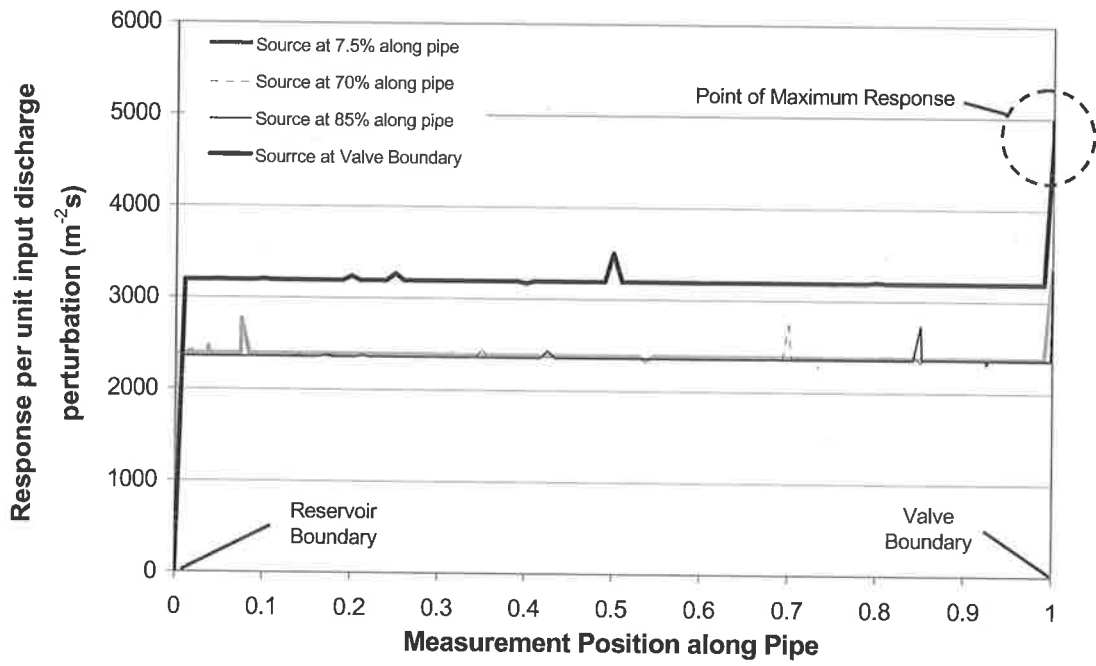


Figure 5-29 – Average response magnitude for varying measurement and generation positions for an anti-symmetric system.

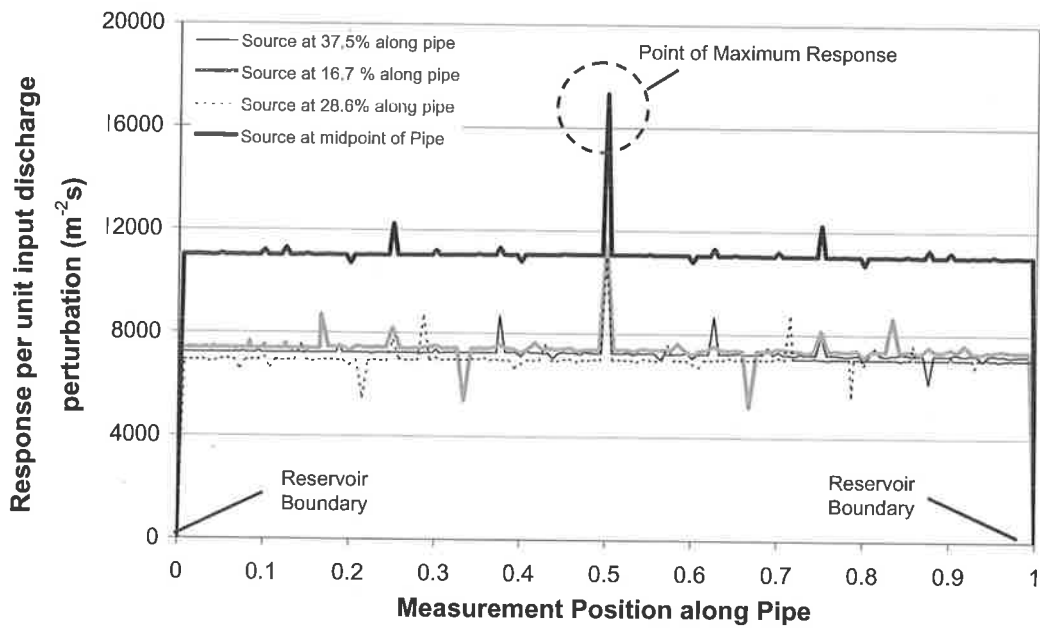


Figure 5-30 – Average response magnitude for varying measurement and generation position for a symmetric system.

5.2.3 Effect of the injected signal

The same system response function will be extracted from a pipeline regardless of the input signal as long as the physical nature of the system remains unchanged and the system operates within the bounds of linearity (refer to Section 5.2.1). This property is illustrated at the beginning of this chapter where the system response function for an injected step was shown to be identical to that from an injected pulse, although the shape of the output for each case is different. While it is true that the same response function can be derived using any injected signal, the accuracy of the extraction process in the presence of background noise can change depending on the energy content of the signal itself.

While an injected transient signal is often described by its shape and duration, a more appropriate approach is to use the amount of information contained in the signal. This property is known as the *bandwidth* of the signal (Lynn 1982, Lee *et al.* 2004). The effect of signal bandwidth in the presence of system noise is investigated in this section and the properties of a signal that allow the most information to be extracted are presented.

In addition to the effect of the signal bandwidth, this section investigates a class of signal often used in transient analysis—the step signal. A step change in pressure and flow is easily generated by a sharp closure of a valve and is popular in the literature on transient behaviour. Problems arise, however, when these types of signals are used in a system extraction procedure, as a step signal is unbounded in time resulting in an invalid signal spectrum using a conventional Fourier transform (Lynn, 1982). This section provides a correction procedure where the results from an injected step signal can be used to determine a valid system response function.

Signal bandwidth

The *bandwidth* of a signal represents its range of detectable frequencies. This property defines the upper limit in the frequency range that can be observed in the measured output (Ibrahim and Mikulcik, 1978). When a signal of a certain bandwidth is injected into a pipeline, the corresponding output from the system only contains useful information up to the bandwidth of the injected signal. This concept can lead to the design of filters for

transient signals where frequency ranges not contained in the input (hence not a direct response to the injected signal) can be removed.

The effect of signal bandwidth on the system response function is illustrated in the following example. A transient signal is introduced into the simulated pipeline using a perturbation of a side-discharge valve located at the downstream (valve) boundary. According to the optimum configuration of the system under an anti-symmetric boundary condition, the transient is measured at the transient source. The $C_d A_v$ of the side-discharge valve is set as 0.00014 m^2 and the transient response is extracted through the method of characteristics model (for 100 reaches, computational time step = 0.0333 s). The valve is first opened and closed in a rapid fashion, as given in Figure 5-31 labelled as “signal #1.”

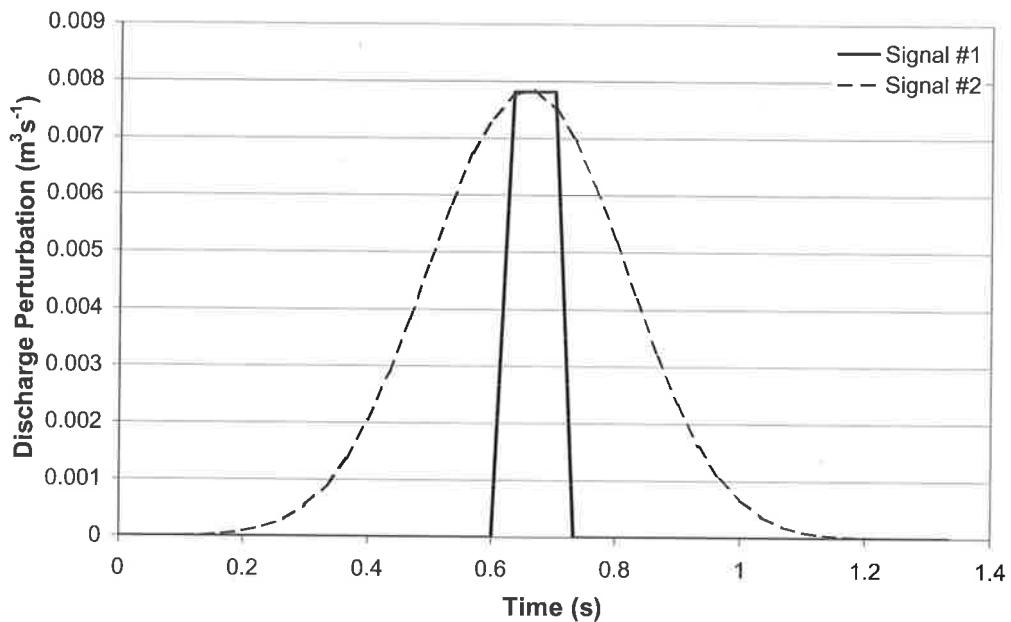


Figure 5-31 – Injected signals for the bandwidth investigation (Data file: C5-8.txt).

The valve is opened from a fully closed position in 0.0333 s , remains open for 0.0666 s and is then closed in 0.0333 s (duration of signal = 0.1332 s). The spectrum of the injected signal and the corresponding measured response from the pipeline are shown in Figure 5-32. The input signal has observable spectral content up to 6 Hz , which results in an output signal that has well-defined resonant peaks up to this frequency. The extracted frequency response for this case is shown in Figure 5-33.

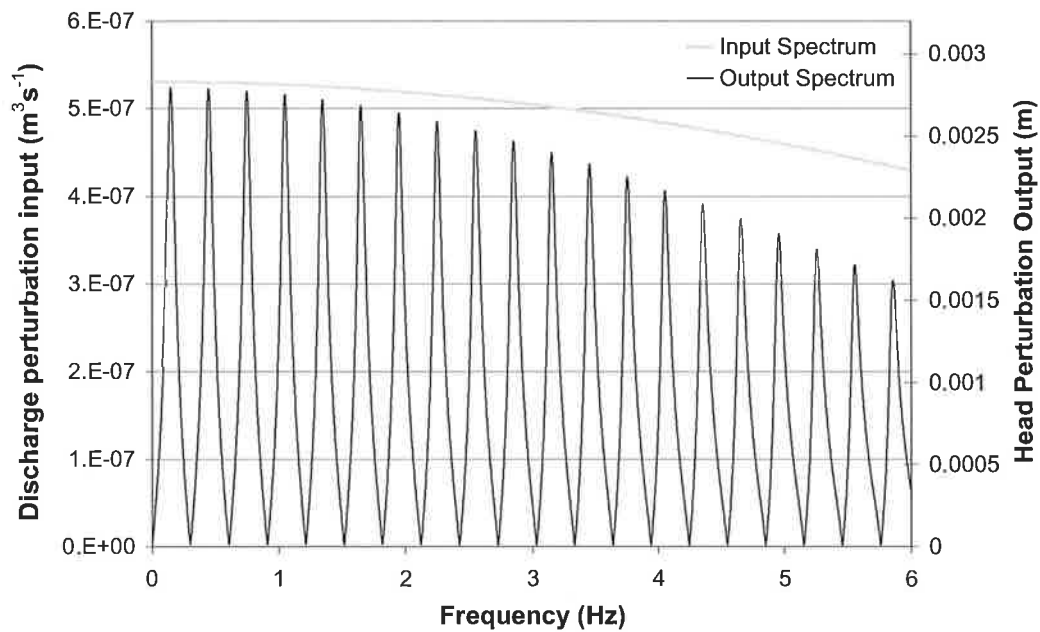


Figure 5-32 – Spectrum of input signal #1 and the corresponding head response spectrum from the system (Data file: C5-9.txt).

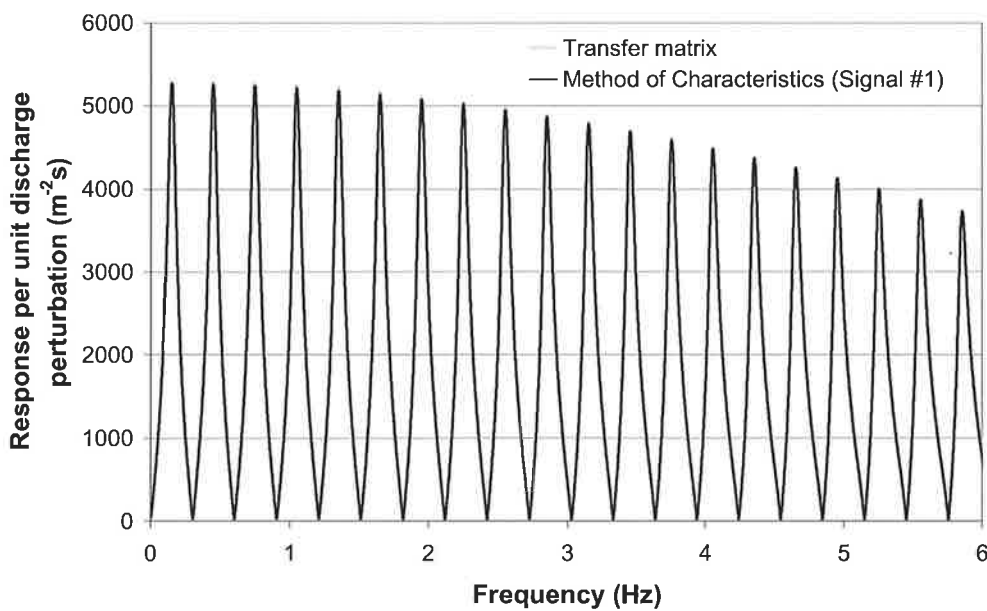


Figure 5-33 – Extracted frequency response function from the system using injected signal #1 (Data file: C5-9.txt).

The slight trend in the peaks of the frequency response function is caused by the small distance between the transient generator / measurement station and the in-line valve boundary, which is equivalent to one node spacing in the method of characteristics model.

The output from the transfer matrix model is shown in the figure to verify the extracted frequency response function and a good match is observed.

Consider now a second example where the injected signal is of the form shown in Figure 5-31 labelled as “signal #2.” The method of characteristics model is discretised with 100 reaches and a computational time step of 0.0333 s. This signal is smoother than signal #1 and, given that the high-frequency content of any signal is contained in the sharp changes in the time trace (Kreuzig 1993), the spectrum of signal #2 has a smaller band of frequencies. The band of frequencies (i.e. the bandwidth of the signal) is shown in Figure 5-34. The spectrum of the input signal indicates that the amplitude of the frequency components contained in the trace decreases to negligible levels by 3 Hz.

The spectrum of the measured head response has a similar range of frequencies to the input and no information was observed from the system beyond 3 Hz. The subsequent frequency response function using this pair of input and output signals is shown in Figure 5-35.

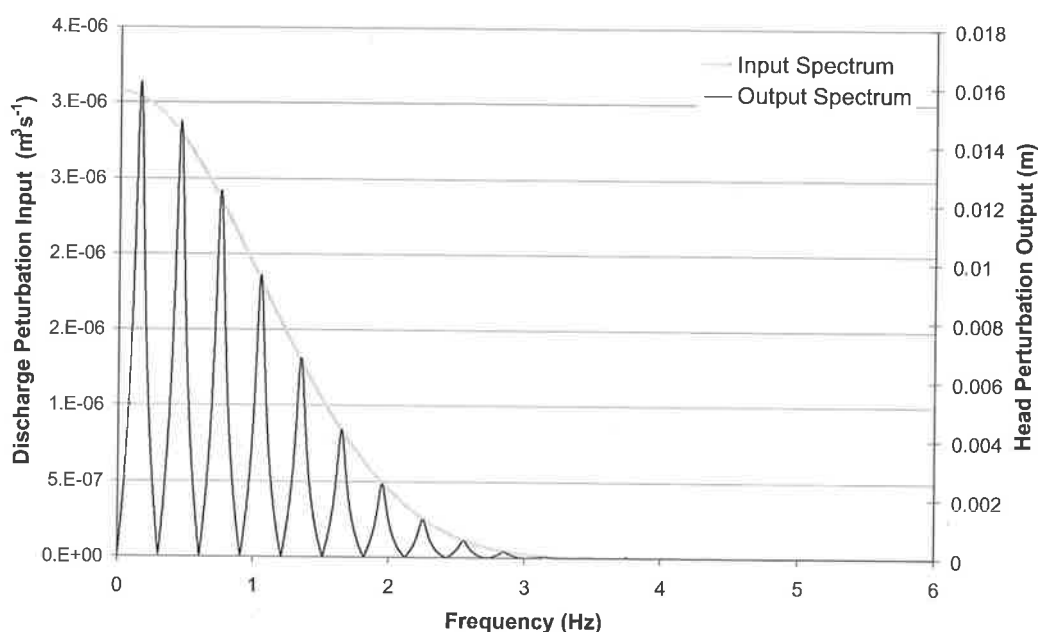


Figure 5-34 – Spectrum of the input signal #2 and the corresponding head response spectrum from the system (Data file: C5-9.txt).

From this investigation, the signal bandwidth represents the upper limit of the range of useful information that can be derived from the extracted response function. It is,

therefore, advantageous to have an injected signal with a large bandwidth to allow the maximum information to be extracted from the system. The injected signal must consist of sharp variations in time (Kreyzig, 1993) that are associated with rapid manoeuvres of the transient-generating valves. Examples of such signals, considered later in this thesis, are generated from sharp discrete perturbations of a side-discharge solenoid valve.

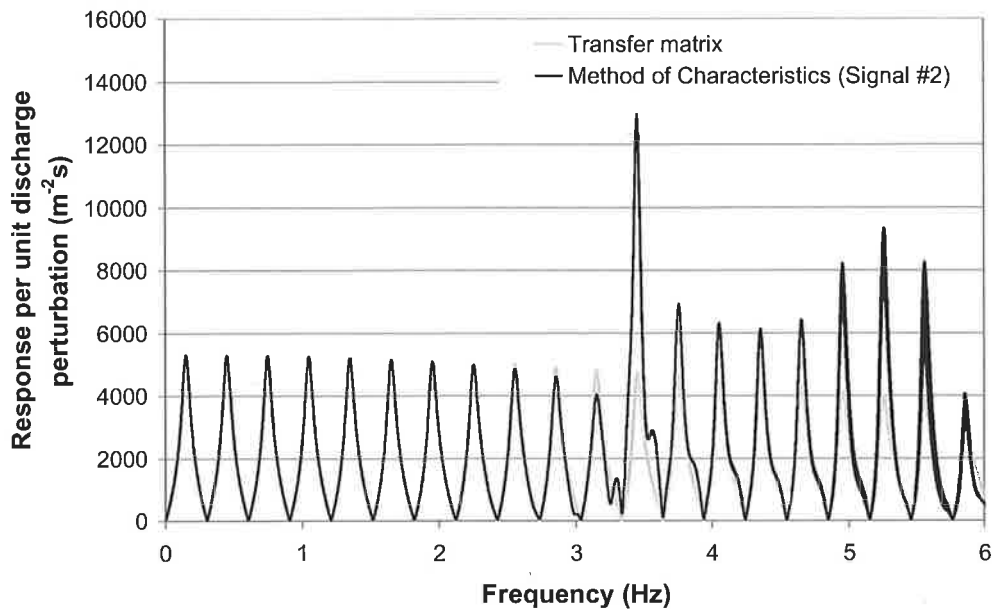


Figure 5-35 – Extracted frequency response function from the system using injected signal #2 (Data file: C5-9.txt).

For the remainder of this thesis, the bandwidth of an input signal is defined as the frequency range where the amplitude of the signal is more than 5% of its maximum level. This definition of the signal bandwidth includes more frequencies than the definition used in electrical engineering and is best suited for the mechanical (slow) transients used in this thesis. In the numerical example above, significant contamination of the data occurred after the point where the spectrum of the input signal had decayed to near zero (much less than 5% of the signal amplitude). Operators should initially investigate the clarity of the response function to determine the range of observable frequencies from the system for a given injected signal.

Infinite energy signals

Infinite energy signals are defined as signals that produce a value of infinity when integrated from $-\infty$ to $+\infty$. For this reason, the spectrums of such signals cannot be

produced by a conventional Fourier transform (Lynn 1982). An example of an infinite energy signal is the step function, commonly generated by the sharp opening or closure of valves in a pipeline, thus inducing a step fall or rise in the pressure head at the generating point. The integration of a step signal, "X", from $-\infty$ to $+\infty$ is,

$$\int_{-\infty}^{\infty} X(t)dt = \infty \quad (5.17)$$

While such a signal is easy to generate, it poses problems for the determination of its spectral content. Ferrante and Brunone (2001) approximated the spectrum of a step closure by the analytical spectrum of a Heaviside function, an instantaneous step rise in time. The use of this function to approximate system input, however, does not correspond to the true nature of valve movement. An additional problem is that the system is forced to change from one flow state to another in direct violation of the underlying linear approximation, which dictates that there is a mean state about which the perturbation takes place. The effect of these problems is shown in Figure 5-36 where the frequency response function from the numerical pipeline is extracted using a step input function and shows discrepancies from the true response function of the system. The transient was generated by the full closure of an initially opened in-line valve with a discharge orifice of $C_d A_L = 0.00014 \text{ m}^2$ ($C_d A_L / A = 1.98 \times 10^{-3}$) placed at the midpoint of the pipeline. The discharge orifice prevents the frequency response function from reaching infinity at the peaks. Figure 5-36 shows the frequency response function from this input and significant deviations are observed from the true response function of the system.

A change in the shape of the transient signal allows the accurate extraction of the response function from data generated from a valve closure. Consider a linear system excited by an input step denoted by $X(t)$ giving a corresponding transient output $Y(t)$. The two series can then be used to determine the frequency response function, $F(\omega)$. To change the input into a finite energy form, an equal and opposite operation is assumed to occur, which changes the step signal into a pulse at a time $t = d$ after the first step operation. The new input function, $X_C(t)$, is given by

$$X_C(t) = X(t) - X(t-d) \quad (5.18)$$

Using the additive and distributive nature of time invariant linear systems, the new corresponding output of the system is given by

$$Y_c(t) = Y(t) - Y(t-d) \quad (5.19)$$

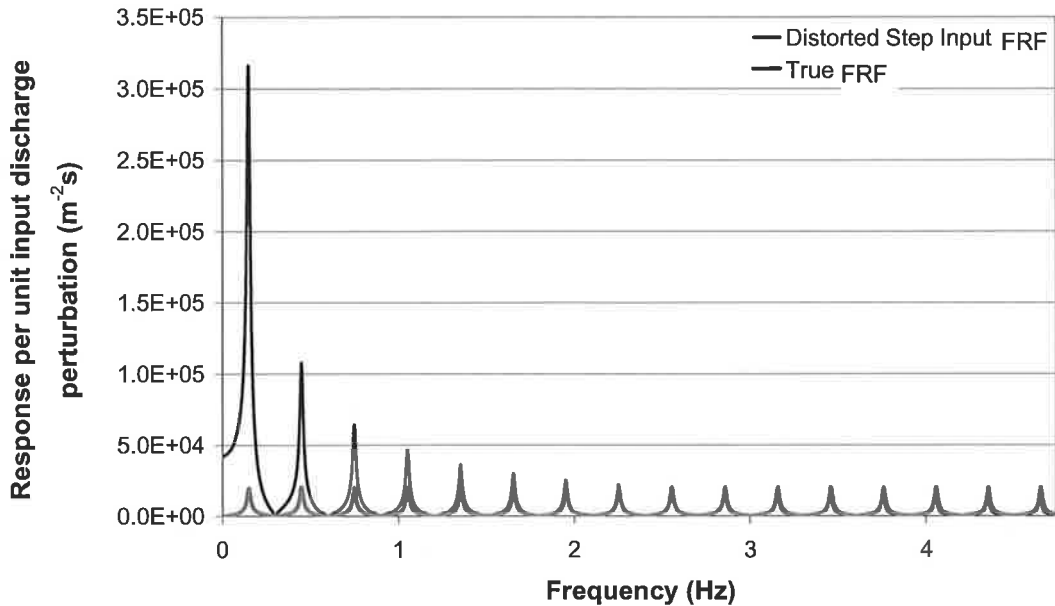


Figure 5-36 – FRF from the uncorrected discharge input from a full in-line valve closure generated using the MOC model.

The use of Eqs. (5.18) and (5.19) as the input and output gives the frequency response of as

$$F_c(\omega) = \frac{\mathfrak{F}\{Y(t) - Y(t-d)\}}{\mathfrak{F}\{X(t) - X(t-d)\}} \quad (5.20)$$

Using the known properties of the Fourier transform operator, Eq. (5.20) now becomes

$$F_c(\omega) = \frac{\mathfrak{F}\{Y(t)\} - e^{-i\omega d} \mathfrak{F}\{Y(t)\}}{\mathfrak{F}\{X(t)\} - e^{-i\omega d} \mathfrak{F}\{X(t)\}} = \frac{\mathfrak{F}\{Y(t)\} [1 - e^{-i\omega d}]}{\mathfrak{F}\{X(t)\} [1 - e^{-i\omega d}]} = F(\omega) \quad (5.21)$$

which indicates that the frequency response of the system remains unchanged as a result of this operation. An illustration of this procedure is shown in Figure 5-37.

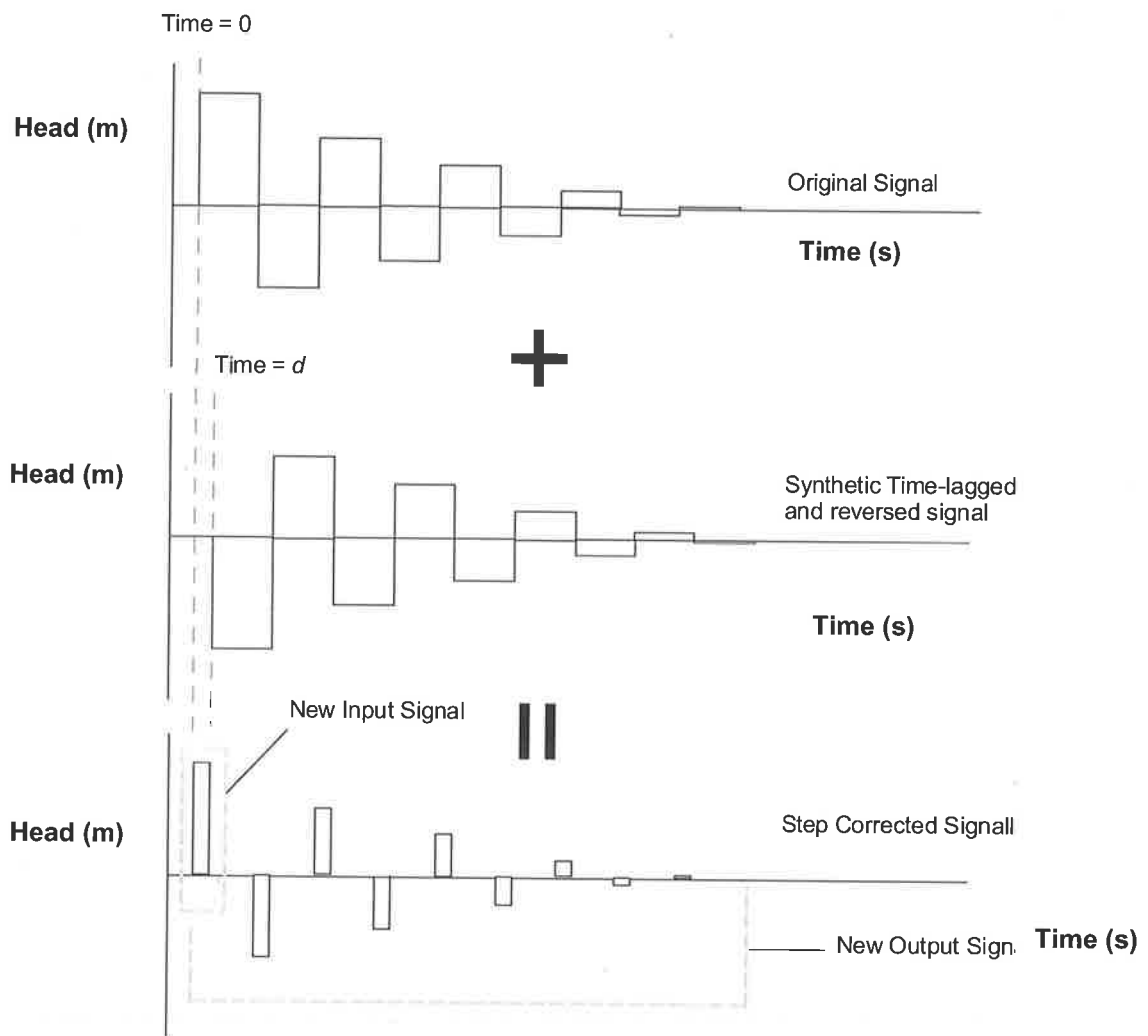


Figure 5-37 – Correction for step input function.

The original input step function can, therefore, be modified into a pulse by adding a delayed and opposite version of itself. If the same procedure is carried out on the output trace of the signal, the frequency response of the system remains unchanged. An application of this approach is presented in Figure 5-38 where Figure 5-36 is converted into a finite energy form using the above procedure and the frequency response function is generated from the result. This frequency response function is compared to the frequency response function generated from the perturbation of the valve about a mean position with excellent agreement. The accuracy of this correction procedure does not depend on the time lag factor, d , except that it must be shorter than the time for the first reflection to arrive at the measurement station.

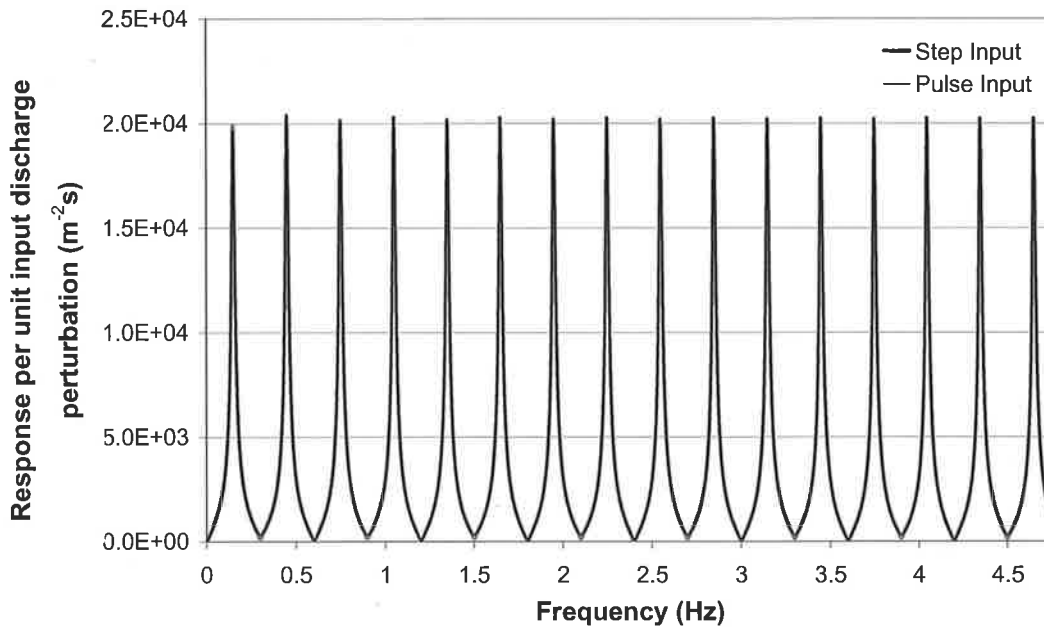


Figure 5-38 – Comparison between MOC generated FRF for an in-line valve closure and an in-line valve perturbation.

5.2.4 Frictional effects on the extracted frequency response function

As mentioned in Section 3.4 pipe friction losses can be modelled in two forms, steady friction and unsteady friction components. Losses induced by a valve in the system can affect the nature of the response function. Each of these loss factors is investigated in this chapter by progressively adding their effect to an initially frictionless numerical pipeline. For this example, a side-discharge valve, of $C_d A_V = 0.00014 \text{ m}^2$ is located directly adjacent to the open in-line valve in the numerical pipeline and is used to generate a transient event. In a system with no losses (excluding both valve and pipe losses), the response function has the form shown in Figure 5-39. The response function in a loss-free system consists of peaks that rise to infinity at the resonant frequencies.

The frequency response function for the pipeline with valve loss included is shown in Figure 5-40 and the peaks now have *finite* values. The valve loss affects all peaks equally in the response diagram, indicating that the valve loss is *frequency-independent*. This behaviour is also the case for steady friction, which causes a uniform decrease in the magnitude of the resonant peaks. In contrast, the incorporation of unsteady friction results in a frequency-dependent reduction in the peak magnitudes, with higher frequencies being

attenuated more than lower. This effect is shown in Vitkovský *et al.* (2003b). The contrast between the effects of different frictional losses is shown in Figure 5-41 where the resonant peak magnitudes are plotted for each case.

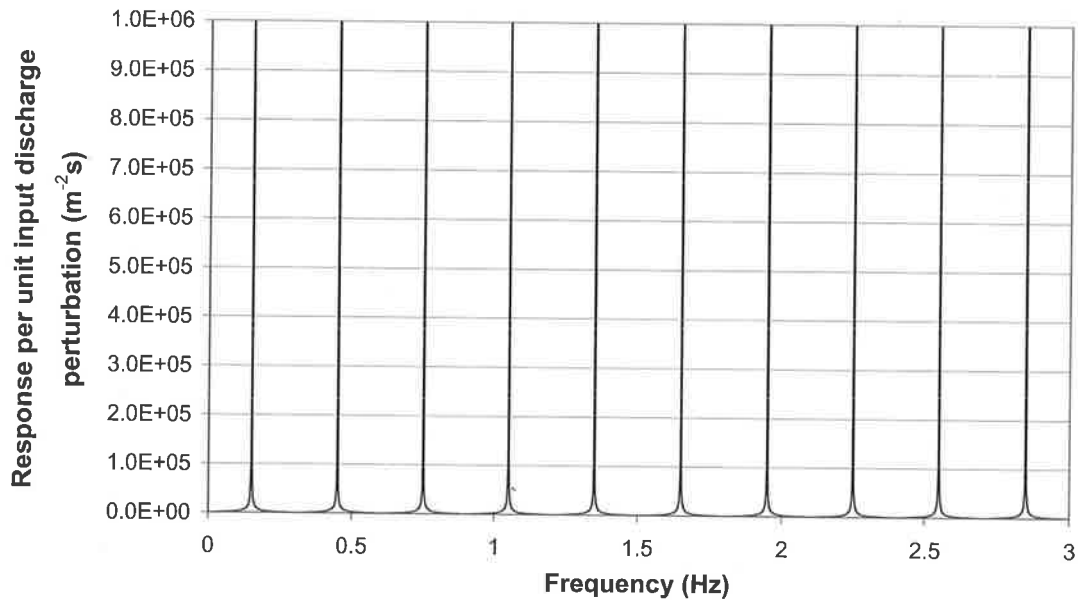


Figure 5-39 – FRF from a pipeline with no losses.

The previous sections have investigated several issues concerning the procedure required for accurate extraction of the system response functions. These issues include procedures for minimising the presence of nonlinear behaviour between the input and the output of the system, the location of the measuring and transient generation stations that provides maximum signal-to-noise ratio in the extracted function, the effect of the signal bandwidth and correction for infinite energy input signals. These findings are applied in the following section for the experimental extraction of the system response function from a pipeline using conventional discrete signals.

The procedure for system response requires only the definition of the input to the system, often described by the nature of the valve movement (i.e. variation in orifice size and pattern of induced discharge variation) and the output from the system, which is the measured transient response. The actual physical location of the input and output (i.e. points of generation and measurement) and the topology of the pipeline do not affect the process. For this reason, the procedure presented in this chapter can be applied in a complex pipe network as well as a simple pipeline.

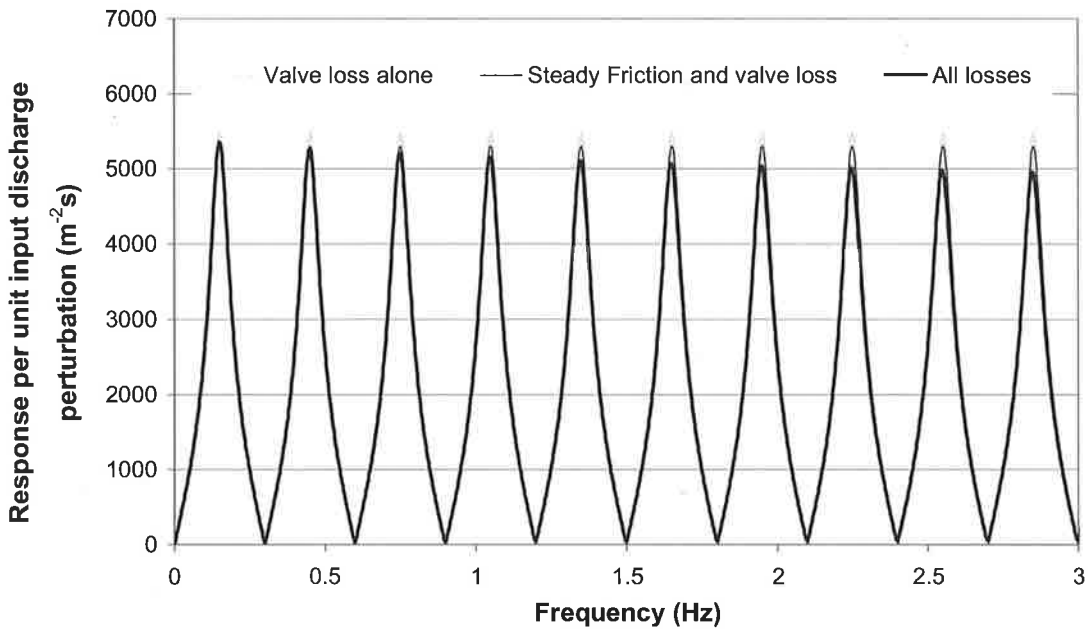


Figure 5-40 – Comparison of the FRF for different friction cases.

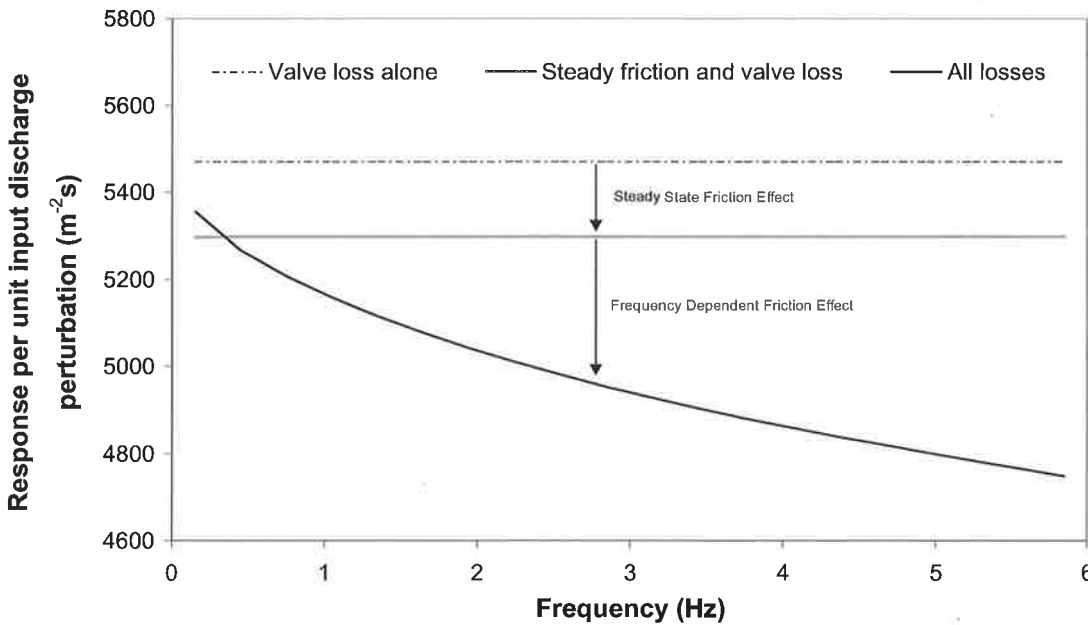


Figure 5-41 – Variation of peak magnitudes across different frequencies for all friction cases.

5.3 EXPERIMENTAL EXTRACTION OF THE SYSTEM RESPONSE FUNCTION

The previous sections have established guidelines for the extraction of the system response function. In this section, the extraction of the response function is investigated experimentally using transients generated by electronic side-discharge valves or manual in-line valves. The properties of these valves are described in Chapter 4. This section investigates the issues with the experimental extraction of the system response functions

5.3.1 Experimentally injected signals for system response extraction

The transients for the validation of the system response extraction procedure were generated by the discrete perturbation of the commercial solenoid valve (refer to Plate 4-4a) and the manual operation of the in-line valve (refer to Plate 4-2a). Chapter 4 describes the valves that are used for generating transients in this thesis. The valves are 1) a side-discharge solenoid valve and 2) an in-line manually-operated valve. The solenoid valve was used to perform sharp closures and pulse perturbations (closed – opened – closed) and the in-line valve was used for full closures. A typical closure profile from the solenoid valve is given in Figure 5-42.

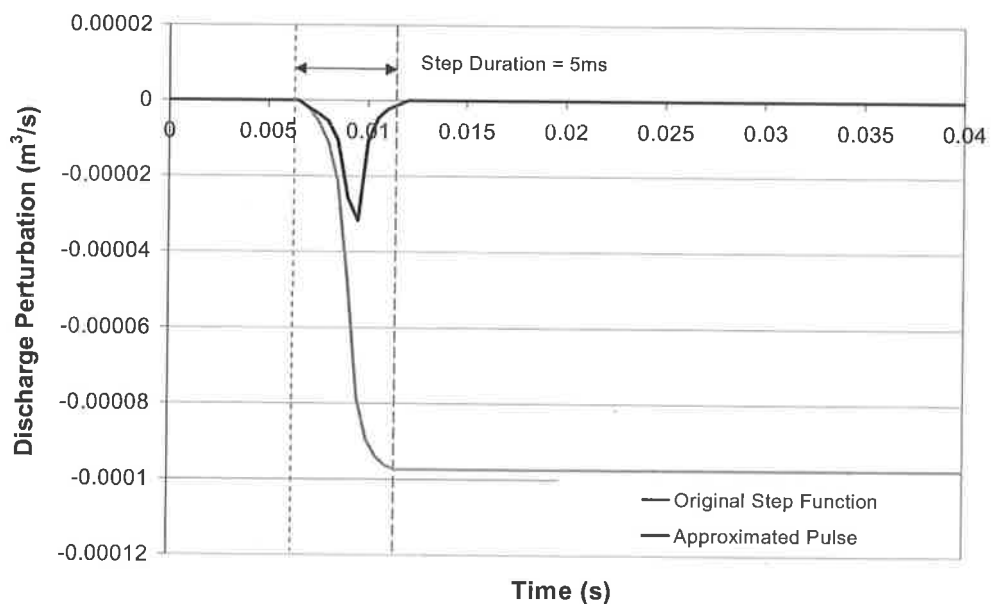


Figure 5-42 – Typical discharge perturbation for a solenoid step closure.

The solenoid valve was placed 0.16 m upstream from a closed in-line valve in the experimental system and the driving head from the upstream reservoir was set at 39.7 m. The discharge perturbation caused by the valve manoeuvre was determined from Eq. (5.11). The duration of the closure was 5 ms and the finite energy correction for this signal (refer to Section 5.2.3) is shown in the figure. An electronic control unit was added to allow pulse perturbations of the valve. This control unit consists of a switch that initiates the valve opening but the power to the solenoid valve is shut off prior to the full opening of the valve. Once the power is shut off, the spring in the solenoid unit returns the valve to the closed position. The control unit is set such that the valve is halfway through its manoeuvre when the power to the solenoid is shut off, creating a pulse that is of a similar duration as the full closure of the valve. The time trace of this pulse perturbation is shown in Figure 5-43; it has a duration of 5.5 ms.

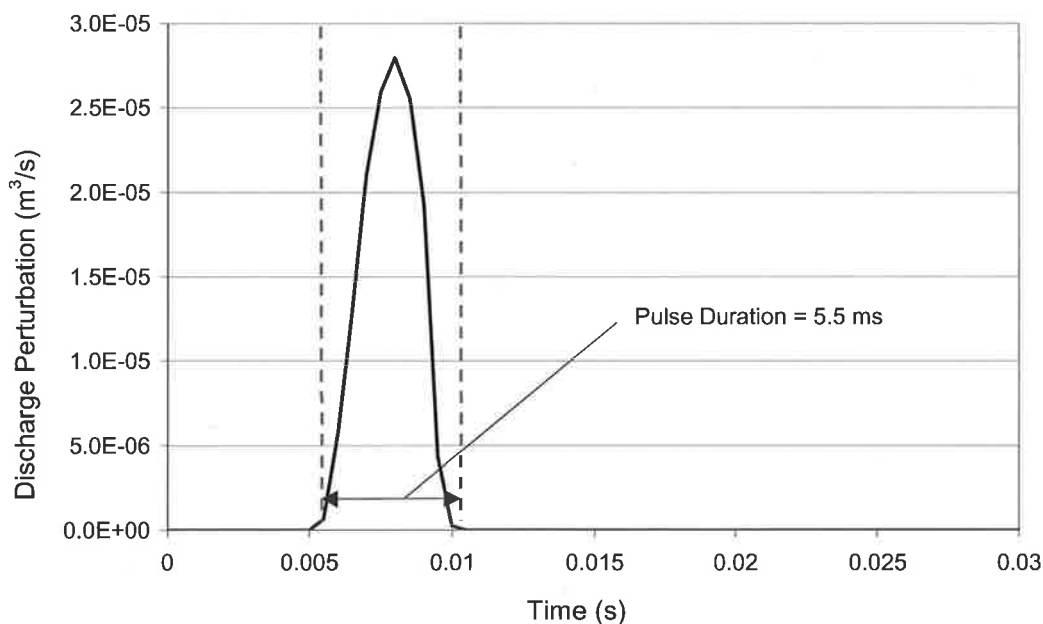


Figure 5-43 – Typical resultant discharge perturbation from a solenoid pulse.

The spectrum of the pulse perturbation input is given in Figure 5-44, which indicates that the spectrum falls below 5% of its maximum magnitude at 300 Hz. This frequency (300 Hz) is taken as the bandwidth of this signal (refer to Section 5.2.3).

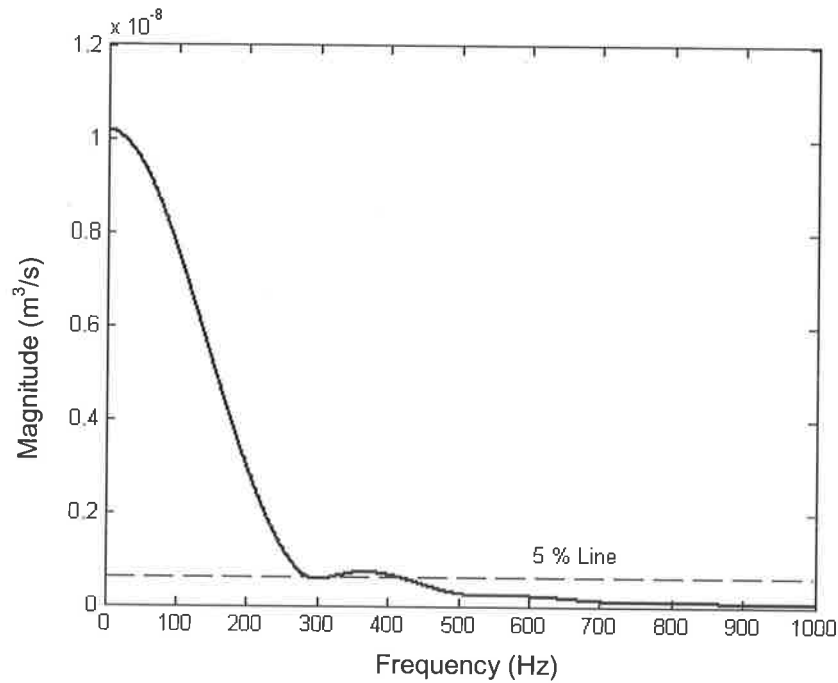


Figure 5-44 – Spectrum of input signal generated by the solenoid valve.

For the step signal the determination of the spectrum cannot be found using a Fourier transform; instead, the bandwidth is estimated from the spectrum of the corrected step signal (of the same duration as the original step function). The resultant spectrum is similar to the generated pulse from the solenoid valve. The step closure produced a bandwidth of 300 Hz.

A similar procedure was carried out for the manual closure of the in-line valve. For this case, the heads were set at 26.6 m at the upstream tank and 26.5 m at the downstream tank. The in-line valve adjacent to the downstream tank was initially fully open and was slammed shut manually. The transient trace in this situation is given in Figure 5-45 along with the corrected step function. The duration of the closure was 13.5 ms, which is longer than the closure generated from the electronic solenoid valve. The spectrum of the corrected step signal is given in Figure 5-46. That spectrum is approximated using the corrected step of the same duration. The slower operation of the in-line valve results in a bandwidth of 120 Hz, lower than the bandwidth of the solenoid valve (300Hz). Given the manual nature of the in-line valve closure (not repeatable), the input signal for each test is expected to vary from the results in Figure 5-45 and Figure 5-46.

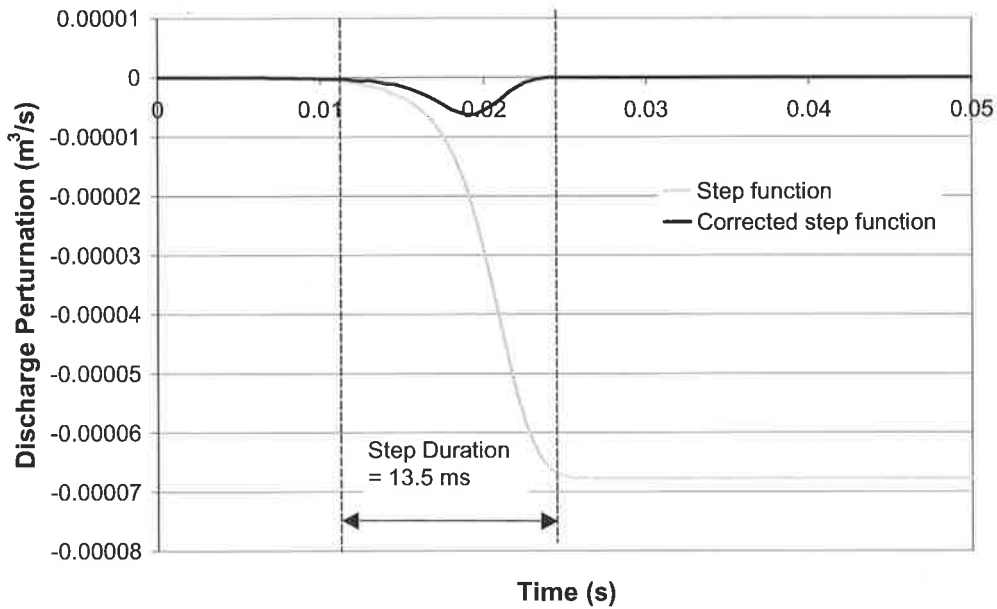


Figure 5-45 – Original and corrected step signal from the manual closure.

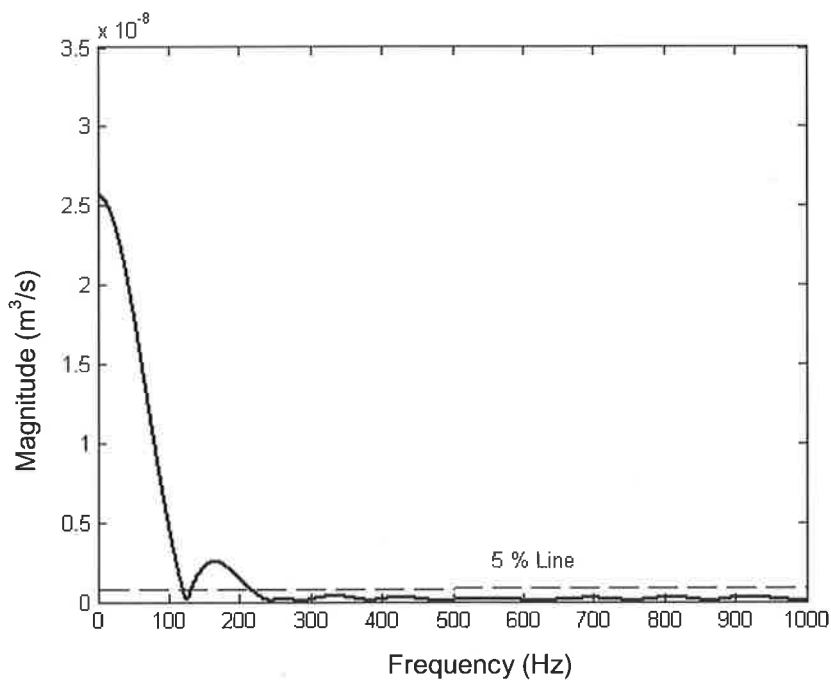


Figure 5-46 – Spectrum of corrected input signal generated by the in-line ball valve.

5.3.2 Experimental frequency response function extraction results

Using the signals described previously, the frequency response function was extracted from the leak-free laboratory pipeline. In these tests, the system was configured anti-

symmetrically, with the upstream tank set at a pressure of 39.7 m and the downstream in-line valve fully closed. The solenoid valve was placed at a position 0.16 m from the in-line valve. The calibrated $C_d A_v$ for the solenoid valve when fully opened is $1.8 \times 10^{-6} \text{ m}^2$ for this head condition. The configuration of the system is shown in Figure 5-47. The transient response from the pipeline when the solenoid valve is perturbed from a closed position is shown in Figure 5-48 and its full closure from an initially opened position is shown in Figure 5-49.

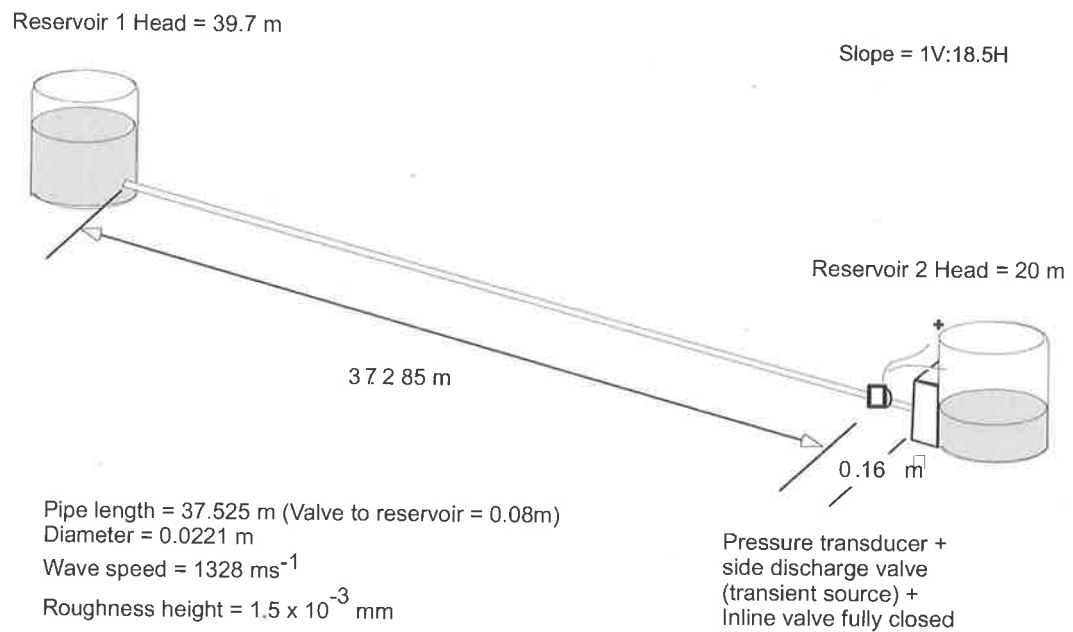
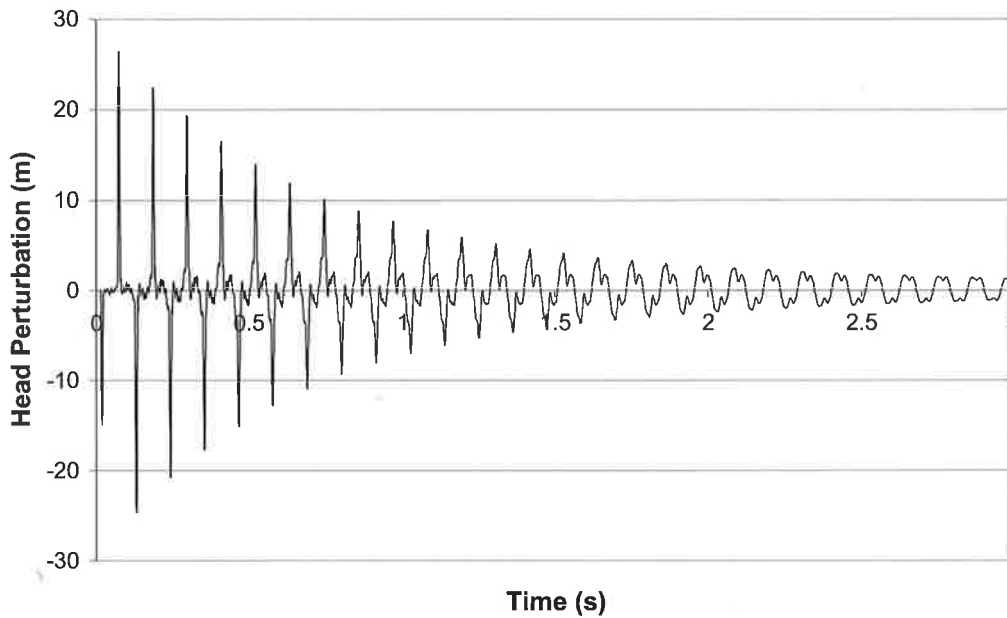


Figure 5-47 – Configuration of the laboratory test validating FRF extraction.

The forms of the transients are different although the pipeline system is the same in each test. A quantitative comparison between the two series is shown in Figure 5-50, with the head response from the injected pulse function plotted on the x -axis and the head response from the injected step function on the y -axis. Functions that are similar in form have data points that are arranged linearly on this graph. The slope of this linear trend should be close to one. The R^2 error of the fit is an indication of the difference between the two sets of data. Figure 5-50 shows that a poor R^2 value of 0.0021 results when a linear trend line is fitted to the data.

The system response functions were extracted for these two transient events. The discharge imposed by the valve manoeuvre was determined for both cases using Eq.

(5.11). These discharge perturbations were used as the inputs to the system and bear a similar form to Figure 5-42 and Figure 5-43 from the previous section. The outputs from the system are the measured transient signals.



**Figure 5-48 – Measured transient response for a pulse signal in the laboratory system
(Data file: C5-10.txt).**

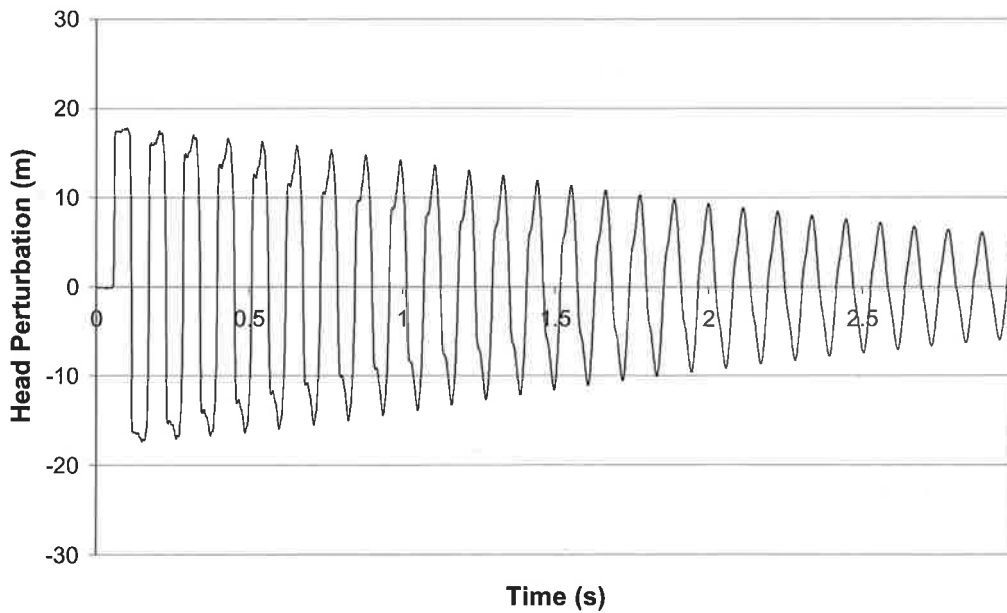


**Figure 5-49 – Measured transient response for a step signal in the laboratory system
(Data file: C5-10.txt).**

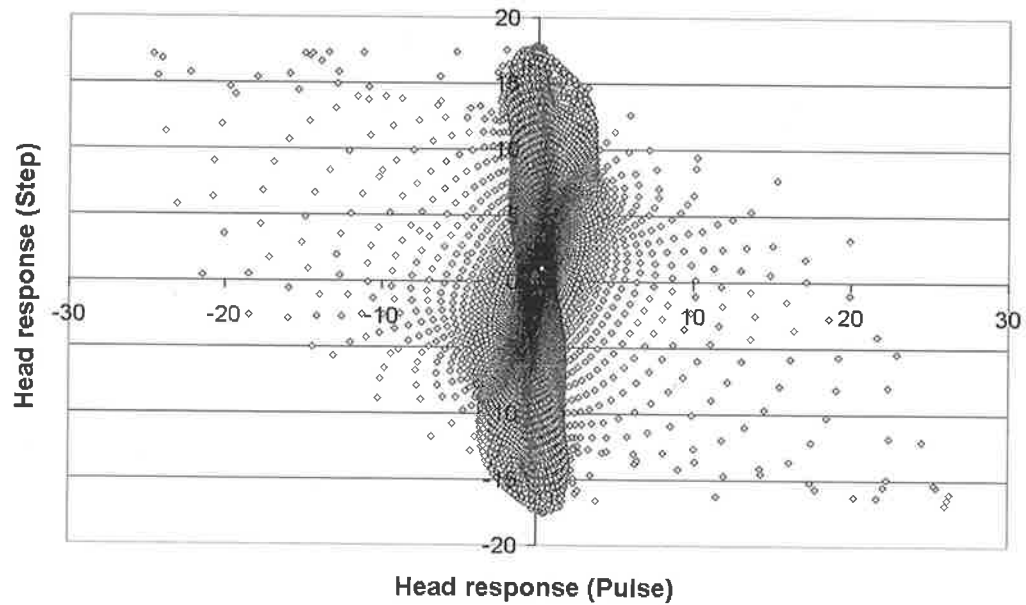


Figure 5-50 – Relationship between the time series of the two transient traces.

The substitution of this set of input and output signals into the linear time-invariant system equation gives the frequency response function of the system, F . The linear time invariant equation is repeated here as

$$F(\omega) = \frac{S_{XY}(\omega)}{S_{XX}(\omega)} \quad (5.22)$$

where S_{XY} = Fourier transform of the input (X) and output (Y) variables and S_{XX} = Fourier transform of the auto-correlation of the input.

The frequency response functions for the two cases are shown in Figure 5-51. The figure shows a good match between the two FRF's, correctly indicating that the underlying system in the two situations is identical. Such a conclusion cannot be reached by comparing the raw measured response from the system alone (refer to Figure 5-48 and Figure 5-49). To quantitatively compare the difference between the resultant FRF's, the magnitude of the FRF from the step input is plotted against the magnitude of the FRF from the pulse input in Figure 5-52.

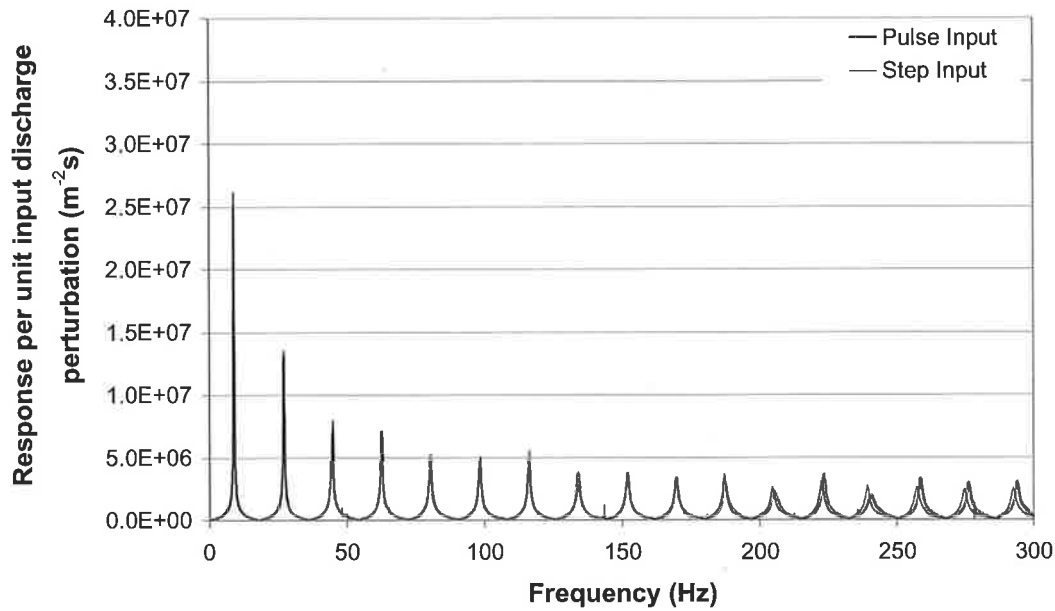


Figure 5-51 – FRF of the experimental pipeline generated by a step in comparison to that generated by a pulse.

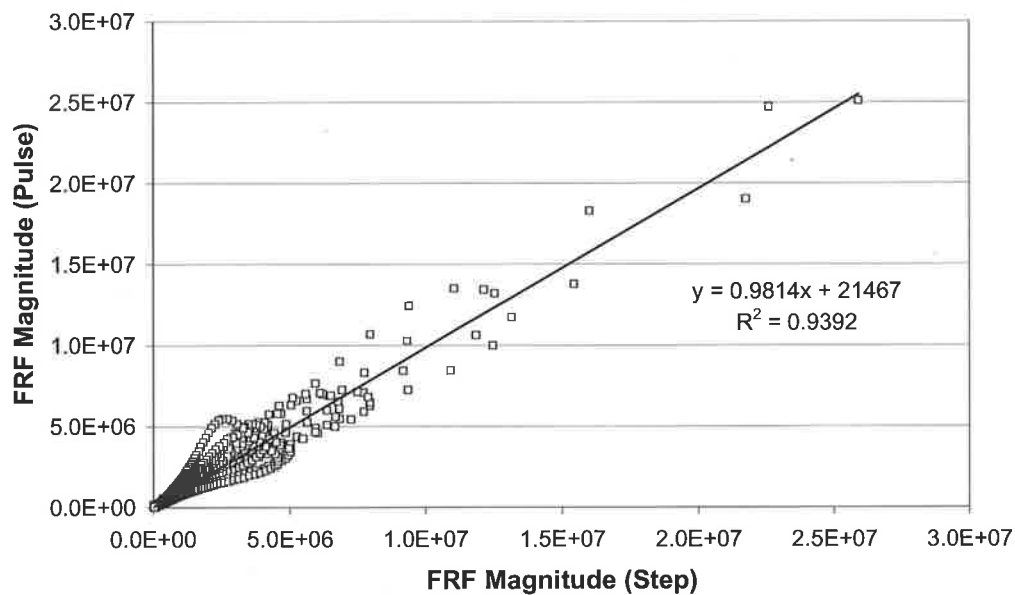


Figure 5-52 – Relationship between the FRF generated by a step and a pulse.

The results show that the relationship between the two FRF's are well approximated by a linear function, with a 0.939 correlation. The slope of the fitted linear function is 0.98, indicating that the two graphs are close to identical. The representation of the system behaviour in terms of the system response functions has correctly shown that the nature of

the system is the same between the two tests, although the raw transient traces are different. This result is an important validation of the advantage in using the system response functions.

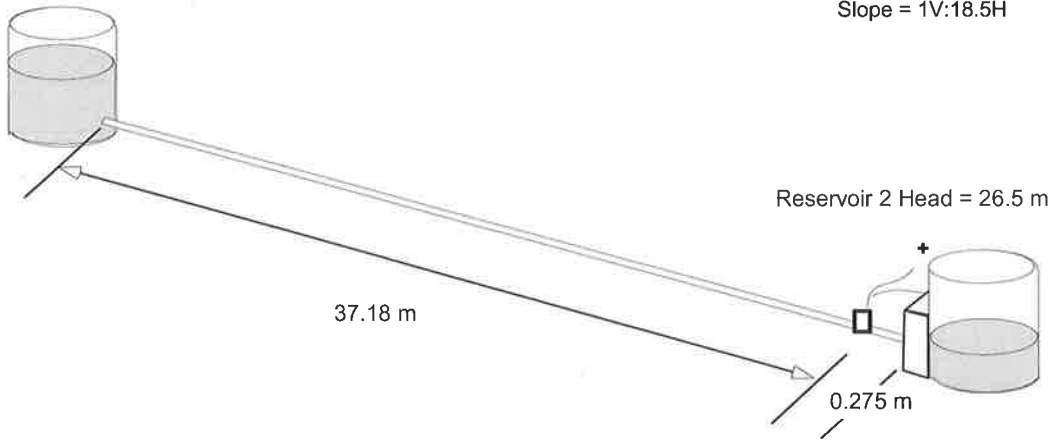
The extracted frequency response function in Figure 5-51 consists of a series of regularly spaced peaks. The positions of these peaks repeat at every odd multiple of 8.9 Hz and correspond well to the theoretical fundamental frequency of 8.76 Hz ($a/4L$). Shifts in the position of the resonant peaks are localised at the high frequencies (frequency > 200 Hz) and may be a result of minor differences in the signal bandwidth between the input signals. The clarity of the response functions was found to deteriorate at higher frequencies, though the effect appears minimal in Figure 5-51.

The effect of the signal bandwidth can be more clearly illustrated using the manual closure of the in-line valve as the input to the system. For this case, the in-line valve was initially fully opened and the upstream and downstream heads were set at 26.6 and 26.5 m, respectively. The initial flow through the valve was $6.01 \times 10^{-5} \text{ m}^3/\text{s}$, giving a Reynolds number of 3471, resulting in smooth-pipe turbulent flow. To generate the transient, the in-line valve was closed manually in 13.5 ms. The configuration of the system, the resultant transient trace and the frequency response function are shown in Figure 5-53, Figure 5-54 and Figure 5-55, respectively. The frequency response function for this situation consists of equally spaced peaks at odd multiples of 8.72 Hz, corresponding well with the theoretical value of 8.87 Hz. The narrow bandwidth of the input signal, however, resulted in a pronounced deterioration of the frequency response function (at high frequencies) when compared with the previous results from the solenoid valve.

The frequency response function was found to be accurate only within the bandwidth of the injected signal, which is 120 Hz for this case (refer to the results of Section 5.2.3). As the physical nature of the generation apparatus is different (for example, the source is in-line and located at the end of the pipeline), the frequency response function for this case is not identical to the results from the solenoid valve operation.

Reservoir 1 Head = 26.6 m

Slope = 1V:18.5H



Pipe length = 37.525 m (Valve to reservoir = 0.07m)

Diameter = 0.0221 m

Wave speed = 1328 ms^{-1}

Roughness height = $1.5 \times 10^{-3} \text{ mm}$

Pressure transducer

Inline valve initially fully open close for transient

Figure 5-53 – System configuration for in-line valve closure test.

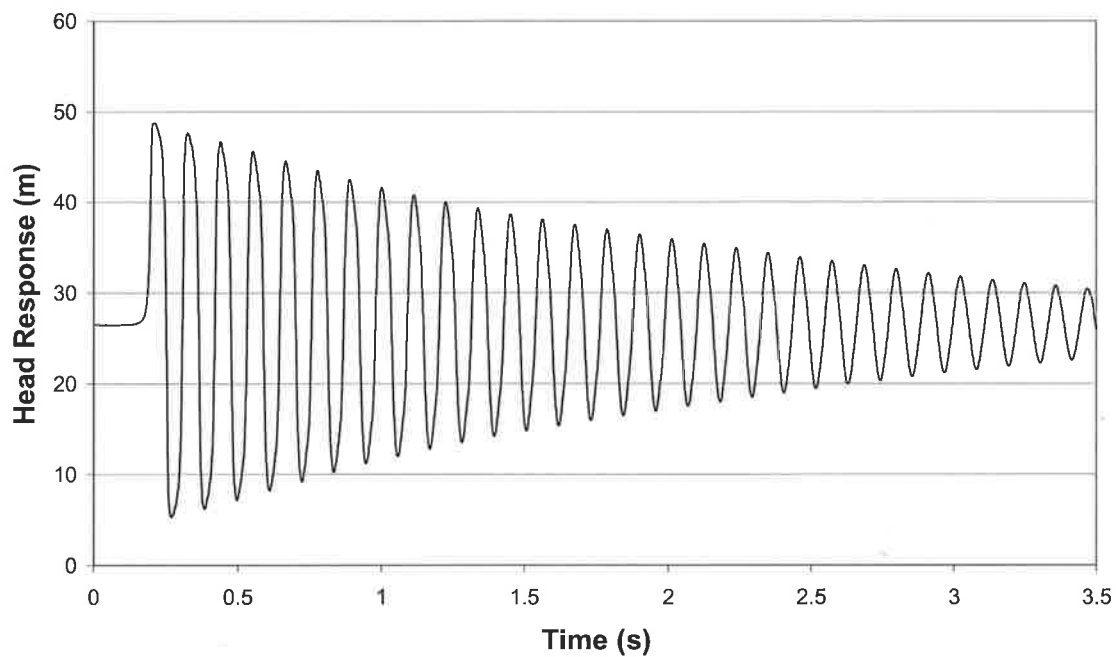


Figure 5-54– Head response from manual closure of the in-line valve

(Data file: C5-11.txt)

To determine the accuracy of the existing transient models, the transient trace from the solenoid valve closure (Figure 5-49) is compared to the predicted response from the method of characteristics (MOC) model in Figure 5-56.

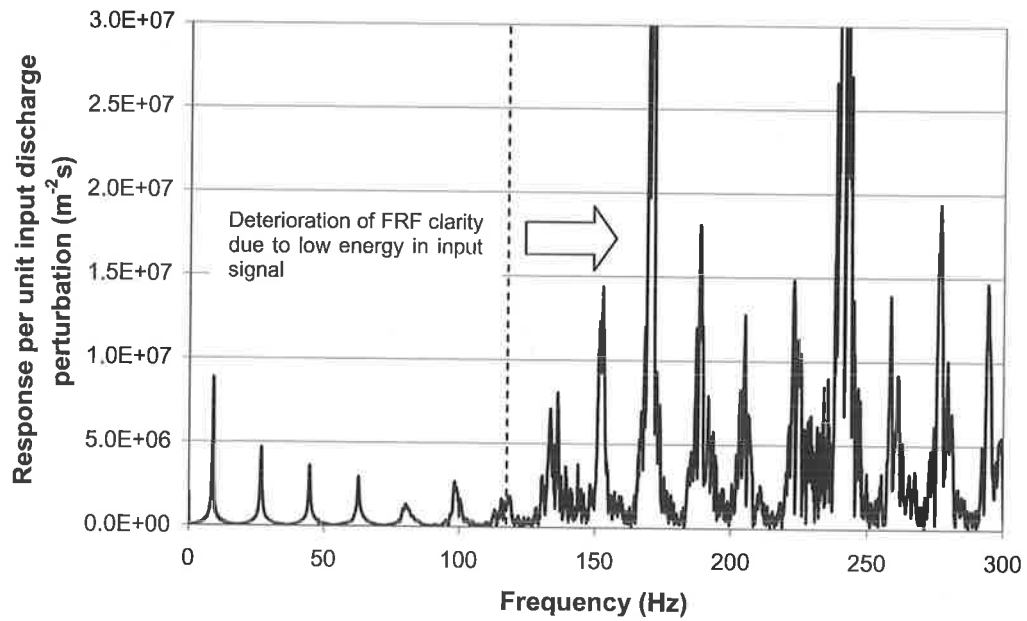


Figure 5-55 – FRF of the experimental pipeline generated by a step using hand closure of the in-line valve (Data file: C5-11.txt).

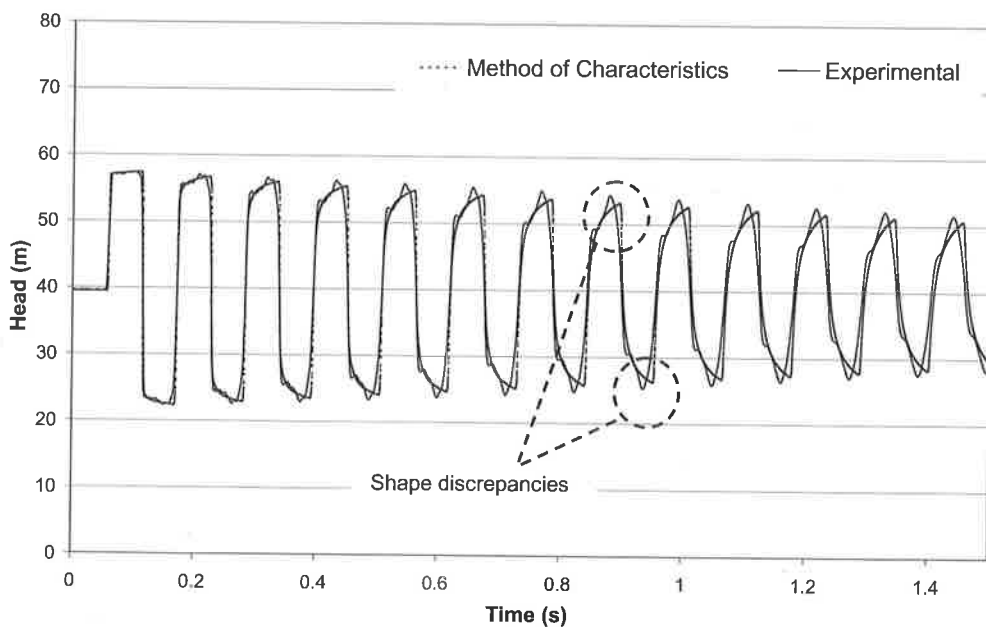


Figure 5-56 – Comparison between time series from experiment and MOC (Data file: C5-12.txt).

The MOC model is discretised into 200 reaches with a computation time step of 0.00014 s. The MOC result incorporates both steady and unsteady friction losses. The unsteady friction is predicted using the Vardy and Brown (1995) model for smooth-pipe turbulent flow. The numerical model provides a good match to the expected transient

response from the pipeline and the rate of attenuation in the transient amplitude was well predicted. A slight difference exists between the *shapes* of the two transient traces. The numerical model predicts that the step function gradually becomes more pointed as the transient progresses. This gradual erosion of the sharp “corners” in the original step function indicates damping of high frequencies in the signal as was predicted by Zielke (1968). The experimental result displays this behaviour, but the rate of this high-frequency damping was more significant and the signal is more sinusoidal in shape than that predicted by the model at the later stages of the transient. The predicted frequency response function is compared to the measured frequency response from the pipeline in Figure 5-57.

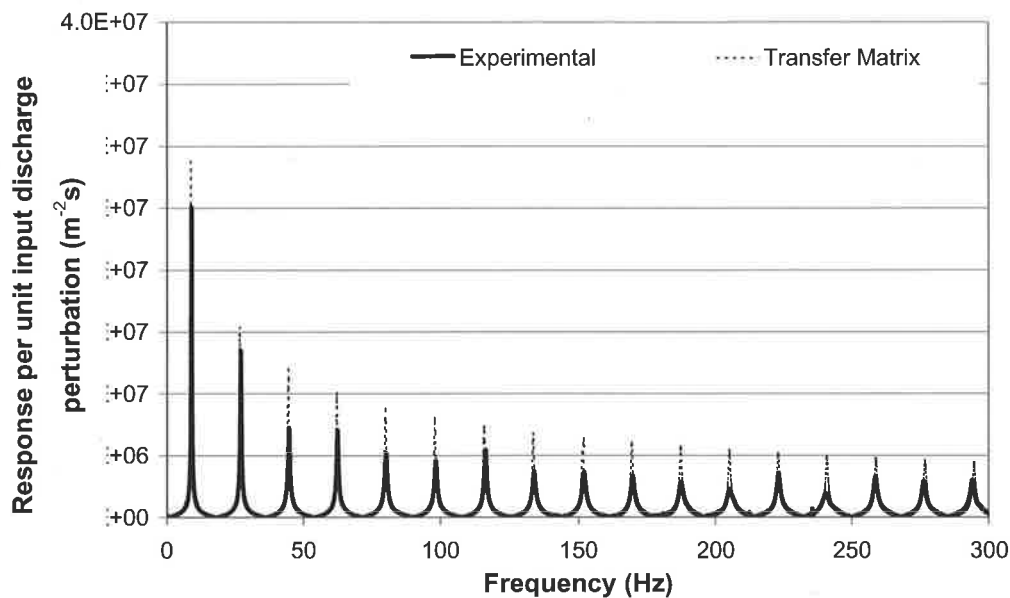


Figure 5-57 – Comparison between theoretical and experimental FRF (Data file: C5-12f.txt).

The comparison indicates that the model can accurately predict the resonance frequencies of the pipeline. Discrepancies can be seen, however, between the magnitudes of the resonant peaks in the numerical and experimental results. Given the close match between the predicted and the measured results in the time domain, this observed discrepancy in the frequency domain must be related to the small shape differences in the transients presented in Figure 5-56. These differences may be due to a number of possible small effects: for example, the presence of varying impedance elements (brass blocks) along the pipe, the presence of possible air pockets within the fluid and small physical vibrations of the pipeline during the transient event.

5.4 CASE STUDY: EXTRACTION OF THE SYSTEM RESPONSE FUNCTION USING PSEUDO-RANDOM BINARY SIGNAL

The previous sections experimentally validated the use of discrete signals for the extraction of the system response functions from the pipeline; the use of continuous signals for this task has been ignored up to this point. While one of the simplest continuous signals is a pure sinusoidal signal, its use is time consuming and can only be applied in situations where the underlying system conditions do not fluctuate during testing. In addition, the generation of such signals requires a driving apparatus that provides a smooth movement, often involving a rotary motor or an existing turbine (Brekke, 1984).

A more attractive type of continuous signal is the pseudo-random binary signal (PRBS), which fluctuates between two set values and conforms well to the sharp on/off nature of inexpensive solenoid valves. The experimental generation of PRBS and its use in the extraction of the system response function is considered in this section.

Pseudo-random binary signals (PRBS), also known as maximum length sequence signals, are used in electrical systems for the determination of system response functions (Niederdränk 1997, Tan and Godfrey, 2001). These signals consist of a series of randomly spaced and equal magnitude pulses. The generation of such a sequence requires a decision to be made at each time step to determine whether a pulse is to be generated. The random sequence of pulses is set to repeat for a PRBS. This periodicity provides the signal with a higher degree of noise tolerance and removes the statistical variability associated with signals of a pure random nature (Liou 1998). Important attributes of a continuous signal of this type is that it allows the power to be spread over a longer time frame and the amplitude of each individual pulse in the signal can be small while maintaining the same signal power (Niederdränk 1997, Liou 1998). The range (travel distance) of a discrete (not continuous) transient signal is governed by its size—the larger the transient event, the greater the power of the signal and hence the further it would travel. To increase the travel distance of a conventional step/pulse perturbation of a valve, the magnitude of the valve movement must be increased, increasing the risk of damaging the valve and the pipeline.

In contrast, the use of a continuous signal such as the PRBS allows the power of the signal to be increased by extending the *duration* of the signal (Niederdränk 1997).

While there have been experimental applications of PRBS for system identification of air ducts (Pande 1982, Dallabetta 1996), the study into the use of PRBS for extracting the system response in hydraulic pipelines has been confined to numerical studies (Liou, 1998). The generation of such a signal in a pipeline and the subsequent extraction of the system response function need to be conducted experimentally. This section employs the procedures developed in the earlier parts of this chapter to validate the extraction of the system response function using such signals.

5.4.1 Experimental apparatus for the generation of PRBS

The extraction of the system response function using the linear time invariant equation,

$$F(\omega) = \frac{S_{xy}(\omega)}{S_{xx}(\omega)} \quad (5.23)$$

requires the creation of an input signal (x) into the system and the subsequent measurement of the output (y). For a transient signal generated by a valve, the input signal can be determined from direct measurement of valve movement. A specially designed solenoid valve was constructed to provide means of generating a PRBS while measuring valve movement. The schematic of this valve is shown in Figure 5-58. The device consists of a brass block with a small diameter hole drilled through the long axis of the block. This hole forms the conduit for water to escape the pipeline. A rod connected to a solenoid controls the hole opening. At rest (solenoid deactivated), the rod is pushed downwards by an internal spring in the solenoid, blocking the conduit. When the solenoid is activated, the rod pulls upwards and clears the flow passage allowing water to flow through the valve. The calibrated lumped valve coefficient ($C_d A_v$) is $4.5 \times 10^{-7} \text{ m}^2$ when fully opened under a head of 41.1 m.

Movement of the rod is measured by a linear voltage displacement transducer and is converted into an equivalent dimensionless valve opening coefficient, τ . The variation in

the dimensionless valve opening throughout the test is used to represent the input to the pipeline. Care must be taken in the use of τ as the input to the system as Section 5.2.1 shows that a large valve perturbation can lead to nonlinear errors. For this investigation, therefore, the perturbation of the valve was kept at the smallest magnitude that could be generated by the solenoid in an attempt to minimise possible nonlinear distortions.

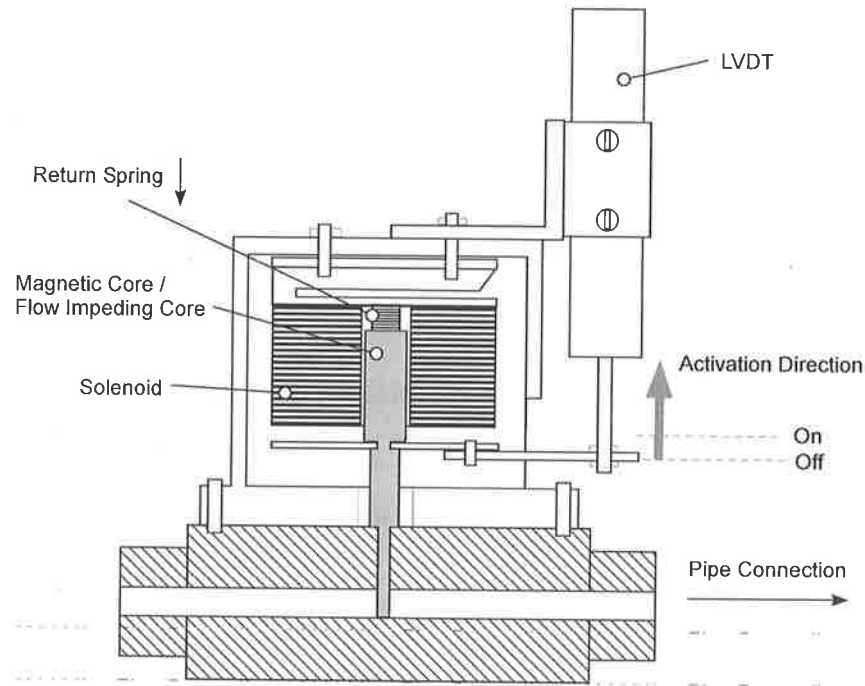


Figure 5-58 – PRBS Signal Generator designed and constructed at the University of Adelaide.

To generate the PRBS signal, the valve was electronically controlled to produce a similar (close to identical) pulse at random intervals. The shape and the duration of one of these pulses are shown in Figure 5-59. Each generated pulse had a duration of 6 ms.

The PRBS consisted of a sequence of these pulses. Their random spacing was regulated by an electric circuit consisting of a series of shift registers (Dallabetta, 1996). The circuit was set such that the sequence repeated after a time of 10.24 seconds (184 fundamental periods), which corresponded to the time required for a single pulse to be fully attenuated in the system (Dallabetta, 1996). The signal was allowed to repeat for a number of periods prior to recording to reduce random fluctuations in the signal spectrum. The minimum time lag between two adjacent pulses is set at 10 ms.

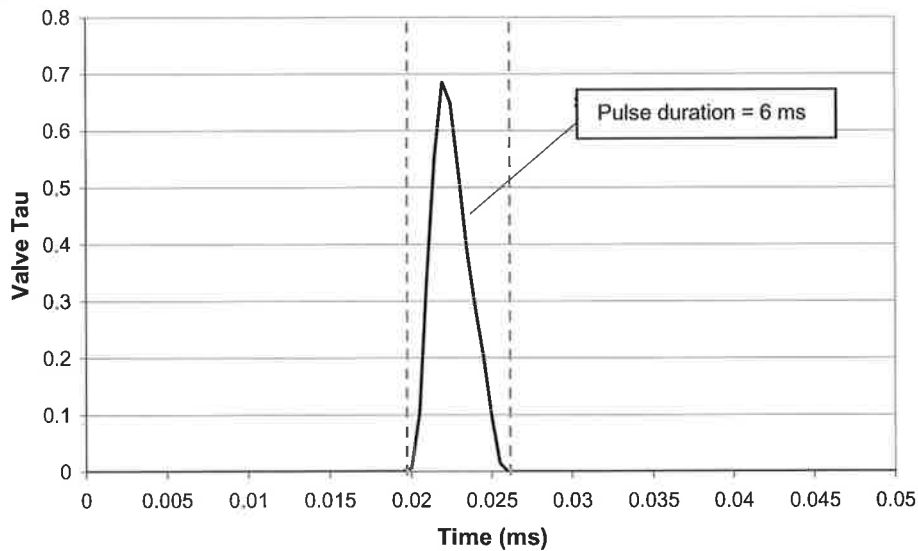


Figure 5-59 – Typical pulses generated by the continuous signal generator.

The PRBS generator was connected to the laboratory system at a position 0.275 m upstream of a closed in-line valve. The upstream reservoir had a driving head of 41.1 m. A schematic of the test is shown in Figure 5-60.

5.4.2 Experimental extraction of the system response function using PRBS

For the experimental investigation, the system response function was determined from the measured head response at the PRBS valve (output) and the measured valve aperture, τ (input). The magnitude of the head response from a single pulse perturbation of the valve in this situation is 2 m. Compared to the size of the transient pulse generated by the commercial solenoid valve in Section 5.3.2 under a similar system configuration, the magnitude of this transient event is 12 m smaller. The PRBS input and output are presented in Figure 5-61.

From Figure 5-61, the measured valve movement and the head response from the system appear to have little visible structure and the transient signal generated by this valve is similar to background noise. Small variations due to the mechanics of the valve were observed in the magnitude of the valve movement. Given that the input sequence is measured and taken into account in Eq. (5.23), this variability is inconsequential in the

accuracy of the resultant frequency response function. The underlying structures of the input and output signals are observed through the correlation functions of the two series shown in Figure 5-62.

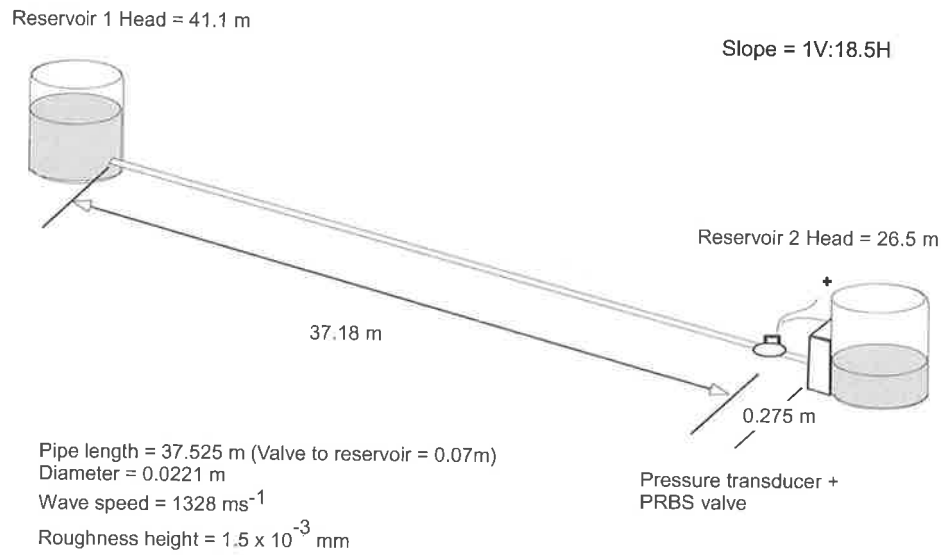


Figure 5-60 – Laboratory configuration for the PRBS test.

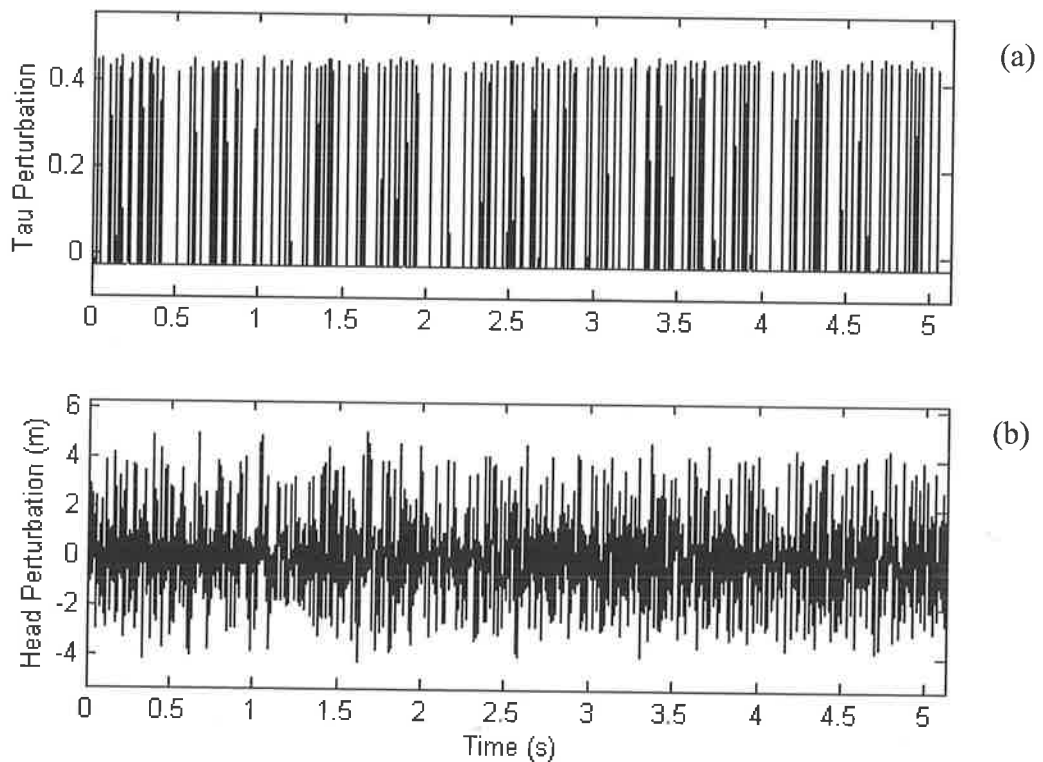


Figure 5-61 – Input (a) and output (b) sequences from the PRBS sequence (Data file: C5-13.txt).

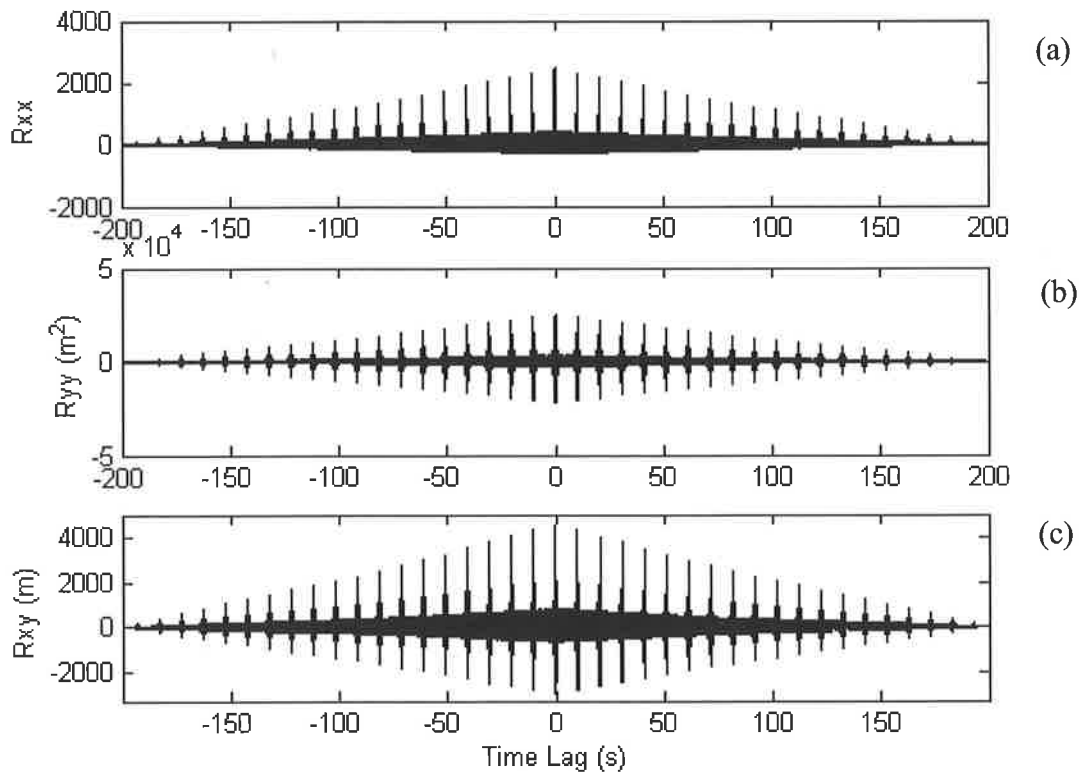


Figure 5-62 – Correlation functions from the injection of the PRBS, (a) auto-correlation of the input, (b) auto-correlation of the output and (c) cross-correlation between the two.

The correlation functions indicate a strong periodic structure in both the input and the output data. These signals have a period of 10.24 seconds, which is the designed period of the PRBS sequence. The spectrums of the input and output series for a single period of the PRBS are given in Figure 5-63. These spectrums have well-defined structures, despite the appearance of the original signals. Frequency spikes, caused by the clock pulse interval of 10 ms and signal period of 10.24 seconds were observed at 100 and 200 Hz (Tan and Godfrey, 2001). These spikes are caused by the low amplitude of the input spectrum at these frequencies.

The frequency response function of the experimental system, calculated using Eq. (5.23), is shown in Figure 5-64 along with the theoretical response function calculated using the transfer matrix method (Chaudhry, 1987). The results are plotted for the frequency range where the input signal has the highest power and is between 0 and 100 Hz. The response

function was smoothed using a centred average filter 0.63 Hz wide to remove spurious fluctuations created by the random nature of the signal (Pande 1982, Dallabetta 1996). The width of this filter was set for minimal reduction in the overall magnitudes of the resonant peaks. A good match is found between the theoretical and experimentally extracted frequency response functions. The positions of the peaks in the frequency response function are clearly defined with the peaks spaced at odd multiples of 8.76 Hz, corresponding well with the theoretical fundamental frequency of the system given by $a / 4L = 8.87$ Hz, where a is the wave speed and L is the pipeline length.

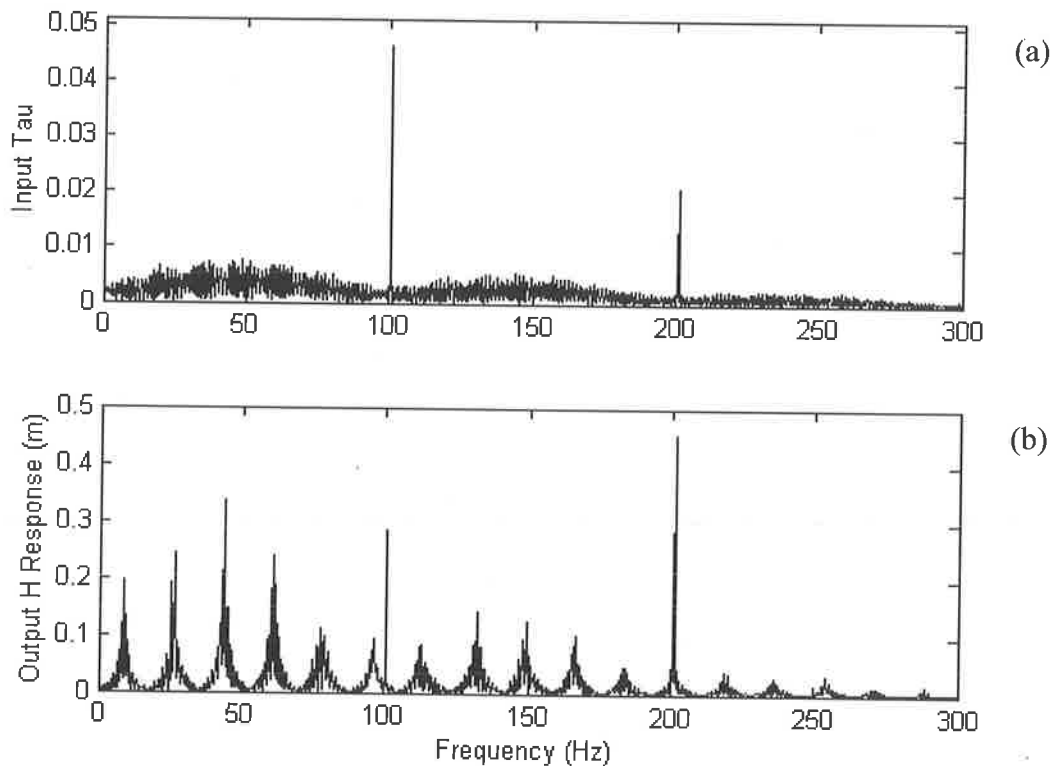


Figure 5-63 – Input (a) and output (b) spectrums from the injected PRBS.

The accuracy of the fit between theoretical and experimental results using the PRBS is better than the accuracy achieved when a discrete perturbation of the commercial solenoid valve is used (refer to Figure 5-57). This improved accuracy is a result of the PRBS valve, which acts as a perturbing leak orifice in the system. The presence of leaks in the experimental pipeline forms one of the dominant sources of energy loss in the system and can lead to improved matches with theoretical predictions. An example is shown later in Section 6.7.3.

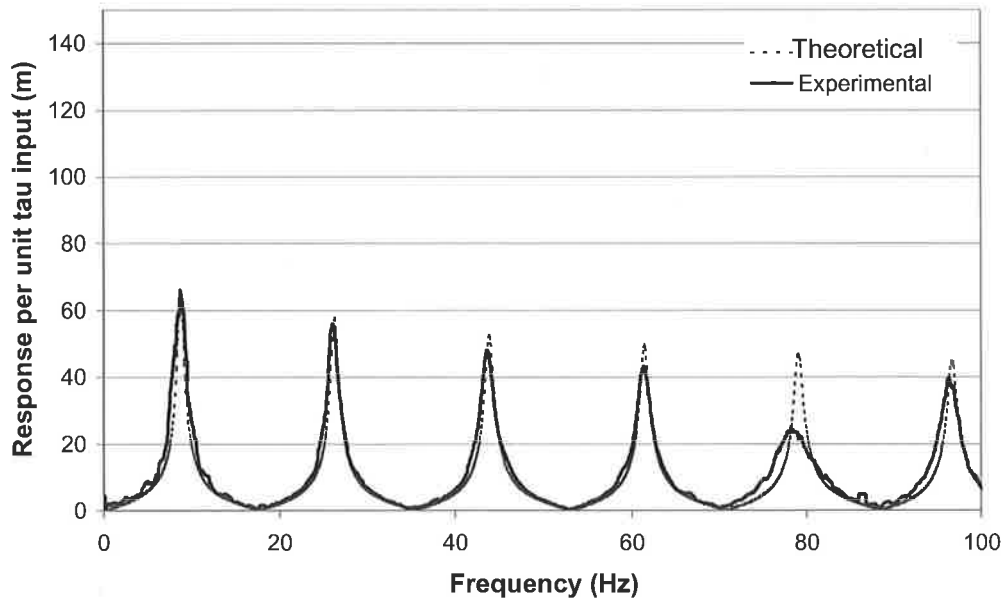


Figure 5-64 – Comparison of PRBS results with theoretical results (Data file: C5-14.txt).

A small deviation exists between the experimentally extracted response function and the theoretical prediction. It is particularly significant for the 5th harmonic peak of the response function. This deviation was also observed when the in-line valve was used to generate the transient and can be related to properties of the pipeline at this boundary (refer to the response function extracted using the in-line valve closure at this boundary in Figure 5-55). Investigations were carried out in the laboratory system to isolate the cause of this problem, which involved fully dismantling the system and inspecting each component and connection in the pipeline. All were found to be in good condition. Also, the bracing support for the system was increased (0.3 m interval) with no improvement to this pipeline behaviour. However, techniques developed later in this thesis do not require a good match between experimental and numerical results; this discrepancy has no effect on the aim of this study. In fact, the inability of the existing numerical models to predict experimental results, even from such a controlled pipeline, illustrates the extent of the problem when transient techniques are applied in a field situation. The need for leak detection methods that do not rely on this match is, therefore, necessary.

This section has experimentally validated the use of PRBS signals for the extraction of frequency response information from a pipeline. The small magnitude of the introduced

signal (12 m smaller than the discrete pulse cases used in section 5.3.2) and its continuous nature provide an attractive means of determining the state of the system on a real-time basis. The nature of PRBS also conforms well with the on/off nature of common solenoid devices. However, for the remainder of this thesis, the system response functions are extracted using the discrete single perturbation of the commercial solenoid valve. This decision was based upon two practical issues with the operation of the customised PRBS valve:

- The bandwidth of the PRBS is 100 Hz and is substantially lower than that produced using the commercial valve (300 Hz). The bandwidth of the signal is governed by the width of individual pulses in the PRBS.
- The random sequence must be allowed to continue for a number of periods before measurement is taken to reduce random distortions in the extracted response function. This requirement means that the valve must operate over a substantially longer period of time than in the generation of a discrete signal, resulting in more water loss from the laboratory system during each test. The reservoir would subsequently need to be refilled at shorter intervals if the valve is used on a regular basis.

5.5 CONCLUSIONS

This chapter presents numerical and experimental results that validate the use of the systems identification theory in hydraulic pipelines. The results indicate that under small valve perturbations, or where a discharge perturbation is used as the input, the pipeline behaves linearly. Also, given that the physical properties of the pipeline remains unchanged, the extracted system response is identical within the bandwidth of any two injected transients. This result illustrates the advantage of using the system response functions for the determination of the system integrity. Certain aspects in the system response extraction process—including (1) the optimum positioning of both the transient source and the measurement station, (2) the selection of the input signal and (3) the correction procedure that can be applied for infinite energy input signals—were investigated.

The extraction procedure is a marked improvement over the use of sinusoidal signals as it can be performed in the time it takes for a single transient event to decay in the pipeline, whereas a sinusoidal signal requires multiple runs to produce a response function of the same resolution. This procedure can be applied using any transient signal and no special apparatus needs to be built especially for this purpose. A variety of signals were used to determine the system response function, including discrete step/pulse signals and a pseudo-random binary signal. A valid representation of the response function was derived for all cases. This study found that the frequency content of an injected transient signal (i.e. the bandwidth) provides the best measure of its suitability for testing the behaviour of a system. The information content of the transient response is related to the bandwidth of the injected signal, with higher bandwidth signals giving higher information content.

The main conclusions from this chapter may be summarised in the following points:

1. System response functions refine transient data such that comparison of the system behaviour from one day to the next can be taken regardless of the type of signal generated. This approach allows the state of the system to be uniquely quantified in both time and frequency domains.

-
2. Given that the amount of information contained in the transient trace is related to the bandwidth of the injected signal, the transient event used to probe the behaviour of the pipeline must be wide-band (i.e. contains a high number of frequencies). The injected signal itself must contain rapid and sharp changes in time (translating to high-frequency content in the signal). The use of slow transient signals, such as those generated by pump trips and slow manual closures of in-line valves should not be used for this purpose. This result has implications on the design of filters for transient data: All frequency content not contained in the input signal (hence not a direct response to the input) can be safely removed.
 3. Signals of a continuous nature should be used for the detection of problems in a field pipeline. The use of continuous signals (e.g. PRBS) distributes the power of the signal over a longer period of time and allows the use of smaller magnitude transients to achieve the same result as from larger discrete signals. An improved design of the PRBS generating valve holds good potential for future application of such signals in leak detection.

The following chapter investigates the use of these response functions to determine the presence and the location of leaks in a pipeline.

CHAPTER 6

LEAK DETECTION USING THE FREQUENCY RESPONSE FUNCTION

6.1 INTRODUCTION

The previous section illustrated the procedure to extract the system response function—in the form of the frequency response function (FRF)—from a pipeline. The response function provides information on the physical configuration and thus the underlying behaviour of a pipeline. The system response functions extracted from different injected signals are identical within the signal bandwidth for the same system and can be used as a clear indication of whether the state of the system has changed from one day to the next. The previous chapter indicates that the linear transfer matrix model will produce identical results to the non-linear method of characteristics model given a careful selection of the input signal. This result was tested on the range of flow conditions considered in this thesis (refer to Figure 5-22, Figure 5-26, Figure 5-27 and Figure 5-33). This chapter continues the study into the use of system response function for detecting leaks in a pipeline. The effect of discrete blockages is also investigated in this chapter.

A number of publications have been written on how leaks modify the frequency spectrum of transients. The effect of a leak on the Fourier spectrum of a measured transient trace is identical to that on the frequency response function as both contain the spectrum of the output signal. Jönsson and Larson (1992) and Covas and Ramos (1999) were amongst the first to suggest using the frequency domain for detection of leaks in pipes. These papers proposed that a leak in a pipeline results in the presence of additional “leak-induced frequencies”, similar to the process that leads to the formation of leak-reflected signals in

the time domain. The position of these leak-induced frequencies on the frequency axis was said to be related to the location of the leak in the pipeline. Results were presented in Jönsson and Larson (1992) to show that a leaking pipeline did appear to have a particular frequency component that is more pronounced than in a non-leaking case. On closer inspection, however, this frequency corresponds to the second system harmonic and is also present in the non-leaking case. The presented difference between leak-free and leaking spectrums can be explained by the use of different signals between the two cases (i.e. the input signal for the leaking case had a wider bandwidth, hence more energy was present in the higher harmonics). The increase in the magnitude of this particular peak, therefore, is not indicative of a new leak-induced frequency as proposed in the paper and its position in the frequency domain does not provide a clue as to the position of the leak.

This idea of the leak-induced frequency was perpetuated in Mpesha *et al.* (2001, 2002) in which they presented a frequency-domain leak detection method based on the existence of additional frequencies. Mpesha *et al.* (2001, 2002) presented numerical results that support the idea and included a leak detection procedure that allows the determination of leak location using their results. Their results, however, appear to contain errors and their form of the frequency response function does not correspond with typical results in Wylie and Streeter (1993) and Chaudhry (1987). A set of results from the publications is presented in Figure 6-1 and Figure 6-2 together with the predicted response from the transfer matrix and method of characteristics models. Note that h is the magnitude of the head perturbation at the valve for a particular frequency and H_0 was defined in Mpesha *et al.* (2001, 2002) as the steady state head at the upstream reservoir. In both the leaking and not leaking cases, significant discrepancies were observed between Mpesha *et al.* (2001, 2002) and the predicted output from the transfer matrix and method of characteristics models. The models predicts the frequency response function with peaks at odd multiples of the fundamental frequency, ω_{th} (Chaudhry 1987, Wylie and Streeter 1993). The results in Mpesha *et al.* (2001, 2002) have peaks at the 1, 7, 13th harmonics only. In the leaking case, an additional frequency spike is present in the Mpesha *et al.* (2001, 2002) results and the position and size of this spike were used as the basis for their leak detection procedure. This spike is located at the fifth harmonic of the system and the reason as to why it was missing in the no-leak case and yet reappears for the leaking case can only be explained by errors in the numerical model used to generate the data.

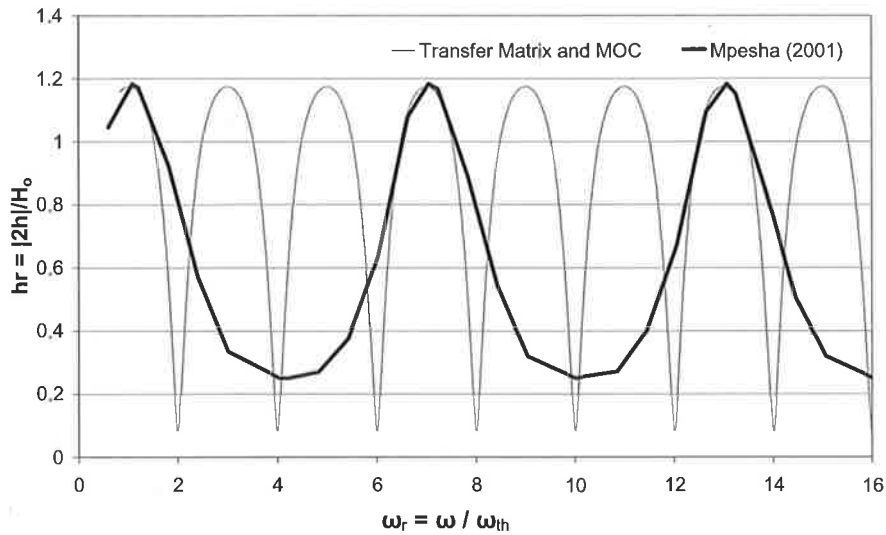


Figure 6-1 – Comparison of the results from Mpesha *et al.* (2001, 2002) with the transfer matrix and MOC models for a leak-free system.

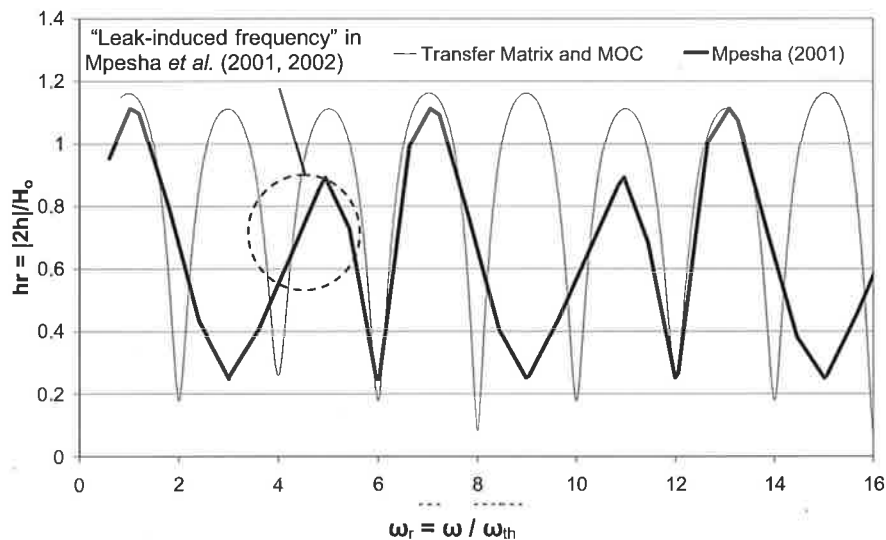


Figure 6-2 – Comparison of the results from Mpesha *et al.* (2001, 2002) with the transfer matrix and MOC models for a leaking system.

These findings with the Mpesha *et al.* (2001, 2002) papers are published as a discussion in Lee *et al.* (2003c). Ferrante and Brunone (2001) presented further results that disprove the existence of leak-induced frequencies. Ferrante and Brunone (2001) increased the size of a leak from small flows up to 80% of the pipe base flow. While the increase of the leak size results in a change in the fundamental frequency of the pipeline, no additional harmonic peaks appeared. The presence of the “leak-induced frequencies” in previous publications has been the result of confusion with the existing harmonics of the pipeline and underlying numerical error.

6.2 EFFECT OF LEAKS ON THE FRF OF PIPELINES

As shown in Section 5.3, the FRF of an intact pipeline consists of equally spaced peaks that attenuate in a smooth fashion with frequency (refer to Figure 5-57). This frequency-dependent attenuation is caused by unsteady friction (Vítkovský *et al.*, 2003b). This section illustrates the effect of a leak on the FRF. To highlight the effect of a leak, the following analysis was performed on the numerical pipeline (in the transfer matrix model) without the effect of pipe friction. The transient was generated by perturbing a side-discharge valve located upstream of the in-line valve in the simulation system. A leak of a $C_d A_L = 1.4 \times 10^{-4} \text{ m}^2$ was placed 1400 m from the upstream boundary. The configuration of the system is shown in Figure 6-3. The extracted frequency response function is shown in Figure 6-4. The response function for the system when no leak exists is shown in the figure for comparison.

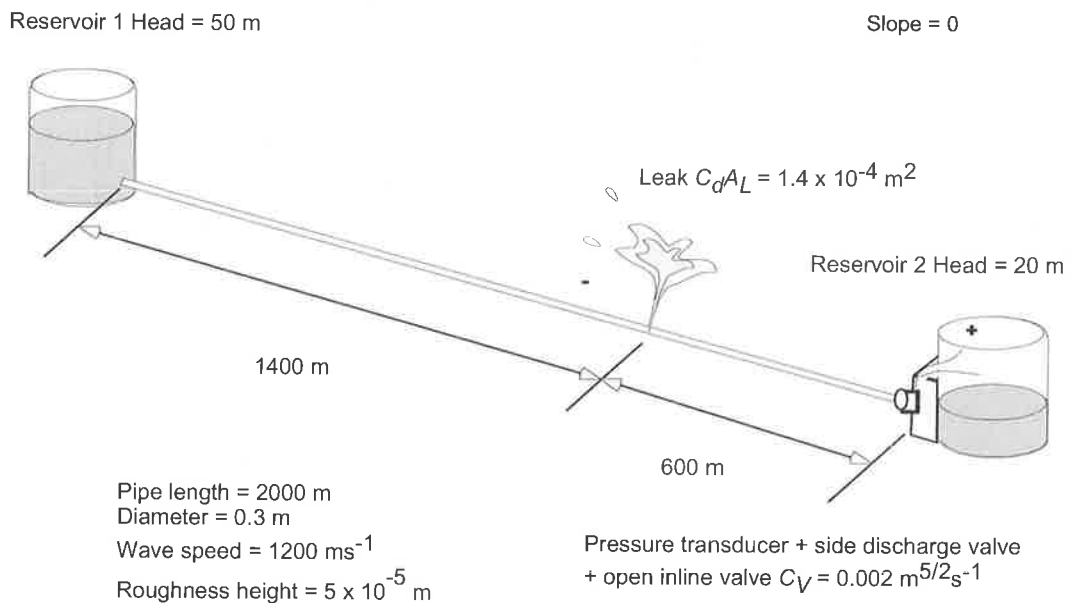


Figure 6-3 – Configuration of the system for test shown in Figure 6-4.

While the FRF of the intact system consists of a series of equally spaced and equal magnitude peaks (for a frictionless pipe), the presence of the leak results in a pattern being imposed onto the peaks of the FRF. These peaks are in the same position as the non-leaking case, but the magnitudes of the resonance peaks are no longer equal; they fluctuate

in a periodic pattern. The FRF of the leaking pipe does not contain additional frequency peaks as predicted by Jönsson and Larson (1992), Covas and Ramos (1999) and Mpesha *et al.* (2001, 2002). In fact, the effect of the leak appears to be localised at the resonant peaks of the pipeline, a behaviour that was predicted in Wang *et al.* (2002). Investigations in air ducts by Smith and Wolfe (2001) presented similar findings where the presence of a hole in the duct was found to accentuate certain harmonics while depressing others. De Salis *et al.* (2002) presented a method of leak detection in depressurised open-ended air ducts based on the shifting of the resonant peaks in the FRF. This shifting was a result of a change in pipe impedance across the leak in this type of system. As shown in Figure 6-4, such shifting does not occur in the pressurised liquid pipelines that are considered in this dissertation.

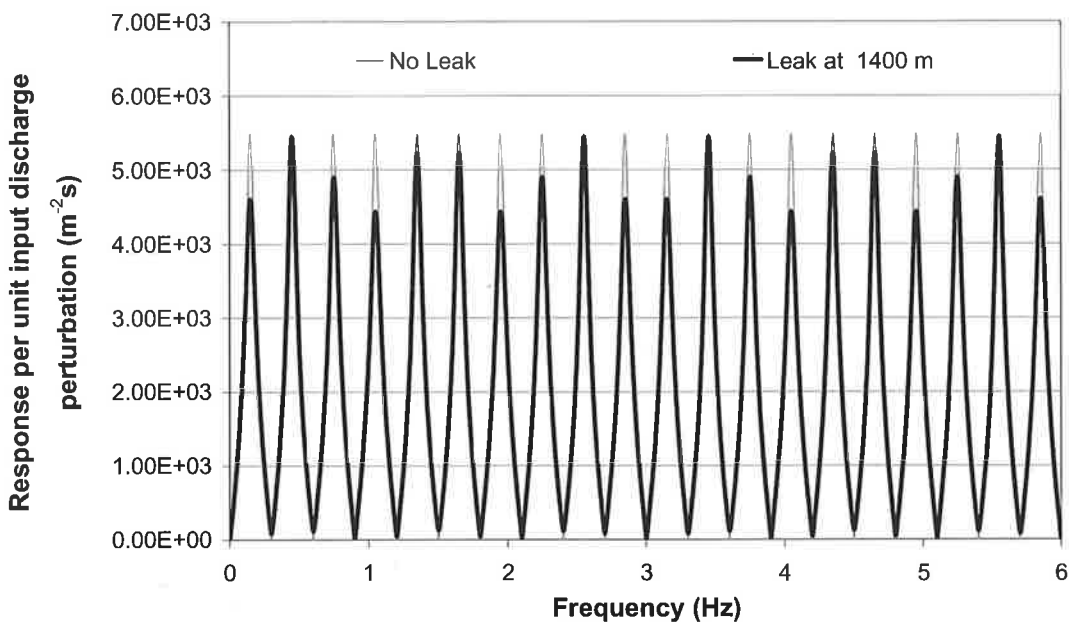


Figure 6-4 – Effect of a leak located at 1400 m from upstream boundary with $C_d A_L = 0.00014 \text{ m}^2$ ($C_d A_L / A = 1.98 \times 10^{-3}$).

The true effect of the leak is investigated further by altering both size and position of a leak in the system. For the same leak at a position 1136 m downstream of the reservoir (refer to Figure 6-5), the extracted FRF from the system is shown in Figure 6-6. The shift in the leak position has resulted in a FRF containing peaks that fluctuate in a different periodic pattern to the one observed in Figure 6-4. A different pattern of the FRF (Figure 6-7) results from the same leak located 500 m from the reservoir boundary (Figure 6-8). Thus, the pattern at peaks of the FRF is a result of leak location in the system.

An additional result is presented in Figure 6-9 where the leak $C_d A_L$ is increased to 0.00042 m^2 ($C_d A_L / A = 5.94 \times 10^{-3}$) with the leak at the same position as Figure 6-7. The size of the leak increases the amplitude of the pattern imposed on the FRF while the shape of the pattern remains unchanged.

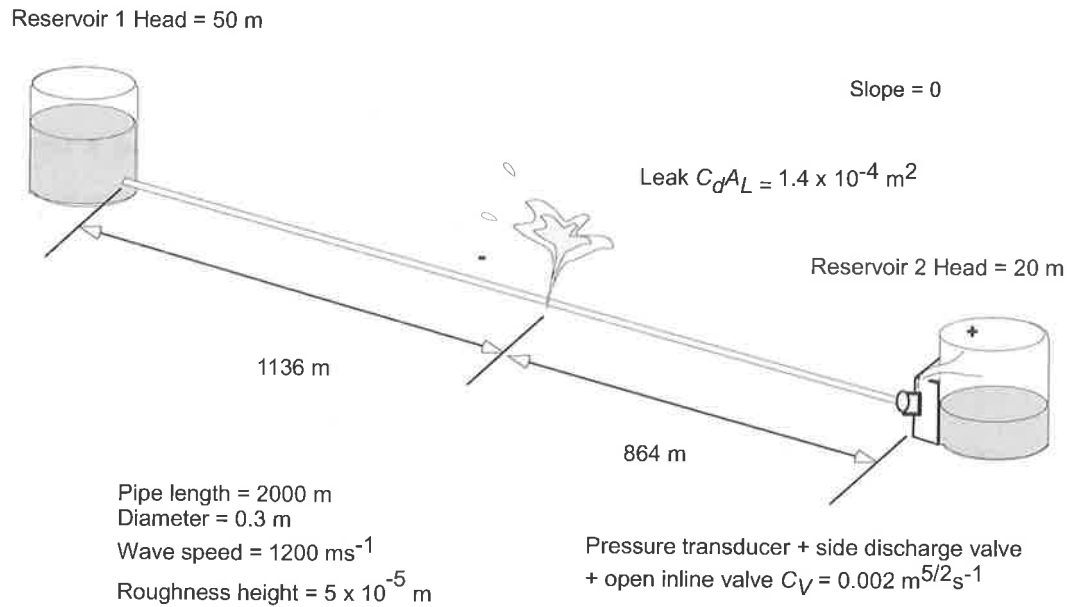


Figure 6-5 – System configuration for Figure 6-4.

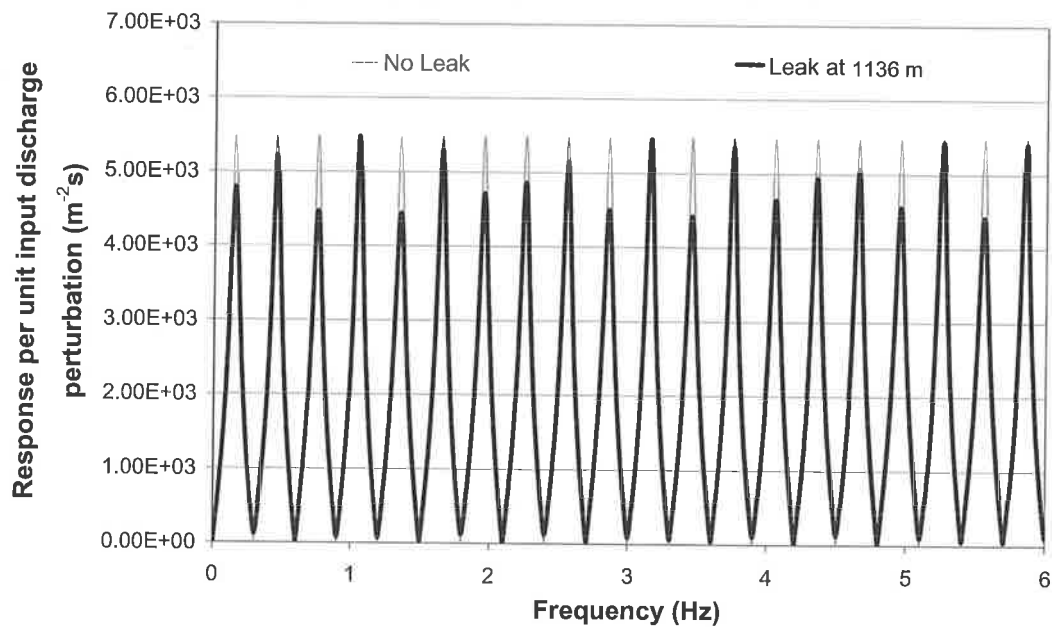


Figure 6-6 – Effect of a leak located at 1136 m from upstream boundary with $C_d A_L = 0.00014 \text{ m}^2$ ($C_d A_L / A = 1.98 \times 10^{-3}$).

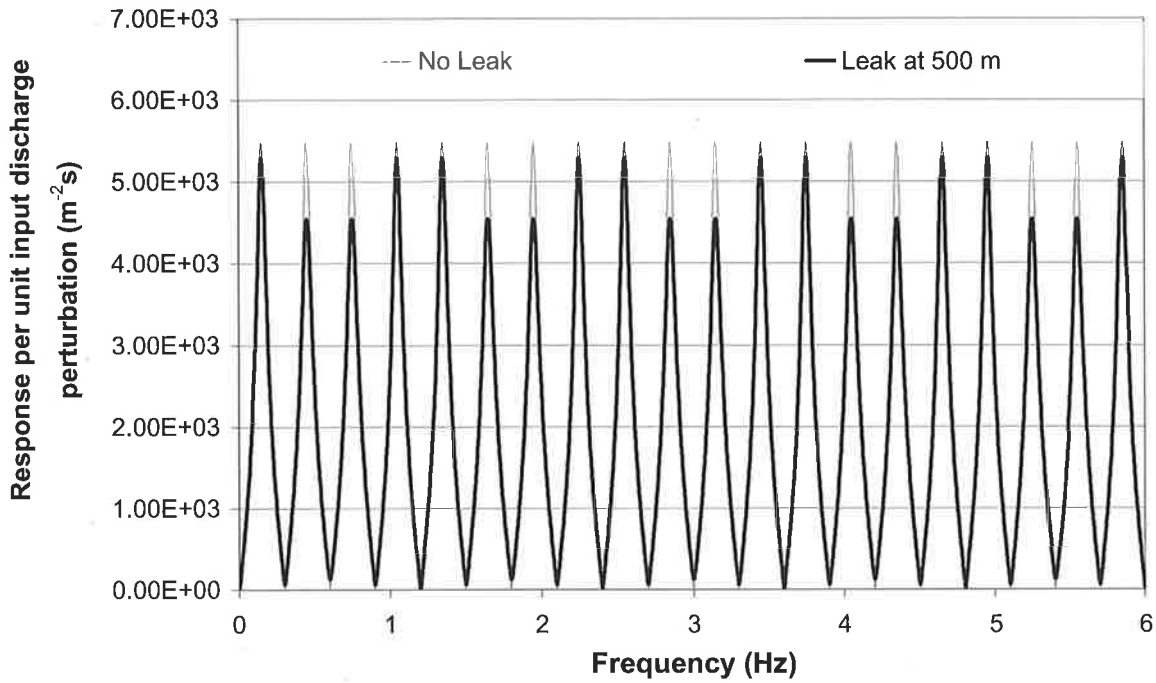


Figure 6-7 – Effect of a leak located at 500 m from upstream boundary with $C_d A_L = 0.00014 \text{ m}^2$ ($C_d A_L / A = 1.98 \times 10^{-3}$).

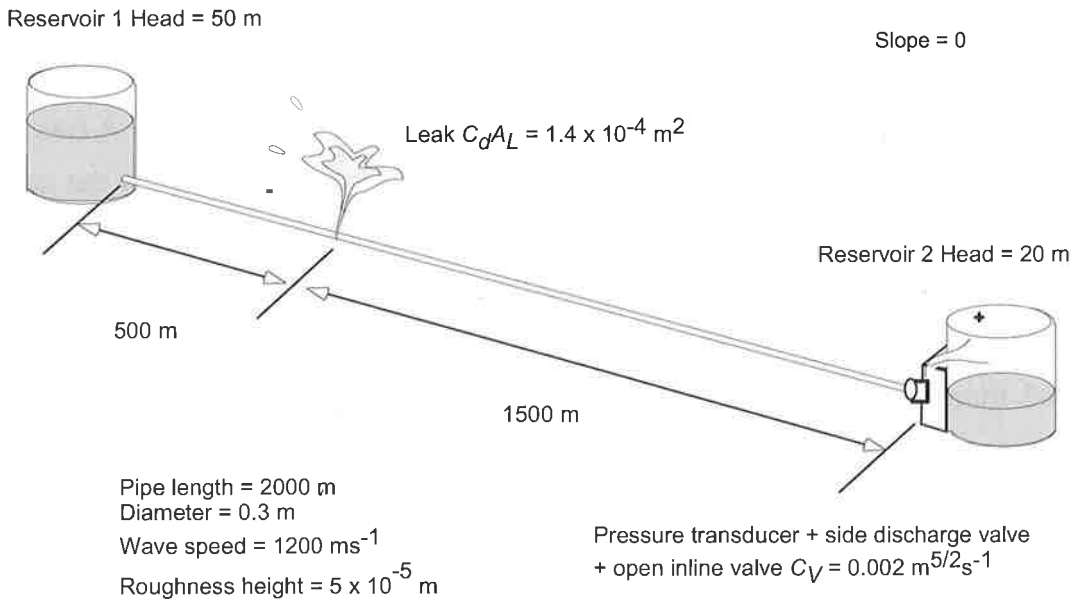


Figure 6-8 – System configuration for Figure 6-7.

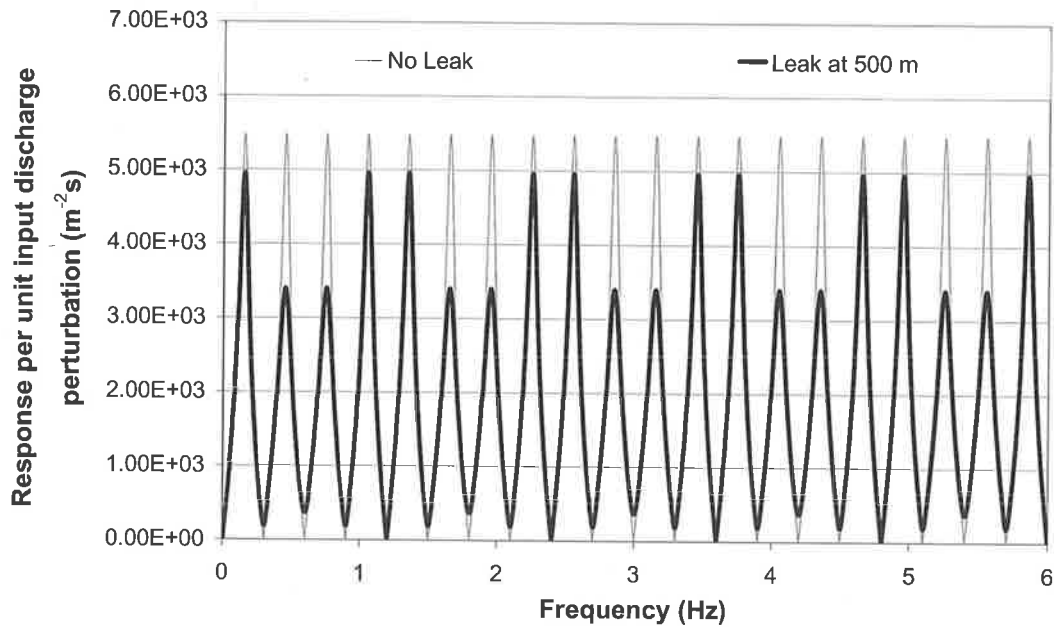


Figure 6-9 – Effect of a leak located at 500 m from upstream boundary with $C_d A_L = 0.00042 \text{ m}^2$ ($C_d A_L / A = 5.94 \times 10^{-3}$).

The effect of leak parameters on the peak magnitudes of a FRF is further tested using the following example. With the measurement and generation point located at the optimum position for this anti-symmetric pipeline (against the downstream in-line valve), the side-discharge valve is forced to oscillate at the frequency associated with the first harmonic peak of the system. This frequency is given by the ratio, $\omega_r = \omega / \omega_{th} = 1.0$. A leak of size $C_d A_L = 0.00014 \text{ m}^2$ ($C_d A_L / A = 1.98 \times 10^{-3}$) is initially placed adjacent to the upstream reservoir and the magnitude of the head response is measured. The leak is then shifted slightly downstream and the response is once again measured. This procedure is illustrated in Figure 6-10. The response measured from the system when the leak is progressively shifted from the upstream to the downstream boundary is given in Figure 6-11. The procedure is repeated for frequencies of oscillation of $\omega_r = 3.0$ and 5.0 (3rd and 5th harmonic peaks). The position of the leak is defined as the dimensionless leak position, x_L^*

$$x_L^* = \frac{x_L}{L} \quad (6.1)$$

where x_L is the distance of the leak from the upstream reservoir.

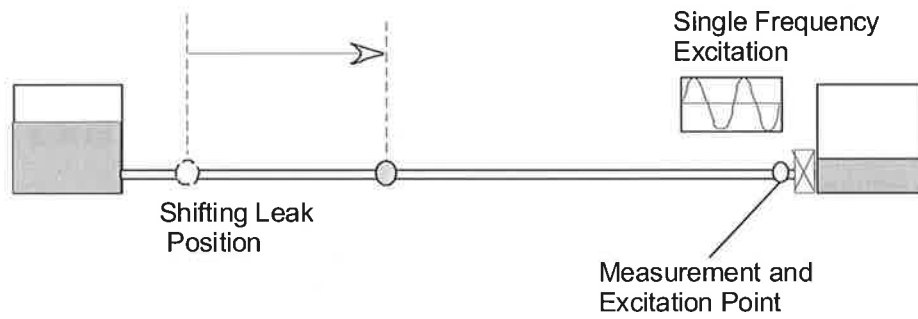


Figure 6-10 – Procedure of testing the effect of the leak position on the measured response magnitude.

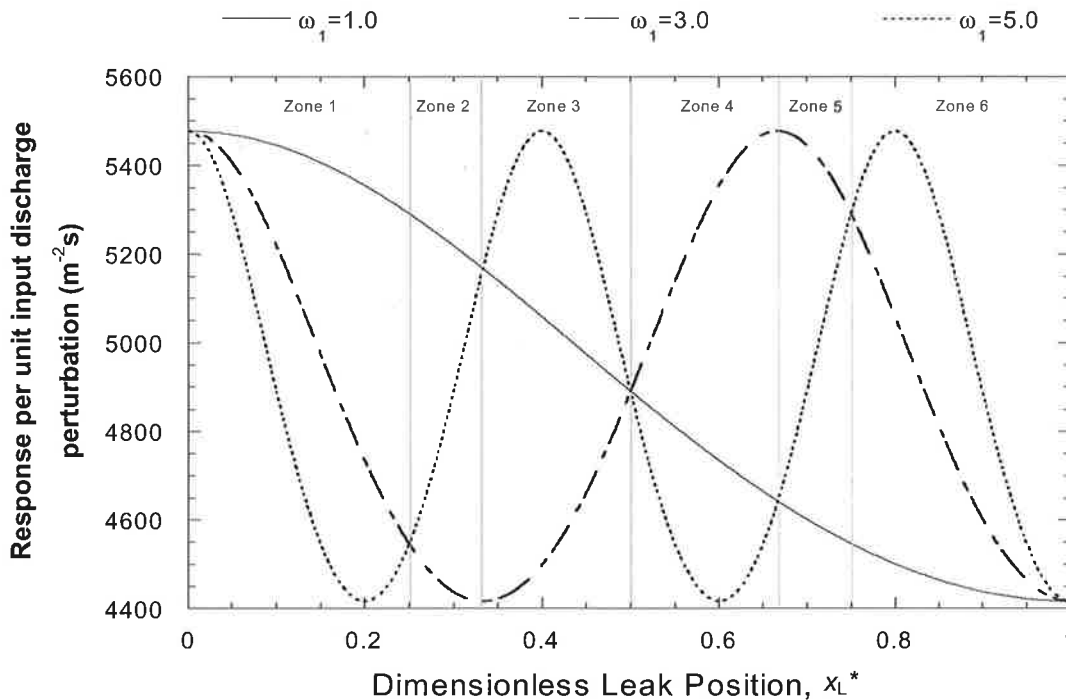


Figure 6-11 – Effect of leak position on the frequency response of the first 3 harmonic peaks.

Figure 6-11 indicates that the response at each of the harmonic peak frequencies varies differently with the position of the leak in the system. Figure 6-11 is divided into 6 zones. In each zone, a specific sequence of peak magnitudes is observed. For example, in zone 1 the response of the first harmonic is greater than the third harmonic, which in turn is greater than the response at the fifth harmonic. In zone 4, the fifth harmonic is greater than the first and both the first and the fifth harmonic responses are greater than the third harmonic. The observation of the relative magnitudes of the peak responses in the FRF can, therefore, lead to an approximate location of the leak. This approach is investigated in more detail in Section 6.3.2

A similar analysis was conducted to determine the effect of leak size on peak response in the FRF. In this case, a leak is positioned at the midpoint of the pipeline and the response of each peak harmonic is plotted against size of this leak. A schematic of this procedure is shown in Figure 6-12.

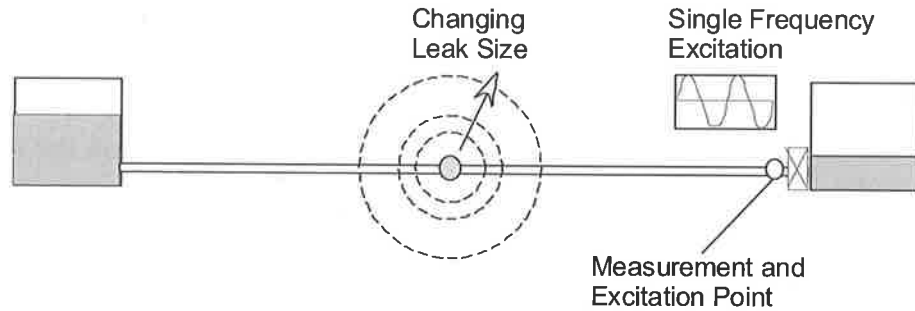


Figure 6-12 – Effect of leak size on the resonance peak responses.

The result of this analysis is shown in Figure 6-13 and it indicates that, unlike the effect of the leak position on the FRF peak responses, the size of the leak results in an identical response in the three different harmonics.

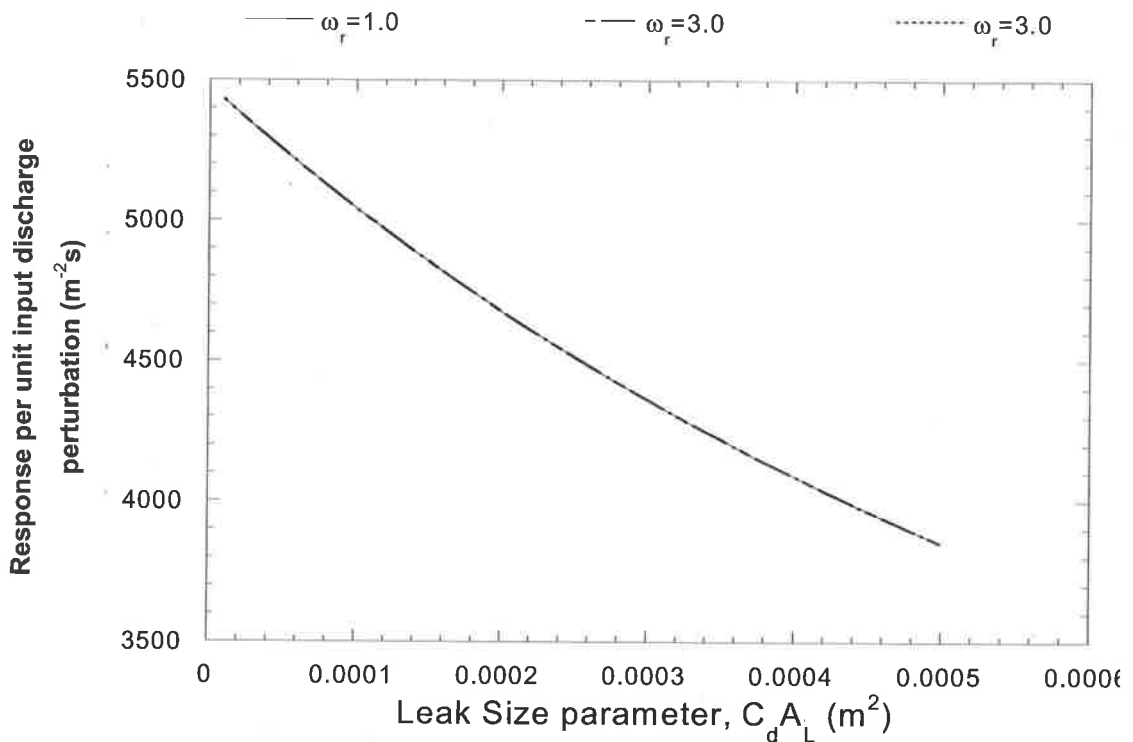


Figure 6-13 – Effect of leak size on the frequency response of the first 3 harmonic peaks (note all three series overlap).

In all three cases, an increase in leak size results in a decrease in the magnitude of the measured responses. This result indicates that the size of the leak does not affect the shape of the pattern on the FRF and its effect is frequency independent.

The effect of a leak on the FRF can, therefore, be summarised as follows:

1. The presence of the leak imposes a pattern onto the peaks of the FRF.
2. The *location* of the leak determines the *shape* of the pattern.
3. The *size* of the leak determines the *amplitude* of the pattern.

These leak-induced effects are incorporated into leak detection procedures in the following section.

6.3 METHODS OF LEAK DETECTION USING THE FRF

The previous section illustrated that the presence of a leak in a pipeline changes the peaks of the frequency response function and no additional “leak-induced frequency peaks” are observed. A leak causes non-uniform damping in the peaks of the FRF and the shape of the pattern is associated with the location of a leak. The magnitude of the deviation between the maximum and minimum values of the induced pattern is related to the size of a leak. This section presents leak detection methods that can determine the position of a leak from the behaviour of the frequency response function. The techniques in this section do not require the derivation of the underlying equations governing the leak-induced modification on the FRF. Two methods are presented:

1. Inverse resonance method—inverse regression of the measured FRF with the output from the numerical model.
2. Peak coding method—code-matching system for determining leak position from observed relative magnitudes of the peaks.

6.3.1 Inverse method

The FRF can be used to detect and locate faults in pipelines through an inverse procedure where the extracted FRF from the pipeline is fitted to the output of a numerical model. As indicated in the previous section, a leak in a single pipeline can lead to a change in the shape of the FRF. Inverse fitting minimises the sum of the squared difference between measured and modelled frequency response functions by varying the value of leak size ($C_d A_L$) and leak position (x_L) in the model. This method is similar to the inverse transient method in Liggett and Chen (1994), but the predicted response function for the system is a unique description of the pipeline and is the same for all injected transient signals (given a careful selection of the input variable to avoid system non-linearities, refer to Section 5.2.1). The objective function of the inverse procedure is given by the least-squares criterion

$$E = \sum_{j=1}^M [h_j^m - h_j]^2 \quad (6.2)$$

where E is the objective function value, h_j^m and h_j are measured and calculated amplitude responses at the j^{th} frequency, respectively and $M =$ number of measurement points. The minimisation algorithm used in this thesis is the shuffled complex evolution (SCE) algorithm (Duan *et al.* 1993). The SCE algorithm performs a global search based on the simplex method and does not require the use of local gradient information.

The application of the inverse method is shown for the pipeline in Figure 6-14. A leak of $C_d A_L = 0.00014 \text{ m}^2$ ($C_d A_L / A = 1.98 \times 10^{-3}$) is located at 1400 m from the upstream boundary with the measurement taken at 800 m from the same boundary.

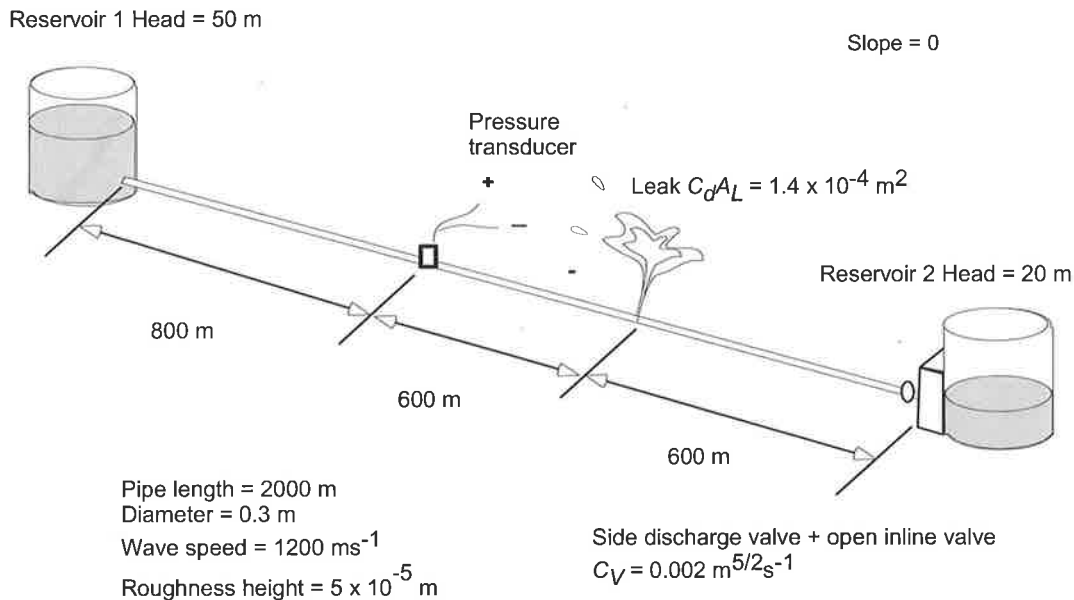


Figure 6-14 – System configuration for Figure 6-15.

The frequency response was extracted from the numerical pipeline with a side-discharge valve located upstream of the in-line valve. The inverse resonance method was performed using “perfect” data generated by the transfer matrix equations. The following examples provide a brief outline of the inverse calibration procedure in the FRF. The result is shown in Figure 6-15.

One hundred data points from the FRF were used in the inverse calculation. The starting guess for the leak size was zero (no leak) and the starting leak position was set at the

midpoint of the pipe. Figure 6-15 shows that the final solution of the inverse resonance method (achieved when the method converged to the minimum of the objective function) corresponds to the measured results. At this final solution, the leak size was determined to be $C_d A_L = 0.00014 \text{ m}^2$ ($C_d A_L / A = 1.98 \times 10^{-3}$) and leak position $x_L = 1400 \text{ m}$.

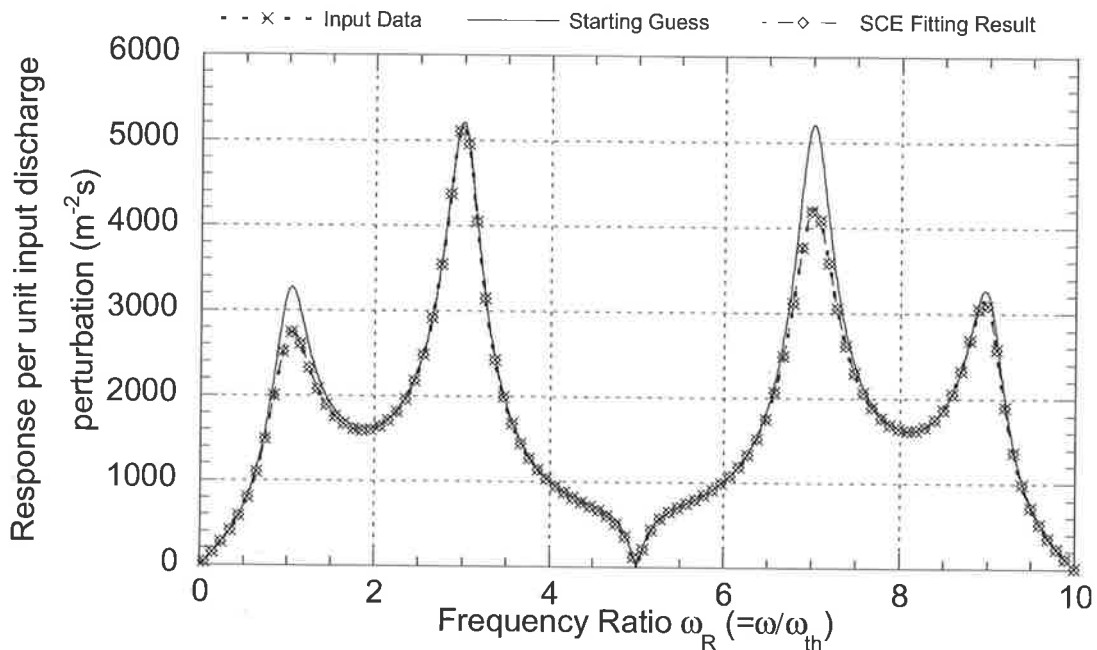


Figure 6-15 – Inverse calibration for the frequency response measured at a location 800 m from the upstream boundary (Data file: C6-1.txt).

This example illustrates the conventional application of inverse transient analysis, where leak parameters can be found by fitting modelled response to measured data. The technique can be made more resilient to contamination in the data by measuring at the position expected to produce the maximum response in the system. From section 5.2.2, this position is located next to the valve boundary (for an anti-symmetric system). The inverse calibration result for the transient source with optimum location of the measurement position (refer to Figure 6-16) is shown in Figure 6-17. Once again, at the optimum solution the leak size and position were correctly found to be 0.00014 m^2 and 1400 m , respectively.

The above investigation has shown the potential of applying an inverse procedure for detecting leaks using the FRF. However, this approach requires the existence of an accurate numerical model and a good understanding of the physical characteristics of the

pipeline along its length. This reliance on an accurate forward prediction can limit its applicability in reality. An alternative technique is to use the relative magnitudes of the peaks in the response function for leak detection without comparing the result to a theoretical output.

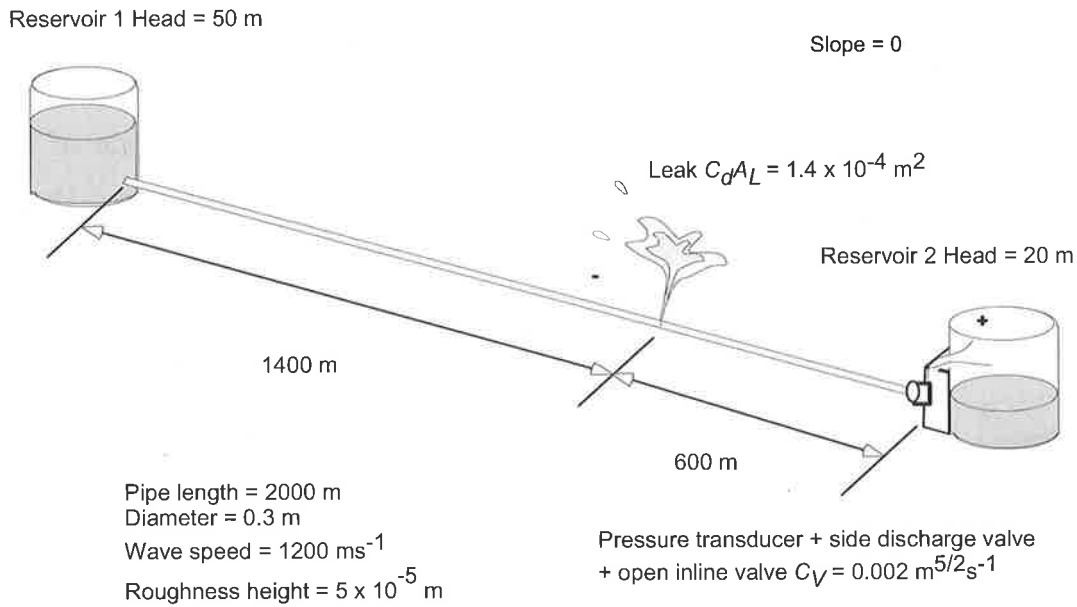


Figure 6-16 – System configuration for Figure 6-17.

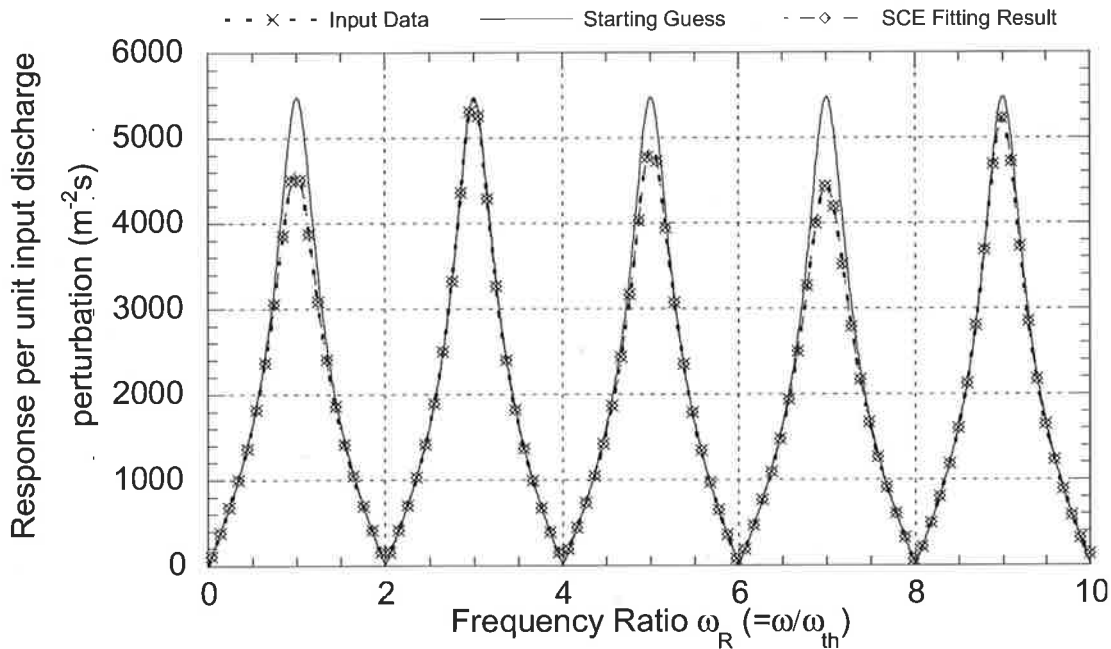


Figure 6-17 – Inverse calibration for the frequency response measured at the optimum position in the pipeline (Data file: C6-2.txt).

6.3.2 Peak sequencing method

The effect of a leak on the FRF is frequency dependent and results in uneven damping of harmonic peaks along the frequency axis. This damping pattern is related to the position of the leak alone and provides a new way of locating a leak based on a study of the relative magnitudes of the peaks in the FRF. This method does not require inverse regression of system responses to a model output, but finds the location of a leak through the matching of rank-sequences to entries in a look-up table. To understand the operation of this method, the FRF from two leaking pipelines of configurations given in Figure 6-18 and Figure 6-19 are presented in Figure 6-20 and Figure 6-21, respectively.

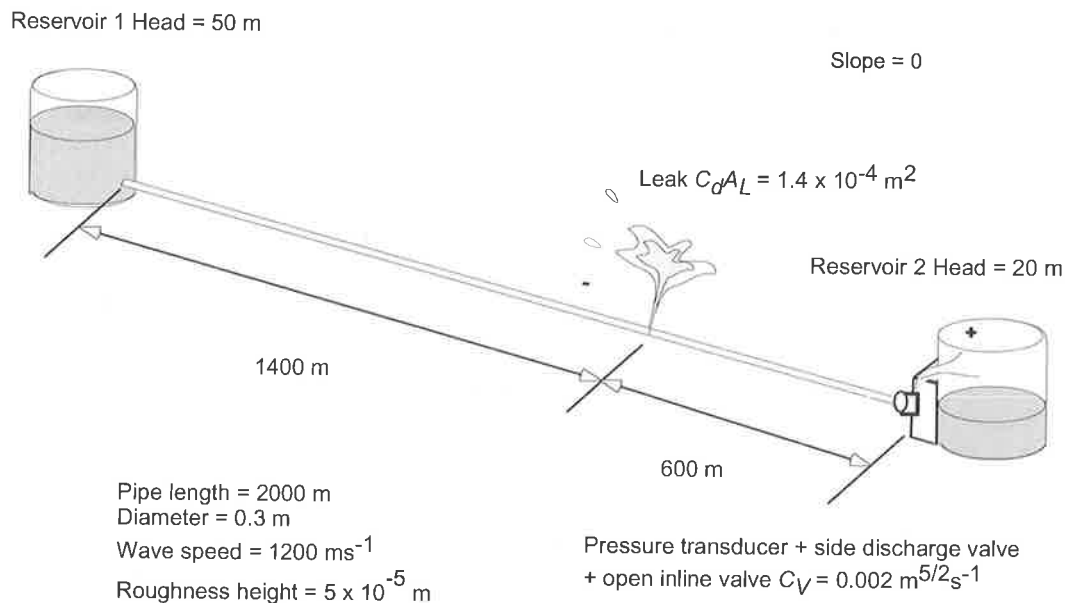


Figure 6-18 – System configuration for Figure 6-20.

To use the shape of the FRF as a means of locating a leak in a system, the shape of FRF must be summarised in a convenient format. The summary can be achieved through ranking the sizes of the resonant peaks in order of magnitude. For example, Figure 6-20 shows that the order of the first three resonant peaks, ranked in terms of magnitude, is [3rd, 5th, 1st] harmonics when the leak is positioned 1400 m from the upper boundary ($x_L^* = 0.7$). In comparison, the change in the shape of the FRF when the leak is shifted to 700 m from the upper boundary ($x_L^* = 0.35$) can be seen through the change in the rank sequence of these three peaks, which is [5th, 1st, 3rd] for this case. The way in which these sequences

can be related to the position of the leak is illustrated by Figure 6-11, which is repeated here as Figure 6-22.

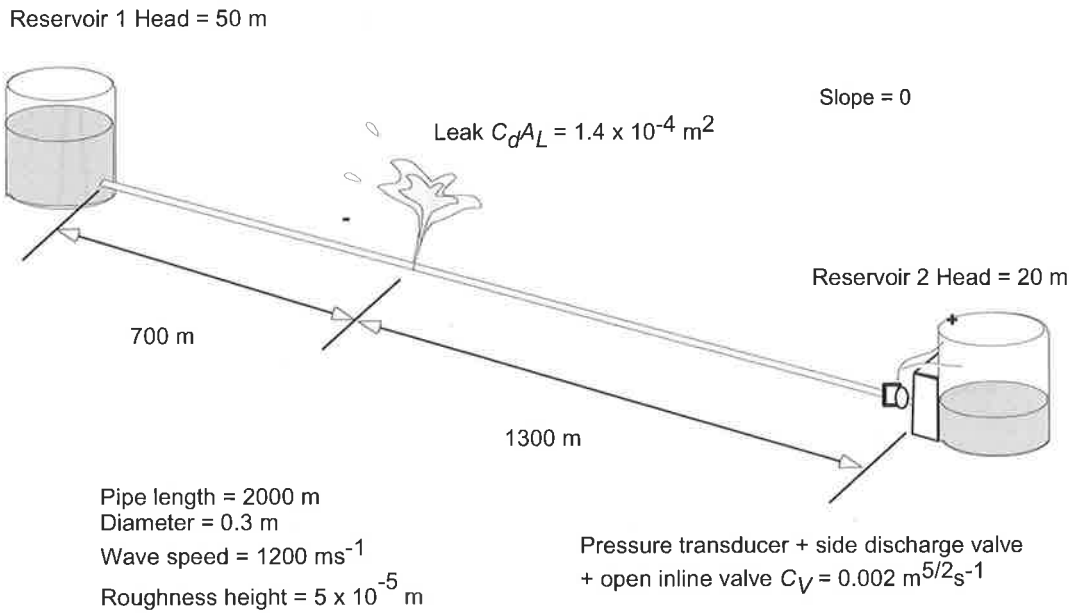


Figure 6-19 – System configuration for Figure 6-21.

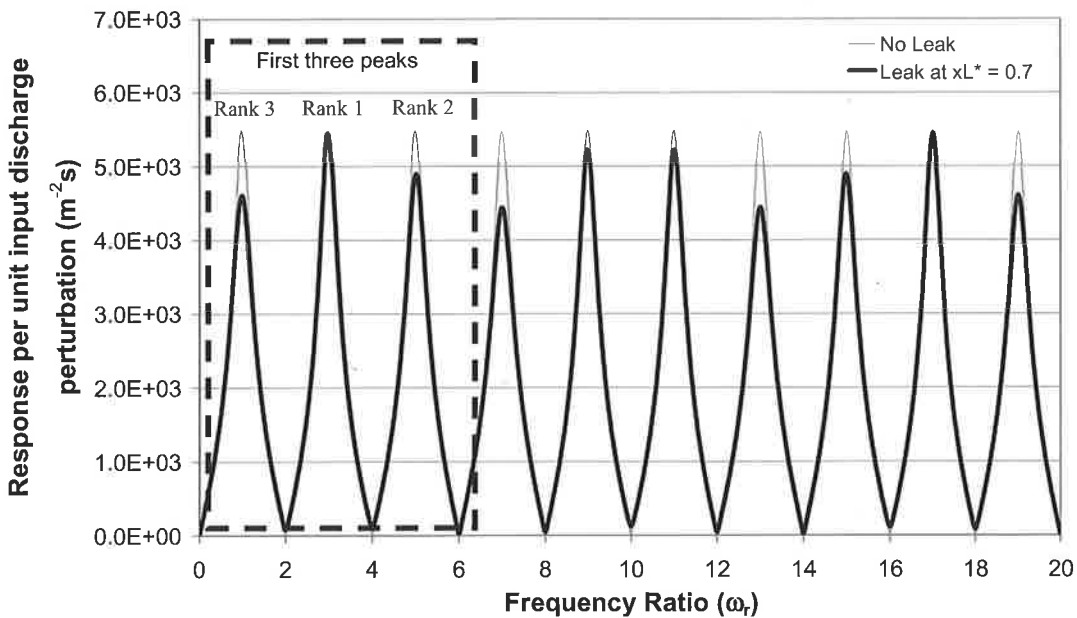


Figure 6-20 – Leak at 1400 m from upstream reservoir (Data file: C6-3.txt).

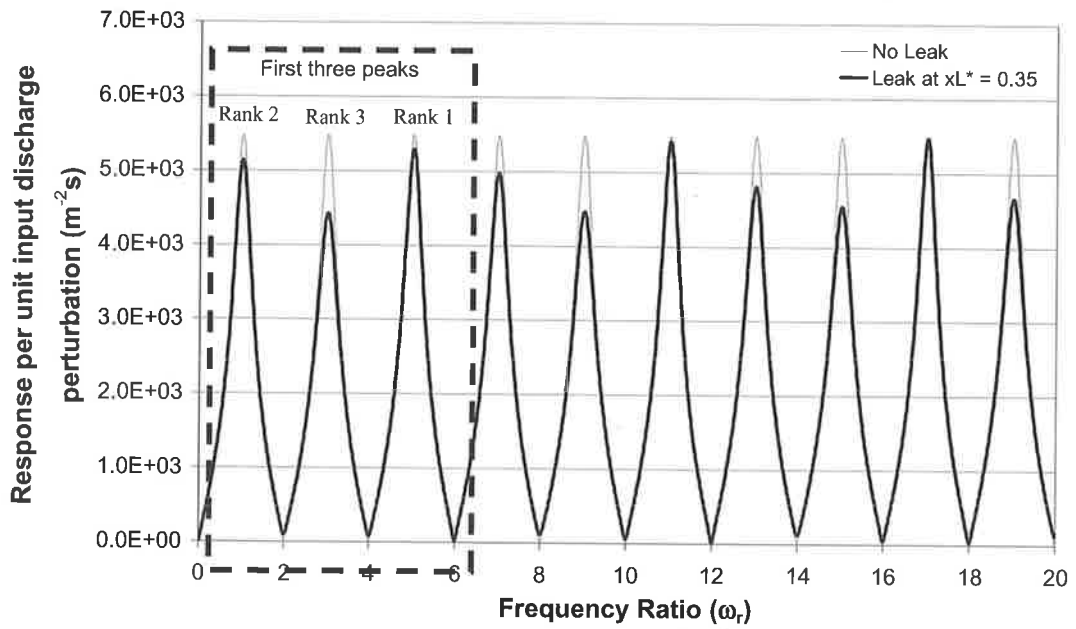


Figure 6-21 – Leak at 700 m from upstream reservoir (Data file: C6-3.txt).

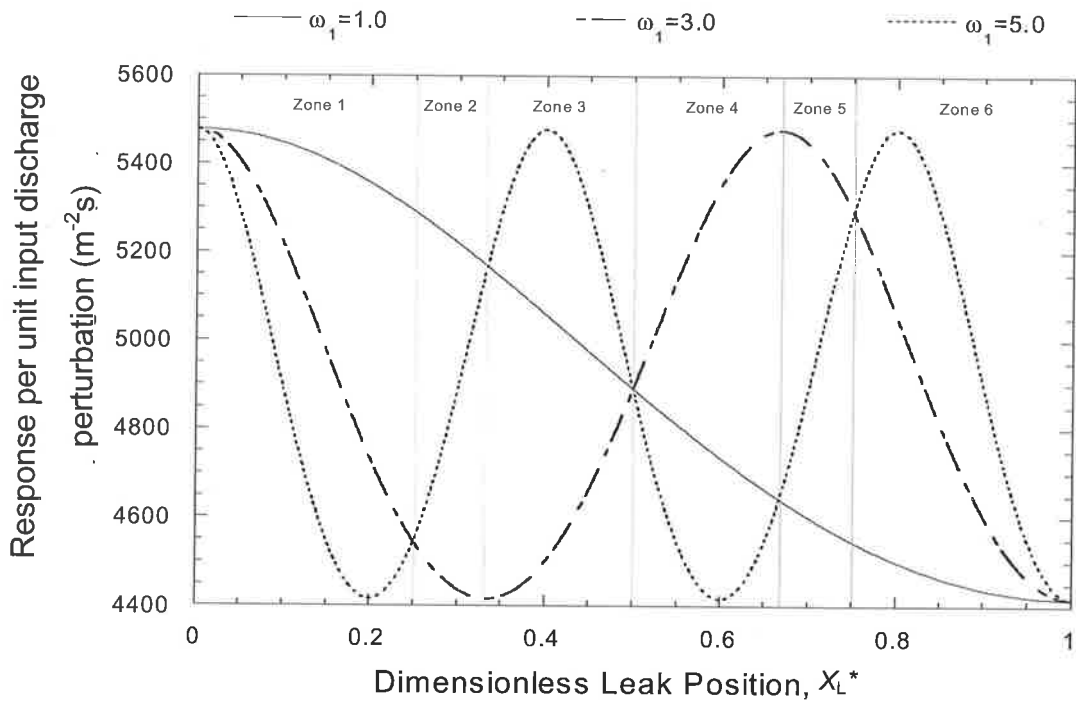


Figure 6-22 – Effect of leak position on the frequency response of the first 3 harmonic peaks.

In Figure 6-22, the responses of the first three harmonic peaks in the FRF with changes in the leak position are given. The resonant peak responses are seen to intersect at five leak positions along the pipe, dividing the system into six unequal sections. Between each pair of intersection points is a region where the first three resonant peaks, when ranked in order of magnitude, are arranged in a specific sequence. When a leak is present in a particular region of the pipe, the shape of the frequency response function follows the rank-sequence for that particular region. For example, in the case where the leak is at a position 1400 m from the upstream reservoir the magnitudes of the peaks are ranked in order as [3rd > 5th > 1st]. From Figure 6-22, to generate this order in the peak magnitudes, the leak has to be positioned in zone 5; that is, $0.66 < x_L^* < 0.75$. The true leak position of $x_L^* = 0.7$ ($x_L = 1400$ m) lies in this predicted region.

The case of $x_L^* = 0.35$ ($x_L = 700$ m) in Figure 6-21 generates peaks ranked in the [5th, 1st, 3rd] sequence and Figure 6-22 correctly indicates that the leak is located between $x_L^* = 0.33$ and 0.5 using this sequence. The shape of a measured FRF can be matched to the expected shapes of the function for a leak located in any particular region of a pipe and be used as a means of locating a leak in a single pipeline. The shapes of the FRF are represented as peak sequences and a summary of these for the first three harmonic peaks are tabulated in Table 6-1. The rank sequences for intersection points are shown in Table 6-1 and correspond to exact leak locations in the pipeline. Similar rank-order tables can be generated for higher numbers of peak harmonics, resulting in a finer discretisation of the pipeline and better location accuracy. For example, the use of the first six harmonic peaks creates 32 divisions of the pipe in which a leak can be located.

The determination of the coding sequences can be performed using the transfer matrix model where the variation in the response magnitude at each resonant peak with leak position is determined. This procedure is described in Figure 6-10 for the generation of the results in Figure 6-22. A similar coding table can be generated for different system configurations (e.g. symmetric) using the same procedure.

The peak sequence method of leak detection does not require accurate forward modelling of the FRF, nor does it require accurate measurement of the function magnitudes. Instead, the procedure uses relative magnitudes between the peaks and given the effects in the pipe are frequency independent, actual sizes of the peaks themselves are irrelevant. Once the

table of sequences is generated, it can be used in any single pipeline of the same boundary configurations to determine the presence and the position of leaks in the system. This technique, however, can only locate a leak in a particular region of the pipeline and does not give an exact location. The resolution of the detection is dependent upon the number of resonance peaks used in the generation of the sequence tables. To extract more definite information concerning the leak from the leak-induced pattern on the FRF, the analytical expressions for the leak-induced pattern on the FRF peaks must be defined.

Table 6-1 – Peak ranking sequence and corresponding leak position. Zones are labelled according to Figure 6-22

Zone	Peak ranking	Leak location range (x_L^*)
1	$h_{ar1} > h_{ar3} > h_{ar5}$	0 – 0.25
1/2	$h_{ar1} > (h_{ar3} = h_{ar5})$	0.25
2	$h_{ar1} > h_{ar5} > h_{ar3}$	0.25 - 0.33
2/3	$(h_{ar5} = h_{ar1}) > h_{ar3}$	0.33
3	$h_{ar5} > h_{ar1} > h_{ar3}$	0.33 - 0.50
3/4	$h_{ar5} = h_{ar1} = h_{ar3}$	0.50 (also 0 or 1)
4	$h_{ar3} > h_{ar1} > h_{ar5}$	0.50 - 0.66
4/5	$h_{ar3} > (h_{ar5} = h_{ar1})$	0.66
5	$h_{ar3} > h_{ar5} > h_{ar1}$	0.66-0.75
5/6	$(h_{ar5} = h_{ar3}) > h_{ar1}$	0.75
6	$h_{ar5} > h_{ar3} > h_{ar1}$	0.75 - 1

6.4 DEVELOPMENT OF AN ANALYTICAL EXPRESSION

DESCRIBING THE LEAK-INDUCED MODIFICATION ON THE FRF PEAKS

The observed leak-induced pattern imposed onto the peaks of the FRF prompted further investigation into the nature of this pattern. The derivation of the leak-induced modification on the FRF is carried out using the transfer matrix equations under two system configurations, symmetric and anti-symmetric. To isolate the effect of the leak on the FRF, the pipeline is assumed to be frictionless with the unit matrix for a length of intact pipeline between points n and $n+1$ given as (refer to Section 3.3)

$$\begin{Bmatrix} q \\ h \end{Bmatrix}^{n+1} = \begin{bmatrix} \cos\left(\frac{la}{\omega}\right) & -\frac{igA}{a} \sin\left(\frac{la}{\omega}\right) \\ -\frac{ia}{gA} \sin\left(\frac{la}{\omega}\right) & \cos\left(\frac{la}{\omega}\right) \end{bmatrix} \begin{Bmatrix} q \\ h \end{Bmatrix}^n \quad (6.3)$$

The overall transfer matrix of the system, U , relates the head and discharge oscillations at the extremities of the system ($a =$ upstream, $b =$ downstream) and is given in Eq. (3.52) repeated here as Eq. (6.4)

$$\begin{Bmatrix} q \\ h \\ 1 \end{Bmatrix}^b = \begin{bmatrix} U_{11} & U_{12} & U_{13} \\ U_{21} & U_{22} & U_{23} \\ U_{31} & U_{32} & U_{33} \end{bmatrix} \begin{Bmatrix} q \\ h \\ 1 \end{Bmatrix}^a \quad (6.4)$$

Eq. (6.4) can be solved using known boundary conditions at a and b . The overall transfer matrix is given by the multiplication of all the unit matrices associated with each element of the pipe (i.e. pipe sections, leaks, valves) starting from the downstream boundary. This procedure is illustrated in Section 3.3 and more details can be found in Chaudhry (1987).

6.4.1 Anti-symmetric boundary conditions

For the derivation of the leak-induced modification on the frequency response function, first consider an arbitrary pipe bounded by a constant head reservoir on the upstream end and an in-line valve on the downstream end (refer to Figure 6-23). The system is excited by a discharge perturbation near the downstream boundary by operating a side-discharge valve or the in-line valve. Two separate cases need to be considered under this system configuration:

- The downstream valve is closed, making the discharge perturbation zero at the downstream valve position.
- The downstream valve throttles the flow, providing head dissipation at the downstream boundary and allowing discharge to fluctuate in this position.

Anti-symmetric boundary with in-line valve fully closed

The schematic of such a situation is shown in Figure 6-23 with subscripts a , b , corresponding to the position of the supply reservoir and the downstream dead end, respectively.

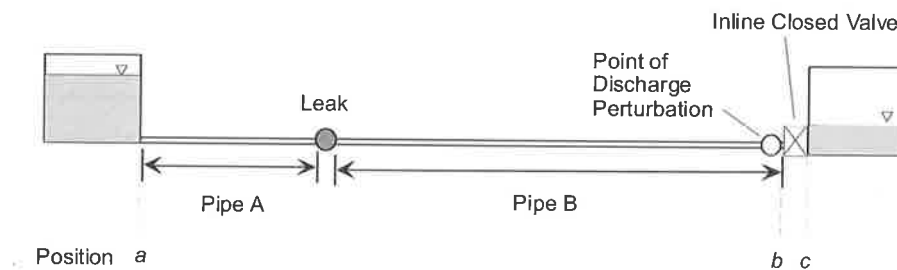


Figure 6-23 – Illustration of the system configuration where a leak exists in the pipeline with a closed downstream valve.

Expanding the discharge and head from Eq. (6.4) gives

$$q_b = U_{11}q_a + U_{12}h_a + U_{13} \quad (6.5)$$

$$h_b = U_{21}q_a + U_{22}h_a + U_{23} \quad (6.6)$$

Using the upstream and downstream boundary conditions where the upstream is a fixed head boundary and the downstream is a fixed discharge boundary,

$$h_a = q_b = 0 \quad (6.7)$$

These boundary conditions simplify Eqs. (6.5) and (6.6) to

$$0 = U_{11}q_a + U_{13} \quad (6.8)$$

$$h_b = U_{21}q_a + U_{23} \quad (6.9)$$

Combining the two equations gives

$$h_b = -\frac{U_{21}U_{13}}{U_{11}} + U_{23} \quad (6.10)$$

Eq. (6.10) is the general head response for a pipe bounded upstream by a reservoir with a dead end at the downstream end. The transient source is a discharge perturbation just upstream of the valve co-located with the pressure measurement according to the optimum system configuration presented in Figure 5-29. The discharge perturbation and the measured head response can be decomposed into a sum of different sinusoids and considered individually.

For an intact length of uniform pipe between the upstream reservoir and the downstream valve, the matrix entries of the pipe unit are given by Eq. (6.3) and the matrix defining a unit discharge oscillation (i.e. $q^{n+1} = q^n + 1$, $h^{n+1} = h^n$, where n = upstream of the transient source, $n + 1$ = downstream of the transient source) is given in Eq. (5.12) and repeated here as

$$\begin{Bmatrix} q \\ h \\ 1 \end{Bmatrix}^{n+1} = \begin{bmatrix} 1 & 0 & 1 \\ 0 & 1 & 0 \\ 0 & 0 & 1 \end{bmatrix} \begin{Bmatrix} q \\ h \\ 1 \end{Bmatrix}^n \quad (6.11)$$

The entries of the system transfer matrix, U , are formed by the multiplication of individual unit matrices in the system starting from the downstream boundary (refer to Chapter 3). Using Eqs. (6.3) and (6.11), the entries of the overall transfer matrix U for an intact pipe system are $U_{31} = U_{32} = U_{23} = 0$ and $U_{13} = U_{33} = 1$. For this situation, Eq. (6.10) becomes

$$h_b = \frac{-\frac{ia}{gA} \sin\left(\frac{l\omega}{a}\right)}{\cos\left(\frac{l\omega}{a}\right)} \quad (6.12)$$

At the resonance peaks, the angular frequency is defined as

$$\omega_{in} = \frac{(2m-1)\pi a}{2L} \quad (6.13)$$

where m is a positive integer ($m = 1, 2, 3, \dots$). Substitution of Eq. (6.13) into Eq. (6.12) produces

$$h_b = \frac{-\frac{ia}{gA} \sin\left(\frac{(2m-1)\pi}{2}\right)}{\cos\left(\frac{(2m-1)\pi}{2}\right)} = \infty \quad (6.14)$$

Indicating that an intact frictionless pipeline with a downstream closed valve produces resonance peaks of infinity. This result is shown in Figure 6-24.

Consider the case where a leak exists in the system as shown in Figure 6-23. The entries of the transfer matrix, U , in Eq. (6.10) are now modified to include the leak in the system. The transfer matrix for the leak unit is given by (refer to Section 3.3)

$$\begin{Bmatrix} q \\ h \end{Bmatrix}^{n+1} = \begin{bmatrix} 1 & -\frac{Q_{L0}}{2(H_{L0} - z_L)} \\ 0 & 1 \end{bmatrix} \begin{Bmatrix} q \\ h \end{Bmatrix}^n \quad (6.15)$$

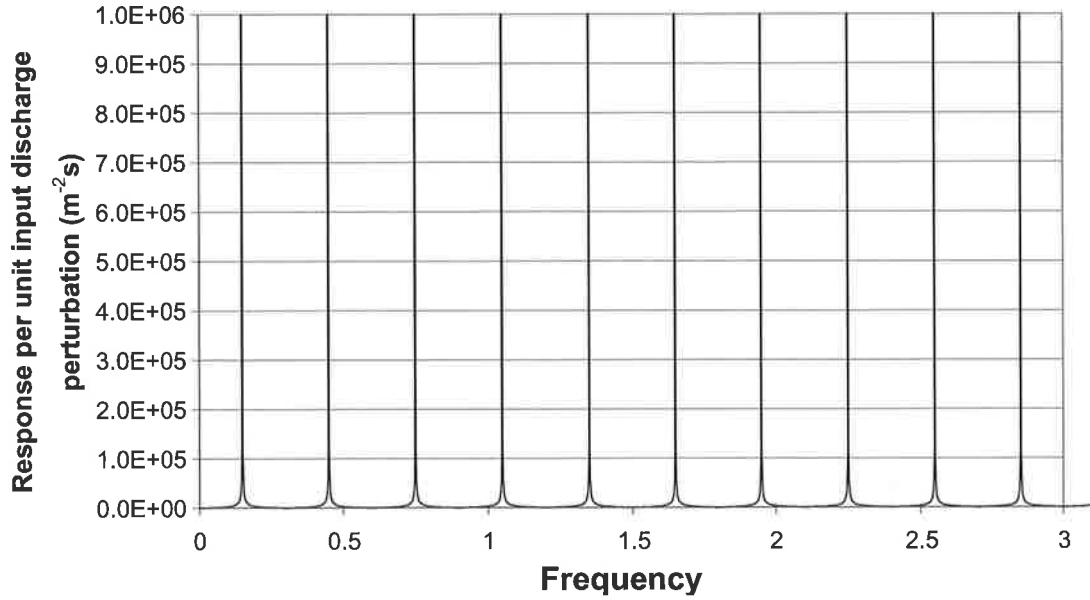


Figure 6-24 – FRF from the pipeline with no losses.

Multiplication of the pipe matrices with the leak matrices is shown in detail in Appendix A and the transfer matrix entries for the system is given by $U_{13} = 1$, $U_{23} = 0$ and

$$U_{11} = \cos\left(\frac{l_A \omega}{a}\right) \cos\left(\frac{l_B \omega}{a}\right) - \frac{ia}{gA} \sin\left(\frac{l_A \omega}{a}\right) \left[-\frac{Q_{L0}}{2(H_{L0} - z_L)} \cos\left(\frac{l_B \omega}{a}\right) - \frac{igA}{a} \sin\left(\frac{l_B \omega}{a}\right) \right] \quad (6.16)$$

Expanding and simplifying give

$$U_{11} = \left[\cos\left(\frac{l_A \omega}{a}\right) \cos\left(\frac{l_B \omega}{a}\right) - \sin\left(\frac{l_A \omega}{a}\right) \sin\left(\frac{l_B \omega}{a}\right) \right] + \frac{Q_{L0}}{2(H_{L0} - z_L)} \frac{ia}{gA} \sin\left(\frac{l_A \omega}{a}\right) \cos\left(\frac{l_B \omega}{a}\right) \quad (6.17)$$

Using the trigonometric argument sum identity,

$$U_{11} = \cos\left(\frac{\omega(l_A + l_B)}{a}\right) + \frac{Q_{L0}}{2(H_{L0} - z_L)} \frac{ia}{gA} \sin\left(\frac{l_A \omega}{a}\right) \cos\left(\frac{l_B \omega}{a}\right) \quad (6.18)$$

At the harmonic peaks, Eq. (6.18) becomes

$$U_{11} = \cos\left(\frac{(2m-1)\pi}{2}\right) + \frac{Q_{L0}}{2(H_{L0} - z_L)} \frac{ia}{gA} \sin\left(\frac{l_A}{L} \frac{(2m-1)\pi}{2}\right) \cos\left(\frac{l_B}{L} \frac{(2m-1)\pi}{2}\right) \quad (6.19)$$

Denoting $l_A/L = x_L^*$ and $l_B/L = (1 - x_L^*)$ and using $\cos(\pi/2) = 0$ give

$$U_{11} = \frac{Q_{L0}}{2(H_{L0} - z_L)} \frac{ia}{gA} \sin\left(\frac{x_L^*(2m-1)\pi}{2}\right) \cos\left(\frac{(1-x_L^*)(2m-1)\pi}{2}\right) \quad (6.20)$$

Using the trigonometric product identity,

$$U_{11} = \frac{Q_{L0}}{4(H_{L0} - z_L)} \frac{ia}{gA} \left[\sin\left(\frac{(2m-1)\pi}{2}\right) + \sin\left(\frac{(2x_L^*-1)(2m-1)\pi}{2}\right) \right] \quad (6.21)$$

After simplifications

$$U_{11} = \frac{Q_{L0}}{4(H_{L0} - z_L)} \frac{ia}{gA} \left[(-1)^{m+1} + \sin\left(2mx_L^*\pi - \pi x_L^*\right) - \frac{\pi}{2}(2m-1) \right] \quad (6.22)$$

Finally, using the sum of arguments identity once again gives

$$U_{11} = \frac{Q_{L0}}{4(H_{L0} - z_L)} \frac{ia}{gA} \left[(-1)^{m+1} + \sin(2mx_L^*\pi - \pi x_L^*) \cos\left(\frac{\pi}{2}(2m-1)\right) - \cos(2mx_L^*\pi - \pi x_L^*) \sin\left(\frac{\pi}{2}(2m-1)\right) \right] \quad (6.23)$$

The entry (1,1) in the overall system transfer matrix is

$$U_{11} = \frac{Q_{L0}}{4(H_{L0} - z_L)} \frac{ia}{gA} \left[(-1)^{m+1} + (-1)^m \cos(2mx_L^*\pi - \pi x_L^*) \right] \quad (6.24)$$

Substituting $U(2,1)$ as shown in Appendix A and simplifying using the procedure above,

$$U_{21} = -\frac{ia}{gA} \left((-1)^{m+1} + (-1)^{m+1} \frac{ia}{gA} \frac{Q_{L0}}{4(H_{L0} - z_L)} \sin(2mx_L^*\pi - \pi x_L^*) \right) \quad (6.25)$$

Substituting the results of Eq. (6.24) and (6.25) into Eq. (6.10) gives the expression for the peaks of the FRF in an anti-symmetric system with a closed in-line valve as

$$h_b = \frac{(-1)^{m+1} + (-1)^{m+1} \frac{ia}{gA} \frac{Q_{L0}}{4(H_{L0} - z_L)} \sin(2mx_L^* \pi - \pi x_L^*)}{\frac{Q_{L0}}{4(H_{L0} - z_L)} [(-1)^{m+1} + (-1)^m \cos(2mx_L^* \pi - \pi x_L^*)]} \quad (6.26)$$

To further simply the equation, the numerator can be shown as approximately constant for reasonable leak sizes by substituting Q_{L0} into the orifice equation, which gives

$$h_b = \frac{(-1)^{m+1} + (-1)^{m+1} \frac{ia}{gA} \frac{(C_d A_L \sqrt{2g(H_{L0} - z_L)})}{4(H_{L0} - z_L)} \sin(2mx_L^* \pi - \pi x_L^*)}{\frac{Q_{L0}}{4(H_{L0} - z_L)} [(-1)^{m+1} + (-1)^m \cos(2mx_L^* \pi - \pi x_L^*)]} \quad (6.27)$$

$$h_b = \frac{(-1)^{m+1} + i(-1)^{m+1} a \left(\frac{C_d A_L}{A} \right) \frac{1}{2^{\frac{3}{2}} \sqrt{g} \sqrt{H_{L0} - z_L}} \sin(2mx_L^* \pi - \pi x_L^*)}{\frac{Q_{L0}}{4(H_{L0} - z_L)} [(-1)^{m+1} + (-1)^m \cos(2mx_L^* \pi - \pi x_L^*)]} \quad (6.28)$$

For typical values of wave speed, leak size and driving head (i.e. wave speed in the range of 1000 ms^{-1} , head at the leak greater than 40 m and $C_d A_L / A$ less than 5×10^{-3}), the imaginary part of the numerator is 0.0893 and is much smaller than 1.0. The numerator of Eq. (6.26) can, therefore, be approximated as $(-1)^{m+1}$. Using this approximation and taking the absolute value, the magnitude of the head oscillation measured upstream of the closed in-line valve is

$$|h_b| = \frac{1}{\frac{Q_{L0}}{4(H_{L0} - z_L)} [1 - \cos(2mx_L^* \pi - \pi x_L^*)]} \quad (6.29)$$

When a leak exists in the system, the peaks of the FRF no longer reach infinity as shown in Figure 6-24, but instead oscillate in a sinusoidal-like pattern as dictated by the denominator of Eq. (6.29). This result is shown in Figure 6-25. The system consists of a

leak of $C_d A_L = 0.00014 \text{ m}^2$ ($C_d A_L / A = 1.98 \times 10^{-3}$) at $x_L^* = 0.7$ in a frictionless pipe of 2000 m. The result of Eq. (6.29) was compared to the output from the numerical model with good agreement between the two, thus validating Eq. (6.29). Note that if the approximation made between Eqs. (6.28) and (6.29) was violated by the size of the leak then additional oscillatory frequency components will be present in the peak values. When these peak values are used in the leak detection procedure (see Section 6.5), the additional frequency components may indicate minute leaks at erroneous positions in the pipe, but the accuracy in locating the real leak will not be compromised.

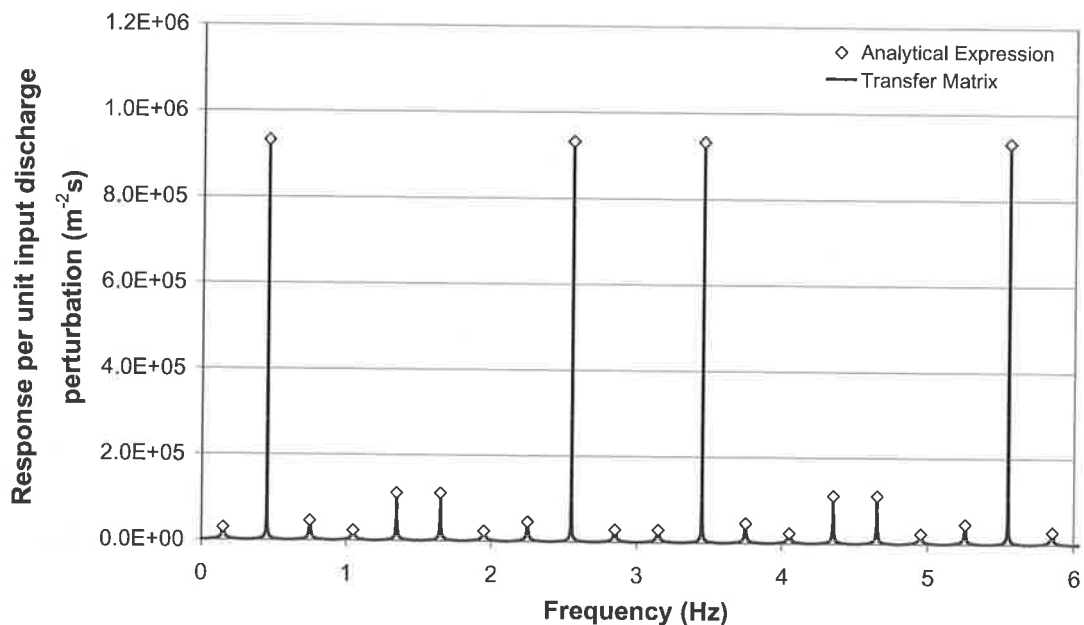


Figure 6-25 – Comparison between Eq. (6.29) and the transfer matrix model.

Anti-symmetric boundary with in-line valve open

A similar expression for the head response can be derived for the case where an anti-symmetric pipeline has an open (yet loss incurring) valve at the downstream boundary. This situation can arise when the in-line downstream valve is throttled, generating a high impedance boundary while maintaining a flow through the pipeline. As only the boundary condition is changed from the previous situation (Figure 6-23), the entries for the transfer matrix, U , remain unchanged and the head response upstream of the valve is solved using the new valve boundary condition. From Chaudhry (1987), the magnitude of the head and discharge oscillation upstream of the valve can be related by the linearised orifice equation,

$$-\frac{2\Delta H_{V0}}{Q_{V0}}q_b + h_b = 0 \quad (6.30)$$

Substituting Eq. (6.30) into the expanded form of the general transfer matrix equation relating the upstream/downstream head and discharge oscillations, Eq. (6.5) becomes

$$\frac{h_b Q_{V0}}{2\Delta H_{V0}} = U_{11}q_a + U_{13} \quad (6.31)$$

Combining this with Eq. (6.6),

$$h_b = \frac{U_{13} - \frac{U_{23}U_{11}}{U_{21}}}{\left(\frac{Q_{V0}}{2\Delta H_{V0}} - \frac{U_{11}}{U_{21}} \right)} \quad (6.32)$$

For an intact pipeline $U_{11} = 0$, the values of the peaks in the FRF are given by

$$h_b = \frac{2\Delta H_{V0}}{Q_{V0}} \quad (6.33)$$

Eq. (6.33) describes the FRF peaks for an intact and frictionless length of pipeline and the peak magnitudes are frequency independent, as is illustrated in Eq. (6.14) for the case where the downstream valve is closed. The validity of Eq. (6.33) is shown in Figure 6-26 and the expression provides a good match to the output of the transfer matrix model. In the case where a leak exists in the system, the entries (1,1) and (2,1) of the transfer matrix are given by Eqs. (6.24) and (6.25), respectively. The head response is now given as

$$h_b = \frac{1}{\left(\frac{Q_{V0}}{2\Delta H_{V0}} - \frac{ia}{gA} \left((-1)^{m+1} + (-1)^{m+1} \frac{ia}{gA} \frac{Q_{L0}}{4(H_{L0} - z_L)} \sin(2mx_L^* \pi - \pi x_L^*) \right) \right)} \quad (6.34)$$

Using $(aQ_{L0})/(4gA(H_{L0}-z_L)) \ll 1$, the expression simplifies to

$$|h_b| = \frac{1}{\left(\frac{Q_{V0}}{2\Delta H_{V0}} + \frac{Q_{L0}}{4(H_{L0} - z_L)} [1 - \cos(2m\chi_L^* \pi - \pi\chi_L^*)] \right)} \quad (6.35)$$

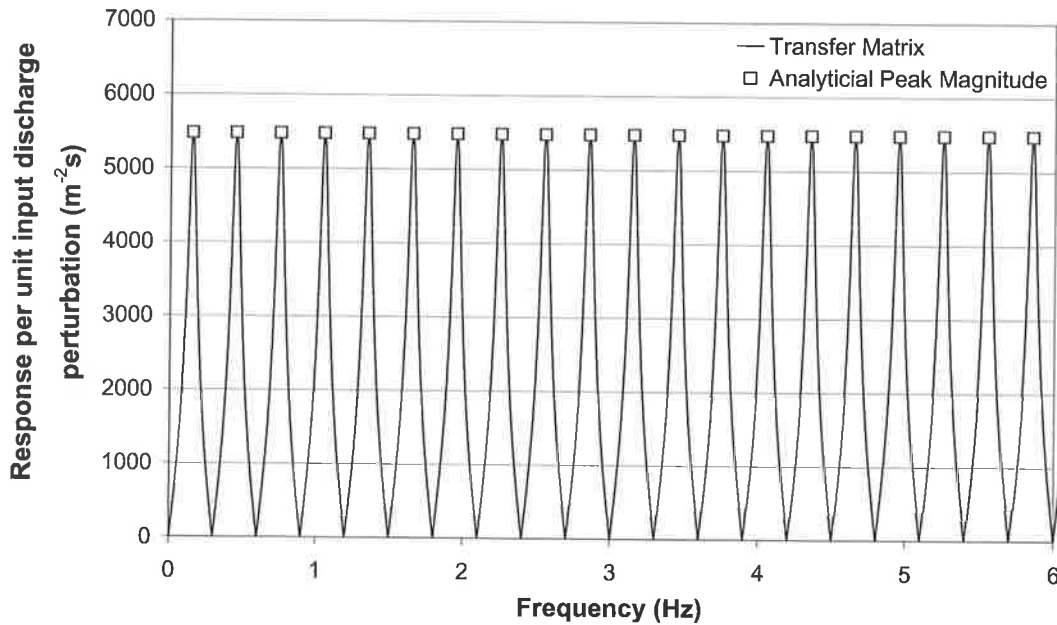


Figure 6-26 – Comparison between analytical peak magnitudes described by Eq. (6.33) and the transfer matrix model.

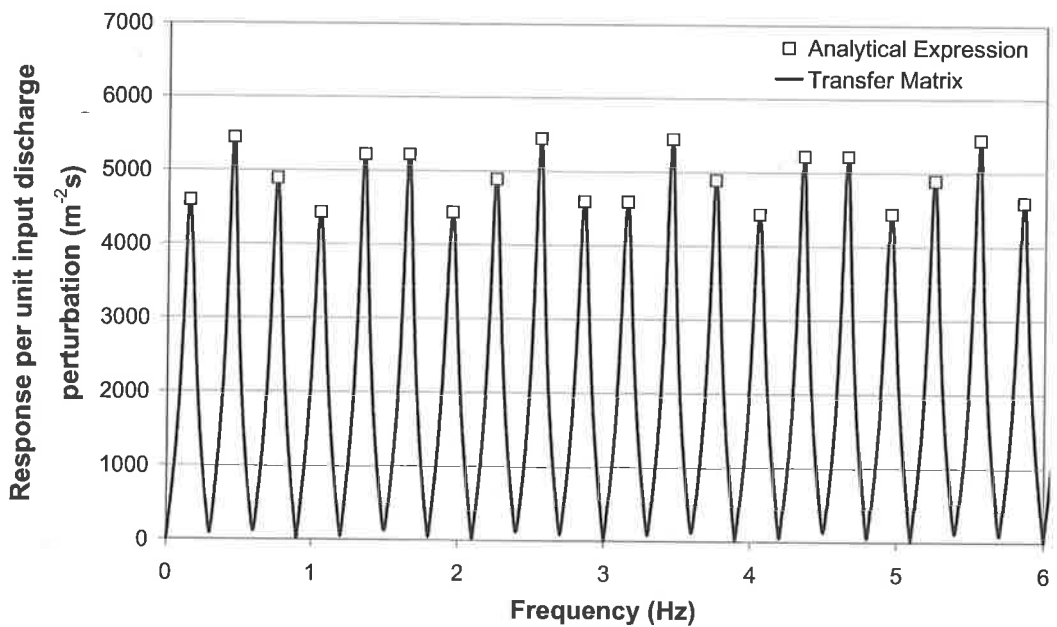


Figure 6-27 – Comparison between analytical peak magnitudes described by Eq. (6.35) and the transfer matrix model.

The peaks of the FRF in a leaking pipeline oscillate in a sinusoidal like pattern as shown in Eq. (6.35). The results agree with the transfer matrix model in Figure 6-27 validating the form of the derived Eq. (6.35). A similar set of equations can be derived for cases where the system boundaries are identical, giving a symmetric system.

6.4.2 Symmetric boundary

Consider the symmetric system in Figure 6-28. The transient source and measurement point are located at the midpoint of the system. The transient source is modelled as a unit discharge oscillation with the transfer matrix given by Eq. (6.11). As in the previous cases, the expressions relating the head and discharge oscillations at the extremities of the system are given by Eqs. (6.5) and (6.6).

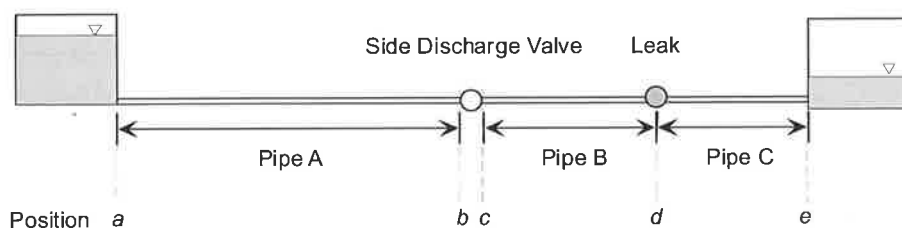


Figure 6-28 – System configuration used for the derivation of the leak-induced modification on a symmetric boundary system.

By substituting the reservoir boundary conditions ($h_a, h_e = 0$), Eq. (6.11) is used to solve for the discharge oscillation at the upstream boundary,

$$q_a = \frac{-U_{23}}{U_{21}} \quad (6.36)$$

The magnitude of the head oscillation at the transient source is determined by multiplying the upstream boundary head and discharge oscillation into the field matrix of pipe section A as indicated in Eq. (6.3) giving

$$h_b = h_c = \frac{ia \sin\left(\frac{l_a \omega}{a}\right) U_{23}}{gA U_{21}} \quad (6.37)$$

When no leak exists in the pipeline, the entries of the transfer matrix, U , are

$$U_{23} = -\frac{ia}{gA} \sin\left(\frac{L\omega}{2a}\right) \quad (6.38)$$

$$U_{21} = -\frac{2ia}{gA} \cos\left(\frac{L\omega}{2a}\right) \sin\left(\frac{L\omega}{2a}\right) \quad (6.39)$$

For a symmetric system, the resonant peaks occur at

$$\omega_{th} = \frac{(2m-1)\pi a}{L} \quad (6.40)$$

Substituting Eq. (6.38), (6.39) and (6.40) into Eq. (6.37) gives

$$h_b = h_c = \frac{-\frac{ia}{gA} \sin\left(\frac{(2m-1)\pi}{2}\right)}{-2 \cos\left(\frac{(2m-1)\pi}{2}\right)} = \infty \quad (6.41)$$

As in the case for an anti-symmetric system, the peaks of the FRF in an intact system are frequency independent and all peaks are of the same value. This finding is illustrated in Figure 6-29.

In the case where a leak exists in the system, the entries of the transfer matrix, U , are given by

$$U_{23} = -\frac{ia}{gA} \left(\sin\left(\frac{(l_b + l_c)\omega}{a}\right) \right) + \frac{Q_{L0}}{2(H_{L0} - z_L)} \left(\frac{a}{gA}\right)^2 \sin\left(\frac{l_b \omega}{a}\right) \sin\left(\frac{l_c \omega}{a}\right) \quad (6.42)$$

$$U_{21} = \frac{-ia}{gA} \sin\left(\frac{(l_a + l_b + l_c)\omega}{a}\right) + \left(\frac{a}{gA}\right)^2 \frac{Q_{L0}}{2(H_{L0} - z_L)} \sin\left(\frac{l_c\omega}{a}\right) \left(\sin\left(\frac{(l_a + l_b)\omega}{a}\right)\right) \quad (6.43)$$

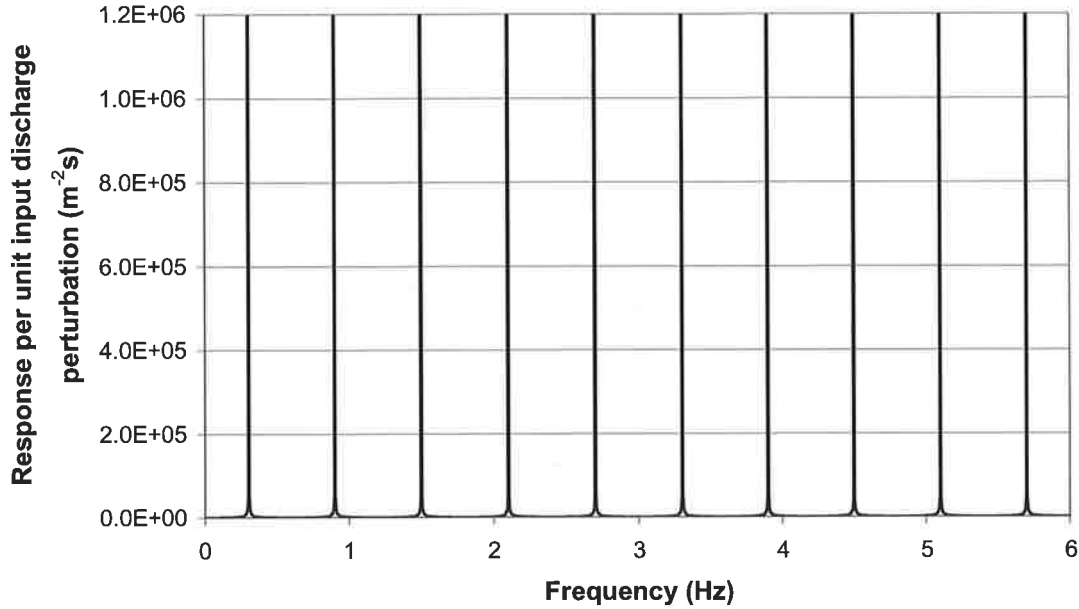


Figure 6-29 – FRF from a frictionless pipeline in a symmetric configuration.

Substituting Eq. (6.40) into Eqs. (6.42) and (6.43) gives

$$U_{23} = -\frac{ia}{gA} \left(\sin\left(\frac{(l_b + l_c)}{L}(2m-1)\pi\right) \right) + \frac{Q_{L0}}{2(H_{L0} - z_L)} \left(\frac{a}{gA}\right)^2 \sin\left(\frac{l_b}{L}(2m-1)\pi\right) \sin\left(\frac{l_c}{L}(2m-1)\pi\right) \quad (6.44)$$

$$U_{21} = \left(\frac{a}{gA}\right)^2 \frac{Q_{L0}}{2(H_{L0} - z_L)} \sin\left(\frac{l_c}{L}(2m-1)\pi\right) \left(\sin\left(\frac{(l_a + l_b)}{L}(2m-1)\pi\right) \right) \quad (6.45)$$

Denoting $l_c / L = x_L^*$ and $(l_a + l_b) / L = (1 - x_L^*)$ and knowing $l_b + l_c = L / 2$,

$$U_{23} = -\frac{ia}{gA} (-1)^{m+1} + \frac{Q_{L0}}{2(H_{L0} - z_L)} \left(\frac{a}{gA}\right)^2 \sin\left(\left(\frac{1}{2} - x_L^*\right)(2m-1)\pi\right) \sin(x_L^*(2m-1)\pi) \quad (6.46)$$

$$U_{21} = \left(\frac{a}{gA}\right)^2 \frac{Q_{L0}}{2(H_{L0} - z_L)} \sin(x_L^*(2m-1)\pi) \left(\sin\left((1 - x_L^*)(2m-1)\pi\right) \right) \quad (6.47)$$

Using the trigonometric product identity,

$$U_{23} = -\frac{ia}{gA}(-1)^{m+1} + \frac{Q_{L0}}{4(H_{L0} - z_L)} \left(\frac{a}{gA}\right)^2 \left(\cos\left(\left(\frac{1}{2} - 2x_L^*\right)(2m-1)\pi\right)\right) \quad (6.48)$$

$$U_{21} = \left(\frac{a}{gA}\right)^2 \frac{Q_{L0}}{4(H_{L0} - z_L)} \left((-1)^m + \cos\left((2x_L^* - 1)(2m-1)\pi\right)\right) \quad (6.49)$$

Simplifying Eq. (6.49) using the trigonometric argument sum identity gives

$$U_{21} = \left(\frac{a}{gA}\right)^2 \frac{Q_{L0}}{4(H_{L0} - z_L)} \left((-1)^m + (-1)^{m+1} \cos(4\pi mx_L^* - 2x_L^*\pi)\right) \quad (6.50)$$

Substituting Eqs.(6.48) and (6.50) into Eq. (6.37) gives the head response at the transient source,

$$h_b = \frac{1 + (-1)^{m+1} \frac{iQ_{L0}a}{4(H_{L0} - z_L)gA} \left(\cos\left(\left(\frac{1}{2} - 2x_L^*\right)(2m-1)\pi\right)\right)}{\frac{Q_{L0}}{4(H_{L0} - z_L)} \left((-1)^m + (-1)^{m+1} \cos(4\pi mx_L^* - 2x_L^*\pi)\right)} \quad (6.51)$$

As $(aQ_{L0})/(4gA(H_{L0} - z_L)) \ll 1$, the expression is simplified to

$$h_b = \frac{1}{\frac{Q_{L0}}{4(H_{L0} - z_L)} \left((-1)^m + (-1)^{m+1} \cos(4\pi mx_L^* - 2x_L^*\pi)\right)} \quad (6.52)$$

and the magnitude of the head oscillation at the midpoint of the pipeline is

$$|h_b| = \frac{1}{\frac{Q_{L0}}{4(H_{L0} - z_L)} \left(1 - \cos(4\pi mx_L^* - 2x_L^*\pi)\right)} \quad (6.53)$$

Eq. (6.53) indicates that the presence of a leak introduces a sinusoidal component to the harmonic peak magnitudes. Due to the symmetry of the system, the same equation applies for a leak located at the other side of the transient source. Eq. (6.53) is a good match to the transfer matrix model (refer to Figure 6-30).

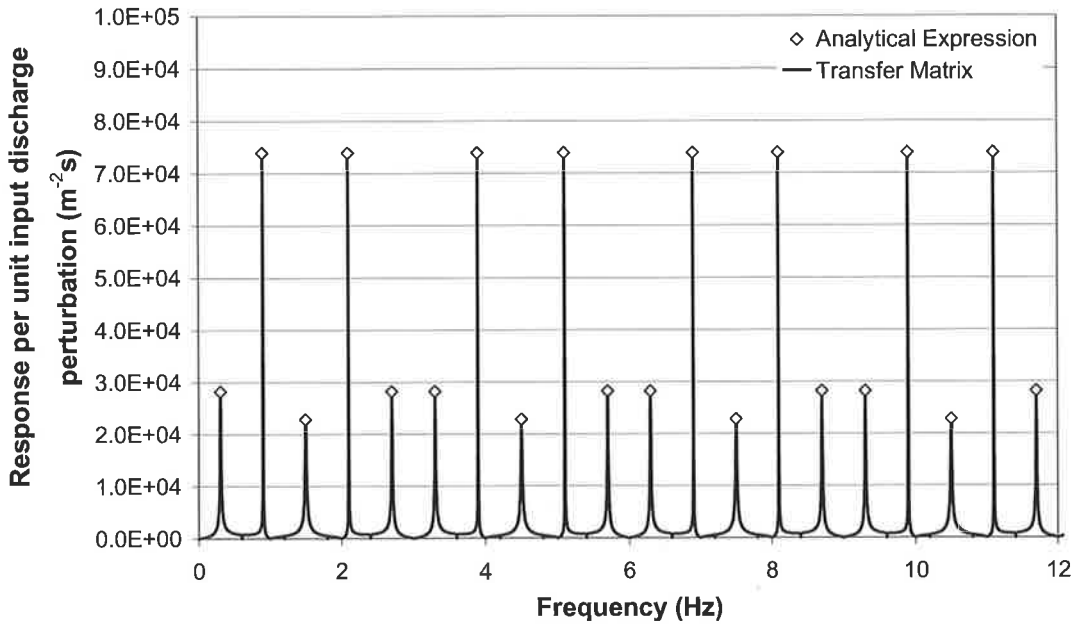


Figure 6-30 – Comparison between analytical peak magnitudes described by Eq. (6.53) and the transfer matrix model.

This section shows the analytical expressions describing the peaks of the FRF under anti-symmetric and symmetric system configurations. In all cases, the peak magnitudes in the FRF from an intact pipe are frequency independent and constant. In the case where a leak exists in the system, the peaks of the FRF are frequency-dependent, given by Eq. (6.29), (6.35) and (6.53) for different boundary conditions. The next section illustrates how this oscillation can be used to determine the location and the size of the leak.

6.5 ANALYTICAL TECHNIQUE OF LEAK DETECTION

The effects of a leak on the FRF from an anti-symmetric system with a closed downstream valve, an anti-symmetric system with a throttled downstream valve and a symmetric system are repeated here as Eq. (6.54), (6.55) and (6.56), respectively.

$$|h_b| = \frac{1}{\frac{Q_{L0}}{4(H_{L0} - z_L)} [1 - \cos(2mx_L^* \pi - \pi x_L^*)]} \quad (6.54)$$

$$|h_b| = \frac{1}{\frac{Q_{V0}}{2\Delta H_{V0}} + \frac{Q_{L0}}{4(H_{L0} - z_L)} [1 - \cos(2mx_L^* \pi - \pi x_L^*)]} \quad (6.55)$$

$$|h_b| = \frac{1}{\frac{Q_{L0}}{4(H_{L0} - z_L)} (1 - \cos(4\pi mx_L^* - 2x_L^* \pi))} \quad (6.56)$$

Using a generic cosine function in t , the form of the function is

$$f(t) = A \cos(2\pi Bt - C) \quad (6.57)$$

where A is the amplitude of the oscillation, B is its frequency in units of $1/t$ and C is the starting phase of the oscillation at $t = 0$. The derived equations [Eqs. (6.54), (6.55) and (6.56)] have oscillatory terms of a frequency—given as the coefficient to m , where m is the peak number in the FRF (e.g. first, second, third peak)—equal to x_L^* , (the dimensionless leak position) for the anti-symmetric cases and $2x_L^*$ for the symmetric case. The oscillation frequency is measured in terms of “per peak interval”, $1/m$. The phase of the oscillatory function is $\pi + \pi x_L^*$ for the anti-symmetric case and $\pi + 2\pi x_L^*$ for the symmetric case. The value of the phase takes into account the phase shift ($+\pi$) generated by the negative sign in front of the cosine terms in Eqs. (6.54), (6.55) and (6.56). For all cases, the amplitude of the oscillation is $Q_{L0} / 4(H_{L0} - z_L)$.

The extraction of this oscillatory function and determination of its frequency, phase and amplitude can lead to the correct location and size of a leak. However, as the frequency of this oscillation is the dimensionless leak position, x_L^* , which can range between 0 to 1.0 (0 = upstream boundary, 1 = downstream boundary), the problem of frequency aliasing must be discussed.

6.5.1 Aliasing of leak-induced oscillations

While Eqs. (6.54), (6.55) and (6.56) indicate that the peaks of the FRF varies sinusoidally, the actual manifestation of this sinusoid suffers distortions from aliasing where the frequency and phase of an oscillation are changed by the discrete sampling process. Given a certain sampling frequency, there is a finite limit to the highest frequency that can be detected in the data. This limit is the frequency of oscillation that completes a full period in the space of three adjacent data points and is equal to half the sampling frequency. This result is the *sampling theorem*, illustrated in Figure 6-31. For a given sampling frequency, Figure 6-31(a) illustrates this highest frequency, known as the *Nyquist frequency*. Any oscillation with a frequency higher than the Nyquist frequency is not detected and is aliased to a lower frequency oscillation as shown in Figure 6-31(b) and (c).

The relationship between the frequency of the original and aliased signals is given in Ambardar (1999) as

$$\omega_{signal}^a = 2\omega_{nq} - \omega_{signal} \quad (6.58)$$

where ω_{signal}^a and ω_{signal} are the distorted and the original signal frequencies, respectively and ω_{nq} is the Nyquist frequency, equal to half the sampling frequency. Eq. (6.58) is derived for the case where, $\omega_{nq} < \omega_{signal} < 2\omega_{nq}$ and for this situation. The phase of the original signal undergoes a reversal after aliasing,

$$\phi_{signal}^a = -\phi_{signal} \quad (6.59)$$

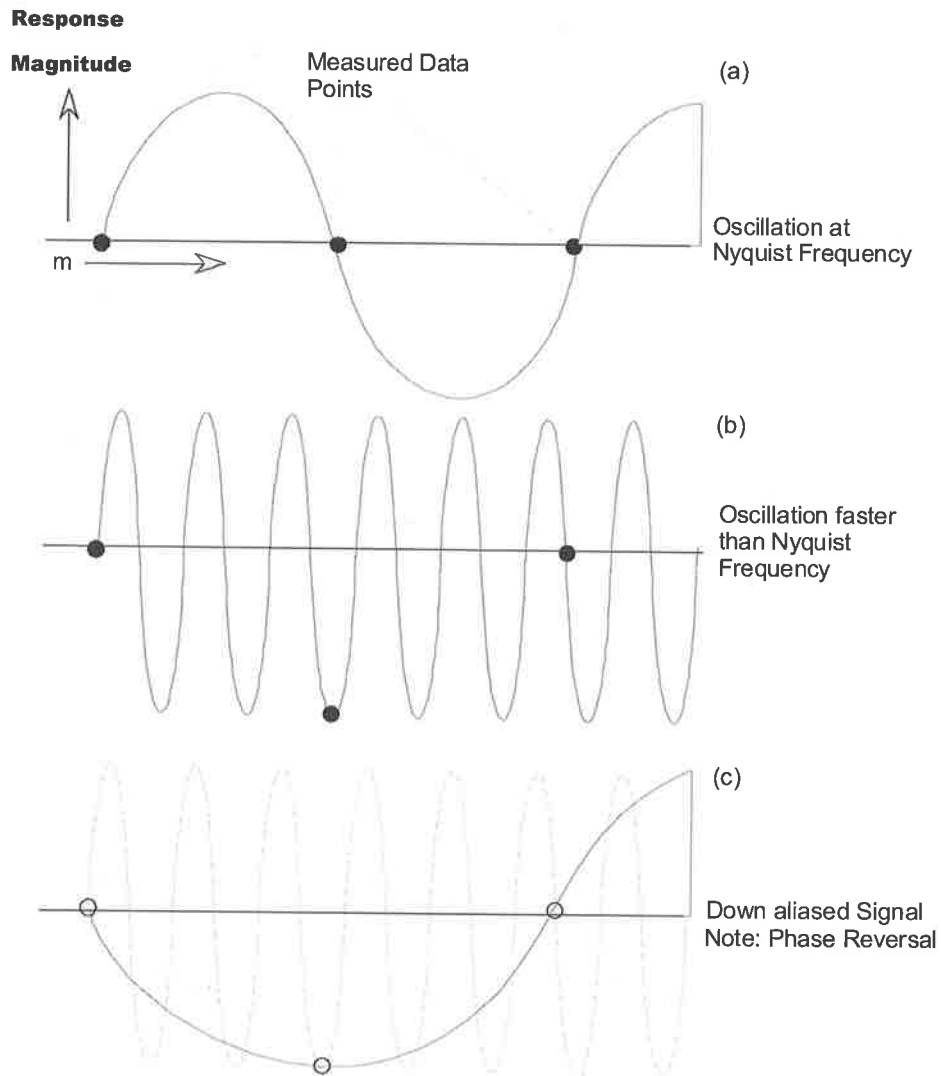


Figure 6-31 – An illustration of the sampling theorem for an oscillation taking place between three consecutive peak values and the effect of aliasing on high-frequency oscillations.

The continuous cosine functions in Eqs. (6.54), (6.55) and (6.56) are represented in the FRF by a series of discrete points spaced according to the fundamental frequency of the system. The observed oscillatory pattern is sampled with a frequency of 1.0, that is, one sample per peak number, m . The corresponding Nyquist frequency is 0.5, the highest detectable frequency in the peak values.

Eqs. (6.54), (6.55) and (6.56), show that the frequency of oscillation is x_L^* for anti-symmetric systems and $2 x_L^*$ for symmetric systems. The dimensionless leak position, x_L^* ,

carries a value between 0 (upstream boundary) and 1 (downstream boundary). In the symmetric system, a leak-induced oscillation at $x_L^* = 0.15$ looks identical to one located at $x_L^* = 0.85$ and the range of considered leak positions is limited to $0 < x_L^* < 0.5$ for this case.

Within this range of possible oscillation frequencies, if an oscillation has a frequency greater than 0.5 (Nyquist frequency), the original signal is aliased to a lower frequency in the range of 0 and 0.5, given by Eq. (6.58). For example, an oscillation frequency of 0.85 will appear in the data as an oscillation at frequency $= 1 - 0.85 = 0.15$. As the oscillation frequency is directly related to the leak position, x_L^* , the physical interpretation of this effect is that any observed frequency of oscillation is associated to a number different leak positions, some associated with an oscillation frequency below the Nyquist frequency and others above. The phase of the oscillation is used to determine whether the signal has undergone aliasing.

From Eq. (6.59) and Figure 6-31, a signal of a frequency in the range of $\omega_{nq} < \omega_{\text{signal}} < 2\omega_{nq}$ undergoes phase reversal at aliasing and can be used to indicate whether the original signal was oscillating with a frequency higher than the Nyquist frequency. Figure 6-32 illustrates the phase of the leak-induced oscillation for all possible leak positions. For example, if the oscillation frequency exceeds 0.5, the phase of the oscillation changes from $\pi + \pi x_L^*$ to $-(\pi + \pi x_L^*)$ for an anti-symmetric system. The phase of a non-aliased signal (frequency < 0.5) is in the 3rd quadrant of the unit circle (π to 1.5π) and for an aliased signal (frequency > 0.5) it is in the 1st quadrant (0 to 0.5π).

This result can be used to divide the unit circle into two zones, distinguishing aliased signals from non-aliased signals. As a typical phase spectrum for an oscillation has sharp discontinuities, the zones in Figure 6-32 are extended to account for possible errors in the phase prediction. Each zone is translated to a region in the pipe where the leak is located. These regions are shown in Figure 6-33.

In an anti-symmetric system the leak-induced oscillations have these properties:

1. The **frequency** of the leak-induced damping pattern **equals** x_L^* for $x_L^* < 0.5$ or $1 - x_L^*$ for $x_L^* > 0.5$

- The **phase** of the leak-induced damping pattern **equals** $\pm\pi(1+x_L^*)$ and the phase is located in zone I when $x_L^* < 0.5$ and in zone II when $x_L^* > 0.5$.
- The **amplitude** of the leak-induced damping pattern **equals** $Q_{L0} / (4(H_{L0} - z_L))$

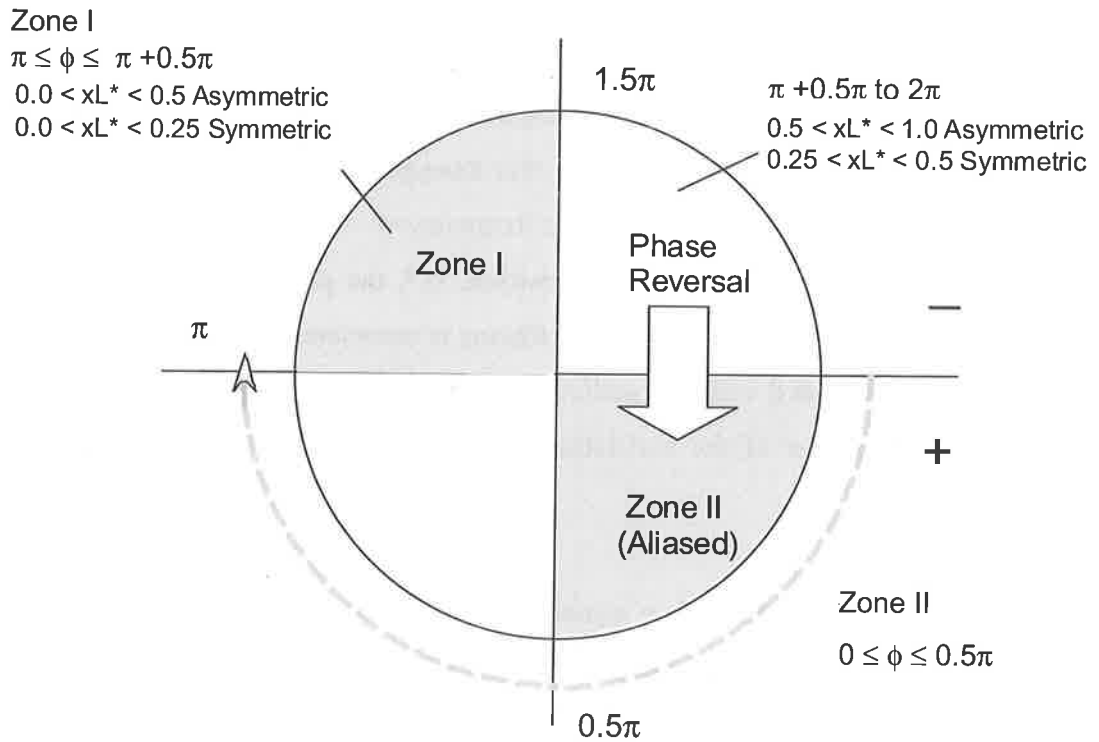


Figure 6-32 – Phase diagram of the different leak positions.

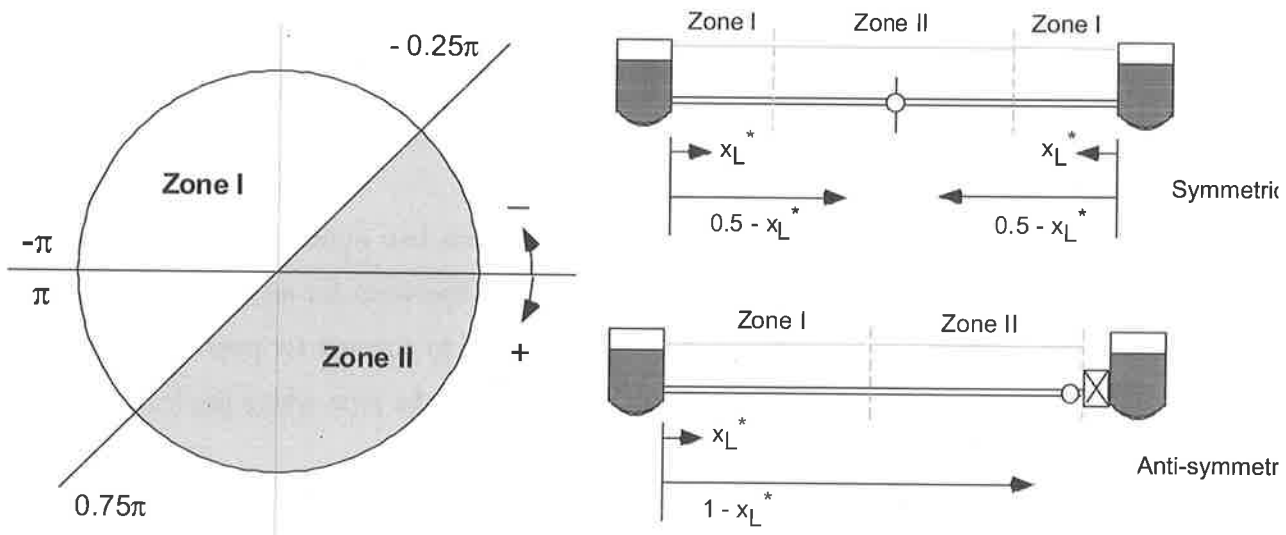


Figure 6-33 – Phase zones to identify leak location.

For the symmetric system configuration:

1. The **frequency** of the leak-induced damping pattern **equals** $2 x_L^*$ for $x_L^* < 0.25$ and $1 - 2 x_L^*$ for $0.5 > x_L^* > 0.25$. Due to the symmetry of the system, for $x_L^* > 0.5$, the results would be identical to that of $x_L^* = 1 - x_L^*$.
2. The **phase** of the leak-induced damping pattern **equals** $\pm\pi (1 + 2 x_L^*)$ and the phase is located in zone I when $x_L^* < 0.25$, $x_L^* > 0.75$ and in zone II when $0.25 < x_L^* < 0.75$.
3. The **amplitude** of the leak-induced damping pattern **equals** $Q_{L0} / (4 (H_{L0} - z_L))$

The sinusoidal function is imposed on the denominator of Eqs. (6.54), (6.55) and (6.56) and for an accurate extraction of the leak-induced oscillation, the peak magnitudes must be inverted.

6.5.2 Proposed leak detection method

The proposed analytical method of leak detection is as follows:

1. Extract the FRF from the pipeline as described in Chapter 5.
2. Select the peaks of the FRF and invert the peak magnitudes.
3. Extract the frequency content of the inverted peak magnitudes and determine whether dominant oscillations exist in the data; if so, a leak is present in the pipe. The method for extracting frequency components from peak data may vary and can involve a Fourier transform of the data. An alternative method of dominant frequency extraction is presented later in the thesis.
4. Determine the frequency of the dominant oscillation, ω_{signal}^d , which provides a number of different possible leak positions as shown in Table 6-2 for both anti-symmetric and symmetric boundaries.
5. Determine whether the phase of the oscillation is in Zone I or Zone II of Figure 6-33.
6. Reduce the number of possible leak locations to one for the anti-symmetric case and two for the symmetric case (at mirrored positions as illustrated in Figure 6-33). The predicted leak locations for each different boundary configuration are shown in Table 6-3.

7. Once the location of the leak is determined, the steady state (initial) head at the leak, H_{L0} , can be approximated assuming a linear hydraulic grade line between the system boundaries. As the amplitude of the oscillation is equal to $Q_{L0} / 4(H_{L0} - z_L)$, the discharge out of the leak can be calculated and the lumped leak parameter found using the orifice equation,

$$C_d A_L = \frac{Q_{L0}}{\sqrt{2g(H_{L0} - z_L)}} \quad (6.60)$$

Table 6-2 – Possible leak positions using the frequency of the oscillation alone.

Possible leak positions (anti-symmetric)		Possible leak positions (symmetric)	
1	$x_L^* = \omega^d_{\text{Signal}}$	1	$x_L^* = \omega^d_{\text{Signal}} / 2$
		2	$x_L^* = 1 - \omega^d_{\text{Signal}} / 2$
2	$x_L^* = 1 - \omega^d_{\text{Signal}}$	3	$x_L^* = (1 - \omega^d_{\text{Signal}}) / 2$
		4	$x_L^* = 1 - (1 - \omega^d_{\text{Signal}}) / 2$

Table 6-3 – Possible leak positions using both phase and frequency of the oscillation.

Possible leak positions (anti-symmetric)		Possible leak positions (symmetric)	
1	$x_L^* = \omega^d_{\text{Signal}}$	1	$x_L^* = \omega^d_{\text{Signal}} / 2$
		2	$x_L^* = 1 - \omega^d_{\text{Signal}} / 2$
2	$x_L^* = 1 - \omega^d_{\text{Signal}}$	3	$x_L^* = (1 - \omega^d_{\text{Signal}}) / 2$
		4	$x_L^* = 1 - (1 - \omega^d_{\text{Signal}}) / 2$

Zone I
Zone II

6.6 NUMERICAL VALIDATION

The method of leak detection proposed in the previous section is validated numerically using the simulation pipeline influenced by steady friction. Leaks occurring in both types of system configurations (anti-symmetric and symmetric) are investigated using the transfer matrix model. For illustrative purposes, the oscillatory components in the inverted peak magnitudes are extracted using a Fourier transform of a large number of data points (4096). This number of data points provides a clear indication of the spectral content of the peak variations.

The validity of the leak detection procedure for the anti-symmetric boundary is illustrated in this example. A leak of a $C_d A_L = 1.4 \times 10^{-4} \text{ m}^2$ ($C_d A_L / A = 1.98 \times 10^{-3}$) is placed at a distance 1511.7 m from the upstream reservoir ($x_L^* = 0.767$) in the anti-symmetric numerical pipeline. The downstream valve is initially closed and remains closed during the transient event. The transient source and the measurement transducer are located next to the closed downstream valve (refer to Figure 6-34). The FRF from the system is shown in Figure 6-35. A distinctive periodic oscillation in the peak values is observed, indicating a leak in the system.

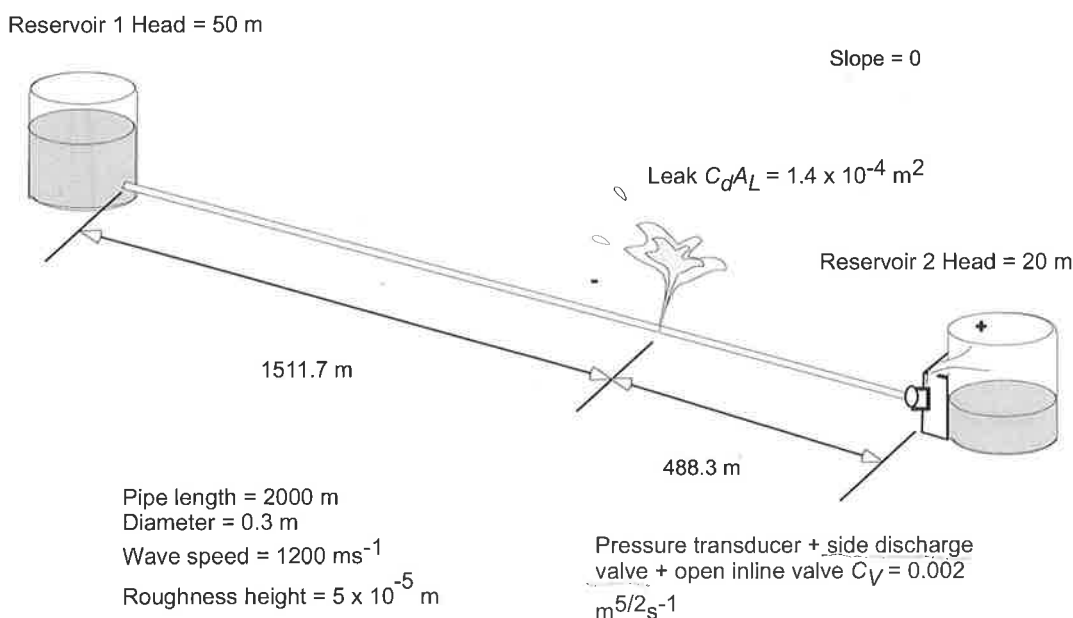


Figure 6-34 – System configuration for numerical validation of the first anti-symmetric system.

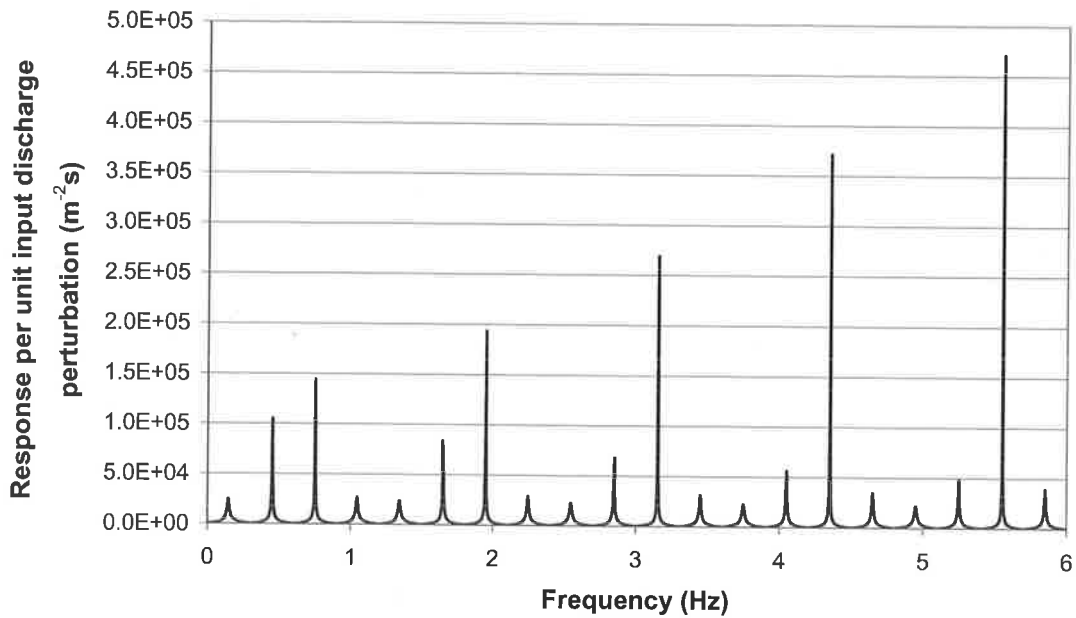


Figure 6-35 – FRF of the pipeline containing a leak at $x_L^* = 0.7559$.

Extracting the peak magnitudes and inverting the values gives the result shown in Figure 6-36 and the inverted peak values are Fourier transformed to produce the spectral content in Figure 6-37.

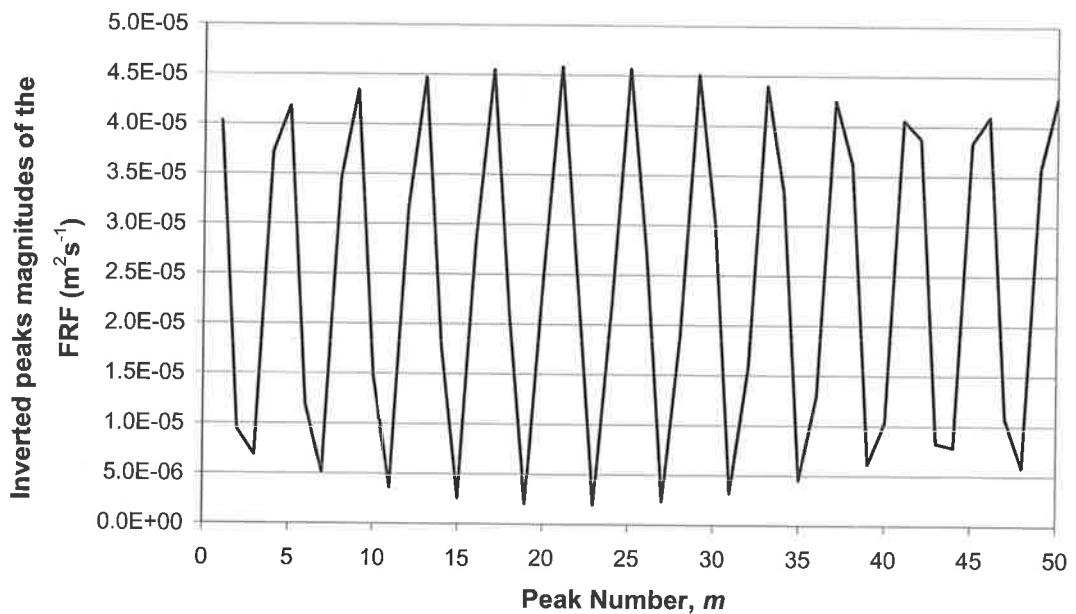


Figure 6-36 – Inverted peak magnitudes of the FRF of Figure 6-35.

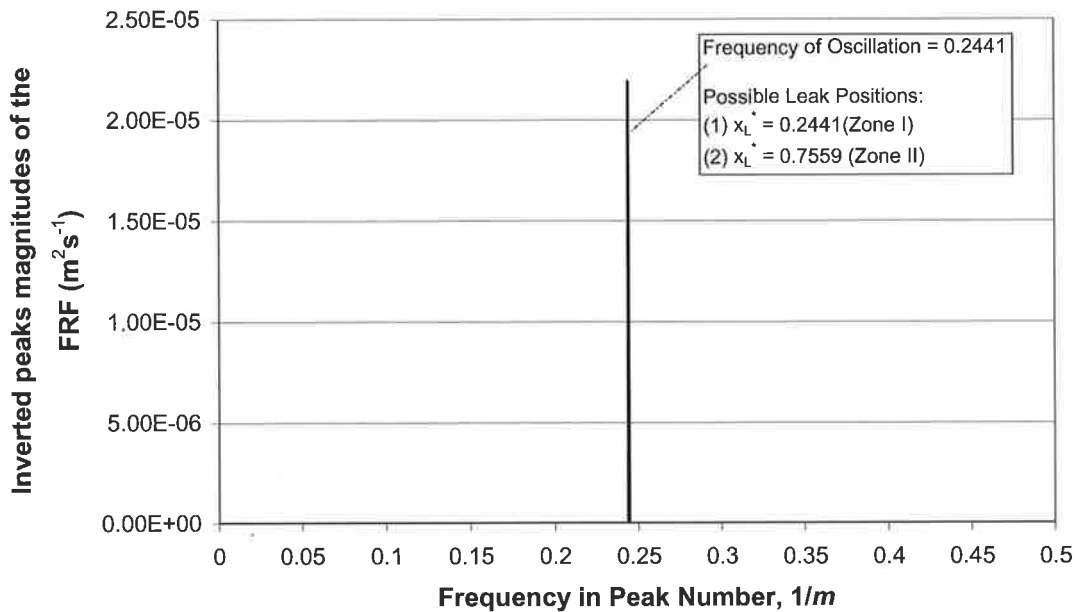


Figure 6-37 – Spectral content of Figure 6-36, showing a dominant leak-induced frequency that is associated with two possible leak positions.

Figure 6-37 shows that the inverted peak magnitudes in the FRF oscillate at a single frequency corresponding to $1/m = 0.2441$. From the previous section, this oscillation frequency is associated with two leak positions, one in Zone I of the pipe and one in Zone II. The two possible leak positions are in Figure 6-37. The phase of the oscillation is used to determine the correct position. The phase spectrum of the oscillation is in Figure 6-38 with the section corresponding to the oscillation frequency expanded in Figure 6-39. At the frequency of oscillation, the phase is equal to 0.767, placing the leak in Zone II according to Figure 6-33. The predicted leak position is $x_L^* = 0.756$ and corresponds to the true position.

From the spectral content of the inverted peak magnitudes, the amplitude of the leak-induced oscillation is $2.192 \times 10^{-5} \text{ m}^2\text{s}^{-1}$. Given the static condition, the head at the leak is approximately equal to the head at the upstream reservoir. Using $H_{L0} = 50 \text{ m}$ and the amplitude of the leak oscillation as $Q_{L0}/(4H_{L0} - z_L)$ with $z_L = 0$, the discharge out of the leak is $4.384 \times 10^{-3} \text{ m}^3\text{s}^{-1}$. Substituting this value into Eq. (6.60) gives the lumped leak parameter, $C_d A_L$, as $1.40 \times 10^{-4} \text{ m}^2$ ($C_d A_L / A = 1.98 \times 10^{-3}$) and is the correct size of the leak.

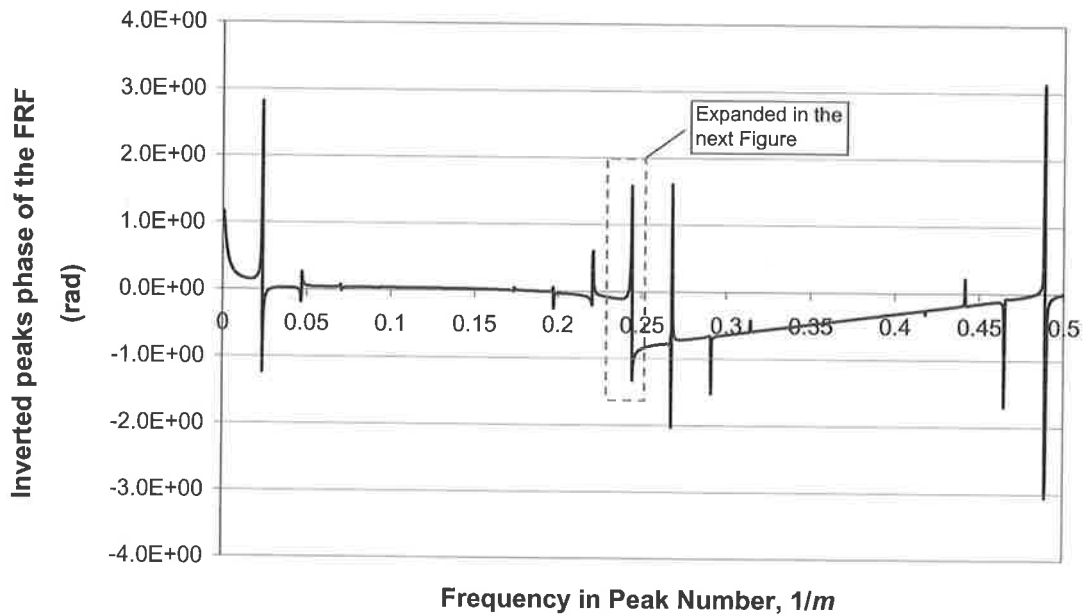


Figure 6-38 – Phase spectrum of Figure 6-36.

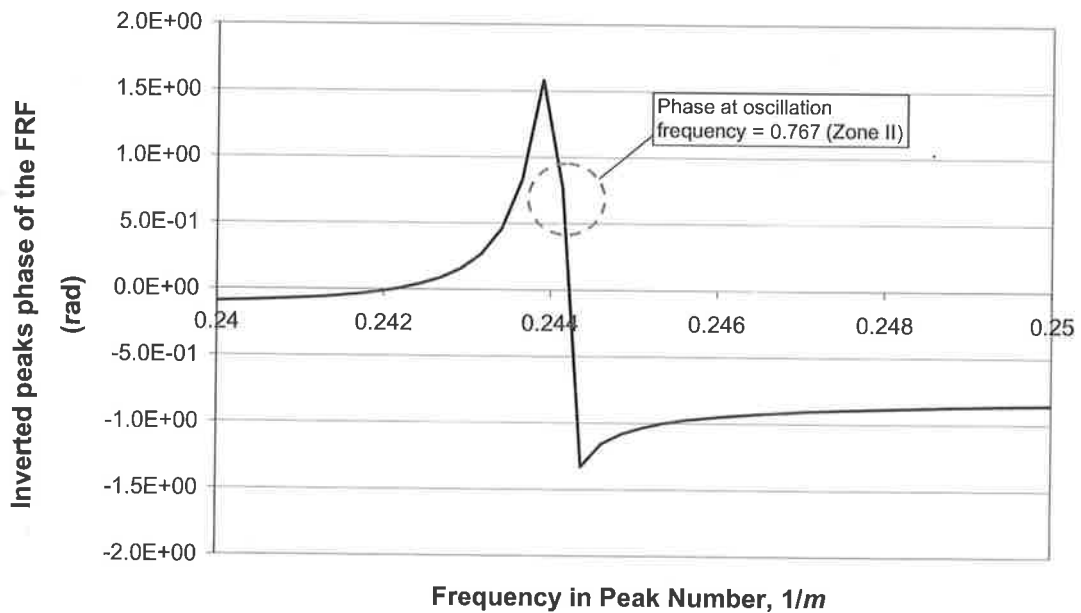


Figure 6-39 – Expanded phase spectrum from Figure 6-38.

Further tests were conducted with this system configuration and a summary of the results is shown in Figure 6-40 with the final leak size and position in Table 6-4. All tests indicate the validity of the technique for both leak sizing and position estimations. Similar tests were performed for the case where the downstream valve is opened ($C_V = 0.002 \text{ m}^{5/2} \text{ s}^{-1}$). Due to the high losses associated with this in-line valve, the system still behaves as an

anti-symmetric system. The results are in Figure 6-41 and Table 6-5. Again the technique was able to detect, locate and size the leak. The size of the leak was determined for each case based on a calculated steady H_L at the predicted leak position for the system assuming no leak exists. As this H_L is slightly different to the actual head at the leak, this discrepancy is carried through to the prediction of the leak size.

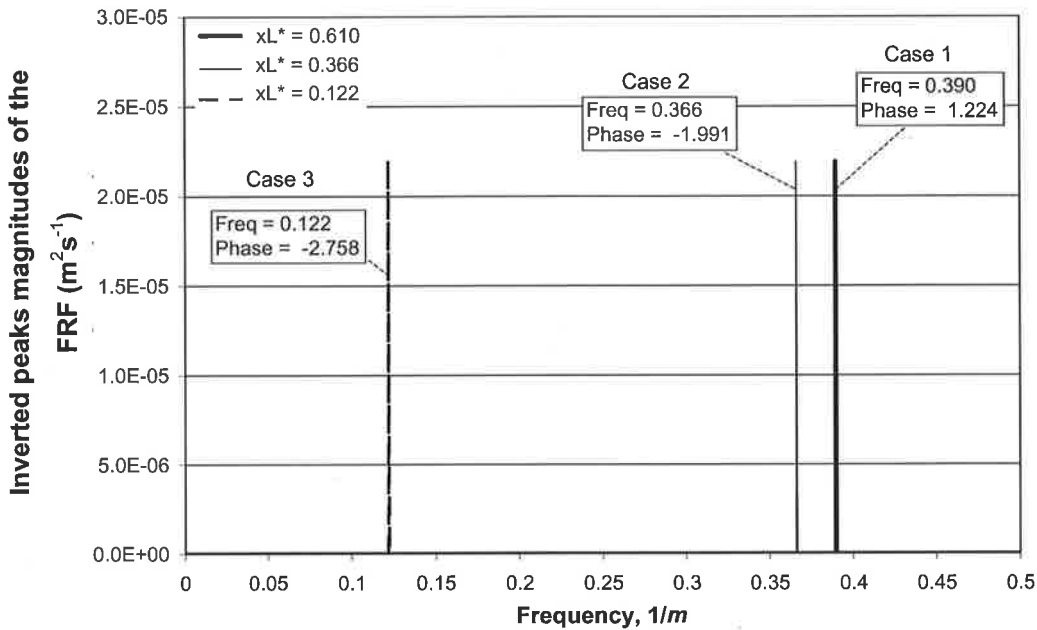


Figure 6-40 – Spectrum of inverted peak oscillations for different leak positions in a static anti-symmetric system.

Table 6-4 – Summary of leak detection in a static anti-symmetric system.

Case Number	True Leak Position	Predicted Leak Position	True Leak Size	Predicted Leak Size
1	$x_L^* = 0.610$	$x_L^* = 0.610$	$C_d A_L = 1.40 \times 10^{-4}$	$C_d A_L = 1.40 \times 10^{-4}$
2	$x_L^* = 0.366$	$x_L^* = 0.366$	$C_d A_L = 1.40 \times 10^{-4}$	$C_d A_L = 1.40 \times 10^{-4}$
3	$x_L^* = 0.122$	$x_L^* = 0.122$	$C_d A_L = 1.40 \times 10^{-4}$	$C_d A_L = 1.40 \times 10^{-4}$

Table 6-5 – Summary of leak detection in a flowing anti-symmetric system.

Case Number	True Leak Position	Predicted Leak Position	True Leak Size	Predicted Leak Size
1	$x_L^* = 0.122$	$x_L^* = 0.122$	$C_d A_L = 0.7 \times 10^{-4}$	$C_d A_L = 0.71 \times 10^{-4}$
2	$x_L^* = 0.244$	$x_L^* = 0.244$	$C_d A_L = 1.40 \times 10^{-4}$	$C_d A_L = 1.40 \times 10^{-4}$
3	$x_L^* = 0.829$	$x_L^* = 0.829$	$C_d A_L = 1.40 \times 10^{-4}$	$C_d A_L = 1.41 \times 10^{-4}$

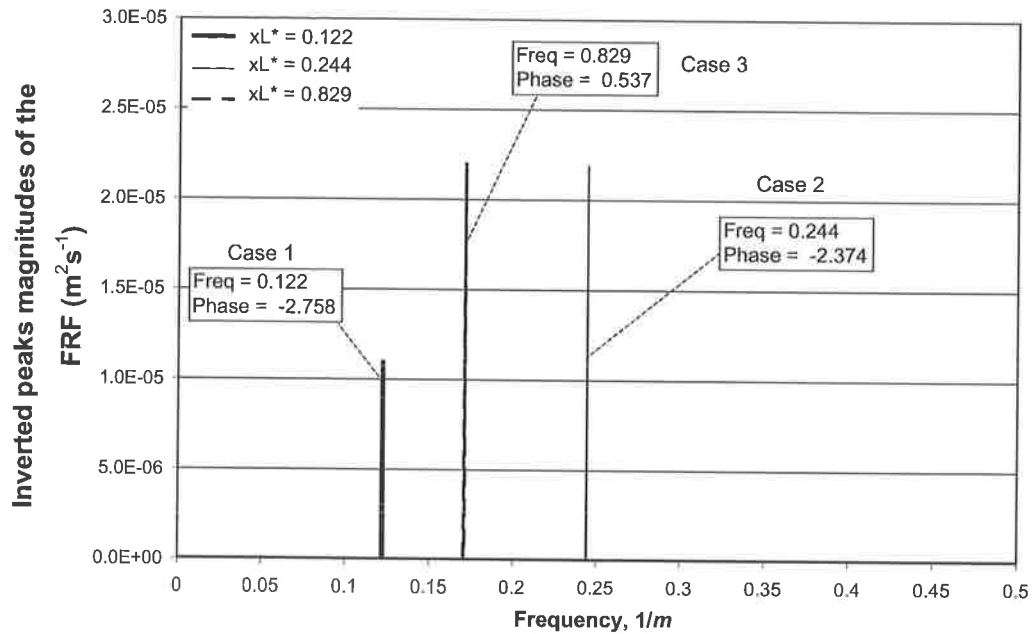


Figure 6-41 – Spectrum of inverted peak oscillations for different leak positions in a flowing anti-symmetric system.

The validation of the technique under symmetric boundary conditions was conducted on the same numerical pipeline with the configuration in Figure 6-42. A leak of size $C_d A_L = 1.4 \times 10^{-4} \text{ m}^2$ ($C_d A_L / A = 1.98 \times 10^{-3}$) is located at $x_L^* = 0.634$ (1268 m from upstream boundary). The FRF for this situation is in Figure 6-43. The peaks of the FRF are inverted (Figure 6-44) and Fourier transformed to give the spectral content shown in Figure 6-45. Unlike the anti-symmetric case, the single frequency of oscillation determined from the spectrum provided four possible leak positions and the phase was once again used to narrow the selection.

The phase spectrum of the data is shown in Figure 6-46 with the phase of the oscillation equal to 0.817, indicating that the leak is in zone II. Its position is $x_L^* = 0.366$, or 0.634 and the second solution corresponds to the true position of $x_L^* = 0.634$. The size of the leak can be estimated using the same procedure as before. The magnitude of the frequency spike in Figure 6-45 is $2.806 \times 10^{-5} \text{ m}^2 \text{ s}^{-1}$. Approximating the HGL between the two reservoirs as a straight line, the head, H_{L0} , at the correct leak position is 31.0 m. Substituting this result into Eq. (6.60) gives the leak parameter as $1.41 \times 10^{-4} \text{ m}^2$, which corresponds to the true leak size, $C_d A_L = 1.40 \times 10^{-4} \text{ m}^2$ ($C_d A_L / A = 1.98 \times 10^{-3}$).

Reservoir 1 Head = 50 m

Slope = 0

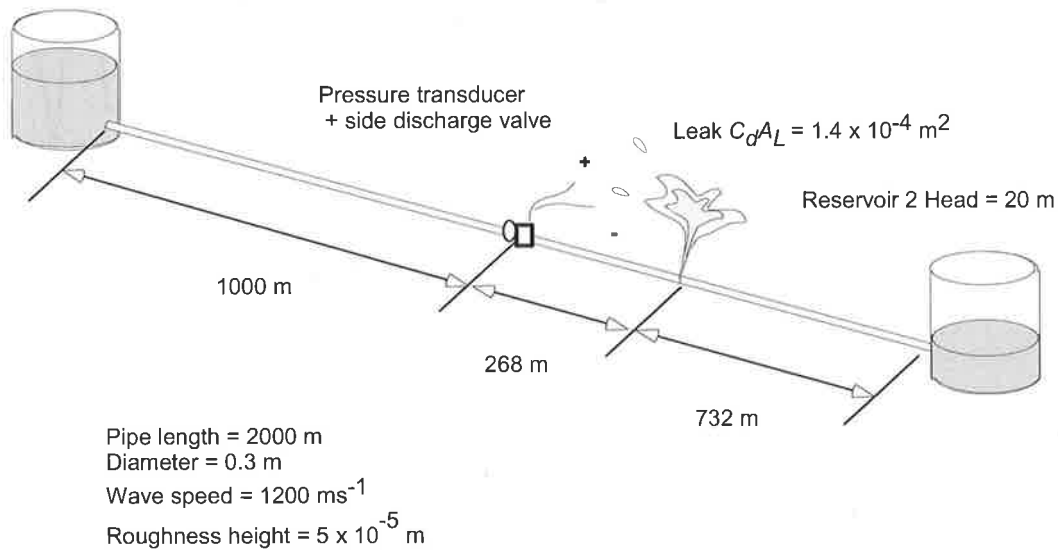


Figure 6-42 – System configuration for the numerical symmetric validation.

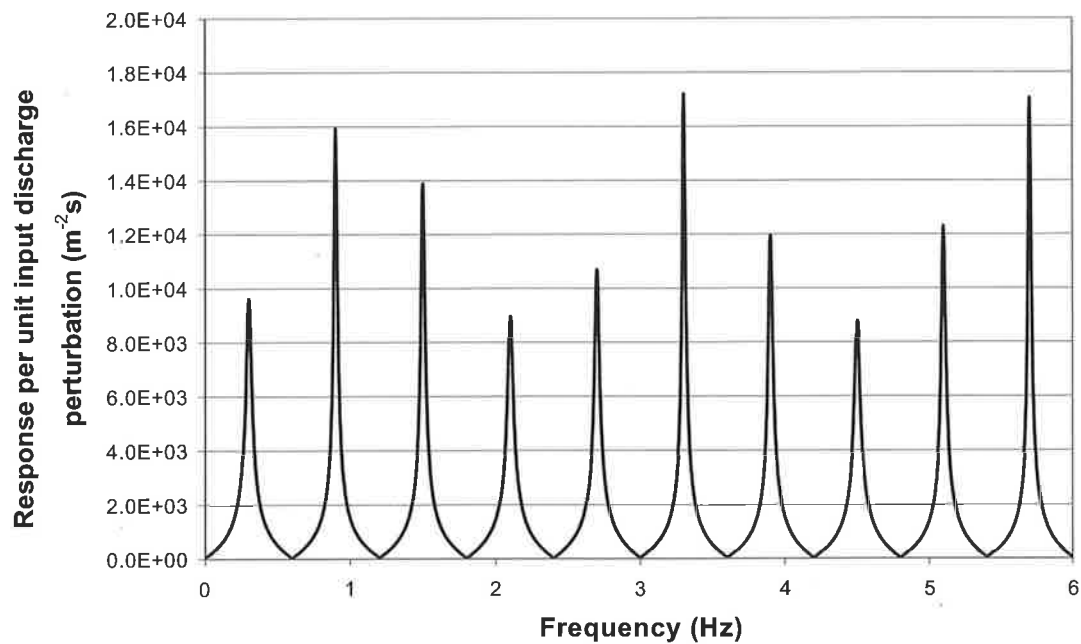


Figure 6-43 – FRF of leaking pipe in a symmetric system with leak located at $x_L^* = 0.634$.

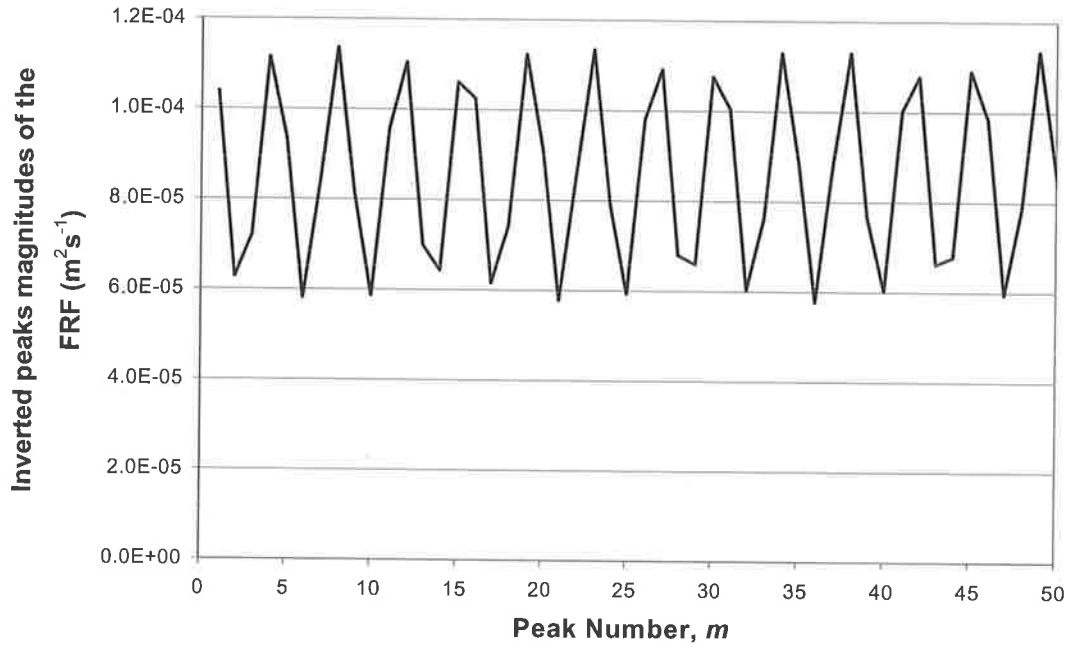


Figure 6-44 – Variation of the inverted peak magnitudes in the FRF of Figure 6-43.

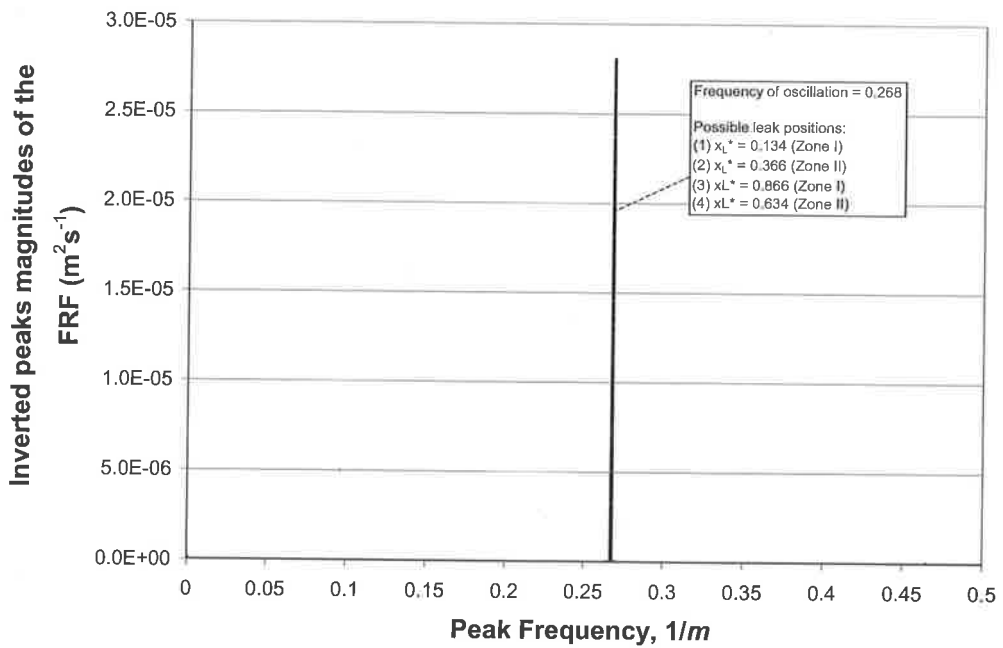


Figure 6-45 – Spectrum of inverted peak oscillations in a symmetric system.

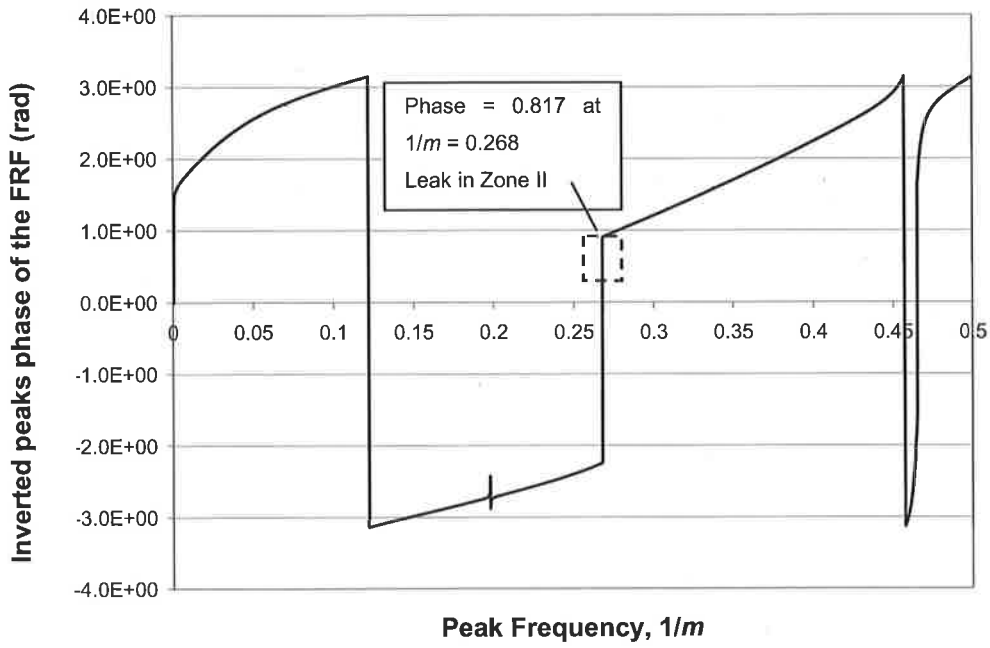


Figure 6-46 – Phase spectrum of inverted peak oscillations for symmetric system.

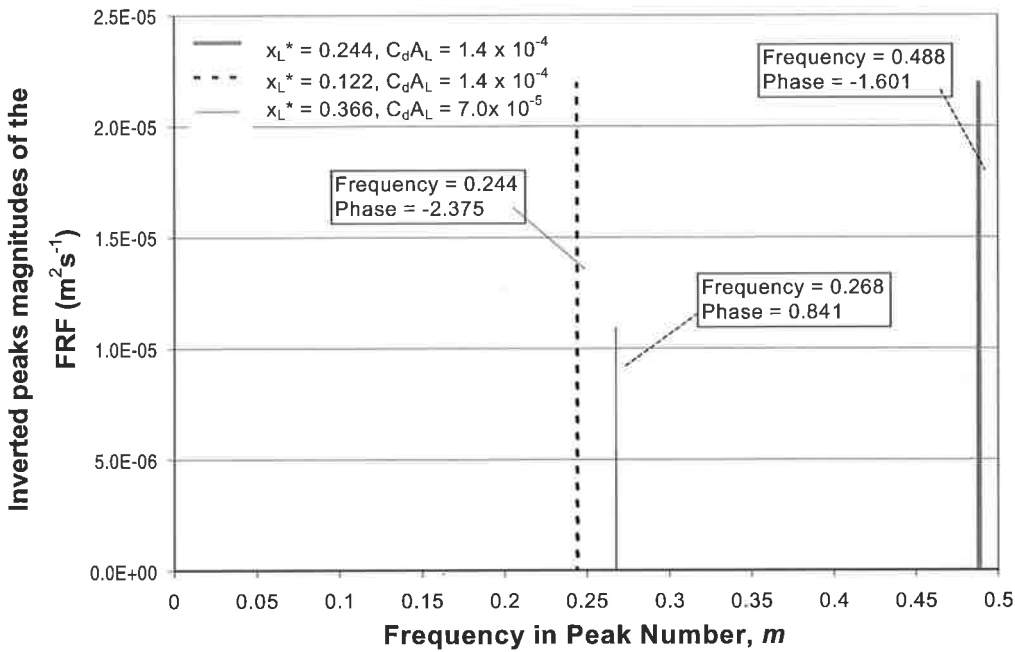


Figure 6-47 – Examples of leak detection in the symmetric system.

The results indicate that for each case the analytical technique of leak detection in the symmetric case is able to provide two possible locations of the leak with one being the correct solution and the other located at the mirror position of the first solution. Given that

the optimum positioning of the measurement station and the transient source is at the centre of the pipeline for a symmetric system, the true leak position cannot be identified. This is an intrinsic problem with the symmetric boundary condition.

This section has provided numerical validation of the proposed analytical leak detection technique and was tested under symmetric and anti-symmetric system boundary conditions. The following section investigates the use of the FRF for leak detection in a physical pipeline.

Table 6-6 – Summary of leak detection in the symmetric system.

Case Number	True Leak Position	Predicted Leak Position	True Leak Size	Predicted Leak Size
1	$x_L^* = 0.244$	$x_L^* = 0.244$ or 0.756	$C_d A_L = 1.40 \times 10^{-4}$	$C_d A_L = 1.41 \times 10^{-4}$
2	$x_L^* = 0.122$	$x_L^* = 0.122$ or 0.878	$C_d A_L = 1.40 \times 10^{-4}$	$C_d A_L = 1.41 \times 10^{-4}$
3	$x_L^* = 0.366$	$x_L^* = 0.366$ or 0.634	$C_d A_L = 0.70 \times 10^{-4}$	$C_d A_L = 0.71 \times 10^{-4}$

6.7 APPLICATION OF THE ANALYTICAL LEAK DETECTION TECHNIQUE IN A PHYSICAL SYSTEM

In the previous sections, three techniques were proposed for the detection of leaks using the FRF. Each of the proposed techniques was validated numerically and can detect and locate leaks in various system configurations. For the remainder of the chapter, the analytical method of leak detection forms the focus of investigation. The advantage of this approach is that the leak can be located exactly without the need for an accurate simulation model. Traditional transient leak detection based on inverse methods requires knowledge of system parameters such as friction factors and valve loss coefficients. Figure 5-57 shows that current numerical models are unable to accurately predict the frequency response function from a laboratory system. The analytical technique proposed here only requires the accurate extraction of the periodic oscillation in the peaks of the FRF. The base line about which this oscillation takes place (given by the absolute magnitude of the FRF) is irrelevant. Later in the thesis, the analytical method is extended to detect and locate multiple leaks in a pipeline. This ability is beyond the scope of the peak sequencing method and cannot be replicated using the inverse FRF technique without an accurate numerical model.

This section investigates how other physical phenomena in a pipeline can affect the shape of the FRF from a leaking pipeline. From Chapter 5, the FRF from the laboratory is affected by a number of factors. These factors include distortion caused by frequency-dependent friction and input signal bandwidth.

6.7.1 Effect of unsteady friction effects on the leak-induced oscillation

The effect of steady and unsteady friction on the FRF is illustrated in Section 5.2.4. While the effect of steady friction is to decrease the magnitude of the peaks in the FRF uniformly, unsteady friction induces a trend in the peak magnitudes, causing the resonant peaks to attenuate with frequency. The effect of unsteady friction on the peaks of the FRF for a leaking anti-symmetric system is shown in Figure 6-48 and is compared with the

case when there is no unsteady friction. The leak is located at $x_L^* = 0.829$ in the numerical pipeline under an anti-symmetric configuration (refer to Figure 6-49).

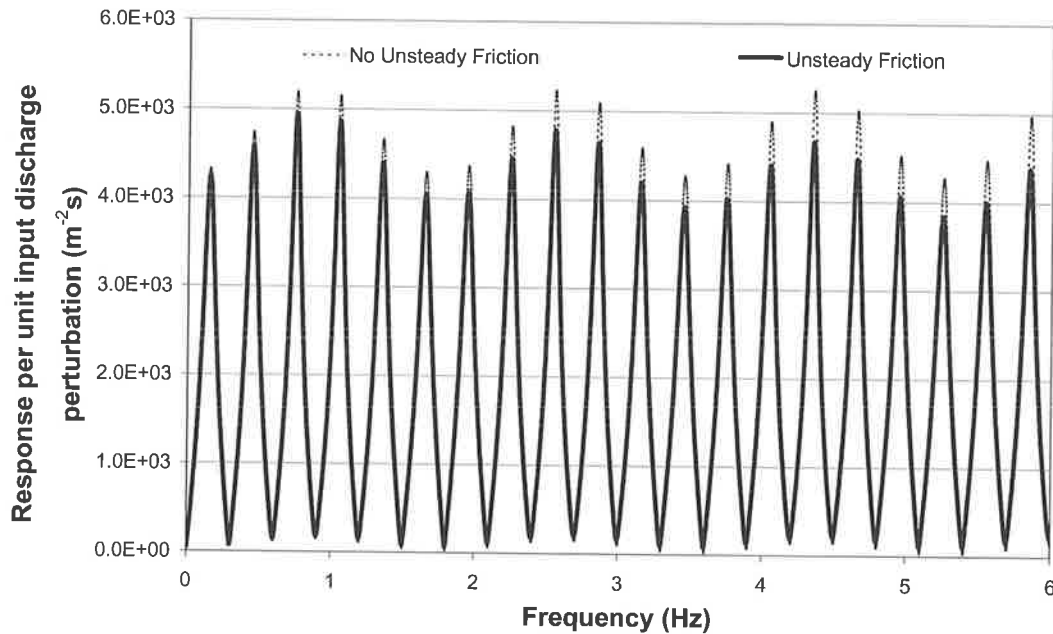


Figure 6-48 – Investigation into the effect of unsteady friction.

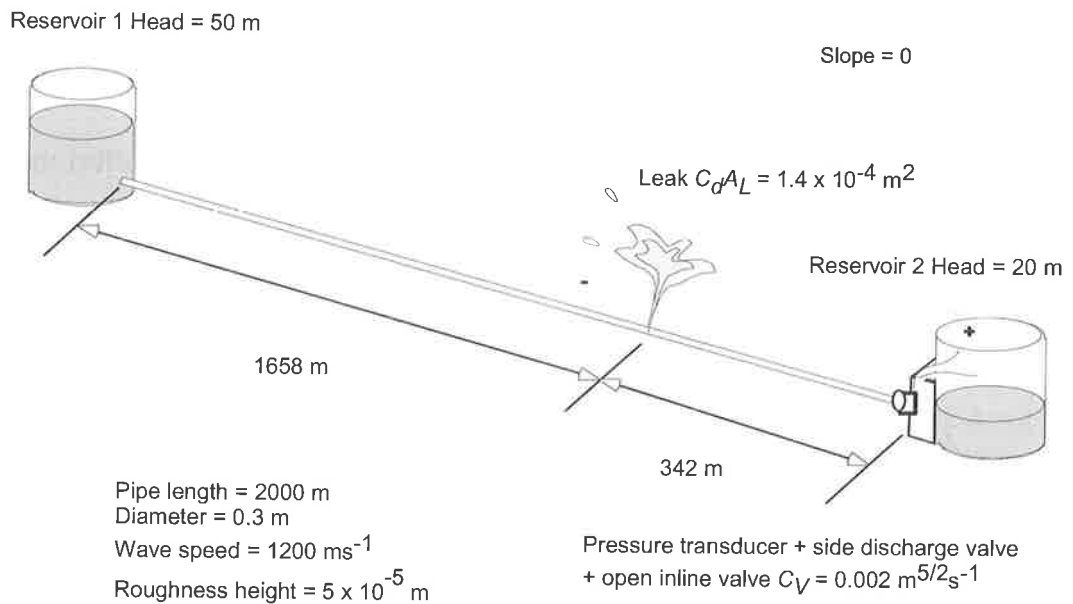


Figure 6-49 – System configuration for investigation into unsteady friction effects on the leak-induced modification on the FRF.

The Vardy and Brown (1995) unsteady friction model was used and was incorporated into the transfer matrix equations. The details of the unsteady friction model are given in Chapter 3, Section 3.4. The inverted peak magnitudes for both cases are shown in Figure 6-50 and the spectrums of the two data are in Figure 6-51.

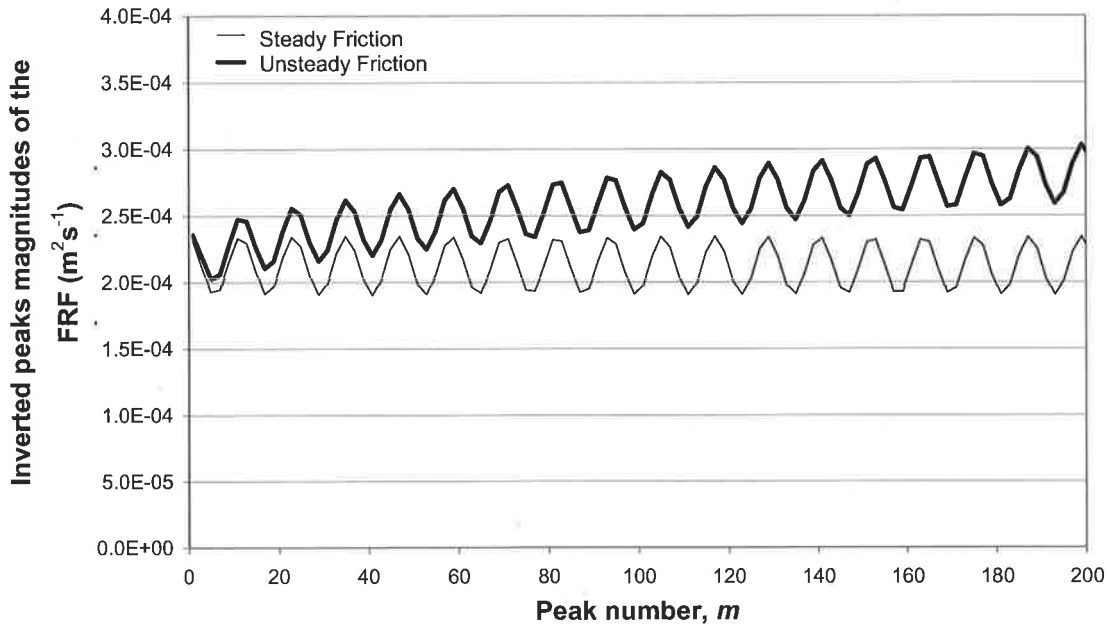


Figure 6-50 – Comparison of the inverted peak magnitudes for a leaking pipeline with and without unsteady friction.

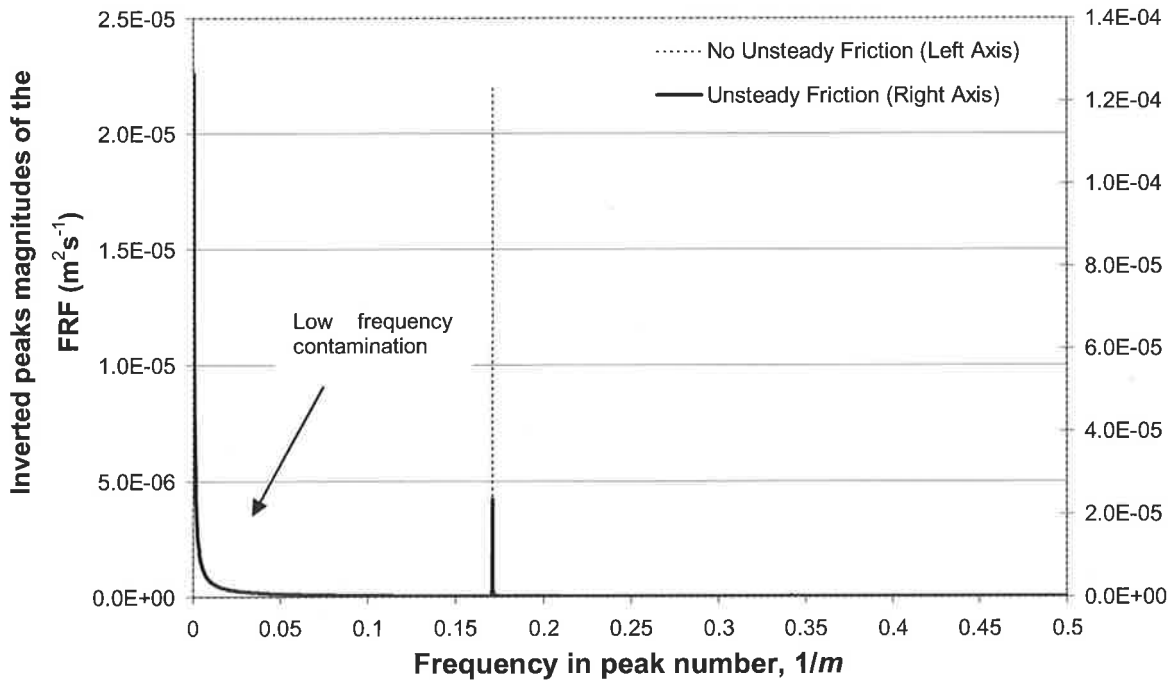


Figure 6-51 – Spectrum of inverted peak magnitudes for the case with and without unsteady friction.

The effect of unsteady friction is superimposed on the original leak-induced oscillation such that the oscillation follows the trend of decay in the peaks of the FRF. For the unsteady friction data series, the slow trend in the data results in contamination by spurious magnitudes at the low frequencies. This trend must be considered during the extraction of the leak position from the FRF and a procedure for doing so is presented later in the thesis.

6.7.2 Effect of signal bandwidth

As mentioned in Chapter 5, the physical extraction of the FRF depends on the frequency content of the input signal. Low energy frequencies in the input signal can be dissipated in the system or masked in the output by background noise. This finding has a major effect on the leak detection technique as it places an upper limit to the number of peaks in the FRF that can be observed. The full FRF from the experimental system with the transient generated by a hand closure of the in-line valve is shown in Figure 6-52. The accuracy of the FRF deteriorates with high frequency and only the initial peaks are free from contamination. The point where the deterioration begins is dependent on the duration and the magnitude of the input transient signal and can be identified from the spectrum of the input.

Two devices were used in the generation of the FRF from the experimental pipeline: the manual operation of an in-line ball valve and a solenoid-actuated side-discharge valve. The input spectrums from both devices are shown in Figure 5-44 and Figure 5-46, respectively. The figures indicate that the operation of the solenoid valve produces an input that has energy distributed at higher frequencies when compared to the spectrum generated by the hand closure. The bandwidth of each input signal is defined in this study as the point where the frequency magnitude falls below 5% of its maximum value, giving the upper limit as 300 Hz for the solenoid generated signal and 120 Hz for the manual operation of the in-line valve. Setting the signal bandwidth at the 5% level is not meant to be the standard for all systems and for situations with different levels of background noise this value may need to be adjusted. It is up to the operator's discretion to decide on a cut-off frequency beyond which the FRF is distorted beyond any practical value.

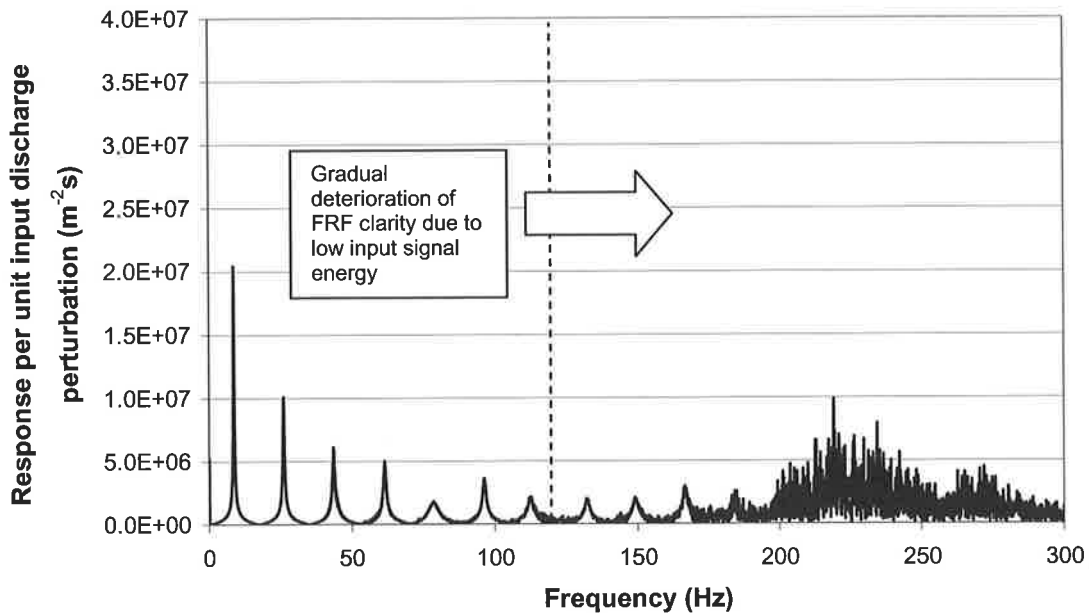


Figure 6-52 – FRF from the experimental pipeline showing the effect of bandwidth.

The finite frequency content of the input signal means that there is a limit as to the number of peaks in the FRF available for the leak detection procedure. Given that the fundamental frequency is 17.7 Hz in the symmetric experimental pipe and 8.8 Hz for the anti-symmetric pipe, the number of useable peaks in the FRF for each generating device and system configuration is summarised in Table 6-7.

Table 6-7 – Number of peaks for leak detection in the laboratory.

Generator	Anti-symmetric	Symmetric
Solenoid	16	8
Manual	7	NA

6.7.3 Effect of pipeline irregularities

Section 5.3.2 shows that discrepancies exist between the predicted FRF and the derived FRF from the pipeline. These discrepancies are noted in the time domain as a small distortion of the original transient shape from the expected behaviour as the transient evolves (refer to Chapter 5, Section 5.3.2, Figure 5-56). The comparison between the

experimental and theoretical FRF for the leaking experimental system is shown in Figure 6-53.

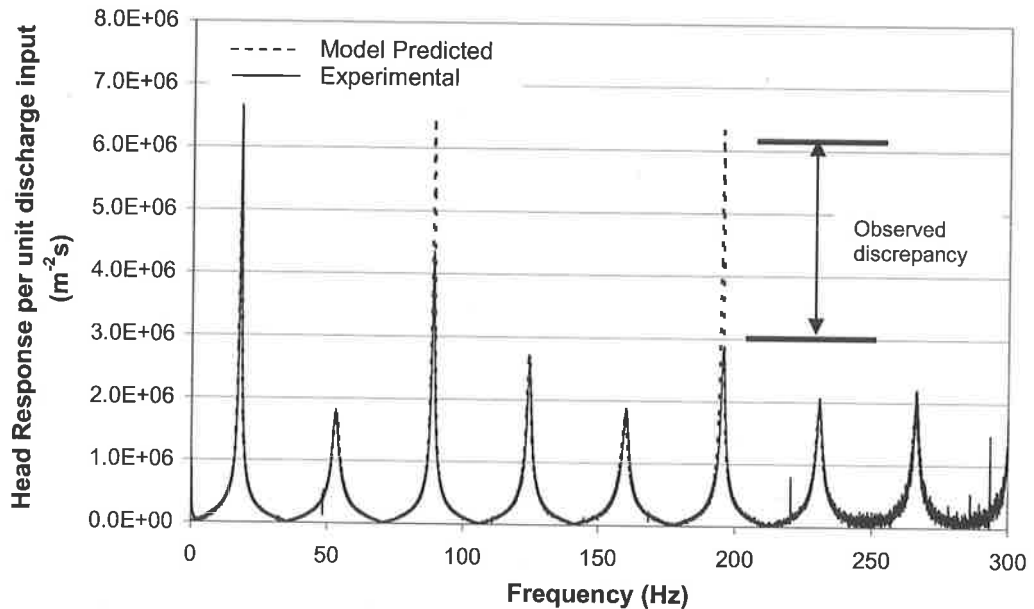


Figure 6-53 – Comparison between model and experimental FRF for a leak symmetric system.

The FRF from the experimental pipeline conforms to the theoretical FRF at the low amplitude portions of the function. Deviations occur, however, at the large magnitude resonant peaks (e.g. 3rd and 6th harmonic peaks). This result suggests that an energy loss—governed by the size of the response (i.e. larger the response, greater the loss)—exists in the pipeline. The amplitude of any peak oscillation pattern is affected by this loss mechanism and its effect cannot be assumed as constant across all frequencies. Possible variations in the oscillation amplitude must be taken into account in the extraction of the leak-induced pattern.

6.7.4 Final leak detection procedure

For accurate frequency and phase extraction of the leak-induced oscillation, the issues of bandwidth limitation and frequency-dependent behaviour described above are taken into account. The number of useful peaks in the FRF is limited by the bandwidth of the injected signal. Using the manual in-line valve closure as an example, Table 6-7 indicates that a maximum of 7 peaks can be used for the leak detection process. The traditional fast

Fourier transform (FFT) of a set of data containing a series of N resonant peaks in the FRF generates frequency data at the following intervals:

$$\Delta \frac{1}{m} = \frac{1}{N} \tag{6.61}$$

The frequency for this case is measured in terms of “per peak interval”, $1/m$. A FFT performed on 7 peak data points creates a coarse spectrum that can locate a leak within 14.3% of the total pipe length and is only acceptable as an initial estimate. In addition, the presence of frequency-dependent effects (e.g. unsteady friction) produces systematic distortions in the leak-induced sinusoid that prevents the direct application of the Fourier transform (refer to Figure 6-51).

Systematic distortions in the leak-induced oscillation can occur in two forms:

1. Trend distortion of resonant peak magnitudes—where the mean of the leak-induced oscillation shifts with frequency. Figure 6-54 illustrates trend distortion where the mean of the oscillation increases nonlinearly. This type of distortion is shown in Figure 6-50 for the effect of unsteady friction.

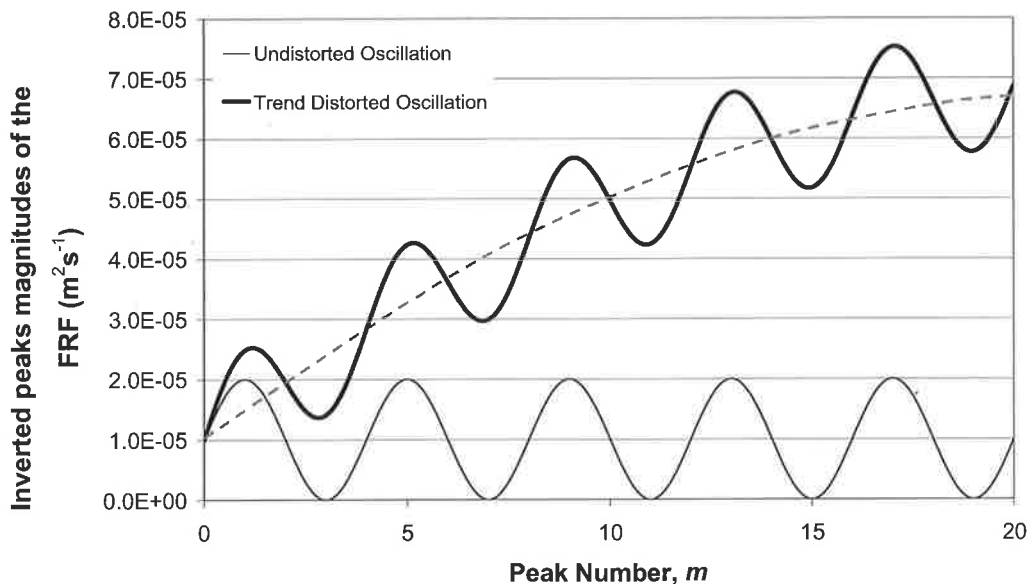


Figure 6-54 – Trend distortion effects on the peak oscillations as a result of unsteady friction.

2. Scale distortion of oscillation magnitudes—where the amplitude of the leak-induced oscillation changes with frequency. The effect of this type of distortion is illustrated in Figure 6-55.

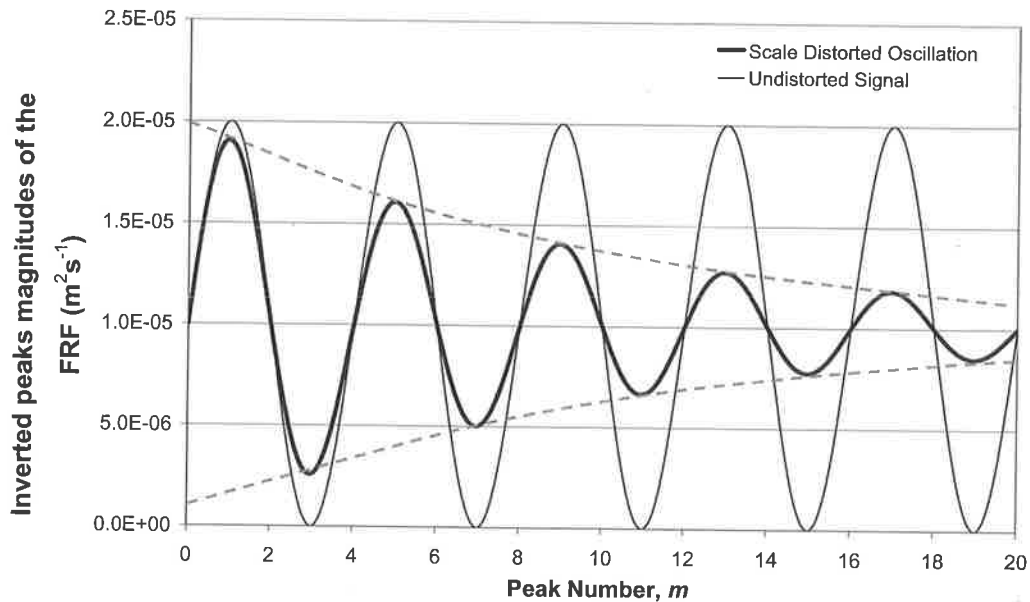


Figure 6-55 – Scale distortion effects on the peak oscillations.

To provide an accurate and flexible leak-induced oscillation extraction procedure, both of these possible distortion effects are considered. As all conventional signal processing algorithms operate upon undistorted sinusoidal signals, a customised procedure is required for situations where systematic scale and trend distortions exist in the data. A least-squares regression of a scale- and trend-corrected sinusoid to the inverted peak magnitudes allow accurate decomposition of the dominant oscillation frequency while taking into account the trend and scaling of frequency-dependent effects. This approach is an improvement to the conventional Fourier transform, which assumes the frequencies in the data as constant amplitude oscillations about a constant value. The fitting function is of the form

$$E(m) = \frac{1}{S(m)} \times X_1 \cos(2\pi m X_2 - X_3) + T(m) \quad (6.62)$$

where X_n are the fitted parameters and m is the resonant peak number. In particular, the parameters X_2 and X_3 are the frequency and phase of the oscillation and are used to

determine the location of a leak. The parameter X_1 is the amplitude of the oscillation. The functions T and S are the trend- and scale-correction functions, respectively. The form of the scale- and trend-correction function must be flexible to include a wide range of possible distortions on the FRF peaks.

As illustrated in Figure 6-50, systematic trend distortion is predominantly the result of unsteady friction effects (Vítkovský *et al.*, 2003b). It is valid, therefore, to base the form of the trend correction function in Eq. (6.63) on the effect of unsteady friction on the FRF. Figure 6-56 shows the effect of unsteady friction on the inverted peaks of the FRF for both laminar and turbulent flow. The Reynolds numbers for the flows are 30 and 44,900 respectively. This trend in the peaks of the FRF may be approximated as a power law function of the form

$$T(m) = X_4 m^{X_5} + X_6 m + X_7 \tag{6.63}$$

and provides a good match with the unsteady friction behaviour in Figure 6-56.

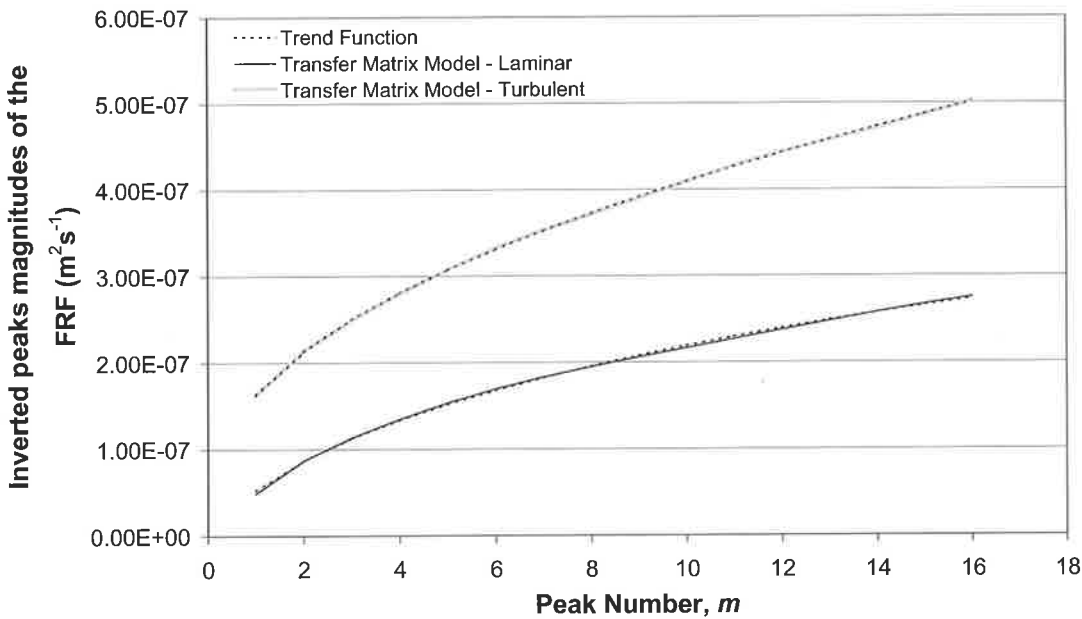


Figure 6-56 – The comparison between the trend correction function for laminar and turbulent flow cases.

Unlike trend distortion, the presence of systematic scale distortions in the oscillation cannot be attributed to a single phenomenon in a pipeline. The extent of this distortion is

dependent on the nature of the system under consideration. In the experimental pipeline, scale distortions are evident. To allow for all possible magnitudes of this distortion, the scale correction is given as a generic power logarithmic function,

$$S(m) = X_8 (\ln(m))^{X_9} + X_{10} + 1 \quad (6.64)$$

Similar polynomial and power-law functions were investigated and were found to have similar leak location accuracies to Eq. (6.63) when incorporated into the fitting function of Eq. (6.62).

The minimisation algorithm selected for least-squares regression is the shuffled complex evolution (SCE) algorithm (Duan *et al.*, 1993) and is used to fit Eq. (6.62) to the inverted peaks magnitudes.

The detailed procedure for detecting and locating leaks using the FRF is as follows:

1. Extract of the pipeline FRF as described in Section 5.3.
2. Isolate peak responses from the FRF and invert the responses.
3. Use the SCE to perform least-squares regression of Eq. (6.63) on the inverted peak responses.
4. Find the dominant frequency and phase of the oscillation.
5. Determine whether a leak exists in the system. To increase confidence of the leak detection result, a leak is “detected” in the system when at least 1.5 periods of the oscillation exist in the data. This guideline prevents spurious fluctuations being detected as true oscillations. However, this safeguard causes low frequency oscillations in the data to be rejected as possible leak candidates and places a limitation on the region of the pipe where leaks can be determined. The feasible regions for both anti-symmetric and symmetric boundaries are shown in Figure 6-57 and Figure 6-58, respectively.

The size of undetectable zones, labelled x_D^* , where $x_D^* = x_D / L$ is related to the number of observable peaks, n_p , by Eq. (6.65) for an anti-symmetric boundary condition as

$$x_D^* = \frac{1.5}{n_p} \quad (6.65)$$

and Eq. (6.66) for a symmetric system

$$x_D^* = \frac{0.75}{n_p} \quad (6.66)$$

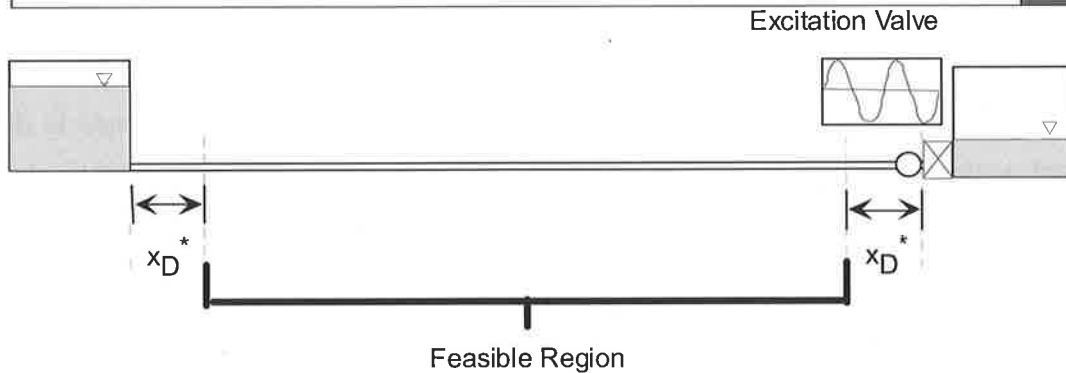


Figure 6-57 – Feasible region for anti-symmetric boundaries.

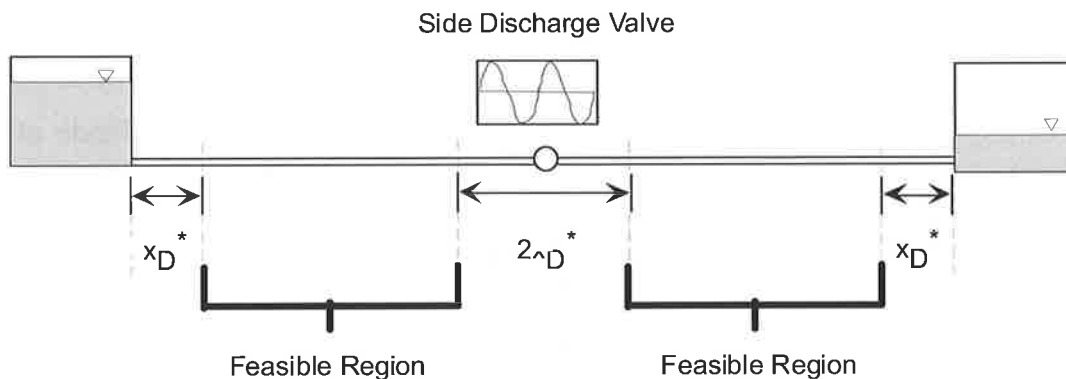


Figure 6-58 – Feasible region for symmetric boundaries.

The x_D^* for the laboratory system is 0.094 for transients generated by the solenoid valve and 0.214 for in-line valve closures. The size of x_D^* will decrease for larger systems with a lower fundamental frequency.

6. Once a leak is detected in a system, use the frequency and phase of the oscillation to determine the location of the leak according to Section 6.5.2.

For a signal of finite bandwidth, the number of available peaks can be low compared to the number of fitted parameters. The accuracy of the fitted parameters is ascertained

through parameter variance, where a small value indicates that the parameter is well determined. The parameter variance is found from the diagonal entries of the covariance matrix formed in the regression process (Vítkovský, 2001). In this thesis, least-squares regression and parameter variances are calculated using a program developed by Kuczera (1994), called “NLFIT”. The variance for each case is converted to a standard deviation value to give confidence limits for the leak position.

Due to the possible low number of data points, the search space was divided into subsections, and the least squares fit for each subsection is found. The best solution out of these is the optimum solution for the entire search space. The search space is divided based on the parameter, X_2 , the oscillation frequency. A search is conducted in each of the 5 possible ranges for X_2 , with bounds for X_2 set as between 0 to 0.1 for the first section, 0.1 to 0.2 for the next and so forth up to the maximum of 0.5. The bounds for the phase of the oscillation (X_3) are set between $-\pi$ to $+\pi$ while all other parameters are unbounded for each of these runs.

As the scaling effect on the leak-induced oscillation cannot be separated from the oscillation amplitude (X_1), an accurate estimation of leak size is not possible. This problem means that any prediction of the size of a leak using the analytical amplitude of leak-induced oscillation would be conservative at best. For this reason, the remainder of this thesis focuses on the prediction of leak position in a pipeline.

6.8 EXPERIMENTAL VALIDATION

A program of experimental tests was conducted in the Robin Hydraulics Laboratory at the University of Adelaide to validate the proposed analytical leak detection technique. The program consists of tests conducted using different transient-generating sources. As mentioned previously, two transient-generating devices were used, the sharp closure of an in-line downstream ball valve and the sharp closure / pulse perturbation of a side-discharge solenoid valve. A summary of the tests is shown in Table 6-8. A selection of these tests is presented in this section; the full set of results can be found in the CD-ROM attached to this dissertation.

Table 6-8 – Summary of test configurations.

Transient Source	Boundary Configuration	Leak Size (orifice diameter, mm)	Leak position ($x_L^* = x_L / L$)	Test Name
Solenoid Valve	Anti-Symmetric	1.5 mm	0.751	C6-L1
	Anti-Symmetric	1.5 mm	0.179	C6-L2
	Anti-Symmetric	1.0 mm	0.751	C6-L3
	Anti-Symmetric	1.0 mm	0.179	C6-L4
	Symmetric	1.5 mm	0.179	C6-L5
In-line Valve	Anti-Symmetric	1.5 mm	0.750	C6-L6
	Anti-Symmetric	1.0 mm	0.750	C6-L7

The leaks are simulated by free discharging orifices and are connected to the pipeline as pictured in Chapter 4. The sizes of leaks range from 1 mm to 1.5 mm diameter orifices, with a $C_d A_L / A$ corresponding to 1.69×10^{-3} and 4.17×10^{-3} ($C_d A_L = 0.65 \times 10^{-6}$, $1.6 \times 10^{-6} \text{ m}^2$, respectively). These sizes of the leak are comparable to those used in the numerical examples of Section 6.6. The experimental results using the actuation of side-discharge ball valves are presented first followed by the results generated using in-line valve closures.

6.8.1 Validation of leak detection technique using a side-discharge solenoid actuated valve

To generate a transient using the side-discharge solenoid valve, the valve was either perturbed in a pulse pattern (closed-open-closed) or shut from a fully opened position. For the following test, the in-line valve at the downstream end of the pipe is shut, creating an anti-symmetric system. The solenoid valve is placed 0.16 m upstream of this closed boundary with the transient being measured at this point (refer to Figure 6-59).

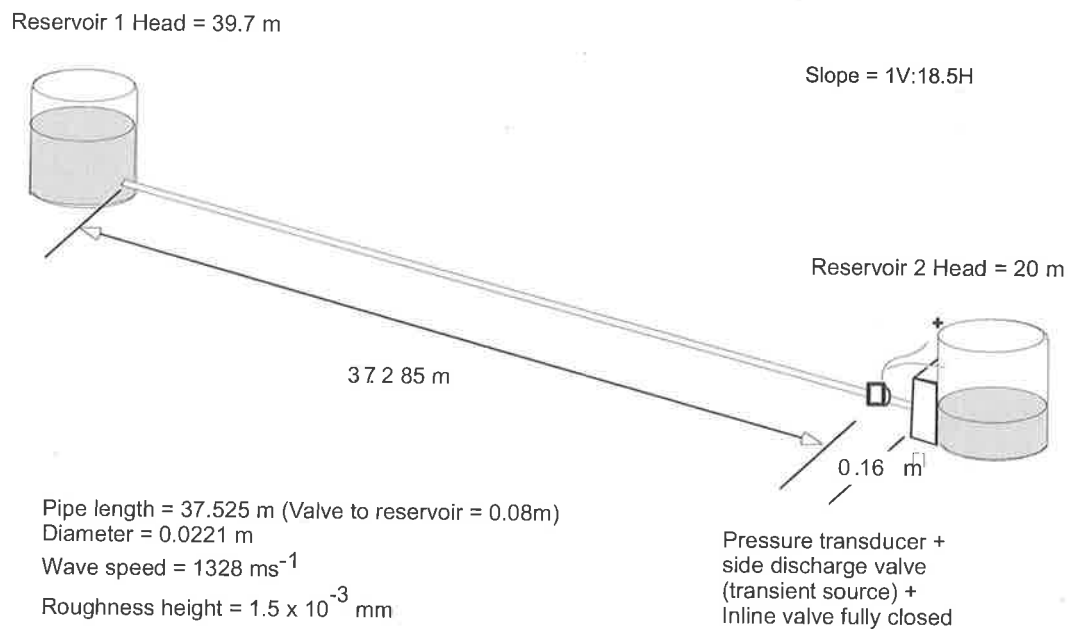


Figure 6-59 – Laboratory configuration for anti-symmetric no-leak test.

The transient trace and the FRF for the *intact* (no leak) pipeline were shown in Section 5.3 and are repeated here as Figure 6-60 and Figure 6-61. The FRF for the intact pipeline contains peaks at odd multiples of the fundamental frequency. The magnitudes of the peaks attenuate with frequency with no clear periodic oscillation. In comparison, consider the case where a 1.0 mm diameter leak ($C_d A_L / A = 1.69 \times 10^{-3}$) is at $x_L^* = 0.751$ (9.39 m upstream of the in-line valve) as shown in Figure 6-62. The transient trace is in Figure 6-63. Figure 6-64 shows the FRF for this situation and its form is different from the leak-free case of Figure 6-61. The magnitude of the peaks of the FRF in the leaking pipeline is lower than those of the intact system and the peaks have a periodic pattern. No additional frequency peaks are generated for the leaking FRF as predicted by Jönsson and Larson

(1992), Covas and Ramos (1999) and Mpesha *et al.* (2001, 2002). Each of the peak magnitudes in the FRF from the leaking pipe were extracted, inverted and plotted in Figure 6-65. The peaks are labelled in the two figures and the leak-induced periodic pattern is shown in Figure 6-65.

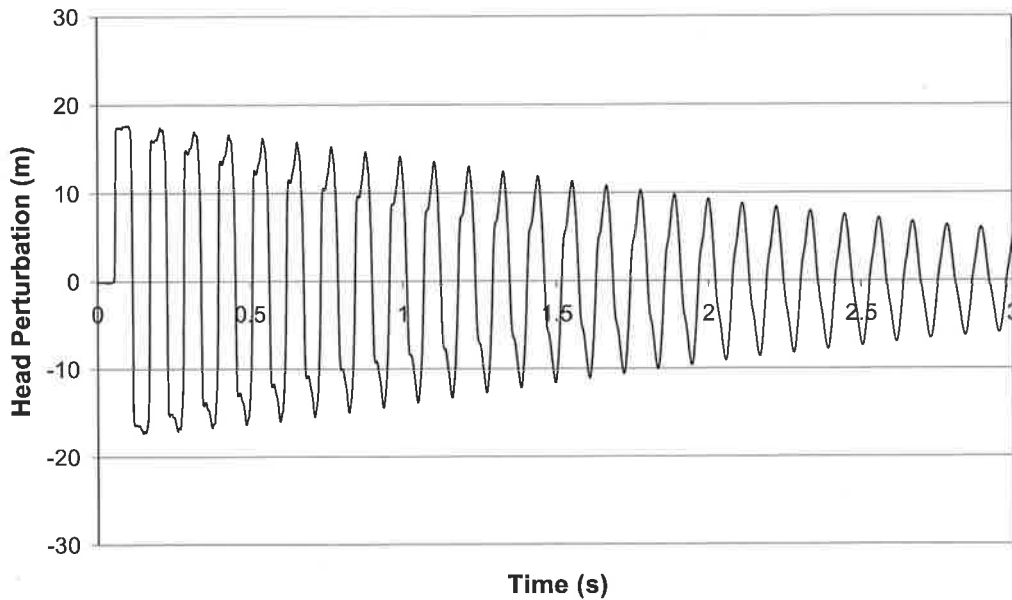


Figure 6-60 – Experimental transient trace for anti-symmetric system with no leak.

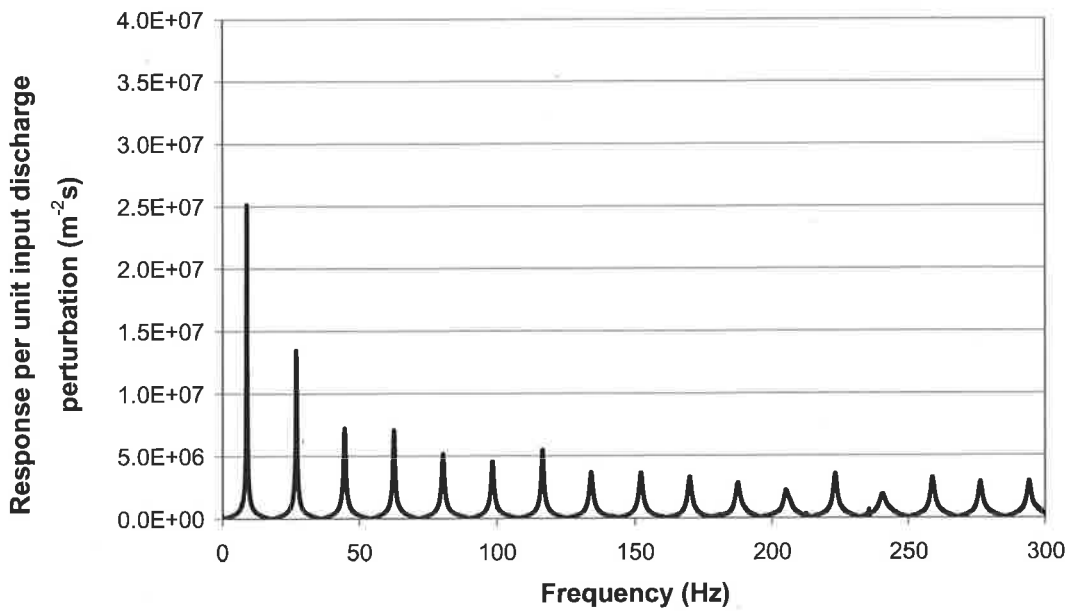


Figure 6-61 – FRF for anti-symmetric experimental system with no leak.

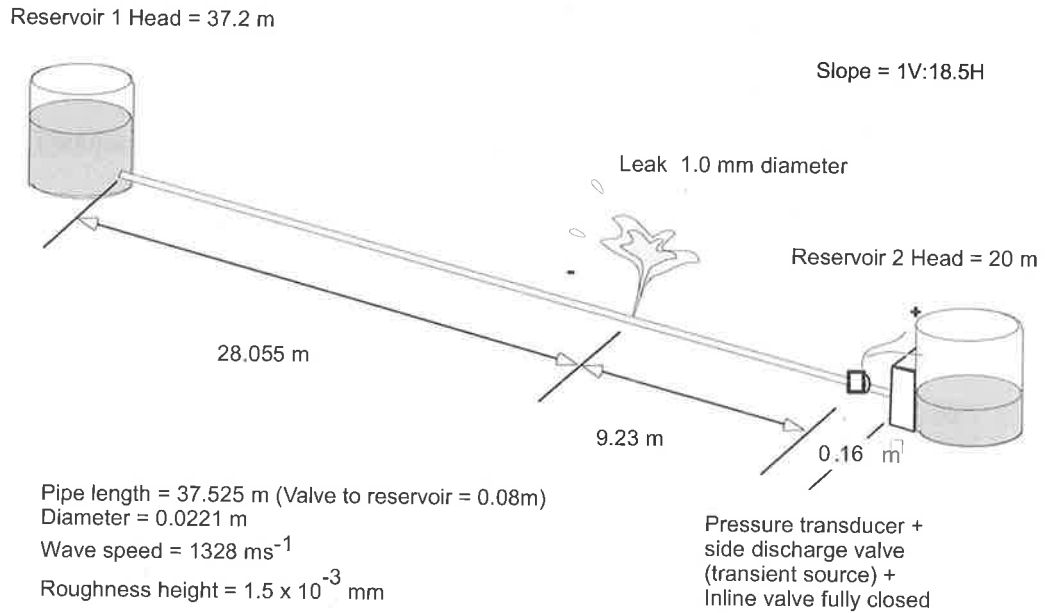


Figure 6-62 – System configuration for the anti-symmetric leaking test with a 1.0 mm ($C_d A_L / A = 1.69 \times 10^{-3}$) leak at $x_L^* = 0.751$.

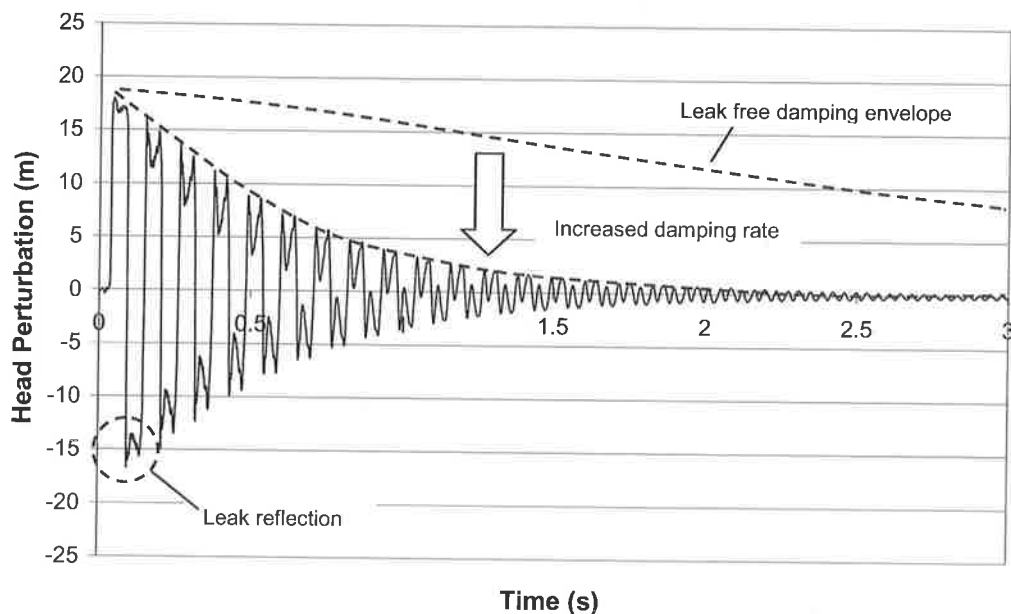


Figure 6-63 – Transient signal for the anti-symmetric leaking test with a 1.0 mm ($C_d A_L / A = 1.69 \times 10^{-3}$) leak at $x_L^* = 0.751$ (Data file: C6-L3.txt).

The frequency and phase of the periodic oscillation was extracted (Figure 6-65) using the least-squares regression procedure. The dominant frequency and phase of the signal was 0.242 and 0.594, respectively. The resultant oscillation is shown in Figure 6-65. The phase result (0.594) places the leak in zone II ($-\pi/4 \leq \phi \leq 3\pi/4$, refer to Figure 6-33) and is

located 9.06 m upstream of the closed valve ($x_L^* = 0.758$). The parameter standard deviation for the leak position is ± 0.22 m (standard deviation of x_L^* as 0.006). For a normal distribution, the 95% confidence interval is set as twice this standard deviation and the error range is ± 0.44 m. The true leak position of 9.39 m upstream of the valve lies within this predicted range of 9.06 ± 0.44 m upstream of the closed valve.

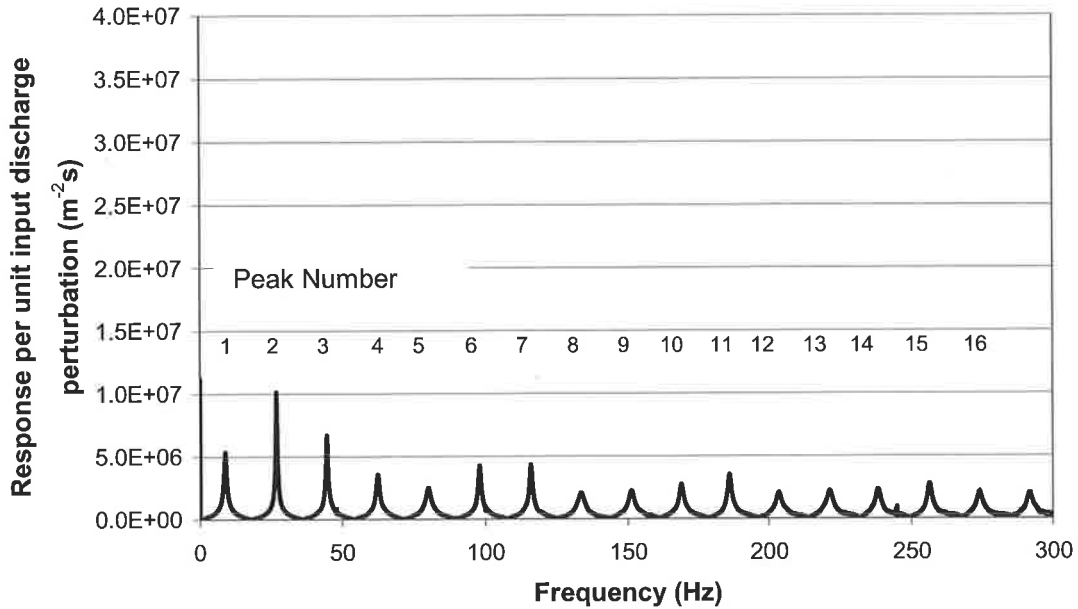


Figure 6-64 – FRF for the anti-symmetric leaking test with a 1.0 mm ($C_d A_L / A = 1.69 \times 10^{-3}$) leak at $x_L^* = 0.751$.

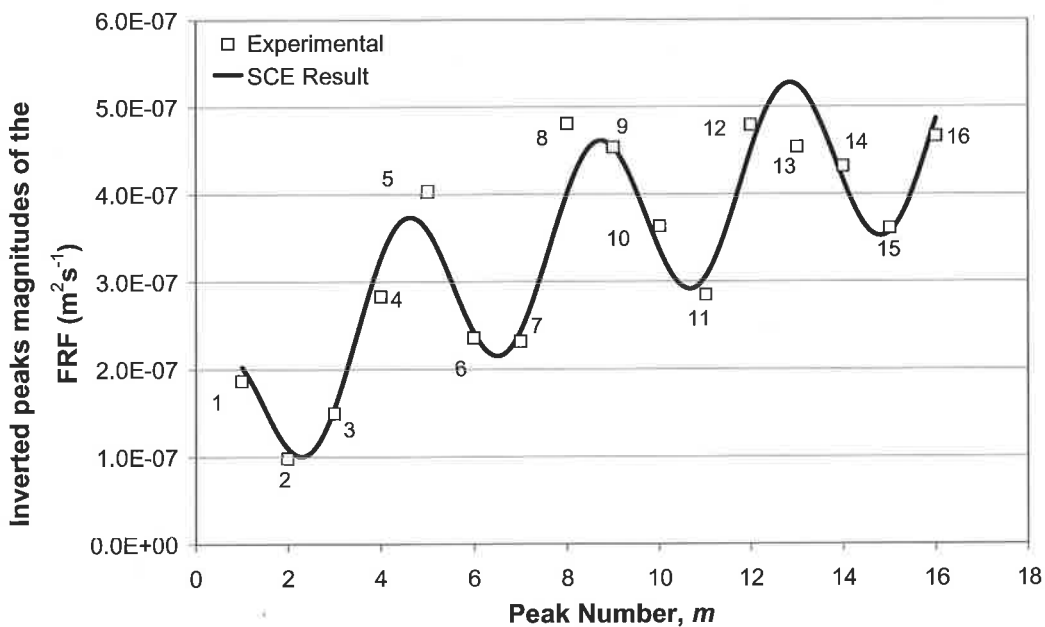


Figure 6-65 – Dominant frequency and phase extraction for the anti-symmetric leaking test with a 1.0 mm ($C_d A_L / A = 1.69 \times 10^{-3}$) leak at $x_L^* = 0.751$.

The regression process provides a single frequency decomposition of the data set and extracts the dominant leak oscillation frequency and phase from the FRF peaks. This procedure should not be confused with conventional inverse transient analysis where a good match in Figure 6-65 is indicative of a good leak location procedure. Instead, the procedure—where distorted oscillations can be found—should be considered as an alternative to a Fourier decomposition of the data. The presence of non-periodic noise is ignored in this search for the dominant frequency and provides the procedure with a degree of noise tolerance.

For the second leak example, a 1.5 mm diameter leak was placed 6.695 m downstream of the reservoir ($x_L^* = 0.179$). The configuration of the system and the transient trace are shown in Figure 6-66, Figure 6-67, respectively. To illustrate the prominence of the leak-induced modification on this signal, the leak-reflected signal is circled in Figure 6-68. The nature of this reflection is similar to other head variations in the signal and is not clearly defined.

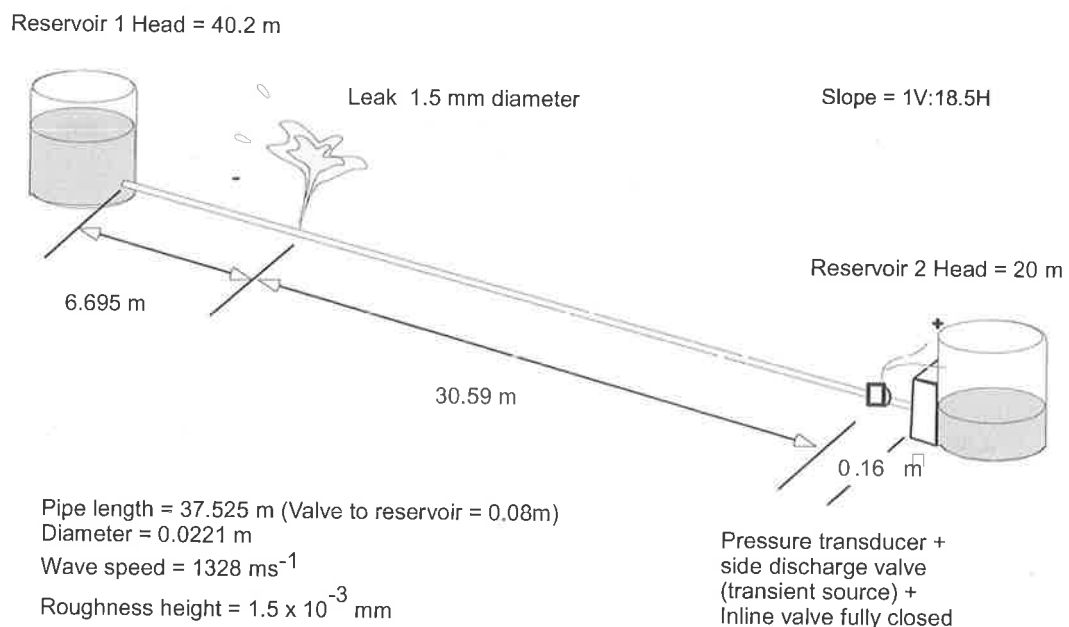


Figure 6-66 – Laboratory configuration for the anti-symmetric leaking test with a 1.5 mm ($C_d A_L / A = 4.17 \times 10^{-3}$) leak at $x_L^* = 0.179$.

The FRF for this leaking system is in Figure 6-69 and the inverted peak magnitudes are shown in Figure 6-70 along with the least-squares regression result. The resultant FRF has a distinctive periodic pattern in the peak magnitudes.

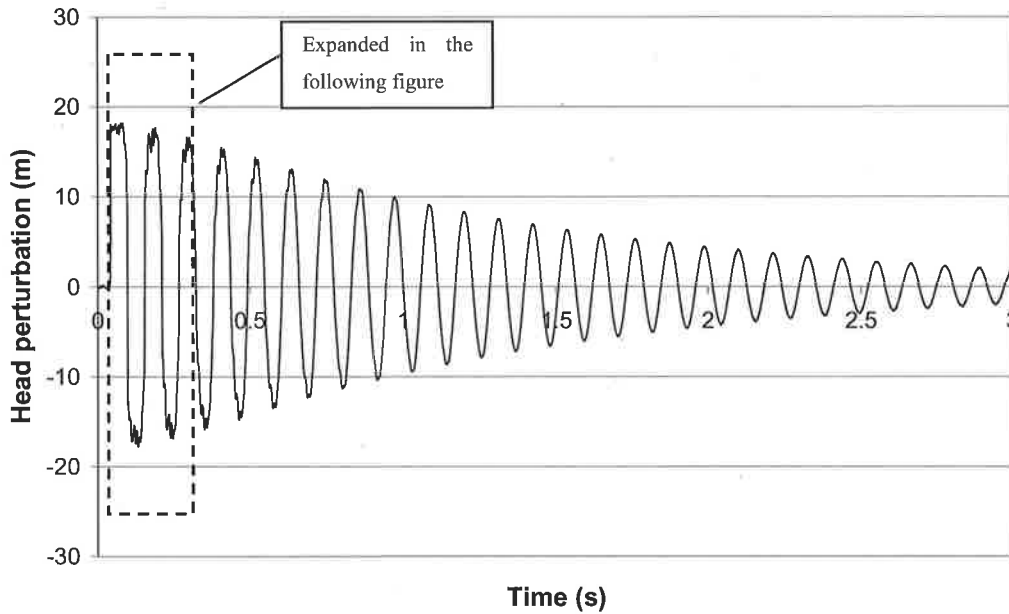


Figure 6-67 – Transient signal for the anti-symmetric leaking test with a 1.5 mm ($C_d A_L / A = 4.17 \times 10^{-3}$) leak at $x_L^* = 0.179$ (Data file: C6-L2.txt).

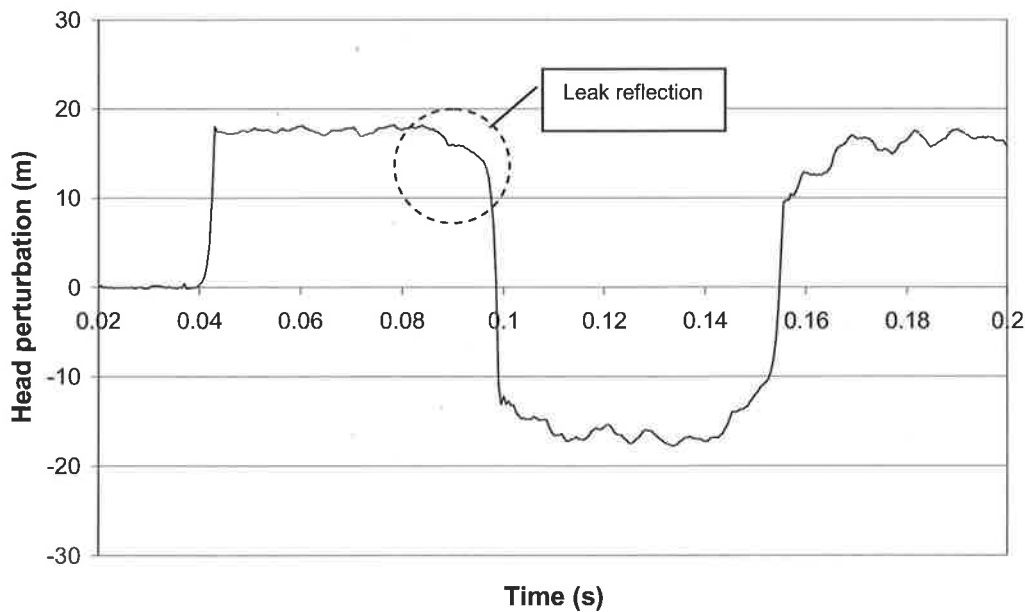


Figure 6-68 – Expanded transient signal for the anti-symmetric leaking test with a 1.5 mm ($C_d A_L / A = 4.17 \times 10^{-3}$) leak at $x_L^* = 0.179$ (Data file: C6-L2.txt).

The dominant oscillation frequency is $x_L^* = 0.185$ with a standard deviation of 0.007 and a phase of -2.40. The phase places the leak in Zone I of the pipeline and the leak is located

at $x_L^* = 0.185 \pm 0.014$ (95% confidence range), corresponding to a distance of 6.927 ± 0.524 m from the upstream reservoir. The true leak location of 6.695 m from the upstream boundary lies within the predicted range.

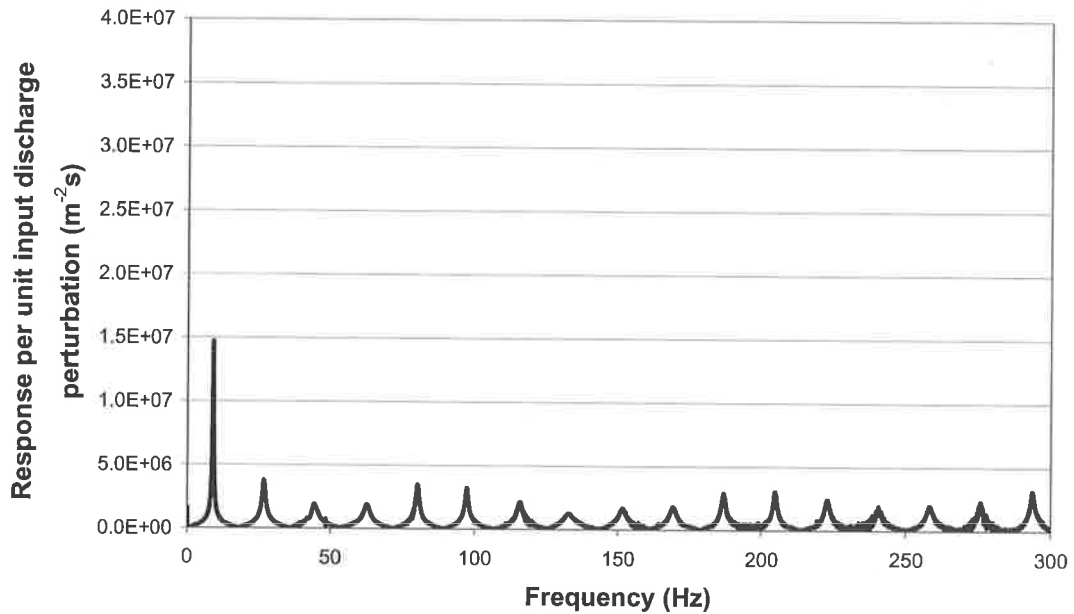


Figure 6-69 – FRF for the anti-symmetric leaking test with a 1.5 mm ($C_d A_L / A = 4.17 \times 10^{-3}$) leak at $x_L^* = 0.179$.

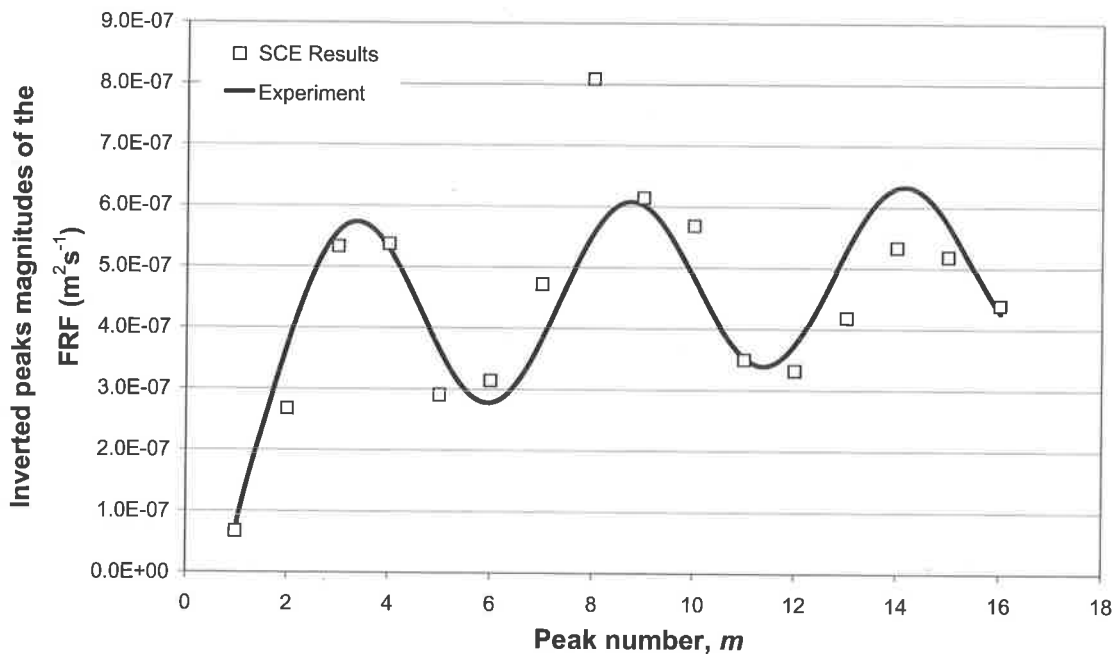


Figure 6-70 – Dominant frequency and phase extraction for the anti-symmetric leaking test with a 1.5 mm ($C_d A_L / A = 4.17 \times 10^{-3}$) leak at $x_L^* = 0.179$.

The same procedure was carried out for the leak-free system in Figure 6-59 with the FRF shown previously as Figure 6-61. The result is in Figure 6-71. Although no clear oscillations can be seen, the SCE routine fitted a weak oscillation of a low frequency to the data to account for the small variation in peak magnitudes. However, as the oscillation did not repeat 1.5 times in the data set, this fit is rejected as a spurious result according to Section 6.7.4. A summary of all the leak detection tests for the anti-symmetric system configuration is shown in Table 6-9. The data of the results not shown in the body of the thesis are included in the attached CD-ROM. In all cases, the technique correctly locates the leak in the system.

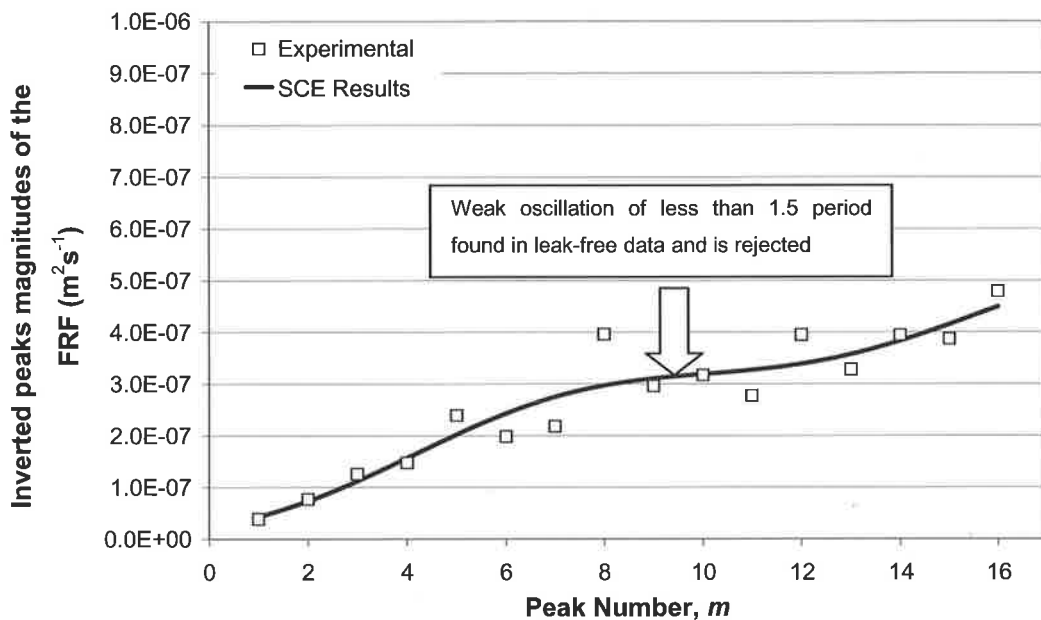


Figure 6-71 – Dominant frequency and phase extraction for the no-leak case in the anti-symmetric system using the solenoid valve as generator.

Table 6-9 – Results for anti-symmetric test with solenoid generator.

Test Configuration	Predicted Frequency		Predicted Phase		Predicted Leak Location
	mean	stdev	mean	stdev	
0.207% Leak at $x_L^* = 0.179$	0.173	0.01	-2.80	0.046	$x_L^* = 0.173$
0.207% Leak at $x_L^* = 0.751$	0.242	0.006	0.594	0.306	$x_L^* = 0.758$
0.465% Leak at $x_L^* = 0.751$	0.244	0.008	0.215	0.419	$x_L^* = 0.756$
0.465% Leak at $x_L^* = 0.179$	0.185	0.007	-2.40	0.334	$x_L^* = 0.185$
No Leak	0.091	1.0	-1.86	6.283	$x_L^* = \text{NA}$

A number of tests were conducted in the system under a symmetric boundary configuration. The in-line valves in the system were fully opened and the boundary heads were set as 36.5 m and 37.0 m. The flow velocity was 0.5 ms^{-1} , giving a Reynolds number of 11,000. A side-discharge valve located close to the midpoint of the system generated the transient. The test has a 1.5 mm diameter ($C_d A_L / A = 4.17 \times 10^{-3}$) leak 6.695m from the upstream reservoir boundary (refer to Figure 6-72).

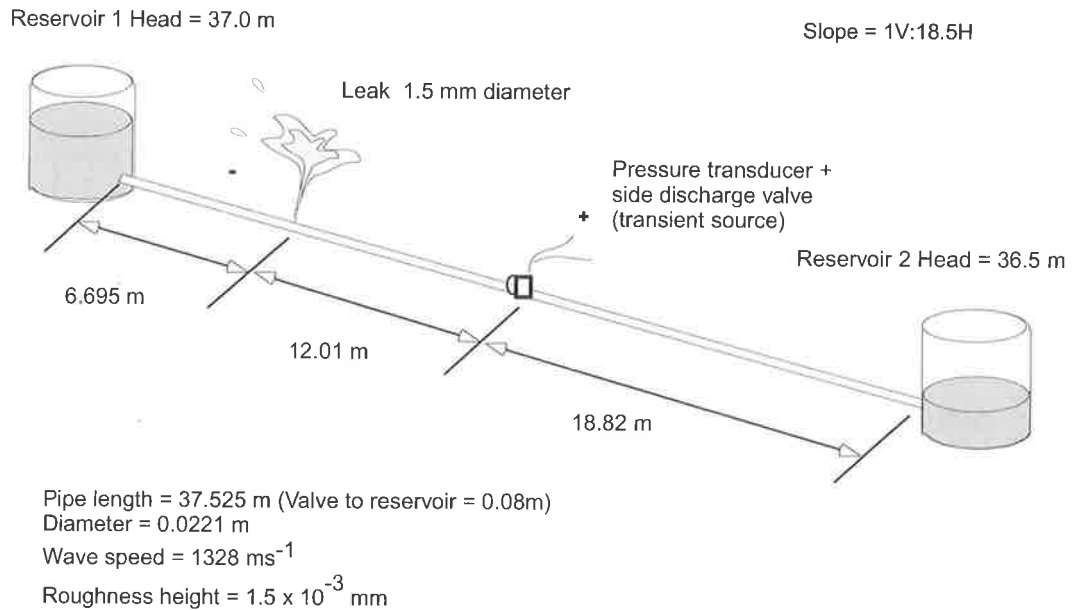


Figure 6-72 – Laboratory configuration for symmetric leaking test with 1.5 mm ($C_d A_L / A = 4.17 \times 10^{-3}$) leak at $x_L^* = 0.179$.

The transient is generated using pulse perturbation of the solenoid valve and the resultant transient as measured at the transient source is shown in Figure 6-73. The FRF of the system is in Figure 6-74. As for the previous leak examples, the peaks of the FRF vary periodically, indicating that a leak exists somewhere in the pipe. The result of the dominant frequency extraction is in Figure 6-75. The resultant dominant frequency was found to be $1/m = 0.358 \pm 0.06$ at the 95% confidence level (parameter standard deviation = 0.03). This frequency of oscillation indicates that a leak can be located at four possible positions in this symmetric system; $x_L^* = 0.179, 0.321, 0.679$ or 0.821 (corresponding to $x_L^* = \omega'_{\text{Signal}} / 2, (1 - \omega'_{\text{Signal}}) / 2, (1 - \omega'_{\text{Signal}}) / 2$ and $1 - \omega'_{\text{Signal}} / 2$, refer to Table 6-3), all with a confidence range of ± 0.03 . The phase of the oscillation was -2.07 rads and according to Figure 6-33 places the leak in zone I of the pipeline. The leak is predicted at 6.695 ± 0.112 m from the upstream reservoir and is at the true leak position.

The transient in this case was generated by a pulse perturbation of the valve and not a full closure as illustrated in the anti-symmetric cases previously. This difference has little effect on the accuracy of the resultant leak positioning and follows the finding given in Chapter 5—that is, the FRF within the bandwidth of the injected signal is a property of the system itself and is unaffected by the shape of the injected transient.

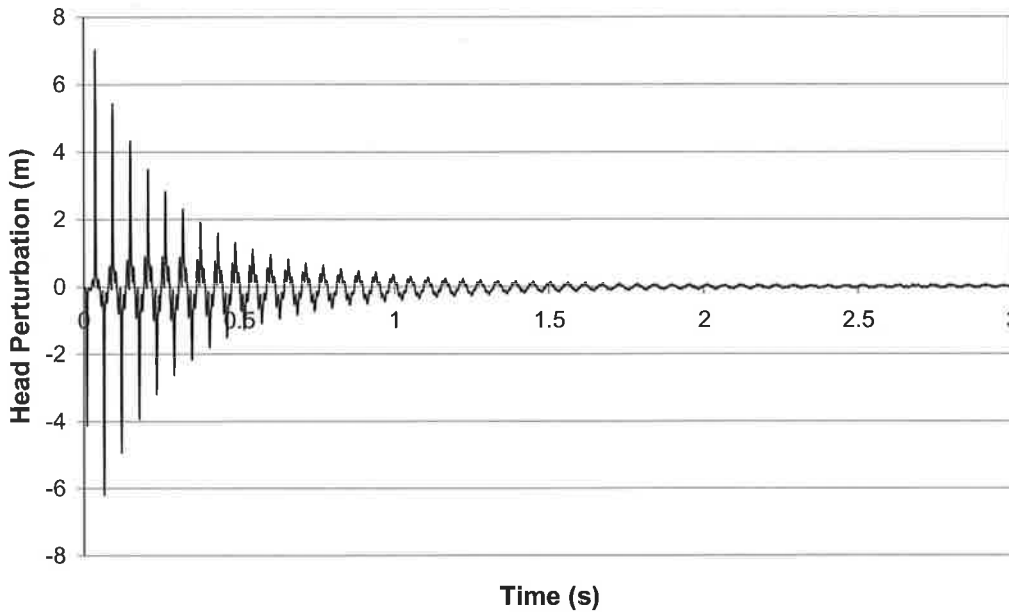


Figure 6-73 – Transient trace for the symmetric leaking test with a 1.5 mm ($C_d A_L / A = 4.17 \times 10^{-3}$) leak at $x_L^* = 0.179$ (Data file: C6-L5.txt).

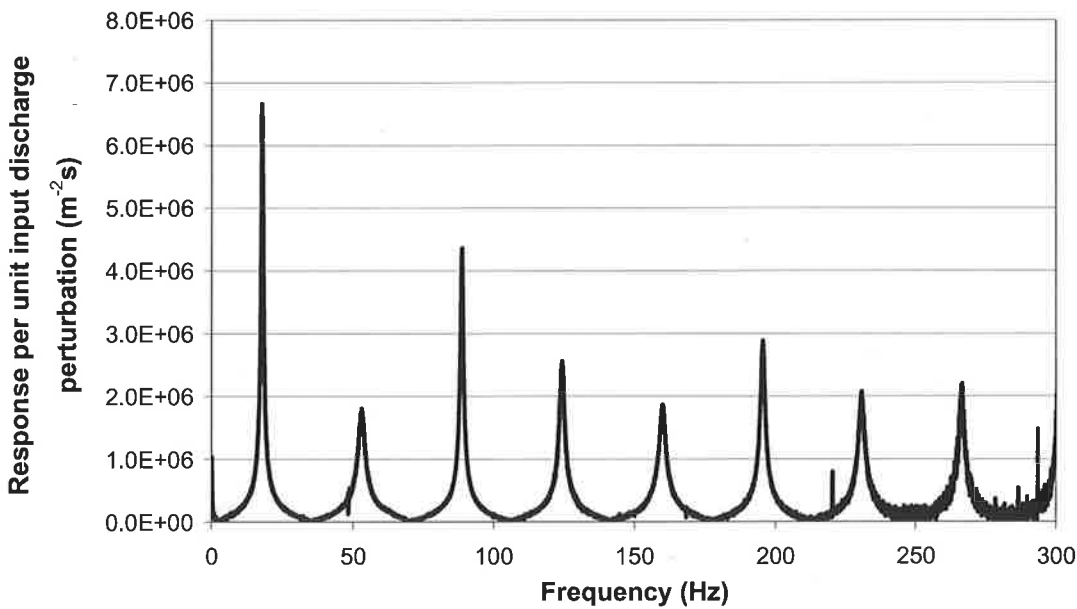


Figure 6-74 – FRF for the symmetric leaking test with a 1.5 mm ($C_d A_L / A = 4.17 \times 10^{-3}$) leak at $x_L^* = 0.179$.

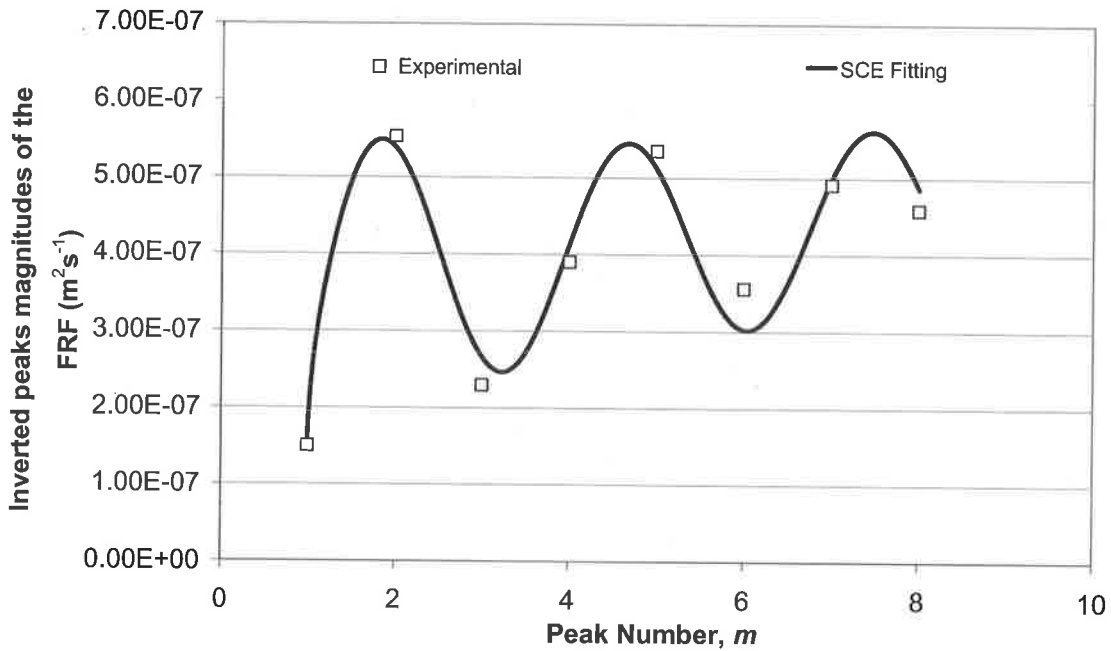


Figure 6-75 – Dominant frequency and phase extraction for the symmetric leaking test with a 1.5 mm ($C_d A_L / A = 4.17 \times 10^{-3}$) leak at $x_L^* = 0.179$.

Due to the low number of data points in the symmetric case, the regression procedure operates on an underdetermined system where the number of parameters is more than the number of available data points. To confirm the validity of the extracted dominant oscillation, two parameters, X_5 and X_7 [refer to Eq. (6.62)], are removed from the regression process, reducing the number of fitted parameters to eight. The value of X_5 is fixed as 0.5 (the result found in Figure 6-56 for the laminar flow case) and X_7 is fixed as 0.396×10^{-7} (the mean of the data). The original fitted values for X_5 and X_7 are 0.16 and 0.207×10^{-11} , respectively. The extracted dominant frequency for this situation is 0.344 ± 0.0140 and is comparable to the fitting using the full ten parameters. For situations where a sufficient number of data points are available, removal of any parameter from the regression is not advised as it places a limitation on the types of scale and trend distortion that the procedure can consider.

The leak detection procedure is repeated for a no-leak system and the FRF is in Figure 6-76. The dominant frequency extraction from the inverted peaks of this FRF gives a trivial solution of $x_L^* = 0.5$ (the Nyquist frequency) and no leak was detected in the system. The summary for the symmetric system is in Table 6-10.

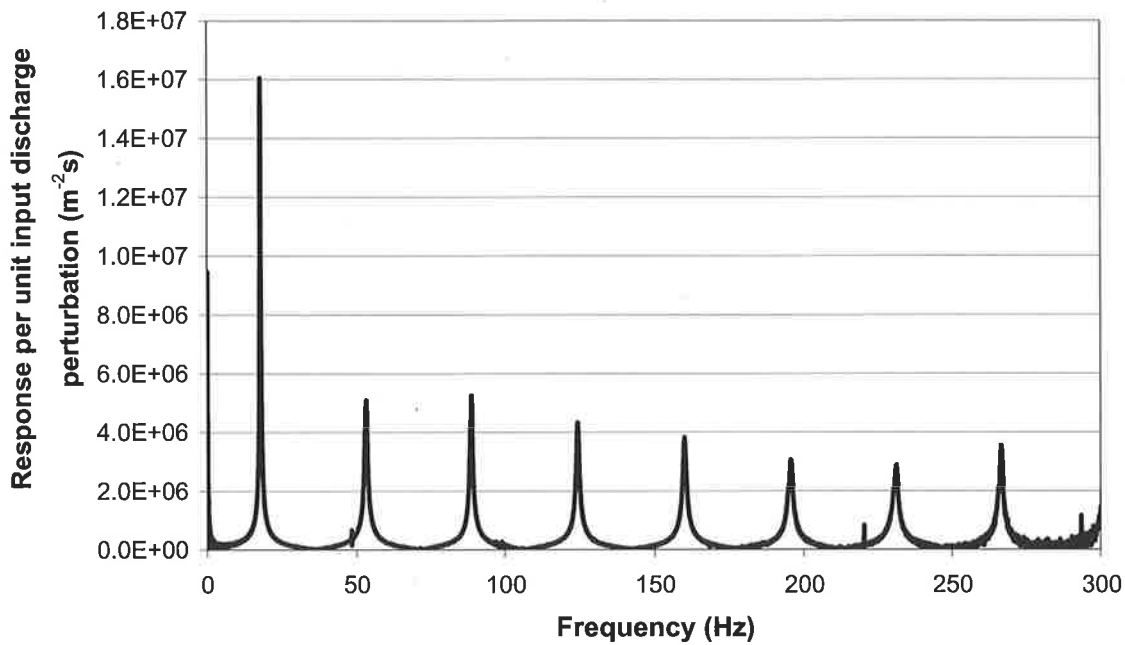


Figure 6-76 – FRF for symmetric system with no leak using solenoid valve as generator.

Table 6-10 – Results for symmetric tests with solenoid generator.

Test Configuration	Predicted Frequency		Predicted Phase		Predicted Leak Location
	mean	stdev	mean	stdev	
1.5 mm Leak at $x_L^* = 0.179$	0.358	0.03	-2.07	1.03	$x_L^* = 0.179$
No Leak	0.500	-	1.57	-	$x_L^* = \text{NA}$

6.8.2 Validation using in-line valve closures

The validation of the leak detection procedure continues with cases in which the transient is generated using an in-line valve. While the bandwidth of such signals is lower than that generated by solenoid valves, this type of transient can be readily generated in a system and has practical advantages. Three experimental tests are presented in this section; they consist of two leak tests and one leak-free test (shown previously in Chapter 5). The leaks are located 9.38 m from the generating valve, giving a $x_L^* = 0.75$ (refer to Figure 6-77). The two leaks are of dimensionless leak sizes $C_d A_L / A = 4.17 \times 10^{-3}$ and 1.69×10^{-3} , respectively (1.5 mm and 1.0 mm diameter leaks). The initial Reynolds numbers for the two situations are 3,924 and 3,148, corresponding to discharges of 6.86×10^{-5} and

$5.50 \times 10^{-5} \text{ m}^3 \text{ s}^{-1}$. The leak-free test has a Reynolds number of 3719 with a base flow of $6.53 \times 10^{-5} \text{ m}^3 \text{ s}^{-1}$. The boundary heads are set close to 26 m with differentials shown in Figure 6-77. The time series data for the three tests are shown in Figure 6-78, Figure 6-79 and Figure 6-80 for leak-free, 1.5 mm leak and 1.0 mm leak tests, respectively.

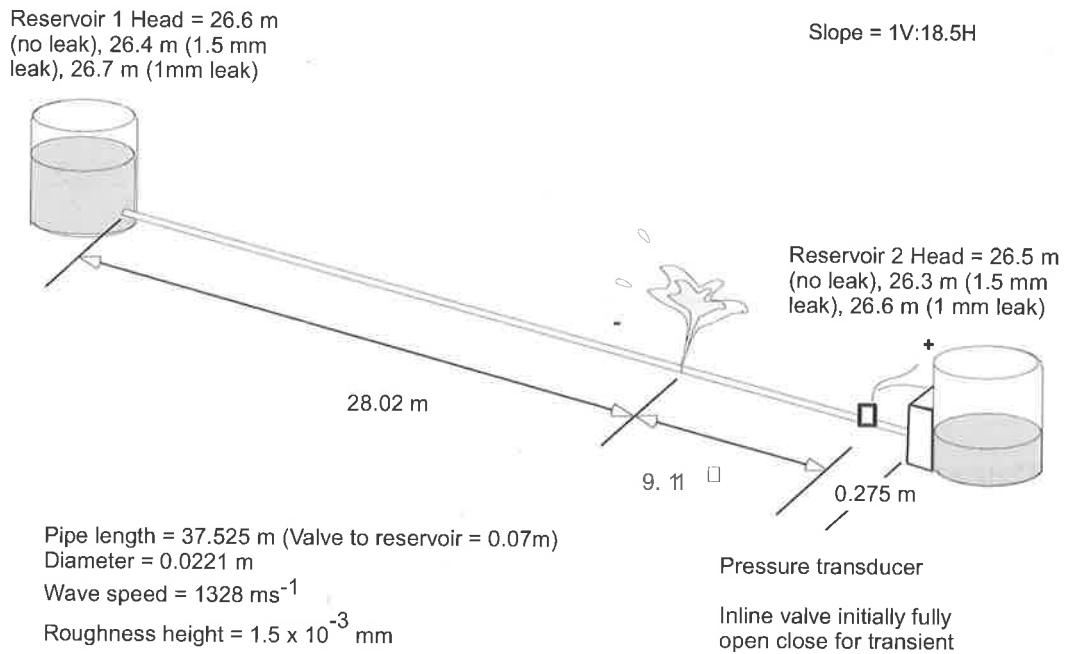


Figure 6-77 – System configuration for the in-line valve leak detection tests.

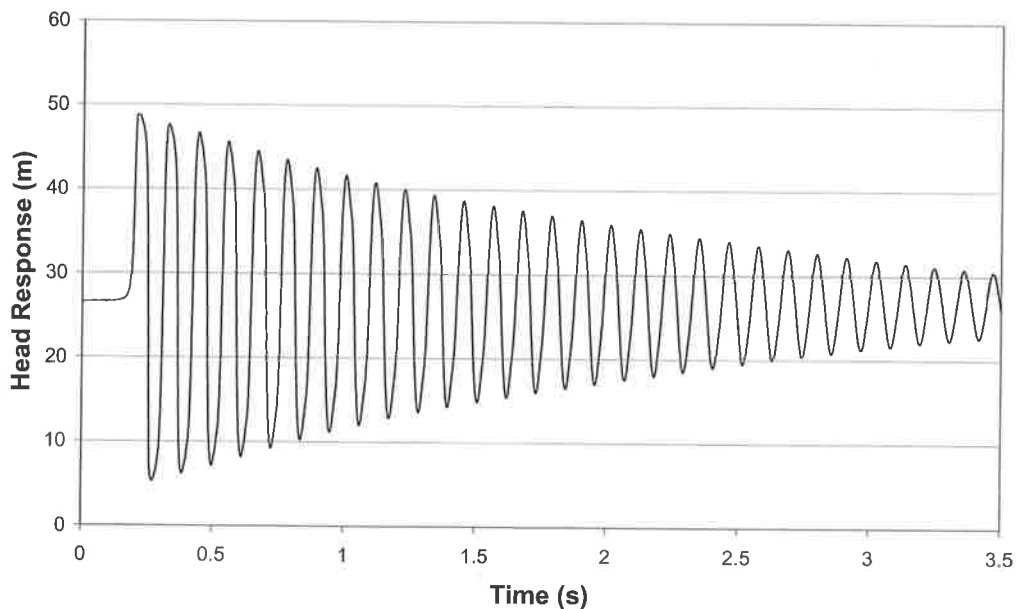


Figure 6-78 – In-line manual valve closure in the leak-free laboratory system.

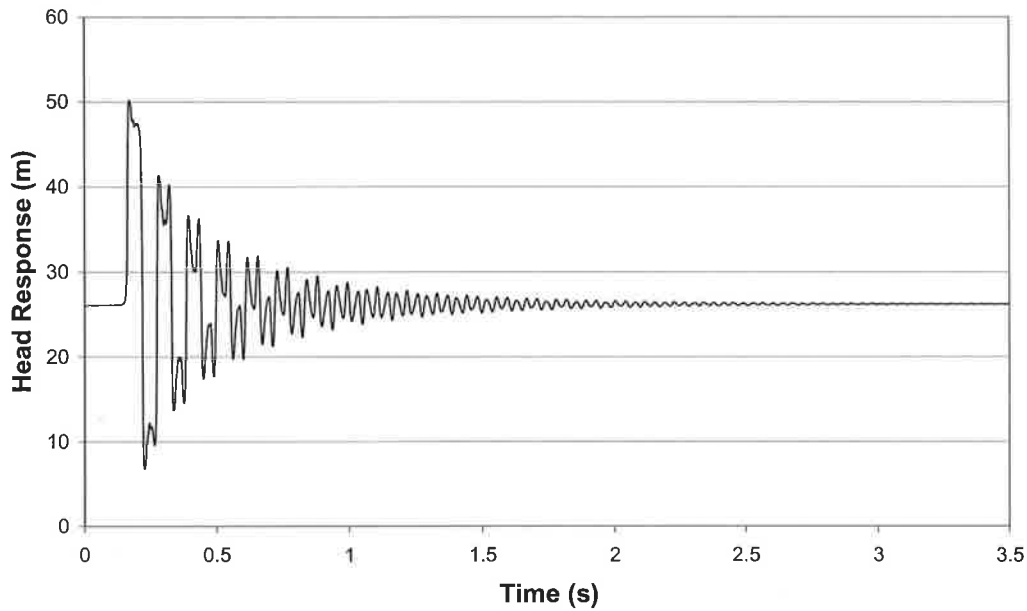


Figure 6-79 – Transient trace for the in-line valve closure leaking test with a 1.5 mm ($C_d A_L / A = 4.17 \times 10^{-3}$) leak at $x_L^* = 0.75$ (Data file: C6-L6.txt).

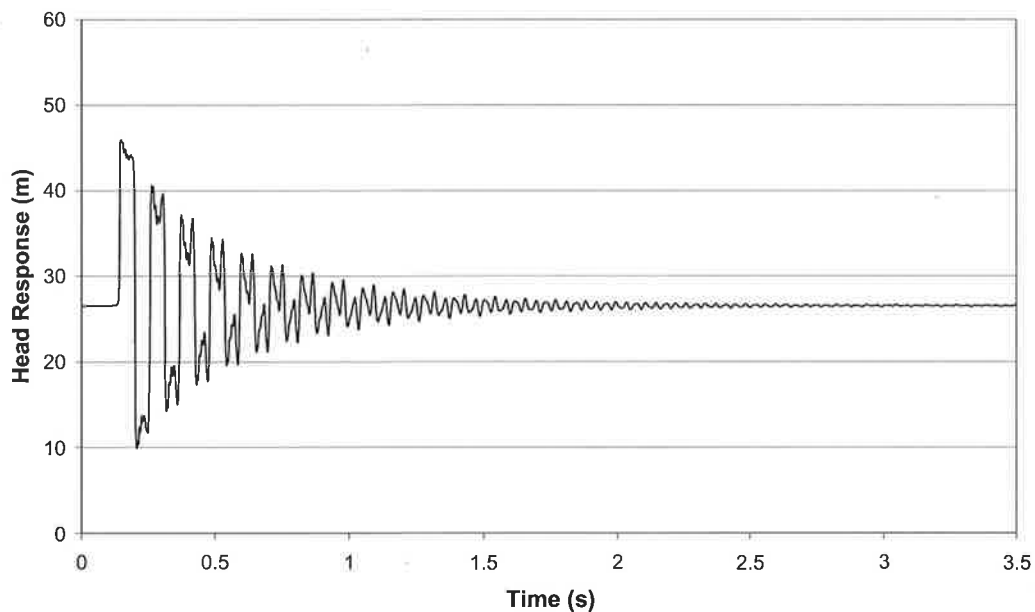


Figure 6-80 – Transient trace for the in-line valve closure leaking test with a 1.0 mm ($C_d A_L / A = 1.69 \times 10^{-3}$) leak at $x_L^* = 0.75$ (Data file: C6-L7.txt).

For all three tests, the in-line valve was initially fully opened then slammed shut manually. This type of transient was used in previous leak detection publications and can be generated in all existing pipelines without the need for specialised equipment.

Following the procedure for FRF, extraction gives the FRF's in Figure 6-81, Figure 6-82 and Figure 6-83.

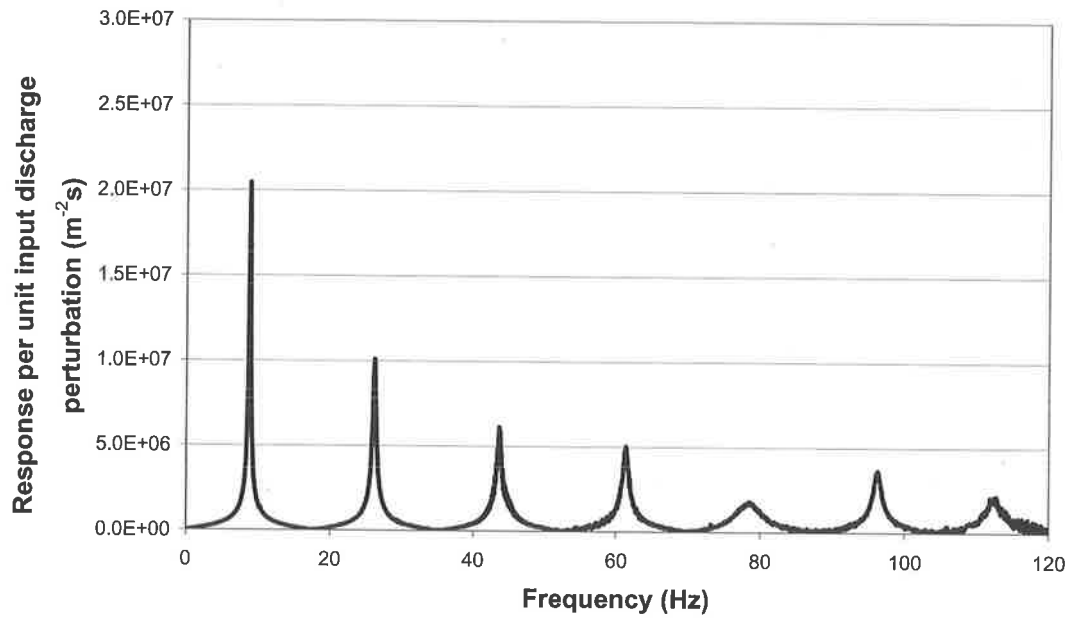


Figure 6-81 – FRF from a non-leaking pipeline generated by the manual closure of the in-line valve.

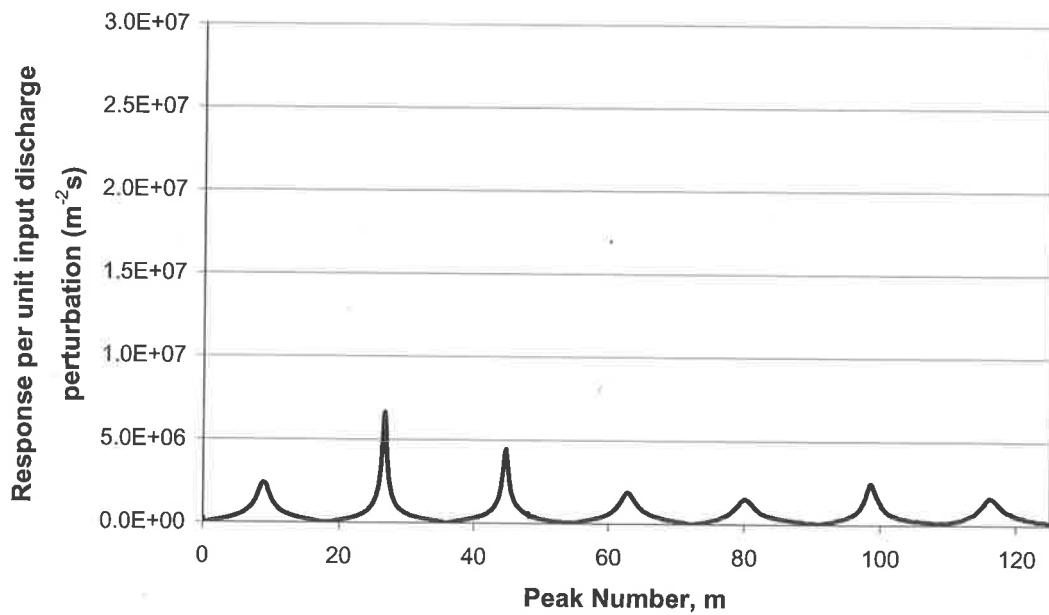


Figure 6-82 – FRF from experimental pipeline with a 1.5 mm leak ($C_d A_L / A = 4.17 \times 10^{-3}$, $x_L^* = 0.75$) using in-line valve closure.

The leak results in the damping of the original FRF and the suppression pattern appears to be periodic, indicating that a leak is present in the pipe. As the size of the leak increase

from 1 mm to 1.5 mm, there was a corresponding decrease in the magnitude of the peaks of the FRF.

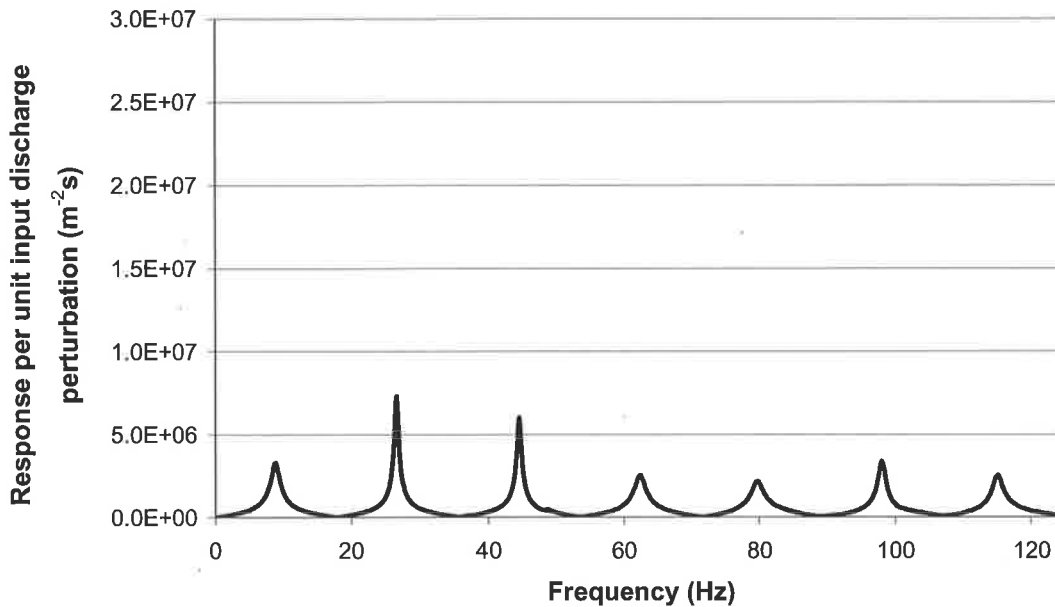


Figure 6-83 – FRF from experimental pipeline with a 1.0 mm leak
 $(C_d A_L / A = 1.69 \times 10^{-3}, x_L^* = 0.75)$ using in-line valve closure.

The least-squares regression of Eq. (6.63) to the data points are shown in Figure 6-84 and Figure 6-85 for the 1.5 mm and 1.0 mm leak, respectively. The results show a good match between the function and the data points and are summarised in Table 6-11. The final prediction of the leak locations for the leaking cases are $x_L^* = 0.754 \pm 0.026$ and 0.746 ± 0.008 for the 1 mm and 1.5 mm leaks, respectively; both are satisfactory estimates of the true leak position of $x_L^* = 0.751$. The same procedure was performed on the intact pipeline. The dominant frequency from the no-leak FRF is a trivial solution of $x_L^* = 0.5$, indicating that the system is leak free.

Table 6-11 – Summary for Experimental Tests.

Test Configuration	Predicted Frequency		Predicted Phase		Predicted Leak Location
	mean	Error	mean	error	
1 mm Leak at $x_L^* = 0.75$	0.246	0.004	0.571	0.12	$x_L^* = 0.754$
1.5 mm Leak at $x_L^* = 0.75$	0.254	0.013	0.772	0.418	$x_L^* = 0.746$
No Leak	0.50	-	1.57	-	$x_L^* = \text{NA}$

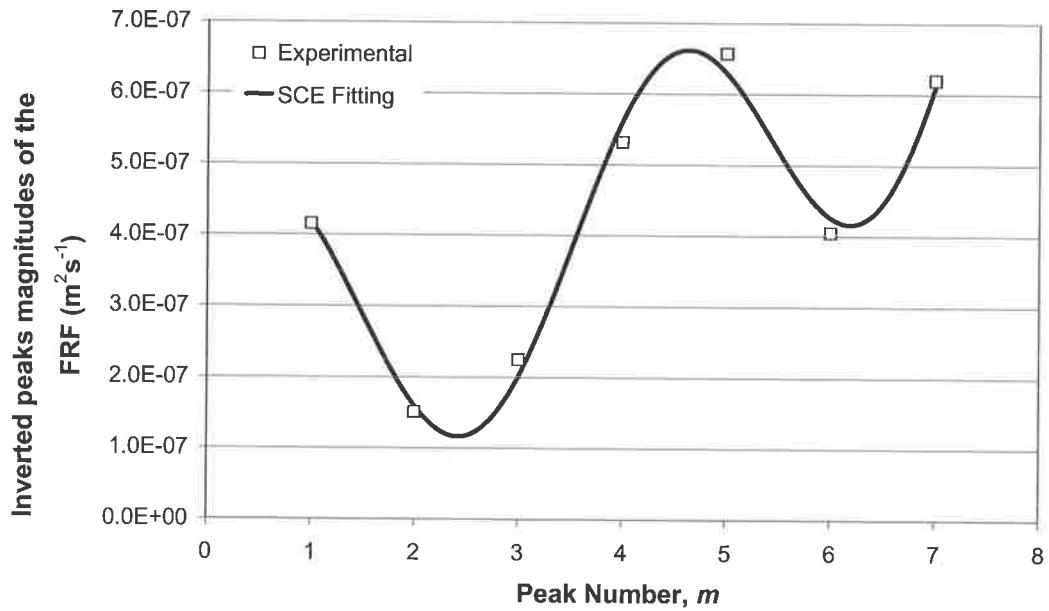


Figure 6-84 – Dominant frequency and phase extraction for leak size $C_d A_L / A = 4.17 \times 10^{-3}$ (1.5 mm) when in-line valve closure is used.

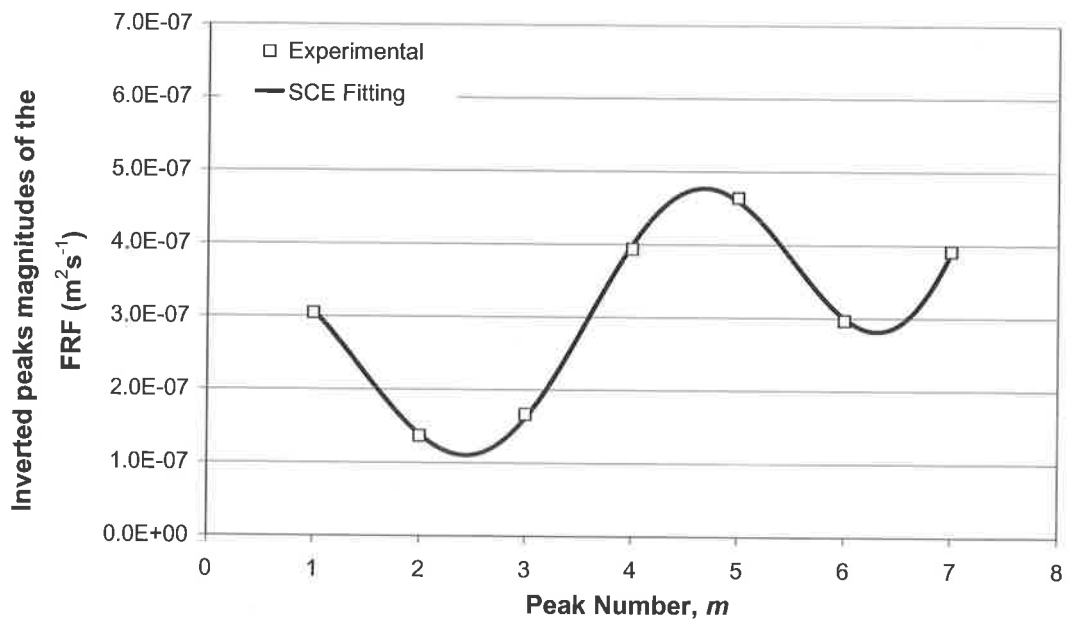


Figure 6-85 – Dominant frequency and phase extraction for leak size $C_d A_L / A = 1.69 \times 10^{-3}$ (1 mm) when in-line valve closure is used.

This section has shown a series of experimental tests for both in-line valve closure and the perturbation of a solenoid-actuated side-discharge valve. These tests (in combination with Section 6.6) provide a comprehensive confirmation of the leak-induced modification on the FRF and the leak detection procedure.

6.9 EXTENSION TO MULTIPLE LEAK DETECTION

Following the procedure for a single leak, an equivalent expression for the effect of multiple leaks in the pipe is derived.

For an anti-symmetric system where the boundary valve is fully closed, the expression for the response measured at the upstream face of the valve, h_{valve} , is given previously in Eq. (6.10) and repeated here as Eq. (6.67),

$$h_{\text{valve}} = -\frac{U_{21}U_{13}}{U_{11}} + U_{23} \quad (6.67)$$

The individual entries for the transfer matrix, U , are given in Appendix A for two leaks in the system. Substitution of these entries into Eq. (6.67) and simplifying the expression in a similar procedure to the single leak case give the response as

$$\frac{1}{|h_{\text{valve}}|} = \sum_{i=1}^{n_{\text{leak}}} \frac{Q_{L0i}}{4(H_{L0} - z_L)_i} (1 - \cos(2\pi m x_{L_i}^* - \pi x_{L_i}^*)) \quad (6.68)$$

where n_{leak} denotes the number of leaks. When the valve is throttled, the expression for the response at the upstream face of the valve, h_b , becomes

$$h_{\text{valve}} = \frac{U_{13} - \frac{U_{23}U_{11}}{U_{21}}}{\left(\frac{Q_{V0}}{2\Delta H_{V0}} - \frac{U_{11}}{U_{21}} \right)} \quad (6.69)$$

Substituting the entries of the transfer matrix in Appendix A and simplifying give

$$\frac{1}{|h_{\text{valve}}|} = \sum_{i=1}^{n_{\text{leak}}} \frac{Q_{L0i}}{4(H_{L0} - z_L)_i} (1 - \cos(2\pi m x_{L_i}^* - \pi x_{L_i}^*)) + \frac{Q_{V0}}{2\Delta H_{V0}} \quad (6.70)$$

Similarly, in a symmetric system, the response at the midpoint of the system, h_m , is

$$h_m = \frac{\frac{ia}{gA} \sin\left(\frac{l_a \omega}{a}\right) U_{23}}{U_{21}} \quad (6.71)$$

Substituting the entries of the transfer matrix when two leaks exist in the system, the expression becomes

$$\frac{1}{|h_m|} = \sum_{i=1}^{n_{leak}} \frac{Q_{L0i}}{4(H_{L0} - z_L)_i} \left(1 - \cos(4\pi m x_{Li}^* - 2\pi x_{Li}^*)\right) \quad 6.72$$

From each equation, each leak generates its own oscillation frequency on the peaks and the final result is a linear summation all these oscillations. As described in the single leak derivations, the equations are bounded by the approximation that the sum of $(Q_{L0} a) / (4(H_{L0} - z_L) g A)$ over all leaks is small. The detection and location of individual leaks in a pipeline depends on accurate extraction of the oscillation associated with each leak as shown in the following numerical and experimental examples.

6.9.1 Numerical validation of multiple leak detection

Three leaks of different sizes ($C_d A_L = 2.8 \times 10^{-7}$, 1.4×10^{-7} , $1.4 \times 10^{-6} \text{ m}^2$) are located at different positions along the 2000 m length simulation pipeline ($x_L^* = 0.244, 0.427, 0.641$). Unsteady friction and other frequency-dependent effects are negligible in the system. The boundaries of the pipeline are configured anti-symmetrically with the downstream valve open ($C_V = 0.002 \text{ m}^{5/2} \text{ s}^{-1}$). The configuration of the system is shown in Figure 6-86. The FRF was generated using the transfer matrix model. The spectrum of peak magnitudes is shown in Figure 6-87. Three distinct spikes appear in the spectrum, each corresponding to a leak. The properties of the three spikes and the corresponding leaks are shown in Table 6-12. The positions for each of the three leaks are accurately determined using the procedure.

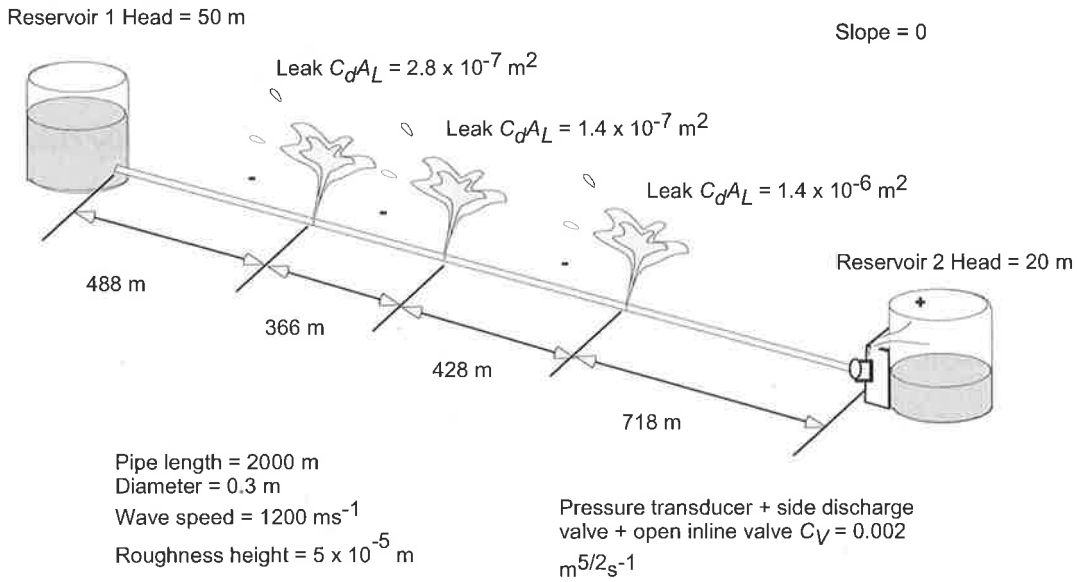


Figure 6-86 – System configuration for the numerical validation of multiple leak detection.

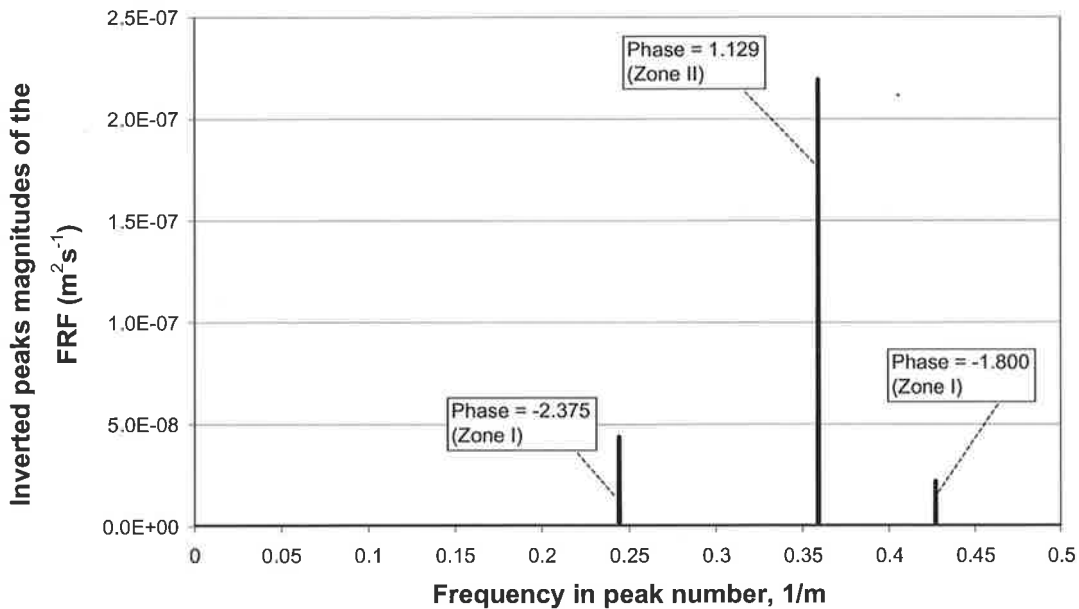


Figure 6-87 – Spectrum of peak magnitudes when three leaks exist in the pipeline.

Table 6-12 – Comparison of prediction accuracy of multiple leaks.

Leak Number	True Leak Position	Predicted Leak Position	True Leak Size	Predicted Leak Size
1	$x_L^* = 0.244$	$x_L^* = 0.244$	$C_d A_L = 2.8 \times 10^{-7}$	$C_d A_L = 2.801 \times 10^{-7}$
2	$x_L^* = 0.427$	$x_L^* = 0.427$	$C_d A_L = 1.4 \times 10^{-7}$	$C_d A_L = 1.402 \times 10^{-7}$
3	$x_L^* = 0.641$	$x_L^* = 0.641$	$C_d A_L = 1.4 \times 10^{-6}$	$C_d A_L = 1.400 \times 10^{-6}$

6.9.2 Experimental validation of multiple leak detection

Two leaks were placed in the laboratory pipe with the downstream valve fully closed. The leaks have $C_d A_L / A = 4.17 \times 10^{-3}$ (1.5 mm) and were located at $x_L^* = 0.179$ and 0.751 (refer to Figure 6-88). The resulting transient trace from the pulse operation of the solenoid valve is shown in Figure 6-89. The FRF of the system derived from this trace is in Figure 6-90.

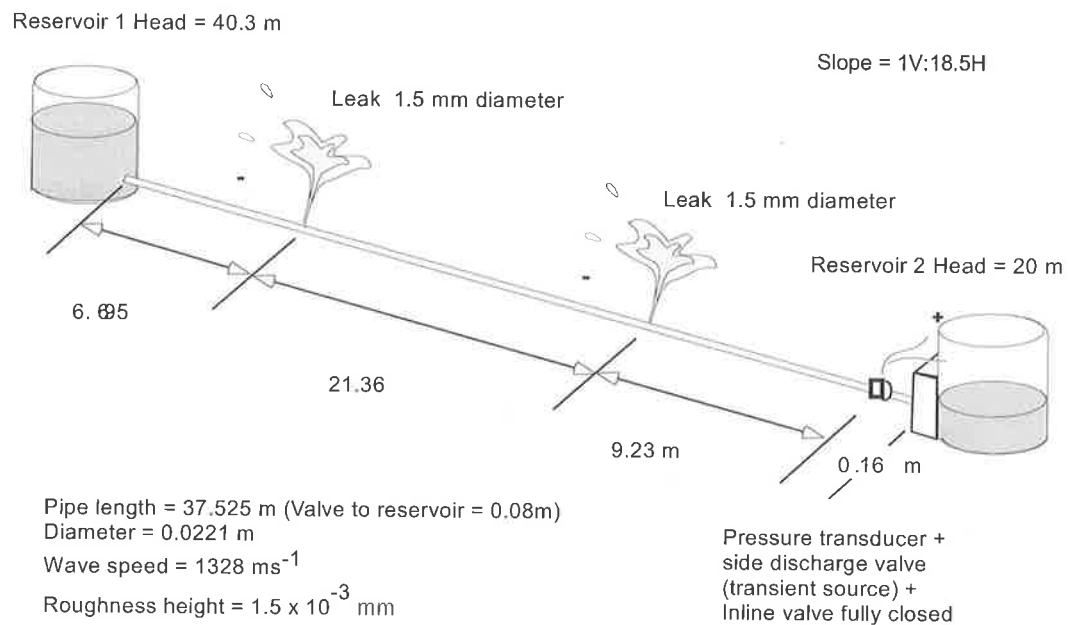


Figure 6-88 – System configuration for the experimental multiple leak detection.

To extract the oscillation frequencies and phases from the peaks of the FRF, the original fitting function in Eq. (6.63) is expanded for the two leak case,

$$E(m) = \frac{1}{S(m)} \times [X_1 \cos(2\pi m X_2 - X_3) + X_{11} \cos(2\pi m X_{12} - X_{13})] + T(m) \quad (6.73)$$

where $x_{11,12,13}$ are new parameters for the additional leak in the system. The forms of the scaling and trend functions remain the same for the multiple leak case. The result of fitting the function to the data is in Figure 6-91 and the leak detection result is summarised in Table 6-13. The data show two dominant oscillations, one with a frequency of 0.185 and the other with a frequency of 0.243. The standard deviations for these frequencies are

0.024 and 0.014, respectively. The phase for the 0.185 frequency is -2.11 , placing the leak in Zone I of the system. The first leak is predicted at $x_L^* = 0.185 \pm 0.048$ (at 95% confidence). The phase for the second frequency is 0.071 and the corresponding leak position is $x_L^* = 0.757 \pm 0.028$. The predicted positions for the leaks are close to the true positions of $x_L^* = 0.179$ and 0.751 .

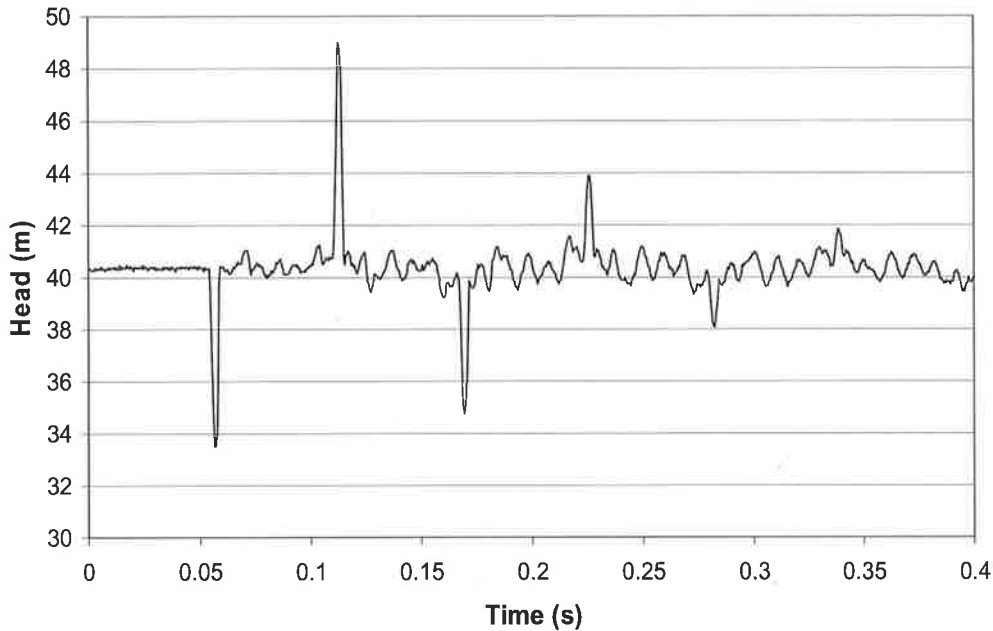


Figure 6-89 – Transient trace from a multiple leak situation in the laboratory pipeline (Data file: C6-L8.txt).

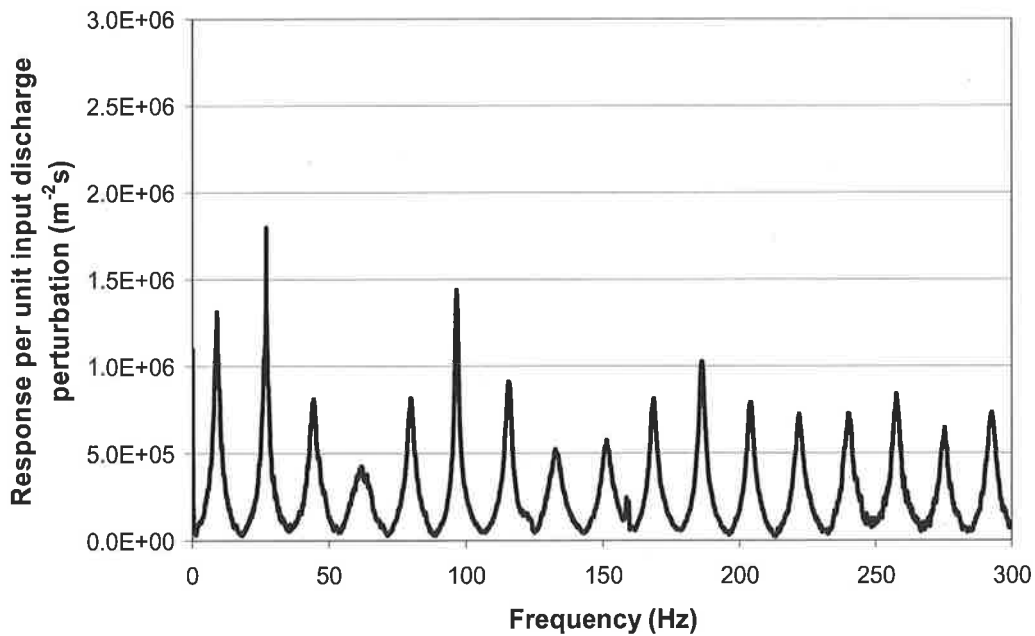


Figure 6-90 – FRF for the multiple leak situation.

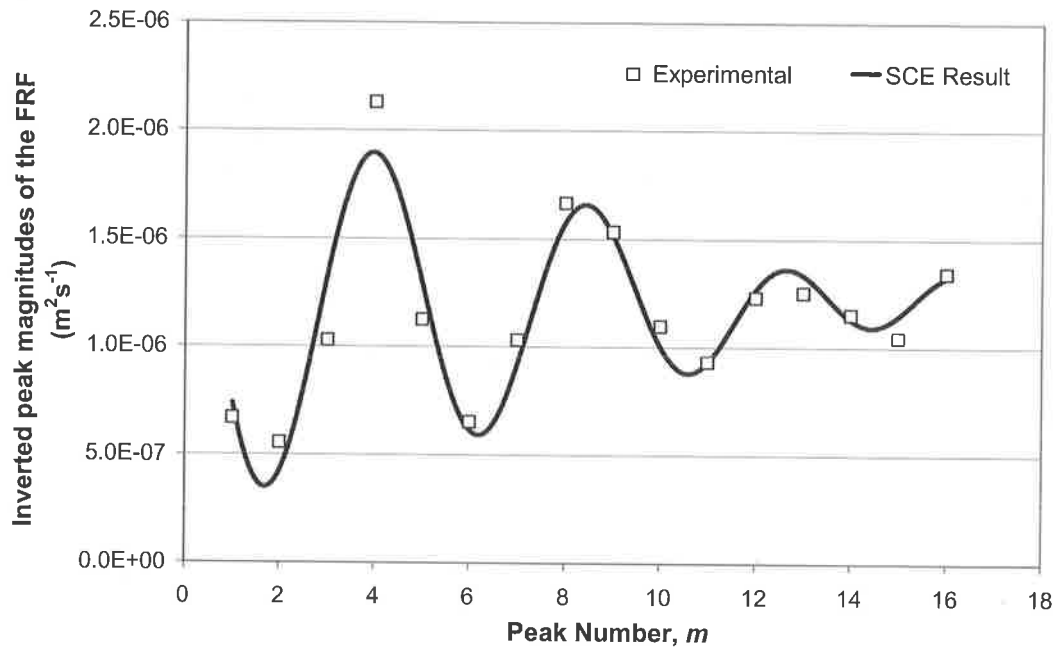


Figure 6-91 – Dominant frequency and phase extraction for the multiple leak case.

Table 6-13 – Summary of results for the experimental multiple leaks test.

Test Configuration	Predicted Frequency			Predicted Phase		Predicted Location
		mean	stdev	mean	stdev	
Leak 1 at $x_L^* = 0.179$	Leak 1	0.185	0.024	-2.11	1.44	$x_L^* = 0.185$
Leak 2 at $x_L^* = 0.751$	Leak 2	0.243	0.014	0.071	0.754	$x_L^* = 0.757$

The fitting function for multiple leaks can be applied for situations where only a single leak exists. This application is illustrated using experimental data from an anti-symmetric system with a single leak at $x_L^* = 0.751$. The result from the fitting using Eq. (6.73) is shown in Figure 6-92 and summarised in Table 6-14. In this case, only one non-trivial solution was found, corresponding to the correct location of the leak.

Table 6-14 – Summary of multiple leak detection with single leak data.

Test Configuration	Predicted Frequency		Predicted Phase	Predicted Location
Leak at $x_L^* = 0.751$	Leak 1	0.500	-	NA
	Leak 2	0.244	0.201 (Zone II)	$x_L^* = 0.756$

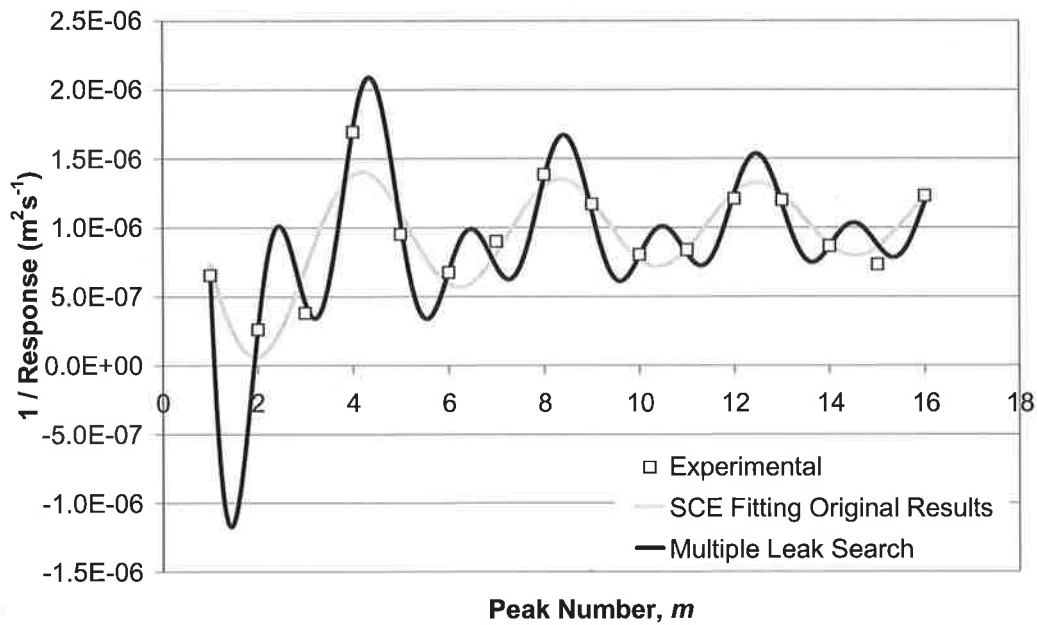


Figure 6-92 – Result of the multiple leak search on a single leak data for anti-symmetric leaking test with 1.5 mm ($C_d A_L / A = 4.17 \times 10^{-3}$) leak at $x_L^* = 0.751$.

This section illustrates how the technique can be used to find multiple leaks. The method is able to determine the location of each leak accurately in numerical and experimental investigations.

6.10 EXTENSION INTO DIFFERENT MEASUREMENT POSITIONS

The proposed leak detection method requires specific configurations of the transient measurement point and the transient source. While this is possible under a controlled laboratory system, the availability of access points for insertion of pressure transducers in a field pipeline can become a limiting factor. This section describes a correction procedure that overcomes this problem. In this procedure, the transient-generating source is assumed to be located at the correct position, whereas the measurement station is placed a distance away from the source. While devices for generating a transient event can often be found at the extremity of a system (e.g. an in-line valve), the location of an access port for the insertion of a pressure transducer adjacent to this device is often problematic.

The use of multiple measurement points can overcome the disadvantages of the measurement being located away from the optimum point. The results from two measurement positions can be combined and used to determine the head and discharge oscillation at the optimum position. The two measurement points should preferably be close together so that the section of pipe between the points can be verified as leak-free. The schematic for this situation is shown in Figure 6-93. The transient event is measured at each of the transducer locations and the corresponding response function determined for each.

The relationship bounding the head and discharge oscillations positions n and $n+1$ in Figure 6-93 is

$$\begin{bmatrix} q \\ h \end{bmatrix}^{n+1} = \begin{bmatrix} T_{11}^a & T_{12}^a \\ T_{21}^a & T_{22}^a \end{bmatrix} \begin{bmatrix} q \\ h \end{bmatrix}^n \quad (6.74)$$

where, T^a is the transfer matrix for pipe length "a." Expanding the bottom row and rearranging give

$$q_n = \frac{h_{n+1} - T_{22}^a h_n}{T_{21}^a} \quad (6.75)$$

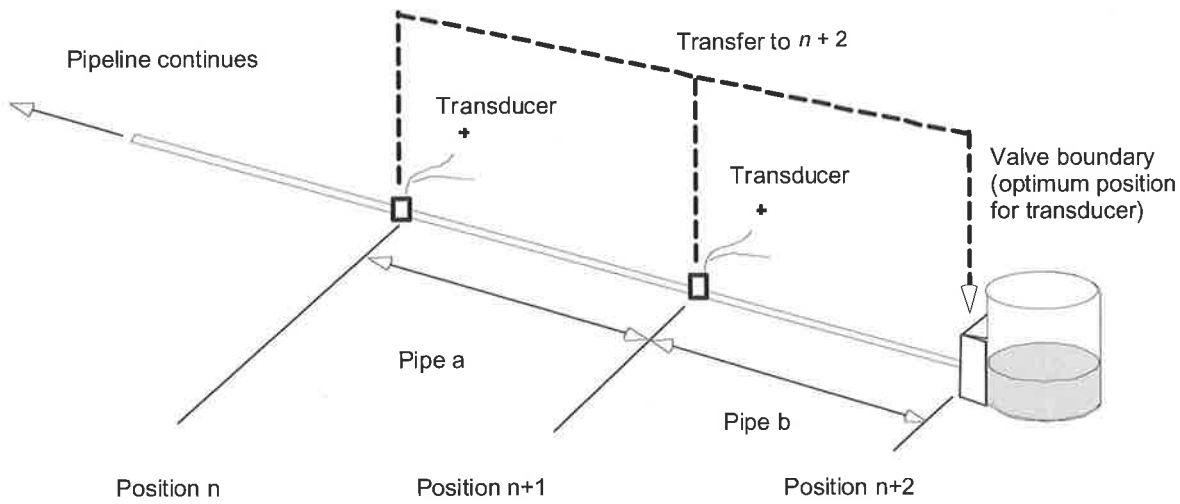


Figure 6-93 – Schematic for the measurement position transfer in an anti-symmetric system with transient generated by in-line valve.

Expanding the top row and substituting Eq. (6.75) for q_n give

$$q_{n+1} = T_{11}^a \left(\frac{h_{n+1} - T_{22}^a h_n}{T_{21}^a} \right) + T_{12}^a h_n \quad (6.76)$$

Consider now the transfer between positions $n+1$ and $n+2$

$$\begin{bmatrix} q \\ h \end{bmatrix}^{n+2} = \begin{bmatrix} T_{11}^b & T_{12}^b \\ T_{21}^b & T_{22}^b \end{bmatrix} \begin{bmatrix} q \\ h \end{bmatrix}^{n+1} \quad (6.77)$$

where, T^b = the transfer matrix for the pipe length between the second measurement point to the perturbation valve. The FRF at the optimum position, h_{n+2} , is given by

$$h_{n+2} = T_{21}^b q_{n+1} + T_{22}^b h_{n+1} \quad (6.78)$$

Substituting Eq. (6.76) for q_{n+1} gives

$$h_{n+2} = T_{21}^b \left(T_{11}^a \left(\frac{h_{n+1} - T_{22}^a h_n}{T_{21}^a} \right) + T_{12}^a h_n \right) + T_{22}^b h_{n+1} \quad (6.79)$$

The entries of both T^a and T^b can be determined from the entries of the transfer matrix for an intact length of pipeline. Using Eq. (6.79) the FRF at the optimum position can be found from two non-optimum measurement points.

The validity of the procedure is illustrated in the following example generated using the transfer matrix model with no unsteady friction. The transient is generated by the perturbation of the boundary valve. The FRF of the 2000 m long pipe is calculated using measurements from two different pressure transducers located 60 m (position “n” in Figure 6-93) and 50 m (position “n+1” in Figure 6-93) upstream of the valve. The optimum response location is the upstream face of the valve, position “n+2” in Figure 6-93. The original pressure responses are measured at both transducers and are shown in Figure 6-94.

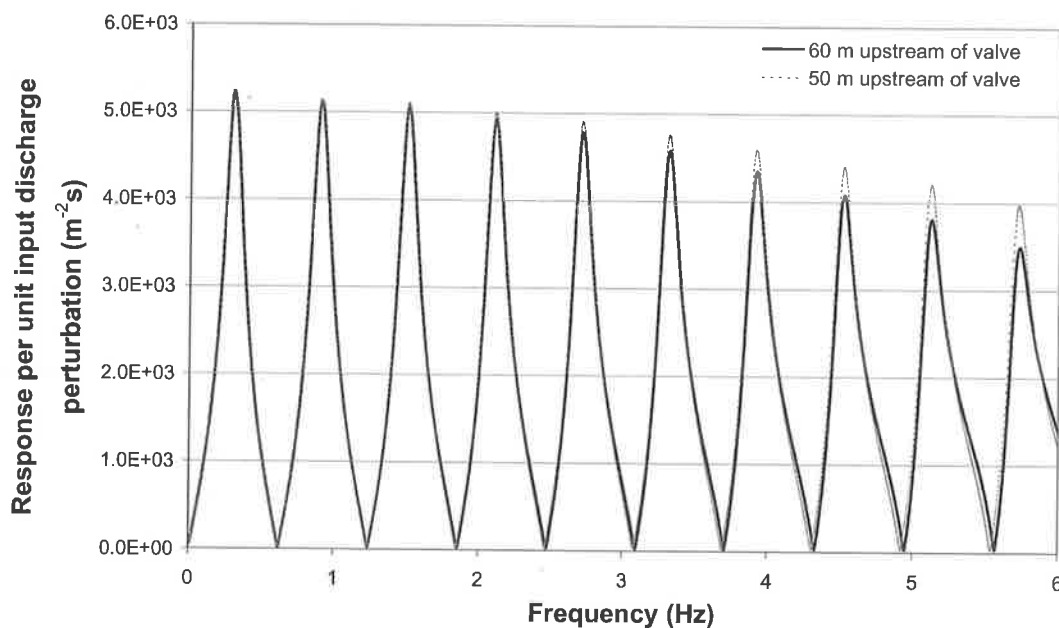


Figure 6-94 – The FRF from different measurement positions.

Combining these two responses in Eq.(6.79), the corrected response is compared to the true response at the valve in Figure 6-95. From the result, the scheme has accurately transferred the original response to the optimum position at the valve.

This scheme can be used in all cases where the pressure transducer is placed away from the optimum point, regardless of the nature of the transient-generating device (i.e. in-line or side-discharge valve). Although Figure 6-93 shows the FRF upstream of the in-line valve, the procedure can be applied to find the FRF at any point in the system given that two different measurement stations are available and the length of pipe between the transducers and the point of interest is intact.

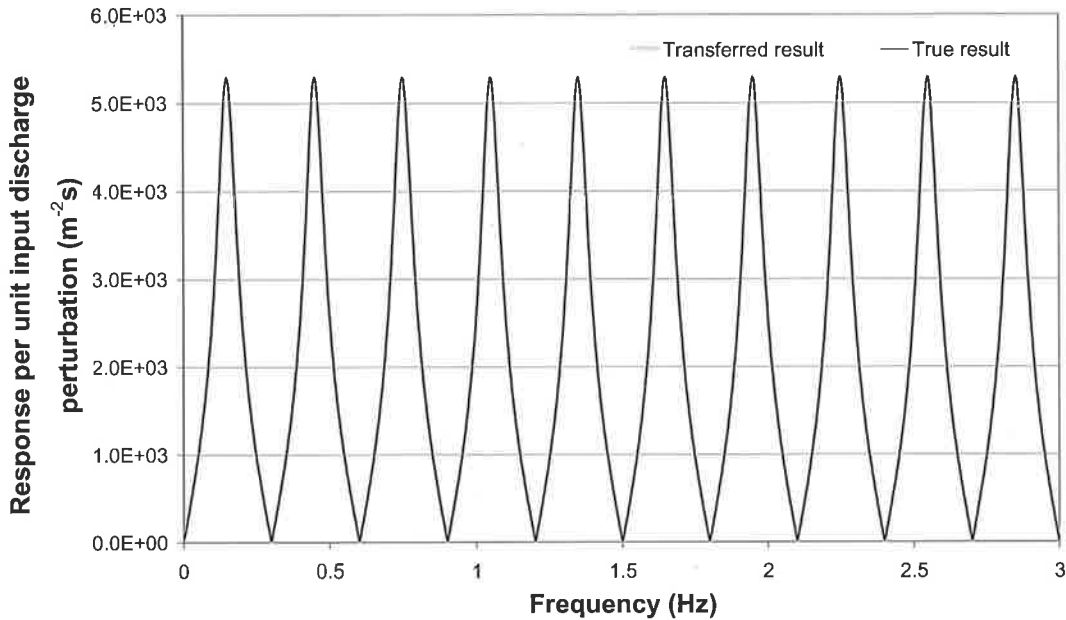


Figure 6-95 – Results of the FRF from single pipeline when the original FRFs from each measurement point are combined in Eq. (6.79) (the results overlap perfectly).

This procedure assumes the transient *generator* is located at the optimum position. In situations where this is not the case, a procedure for correcting the resultant FRF to give the FRF at the optimum configuration is not available. The system response function in the time domain—the impulse response function—is required for these cases (refer to Chapter 7).

6.11 EXTRACTION OF RESPONSE FUNCTION FOR PIPE SEGMENTS CONTAINED IN COMPLEX NETWORKS

The proposed leak detection method relies on the existence of well-defined boundaries at each end of a pipeline with the excitation valve at one end and a reservoir at the other. However, pipelines often contain multiple pipe sections or exist in complex networks. In such cases, the network is divided into pipe segments and the FRD for each individual pipe is determined.

To illustrate this procedure, consider the section of a pipeline network shown in Figure 6-96.

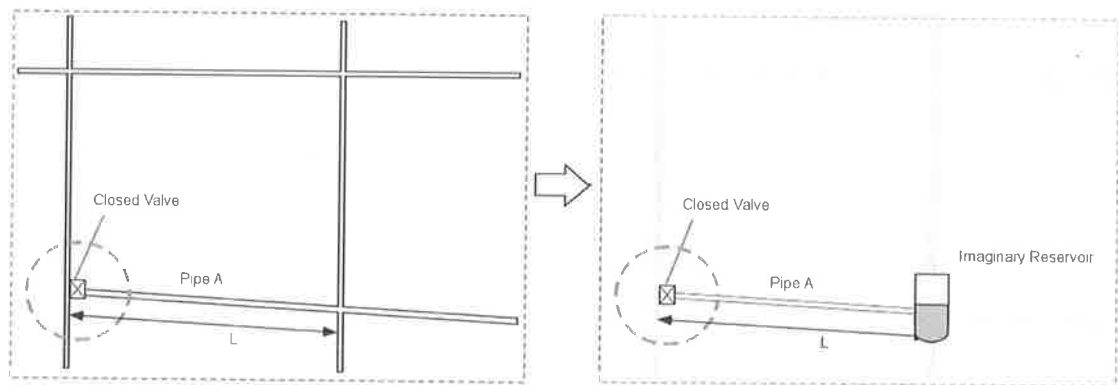


Figure 6-96 – Illustration of network analysis using the proposed procedure.

The network is a combination of individual single pipelines that can be partially separated from the main network by closing a single valve at one boundary of the pipe section. In Figure 6-96 only the indicated valve is closed. The closure of this valve defines a system boundary for the pipeline labelled “A” and a perturbation injected adjacent to the closed valve generates the transient signal needed for the analysis. The resultant transient trace from the injection of a pressure pulse at this position consists of the initial input pressure pulsation followed by possible reflections from pipe “A” up to a time of $2L/a$ seconds after which dispersed reflections from the rest of the network contaminate the trace.

To extract only the information related to the pipe “A”, the initial length of data ($t = 0$ to $t = 2L/a$) can be extrapolated to produce a synthetic signal that oscillates at the fundamental period of the pipe section by assuming a reservoir at the far boundary as shown in Figure

6-96. As the period of an anti-symmetric pipe is $4L/a$, the original $2L/a$ section of data needs to be extended to cover the complete period of the transient. An approximate reconstruction of the second half of the period for a reservoir boundary reflection is given by the inverted (upside down) version of the first $2L/a$ section of data, which is then attached to the end of the original section to produce the full period. This full period is then duplicated repeatedly until the number of data points needed for the desired resolution in the Fourier domain is reached. The reconstructed transient signal is analysed using the conventional procedure to produce the system response for this pipeline section.

This procedure is illustrated using the following numerical example. A leaking pipeline of length 2000m and internal diameter 0.3 is embedded in a complex network as shown in Figure 6-96. The configuration of the pipeline section is shown in Figure 6-97.

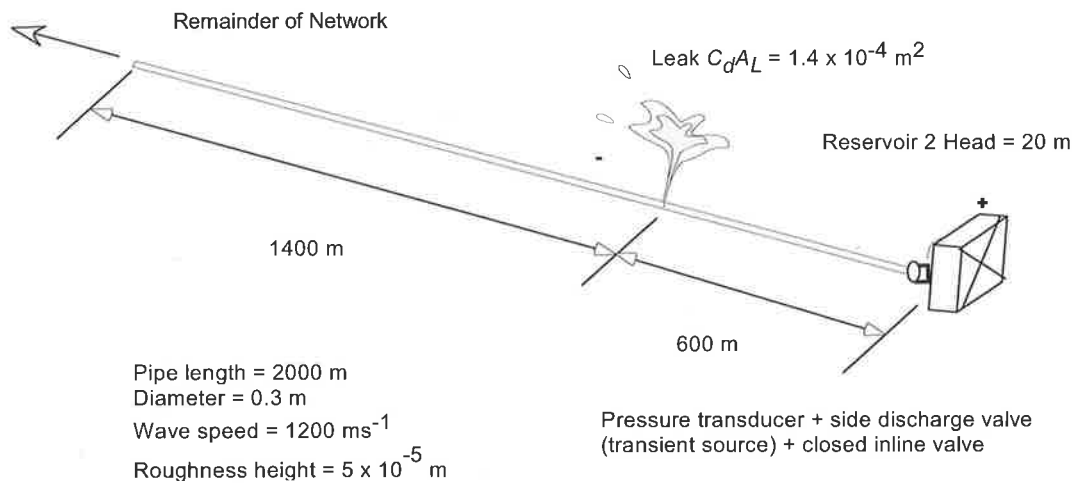


Figure 6-97 – Configuration of pipeline section.

To extract the FRF for this pipe section, the in-line valve is closed at one end to produce a definable boundary. A leak is located 600 m from the in-line valve with $C_d A_L / A = 1.98 \times 10^{-3}$. A transient is generated by perturbing a side-discharge valve located adjacent to the closed valve (duration of pulse perturbation = $6.66 \times 10^{-3} \text{ s}$). The transient trace is generated by the method of characteristics model with a discretisation of 500 and a computational time step of 3.33×10^{-3} seconds. The system is modelled as a single pipeline with randomly placed reflections after the time = $2L/a$ to simulate the response from the remainder of the pipeline network. The positions and sizes of these network reflections (hence the nature of the network itself) play no part in this analysis and were

created strictly for illustrative purposes. The resultant transient signal from the arbitrary network is shown in Figure 6-98.

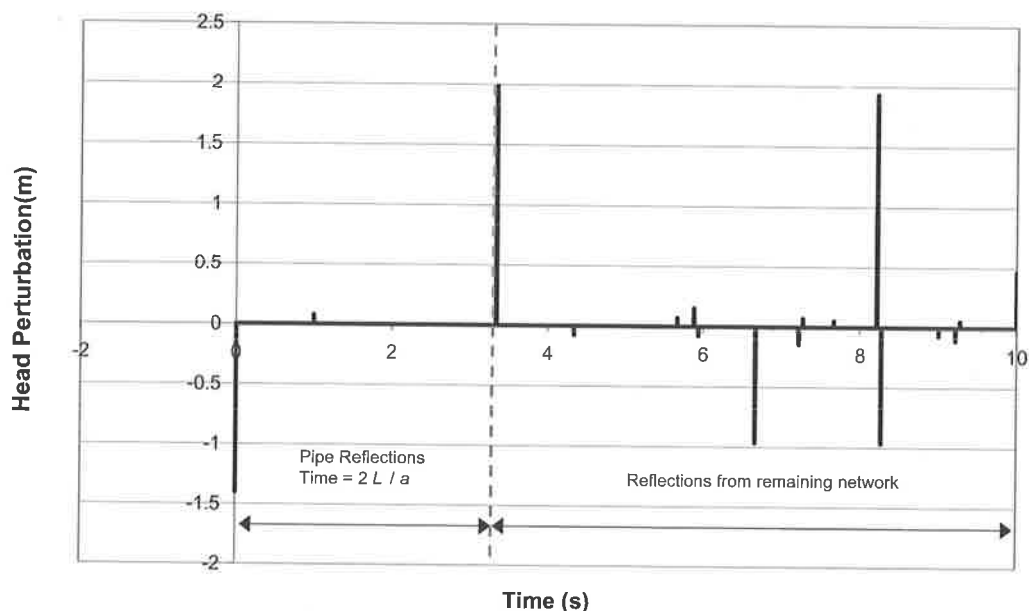


Figure 6-98 – Typical numerical results from an arbitrary network shown in Figure 6-96

Extrapolating the first $2L/a$ of the transient signal gives the trace of Figure 6-99 (extended into Figure 6-100) with the FRF in Figure 6-101. The resultant FRF has peaks at the odd multiples of the pipe fundamental frequency and the magnitudes of the peaks oscillate in a periodic pattern. The FRF of the same pipeline existing as a *single* pipeline (bounded by a reservoir on the upstream and a valve on the downstream) is shown in Figure 6-102. Comparison between the two results indicates that the extension of the first half period of the original signal from a network produces peaks in the FRF that vary in the same pattern as the FRF from the independent pipeline. This procedure can modify the network trace into a form that approximates a transient signal propagating between two well-defined boundaries, thus allowing the direct application of the leak detection procedures derived in this chapter. In addition, this procedure does not require the full isolation of the pipeline from the remaining network and supply can be maintained for the offtakes along the pipe.

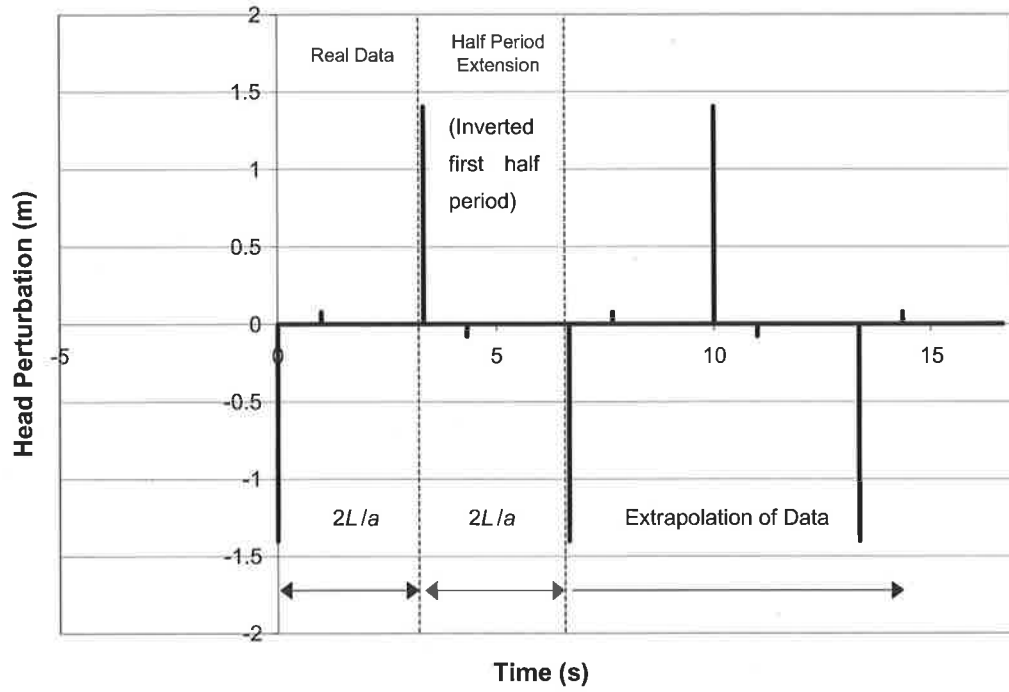


Figure 6-99 – Extension of the first half period data in Figure 6-97.

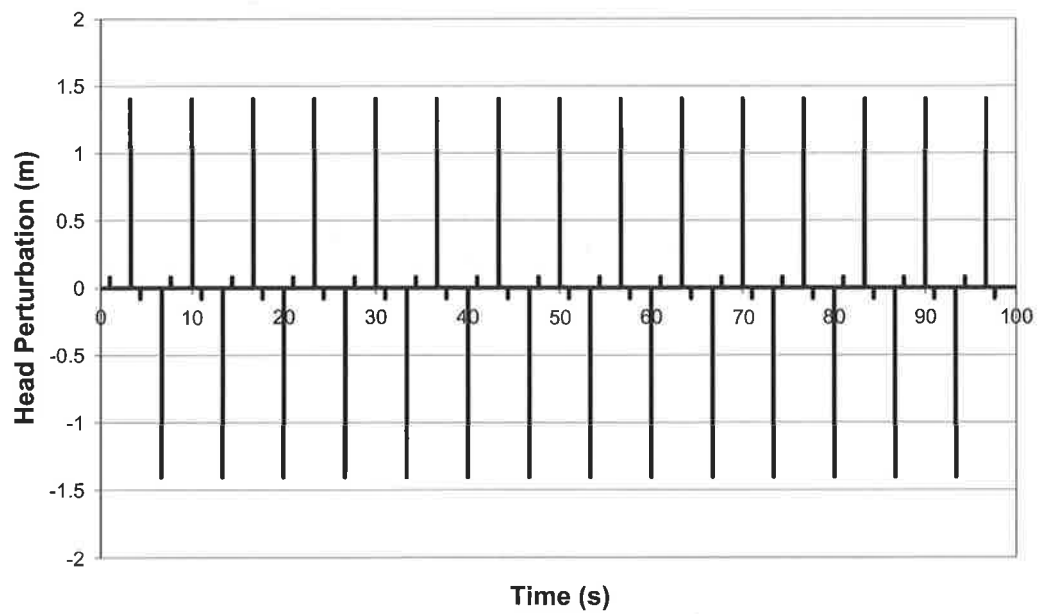


Figure 6-100 – Synthetically extended data for the extraction of the pipe FRF.

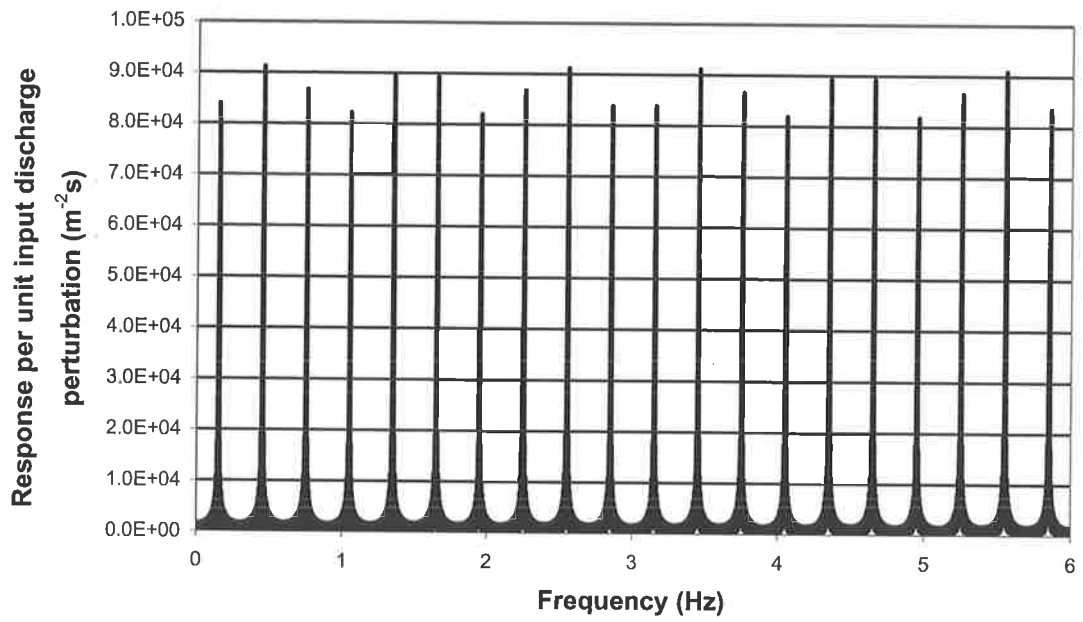


Figure 6-101 – Approximate FRF of pipeline using half-period extension procedure.

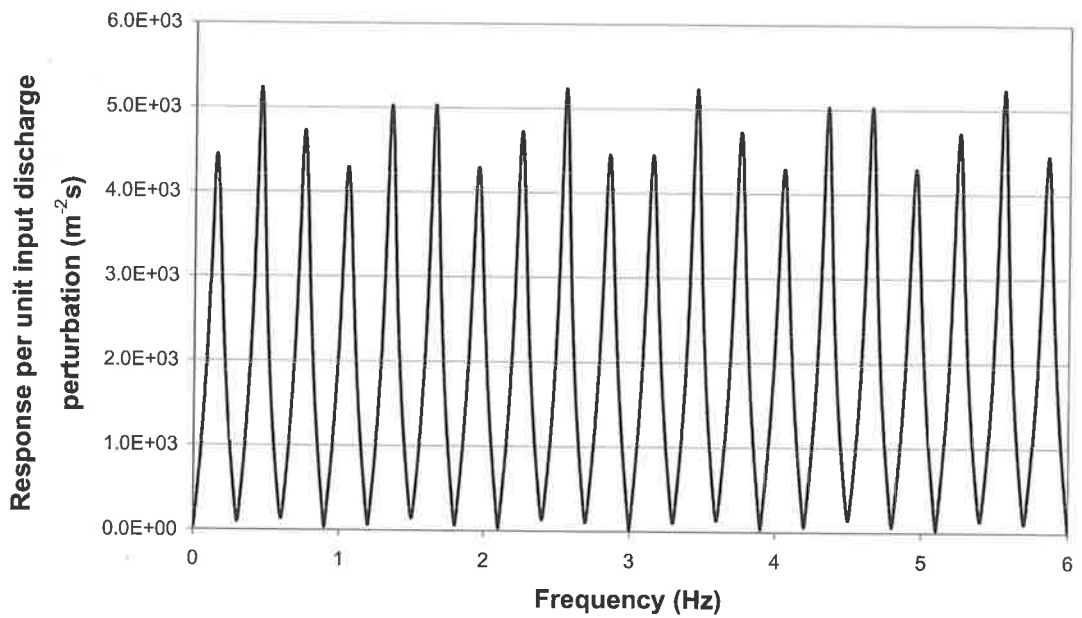


Figure 6-102 – FRF of the pipeline existing as a separate pipeline.

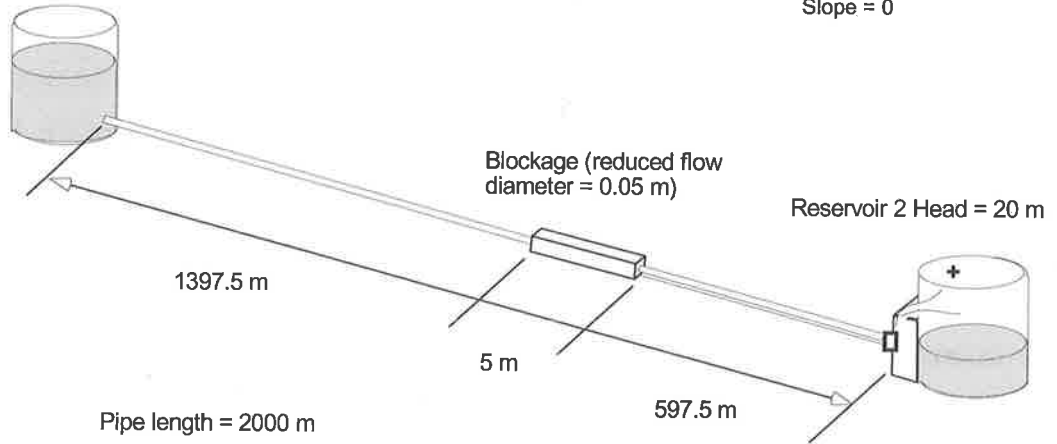
6.12 DISCRETE BLOCKAGE DETECTION

The technique of leak detection presented in this chapter can be modified for the detection of discrete blockages in a system. Amongst the types of faults that can occur in a pipeline, the formation of (partial) blockages poses an elusive problem for existing fault detection technologies. Unlike leaks in piping systems, the presence of a block does not generate clear external indicators for its location and such faults cannot be easily located unless intrusive procedures, such as the insertion of a closed-circuit camera or a robotic pig, are applied.

The medical field was amongst the first to use the FRF of pipe-like systems for measurement in the human vocal tract (Schroeder 1967, Mermelstein 1967). Schroeder (1967) found that prolonged changes in the area of the tract impose shifts in the position of the resonance peaks in the frequency response function of a system and Mermelstein (1967) provided a numerical explanation of this finding. Antonopoulous-Domis (1980), Qunli and Fricke (1989, 1991) and De Salis and Oldham (1999, 2001) further improved the method and applied it to detection and location of extended blockages in gas pipelines. These techniques rely on the measured shifts in the resonant frequencies for the detection of extended blockages in gas transmission ducts. A series of numerical investigations were conducted to determine the extent of these peak shifts in a pressurised liquid system. Figure 6-103 shows the configuration of the system and Figure 6-104 shows the FRF of the numerical pipeline when a blockage of 5 m length exists between 1397.5 and 1402.5 m from the upstream boundary. The blockage results in a reduced flow diameter of 0.05 m in the blocked section. The FRF of the system when no blockage exists is shown in the figure. The system has anti-symmetric boundaries with the in-line valve at the downstream end fully opened ($C_v = 0.002 \text{ m}^{5/2}\text{s}^{-1}$). The FRF from the partially blocked pipeline is significantly different from the normal response with deviations found in both magnitudes and positions of the peaks. When the extent of the blockage is reduced to 3m (while keeping the central point of the blockage at the same position), the resultant FRF is shown in Figure 6-105 and when the blockage is of a 0.5 m length in Figure 6-106.

Reservoir 1 Head = 50 m

Slope = 0



Pipe length = 2000 m

Diameter = 0.3 m

Wave speed = 1200 m s^{-1}

Roughness height = $5 \times 10^{-5} \text{ m}$

Perturbing inline valve

Inline valve $C_V = 0.002 \text{ m}^{5/2} \text{ s}^{-1}$

Figure 6-103 – System configuration of the blockage example.

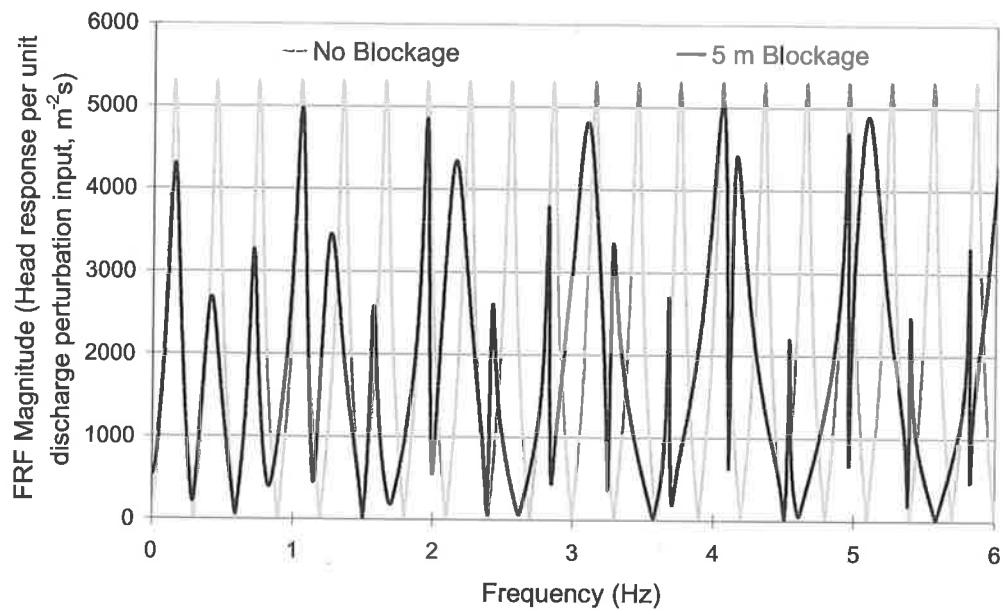


Figure 6-104 – Illustration of the resonant peaks shift as a result of a 5 m blockage in the numerical pipeline with a reduced flow diameter of 0.05 m.

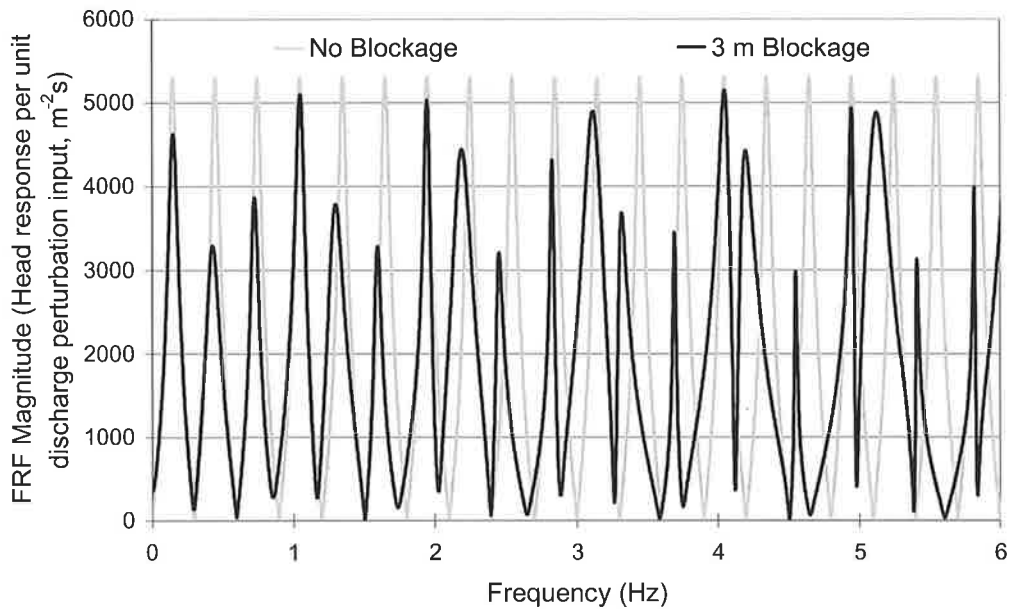


Figure 6-105 – Illustration of the resonant peaks shift as a result of a 3 m blockage in the numerical pipeline with a reduced flow diameter of 0.05 m

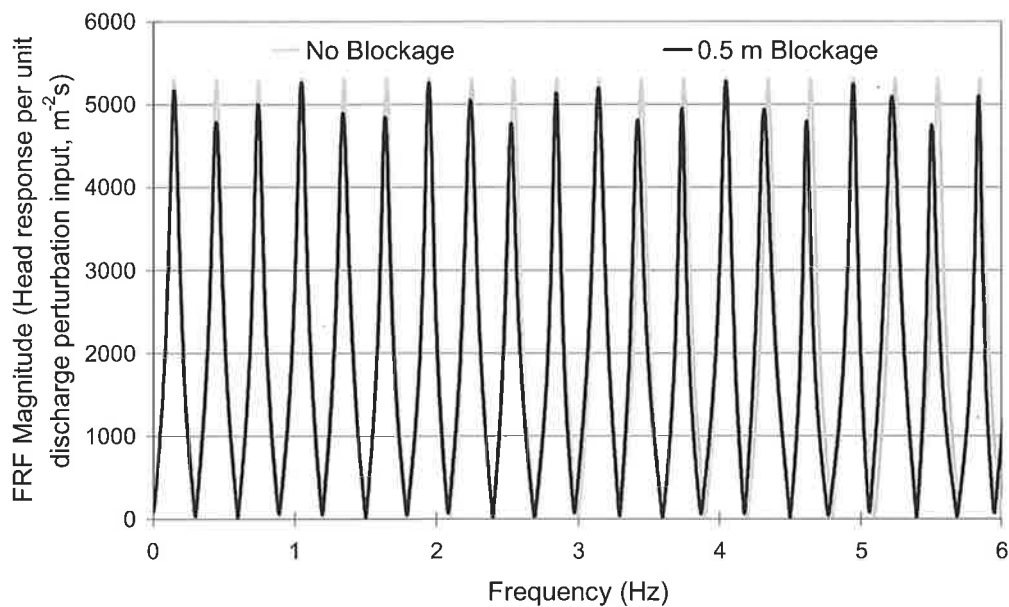


Figure 6-106 – Illustration of the resonant peaks shift as a result of a 0.5 m blockage in the numerical pipeline with a reduced flow diameter of 0.05 m.

The results indicate that, as the length of the blockage decrease, the magnitude of the shifts in the position of the resonant peaks becomes less noticeable; instead, only a periodic damping pattern in the resonant peaks remains. In cases where the extent of the blockage is not substantial in relation to the scale of the pipeline, techniques that rely on

these resonant shifts as a means of blockage location are not applicable. For these mild blockage cases in large systems, each block can be considered as a discrete blockage, similar to that generated by a partially closed in-line valve. In the next section an analytical expression is derived that allows discrete blockages to be detected in a single pipeline using the shape of the FRF.

6.12.1 Effect of blockage on the peaks of the FRF

The behaviour of a discrete blockage can be considered similar to an in-line valve having a transfer matrix of the form

$$\begin{Bmatrix} q \\ h \end{Bmatrix}^{n_3} = \begin{bmatrix} 1 & 0 \\ -\frac{2\Delta H_{B0}}{Q_{B0}} & 1 \end{bmatrix} \begin{Bmatrix} q \\ h \end{Bmatrix}^{n_2} \quad (6.80)$$

where, Q_{B0} , ΔH_{B0} = steady state (initial) flow through the blockage and steady state (initial) head loss across the block, respectively. The effect of a discrete blockage on the anti-symmetric numerical pipeline in Figure 6-107 is shown in Figure 6-108.

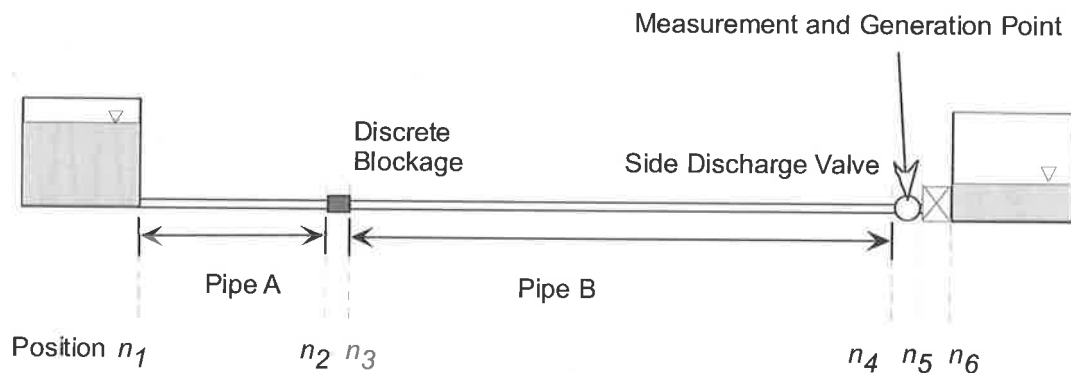


Figure 6-107 – Pipeline under consideration.

The extent of the blockage is measured by the impedance, $Z_B = 2\Delta H_{B0} / Q_{B0} = 1527.8 \text{ m}^{-2}\text{s}$, where ΔH_{B0} = the head loss across the blockage and Q_{B0} = the discharge through the blockage. The location of the block is defined as

$$x_b^* = \frac{L_A}{L_A + L_B} \quad (6.81)$$

where L_A, L_B = lengths of the pipe section upstream and downstream of the blockage, respectively and for this case $x_b^* = 0.878$.

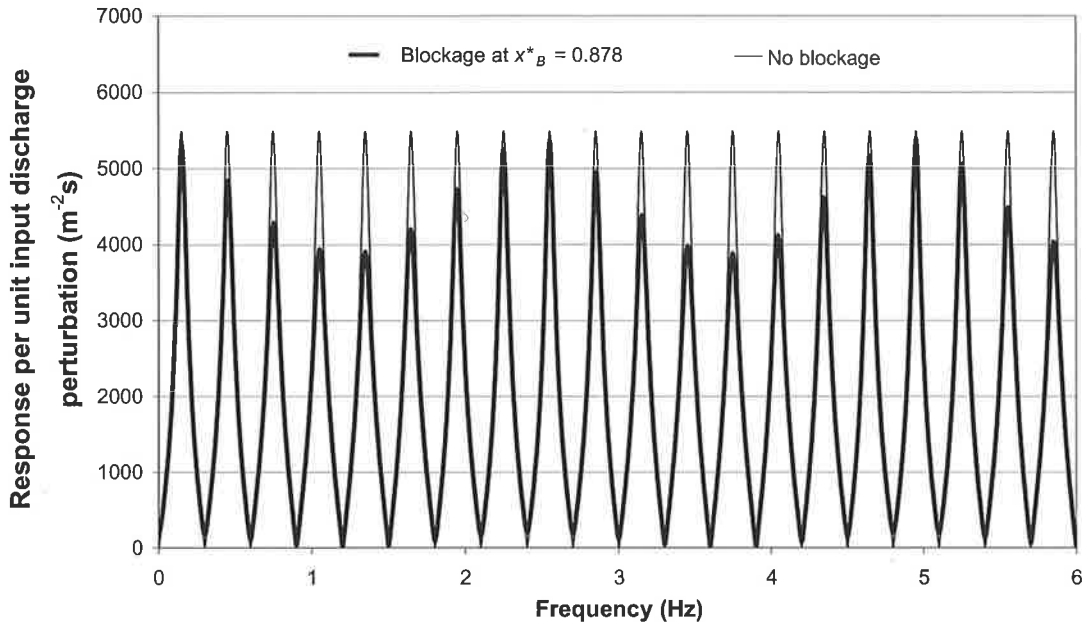


Figure 6-108 – FRF of the blocked and unblocked numerical pipeline.

For the purpose of isolating the effect of the block on the FRF, the pipeline is assumed to be frictionless. The result in Figure 6-108 indicates that the presence of a discrete blockage in the system induces a sinusoidal-like oscillation on the peaks of the FRF (as in the case for a leak). The analytical expression for this blockage-induced pattern on the peaks of the FRF can be determined using the same procedure as the analytical expression for the leak-induced modification on the FRF. The derivation is carried out in the anti-symmetric system of Figure 6-107.

For an anti-symmetric system with an in-line valve, the frequency response function measured at a position just upstream of the boundary valve is given in Eq. (6.32) and repeated here as

$$h_b = \frac{U_{13} - \frac{U_{23}U_{11}}{U_{21}}}{\left(\frac{Q_{V0}}{2\Delta H_{V0}} - \frac{U_{11}}{U_{21}} \right)} \quad (6.82)$$

The entries of the transfer matrix, U_{13} , U_{23} , U_{11} and U_{21} can be found by progressively multiplying together the matrices of each hydraulic element starting from the downstream end as illustrated in Section 3.3.1. The resultant simplified entries for U are

$$U_{23} = 0 \quad (6.83)$$

$$U_{13} = 1 \quad (6.84)$$

$$U_{11} = (-1)^{m+1} \frac{igA\Delta H_{B0}}{aQ_{B0}} + (-1)^{m+1} \frac{igA\Delta H_{B0}}{aQ_{B0}} \cos(2\pi x_B^* m - \pi x_B^*) \quad (6.85)$$

$$U_{21} = \frac{-ia}{gA} (-1)^{m+1} + \frac{2\Delta H_{B0}}{Q_{B0}} (-1)^{m+1} \sin(2\pi x_B^* m - \pi x_B^*) \quad (6.86)$$

Substituting these entries into Eq. (6.82) gives

$$h_{ns} = \frac{2\Delta H_{V0}}{Q_{V0} - 2\Delta H_{V0} \left[\frac{(-1)^{m+1} \frac{igA\Delta H_{B0}}{aQ_{B0}} + (-1)^{m+1} \frac{igA\Delta H_{B0}}{aQ_{B0}} \cos(2\pi x_B^* m - \pi x_B^*)}{\left[\frac{-ia}{gA} (-1)^{m+1} + \frac{2\Delta H_{B0}}{Q_{B0}} (-1)^{m+1} \sin(2\pi x_B^* m - \pi x_B^*) \right]} \right]} \quad (6.87)$$

where g = acceleration due to gravity, a = pipeline wave speed, A = cross-section pipe area, $i = \sqrt{-1}$ and the variable m = harmonic peak number in the FRF. For discrete blockages that do not result in a total constriction of the flow through the pipe, the term $2\Delta H_{B0}/Q_{B0}$ is small compared to $a/(gA)$ and Eq. (6.87) simplifies to

$$h_{n_5} = \frac{2\Delta H_{V0}}{Q_{V0} - 2\Delta H_{V0} \left[\frac{(-1)^{m+1} \frac{igA\Delta H_{B0}}{aQ_{B0}} + (-1)^{m+1} \frac{igA\Delta H_{B0}}{aQ_{B0}} \cos(2\pi x_B^* m - \pi x_B^*)}{\left[\frac{-ia}{gA} (-1)^{m+1} \right]} \right]} \quad (6.88)$$

Inverting the magnitude of this result and defining $Z_B = 2\Delta H_{B0} / Q_{B0}$ as the block impedance value, $Z = a / gA$ as the pipe characteristic impedance for a frictionless system and using $Z_V = 2\Delta H_{V0} / Q_{V0}$ as the valve impedance give an expression for the inverted peaks in the FRF as

$$\frac{1}{|h_{n_5}|} = \frac{1}{Z_V} + \frac{Z_B}{2Z^2} (1 + \cos(2\pi x_B^* m - \pi x_B^*)) \quad (6.89)$$

where the frequency of the oscillation (in “per peak interval”, $1/m$) is x_B^* , which is the coefficient to m and the phase is πx_B^* . Eq. (6.89) indicates that a blockage induces a sinusoidal oscillation on the inverted peaks of the FRF, similar to the effect of a leak. The properties of this block-induced oscillation are as follows:

- The **frequency** of the block-induced damping pattern from Eq. (6.89) is x_B^* . As in the leak situation, frequency aliasing means that for oscillation frequencies greater than the Nyquist frequency of 0.5, the signals appear with frequencies of $(1 - x_B^*)$. Each observed oscillation in the peaks of the FRF can be caused by two possible frequencies, one above the Nyquist frequency and one below.
- The **phase** of the block-induced damping pattern is πx_B^* and when the signal is aliased, the phase is $-\pi x_B^*$. This parameter can be used to indicate whether the frequency has experienced aliasing and the sign of the phase determines the correct blockage position. Signals with phase located near or in the first quadrant of the unit circle ($-\pi/4 \leq \text{phase} \leq 3\pi/4$) have the blockage in the upstream half of the pipe and phases near or in the third quadrant ($-\pi/4 \geq \text{phase} \geq -5\pi/4$) have the blockage in the downstream half (refer to Figure 6-109). The phases for the blockage are opposite to that from a leak (refer to Section 6.5.2).

- The **amplitude** of the blockage-induced damping pattern is $Z_B / (2Z^2)$, given in Eq. (6.89) as the coefficient to the block-generated cosine function.

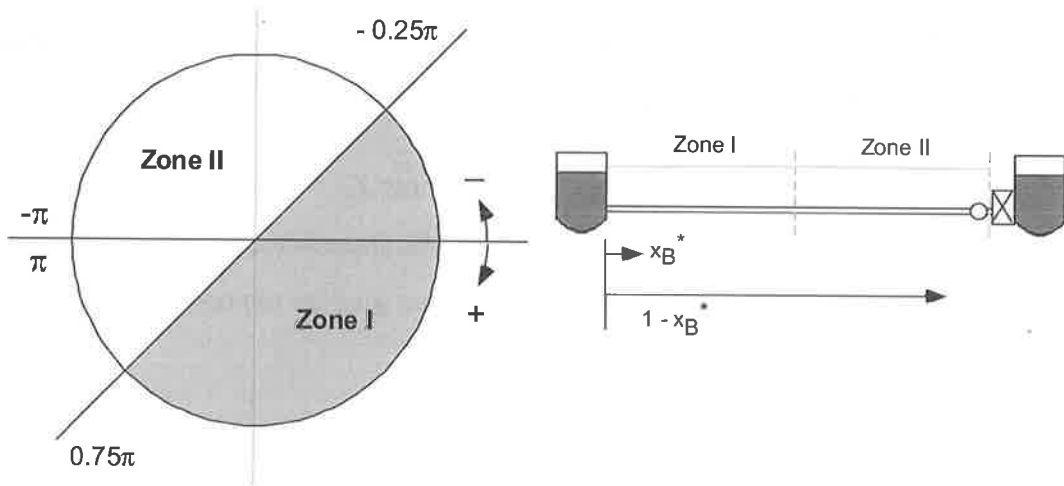


Figure 6-109 – Phase relationship with the block location.

The extraction of the frequency, phase and amplitude of the block-induced pattern from the inverted peaks of the FRF can be carried out using a Fourier transform or a least-squares regression procedure as shown previously. The procedure for blockage detection is as follows:

1. Generate the frequency response function (FRF).
2. Extract the magnitudes of the peaks in the FRF and invert them.
3. Determine frequency, phase and amplitude of the blockage-induced pattern.
4. Use the frequency to determine the two possible blockage locations, then use the value of the phase to determine the correct location.
5. Using the amplitude of the oscillation, determine the severity of the blockage, given by I_B .

6.12.2 Numerical validation of blockage detection technique

The validation of the analytical blockage effect on the FRF and the subsequent detection method is carried out numerically for an anti-symmetric system (refer to Figure 6-107). Three individual cases are considered with the block impedances and locations given in Table 6-15. The FRF of one of the cases is shown in Figure 6-108. The peaks of the FRF

for each blockage case were first inverted and then a Fourier transform was performed, the result of which is shown in Figure 6-110. For all cases, the oscillatory pattern in the inverted peaks have a frequency corresponding to either x_B^* or $(1-x_B^*)$ and for blocks located in the first half of the pipeline, the phase is in the first quadrant of the unit circle; it is in the third quadrant when the blockage is located in the downstream half. Using the above blockage detection procedure, the blockage is correctly located in the pipeline for all three cases. The severities of the blockages are determined within 0.5% of the true block impedance. The small discrepancy in the sizing of the blockage is a result of the approximation made between Eq. (6.87) and (6.88), where a small term was eliminated from the equation but has no effect on the accuracy of the block location. The oscillatory pattern imposed by the presence of a blockage is identical to that of a leak.

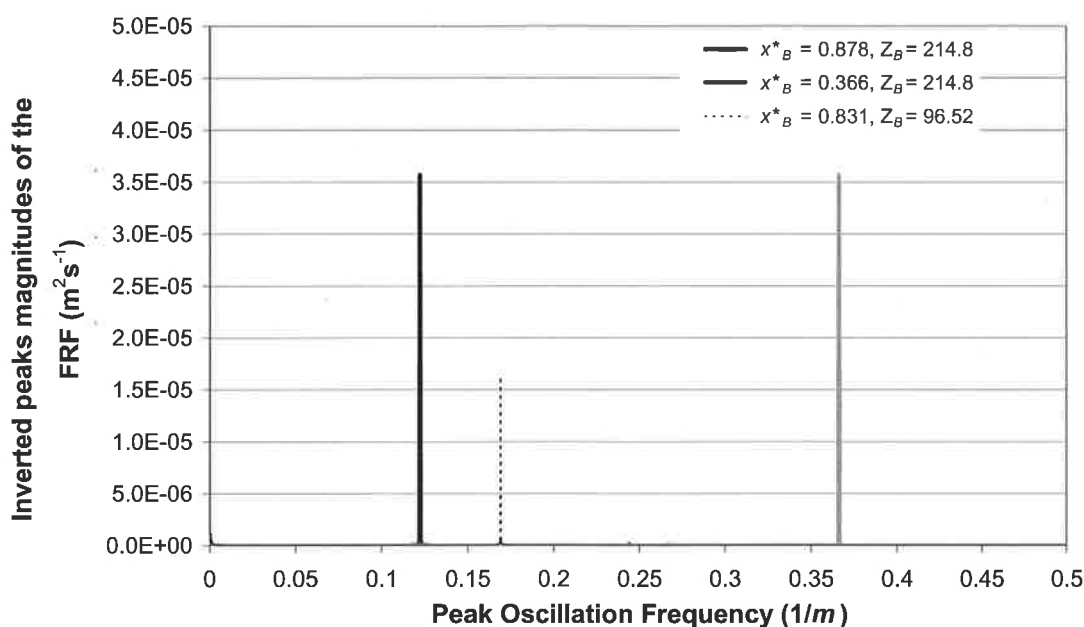


Figure 6-110 – Spectrum of the inverted peaks magnitudes for three different blockage conditions.

Table 6-15 – Results of single blockage detection.

Test Configuration		Pattern Properties			Predicted Blockage Properties
Position	Size	Freq.	Phase	Amplitude	
$x_B^* = 0.878$	$Z_B = 214.8$	0.122	-2.711	3.566×10^{-5}	$x_B^* = 0.878, Z_B = 213.8$
$x_B^* = 0.366,$	$Z_B = 214.8$	0.366	1.120	3.567×10^{-5}	$x_B^* = 0.366, Z_B = 213.8$
$x_B^* = 0.831,$	$Z_B = 96.52$	0.169	-2.500	1.600×10^{-5}	$x_B^* = 0.831, Z_B = 95.92$

Multiple Blockage detection

As in the leak detection case, the technique can be expanded to a multiple blockage situation. For this case, the entries of the system transfer matrix need to be reformulated. The resultant entries for the matrix are then substituted into Eq. (6.82) and the expression for the response, measured upstream of the valve, is rewritten as

$$\frac{1}{|h_{n_s}|} = \frac{1}{Z_V} + \frac{1}{2} \left(\frac{1}{Z} \right)^2 \sum_{k=1}^{n_{block}} [Z_{Bk} (1 + \cos(2\pi\alpha_{B_k}^* m - \pi\alpha_{B_k}^*))] \quad (6.90)$$

where n_{block} = number of blocks in the system. The subscript k indicates the property is associated with the k^{th} block. Eq. (6.90) shows that each block induces its own oscillatory pattern on the inverted peaks of the FRF, which can be separated in the Fourier spectrum as distinct effects from the different blockages. This approach is illustrated in the multiple block example in Figure 6-111. Two blocks of $Z_B = 34.96 \text{ m}^{-2}\text{s}$ are located in the pipe and details are shown in Figure 6-111 and Table 6-16. The Fourier spectrum of the inverted FRF peaks in Figure 6-112 indicates two frequencies, each associated to a particular blockage in the pipe. Applying the same procedure to each oscillation signal gives the correct position and size of the blockages in Table 6-16. As in the single block case, excellent accuracy was shown for the location and sizing of the blockages.

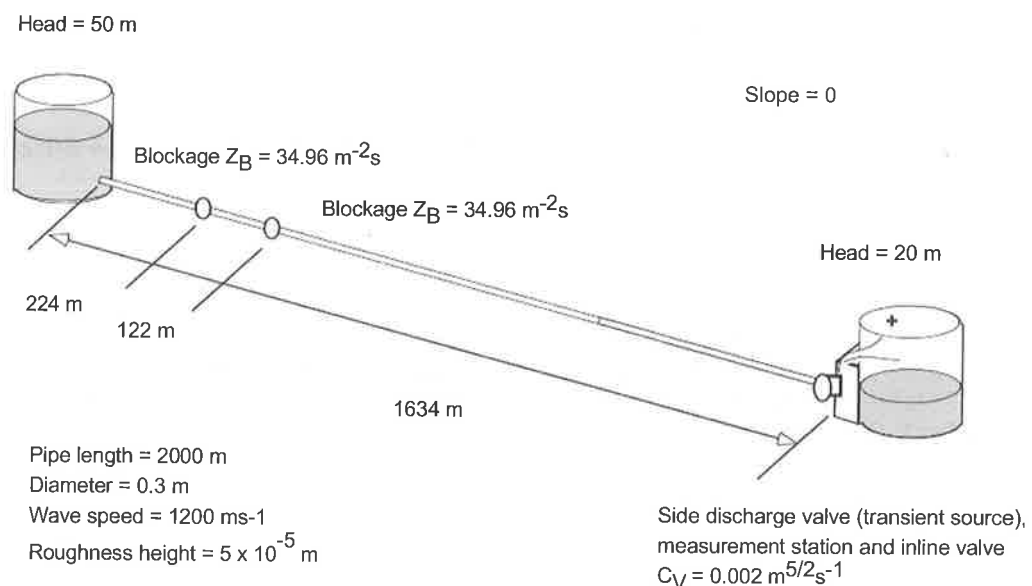


Figure 6-111 – System configuration for multiple block test.

This section developed and numerically validated the effect of a discrete blockage on the FRF of a pipeline. The effect is similar to that from a leak and is limited to the peaks of the response function. The presence of the discrete blockage can be identified by a periodic variation in the peak magnitudes in the FRF. The application of such a technique allows the detection and location of partially closed in-line valves or short sections of blockages (<0.5 m in a 2000 m pipeline). Additional experimental testing is required to determine the applicability of such a technique in a physical system.

The effect of a blockage is opposite to that produced by a leak. For example, the effect of a blockage at $x_B^* = 0.75$ is identical to the effect generated by a leak at $x_L^* = 0.25$ (i.e. at the mirror position from the blockage). This issue highlights a possible problem in applying the FRF method for fault detection as each detected oscillation indicates either a leak at one position or a blockage at the mirror position.

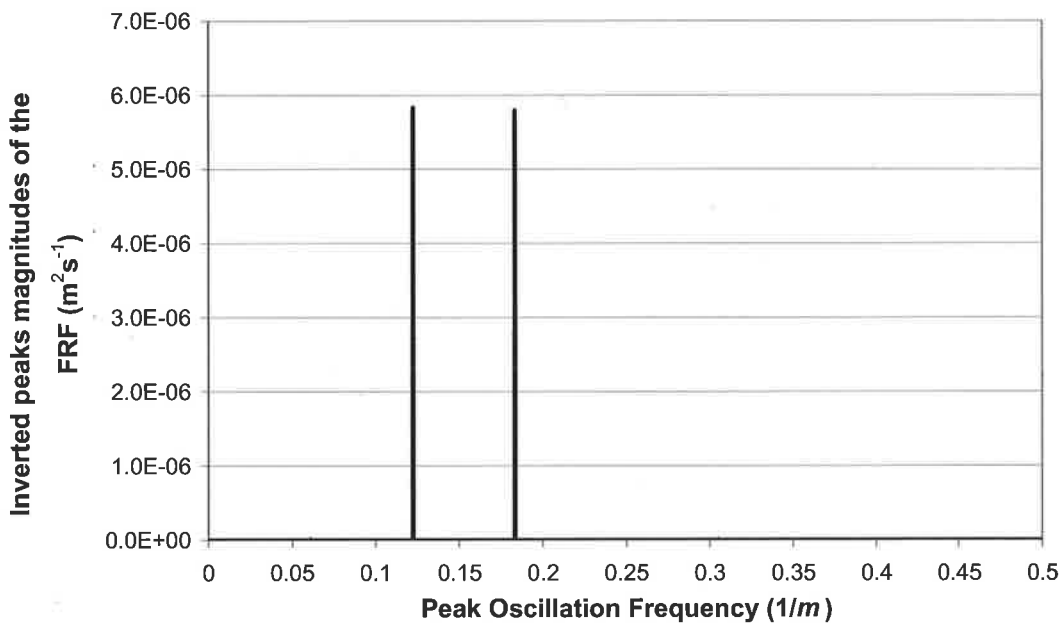


Figure 6-112 – Spectrum of the inverted peaks magnitudes for multiple blockages.

Table 6-16 – Results of multiple blockage detection.

Test Configuration		Pattern Properties			Predicted Block Properties
		Freq.	Phase	Amplitude	
Blockage #1	$x_{B1}^* = 0.122,$ $Z_{B1} = 34.96$	0.122	0.383	0.589×10^{-5}	$x_{B1}^* = 0.122, Z_{B1} = 35.32$
Blockage #2	$x_{B2}^* = 0.183,$ $Z_{B2} = 34.96$	0.183	0.575	0.579×10^{-5}	$x_{B2}^* = 0.183, Z_{B2} = 34.72$

6.13 LIMITATIONS TO THE FRF TECHNIQUE

This chapter has proposed a method of leak and discrete blockage detection in a pipeline that can accurately locate faults under both numerical and experimental conditions. The limitations of this approach, however, must be discussed.

One of the main limitations of the leak and discrete blockage detection procedure in the frequency domain is that the effect of a fault is limited to the harmonic peaks of the FRF and the accuracy of the procedure is heavily dependent upon the bandwidth of the input signal. For the experimental results, the fundamental frequency of the pipe is high in relation to the bandwidth of the input signal, leading to a low number of peaks for analysis. The technique is, therefore, most applicable in large-scale systems where the fundamental frequency of the system is low compared to the injected signal bandwidth.

Leaks and blockages located near particular positions in the pipeline generate very low frequency oscillations in the peaks of the FRF and may not be detected. For a symmetric system, these positions are the system boundaries, the quarter points and the midpoint of the system, whereas in the anti-symmetric case, the positions are the system boundaries and the midpoint. The technique relies on a particular location of the transient source and significant deviation from this configuration leads to distortions in the observed peak pattern. Finally, the phase of a leak-induced oscillation on the peaks of the FRF is opposite to that generated by a blockage located at the same position in the system. This finding means that each detected oscillation in the FRF peaks indicates either a leak at one position or a blockage at a mirror position.

Many of the limitations associated with leak detection using the FRF can be solved using the time equivalent of this function—the impulse response function. The use of the impulse response function for leak detection retains the advantages associated with the system response function described in Chapter 5. However, it places no limit on the arrangement of the transient source and measurement station, no limit on the number of faults that can be detected and can distinguish between faults of different nature (i.e. leaks and blockages). The application of the impulse response function is described in the next chapter.

6.14 CONCLUSIONS

This chapter investigated the effect of a leak on the frequency response function (FRF) of a pipeline. The presence of a leak does not generate additional “leak harmonics” as proposed in previous publications. Instead, the leak imposes a periodic pattern on the peaks of the FRF. The analytical expression for this leak-induced pattern was derived for a number of system boundary configurations and is in the form of an inverted cosine function. The frequency and phase of this function provide information on the leak position in the system. A new leak detection procedure was proposed and was validated both numerically and experimentally. This procedure does not require a numerical model, nor does it require knowledge of the losses in the system.

This procedure is extended to multiple leaks in a pipeline, to different measurement / transient-generating positions and to networks. A new technique of discrete blockage detection was proposed and was successfully validated using numerical results.

The main conclusions from this chapter are summarised in the following points:

1. As leaks and blockages in a pipeline only affect the peaks in the FRF, the injected transient signal must have a large bandwidth to increase the number of data points for analysis. In this respect, a system configured anti-symmetrically is more suited to the application of this procedure (in contrast to symmetric systems) as the fundamental frequency is lower, thus giving more observable peaks for a given signal bandwidth.
2. As a result of the finite number of observable peaks in the extracted FRF, there is a limit to the maximum number of faults that can be detected from a pipeline using this procedure.

This investigation of the leak-induced modification on the frequency response from a pipeline is followed by the investigation of the leak-induced modification on the impulse response function.

CHAPTER 7

LEAK DETECTION USING THE IMPULSE RESPONSE FUNCTION

7.1 INTRODUCTION

The previous chapter shows that by using the system response function, problems in a pipeline can be identified without need for a numerical simulation. This chapter focuses on leak-induced modification of the time-domain response of a pipeline and investigates a leak detection procedure known as time-domain reflectometry. As discussed in Section 2.3.2, time-domain reflectometry is a procedure where the presence and location of leaks are determined by detecting leak-reflected signals in a transient trace. Given that the wave speed of the system is known, the arrival time of reflected signals can be used to determine the position of a problem in a pipe. This technique is mathematically intuitive, does not require knowledge of frictional losses and a numerical model is needed only for identification of reflected signals in the trace. In this chapter, the procedure for detecting and locating leaks using time-domain reflectometry was experimentally tested to identify problems associated with this approach. This procedure is then improved using the system response function in the time domain, the *impulse response function* (IRF). The effect of the impulse response function on the accuracy of the time-domain reflectometry procedure was investigated experimentally.

7.2 BACKGROUND

Time-domain reflectometry is used in a range of applications and includes detection of remote objects in radar and sonar systems (Ahmad, 1995), determination of structural integrity (Okanla *et al.* 1997, Liu *et al.* 2001), determination of electrical cable faults (Maloney 1973, Harding 1974), detection of soil movement (O'Connor and Wade 1994, Beck and Kane 1996, Kane and Beck 1999, O'Connor and Dowling 1999), geoseismic surveys (Martinez, 2002) and measurement of soil moisture / pollutant profiles (Heimovaara 2001, Chambarel *et al.* 2001, Said *et al.* 2001). In all these cases, a signal is sent from a source to detect objects or abnormalities in the area. The signal propagates away from the source and upon meeting a change in the media (caused by the presence of defects or other objects), part of the signal is reflected back towards the source. The arrival time provides the distance the wave has travelled to the object and back to the detection station. The operation of a conventional radar system is shown in Figure 7-1.

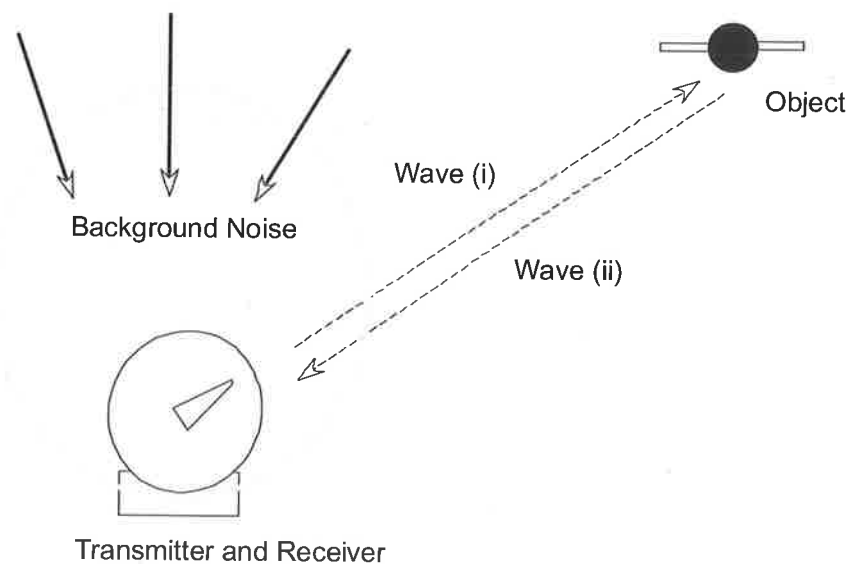


Figure 7-1 – Operation mechanism for a conventional radar system.

For a transient signal in a simple pipeline, the situation is more complex (refer to Figure 7-2). In this case, the transient wave travels back and forth along the pipe, reflecting off system boundaries and generating an oscillation in head at all locations in the system. The signal travels past any system abnormality repeatedly, creating a reflected signal at regular time intervals. In this respect the pipeline behaviour is unlike TDR in radar and sonar where there are no system boundaries.

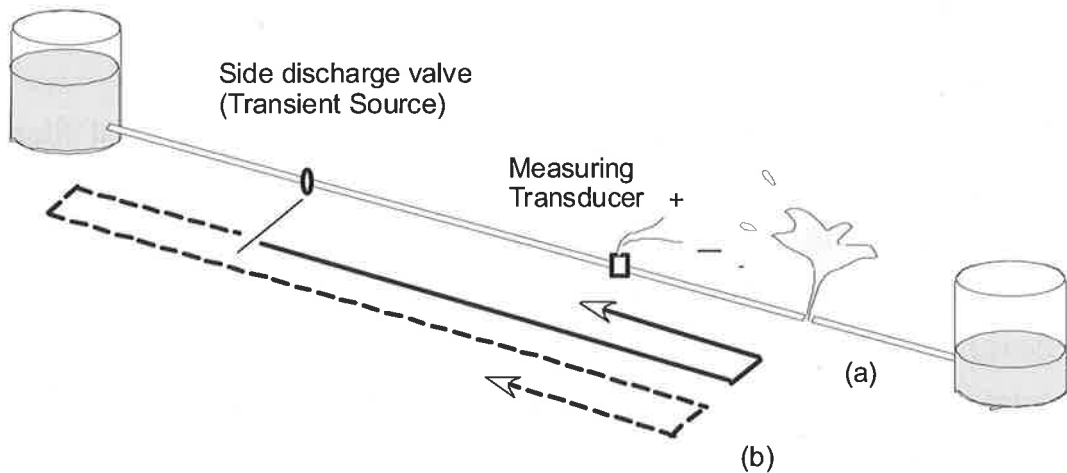


Figure 7-2 – Operation mechanism of TDR in pipelines.

This travel pattern of transient waves imposes an additional complexity to the problem. In the case of a radar, the travel path of the generated signal to the target and back to the detection point is known (Figure 7-1). In the case of a transient wave in a pipeline, the leak-reflected signals can take multiple wave paths due to a complex series of possible reflections. A transient event in a pipeline is shown in Figure 7-2. The figure illustrates two different wave travel patterns that can generate the same leak-reflected signal, labelled (a) and (b). The time of arrival of the reflected signal can be associated with either one of these travel patterns, each indicating a different position of the leak.

In a pipeline the pressure response consists of a series of reflections from system boundaries even without leaks in the pipe. Some knowledge of the nominal response to a transient event is required so that leak-reflected signals in the trace can be distinguished from other reflections. An expected nominal response can be produced numerically using a method of characteristics model. Alternatively, if the transient event can be controlled and made repeatable, then a comparison between the current trace and a trace generated previously—when the system is known to be leak free—can achieve the same outcome. The nature of the reflection can provide clues as to the nature of the object. For example, an object with a low impedance in relation to the pipeline impedance will give a negative wave reflection (i.e. one that is of opposite phase to the incident wave), whereas an object with a higher impedance will give a positive reflection (Harding, 1974). The following section investigates the mechanism that allows these leak-reflected signals to be recognisable in a transient trace.

7.3 ILLUSTRATION OF THE CONVENTIONAL TDR PROCEDURE

A 2000 meters long simulation pipeline was used for the following numerical illustration. The bounding reservoirs have heads of 50 m and 20 m, giving the steady state velocity through the downstream valve as 0.22 ms^{-1} with the discharge through the valve of $Q_{V0} = 0.0136 \text{ m}^3 \text{ s}^{-1}$ and the head loss through the valve of $H_{V0} = 29.78 \text{ m}$. The friction factor of the flow, f , was 0.02 and resulted in a loss of 0.222 meters of head along the pipe. The Reynolds number was 65,540, placing the flow in the smooth turbulent flow regime for a roughness height of $5 \times 10^{-2} \text{ mm}$. The transient was generated by the sudden closure of an initially open side-discharge valve located 500 m from the upstream boundary with a discharge coefficient of $C_{dA_V} = 7 \times 10^{-5} \text{ m}^2$. A leak of size $C_{dA_L} = 1.4 \times 10^{-4} \text{ m}^2$ ($C_{dA_L} / A = 1.98 \times 10^{-3}$) was located 1500 m from the upstream boundary and the pressure trace was measured at the transient source. A schematic of the system is shown in Figure 7-3.

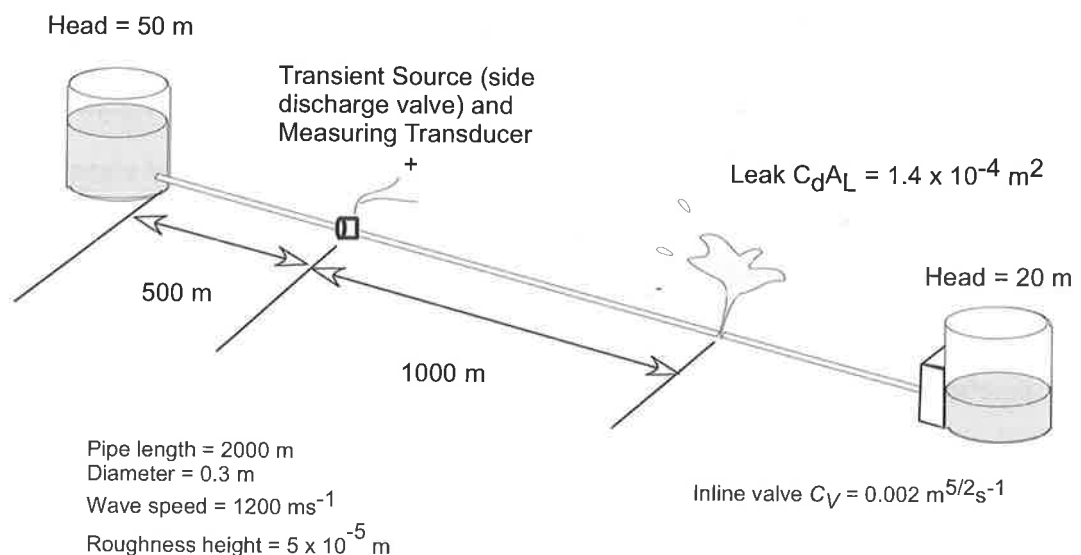


Figure 7-3 – Schematic of pipeline for illustrating the generation of leak-reflected signals in a transient trace.

The transient trace was numerically generated using the method of characteristics with a discretisation of 150 intervals and a computational time step of 1.12×10^{-2} seconds. The transient traces for the leaking and intact pipeline are shown in Figure 7-4. The figure shows that a leak causes additional reflections, circled in the figure, in the transient trace.

These reflections are leak-induced and the sequence of events leading up to the occurrence of the reflections in the signal is considered below.

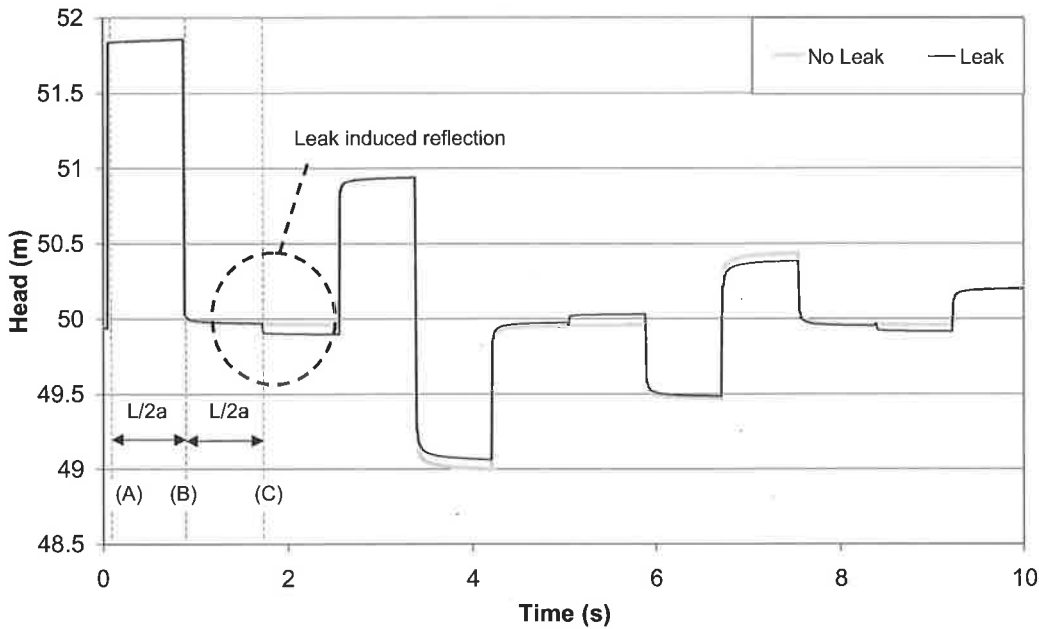


Figure 7-4 – Numerical comparison of transient traces from leaking and intact pipes (Data file: C7-1.txt).

Figure 7-5 shows the propagation of the transient wave away from the source at $t = 0$ after the generation of the transient event at the first-quarter point, corresponding to the time labelled (A) in Figure 7-4.

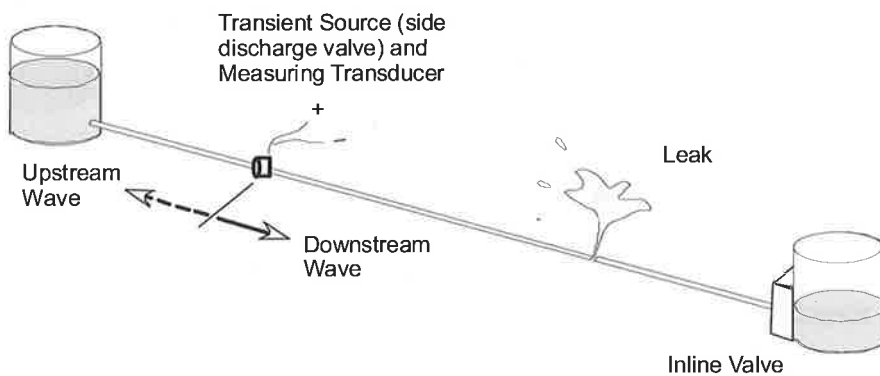


Figure 7-5 – Transient propagation at $t = 0$ s.

Closure of the side-discharge valve induced a rise in the hydraulic grade line at the first-quarter point that is detected immediately by the pressure transducer located in the same position. Note that two distinct wave fronts were generated from the transient event, one propagating upstream of the source and the other downstream, labelled in Figure 7-5.

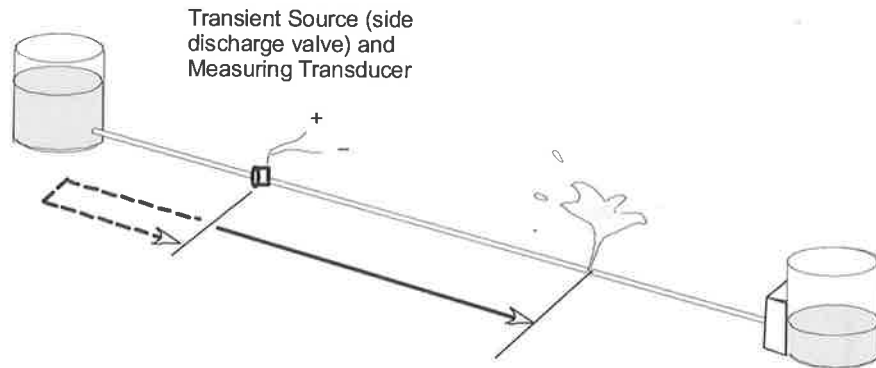


Figure 7-6 – Transient propagation at $t = L / (2a)$ s.

Figure 7-6 shows the pipeline $0.833 \text{ s } [L/(2a)]$ after the transient generation. The upstream propagating wave front has reflected from the upstream reservoir and has arrived back at the first-quarter point, illustrated in Figure 7-4 as the time labelled (B). The downstream propagating wave front is at the leak and is partially reflected. This leak-reflected signal begins to propagate upstream while the original transmitted signal continues to move downstream.

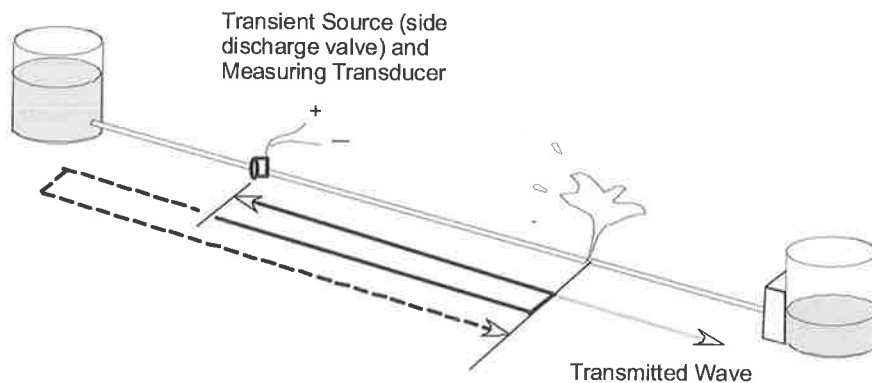


Figure 7-7 – Transient propagation at $t = L/a$ s.

Figure 7-7 shows the pipeline at $1.667 \text{ s } [L/(a)]$ when the leak-reflected wave has arrived back at the measuring point, giving the leak-reflected signal at the time labelled as (C) in Figure 7-4.

From the above analysis, the disturbance in the transient trace is generated by the arrival of the leak-reflected signal at the measuring transducer. The position of this disturbance in the trace provides an indication of the arrival time of the leak-reflected signals and signifies the time needed for the transient signal to travel away from the transient source, reflect off the leak and return to the measurement transducer. This approach was used in

Jönsson and Larson (1992), Brunone (1999), Covas and Ramos (1999), Jönsson (2001) and Ferrante and Brunone (2001). Once the reflection arrival time is determined, the distance travelled by the wave is found by using the wave speed of the pipeline. The procedure for locating a leak in the pipeline using time-domain reflectometry (TDR) consists of two stages,

1. Reflection Detection - Compare the transient trace to a numerically generated leak-free trace of the system or a known response to detect a possible leak-reflected disturbance in the signal.
2. Leak Location - Using the wave speed, determine the position of the leak in the pipeline from the arrival time of the leak-reflected signals.

7.3.1 Detection of reflected signals

TDR requires detection of a leak-reflected disturbance in a transient trace and accurate determination of the arrival times of these reflections. In Jönsson and Larson (1992), Brunone (1999), Covas and Ramos (1999), Jönsson (2001), these signals were detected by visually comparing the leak-free transient response and the observed trace. While simple to apply, this procedure is only applicable under experimental conditions where a reflection from the system can be easily discerned. For real pipelines, disturbances from non-leak related sources—such as pipeline vibrations, background transients and instrument noise—can create traces where the existence of leak-reflected signals cannot be easily recognised.

Leak reflections can be detected more consistently through an automated comparison of the measured transient signal with a benchmark transient for the system when no leak exists. Any significant deviations between the measured and expected trace are detected as possible leak-reflected signals. In this study, the cumulative sum algorithm (CUSUM) is used to detect these deviations. CUSUM is a popular change detection algorithm that allows recognition of small, yet prolonged, differences between two data sets. It is commonly used in online monitoring of chemical processes (Basseville *et al.*, 1993). Misiunas *et al.* (2003, 2004) have used this algorithm for detecting bursts in a pipeline. CUSUM operates on the sum of the past significant differences between the measured and

modelled results, detecting a change only when the cumulated differences over the past few time steps are consistently in the same direction and the magnitude exceeds the expected variance level in the data. Spurious errors in the data are unlikely to be detected as a change.

The two-sided CUSUM algorithm operates as follows:

$$g_t^1 = \max(g_{t-1}^1 + s_t^1 - \nu, 0) \quad (7.1)$$

$$g_t^2 = \max(g_{t-1}^2 + s_t^2 - \nu, 0) \quad (7.2)$$

where g_t^1, g_t^2 = positive and negative cumulative sum of differences between the modelled and measured results at time t and ν = expected variance level. Eqs. (7.1) and (7.2) returns the larger value between zero and the expression within the bracket. The positive and negative residual errors, s_t^1, s_t^2 are defined as

$$s_t^1 = (h_E(t) - h_M(t)) \quad (7.3)$$

$$s_t^2 = -(h_E(t) - h_M(t)) \quad (7.4)$$

where h_E and h_M are the observed and modelled head responses at time t . The positive CUSUM detects changes in the positive direction, whilst the negative CUSUM detects changes in the negative direction. A change is detected when the value of g_t^1 or g_t^2 grows beyond a pre-set tolerance level, in which case the change time is recorded and the alarm triggered. The value of the cumulative sum increases from one time step to the next only if the deviation is greater than the value of the expected variance, ν . The length of data, T_A , over which the CUSUM is applied is limited to the maximum time it takes for a leak-reflected signal to travel back to the measurement station since the start of a transient trace. This analysis time is defined as $2L/a$ for all boundary conditions.

The operation of the CUSUM algorithm is shown in Figure 7-8. The figure shows the value of the negative CUSUM for a sequence of residual errors [s_t^2 from Eq. (7.4)]. The value of CUSUM is greater than zero only when the residual error exceeds the expected

variance, υ (at “A” and “B”). The value of CUSUM increases when the magnitude of the residual errors for subsequent time steps are also above the expected tolerance level (i.e. a sustained and significant change) and occurs for the deviation at point “B.”

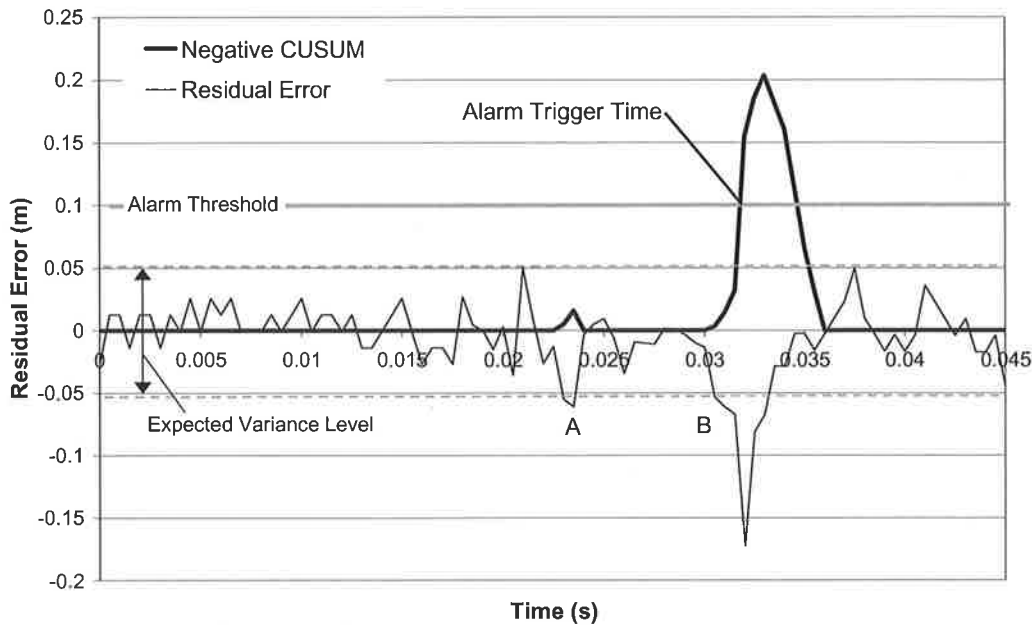


Figure 7-8 – Illustration of the operation of the negative CUSUM.

The expected variance level, υ , and the tolerance level have a significant effect on the accuracy of the CUSUM procedure. For the greatest change detection accuracy, the value of the tolerance level should be determined directly from the measured trace taking into account the background electrical and mechanical noise in the system. Before the application of the leak detection procedure, the minimum size leak that can be detected using the input transient must be determined in-situ by placing artificial leaks of different sizes (simulated by side discharge orifices) in the pipe. The smallest leak-reflected signal that can be detected is set as the threshold with υ as half the size of this threshold. The threshold determines the lower limit of the leak detection sensitivity.

This procedure was applied in the laboratory system to determine the threshold for the CUSUM algorithm. The transient was generated using a solenoid valve placed at the centre of the pipeline (Figure 7-9). The boundaries were symmetric with heads at the reservoirs of 36.5 m and 37.0 m. The flow velocity was in the range of 0.5 ms^{-1} , giving a Reynolds number of 11,000. Leaks of various sizes were placed 6.695 m from the upstream boundary. Figure 7-10 shows a transient trace generated in this situation with the smallest observable leak reflection highlighted. This reflection, expanded in Figure 7-11,

was from a leak of orifice diameter of 1 mm ($C_d A_L / A = 1.69 \times 10^{-3}$). The magnitude of the reflection was 0.37 m compared to the incident transient of magnitude 10.67 m.

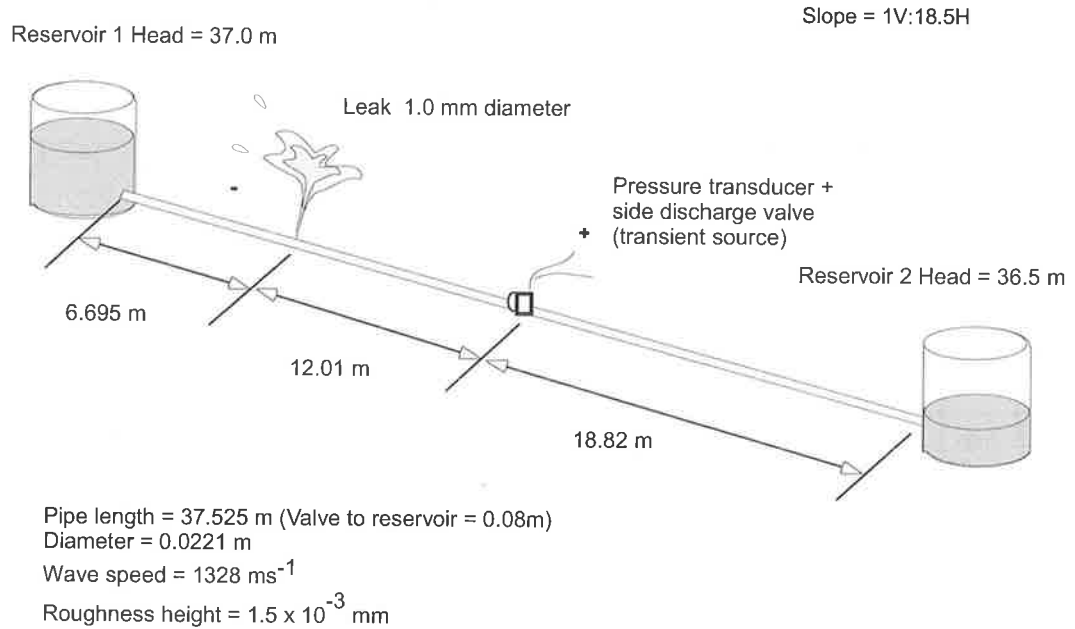


Figure 7-9 – System configuration for determination of the threshold value in the CUSUM algorithm in the laboratory.

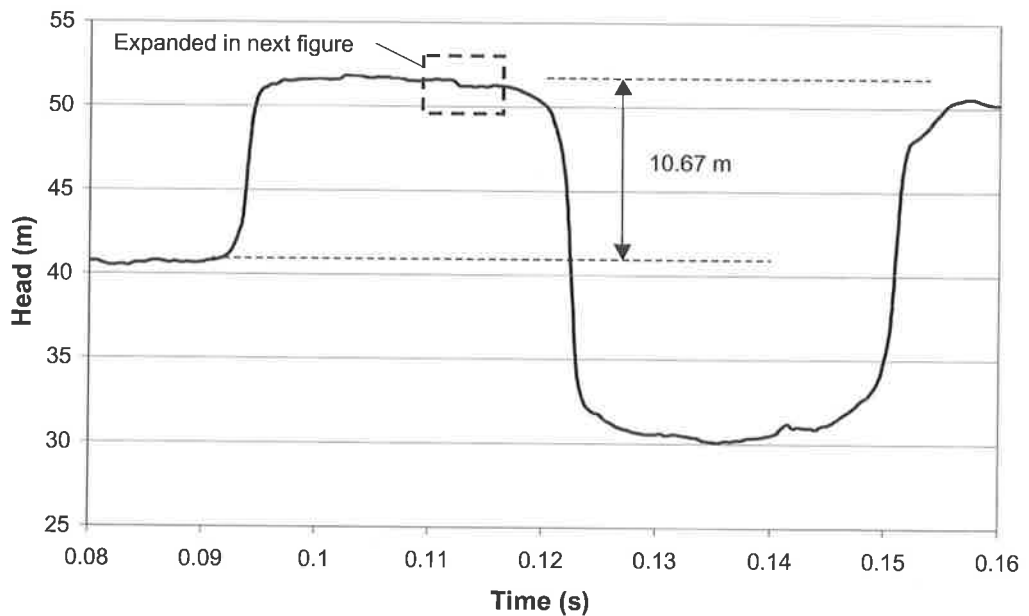


Figure 7-10 – Smallest detectable leak reflection in the experimental system.

The magnitude of the smallest detectable leak reflection in the laboratory system is 3.5% of the magnitude of the incident transient signal and is set as the threshold for the CUSUM detection procedure. The expected variance of the signal is half the size of this threshold.

The trigger time for the CUSUM alarm is not the arrival time of the leak-reflected signal as the alarm is triggered only when the accumulated error over a number of time steps exceeds the threshold. The cumulative sum must be traced back from the trigger time to the point where it was just starting to increase to obtain the true arrival time.

Apart from these issues, this technique hinges on the accuracy of the leak-free benchmark, which is generated from a numerical model for this study. The accuracy of the numerical model in predicting the transient trace in the laboratory system is discussed in Chapter 5. This result is repeated in Figure 7-13, with the transient trace from the method of characteristic model, incorporating Zielke (1968) weighting function unsteady friction. The pipeline was discretised into 150 reaches in the model with a computational time step of 1.89×10^{-4} s. The configuration of the system is shown in Figure 7-12 with the transient trace in Figure 7-13.

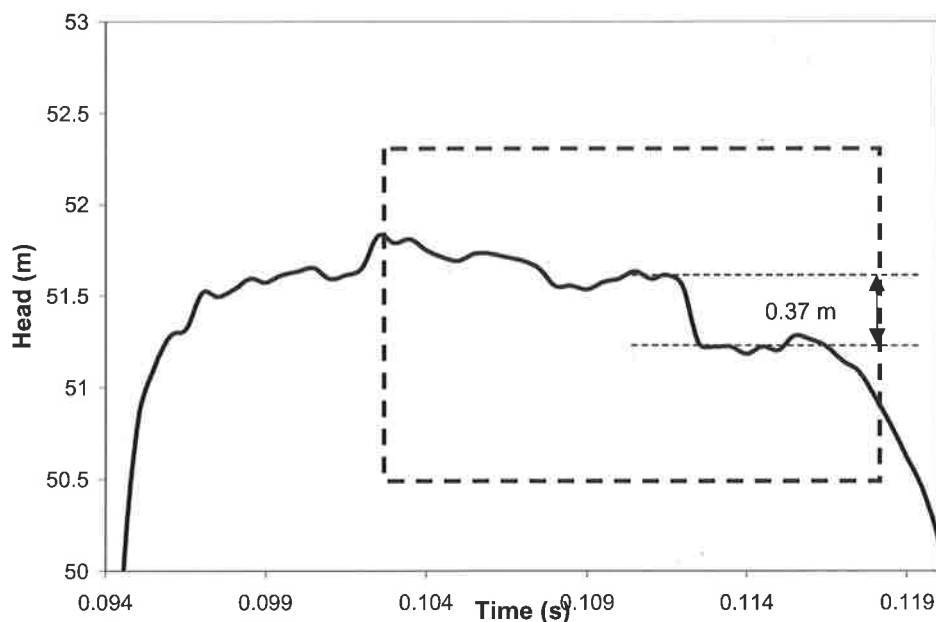


Figure 7-11 – Expanded view of the leak reflection.

The trace was generated by the closure of a brass solenoid side-discharge valve with the system arranged anti-symmetrically. The upstream reservoir was set at 39.7 m and the

downstream valve was fully closed. The solenoid valve was placed 0.16 m from the in-line valve. From Figure 7-13, the MOC numerical results closely follow the experimental data in the first $t = 2L/a$ of the trace.

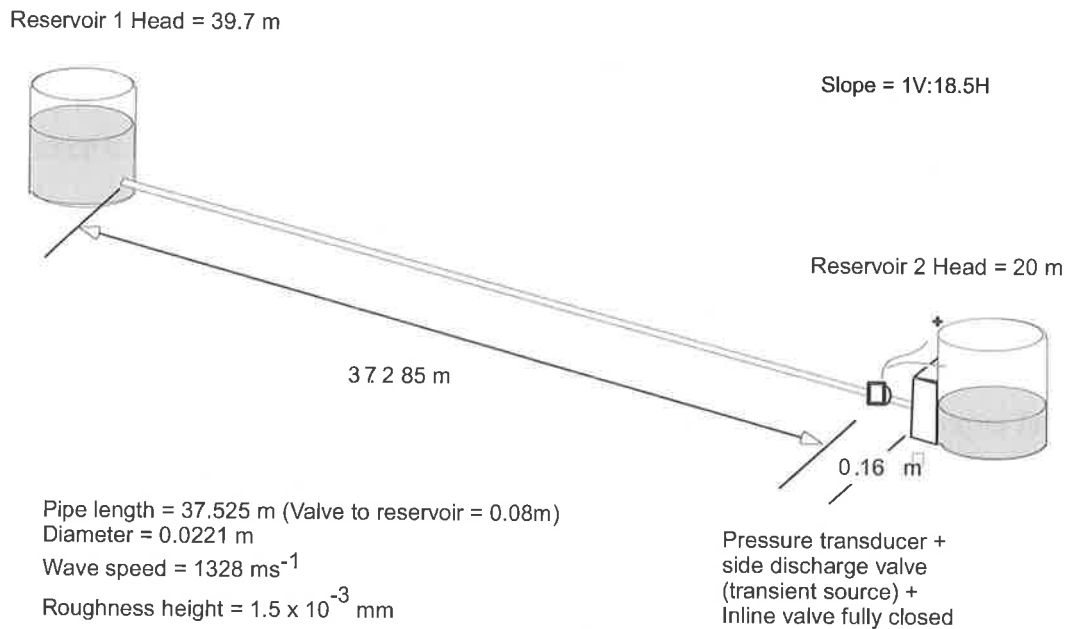


Figure 7-12 – Configuration of the anti-symmetric system for the determination of model accuracy.

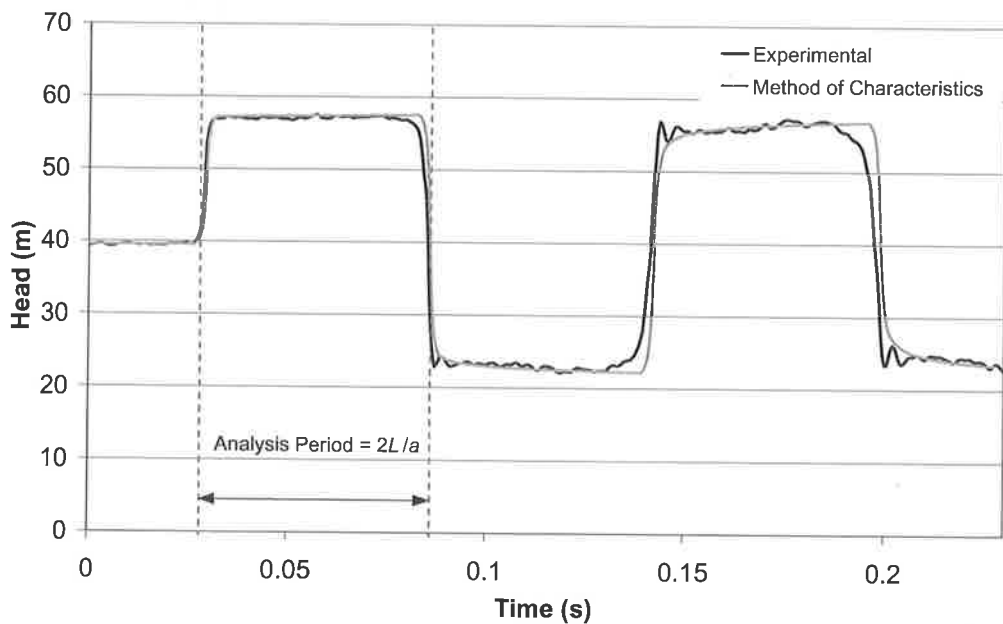


Figure 7-13 – Comparison between experimental results and method of characteristics prediction with Zielke (1968) unsteady friction model for a no-leak situation (Data file: C7-3.txt).

7.3.2 Location of the leak from the arrival time of the reflected signal

Once the leak-reflected signal is found, the arrival time of the signal is used to locate the leak. In the case of a simple pipeline with the transient generation point and the measuring transducer both located at the same position (refer to Figure 7-14), the distance of the leak from the measurement point is given by

$$|D_{Leak}| = \frac{aT_0}{2} \quad (7.5)$$

where $|D_{Leak}|$ is the distance of the leak from the transducer and T_0 is the occurrence time of the disturbance, measured from the start of the transient to the time of the leak-induced disturbance.

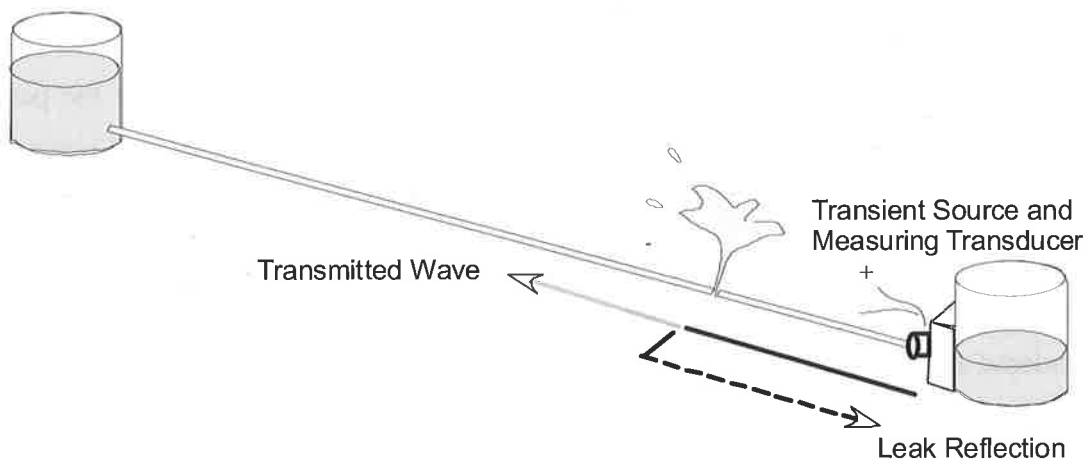


Figure 7-14 – Illustration of the operation of time-domain reflectometry.

However, while most single pipelines have flow controlling devices at boundaries that can be adapted for transient generation, the availability of tapping ports for pressure transducers can be problematic. In these situations, Eq. (7.5) cannot be used. For example, the use of Eq (7.5) for locating the leak in Figure 7-2 (repeated here as Figure 7-15) when the reflection has travelled on (b) indicates a leak much closer to the measurement point than it really is.

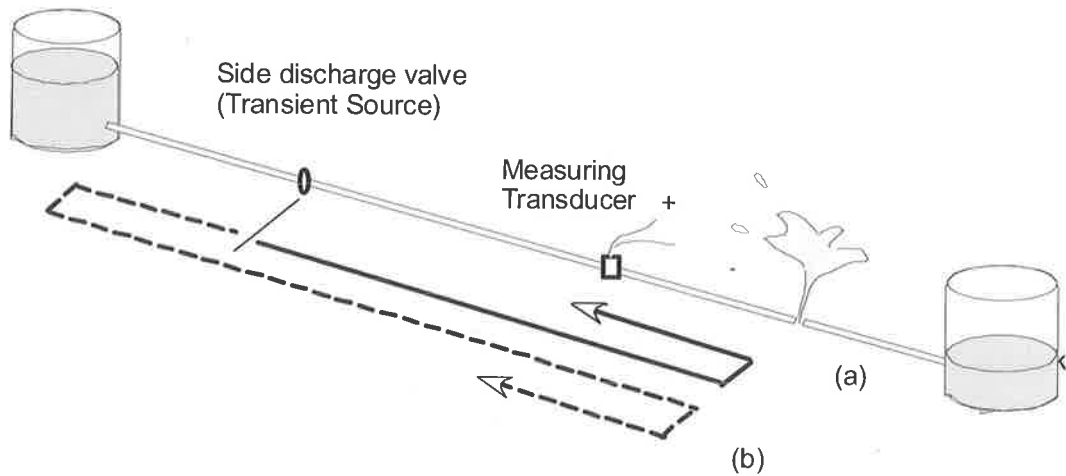


Figure 7-15 – Operation mechanism of TDR in pipelines under non-optimum configuration.

A set of mathematical equations describing the relationship between the arrival time of the leak-reflected wave front and the location of the leak can be derived to allow the application of the TDR procedure for all system configurations. The arrival time of the first reflected wave front at the measuring point can be associated with all the possible ways the reflected wave is expected to have travelled. For a measurement point and a transient source in a single pipeline, a leak can be located in three zones: between a boundary and the measuring point, between a boundary and the transient source and between the transient source and the measuring transducer. All three zones need to be considered as potential locations for the leak. The derivation is illustrated with the pipeline shown in Figure 7-16 with the leak located between the transient generation point and the pressure transducer.

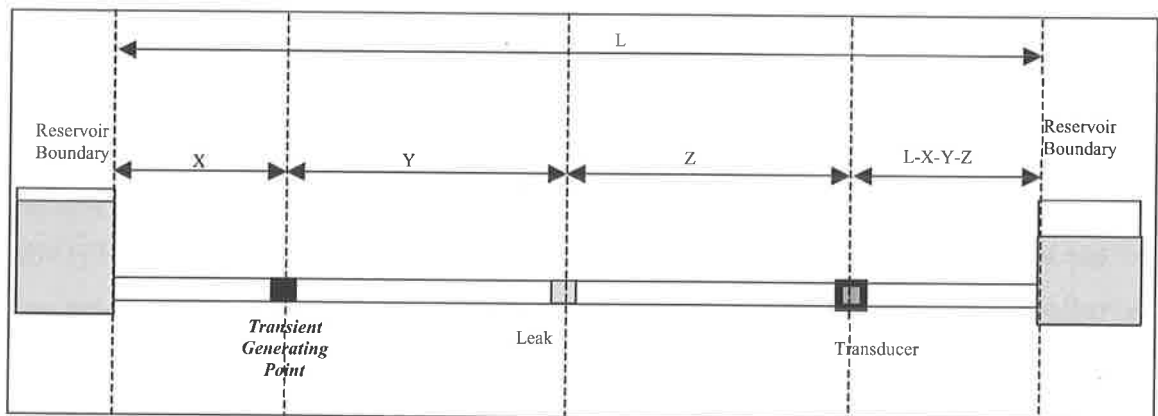


Figure 7-16 – Configuration of the system used for mathematical derivation of the relationship between occurrence time and leakage location.

The known distances in Figure 7-16 are X , $(L-X-Y-Z)$ and L . Figure 7-17 and Figure 7-18 (which, for the purpose of nomenclature, are called scenarios #1 and #2) are two possible sequences of events.

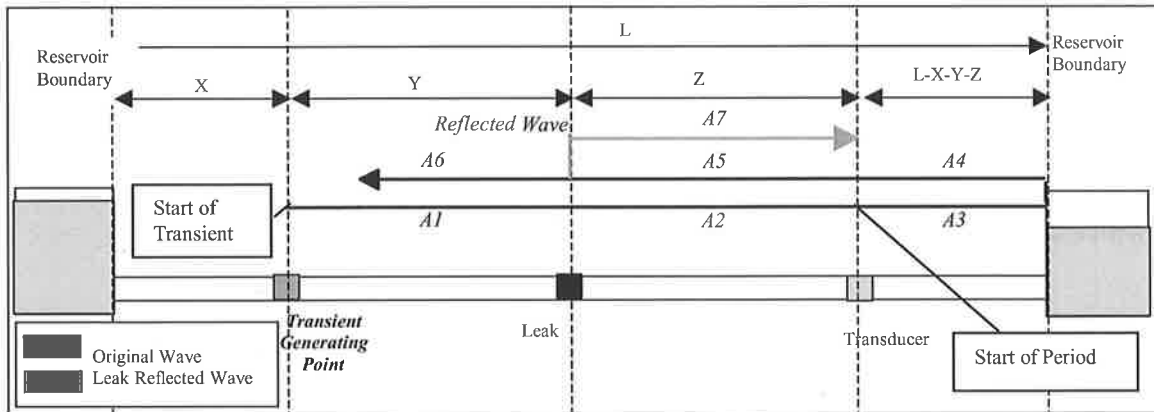


Figure 7-17 – Scenario #1 for generating a leak-induced disturbance in the transient trace measured at the transducer.

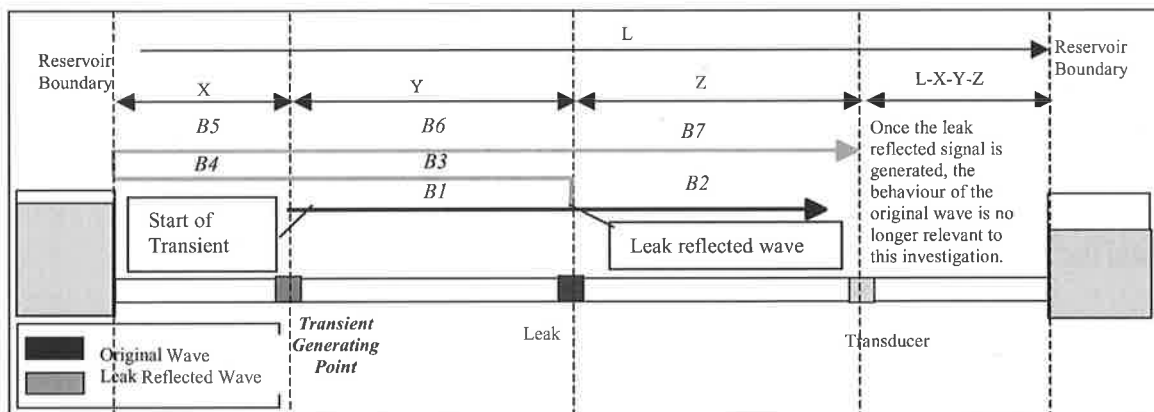


Figure 7-18 – Scenario #2 for generating a leak-induced disturbance in the transient trace measured at the transducer.

In Figure 7-17 (scenario #1) the time between the generation of the transient and the arrival of the leak-reflected wave at the transducer is given by the summation of the total distance travelled along paths ($[A1, A2, A3]$, $[A4, A5]$, $A7$) divided by the wave speed,

$$T_T = \frac{Y}{a} + \frac{3Z}{a} + \frac{2(L-X-Y-Z)}{a} \quad (7.6)$$

The time of commencement of the transient oscillation, as measured by the transducer, occurs after a time lag of $(Y+Z)/a$ following the generation of the transient (paths [A1, A2]). The arrival time of the leak-reflected signal, T_o , measured from the start of the transient trace for scenario #1 is

$$T_o = \frac{Y}{a} + \frac{3Z}{a} + \frac{2(L - X - Y - Z)}{a} - \frac{(Y + Z)}{a} \quad (7.7)$$

which simplifies to

$$T_o = \frac{2L}{a} - \frac{2X}{a} - \frac{2Y}{a} \quad (7.8)$$

Now, considering Figure 7-18 for scenario #2, the total travel time along paths ([B1], [B3, B4], [B5, B6, B7]) is given by

$$T_T = \frac{3Y}{a} + \frac{2X}{a} + \frac{Z}{a} \quad (7.9)$$

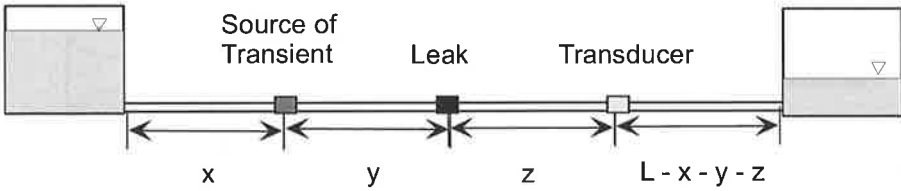
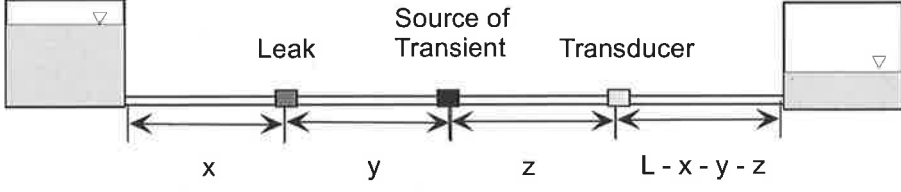
and the time of arrival after subtracting the time lag of $(Y+Z)/a$ is ([B1, B2])

$$T_o = \frac{2Y}{a} + \frac{2X}{a} \quad (7.10)$$

Eqs (7.8) and (7.10) describe the shortest possible arrival time of a leak-reflected signal for a leak located between the measurement transducer and the transient source. To consider all cases, similar derivations were performed for leaks located in other zones with the aim of producing a comprehensive set of equations that can detect leaks located anywhere in a pipeline. The details of these derivations follow the same procedure as previously shown with the results in Table 7-1. A given time of detection results in four possible leak locations. For the case where the transient source and measurement transducer are coincident, Eq. (7.5) should be used to determine the distance of the leak from the source/measurement point. This special consideration is required because the

results of Table 7-1 cannot produce the two solutions (one on each side of the transient source/transducer position) required for this situation.

Table 7-1 –The complete set of leak location equations.

Diagram of Configurations		Equations
	A	$Y = \frac{-aT_o}{2} + L - X$
	B	$Y = \frac{aT_o}{2} - X$
	C	$Y = \frac{aT_o}{2}$
	D	$Y = \frac{aT_o}{2}$

7.3.3 Experimental verification of the improved TDR technique

The experimental validation of the above TDR leak detection procedure was undertaken for both symmetric and anti-symmetric boundary configurations. For each test, the transient traces from measurement transducers are compared to the model-predicted results for a no-leak system. The error between the two is entered into the CUSUM algorithm to determine the arrival times of leak reflections. Using these arrival times, the corresponding leak positions are calculated using Table 7-1.

Symmetric boundary configuration

The symmetric system test was conducted with the boundary heads of 49.2 m and 39.6 m, giving a flow with a Reynolds number of 26,200 and a velocity of 1.2 ms^{-1} . The system layout is shown in Figure 7-19.

Reservoir 1 head = 49.2 m

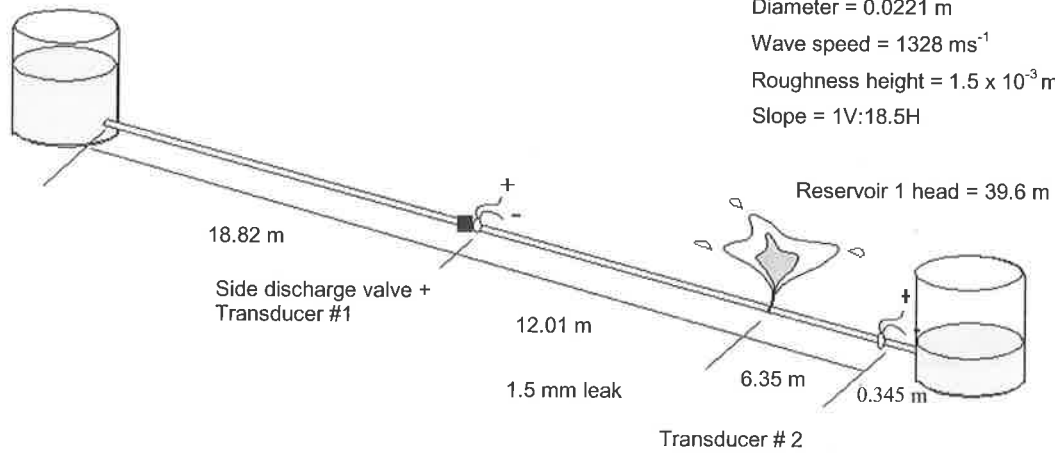


Figure 7-19 – System layout for the symmetric test.

The transient was generated by closure of the initially open, side-discharge valve located at the midpoint of the system. A leak of a $C_d A_L / A = 4.17 \times 10^{-3}$ (orifice diameter of 1.5 mm) was placed 30.83 m downstream of the supply tank. The transient was measured by two transducers, one located at the transient source and the other 0.345 m upstream of the downstream tank. The model prediction (leak-free benchmark) was determined by the method of characteristics with a discretisation of 300 and a computational time step of 2.27×10^{-4} s. The Vardy and Brown (1995) unsteady friction model was incorporated in the model. The measured transient trace, model prediction, residual and alarm status for transducers 1 and 2 are shown in Figure 7-20 and Figure 7-21, respectively. The alarm statuses from the CUSUM algorithm are plotted on these figures where “1” represents the activated status. The point where the alarm was first activated is stored. To determine the beginning of the disturbance, the time was traced back from this alarm activation time to the time when the residuals have just started to increase. This time is the predicted arrival time of disturbance, which is 0.020 s for Figure 7-20 and 0.0105 s for Figure 7-21. For Figure 7-20 the leak was located at 13.28 m away from the transient source, which is either 5.54 m or 32.10 m downstream from the supply tank using Eq. (7.5). For Figure 7-21 the leak is located 30.54 m from the upstream boundary using equation A in Table 7-1. For this situation, equations B, C and D in Table 7-1 yield results that are either negative or outside the physical boundaries of the system and these predictions are ignored.

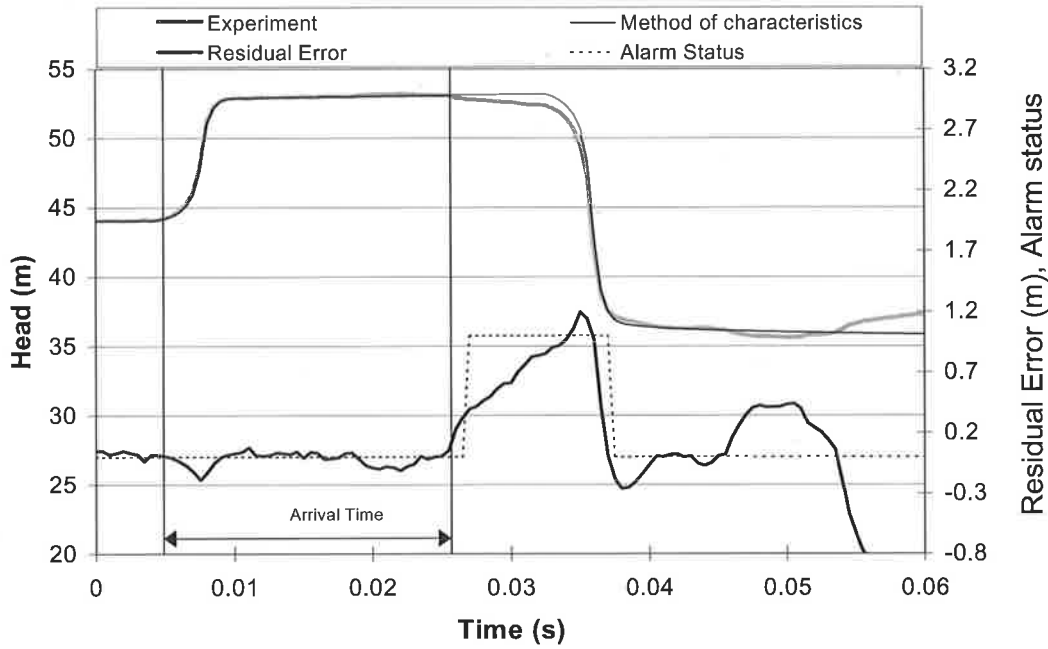


Figure 7-20 – Transient trace at the measuring station 18.82 m from upstream reservoir for symmetric system test (Transducer 1) – (Data file: C7-L1.txt).

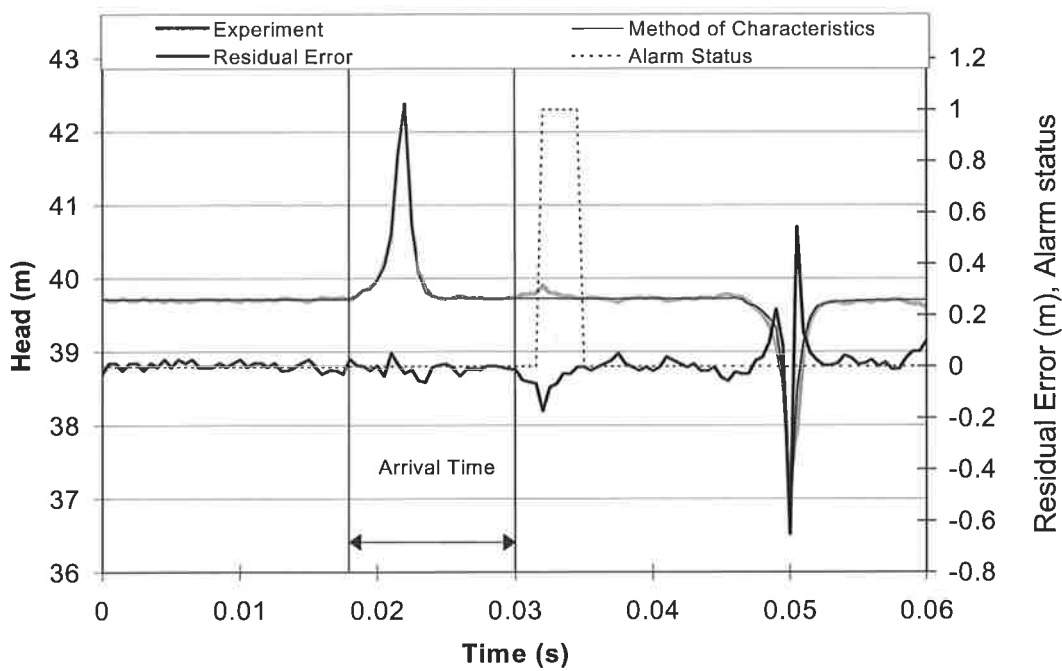


Figure 7-21 – Transient trace measured 0.345 m from the downstream reservoir for symmetric system test (Transducer 2) – (Data file: C7-L1.txt).

The three possible leak locations from the CUSUM analysis are 5.55 m and 31.10 m for Figure 7-20 or 30.54 m from the upstream boundary for Figure 7-21. As the true leak position must be consistent with the results observed from both transducers, the leak location of 5.55 m is discarded. Comparing the predicted leak locations with the true value of 30.83 m, the errors in both cases are 0.27 m and 0.29 m for the results of Figure 7-20 and Figure 7-21, respectively. The possible causes of this error are described later in the chapter.

Anti-symmetric test

The anti-symmetric system test was conducted with the upstream reservoir set at a head of 39.6 m with the downstream valve closed. The transient was generated by closure of the initially-open brass side-discharge solenoid valve located 37.30 m from the upstream boundary. Two transducers were used to measure the transient, one 18.71 m and the other 37.30 m from the upstream boundary. A leak of $C_d A_L / A = 4.17 \times 10^{-3} \text{ m}^2$ (orifice diameter = 1.5mm) was located 6.70 m downstream from the supply tank. The system layout for this test is shown in Figure 7-22. To generate the leak-free benchmark from the MOC, the pipeline was discretised into 300 reaches with a computation time step of $2.27 \times 10^{-4} \text{ s}$.

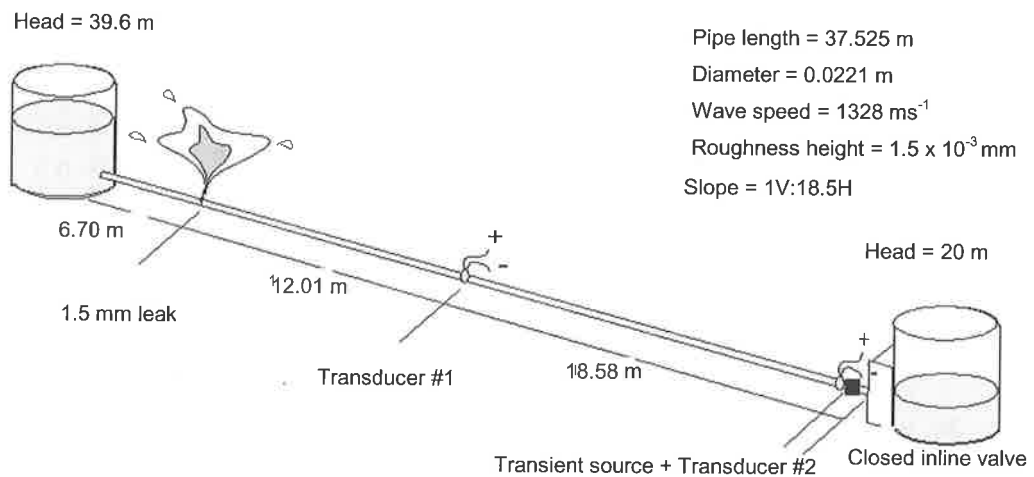


Figure 7-22 – System layout for the anti-symmetric test.

The results 18.71 m (transducer 1) and 37.30 m (transducer 2) from the upstream boundary are shown in Figure 7-23 and Figure 7-24. The corresponding predicted leak

locations for the two measurement stations are 6.42 m and 5.76 m from upstream boundary [using Table 7-1, equation D and Eq. (7.5)] and differ from the true leak position of 6.70 m by 0.28 m and 0.94 m.

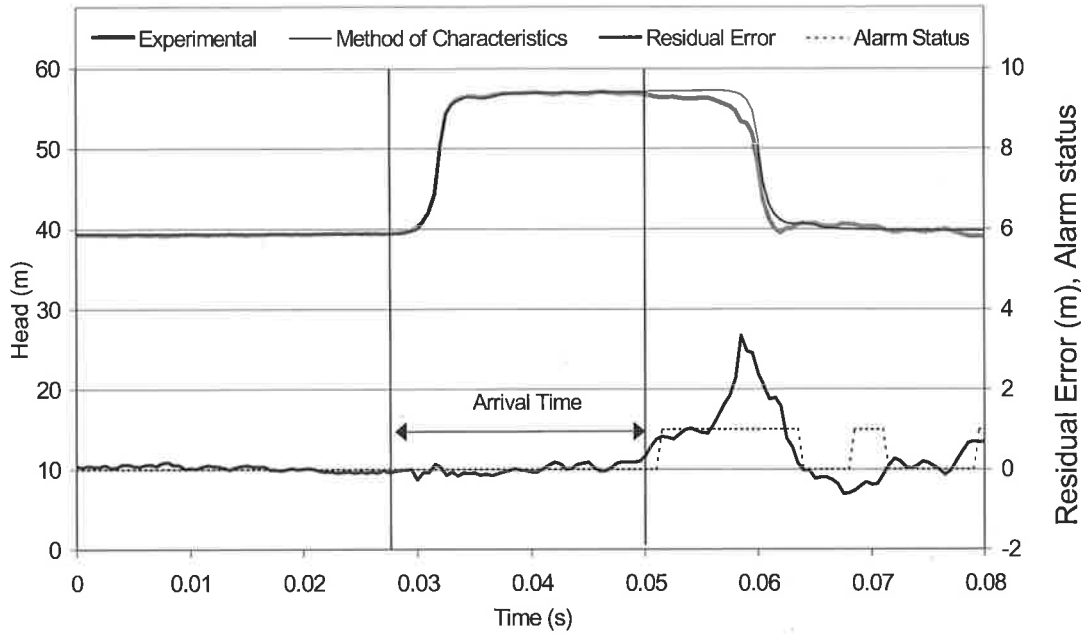


Figure 7-23 – Transient trace measured 18.71 m from upstream reservoir for the anti-symmetric system test (Transducer 1) – (Data file: C7-L2.txt).

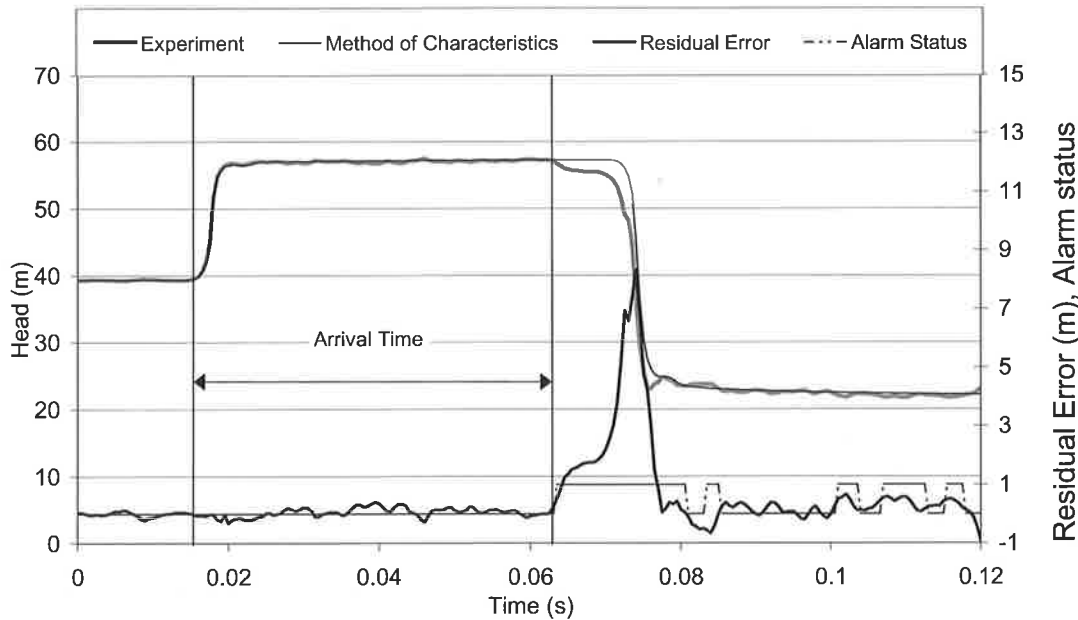


Figure 7-24 – Transient trace measured at the transient source (0.16 m from closed valve) for anti-symmetric system test (Transducer 2) – (Data file: C7-L2.txt).

The use of two measurement stations for each test has the advantage of confirming the location of the leak, especially for the cases where the transient source and the measurement station are at the same position. The errors of the leak location for both tests range between 0.27 m to 0.94 m from the leak, corresponding to 0.7% to 2.5% of the pipe length. The accuracy of this leak detection procedure is affected by a number of anomalies that are discussed in the following section.

7.3.4 Limitations of the conventional TDR technique

The previous tests show that the conventional TDR procedure can detect and locate a leak in a pipeline under symmetric and anti-symmetric boundary configurations. Unlike the frequency-domain leak detection procedure of Chapter 6, the arrangement of the transient source and the measurement stations has no effect on the accuracy. Also, multiple measurement stations provide additional information that can be used to increase accuracy and eliminate ambiguities. However, a problem associated with the conventional TDR approach is that the accuracy and the applicability of this procedure are dependent on the existence of a leak-free benchmark. In addition, the results from two different tests cannot be compared directly unless the injected signals are identical. All deviations from the benchmark, including factors that are not leak related—for example, a difference in the frictional losses in the system—are detected as a leak reflection.

Apart from the reliance on a benchmark, the estimation of the arrival time of leak-reflected signals in the conventional TDR procedure is prone to error. Due to the mechanical inertia associated with transient-generating valves, the injected transient signal is often smooth and contains no distinguishing points that can be used as a reference. The estimation of the arrival time can be taken between points that do not correspond to the beginning of the transient signal and the beginning of the leak reflection. To illustrate, Figure 7-25 shows the beginning of the transient in Figure 7-24. Figure 7-25 indicates four different data points that could be nominated as the “start” of the transient. The arrival of the leak-reflected signal is expanded in Figure 7-26, which shows a number of points that might signal the arrival of the reflected signal. The decision as to which point is chosen from the CUSUM algorithm depends on background noise and the error in both the measured and modelled results.

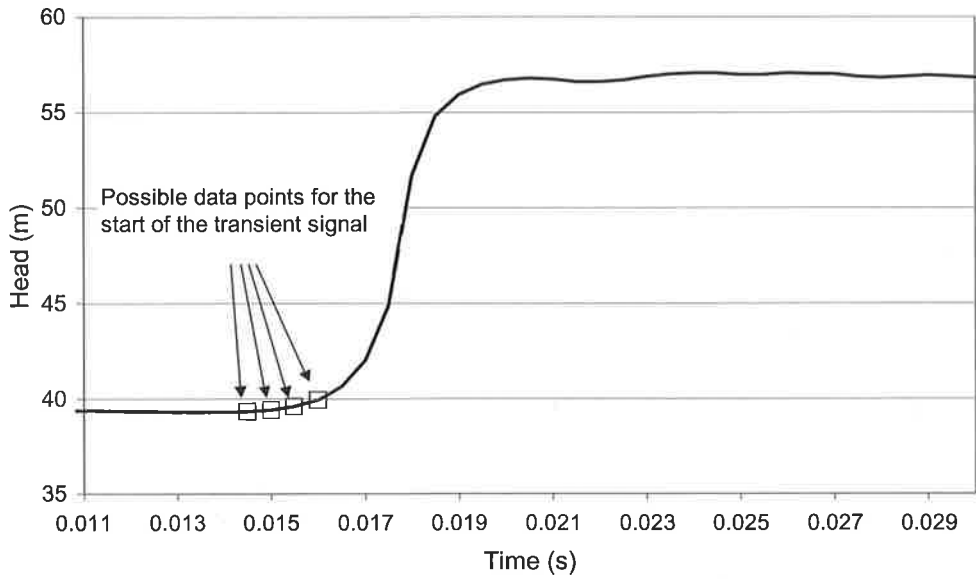


Figure 7-25 – Possible start points of the transient signal in Figure 7-24.

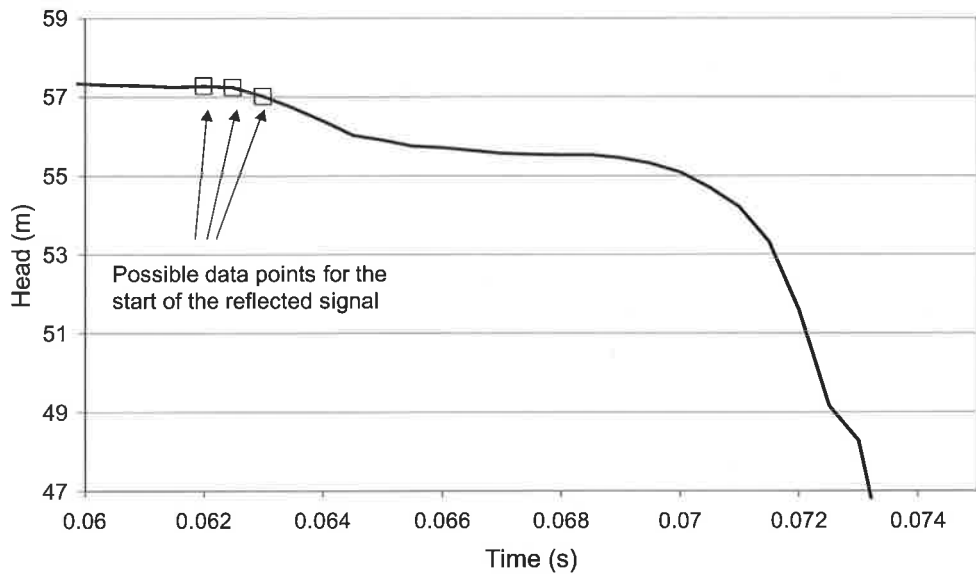


Figure 7-26 – Possible arrival points of the reflected signal in Figure 7-24.

This reliance on a leak-free bench mark and the uncertainty associated with the estimation of the arrival time pose problems for the application of this procedure. These problems can be removed through the use of the system response function in place of the original transient output.

7.4 IMPULSE RESPONSE FUNCTION FOR THE APPLICATION OF TDR

From Chapters 5 and 6, the frequency response function from all intact pipelines has peaks that smoothly decay with frequency and is noticeably different from the case when a leak exists. The shape of the system response function for an intact pipeline is the same for varying levels of frictional loss in the system, different lengths or sizes of the pipeline and for all different types of the injected signal (given a careful selection of the input variable to avoid system non-linearities, refer to Section 5.2.1). A leak can be identified through any deviation from this known form of the response function as was illustrated in the leak detection procedure in Chapter 6. The remainder of this chapter investigates the use of the time-equivalent of the frequency response function, that is, the *impulse response function* for detecting leak-reflected signals in a transient trace. While there have been publications in other fields that make use of the impulse response function for the determination of system characteristics (Sharp 1996), examples of this approach for fluid hydraulic systems are few.

Liou (1998) illustrated the extraction of the impulse response function from a numerical system at different positions along a pipe. The maximum magnitude of the impulse response for each measurement position is then plotted and the linear decrease in the maximum response with distance of measurement position from the transient source is noted. This decrease in the response magnitude is caused by frictional losses in the pipe section joining the transient source and the measurement point and is proportional to distance from the source. A leak imposes a change in the pipe flow, giving a different value of the frictional loss upstream and downstream of the leak. The leak can be detected as the point where the slope of the energy line changes. In essence, this approach resembles the steady state hydraulic grade line measurement approach and the use of the impulse response function for this purpose brings little improvement. Le *et al.* (1998) and Beck and Staszewski (2004) proposed the use of a function similar to the impulse response function for leak detection. This function, known as the “cepstrum” of the measured pressure signal, is defined as

$$C(t) = \mathfrak{F}^{-1}(\log(Y(\omega))) \quad (7.11)$$

where, C is the cepstrum of the signal. The relationship between cepstrum and the impulse response function can be illustrated by substituting $Y(\omega) = H(\omega)X(\omega)$ into Eq. (7.11) giving

$$C(t) = \mathfrak{F}^{-1}(\log(H(\omega)X(\omega))) \quad (7.12)$$

Using a property of the logarithmic function, the equation becomes

$$C(t) = \mathfrak{F}^{-1}(\log(H(\omega))) + \mathfrak{F}^{-1}(\log(X(\omega))) \quad (7.13)$$

The cepstrum of the signal consists of a summation of the inverse Fourier transform of the logged frequency response function (which is an approximation of the impulse response function) and a second term, which is related to the nature of the input signal. The equation can be rewritten as

$$C(t) = I'(t) + \mathfrak{F}^{-1}(\log(X(\omega))) \quad (7.14)$$

where I' is the approximation of the impulse response function. The cepstrum of the signal is of a similar form to the impulse response function and can be used to determine the position of faults in the pipeline. However, while the cepstrum produces an approximation of the impulse response function, it is still dependent on the nature of the input signal and is not a true representation of system behaviour. Given a different input signal, the second term in Eq. (7.15) is different and the cepstrum changes as a result. For a proper extraction of the system response behaviour, the true impulse response function, which is independent of the input signal, should be used. The following section describes a procedure where the impulse response function can be extracted from a pipeline.

7.4.1 EXTRACTION OF THE IMPULSE RESPONSE FUNCTION (IRF)

From Chapter 5, the frequency response function (F) relates the correlation spectrums of the input, X , and output, Y , of a system by

$$S_{XY}(\omega) = S_{XX}(\omega)F(\omega) \quad (7.15)$$

The time equivalent of this equation is

$$r_{xy}(t) = \int_{-\infty}^{\infty} r_{xx}(t^*)I(t-t^*)dt^* \quad (7.16)$$

where $I(t)$ is the impulse response function, S_{XX} = Fourier transform of the auto-correlation of the input signal, S_{XY} = the Fourier transform of the cross-correlation between the input and the output, r_{xy} = the cross-correlation function between x and y , r_{xx} = auto-correlation function of the input, and the integral in Eq. (7.16) is known as the *convolution integral*. From Eq. (7.15), the frequency response function can be extracted from the input and output of a system by dividing the auto-correlation spectrum of the input into the cross-correlation spectrum as was shown in Chapter 5. The extraction of the impulse response function from the original time series, however, can become complicated using Eq. (7.16); it involves a process known as *deconvolution*, where $I(t)$ is extracted from the convolution integral of Eq. (7.16).

Li *et al.* (1994) and Liou (1998) and Dallabetta (1996) approximated the auto-correlation of the input time series in Eq. (7.16) (r_{xx}) by a dirac impulse when a wide band signal was injected into the system. The convolution of any function with the dirac pulse is the signal itself. The impulse response function of the system is, therefore, proportional to the cross-correlation between the input and output signals. However, as indicated in Chapter 5, the generation of a transient signal that has a bandwidth approximating a dirac impulse is difficult to produce in hydraulic systems. The use of a solenoid side-discharge valve can only produce signals of 300 Hz bandwidth (refer to Chapter 4). The approximation used in Li *et al.* (1994), Liou (1998) and Dallabetta (1996) cannot be applied in this situation.

Alternatively, in the case where the bandwidth of the injected signal is not close to the Nyquist frequency (1000 Hz for a sampling frequency of 2000 Hz), a fast deconvolution method, known as the *Fourier-quotient method*, can be used (Starck *et al.* 2002, Sharp 1996). This approach takes advantage of the fact that the impulse response function and the frequency response function are a Fourier transform pair,

$$I(t) = \mathfrak{S}^{-1}[F(\omega)] \quad (7.17)$$

The extraction of the system impulse response can be carried out by first extracting the FRF as illustrated in Chapter 5 and then taking an inverse Fourier transform (Sharp, 1996). Care must be taken to remove any high-frequency components beyond the bandwidth of the injected signal prior to taking the inverse Fourier transform. Failure to do so results in the contamination of the impulse response function as is discussed later in the chapter. In addition, the FRF must remain in complex form prior to the inverse Fourier transform to preserve the phase information contained in the function. The nature of the extracted impulse response function is illustrated in the following section.

7.4.2 PROPERTIES OF THE IMPULSE RESPONSE FUNCTION (IRF)

The process of impulse response extraction can be considered as a procedure that refines the shape of the output signal such that each reflected signal in the trace is replaced by a unit impulse having a sharp, well-defined spike (Lynn, 1982). The definition of the impulse response of a system is the response measured at the output when a unit impulse (a sharp spike of a magnitude of 1.0) is applied at the input. The definition of the impulse response function is illustrated in Figure 7-27.

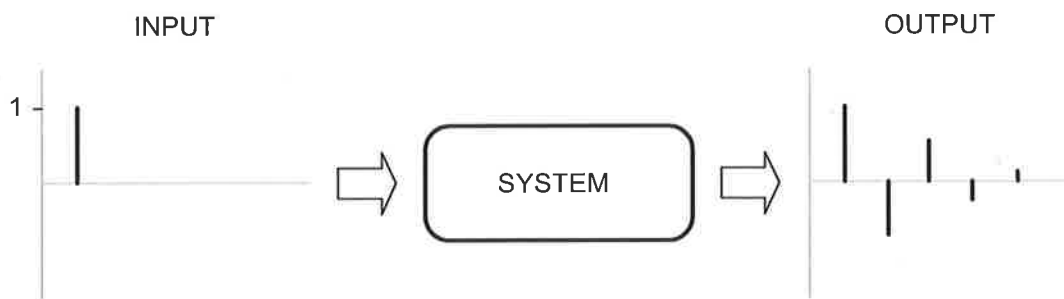


Figure 7-27 – Impulse response function from a system.

Consider the response of a system when a complex signal is applied at the input. Each input may be considered as a sequence of weighted impulses, hence each point on the input generates a scaled version of the impulse response at the output. The overall response from the entire input signal is given by the sum of these individual scaled impulse responses. This fundamental property is shown in Figure 7-28 where a signal,

consisting of three points (A, B, C), is used as the input. The output is given by the sum of the expected responses from each of the three individual impulses. This method of graphically summing the responses from each data point at the input to produce the overall output is mathematically equivalent to the convolution process in Eq. (7.16).

For any input / output pair from a pipeline, the impulse response can be extracted using Eq. (7.17) to give an indication of system behaviour and hence determine the possible presence of faults. The extraction of the impulse response function from the numerical pipeline (refer to Figure 7-29) is illustrated in Figure 7-30 to Figure 7-33.

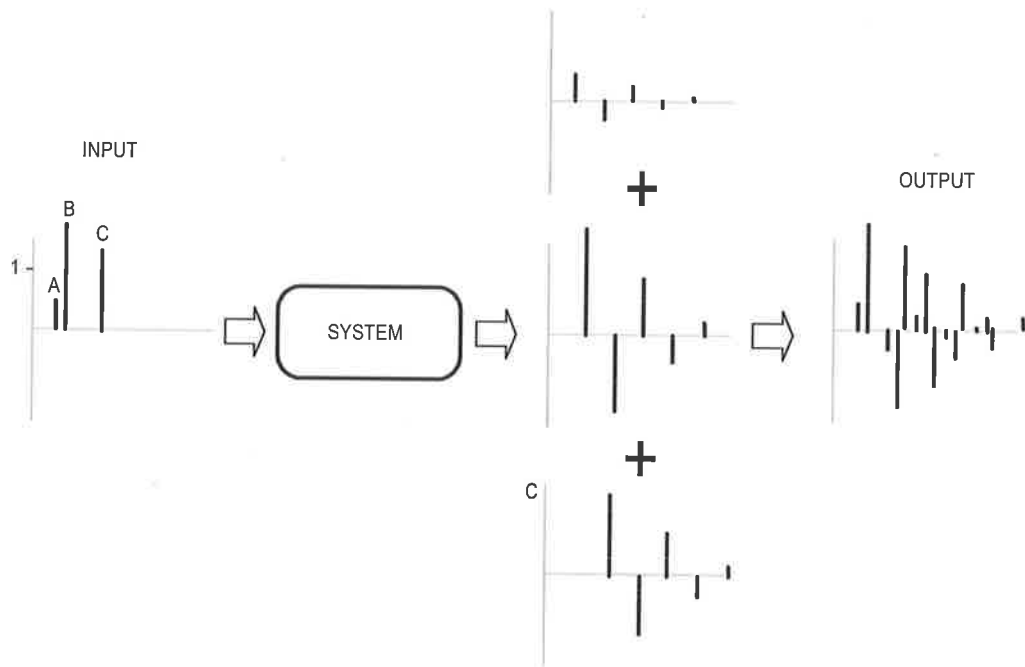


Figure 7-28 – The overall response from the system when a complex single is applied at the input.

The results were generated numerically using the method of characteristics model with a discretisation of 100 and a computational time step of 0.0333 s. The pipeline was configured symmetrically with the transient-generating side-discharge valve at the centre of the pipeline (refer to Figure 7-29). The side-discharge valve was made to perturb in the pattern shown in Figure 7-30 , giving the response at the midpoint as Figure 7-31. For illustrative purposes, unsteady friction is assumed negligible. To extract the impulse response, the input and output signals were first used to determine the FRF from the pipeline in a procedure described in earlier chapters. The magnitude of the FRF from this system is shown in Figure 7-32. This FRF (in complex form) was put through an inverse

Fourier transform algorithm according to Eq. (7.17) giving the impulse response as shown in Figure 7-33. To provide a clear comparison with the original time series trace, the IRF is translated forward in the time axis to match the starting position of the initial transient.

Reservoir 1 Head = 50 m

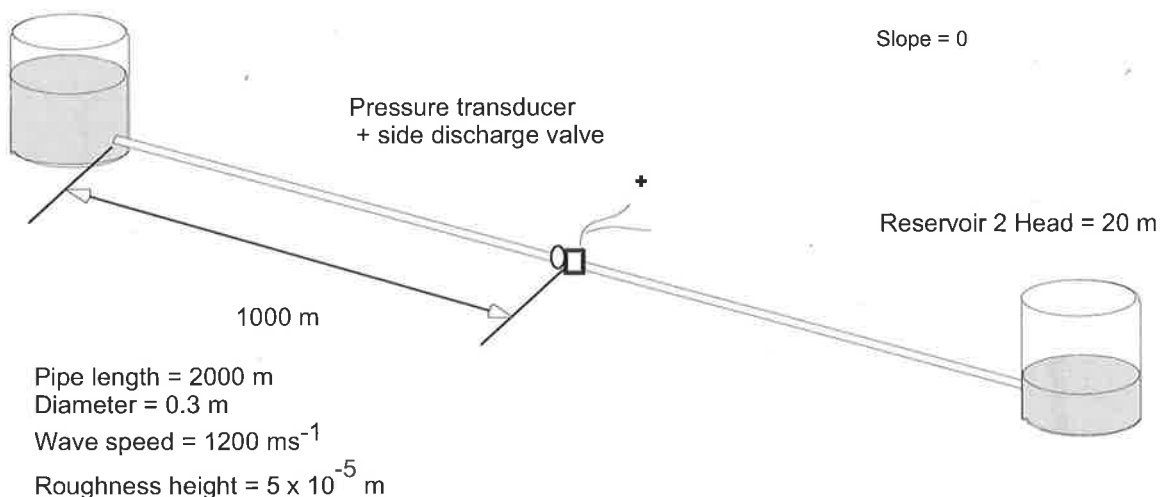


Figure 7-29 – System configuration for numerical extraction of the impulse function.

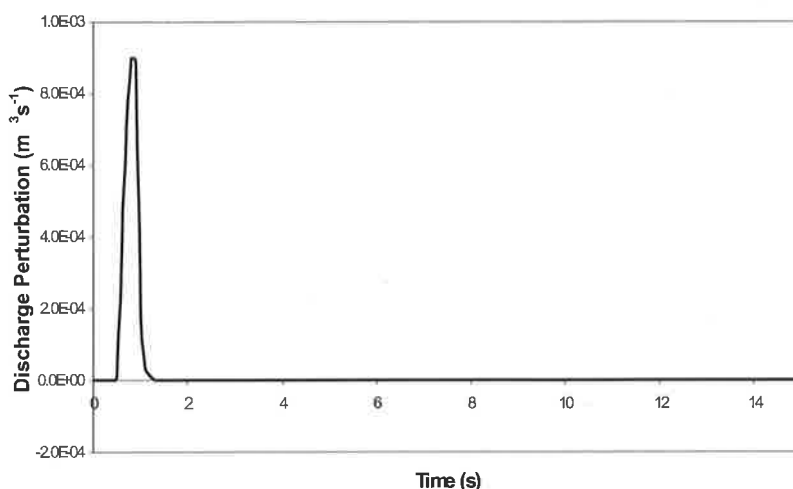


Figure 7-30 – Input to the leak-free numerical system (Data file: C7-I1.txt).

Through the method of impulse response extraction, each occurrence of the input pulse in the original transient trace is replaced by a perfect impulse, each with a width of a single time step. The same procedure is carried out where a leak exists 1500 m from the upstream boundary with a $C_d A_L / A = 3.96 \times 10^{-3}$ (refer to Figure 7-34). For a similar input

signal (Figure 7-30), the output of the leaking system is shown in Figure 7-35. The leak-reflected signals are circled in Figure 7-35. The impulse response is shown in Figure 7-36, again with the leak reflections circled. A set of leak-reflected signals from the original transient trace and the impulse response are superimposed in Figure 7-37 showing the refinement of the pulse width using the impulse response.

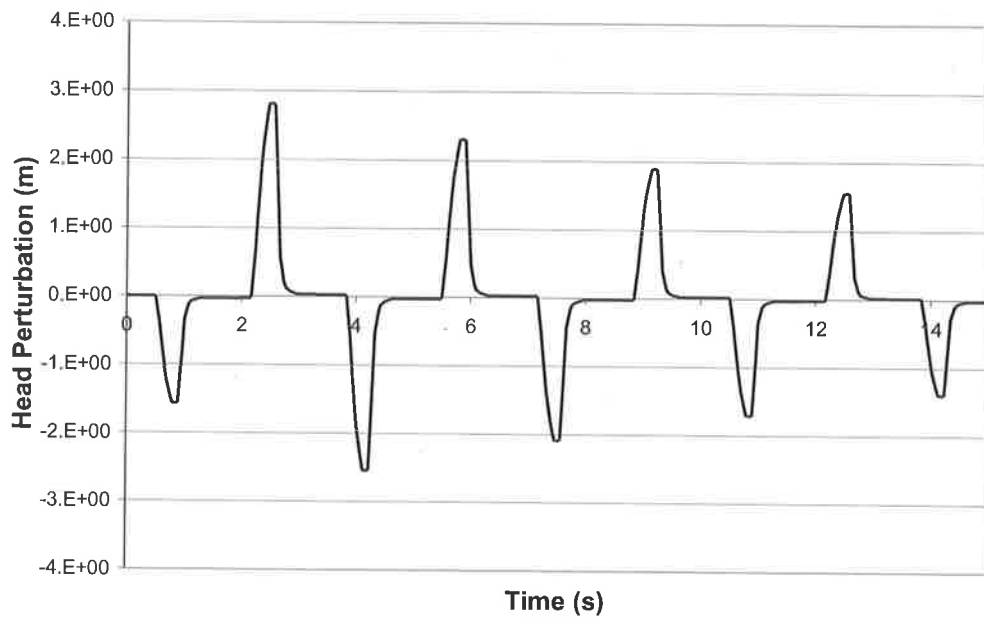


Figure 7-31 – Output from the leak-free numerical system (Data file: C7-11.txt).

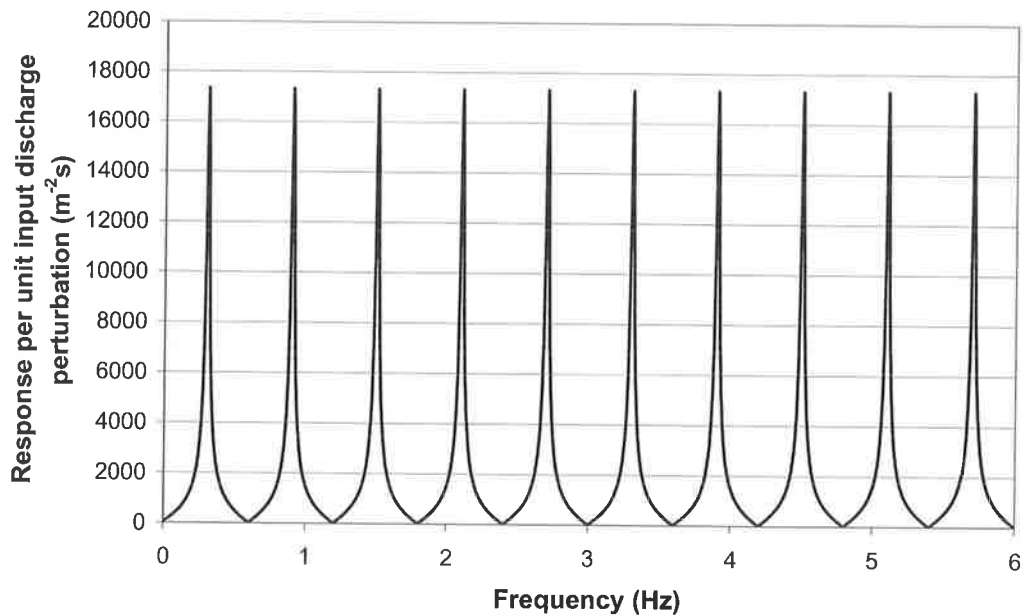


Figure 7-32 – FRF from the symmetric leak-free pipeline.

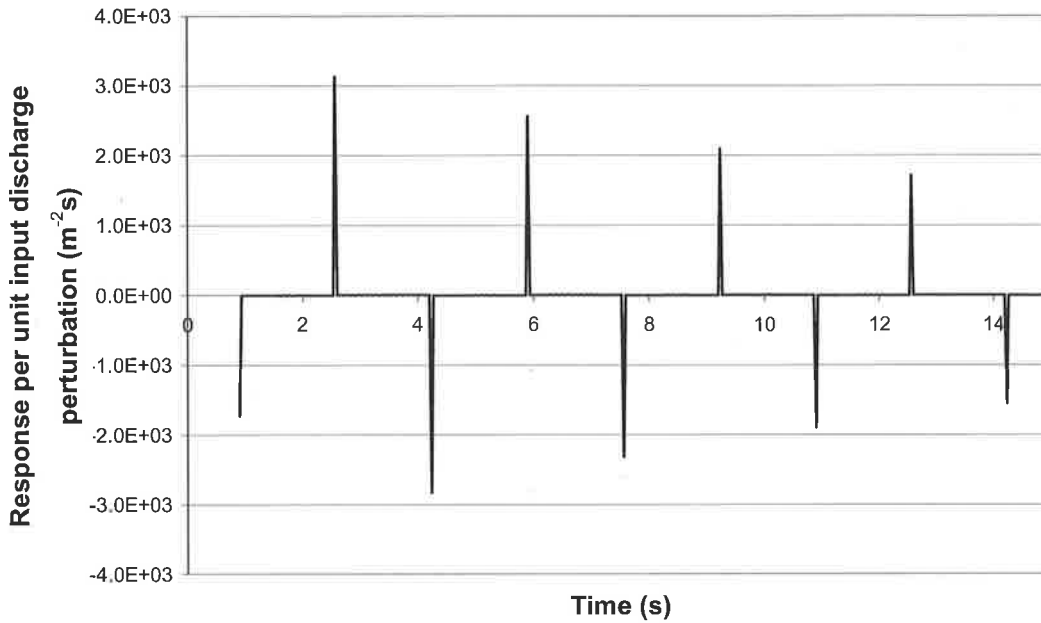


Figure 7-33 – Impulse response extracted from the input and output pair.

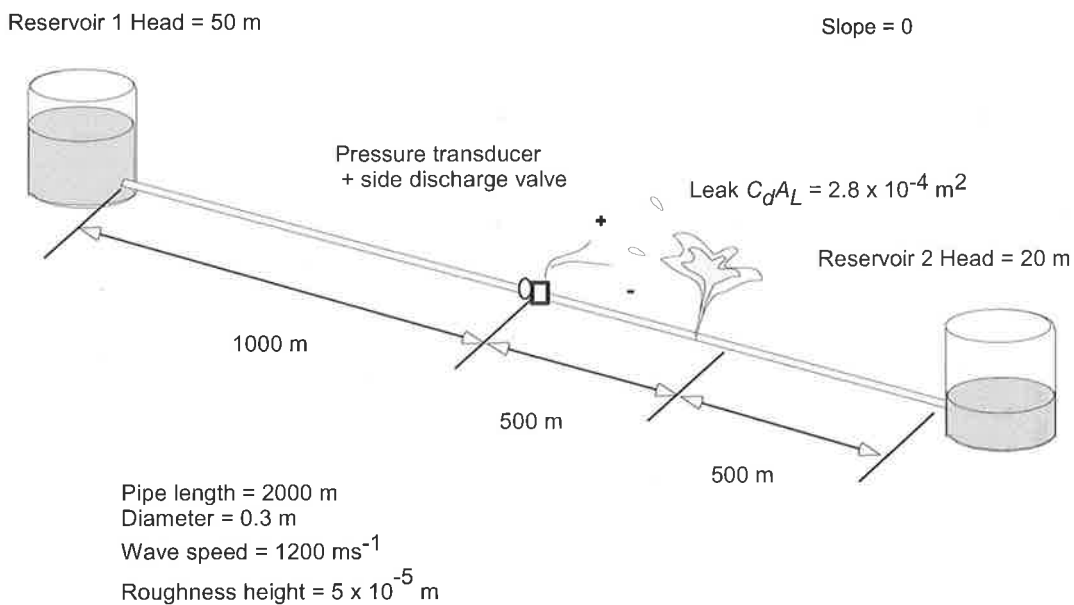


Figure 7-34 - Configuration for numerical extraction of the impulse response function in a leaking system

This refinement can improve the accuracy of the TDR procedure if the impulse response function is used in place of the original transient trace for the estimation of arrival time of a leak-reflected signal. When an injected transient is in the form of a pulse, the arrival time of a signal can be estimated from a raw transient trace by the time lag between the peak of the injected signal and the peak of the reflected signal. These peak positions on the

reflected signals, however, can be taken as either of the two data points, labelled “A” and “B,” circled in Figure 7-37.

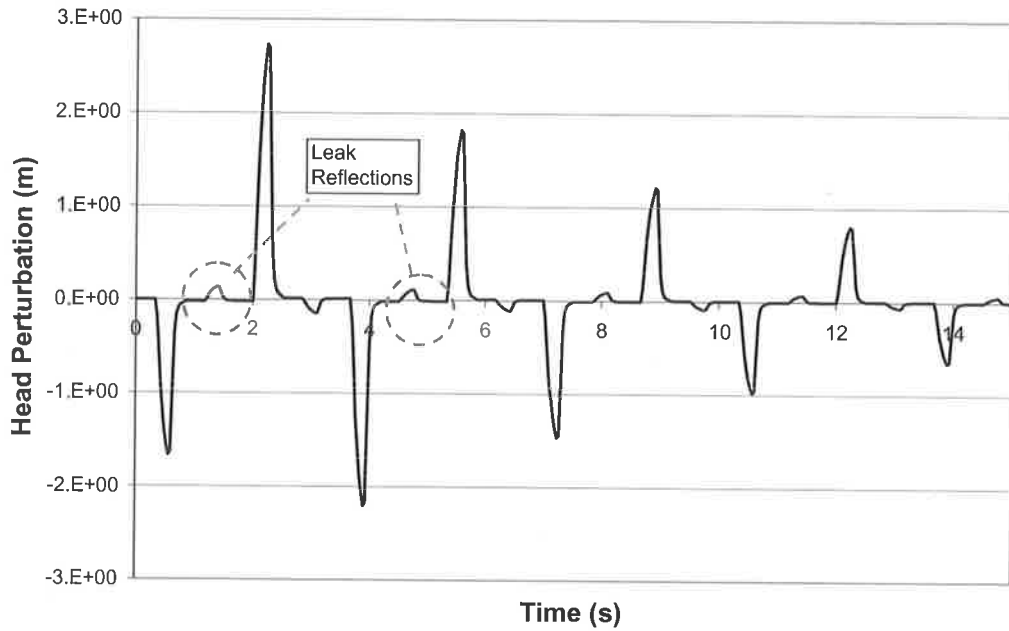


Figure 7-35 – Output from the leaking system with a leak 1500 m from upstream boundary, $C_d A_L / A = 3.96 \times 10^{-3}$ (Data file: C7-I2.txt).

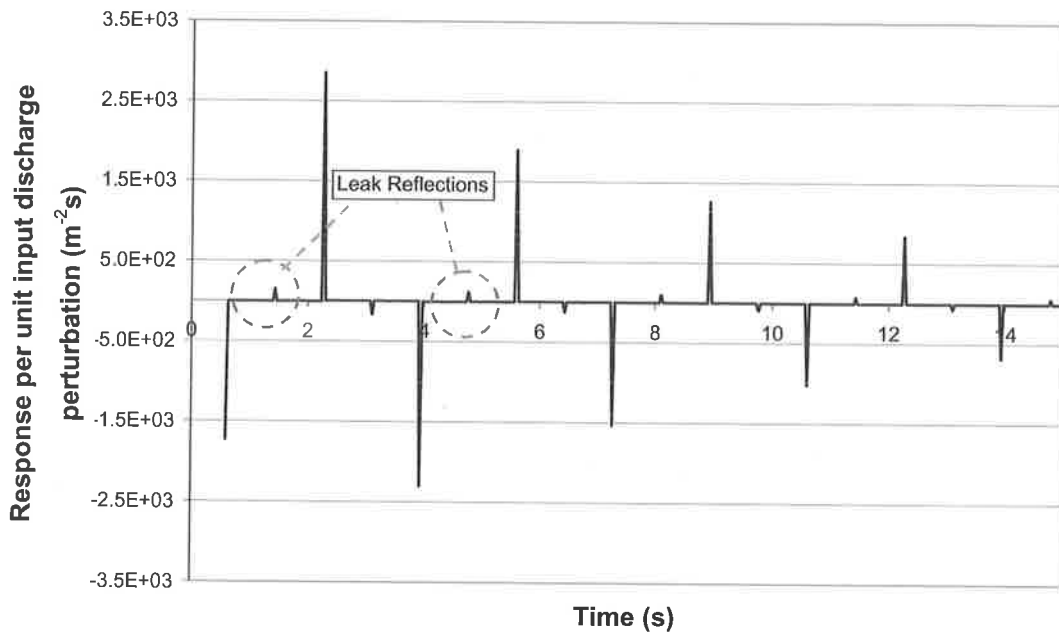


Figure 7-36 – Impulse response from the leaking system with a leak 1500 m from upstream boundary, $C_d A_L / A = 3.96 \times 10^{-3}$.

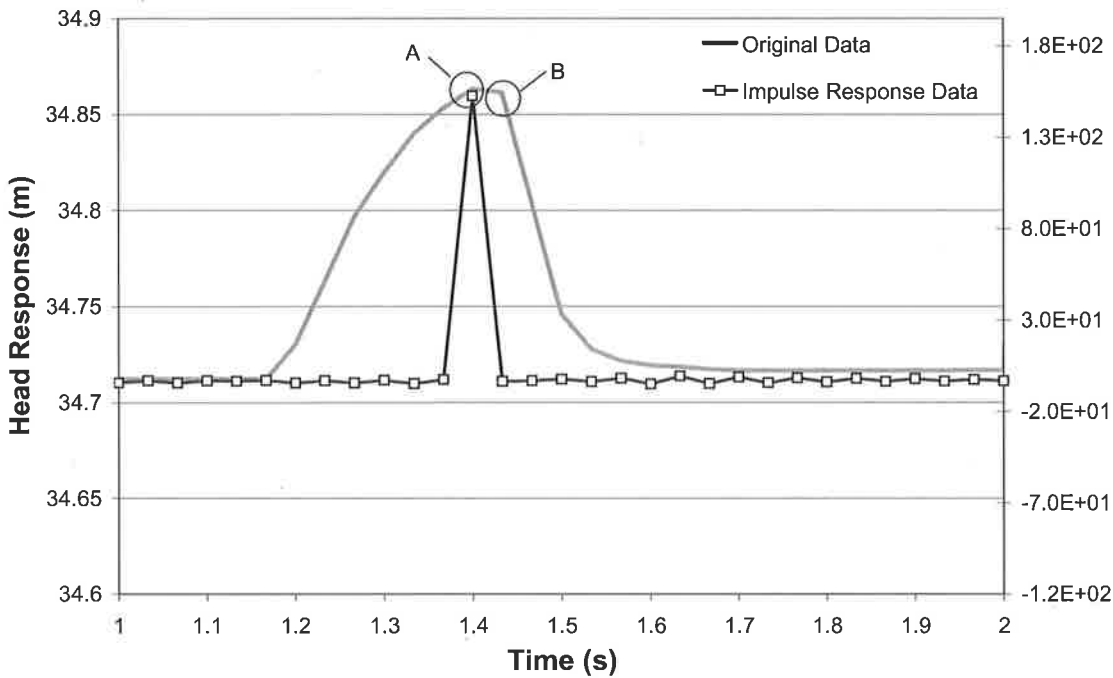


Figure 7-37 – Refinement of leak-reflected pulse using the impulse response function.

These two points are of similar magnitudes and, in the presence of system noise, either of these can be identified as the “peak” of the transient pulse. The estimation of the signal arrival time can be in error by 0.067 s for this sampling frequency (30 Hz) and corresponds to a wave travel distance of 80 m in this numerical pipeline of length 2000 m.

In comparison, the refinement of the signal using the impulse response extraction procedure removes this ambiguity in the estimation of arrival time. The original and reflected signals in the IRF are refined to sharp spikes with widths equal to the sampling interval. The exact timing of the reflected signal can now be determined with minimal error.

As mentioned in Chapter 5 and Chapter 6, another important advantage in using the system response functions for leak detection is that the nature of the functions represents the underlying behaviour of the system. To illustrate this property, a different signal, generated by the closure of the solenoid valve, is injected into the same leaking pipeline. The measured transient output for this situation is shown in Figure 7-38. This output is clearly different than the one shown in Figure 7-35, although the physical properties of the pipeline remain unchanged. The detection of the leak-reflected signal using TDR in these

two cases would require two different leak-free benchmarks. The IRF of the system for the two cases is shown in Figure 7-39. A good match is observed indicating that the form of the IRF is not dependent on the shape of the injected signal.

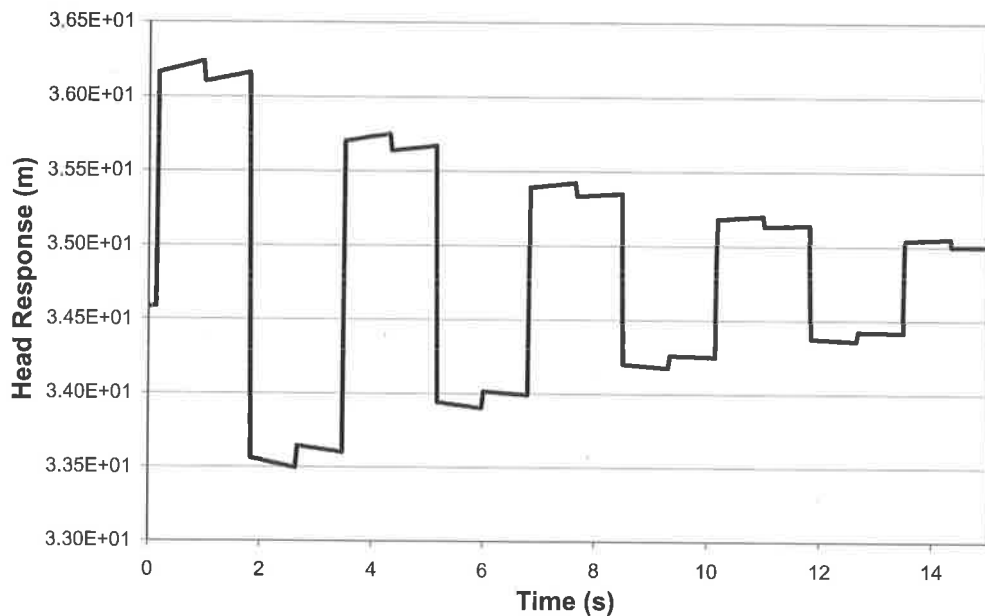


Figure 7-38 – Output from the same leaking system using a step closure of the valve as the injected signal.

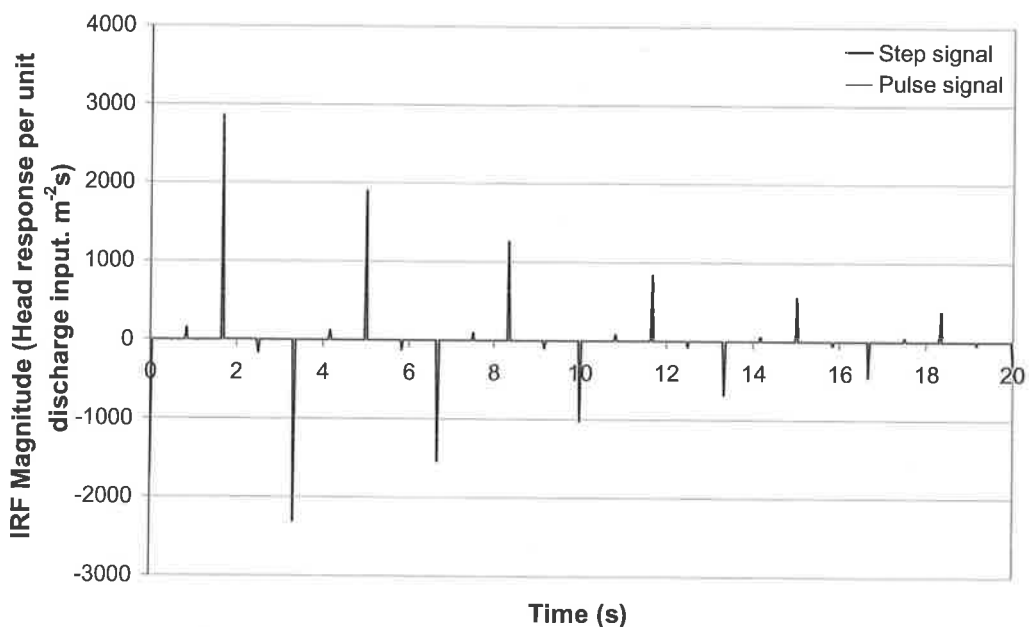


Figure 7-39 – Comparison of the impulse response function using the two different injected signals in Figure 7-35 and Figure 7-38 (the series overlap perfectly).

As the impulse response for different signals is of the same form, the application of the TDR procedure using the IRF can remove the previous reliance on the leak-free benchmark for comparison. For example, from the leak-free IRF in Figure 7-33, the impulse response function is zero except when a system reflection arrives at the measurement point. As arrival times of boundary reflections in any pipeline are known, detected reflections that do not correspond to these arrival times are fault-generated reflections. The benchmark for comparison is no longer necessary when the impulse response function is used. The CUSUM algorithm can be set to detect any significant deviations from zero in regions where reflections from the system are not expected.

The following section investigates the application of this technique in an experimental system and presents additional modifications to the procedure required to produce a clean IRF in a physical system.

7.5 EXPERIMENTAL EXTRACTION OF THE IMPULSE RESPONSE FUNCTION (IRF)

To validate the IRF extraction procedure under experimental conditions, the laboratory system was arranged symmetrically with the downstream valve fully opened. The boundary heads were set at 37 and 36.5 m giving a flow velocity in the range of 0.5 ms^{-1} and a Reynolds number of 11,000 (refer to Figure 7-40). The transient was generated by a pulse perturbation of a side-discharge valve located close to the midpoint of the pipe (18.705 m from one boundary) and the transient was measured at this position. The resultant transient trace and the extracted IRF (using the procedure described in the previous section) are shown in Figure 7-41 and Figure 7-42.

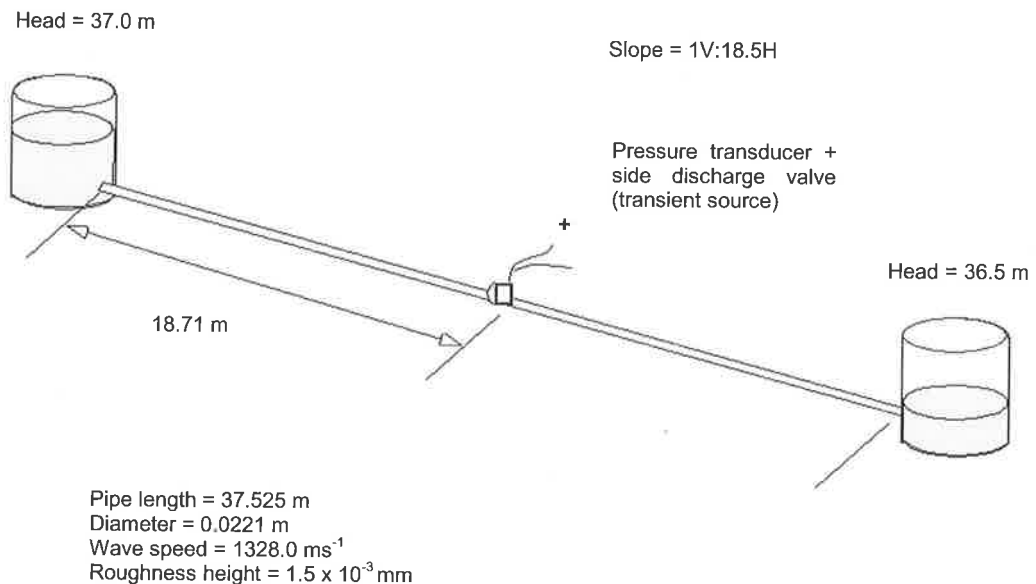


Figure 7-40 – System configuration for the experimental extraction of the IRF.

Unlike the numerical results in the previous section, the experimentally extracted IRF displays a significant level of distortion and the spikes in the IRF are no longer visible as discrete boundary reflections. The cause of this distortion can be explained by the bandwidth of the injected signal. As discussed in Section 5.2.3, the experimentally derived FRF is affected by the bandwidth of the input signal. Every input signal contains a finite amount of energy that attenuates with frequency. The input signal from the solenoid valve has a bandwidth of 300 Hz. At higher frequencies, the energy of the input approaches zero

and introduces errors in the FRF (through the division of the output spectrum by small values). This result is illustrated in the full FRF for the experimental data with frequencies ranging from zero to 1000 Hz (the Nyquist frequency for a sampling frequency of 2000 Hz) in Figure 7-43. From the FRF, the lower frequencies consist of regular harmonic peaks (as shown in Chapter 5 and 6) whereas the higher frequencies contain only random noise.

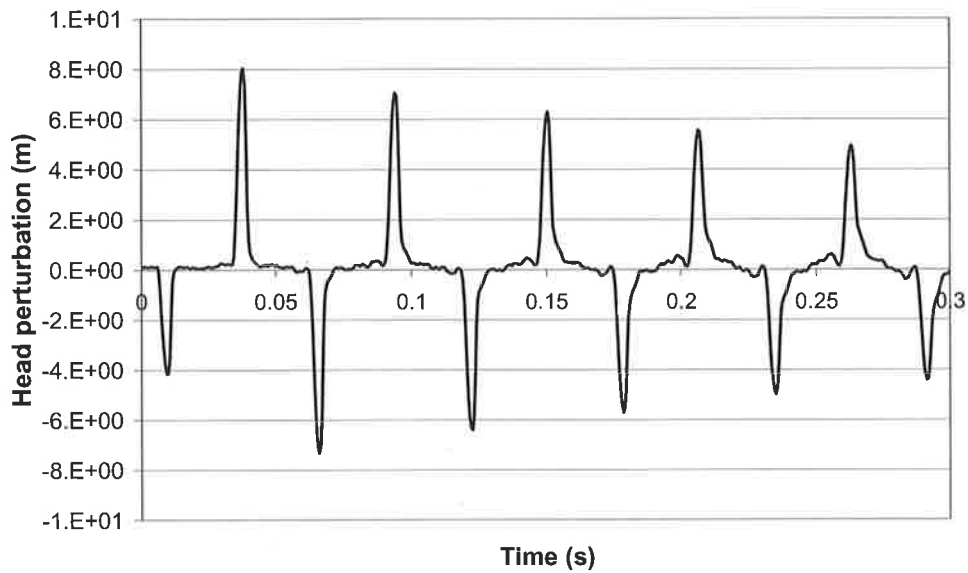


Figure 7-41 – Transient trace from the experimental system (Data file: L7-I3.txt).

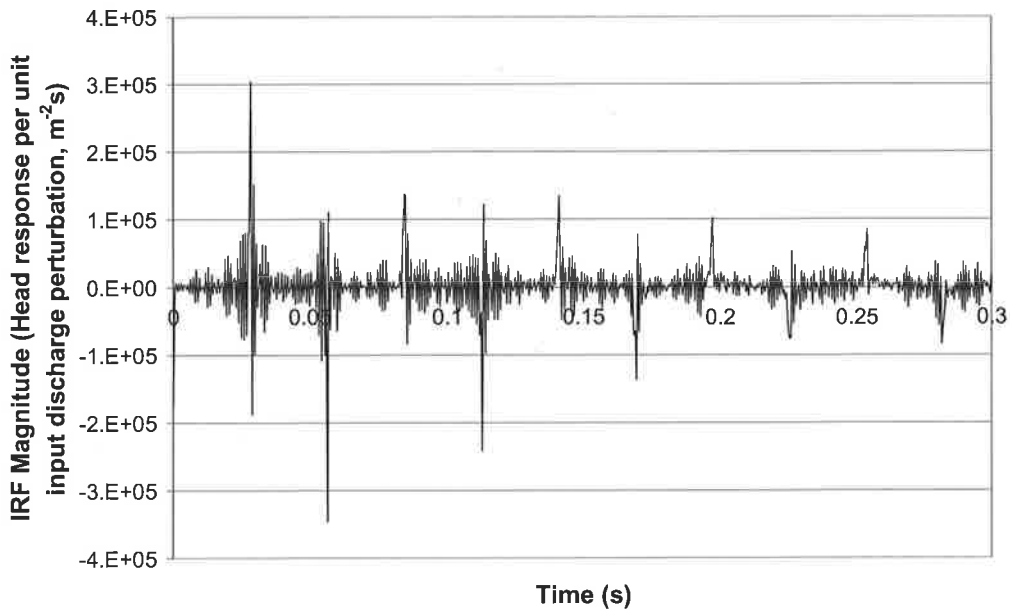


Figure 7-42 – Unsmoothed IRF from leak-free experimental pipeline.

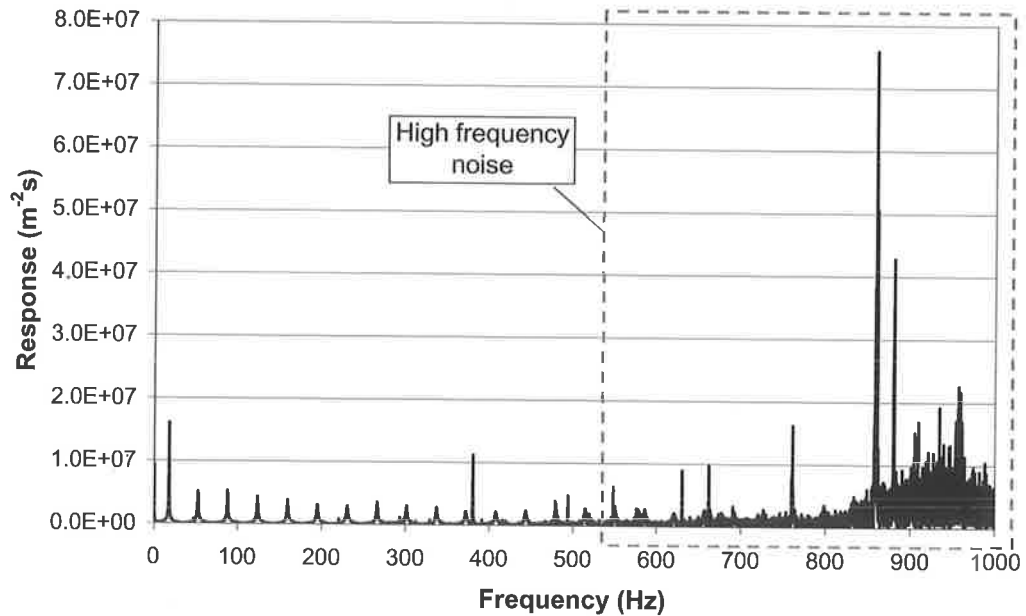


Figure 7-43 – Bandwidth-related high-frequency noise in FRF.

In Sharp (1996), this distortion of the FRF was reduced by adding a small non-zero term to the input spectrum across all frequencies, which prevents the division of the output spectrum by small values in the extraction of the FRF. A procedure that can achieve a similar result is to multiply the FRF by a filter, thus removing the noise component at high frequencies. Two filter types are chosen for their ability to generate a smooth reduction of magnitudes at high frequencies, the Hamming filter and the Blackman filter (Oppenheim and Schaffer, 1989). The shapes of the Hamming and Blackman filters for 10,000 data points are shown in Figure 7-44.

Both filters are symmetric and can be multiplied into the frequency data generated from a conventional Fourier transform where zero frequency is at the centre with positive and negative frequencies responses on either side. The shapes of the two filters differ slightly. The Blackman filter produces a faster reduction in magnitudes near the tails of the filter. The equation for the impulse response function, taking into account the filtering process, is

$$I(t) = \mathcal{F}^{-1}[W(\omega)F(\omega)] \quad (7.18)$$

where W = the filter function.

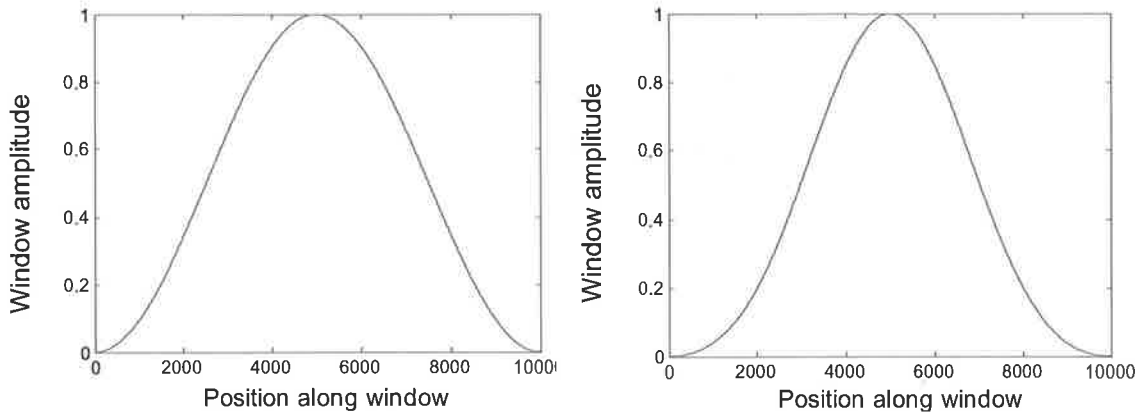


Figure 7-44 – Shape of the (a) Hamming and (b) Blackman filter.

The effect of multiplying the Blackman filter into the FRF is shown in Figure 7-45. The filter has resulted in the removal of most of the noise from the FRF. The effect of each filter on the resultant IRF of the system is shown in Figure 7-46. The results show that, although both filters produce a marked improvement, the Blackman filter gives a cleaner response function.

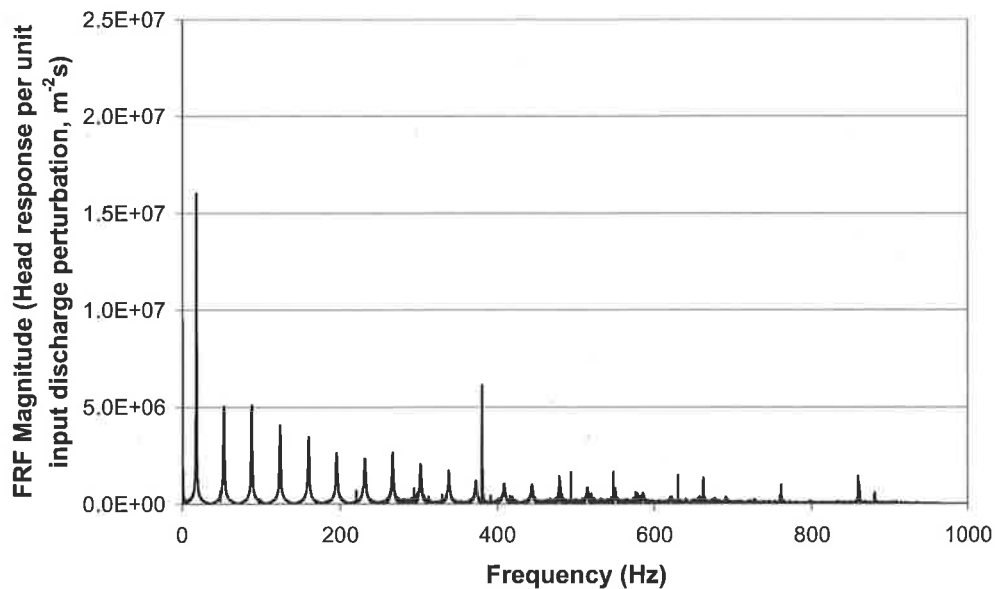


Figure 7-45 – Filtered FRF result using the Blackman filter.

A boundary reflection from the original signal is shown with the same reflection in the IRF in Figure 7-47. As in the numerical investigation, the reflection from the IRF is sharper than that in the original signal. Unlike the numerical study, however, the widths of the reflected pulses in the IRF are no longer at the width of the sampling interval. Instead,

the Blackman filter has smoothed the overall IRF and the pulses are now wider than the numerical example.

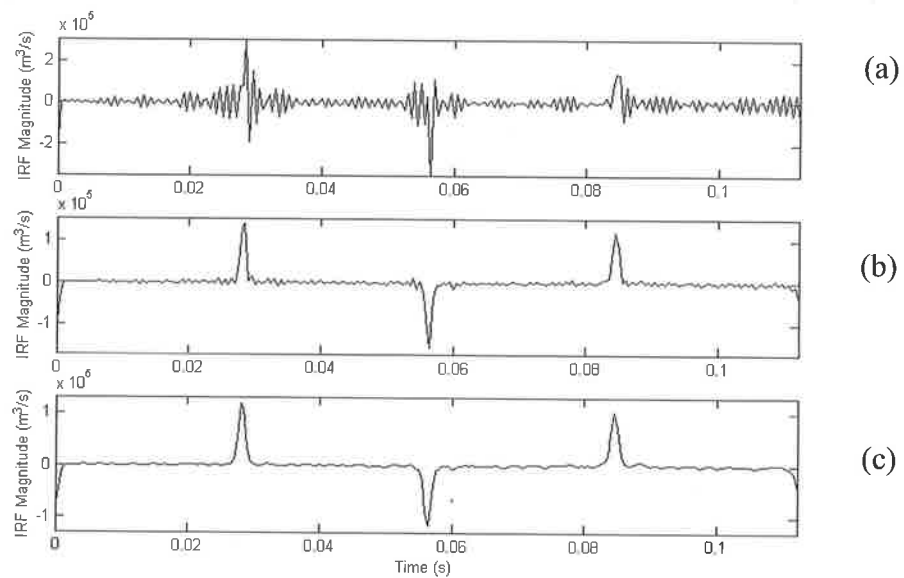


Figure 7-46 – Effect of each filter on the form of the IRF, with (a) the unfiltered IRF, (b) the filtered IRF using Hamming and (c) the filtered IRF using Blackman.

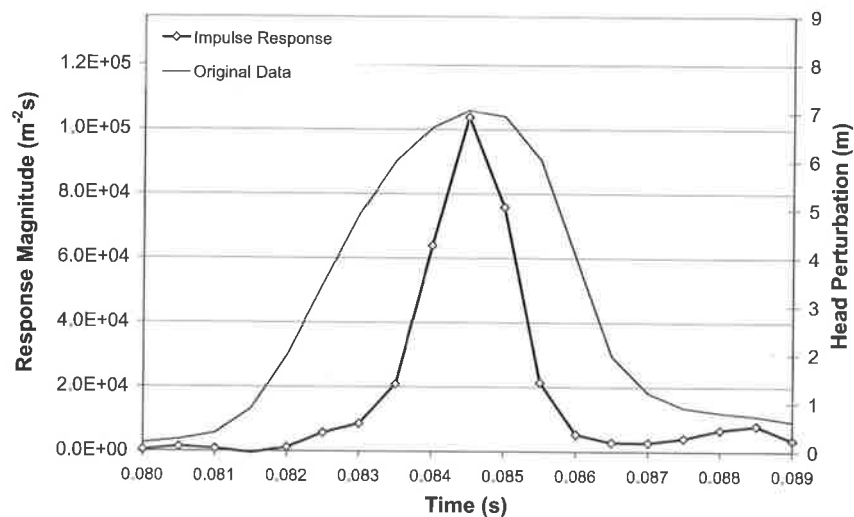


Figure 7-47 – Comparison of reflection shapes between the original signal and the filtered IRF

In summary, the procedure for extracting the IRF from a pipeline is as follows:

1. Extract the frequency response function from the pipeline (refer to Chapter 5).
2. Multiply the resultant complex FRF by a Blackman filter according to Eq. (7.18).

3. Inverse Fourier transform the result.

The schematic of the IRF extraction procedure is shown in Figure 7-48. The following section presents the procedure for leak detection using the IRF.

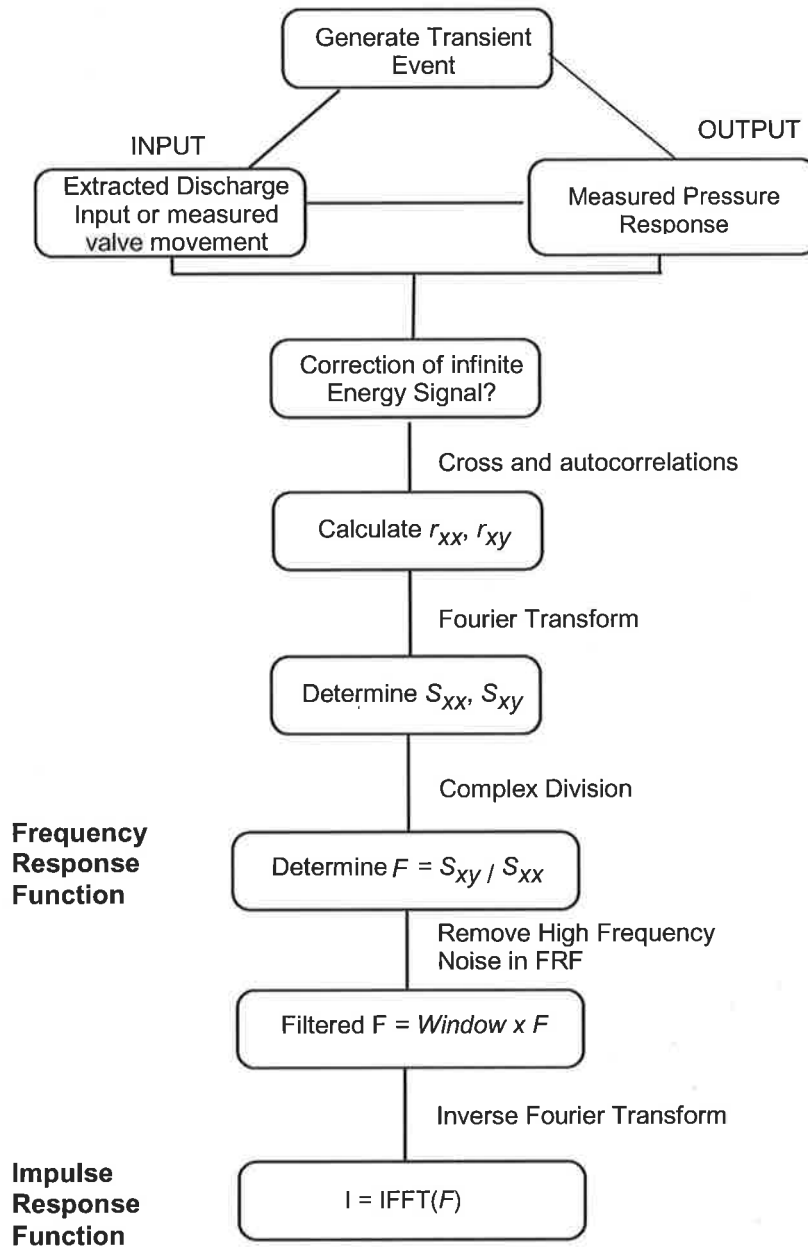


Figure 7-48 – Procedure for extracting the impulse response function from the pipeline

7.6 METHOD OF LEAK DETECTION USING THE IMPULSE RESPONSE FUNCTION (IRF)

The conventional TDR procedure can be modified to take advantage of the properties of the impulse response function. Two modifications are made that include (1) the removal of the leak-free benchmark and (2) the refinement of the signal reflections.

7.6.1 Removal of the need for a leak-free benchmark

For any injected transient signal the resultant IRF of an intact pipeline consists of a series of sharp pulses about zero. Each of these pulses corresponds to a reflection from the system. Detection of pulses at times that do not correspond to arrival times of boundary reflections indicates the possible presence of a leak in the system. This fixed shape of the IRF in an intact system can allow reflected signals in a pipeline to be detected regardless of the nature of the injected signal and without the need for a leak-free benchmark. A leak reflection arriving in close proximity to a boundary reflection may not be distinguishable as a separate waveform. The detection regions, illustrated in Figure 7-49, in the IRF should take place away from the boundary reflections.

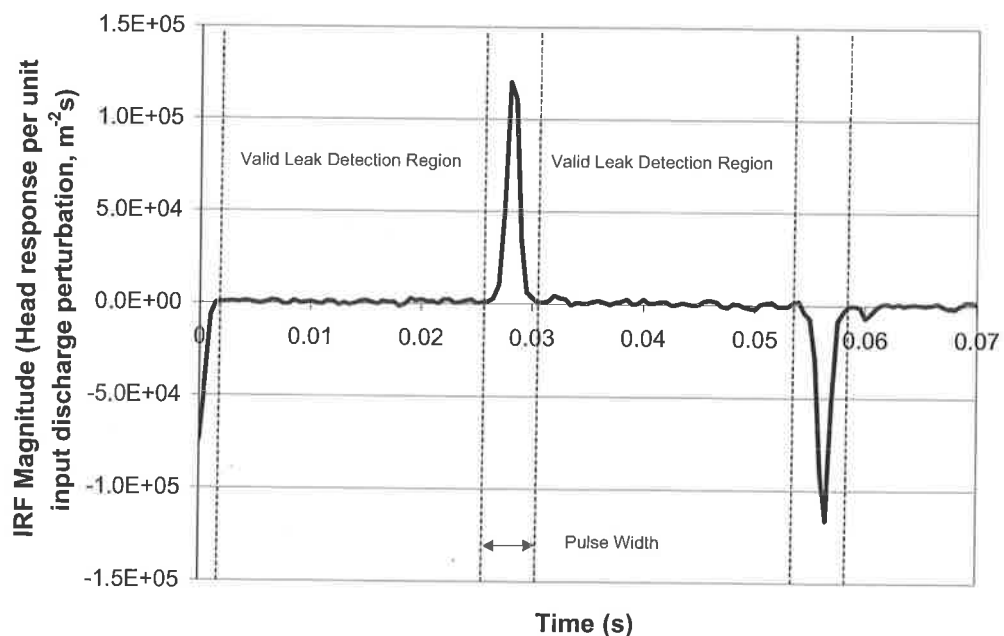


Figure 7-49 – Regions for leak detection in the IRF.

Multiple measurement stations can be used to measure the same transient event giving the IRF at different positions in the pipeline. The valid extraction of the system response function requires only a set of input and output time series, the location of which does not affect the accuracy of the approach. The predicted leak location that is common to results from different measurement stations is the true position of the fault. This approach is an improvement to the leak detection procedure in the frequency domain where the transient source and measurement station must be placed at certain positions to locate a leak.

7.6.2 Refinement of transient reflections

The smooth nature of an injected transient signal can lead to errors in the estimation of reflection arrival times (refer to Section 7.3.4). An impulse response function removes this ambiguity as all reflections are converted into sharp pulses, each with a clearly defined maximum point. The form of the IRF is automatically time-shifted such that the start of a transient signal corresponds to $t = 0$ in the IRF. The time lag between an injection of a signal and the arrival of any reflection is simply given as the time at the peak of the reflected pulse and can be used to determine the leak position. This improvement is shown in Figure 7-50 (shown previously as Figure 7-36).

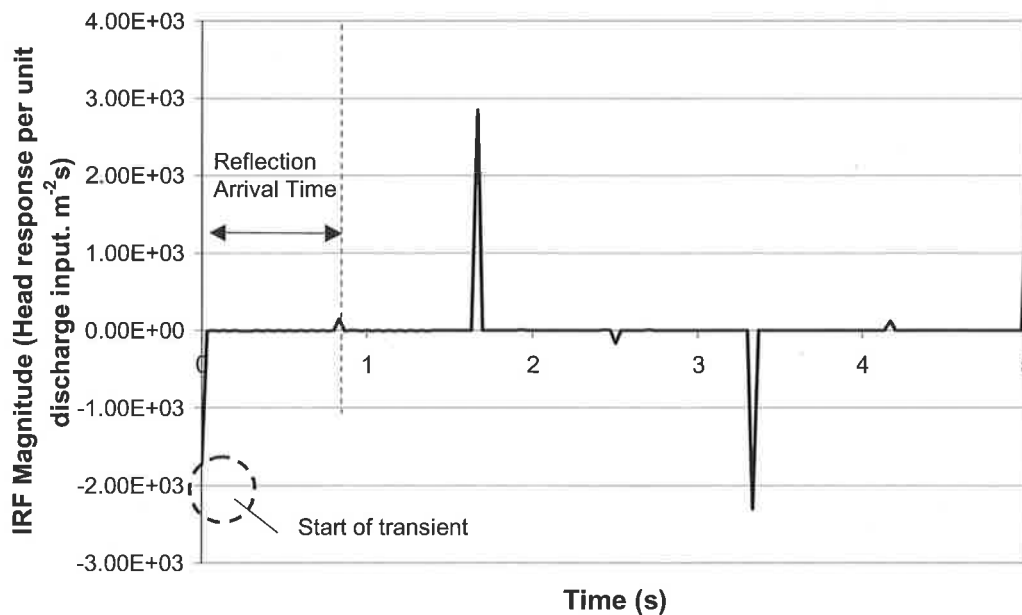


Figure 7-50 – Estimation of the arrival time of leak-reflected signals using the IRF.

7.7 EXPERIMENTAL VALIDATION OF THE IMPROVED TDR PROCEDURE FOR LEAK DETECTION

Experiments of leak detection using the impulse response were conducted for both anti-symmetric and symmetric boundary configurations. Given that the TDR procedure is only concerned with the first reflection from the system, the first half period of oscillation is shown for each of the following results.

7.7.1 Anti-symmetric System Tests

The anti-symmetric tests were conducted in the experimental apparatus with the in-line valve fully closed and the upstream reservoir set at 39.6 m. A leak 28.06 meters from the upstream boundary has an orifice diameter 1.5 mm and $C_d A_L / A = 4.17 \times 10^{-3}$. Two pressure transducers, labelled “Transducer #1 and Transducer #2,” were placed in the system to measure the transient response 0.16 m from the valve and at the midpoint of the pipe. The layout for this test is shown in Figure 7-51.

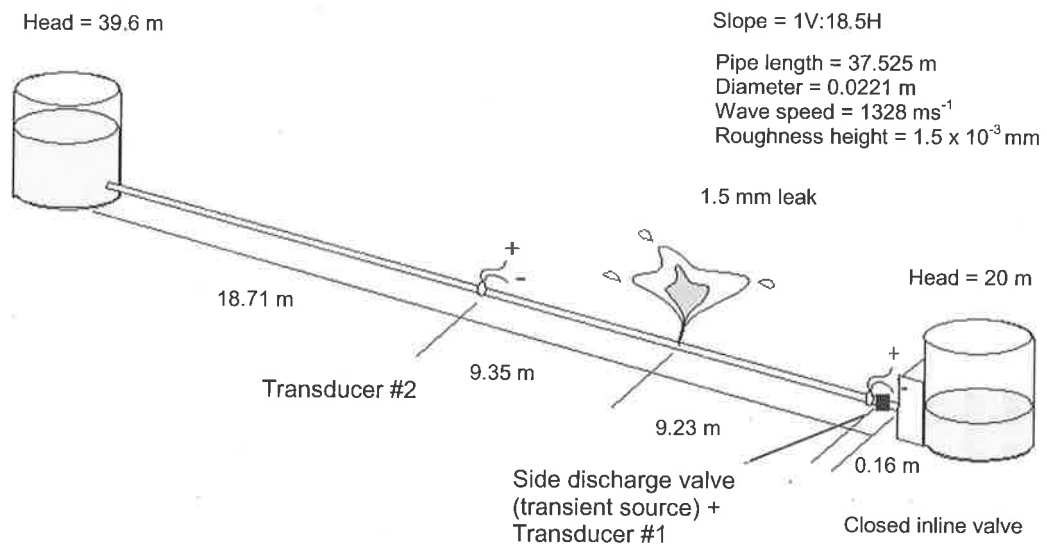


Figure 7-51 – System layout for the anti-symmetric test #1 using the improved TDR procedure.

The transient was generated by the pulse perturbation (close – open – close) of a side-discharge solenoid valve located 0.16 m upstream of the closed valve (same position as

transducer #1). The transient trace for the test measured using transducer #1 is shown in Figure 7-52. For the purpose of comparing the shapes of the reflected signals between the transient trace and the IRF, the leak reflection in the original transient trace in Figure 7-52 is circled. Using this measured head response as output, the IRF of the system is shown in Figure 7-53 with the leak reflection once again circled. Comparing the form of the reflections between the original signal and the IRF, the reflection is noticeably sharper in the case of the IRF.

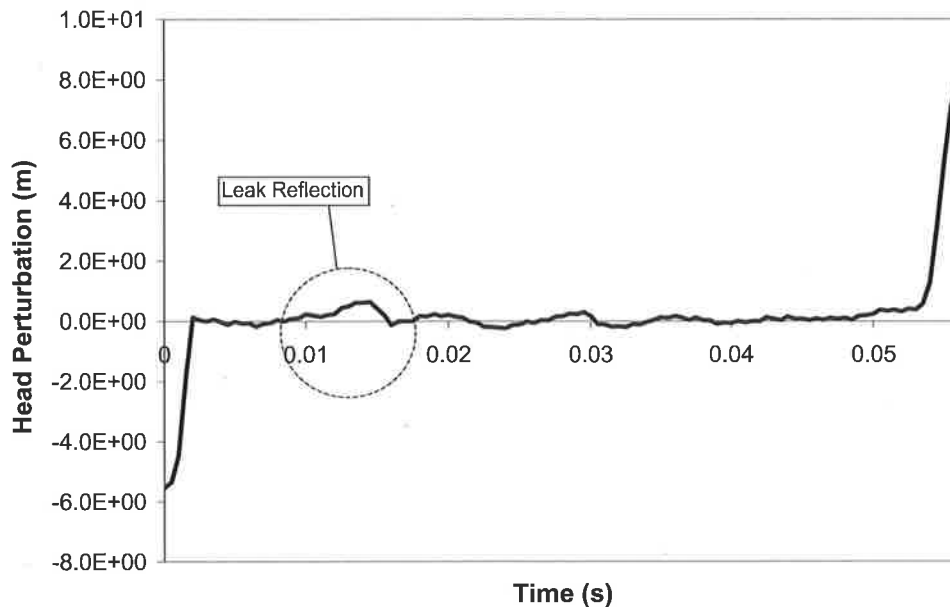


Figure 7-52 – Original transient trace for the anti-symmetric example for transducer #1 (Data file: C7-IL1.txt).

Applying the CUSUM change detection algorithm on the impulse response gives the results shown in Figure 7-54 where a non-zero value in the CUSUM alarm status indicates that the alarm has been triggered. For this leak position, the alarm was triggered at two places in the IRF, once at 0.014 s another at 0.0285 s. Substituting the arrival time of the first reflected signal into Table 7-1, the leak is located 9.29 m upstream of the measurement transducer #1 and corresponds well with the true leak location of 9.23 m. The cause of the second reflection is illustrated later in the thesis.

For comparison, the arrival time of the first leak reflection is estimated from the original transient signal (Figure 7-52). This arrival time was measured as the time lag from the start of the transient to the start of the reflected signal (see Figure 7-55) and also as the

time lag between the peak of the injected signal and the observed reflection (see Figure 7-56). In both cases, the estimated arrival time is 0.0145 s, placing the leak 9.63 m upstream of the transient source. This leak location is less accurate than the result from the IRF, which predicts 9.29 m with the true leak position 9.23 m upstream of the source. The accuracy is increased through the use of the IRF.

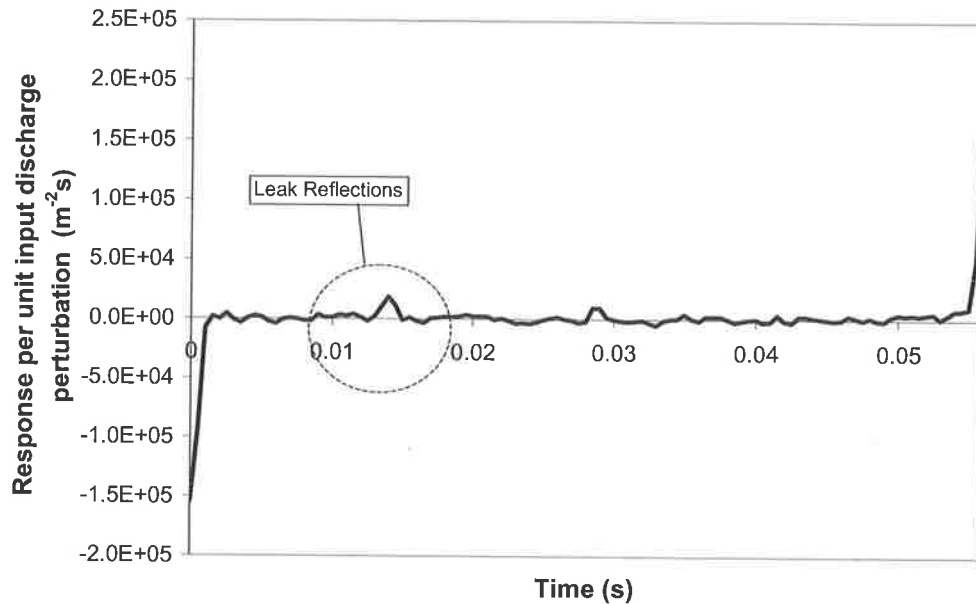


Figure 7-53 – Improvement of the reflection form using the IRF for transducer #1.

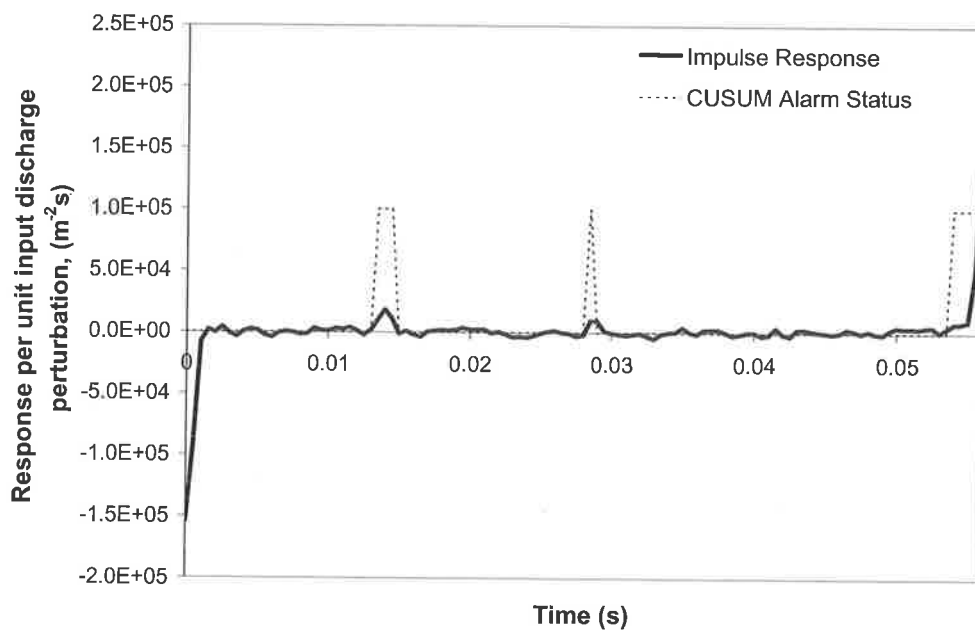


Figure 7-54 – CUSUM results of anti-symmetric example for transducer #1.

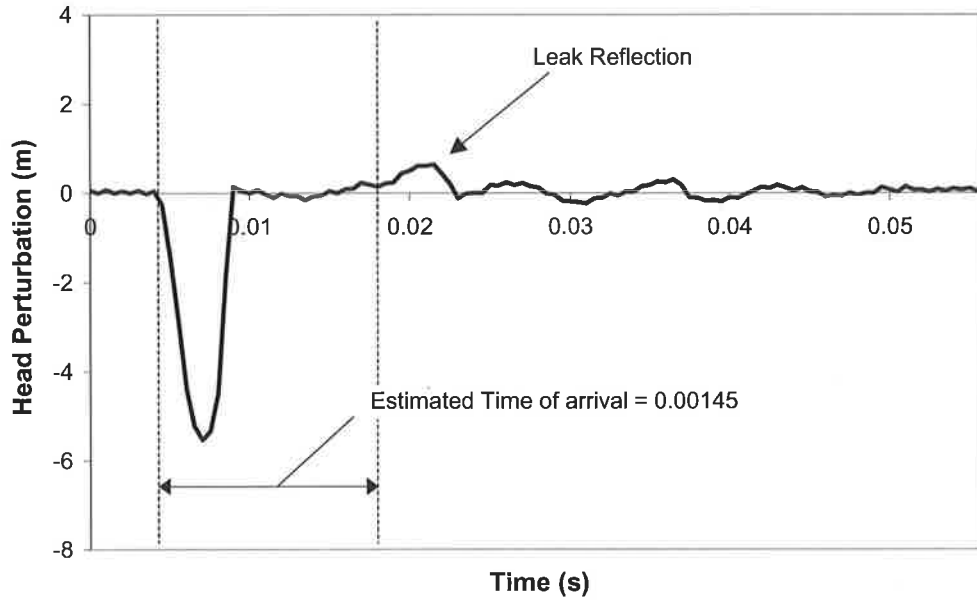


Figure 7-55 – Estimation of the arrival time from the transient trace from estimated start times of the signals for transducer #1.

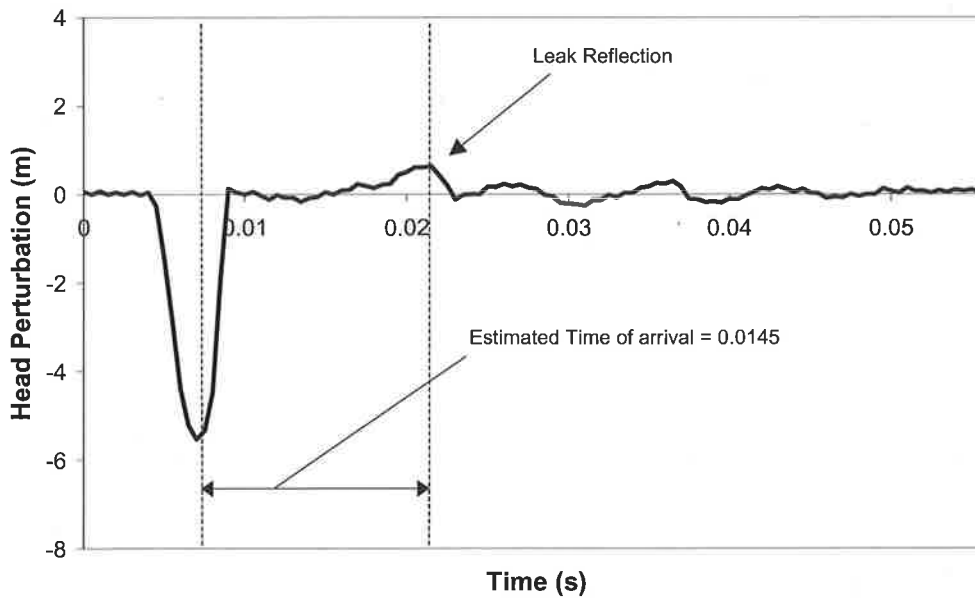


Figure 7-56 – Estimation of the arrival time from the transient trace from signal peaks for transducer #1.

The IRF from the same transient event measured at the midpoint of the pipeline (Transducer #2) is shown in Figure 7-57 along with the CUSUM results. The results show that a reflection is detected at $t = 0.014$ s from the first arrival of the main transient wave at transducer #2. Using Table 7-1, the leak is located either 9.29 m upstream of the transient source or 9.29 m upstream of transducer #2.

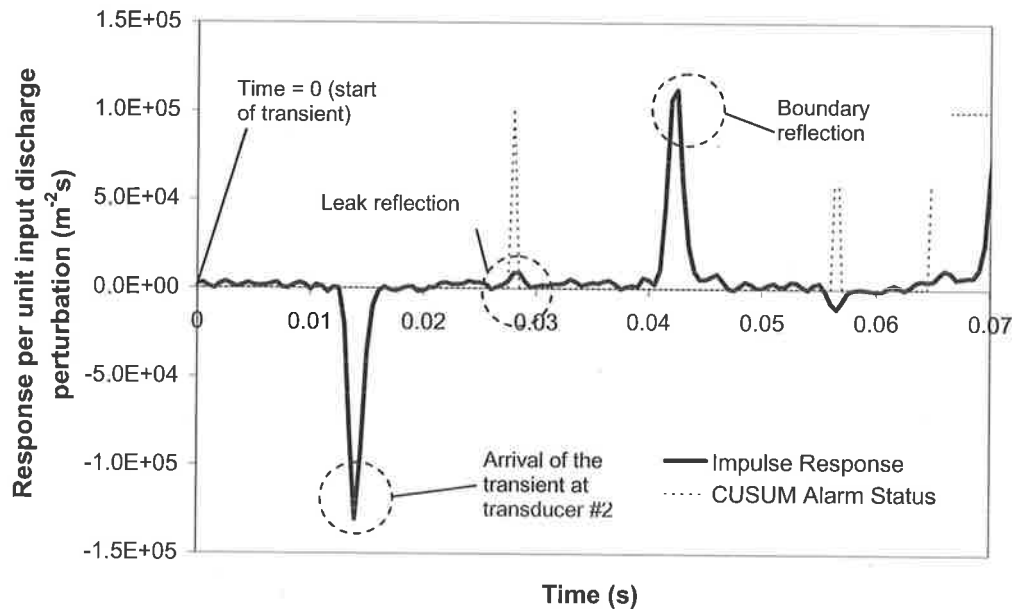


Figure 7-57 – IRF measured from transducer #2 in the anti-symmetric system (Data file: C7-IL1b.txt).

The first solution corresponds exactly with the predicted leak position from transducer #1, and corresponds well with the true solution of 9.23 m upstream of the transient source. Unlike the FRF, the form of the leak-induced modification on the IRF remains unchanged with different arrangements of the transient source and measurement station. In a second example, the same leak is positioned at the midpoint of the pipeline (18.71 m from the upstream boundary) and both the transient source and the measurement point are located at the closed in-line valve (refer to Figure 7-58).

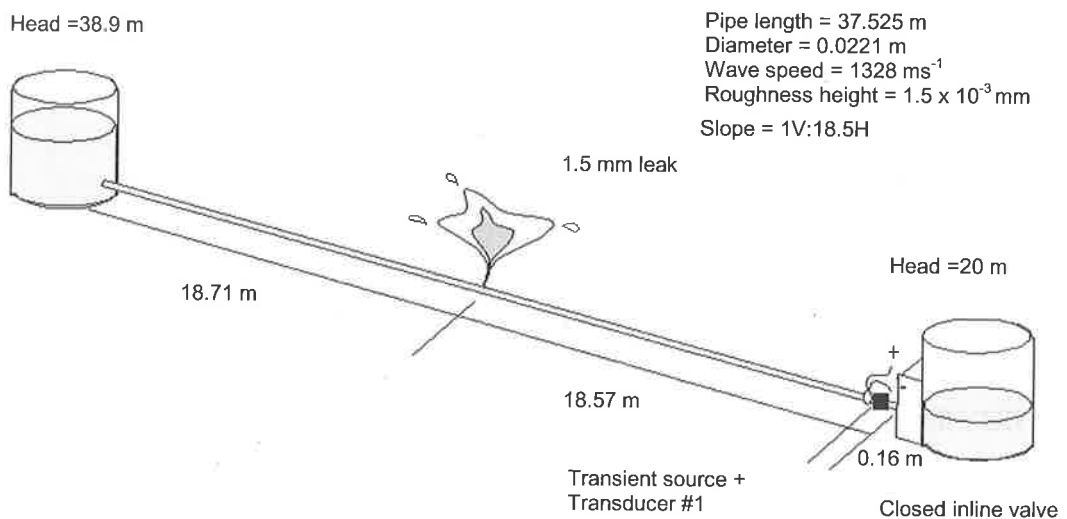


Figure 7-58 – Configuration of the second anti-symmetric example.

The IRF from this case is shown in Figure 7-59 along with the CUSUM results. From Figure 7-59, a reflection is detected 0.028 s from the start of the transient, placing the leak 18.59 m upstream of the transient source, which agrees with the true position of 18.58 m.

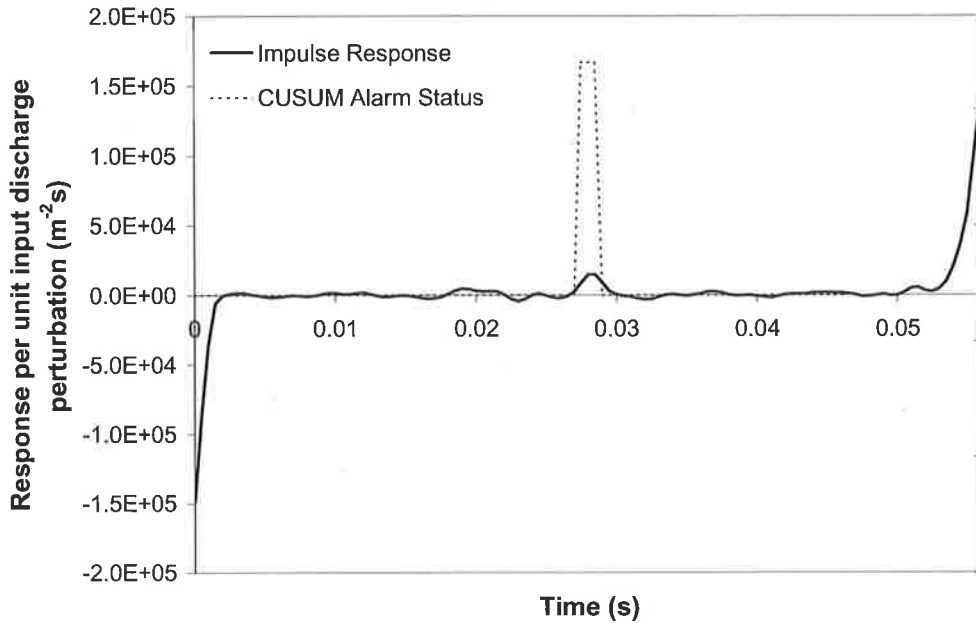


Figure 7-59 – CUSUM result for 1.5mm leak at the mid point of a pipe with anti-symmetric boundaries (Data file: C7-IL2.txt).

7.7.2 Symmetric boundary conditions

The procedure is now repeated under a symmetric boundary condition where the downstream valve of the pipeline is fully opened with boundary heads of 39.6 and 39.0 m, resulting in a flow with velocity of 0.5 ms^{-1} and Reynolds number of 11,000. The transient source and the measurement points were positioned at the centre of the pipeline (18.82 m from upstream boundary) with a 1.5 mm diameter leak ($C_d A_L / A = 4.17 \times 10^{-3}$) 6.695 m from the upstream reservoir, or 12.01 m upstream of the transient source. The configuration of the system is shown in Figure 7-60. The IRF of this situation is shown in Figure 7-61 along with the CUSUM results.

In a second example the leak was moved to a position 9.35 m downstream from the transient source (refer to Figure 7-62). The IRF and the CUSUM results, Figure 7-63,

indicate that the arrival time of the first leak-reflected signal is 0.0145 s, putting it 9.63 m away (both upstream and downstream) from the transient source [using Eq.(7.5)]. The solution corresponds well with the true location of 9.35 m downstream from the source.

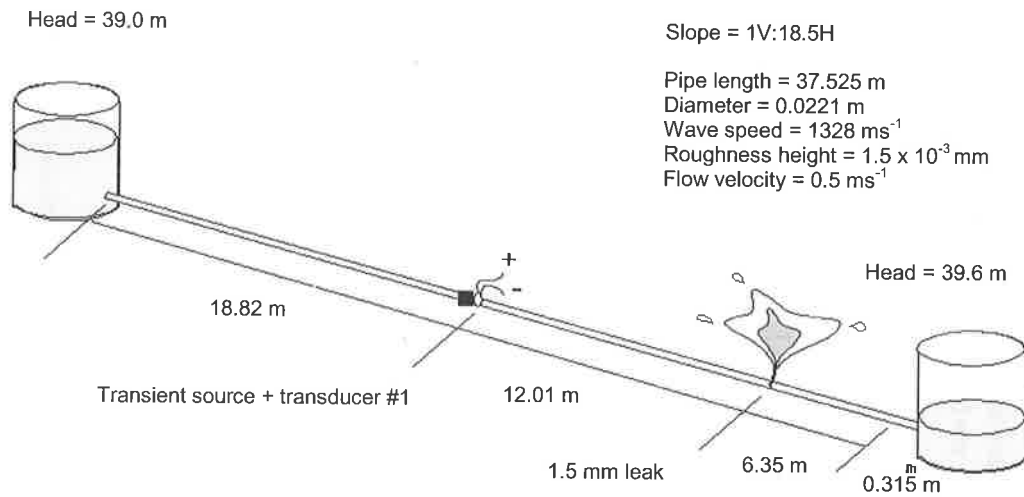


Figure 7-60 – Configuration of the first symmetric test example.

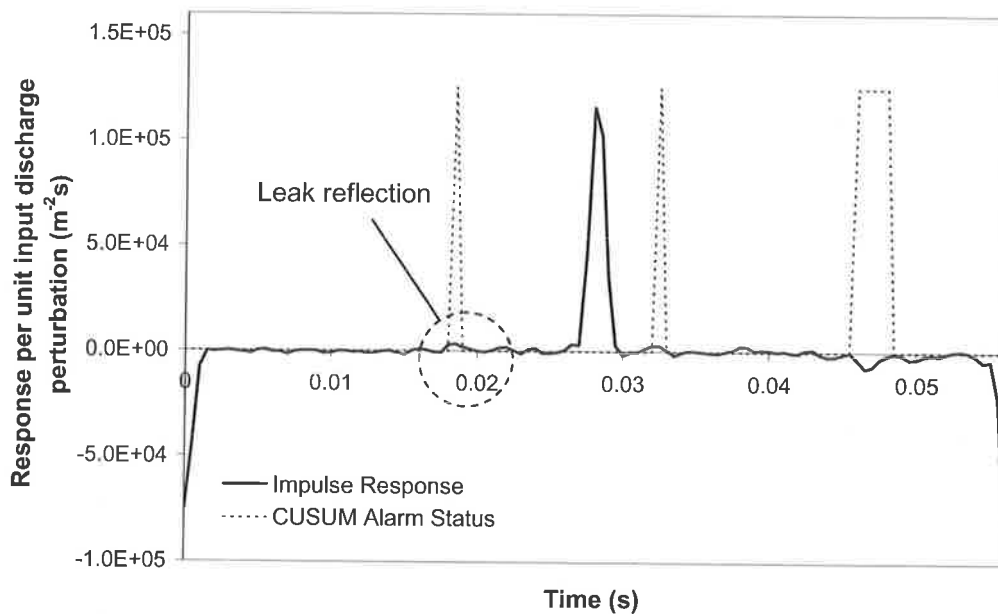
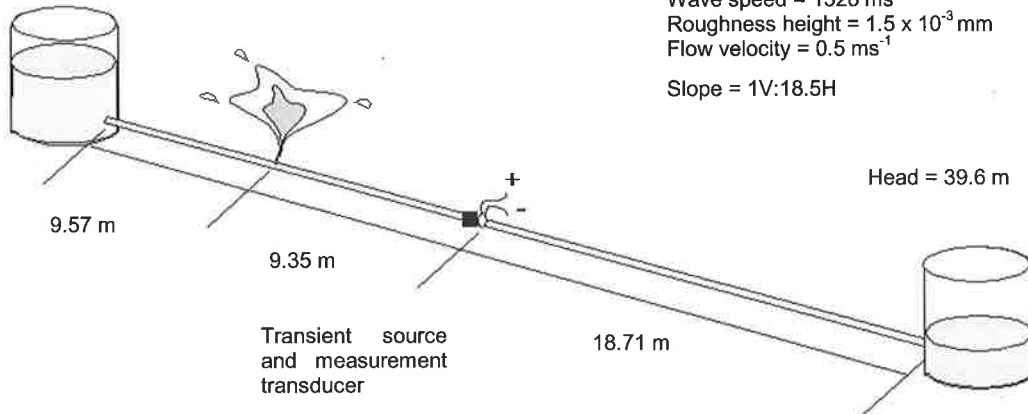


Figure 7-61 – Symmetric test example 1 (Data file: C7-IL3.txt).

This study shows that the IRF is able to locate a leak with an error of 0.05 % - 0.7 % of the pipe length without the use of a leak-free benchmark. The TDR procedure can detect leaks located at all positions in the pipeline, unlike the leak detection procedure in the frequency domain where leaks at the quarter points are not detectable.

Head = 39.0 m



Pipe length = 37.525 m
Diameter = 0.0221 m
Wave speed = 1328 ms⁻¹
Roughness height = 1.5 x 10⁻³ mm
Flow velocity = 0.5 ms⁻¹
Slope = 1V:18.5H

Figure 7-62 – Configuration of the second symmetric test.

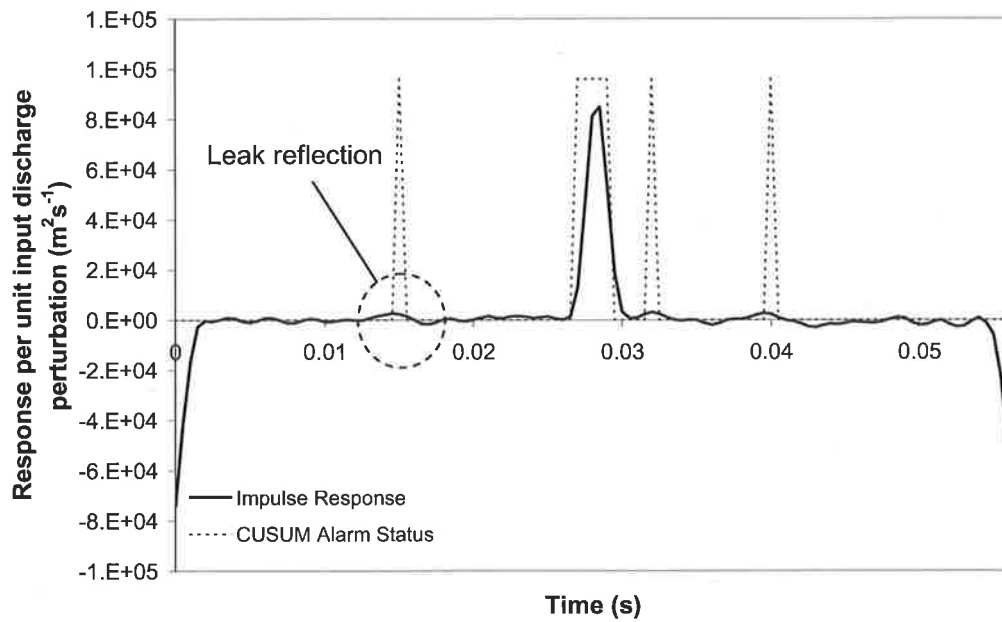


Figure 7-63 – Results of the second symmetric test (Data file: C7-IL4.txt).

7.8 IMPROVEMENTS TO THE APPLICABILITY OF IRF

This section presents two possible extensions to the proposed IRF leak detection procedure to generalise the scope of its application.

7.8.1 Extension to discrete blockage detection

The leak detection procedure described in this section is based on detection of fault-reflected signals. This procedure can be adapted to other types of faults, given that their presence results in partial reflections of the original transient signal, using Table 7-1 for fault location.

A discrete blockage can be modelled with the orifice equation. It generates reflected signals in the transient trace in much the same way as a leak (Liou 1998, Vítkovský *et al.* 2003a). Harding (1974) proposed that the nature of the reflection from any object in the system is dependent upon its impedance. A low impedance element (a leak) generates reflections that are reversed in sign to the original signal, whereas a high impedance element (a block) results in reflections of the same sign as the incident wave.

The effect of a blockage on the IRF is compared to that of a leak in Figure 7-64. The transient is generated by closure of the downstream in-line valve. A leak of size $C_d A_L = 1.4 \times 10^{-4} \text{ m}^2$ ($C_d A_L / A = 1.98 \times 10^{-3}$) is placed 1250 m upstream from the valve along with a block of impedance $Z_B = 141.4 \text{ m}^{-2} \text{ s}$ 625 m upstream of the valve. The configuration of the system is shown in Figure 7-65.

The two-sided CUSUM algorithm can detect both positive and negative changes in the IRF and the same TDR procedure can locate these blockages. As the sign of these deviations are different between a leak and a block, the nature of the problem can be ascertained from the direction of the deviation. Additional details of this approach can be found in Vítkovský *et al.* (2003a). The IRF is different than the FRF in that reflections from a blockage cannot be confused with a leak reflection from another position in the pipeline (refer to Section 6.13). This result highlights one of the advantages for detecting

faults using the IRF in the time domain compared to using the FRF in the frequency domain.

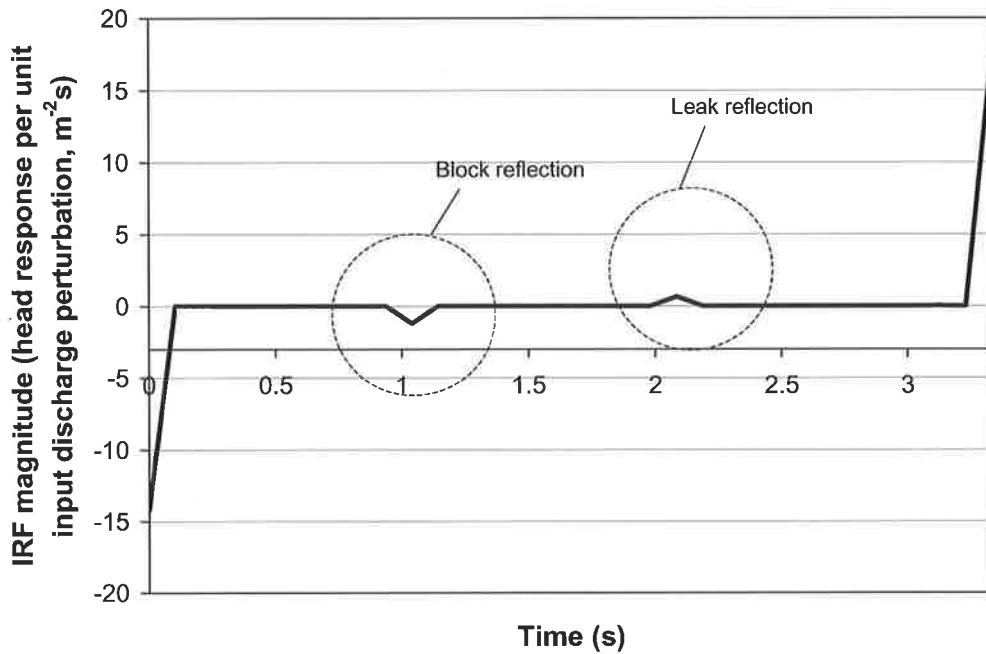


Figure 7-64 – Impulse response function comparing the reflection from a leak and from a discrete blockage.

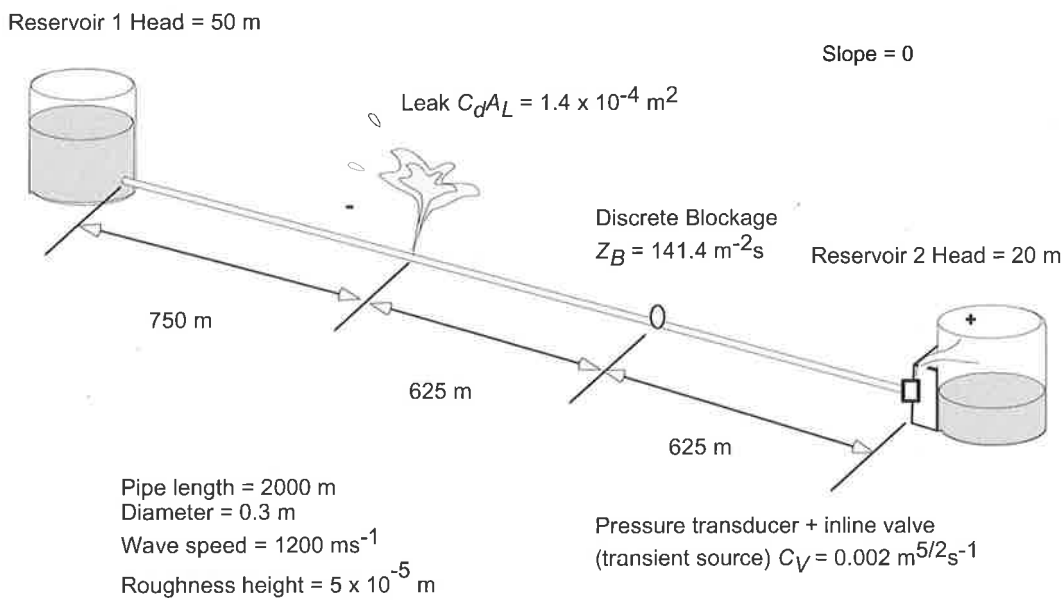


Figure 7-65 – System configuration for results shown in Vítkovský *et al.* (2003a).

7.8.2 Detection of multiple faults

The previously described procedure for a single leak using the FRF can be extended to detection of multiple leaks. Given that each individual element with a different impedance generates a discrete reflection in the transient trace (Harding, 1974), the presence of multiple leaks can be approached in the same manner as the detection of a single leak. Figure 7-66 illustrates the situation where three leaks result in the arrival of three distinct reflections at the measurement station. The arrival time of each of these reflections can be used in the TDR procedure to determine the location of each of the faults.

The application of the TDR procedure for detecting multiple leaks is illustrated for the experimental configuration in Figure 7-67. The system is arranged anti-symmetrically with two leaks, both of orifice diameters of 1.5 mm ($C_d A_L / A = 4.17 \times 10^{-3}$), located 9.23 m and 30.59 m upstream of the transient source. The transient event was generated by the pulse perturbation of the side-discharge valve. The resultant transient trace is shown in Figure 7-68 and the extracted IRF is in Figure 7-69 along with the CUSUM detection results. The IRF indicates that two distinct reflections from the system exist in the signal, one at 0.014 s and the other at 0.0465 s. These times correspond to leaks 9.29 m and 30.87 m upstream of the transient source. The results are good estimates of the true positions of 9.23 m and 30.59 m with errors of 0.16 % and 0.7 % of the pipeline length.

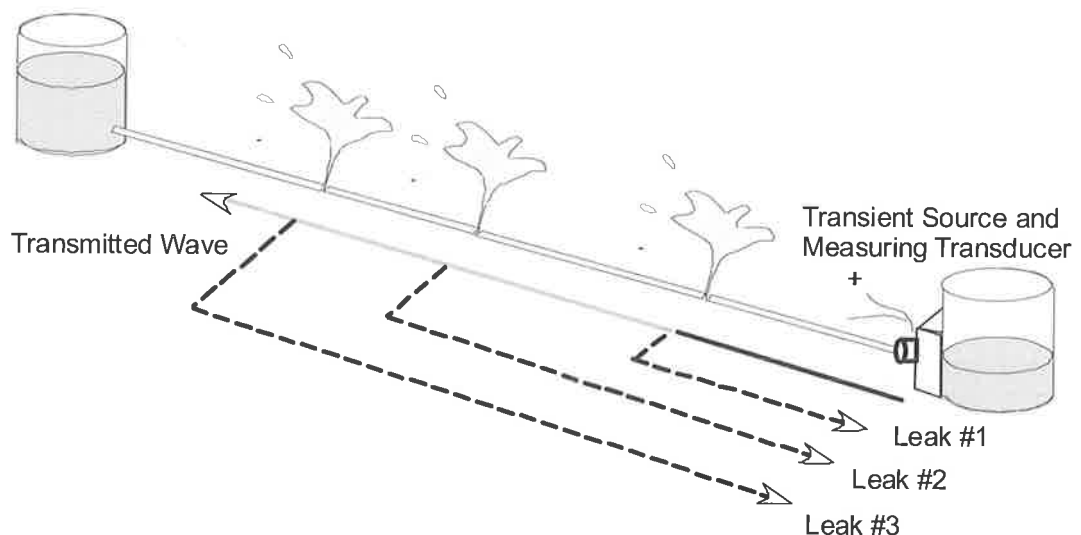


Figure 7-66 – Multiple leak detection in an anti-symmetric system.

Reservoir 1 Head = 40.3 m

Slope = 1V:18.5H

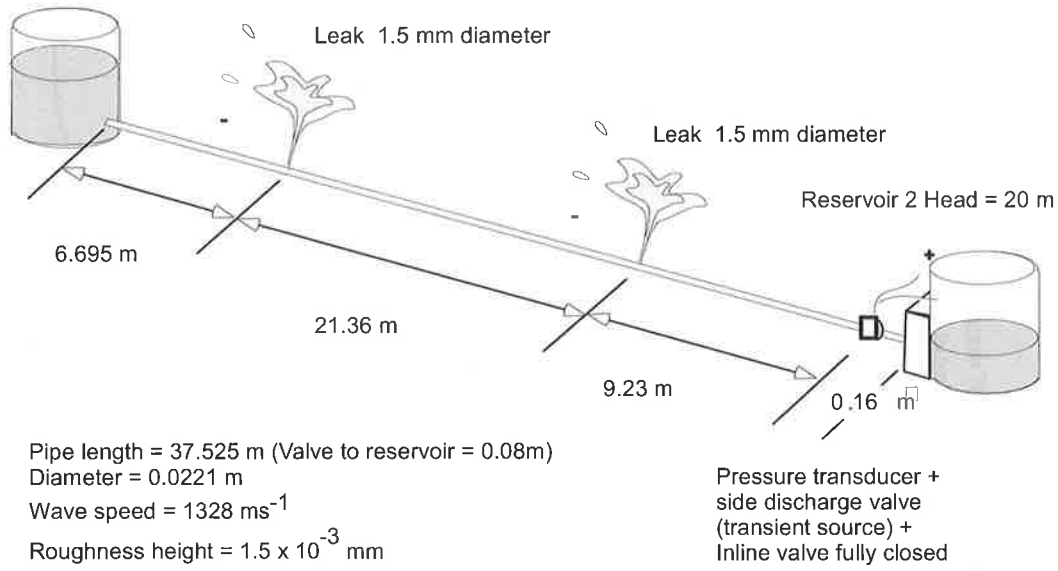


Figure 7-67 – System configuration for experimental multiple leak detection.

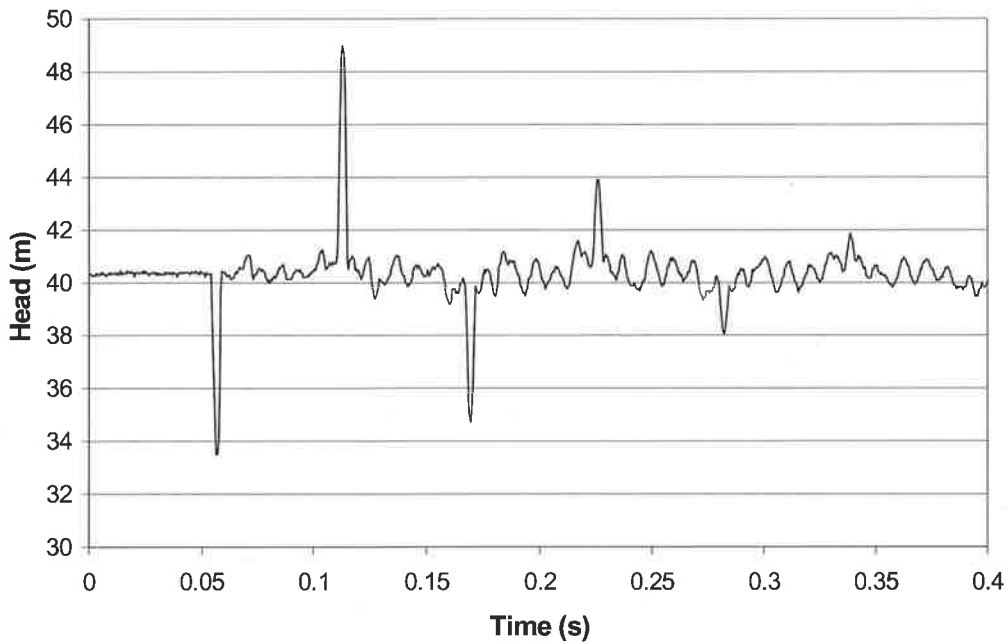


Figure 7-68 – Original transient signal for the multiple leak case shown in Figure 7-67 (Data file: C6-L8.txt).

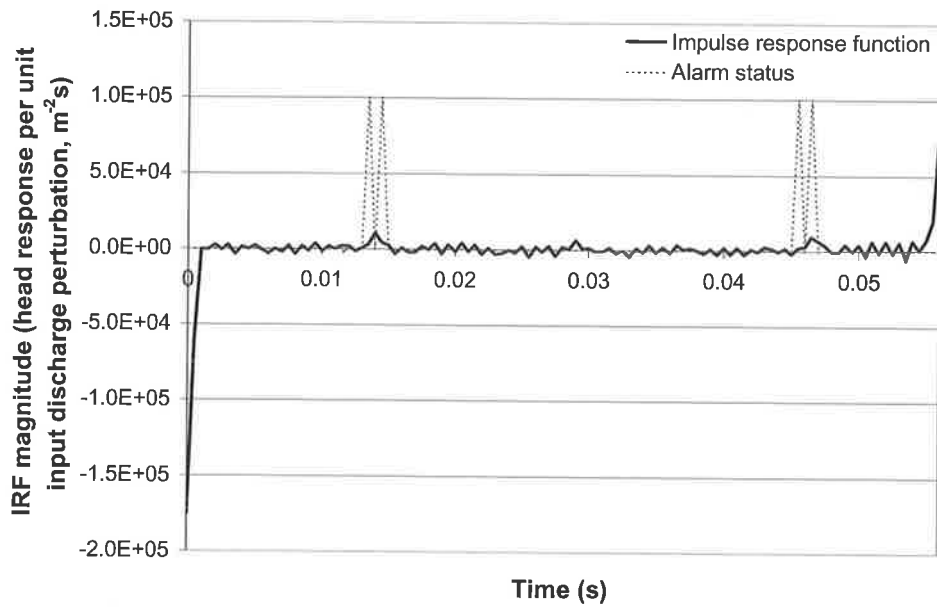


Figure 7-69 – Leak detection using the IRF for system shown in Figure 7-67.

Presence of higher order reflections

The previous example illustrates how every detected reflection in the IRF can be used to determine an associated leak position. However, repeated reflections from the same leak lead to complications. The formation of these higher order reflections are illustrated in Figure 7-70 where the original leak reflection passes through the leak again, thus generating an additional reflection.

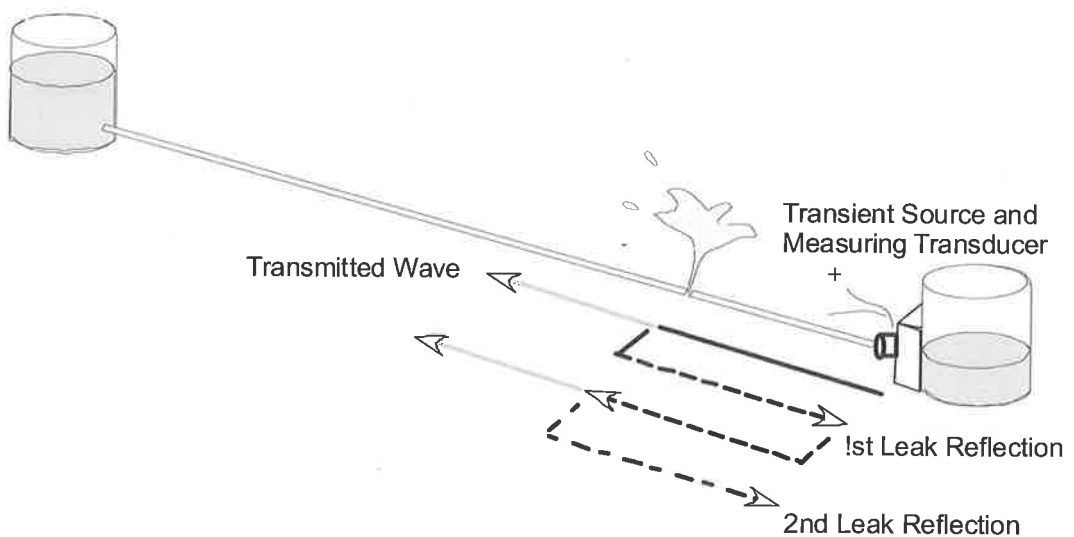


Figure 7-70 – Diagram showing higher order reflections from the leak.

Each detected disturbance occurring *after* detection of the first can be either (1) a higher order reflection from the same leak or (2) a primary reflection from a different leak. To illustrate, the experimental result shown in Figure 7-54 is repeated here as Figure 7-71. The system configuration, shown in Figure 7-72, consists of a pressure transducer and a transient source (side-discharge valve) located adjacent to the closed in-line valve. A single leak of 1.5 mm diameter ($C_d A_L/A = 4.17 \times 10^{-3}$) is located 9.23 meters upstream of the transducer. Two reflections, measured at transducer #1, are detected in the resultant IRF. The first reflection correctly indicates a leak 9.29 m upstream of the transducer and the second indicates another leak at 18.58 m. As only one leak exists in the system, the second reflection is a higher order reflection from the leak, generated when the original leak-reflected signal travelled through the leak again (refer to Figure 7-70).

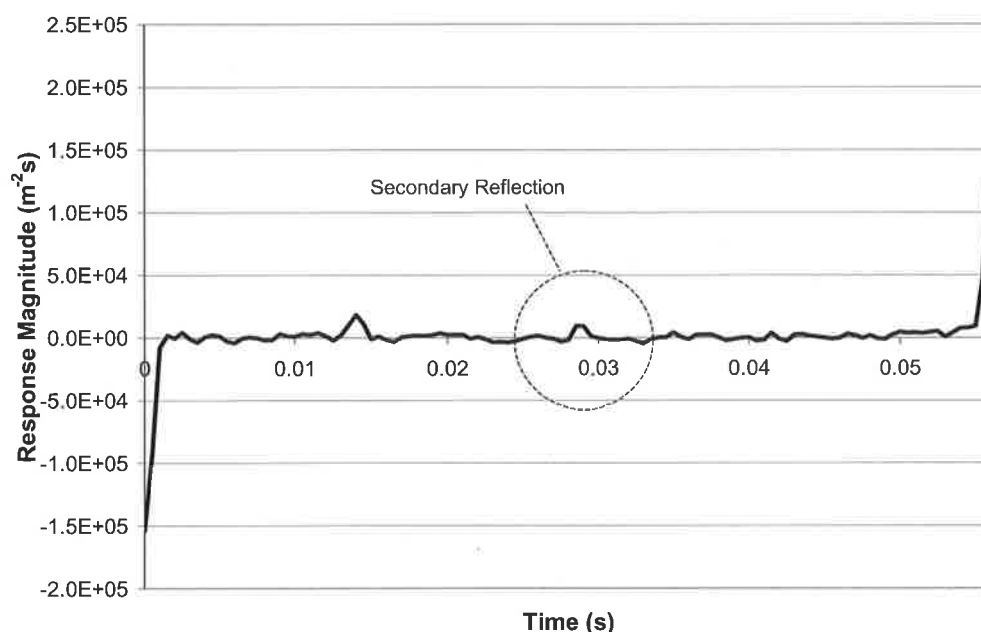


Figure 7-71 – Expanded impulse response for the first $2L/a$ seconds for transducer #1 system shown in Figure 7-72.

The higher order reflection from the leak is of a similar form to a true leak reflection at the same position and poses a potential problem for the detection of multiple leaks using the TDR method. This problem can be overcome in the anti-symmetric pipeline shown in Figure 7-70 by ensuring that each detected leak reflection in the IRF does not have an arrival time that is an integer multiple of the arrival time of an earlier reflected signal. For example, the reflection predicting a leak 18.58 m upstream of the source is an integer

multiple of a lower leak position of 9.29 m. Given that it is unlikely for two leaks to be located at such regular spacing, the reflection pointing to a leak 18.58 m upstream of the source can be assumed to be a higher order reflection and is ignored.

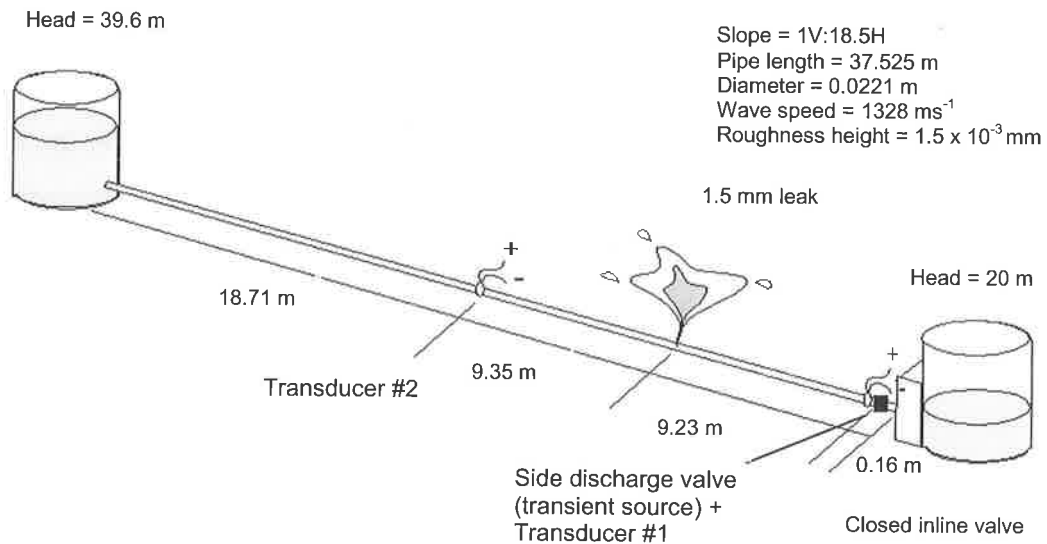


Figure 7-72 – System layout for the illustration of the effect of higher order reflections.

7.8.3 IRF for the application of complex signals

This chapter illustrates how the IRF can be used to refine the raw transient trace such that leak-reflected signals in a pipeline can be better identified. Although this approach may appear intuitive for simple signals such as single pulses and steps, its value becomes more evident when complex signals are injected into the system. In Chapter 5, a continuous transient was injected into a pipeline as an alternative to a single discrete signal. The advantage of this approach is that the energy of the signal is spread over a longer time and the amplitude of the injected transient can be small while retaining the same amount of information in the measured response. From experimental tests presented in Chapter 5, a pseudo-random binary sequence contains the same information as a discrete signal that is 7 times its amplitude. This type of signal may be necessary in situations where the amplitude of the induced transient is of concern. To illustrate the application of the IRF in this situation, consider the following numerical example.

A transient is generated by perturbing (close – open – close) a downstream in-line valve in the simulation pipeline in which a leak of $C_d A_L = 1.4 \times 10^{-4} \text{ m}^2$ ($C_d A_L/A = 1.98 \times 10^{-3}$) is located 1400 m from the upstream boundary. The layout of the system is shown in Figure 7-73. The transient data are generated using the method of characteristics model with a computational time step of 0.167 seconds (100 reaches). The resultant input (valve tau fluctuation) and the output (measured head response) are given in Figure 7-74. From the measured transient trace, the form of the signal is complex and the detection of a leak reflection using this raw transient data without an accurate leak-free benchmark is not possible. In comparison, the IRF extracted from this transient event is shown in Figure 7-75. From the IRF, the position of the leak-reflected signal is evident and is circled. In cases where complex signals are used, the IRF simplifies the data such that the leak reflections can be determined. The refinement of the extracted information using a complex signals can only be carried out using the procedures presented in this dissertation.

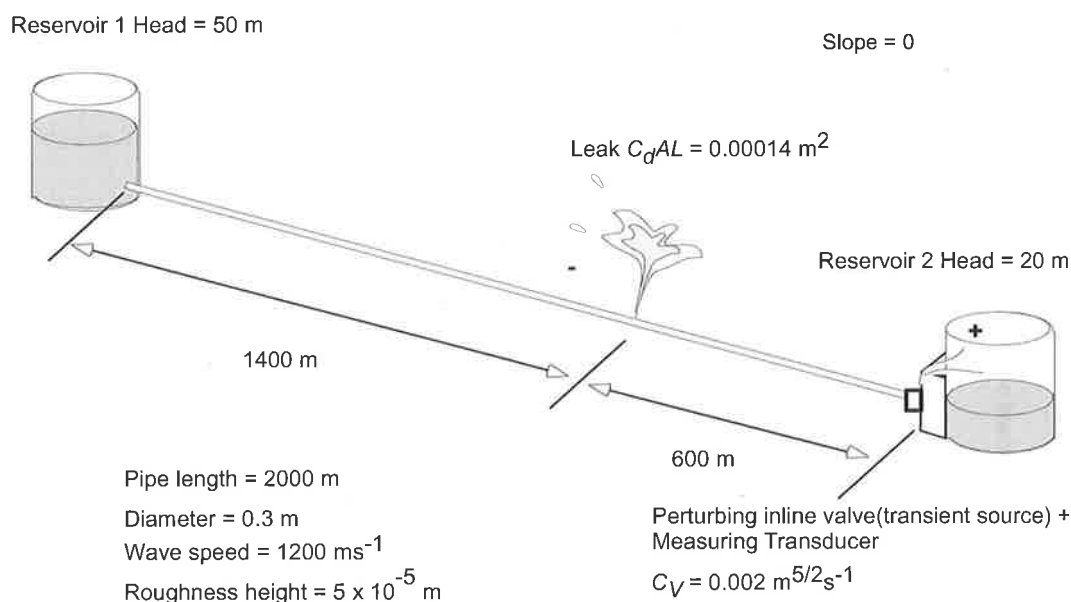


Figure 7-73 – Numerical simulation of PRBS analysis using IRF.

7.8.4 Application in a complex system

The same reflectometry procedure can be applied in a complex system consisting of pipes of different properties. The leak-induced modification in a complex system is identical to that in a simple pipeline where the arrival time of any reflected signal provides an indication of the distance the wave has travelled since the start of the transient.

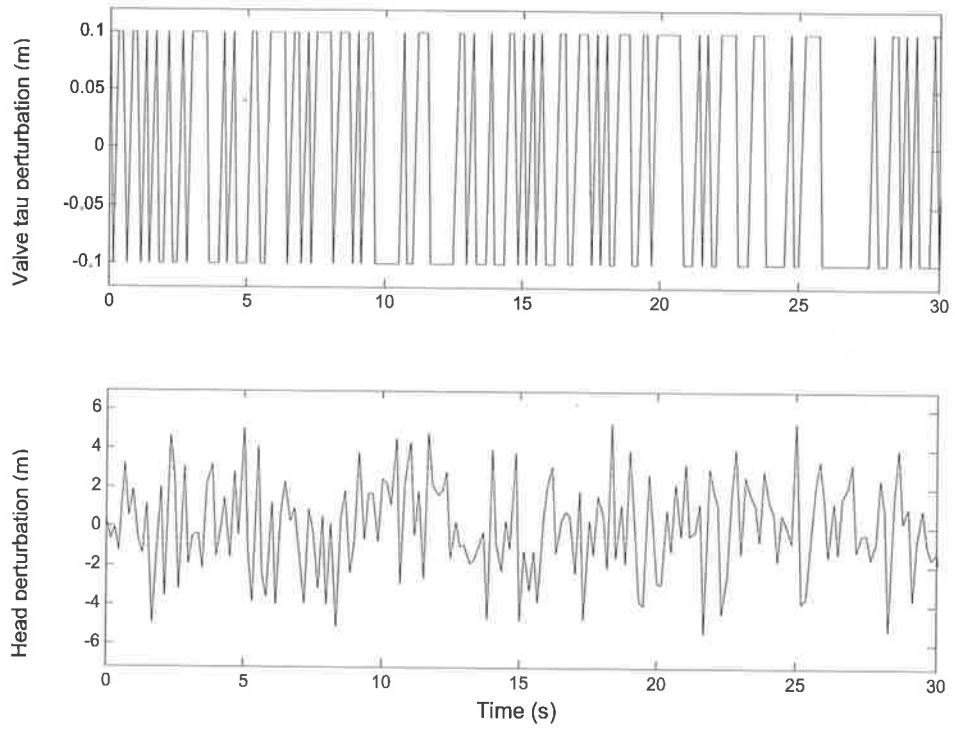


Figure 7-74 – Input and output sequences for PRBS signal.

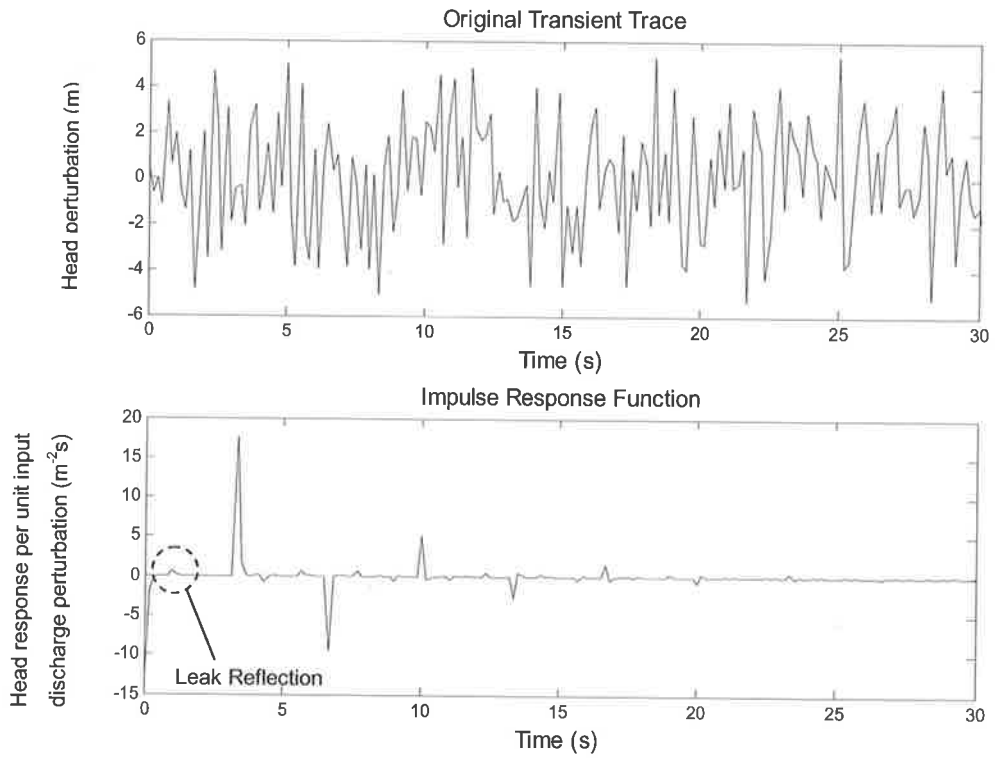


Figure 7-75 – Comparison between raw transient trace and IRF.

7.9 CONCLUSIONS

This chapter presents the conventional time-domain reflectometry (TDR) for leak detection in a pipeline and presents two modifications to the TDR procedure that allow leaks to be detected and located automatically regardless of system configuration. The shortfalls of this technique, including a reliance on a leak-free benchmark of the system and inaccuracies in the estimation of the true arrival time of the leak-reflected signals, are presented.

These shortfalls are overcome by using the impulse response function in place of the original transient trace for this procedure. The process of impulse response extraction allows the shape of the original signal to be refined such that each reflection from the system is converted into the form of a sharp pulse, allowing accurate determination of the reflection arrival time. In addition, the form of the system response function is independent of the nature of the injected signal, thus removing the necessity of a leak-free benchmark.

The improved TDR procedure using the impulse response function was validated experimentally, illustrating that it can locate leaks in the experimental pipeline to a greater accuracy than use of the original signal. The technique can be applied to multiple leaks and the detection of discrete blockages.

The main conclusions from this chapter can be summarised in the following points:

1. Given its ability to analyse complex injected signals, refinement of system reflections and its independence to the shape of the injected signal, the *impulse response function* should be used in place of the original transient for existing time-domain reflectometry methods of leak detection.
2. The impulse response function, unlike the frequency response function, clearly distinguishes leak reflections from blockage reflections and should be used in situations where a number of different faults exist in the system. The nature of the leak-induced modification on the IRF (i.e. a reflection) is the same for all arrangements of the transient source and measurement station; hence, multiple

measurement stations can be used to increase confidence in the leak detection procedure.

The previous two chapters illustrate the application of the system response functions in the time and frequency domains for the detection of leaks in the pipeline. These two procedures were validated experimentally. The next chapter conducts a comparison between the procedures and determines the technique best suited for detecting faults in pipelines.

CHAPTER 8

COMPARISON BETWEEN TIME- AND FREQUENCY-DOMAIN LEAK DETECTION

8.1 INTRODUCTION

Chapter 6 and Chapter 7 illustrate two different leak detection procedures, one in the frequency domain and the other in the time domain. Both techniques were experimentally tested and can detect leaks under laboratory conditions. In the frequency domain, a leak in a pipeline causes the peaks of the frequency response function to oscillate periodically. The frequency and phase of the oscillatory pattern are used to predict the position of the problem through a series of derived analytical expressions. In the time domain, a leak is located through the arrival time of the leak-reflected signal in the impulse response function. A common feature of both techniques is that they do not require the use of a numerical model or an existing leak-free benchmark for comparison. All injected transient signals in the pipeline produce the same response function given that the physical nature of the system remains unchanged and the input signal is chosen to avoid system nonlinearities (refer to Section 5.2.1). For an intact pipeline, the shape of the response function is initially known. For example, the frequency response function for an intact pipe contains peaks that attenuate smoothly with frequency, whereas the impulse response function contains spikes that correspond only to boundary reflections from the system. Any significant deviations from these known forms indicate problems in the pipe. This chapter directly compares the two leak detection procedures and determines when each approach is most appropriate. The relationship between the two different leak-induced modifications, one in the frequency and the other in the time domain, is investigated first.

8.2 RELATIONSHIP OF LEAK-INDUCED MODIFICATION ON THE FRF AND THE IRF

Both the frequency response function (FRF – frequency domain) and the impulse response function (IRF – time domain) operate on the information derived from the measured transient response of the system. For this reason, leak-induced modifications in the system response functions must stem from certain behaviour in the raw transient trace. From Chapter 2, the effects of a leak on the transient trace are:

- A leak creates reflections in the transient trace.
- A leak induces additional damping on the transient data.

To determine the cause of the leak-induced damping pattern in the frequency domain, consider the following numerical example. A transient event was generated in the simulation pipeline with the boundaries arranged anti-symmetrically. The transient was generated by a side-discharge valve located adjacent to an opened in-line valve and a leak—size $C_d A_L = 1.4 \times 10^{-4} \text{ m}^2$ ($C_d A_L / A = 1.98 \times 10^{-3}$)—is placed 1400 m from the upstream boundary (refer to Figure 8-1). The closed side discharge valve was fully opened and closed again in 8.33 ms (refer to Figure 8-2 producing the transient trace in Figure 8-3). The simulation was carried out using the method of characteristics with a discretisation of 400 and a computational time step of 4.17 ms. The leak-induced reflections in the signal, along with the increased damping of the transient as a result of the leak are identified in the transient trace. The corresponding FRF of this situation is shown in Figure 8-4. To determine which of the two leak-induced effects (reflections and damping) resulted in the formation of the oscillation pattern in the FRF peaks, the leak reflections in the transient trace are removed by replacing each reflection with the steady state (initial) head value. The resultant transient trace with only the leak-induced damping in the signal is shown in Figure 8-5. The FRF for this situation is in Figure 8-6.

The FRF shows that when the leak reflections are removed from the original transient trace, the leak-induced oscillations in the peaks of the FRF are no longer present, although the damping effect of the leak still exists. This result indicates that leak-induced oscillations in the FRF peaks are a result of the leak-reflected signals in the original

transient trace. As the procedure in the time domain using the impulse response function also operates on the location and the presence of these leak-reflected signals, both the time and frequency-domain techniques for leak detection in the pipeline are linked to the detection of fault reflections in the original transient trace.

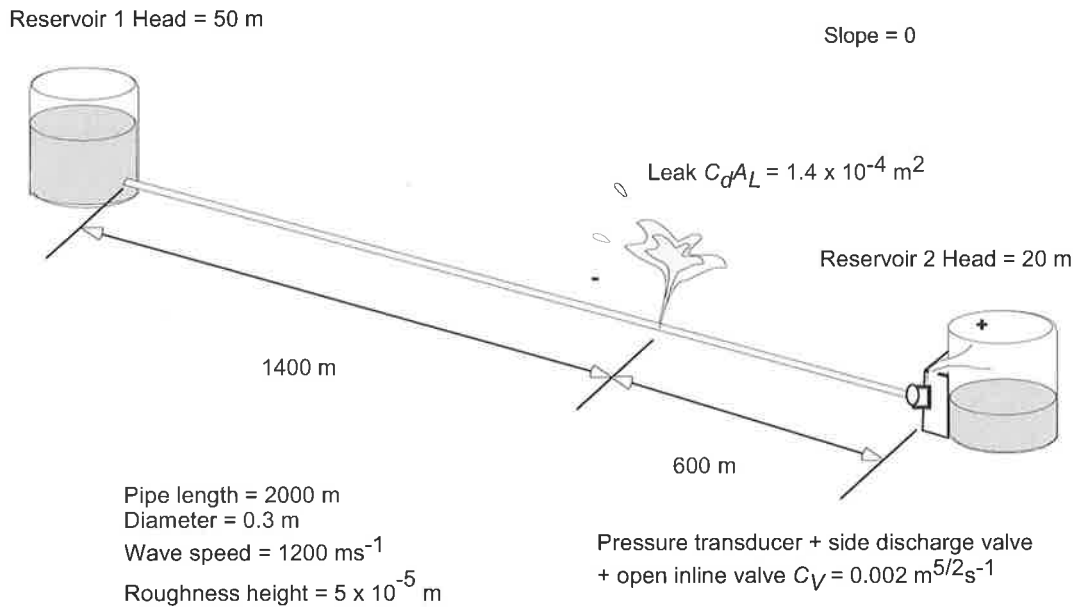


Figure 8-1 – System configuration for investigation.

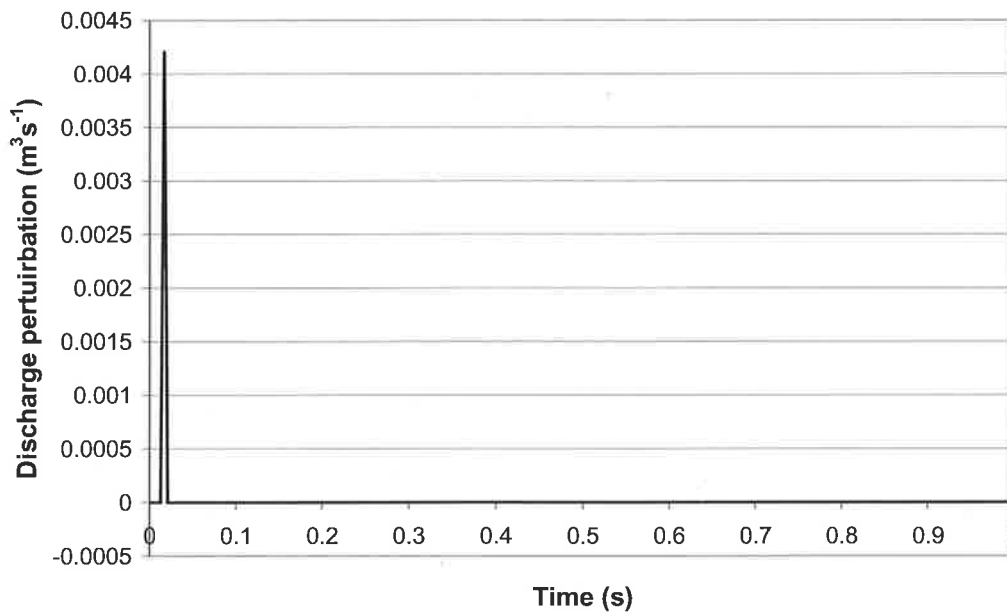


Figure 8-2 – Input discharge perturbation at the side-discharge valve.

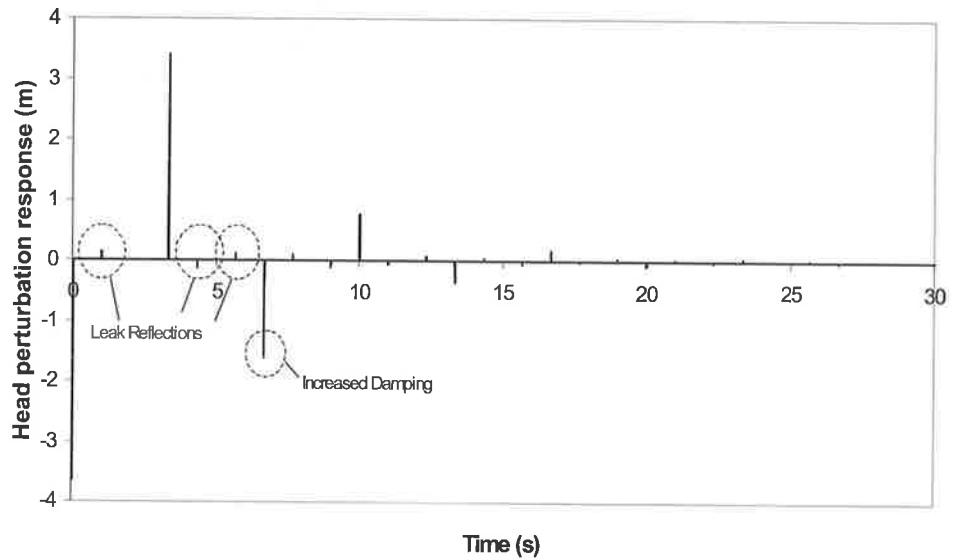


Figure 8-3 – Transient response from the leaking pipeline measured upstream of the in-line valve.

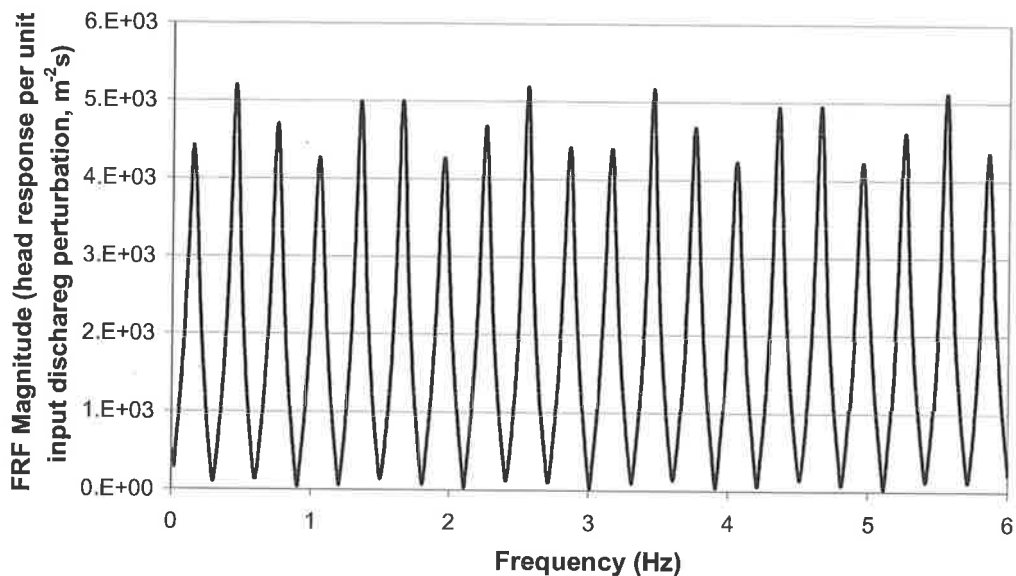


Figure 8-4 – FRF of the transient event.

The FRF shows that when the leak reflections are removed from the original transient trace, the leak-induced oscillations in the peaks of the FRF are no longer present, although the damping effect of the leak still exists. This result indicates that leak-induced oscillations in the FRF peaks are a result of the leak-reflected signals in the original transient trace. As the procedure in the time domain using the impulse response function also operates on the location and the presence of these leak-reflected signals, both the time

and frequency-domain techniques for leak detection in the pipeline are linked to the detection of fault reflections in the original transient trace.

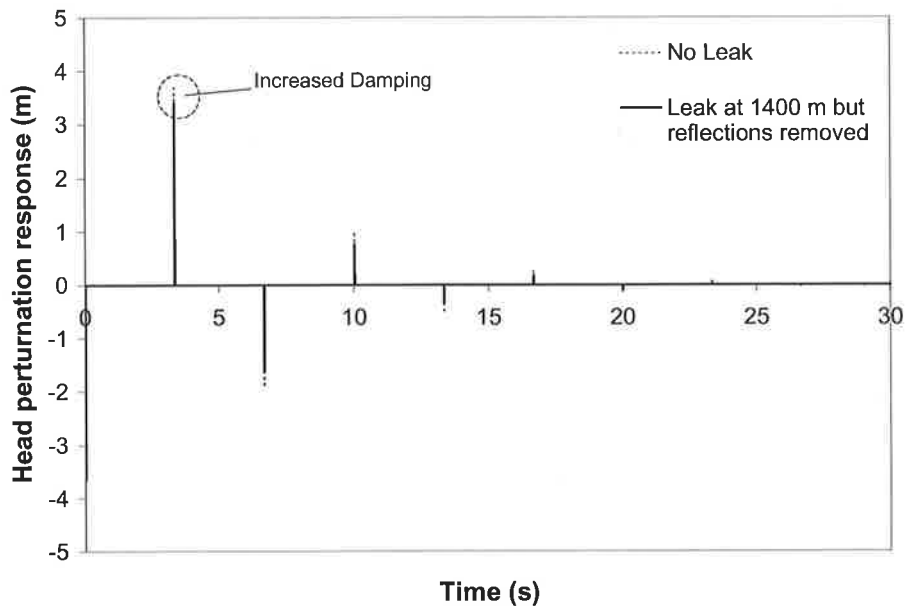


Figure 8-5 – Modified transient response with leak reflections removed.

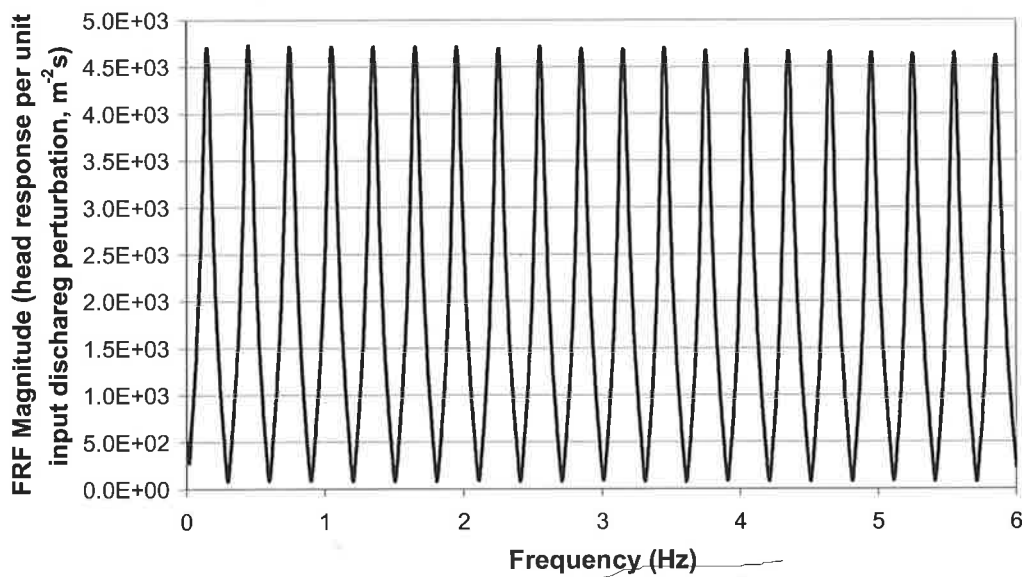


Figure 8-6 – FRF of transient trace with leak reflections removed.

There is a difference, however, in the way this reflection information is used in the procedures. The IRF procedure (time domain) operates on the detection of those leak reflections in the initial sections of the transient trace ($0 < t < 2L/a$). Any detectable

discrepancy from zero is noted as a reflection and the arrival time of the reflection gives the position of the leak. Consider an example where the same transient event in Figure 8-3 is modified so that the first reflection from the leak is removed (by replacing the reflection in $0 < t < 2L/a$ with the steady state head value), but the subsequent reflections are unchanged (Figure 8-7). The resultant IRF of the system is shown in Figure 8-8. Due to the speed of the injected transient pulse (8.33×10^{-3} s) in respect to the fundamental frequency of the system (6.67 s), the IRF is of a similar form to the modified transient signal.

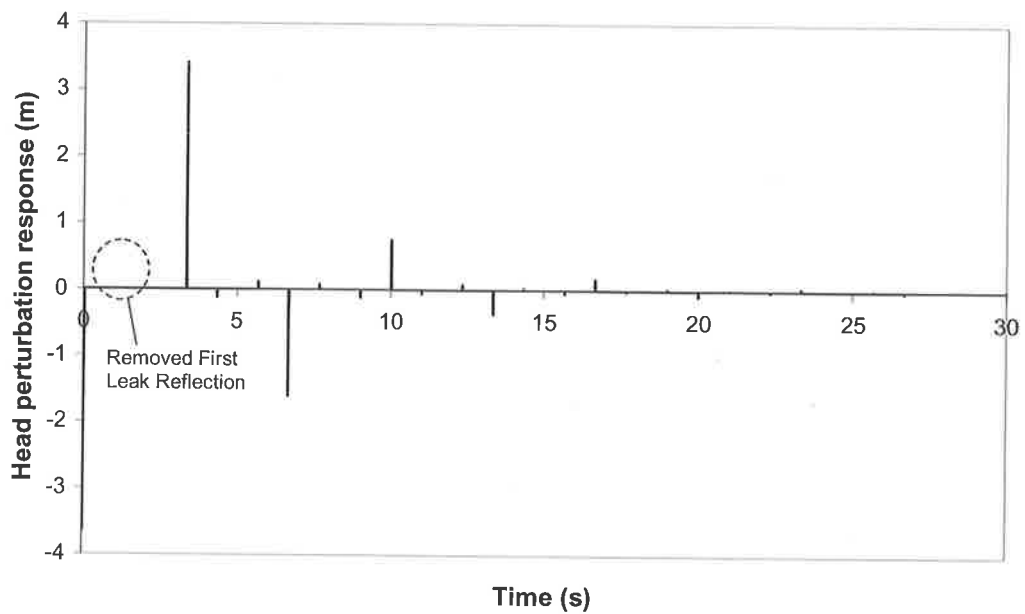


Figure 8-7 – Corrected transient trace with the first reflection from the leak removed.

The IRF from the modified transient trace has no reflection from the leak in the first $2L/a$ of the response. The removal of the leak-reflected signal in the analysis period of the TDR procedure can falsely identify the pipeline as leak free. In comparison, consider the FRF from the same modified transient output shown in Figure 8-9. The FRF displays oscillating peaks, indicating that a leak is present in the pipeline. A leak can be correctly located despite having the first leak reflection removed from the transient signal. This procedure can be repeated for any other leak reflection in the signal and the shape of the leak-induced pattern will remain unchanged. The leak-induced pattern on the FRF is caused by an agglomeration of all the leak reflections in the transient signal, and the removal of a single reflection has no effect on the leak detection procedure.

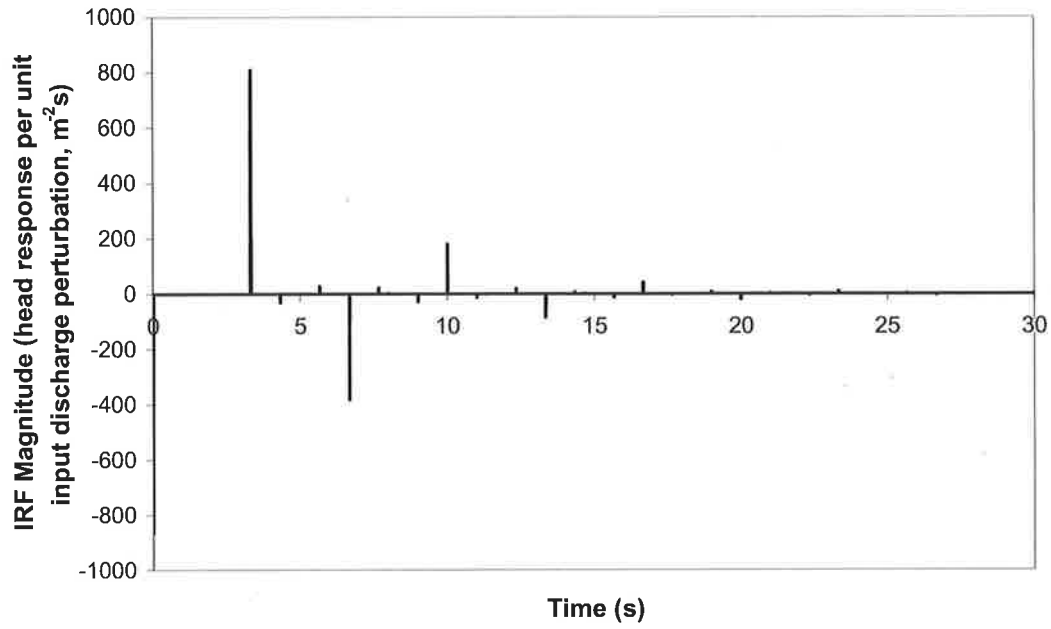


Figure 8-8 – IRF for the modified transient signal with the first reflection removed.

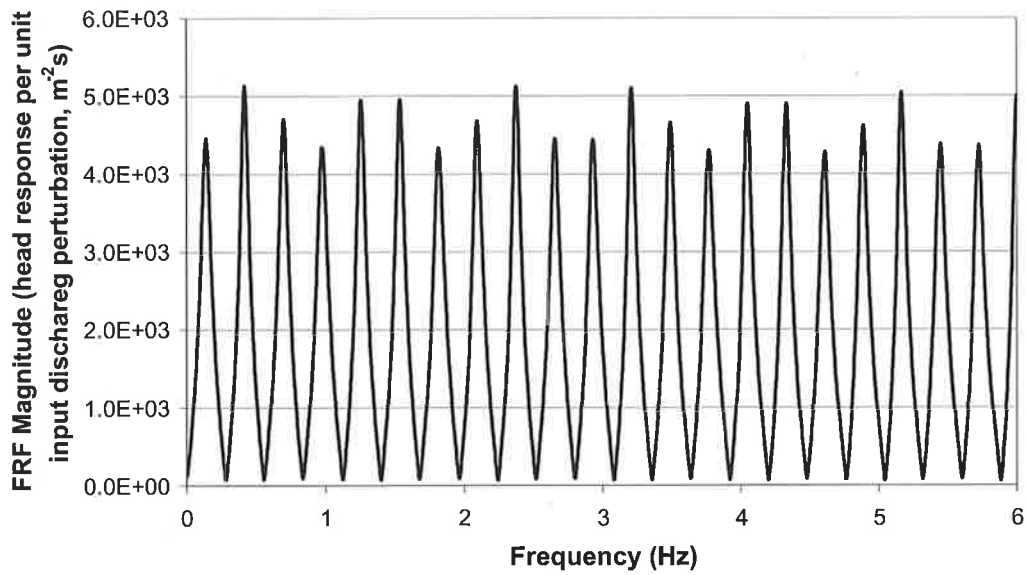


Figure 8-9 – FRF of transient signal with first reflection removed.

8.3 SENSITIVITY OF TECHNIQUES TO SYSTEM NOISE

The term “noise” in the transient data for the purpose of fault detection refers to any contamination of the transient signal that is unrelated to the *physical* nature of the pipeline. Noise can be generated by fluctuating demand, the operation of hydraulic devices and electrical contamination in the transducer output. The presence of noise can lead to inaccuracies and forms an important study. Two types of noise are considered, random noise and sinusoidal noise.

The experimental data are generated using the solenoid valve at the centre of the pipeline with symmetric boundary conditions. The heads at the upstream and downstream reservoirs are 37.0 and 36.5 metres. A leak from an orifice of diameter 1.5 mm ($C_d A_l/A = 4.17 \times 10^{-3}$) is 6.695 m from the upstream reservoir, producing a Reynolds number of 11,000 and a velocity of 0.50 ms^{-1} . The configuration of the system is shown in Figure 8-10.

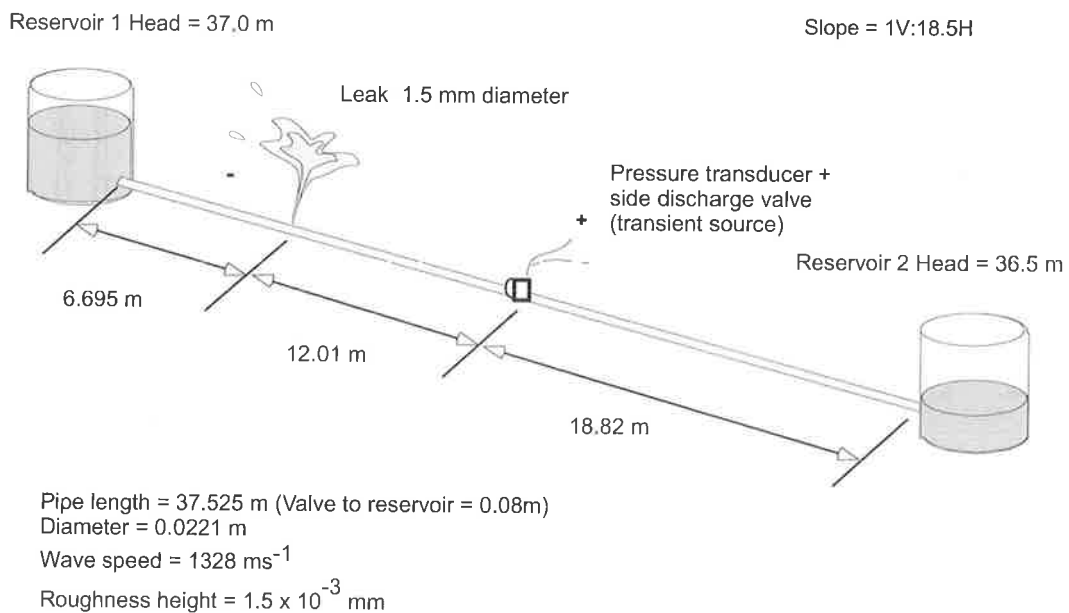


Figure 8-10 – System configuration for testing the effect of noise in data

The measured transient event at the transient source is shown in Figure 8-11. To illustrate the effect of random system noise on the leak detection procedures, a uniformly distributed random perturbation of maximum amplitude of 1.0 metre is added onto the

measured signal. The resultant contaminated signal is shown in Figure 8-12. The FRF (frequency domain) and the IRF (time domain) of both the original and the contaminated signals are shown in Figure 8-13 and Figure 8-14.

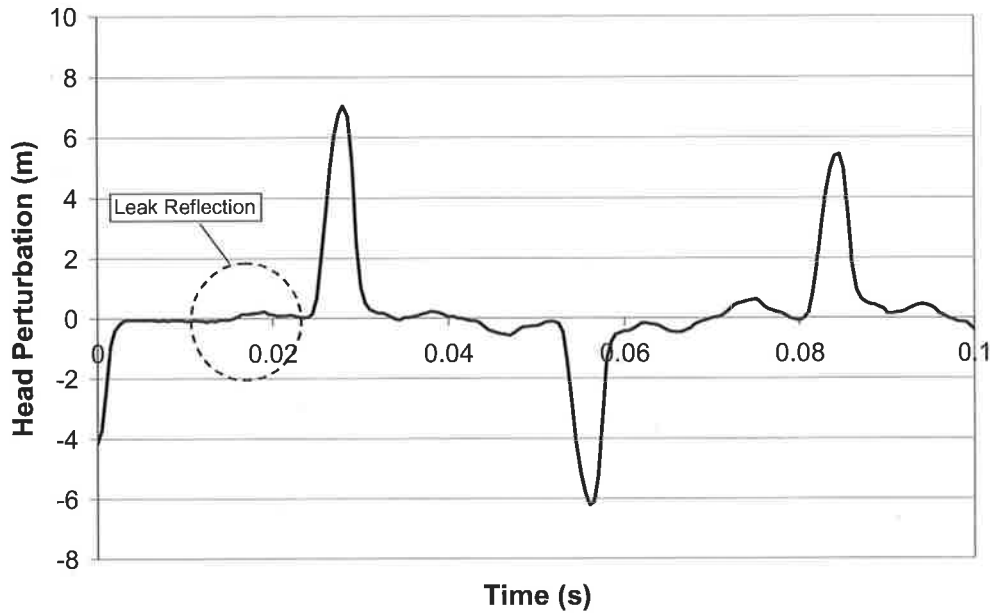


Figure 8-11 – Original transient signal (Data file: C6-L5.txt).

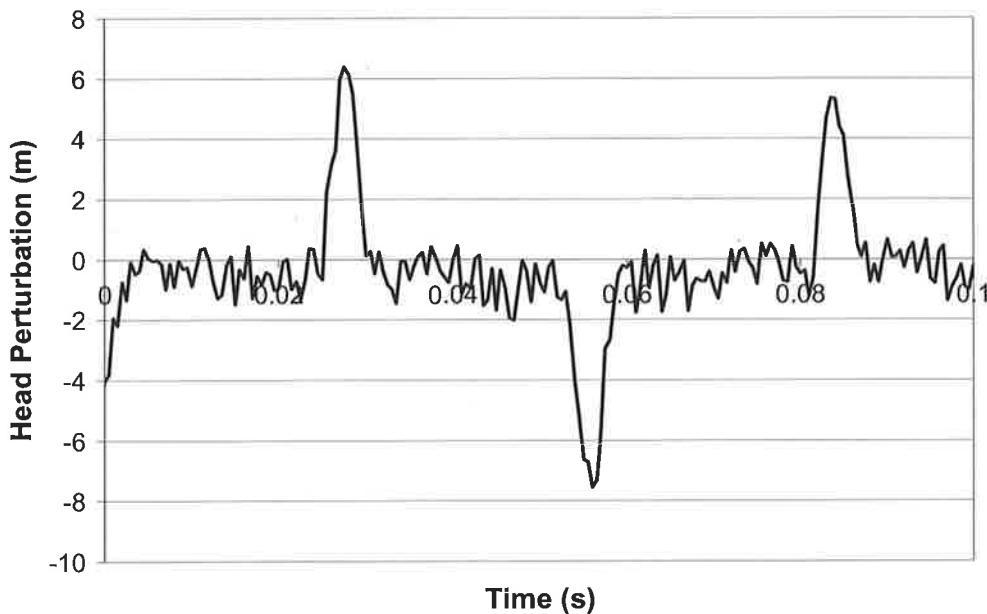


Figure 8-12 – Contaminated transient signal.

In the contaminated transient signal (Figure 8-12), the leak reflections in the signal are completely masked (refer to Figure 8-13 and Figure 8-14). For the FRF in Figure 8-13, the noise distorts the form of the response function and the peaks at the higher frequencies are

masked. However, the magnitudes at the lower harmonic peaks (i.e. first 5 peaks) remain largely unchanged. The use of these peaks in the leak detection procedure correctly locates the leak. The harmonic peaks in the FRF are indicative of components of the original transient signal that repeat at the fundamental frequency of the pipeline. In the case of random noise, which is not periodic, the effect on peak magnitudes is minimal.

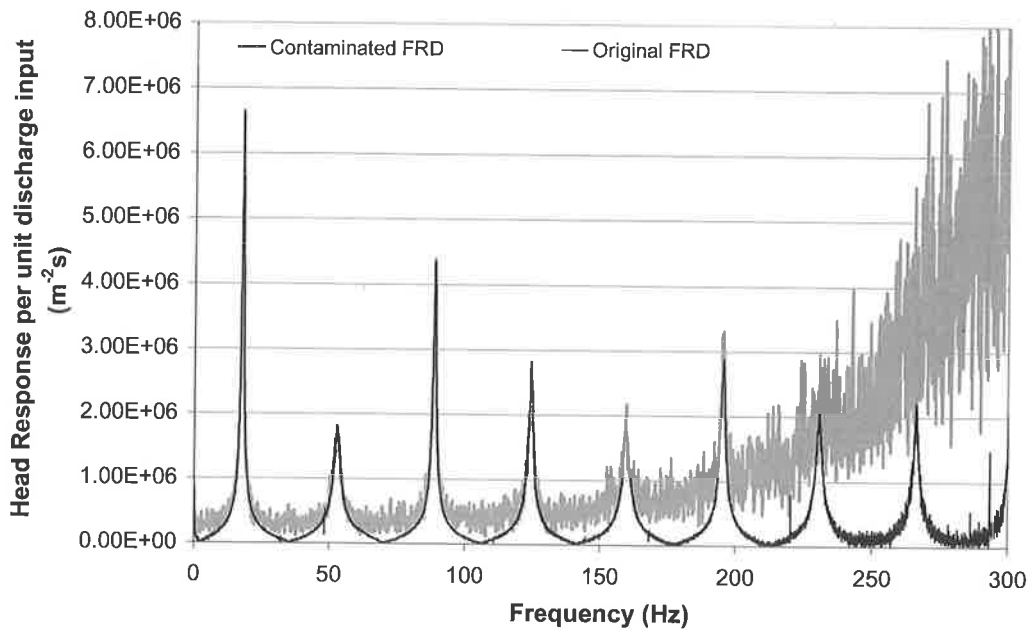


Figure 8-13 – Comparison between the FRF of contaminated and original signals.

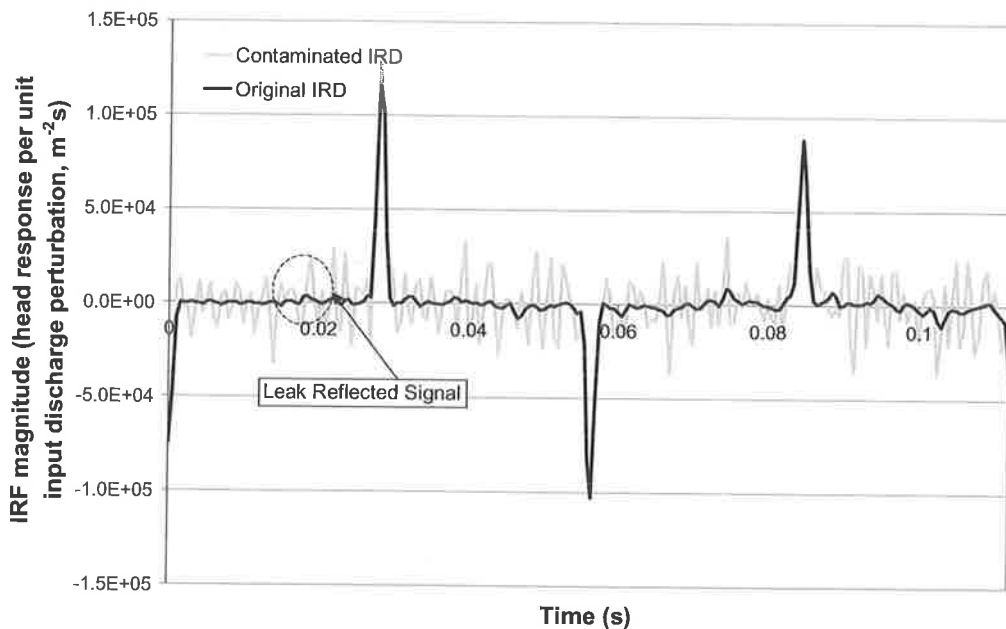


Figure 8-14 – Comparison between the IRF of contaminated and original signals.

In comparison, the IRF from the contaminated signal (refer to Figure 8-14) has severe distortions throughout. Leak reflections are no longer discernible and the use of the TDR procedure in any period of this IRF will not result in the correct determination of the leak position.

Another type of signal contamination is oscillatory noise and may be the result of poorly earthed appliances that use mains AC power. A sine signal of magnitude 1 m with frequency 100 Hz was added to the original transient trace as shown in Figure 8-15. This frequency was selected as it provides the maximum level of distortion to the leak-reflected signals. The transient trace and the FRF are shown in Figure 8-16 and Figure 8-17.

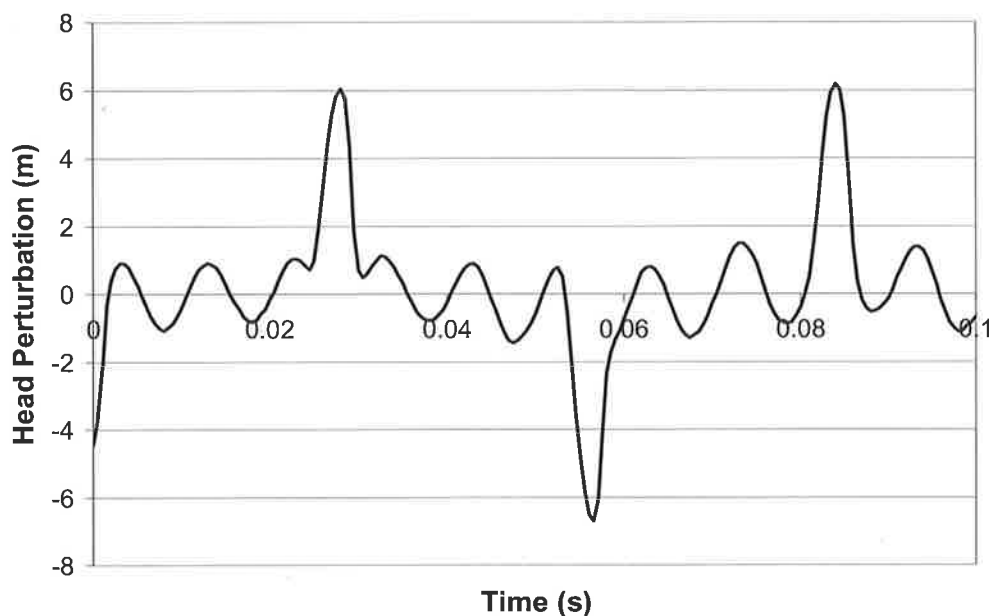


Figure 8-15 – Contaminated transient signal with a sinusoidal function.

The FRF (Figure 8-16) indicates that the sinusoidal contamination in the original transient appears as a discrete spike (at 100 Hz). The responses at other positions in the function are unchanged. If the frequency of the noise does not correspond to a fundamental frequency, the contamination from sinusoidal noise has minimal effect on the accuracy of the leak detection procedure in the frequency domain. The effect on the IRF, however, is not localised and as it creates a sinusoidal oscillation (Figure 8-17). The presence of leak reflections cannot be ascertained from the IRF. The application of the CUSUM algorithm in this case detects changes near the peak / trough of the sinusoidal contamination and does not correspond to correct positions of the leak reflections.

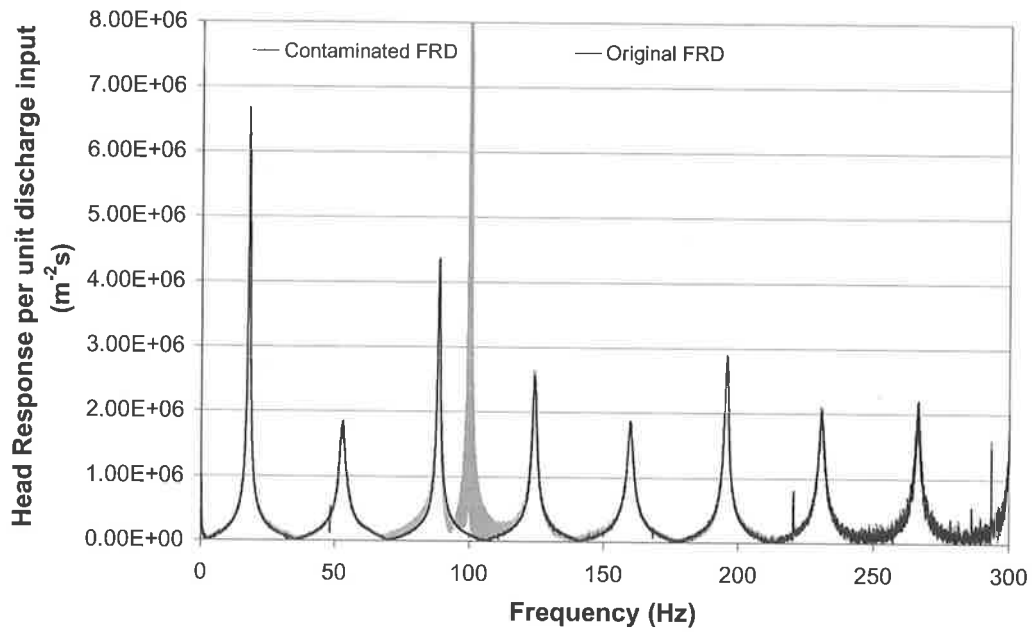


Figure 8-16 – FRF of sine-function contaminated transient data.

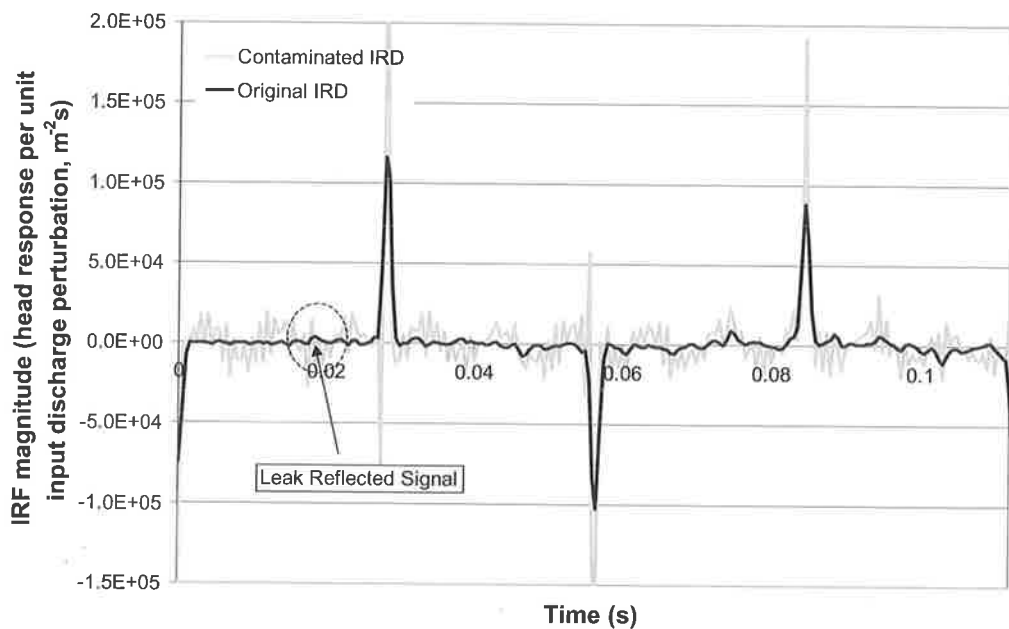


Figure 8-17 – IRF of a sine-contaminated transient data.

The contamination of the transient trace through random and sinusoidal noise has minimal effect on the FRF (frequency domain) and significant effect on the IRF (time domain). The leak detection procedure in the frequency domain using the relative peak magnitudes of the FRF is more noise tolerant than the time-domain procedure using the IRF.

8.4 SUMMARY OF PROPERTIES OF TIME- AND FREQUENCY-DOMAIN TECHNIQUES

The previous sections illustrate the relationship between the leak-induced modifications in the frequency response function (FRF) and the impulse response function (IRF). This final section provides a summary of the advantages and disadvantages of the analysis using the two different forms of the system response function.

8.4.1 Frequency-domain techniques

The leak detection procedure in the frequency domain is more tolerant to the presence of random and harmonic noise. While the approach is advantageous in this respect, it is strongly dependent on the bandwidth of the injected signal (refer to Chapter 6), which limits the number of observable peaks and hence the amount of information that can be used.

The number of leaks (oscillation frequencies) detected in the system is fixed by the form of the fitting function, repeated here as

$$E(m) = \frac{1}{S(m)} \times [X_1 \cos(2\pi m X_2 - X_3) + X_4 \cos(2\pi m X_5 - X_6)] + T(m) \quad (8.1)$$

where, S is the scale correction function, T is the trend correction function and X is the vector of fitting parameters. Each additional fault to be detected in the system requires an additional three parameters that correspond to the magnitude, frequency and phase of the leak / block generated oscillation (e.g. X_1 , X_2 and X_3). Eq. (8.1) shows the fitting function for the detection of two oscillations. From Section 6.9, the number of search parameters should ideally be fewer than the number of available data points. For a given number of peaks, the number of oscillations that can be included is limited as is the number of faults that can be detected simultaneously.

The FRF leak detection procedure has difficulty finding leaks that are located at certain positions in the pipe, depending on the boundary conditions. For example, in a symmetric system, fault locations with a x_L^* that is an integer multiple of 0.25 create patterns on the peaks that have oscillation frequencies either near the Nyquist or zero frequency [refer to Eq. (6.56)]. Oscillations at these frequencies are difficult to detect. Faults located near the midpoint or boundaries have a similar problem for anti-symmetric systems. As the frequency response method of leak detection was specifically derived for two system configurations (an anti-symmetric system where a transient source and a measurement station are adjacent to a closed boundary, and a symmetric system where both are located at the pipe centre point), large deviations from these configurations can lead to distortions in the resultant leak-induced pattern.

Finally, leaks and blockages existing simultaneously in the pipeline pose a problem for the technique as a blockage at one position is indistinguishable from a leak at the mirror position in the system.

In summary, the frequency-domain procedure for leak detection has benefit in situations where the input bandwidth is high compared to the fundamental frequency of the system, providing a large number of resonance peaks for analysis. Examples of such systems are large-scale transmission pipes. To accurately differentiate between leaks and blockages the FRF technique should always be used in conjunction with a time-domain technique.

8.4.2 Time-domain techniques

One of the advantages of the time-domain (IRF) approach is that there are no limits to the maximum number of faults that can be detected in the system. Each fault generates an individual reflection in the IRF and can be located using its arrival time. The nature of these faults (i.e. leaks or blockages) can be determined from the sign of the reflected signal. In addition, faults at all positions in the pipeline can be detected regardless of the system configuration. Multiple measurement stations can be used to measure the same transient event to increase the confidence in the predicted leak location. However, the main disadvantage to the time-domain approach is that it provides little tolerance to noise

contamination, as shown in the Section 8.3. Any distortion of the original transient signal remains in the resultant IRF of the system.

8.4.3 A comparison of time- and frequency-domain techniques

The properties of both procedures are shown in Table 8-1.

Table 8-1 – Properties of FRF and IRF procedures for leak detection.

	Frequency Response Method	Impulse Response Method
Advantages	<ul style="list-style-type: none"> Noise Resistant 	<ul style="list-style-type: none"> Independent of system configuration and number of faults in system Nature of each reflection indicates the location and nature of each fault (leaks and blockages can be detected simultaneously)
Disadvantages	<ul style="list-style-type: none"> Bandwidth limits accuracy of leak detection and number of detectable faults Leaks at one position can be confused with blockages at a mirror position Specific to certain system configurations 	<ul style="list-style-type: none"> Susceptible to noise

From these findings, the frequency-domain fault detection has a real advantage only in cases where the noise contamination of the data is significant. In most situations, the detection of faults in the time domain can lead to the simultaneous detection of any number of faults in the system and the position and nature of each fault can be determined independently. The time-domain approach of leak detection using the impulse response function is more versatile and is better suited to detecting faults in a field situation than the detection procedure in the frequency domain. In reality as the FRF needs to be determined prior to the IRF, both techniques can be applied together for each situation to minimise the possibility of false detection using either technique.

CHAPTER 9

CONCLUSIONS AND RECOMMENDATIONS

9.1 SUMMARY AND CONCLUSIONS

The major aim of this dissertation was to provide new methods for detecting leaks using injected fluid transient signals in pressurised water pipelines. The use of fluid transients for this purpose is non-intrusive and has the potential for testing large stretches (kilometres) of a pipeline within a short period of time (in seconds, depending on system size). Fluid transients can be generated by the operation of in-line or side-discharge valves. The measurement of the pressure fluctuations in time can be analysed to determine the presence and positions of leaks and blockages. The detection range of this type of approach is unmatched by any other existing method of fault detection (e.g. the leak correlators).

Previous techniques in the field of transient leak detection require all features of the flow have to be modelled accurately, including steady and unsteady friction as well as the dynamics of flow that is approximated as one dimensional. However, the state of the art in mathematically modelling flow in pipes is not sufficiently accurate to provide a basis for reliable leak detection. From a practical point of view the following factors inhibit accurate modelling: unsteady friction; knowledge of the detailed geometry and (rheological) properties of the pipe and its fittings; contamination of the fluid (for example, with air) and status of flow control valves. As the state of any pipeline is usually unknown, the reliance on such a good understanding of pipeline topology may limit the application of these techniques.

This thesis describes new techniques where faults can be detected without a good knowledge of the leak-free system behaviour. These techniques were developed in both the frequency domain and the time domain and allow the detection of leaks of a $C_d A_L / A = 1.69 \times 10^{-3}$ (1 mm diameter) under laboratory conditions, where C_d is the coefficient of discharge for the leak, A_L is the area of the leak and A is the area of the pipeline. The work in this thesis can be divided into two sections, the extraction of the system response function from a pressurised hydraulic system and the development of new leak detection techniques in the time and frequency domains.

9.1.1 Summary and conclusions of system response extraction in hydraulic systems

The system response functions provide insight into behaviour of a pipeline by reducing measured output to a form that is solely dependent on the system and independent of flow changes, including introduced transients. Any change in the system from one day to the next can be detected as a change in the system response function even though the injected signals on those two days are different. The shape of the system response function for a perfect pipeline was determined in this thesis. For a leak-free pipe the system response function in the frequency domain (the frequency response function) consists of regularly spaced peaks that attenuate smoothly with frequency whereas in the time domain, it consists of a series of reflections that corresponds only to boundary reflections. A deviation from these known shapes indicates a possible fault.

In the past, the determination of the frequency response involved the repeated injection of a single frequency (sinusoidal) signal. The generation of a high resolution frequency response function using this procedure requires a large number of runs and is time consuming. By considering every complex transient signal as a summation of different frequencies, a procedure was developed in this thesis that allows the accurate extraction of the system response function using a single transient run.

The system response extraction procedure applies linear time-invariant system equations to the measured input and output from the pipeline during the transient event. The output is the measured transient response from the pipeline and the input can be any parameter that describes the valve movement generating the transient. The selection of the input

parameter (i.e. the dimensional valve opening coefficient, τ , or the induced discharge perturbation) can affect the accuracy of the resultant response function. The use of the valve opening coefficient is valid only in cases where the valve movements are small, reducing nonlinearity of the valve orifice equation. In comparison, the use of the induced discharge perturbation as the input eliminates the nonlinear valve equation and good matches between the nonlinear method of characteristics model and the linear transfer matrix model can be found for all magnitudes of valve movement. For these reasons, the induced discharge perturbation should be used to describe any discrete transient event.

The amount of information contained in the measured transient response is governed by the bandwidth—range of frequencies—in the input signal. The input signal should contain sharp changes of pressure in time (translating to high-frequency content). Slow transient signals, such as those generated by pump trips and slow manual closures of in-line valves, are generally not suitable for fault detection. This finding has implications on filter design for extracting relevant information from transient signals as all frequency content that is outside the bandwidth of the input signal (hence not a direct response to the input) should be removed.

The procedure for system response extraction was experimentally validated using different input signals such as step signals, pulse signals and pseudo-random binary signals (PRBS). The frequency response function was accurately extracted displaying resonant peaks at the correct frequencies. PRBS was advantageous in regards to the required maximum head variations induced into a pipe. For a given pipeline, the use of PRBS as the excitation signal can provide the same information as a discrete signal many times its size. The application of such signals in the field may be of benefit as the range of the transient signal can be increased without increasing the pressure change of the transient event.

9.1.2 Summary and conclusion of leak detection procedures using the system response functions

Two new techniques of leak detection were developed in this thesis, one in the frequency domain and the other in the time domain. These techniques do not require leak-free results for comparison nor an accurate prediction of transient behaviour.

Previous publications proposed that a leak generates additional resonant peaks in the frequency response function and the position of these peaks can be used to locate the leak. Experiments conducted in this dissertation show that extra peaks are not generated. A leak was found to impose a non-uniform pattern on the peaks of the frequency response function. The imposed pattern is periodic and is indicative of the location of the leak. This pattern is a result of leak reflections in the transient signal. A new leak detection technique based on the observed pattern of the resonant peaks is validated using both numerical and experimental results. The technique can detect and locate single or multiple leaks and was extended to the detection of discrete blockages. It is tolerant of random and harmonic noise in the data.

The application of the leak detection procedure in the frequency domain requires a transient signal of large bandwidth to provide a sufficient number of peaks for analysis. For a given number of observable peaks, there is an upper limit as to the maximum number of faults that can be detected. In this respect, a system configured anti-symmetrically is better suited for this procedure due to its lower fundamental frequency. For the same reason the method works better in long pipelines than in short ones.

The impulse response function—the time-domain representation of the system response function—was used to detect the occurrence and locate the position of leak-reflected signals in the transient trace. Leaks were found using the known wave speed and arrival time of leak reflections. The use of the impulse response function in this procedure increases the accuracy of the predicted leak location as well as providing a way to detect reflections without a leak-free benchmark for comparison. The impulse response function can also be used with complex signals (e.g. PRBS) for this purpose.

Leak detection procedures in the time and frequency domains were compared in the thesis. The conclusion is that while the procedure in the frequency domain is more tolerant of data contamination, it should only be applied as a supplement to the time-domain methods of leak detection due to the low number of available data points for analysis, high sensitivity to bandwidth / fundamental frequency of the system and its inability to distinguish between a leak and a blockage at mirror positions in the pipe. In contrast, fault detection using the impulse response function (time domain) has none of these disadvantages and is the better technique.

9.2 RECOMMENDATIONS FOR FUTURE WORK

This thesis illustrates that the information contained within a transient trace is governed by the bandwidth (frequency content) of the injected transient event. A high bandwidth signal translates to sharp impulses in the impulse response function in the time domain and provides more information about the system. Electronic solenoid valves used in this thesis can generate transients that have a duration of 4 ms. Given the high wave propagation speed, this translates to a physical distance of 5.3 meters in the pipe. Objects spaced closer than this distance may be difficult to separate as distinct objects and fine details concerning the object cannot be extracted. Investigations of devices capable of generating higher frequency (shorter duration) signals should be conducted to increase the information content of the transient signal. Questions that need to be answered concerning the use of high frequency signals for fault detection include,

- What is the level of energy dispersion at these high frequencies? That is, how far can these signals propagate through the system?
- Is there an upper limit to the frequencies that can be generated in a fluid transient signal? What is the maximum information resolution that can be expected using transient techniques?
- Do leaks and blockages have detailed signatures in their reflections that will distinguish them from other objects in the pipe?
- How do corners, junctions, air valves and other common elements in pipeline affect the behaviour of transient signals?

The investigation should involve the design of new transient generators, including the testing of piezoelectric speakers and also improved designs of solenoid valves. Signals of progressively greater bandwidths should be injected into system to determine if an upper frequency limit exists for the pipe frequency response. Reflections from leaks, blockages, air pockets and other common hydraulic elements using these high bandwidth signals should be analysed to determine if unique characteristics exist that can allow identification of the problem. Currently, all transient based leak detection techniques are unable to provide conclusive identification of objects in the pipeline based on the nature of the reflection. Advances in this area are vital for future development of the field.

Field testing of the techniques is also necessary to determine the range of the transient technique in a field system. The attenuation caused by corners and junctions may result in the dispersion of reflected signals. Such dispersion can distort the form of the reflected signals, making them difficult to detect using the current procedure. A modified system response extraction procedure using the wavelet transform in place of the Fourier transform is presented in Young (1995) and may be required in this situation. This procedure takes into account of all possible levels of signal dispersion and unlike the Fourier transform, it does not assume that the reflected signal is of the same form as the input signal.

REFERENCES

1. Ahmad, A. (1995). "Detection and Identification of Underground Objects." *IE(I) Journal-ET*, **76**, pp. 7 – 10.
2. Akiyama, T. (1986). "Pressure Estimation from Oscillatory Signals Obtained Through BWR's Instrument Lines." *Journal of Dynamic Systems, Measurement and Control*. **108** (3), pp. 80 – 85.
3. Alaskan Department of Environmental Conservation – ADEC (2000). *Technical Review of Leak Detection Technologies- Volume 1 – Crude Oil Transmission Pipelines*. Research report.
4. Ambardar, A. (1999). *Analog and Digital Signal Processing. Second Ed*, Brooks/Cole Publishing Company, U.S.A.
5. American Water Works Association (1987). *Leaks in Water Distribution Systems: A Technical/Economic Overview*, AWWA, Denver.
6. Antonopoulous-Domis, M. (1980). "Frequency Dependence of Acoustic Resonances on Blockage Position in a Fast Reactor Subassembly Wrapper." *Journal of Sound and Vibration*. **72**(4), pp. 443 – 450.
7. Atherton, D., Morton, K. and Mergelas, B. (2000). "Detecting Breaks in Prestressing Pipe Wire." *Journal of AWWA*. **92**(7), pp. 50 – 56.
8. Axworthy, D.H., Ghidaoui, M.S. and McInnis, D.A. (2000). "Extended Thermodynamics Derivation of Energy Dissipation in Unsteady Pipe Flow." *Journal of Hydraulic Engineering*, ASCE. **126**(4), pp. 276 – 287.
9. Baghdadi, A.H. and Mansy, H.A. (1988). "A Mathematical Model for Leak Location in Pipelines." *Applied Math. Modelling*. **12**, pp. 25 – 30.
10. Basseville, M. and Nikiforov, I. (1993). *Detection of Abrupt Changes: Theory and Application*. Englewood Cliffs, NJ: Prentice-Hall.
11. Beck, S. and Staszewski, W. (2004). "Cepstrum Analysis for Identifying Reflection Points in Pipeline Networks." *The Practical Application of Surge Analysis for Design and Operation, 9th International Conference on Pressure Surges*. Chester, UK, 24 – 26 March, 2004, pp. 199 – 209.
12. Beck, T. and Kane, W. (1996). "Current and Potential Uses for Time Domain Reflectometry for Geotechnical Monitoring." *47th Highway Geology Symposium*, Cody, Wyoming, pp. 94 – 103.
13. Bergant, A. and Simpson, A.R. (1995). *Water Hammer & Column Separation Measurements in an Experimental Apparatus*. Research Report No. R128, Department of Civil and Environmental Engineering, University of Adelaide, South Australia.
14. Bergant, A., Simpson, A.R. and Vítkovský, J.P. (1999). "Review of Unsteady Friction Models in Transient Pipe Flow." *9th International Meeting of the Work Group on the Behaviour of Hydraulic Machinery Under Steady Oscillatory Conditions*, IAHR, 7-9 September, Brno, Czech Republic.
15. Black, P. (1992). "A Review of Leak Detection Technologies." *Pipeline System – Fluid Mechanics of Its Application*, Kluwer Academic Publishers, pp. 287 – 298.
16. Brekke, H. (1984). *A Stability Study on Hydro Power Plant Governing Including the Influence from a Quasi Nonlinear Damping of Oscillatory Flow and from the Turbine Characteristics*. PhD dissertation, University of Trondheim, The Norwegian Institute of Technology.

-
17. Brown, F. (1984). "On Weighting Functions for the Simulation of Unsteady Turbulent Flow." *Forum on Unsteady Flow*, ASME, New Orleans, USA, FED. **15**, pp. 26 – 28.
 18. Brunone, B. (1999). "Transient Test-based Technique for Leak Detection in Outfall Pipes." *Journal of Water Resources Planning and Management*, ASCE. **125**(5), pp. 302 – 306.
 19. Brunone, B., Golia, U.M. and Greco, M. (1991). "Some Remarks on the Momentum Equations for Fast Transients." *International Meeting on Hydraulic Transients with Column Separation, 9th Round Table*, IAHR, Valencia, Spain, 201-209.
 20. Chambarel, A., Ferry, E., Chanzy, A., Laurent, J., Todoroff, P. and Ferrari, P. (2001). "TDR Signal Modelling Using the Electric Line Approach: Model Validation and Signal Inversion to Retrieve Soil Moisture Profile." *Second International Symposium and Workshop on Time domain Reflectometry for the Detection of Liquid Spills*.
Online proceedings – <http://www.iti.northwestern.edu/tdr/tdr2001/proceedings>
 21. Chaudhry, M. H. (1987). *Applied Hydraulic Transients*. Van Nostrand Reinhold Company Inc, New York.
 22. Chaudhry, M.H. (1970). "Resonance in Pressurized Piping Systems." *Journal of the Hydraulics Division*, ASCE. **96**(HY9), pp. 1819 – 1839.
 23. Chen, L. (1995). *Pipe Network Analysis – The Forward and Inverse Problems*. PhD dissertation, August, Cornell University, USA.
 24. Colombo, A. and Karney, B. (2002). "Energy and Costs of Leaky Pipes: Toward a Comprehensive Picture." *Journal of Water Resources Planning and Management*, November/December, pp. 441 – 450.
 25. Covas, D. and Ramos, H. (1999). "Leakage Detection in Single Pipelines Using Pressure Wave Behaviour." *Water Industry System: Modelling and Optimisation Application*. **1**, pp 287 – 299.
 26. Covas, D., Graham, N., Maksimovic, C., Kapelan, Z., Savic, D. and Walters, G. (2003), "An Assessment of the Application of Inverse Transient Analysis for Leak Detection: Part II - Collection and Application of Experimental Data." *Proc. Computer Control for Water Industry (CCWI)*, London (UK), C. Maksimovic and N. Graham, eds.
 27. Covas, D., Ramos, H., Brunone, B. and Young, A. (2004). "Leak Detection in Water Trunk Mains Using Transient Pressure Signals: Field Tests Scottish Water." *The Practical Application of Surge Analysis for Design and Operation, 9th International Conference on Pressure Surges*. Chester, UK, 24 – 26 March, 2004, pp.185 – 198.
 28. Cowan, G. (1975). "Digital Processing Adds Accuracy to TDR." *Microwaves*. December, pp. 47 – 51.
 29. D'Souza, A. and Oldenburger, R. (1964). "Dynamic Response of Fluid Lines." *Journal of Basic Engineering*. September, pp. 589 – 596
 30. Daily, J.W., Hankey, W.L., Olive, R.W. and Jordaan, J.M. (1956). "Resistance Coefficients for Accelerated and Decelerated Flows Through Smooth Tubes and Orifices." *Transactions of the ASME*, Vol. 78, 1071-1077.
 31. Dallabetta, M. J. (1996). "Using Cross-correlation Techniques to Determine the Impulse Response Characteristics of Linear Systems." *Dissertation submitted for the Degree of Master of Science*, The University of Idaho.
 32. De Salis, M., Movchan, N. and Oldham, D. (2002). "Characterizing Holes in Duct Walls Using Resonance Frequencies." *Journal of the Acoustical Society of America*. **111**(6), pp. 2583 – 2593.
-

-
33. De Salis, M.H. and Oldham, D.J. (1999). "Determination of the Blockage Area Function of a Finite Duct from a Single Pressure Response Measurement." *Journal of Sound and Vibration*. **221**(1), pp 180 – 186.
 34. De Salis, M.H. and Oldham, D.J. (2001). "The Development of a Rapid Single Spectrum Method for Determining the Blockage Characteristics of a Finite Length Duct." *Journal of Sound and Vibration*. **243**(4), pp. 625 – 640.
 35. Deutsch, R. (1969). "System Analysis Techniques." *Prentice-Hall, Inc., Englewood Cliffs, N.J.*
 36. Duan, Q.Y., Gupta, V.K. and Sorooshian, S. (1993). "Shuffled Complex Evolution Approach for Effective and Efficient Global Minimisation." *Journal of Optimization Theory and Applications*. **76**(3), pp. 501 – 521.
 37. Dunn, C. and Hawksford, M. (1993). "Distortion Immunity of MLS-derived Impulse Response Measurements." *Journal of Audio Engineering Society*. **41**(5), pp 314 – 335.
 38. Eiswirth, M. and Burn, L.S. (2001). "New Methods for Defect Diagnosis of Water Pipelines." *4th International Conference on Water Pipeline Systems*. 28 – 30th March, York, UK.
 39. Fan, D. (1989). *Fluid Structure Interactions in Internal Flows*. A thesis presented in application for the degree of Doctor of Philosophy in the University of Dundee.
 40. Fanelli, M. Angelico, G. and Escobar, P. (1983). "Comprehensive Experimental Confirmation of Transfer Matrix Theory for Uniform Pipelines under Steady Pulsating Conditions." *4th International Conference on Pressure surges*." September 21 – 23, 1983, pp. 379 – 391.
 41. Ferrante, M. and Brunone, B. (2001). "Leak Detection in Pressurised Pipes by Means of Wavelet Analysis." BHR Group. *4th International Conference on Water Pipeline System - Managing Pipeline Assets in an Evolving Market*. York, UK: 28-30 March, 2001.
 42. Ferrante, M., Brunone, B. and Rossetti, A.G. (2001). "Harmonic Analysis of Pressure Signal during Transients for Leak Detection in Pressurized Pipes." BHR Group. *4th International Conference on Water Pipeline System - Managing Pipeline Assets in an Evolving Market*. York, UK: 28-30 March, 2001.
 43. Foster, K. and Parker, G. (1964). "Transmission of Power by Sinusoidal Wave Motion through Hydraulic Oil in a Uniform Pipe." *Proceedings of the Institution of Mechanical Engineers*. **179**, Pt. 1, No. 19, pp. 599 – 614.
 44. Fox, J. A. (1989). *Transient Flow in Pipes, Open Channels and Sewers*. Ellis Horwood Limited, England.
 45. Fuchs, H. and Riehle, R. (1991). "Ten Years of Experience with Leak Detection by Acoustic Signals Analysis." *Applied Acoustic*. **33**, pp. 1 – 19.
 46. Furness, R. and van Reet J. (1998), *Pipe Line Rules of Thumb Handbook*, Gulf Publishing Company, Houston, Texas.
 47. Ghidaoui, M. S., G. S. Mansour, Zhao, M. (2002). "Applicability of Quasi-Steady and Axi-Symmetric Turbulence Models in Water Hammer." *Journal of Hydraulic Engineering, ASCE* **128**(10): 917-924.
 48. Harding, R. (1974). "Use Pulse instead of CW Signals." *Electronic Design*. **11**, May, pp. 60 – 67.
 49. Heimovaara, T. (2001). "Frequency domain Modelling of TDR Waveforms in order to obtain Frequency Dependent Dielectric Properties of Soil Samples: A Theoretical Approach." *Second International Symposium and Workshop on Time Domain Reflectometry for Innovative Geotechnical Applications*.
<http://www.itn.northwestern.edu/tdr/tdr2001/proceedings>
-

-
50. Heutschi, K. and Rosenheck, A. (1997). "Outdoor Sound Propagation Measurements using an MLS Technique." *Applied Acoustic*. **51**(1), pp 13 – 32.
 51. Hovey, D. and Farmer, E. (1999). "DOT Stats Indicate Need to Refocus Pipeline Accident Prevention." *Oil and Gas Journal*. **47**(11). pp. 52-57.
 52. Hsuing, J. (1992). "Fault Detection via Acoustic Noise." *A dissertation submitted to The University of Texas for the partial fulfilment of the degree of Doctor of Philosophy*.
 53. Hwang, H. and Kim, C. (2004). "Damage Detection in Structures using a Few Frequency Response Measurement." *Journal of Sound and Vibration*. **270**, pp. 1 – 14.
 54. Ibrahim, S. and Mikulcik, E. (1978). "Time Domain Identification of Standing Wave Parameters in Gas Piping Systems." *Journal of Sound and Vibration*, **60**(1), pp. 21 – 31.
 55. Ivetić, M. and Savic, D.A. (2002). "Practical Implications of Using Induced Transients for Leak Detection." *3rd World Water Forum, Kyoto, Session "Integrated River Basin Environment Assessment"*,
http://river4.kuciv.kyoto-u.ac.jp/member/hosoda/vwf/Hosoda_art.pdf.
 56. Jaeger, C. (1977). *Fluid Transients*. Blackie & Son Limited, Bishopbriggs, Glasgow.
 57. Jönsson, L. (2001). "Experimental Studies of Leak Detection using Hydraulic Transients." *29th IAHR Congress Proceedings*, IAHR, Sept. 16 – 21, 2001, Beijing, China.
 58. Jönsson, L. (1995). "Computer and Laboratory Studies of Leak Detection Using Hydraulic Transients." *Water Resources Management under Drought or Water Shortage Conditions*, N.T. Tsiourtis (Editor), Balkema, Rotterdam, pp. 119 – 126.
 59. Jönsson, L. and Larson, M. (1992). "Leak Detection through Hydraulic Transient Analysis." *Pipeline Systems*, B. Coulbeck and E. Evans, eds., Kluwer Academic Publishers, pp. 273 – 286.
 60. Kagawa, T., Lee, I., Kitagawa, A. and Takenaka, T. (1983). "High Speed and Accurate Computing Method of Frequency-Dependent Friction in Laminar Pipe Flow for Characteristic Method." *Transactions of the Japanese Society of Mechanical Engineers*. **49**(447), pp. 2638 – 2644.
 61. Kane, W. and Beck, T. (1999) "Advances in Slope Instrumentation: TDR and Remote Data Acquisition Systems." *Field Measurements in Geomechanics, 5th International Symposium on Field Measurements in Geomechanics*, Singapore, pp. 101 – 105.
 62. Kapelan, S.Z., Savic, D.A., Walters, G.A., Covas, D., Stoianov, I., Graham, N., Maksimovic, C. and Butler, D. (2003). "Inverse Transient Analysis in Pipe Networks for Leakage Detection, Quantification and Roughness Calibration", *Proc. 30th IAHR Congress*, Thessaloniki (Greece).
 63. Karney, B. and McInnis, D. (1990), "Efficient Calculation of Transient Flow in Simple Pipe Networks," *Journal of Hydraulic Engineering*, ASCE. **118**(7), pp. 1014 – 1030.
 64. Kreyzig, E. (1993). *Advanced Engineering Mathematics*. Wayne Anderson Publisher, 7th edition.
 65. Kuczera, G. (1994). *NLFIT – A Bayesian Nonlinear Regression Program Suite – V 1.00g*, Department of Civil Engineering and Surveying, University of Newcastle, New South Wales, Australia.
 66. Lampton, M. (1978). "Transmission Matrices in Electroacoustics." *Acoustica*. **39**, pp. 239 – 251.
-

-
67. Le, T., Watton, J. and Pham, D. (1998). "Fault Classification of Fluid Power Systems using a Dynamic Feature Extraction Technique and Neural Networks." *Proceedings of the Institution of Mechanical Engineer.* **212**(1), pp. 87 – 97.
 68. Lee, P.J., Vítkovský, J.P., Simpson, A.R., Lambert, M.F. and Liggett, J.A. (2003c). Discussion to "Leak Detection in Pipes by Frequency Response Method Using a Step Excitation, 2002, 40(1), 55-62." *Journal of Hydraulic Research, IAHR,* 41(2), 221-223.
 69. Lee, P.J., Vítkovský, J.P., Lambert, M.F., Simpson, A.R. and Liggett, J.A. (2004). "Experimental Validation of Frequency Response Coding for the Location of Leaks in Single Pipeline Systems." *The practical application of surge analysis for design and operation, 9th international conference on pressure surges*, BHR Group. Chester, UK, 24 – 26 March 2004, pp. 239 – 253.
 70. Lee, P.J., Vítkovský, J.P., Lambert, M.F., Simpson, A.R. and Liggett, J.A. (2003a). "Frequency Response Coding for the Location of Leaks in Single Pipeline Systems." *International Conference on Pumps, Electromechanical Devices and Systems Applied to Urban Water Management*, IAHR and IHR, Valencia, Spain, April 22 – 25, 2003. pp. 371-378.
 71. Lee, P.J., Vítkovský, J.P., Lambert, M.F., Simpson, A.R. and Liggett, J.A. (2003b). "Detection of Leaks in a Fluid Pipelines using a Linear System Transfer Function." Submitted to *Journal of Hydraulic Engineering*, ASCE.
 72. Li, H., Dallabetta, M. and Demuth, H. (1994). "Measuring the Impulse Response of Linear Systems using an Analog Correlator." *Proceedings – IEEE International Symposium on Circuits and Systems*, **5**, pp. 65 – 68.
 73. Liggett, J.A. and Chen, L. (1994). "Inverse Transient Analysis in Pipe Network." *Journal of Hydraulic Engineering*, ASCE. **120**(8), pp. 934 – 955.
 74. Liou, J.C. and Tian, J. (1995). "Leak Detection-transient Flow Simulation Approaches." *Journal of Energy Resources Technology*, ASME. **117**, pp. 243 – 248.
 75. Liou, J.C. (1998). "Pipeline Leak Detection by Impulse Response Extraction." *Journal of Fluids Engineering*, ASME. **120**, pp 833 – 838.
 76. Liou, J.C. (1996) "Pipeline Integrity Monitoring using System Impulse Response." *International Pipeline Conference – Volume 2* ASME. pp. 1137 – 1141.
 77. Liu, W., Hunsperger, R., Chajes, M. and Kunz, E. (2001). "An Overview of Corrosion Damage Detection in Steel Bridge Strands using TDR." *Second International Symposium and Workshop on Time domain Reflectometry for the Detection of Liquid Spills*. <http://www.iti.northwestern.edu/tdr/tdr2001/proceedings>
 78. Lynn, P. (1982). *An Introduction to the Analysis and Processing of Signals*. The Macmillan Press Ltd, London and Basingstoke.
 79. Maclean, A., Moran, C., Johnstone, W., Culshaw, B., Marsh, D. and Andrews, G. (2001). "Distributed Fibre Optic Sensors for the Detection of Liquid Spills." *Second International Symposium and Workshop on Time domain Reflectometry for the Detection of Liquid Spills*. Online proceedings – <http://www.iti.northwestern.edu/tdr/tdr2001/proceedings>
 80. Maloney, C. (1973). "Locating Cable Faults." *IEEE Transactions on industry applications*, **IA-9**(4), pp. 380 – 394.
 81. Martinez, V. (2002). *Seismic Response of Coal Seams in the Western Canadian Basin*. Master of Science Dissertation, Department of Physics, University of Alberta, Edmonton, Canada.
 82. Mermelstein, P. (1967). "Determination of the Vocal-tract Shape from Measured Formant Frequencies." *The Journal of the Acoustical Society of America*, **41**(5), pp 1283 – 1294.
-

-
83. Misiunas, D., Vítkovský, J., Olsson, G., Simpson, A.R. and Lambert, M. (2003). "Pipeline Burst Detection and Location using a Continuous Monitoring Technique." *International Conference on Advances in Water Supply Management*, CCWI, 15 – 17 September, 2003, Imperial College London, UK.
 84. Misiunas, D., Vítkovský, J.V., Olsson, G., Simpson, A.R. and Lambert, M.F. (2004). "Burst Detection and Location in Pipe Networks using a Continuous Monitoring Technique." *The Practical Application of Surge Analysis for Design and Operation*, 9th International conference on pressure surges. Chester, UK, 24-26 March, 2004, pp. 225 – 237.
 85. Mpesha W., Chaudhry, M.H. and Gassman, S.L. (2002) "Leak Detection in Pipes by Frequency Response Method Using a Step Excitation." *Journal of Hydraulic Research*, IAHR. **40**(1), pp. 55 – 62.
 86. Mpesha, W. (1999). *Leak Detection in Pipes by Frequency Response Method*. Dissertation submitted to the University of South Carolina in partial fulfilment of Doctor of Philosophy, Columbia, SC. USA.
 87. Mpesha, W., Gassman, S.L. and Chaudhry, M.H. (2001). "Leak Detection in Pipes by Frequency Response Method." *Journal of Hydraulic Engineering*, ASCE. **127**(2), pp. 134 – 147.
 88. Mukherjee, J. and Narasimhan, S. (1996). "Leak Detection in Networks of Pipelines by the Generalized Likelihood Ratio Method." *Ind. Eng. Chem. Res.* **35**, pp. 1886 – 1893.
 89. Muto, T. and Kanei, T. (1980). "Resonance and Transient Response of Pressurised Complex Pipe Systems." *Bulletin of the JSME*, **23**(184), pp. 1610 – 1617.
 90. Nash, G. and Karney, B. (1999). "Efficient Inverse Transient Analysis in Series Pipe Systems." *Journal of Hydraulic Engineering*, ASCE, **125**(7), pp. 761 – 764.
 91. Niederdränk, T. (1997). "Maximum Length Sequences in Non-destructive Material Testing: Application of Piezoelectric Transducers and Effects of Time Variances." *Ultrasonics*. **35**, pp 195 – 203.
 92. Norton, M. P. and Greenhalgh, R. (1986). "On the Estimation of Loss Factors in Lightly Damped Pipeline Systems: Some Measurement Techniques and their Limitations." *Journal of Sound and Vibration*. **105**(3), pp. 397 – 423.
 93. O'Connor, K. and Wade, V. (1994). "Application of Time Domain Reflectometry in the Mining Industry." *Symposium and workshop on time domain reflectometry in environmental, infrastructure and mining applications*, Northwestern University, Evanston, Illinois, September 17 – 19.
 94. O'Connor, K. and Dowding, C. (1999). *Geomeasurements by Pulsing TSR Cables and Probes*. CRC Press, Boca Raton.
 95. OFWAT - Office of Water Services (2001). "Leakage and the Efficient Use of Water – 2000-2001 report". Office of Water Services, UK, Annual Report.
 96. Ogawa, N., Mikoshiba, T. and Minowas, C. (1994) "Hydraulic Effects on a Large Piping System during Strong Earthquakes." *Journal of Pressure Vessel Technology*, ASME. **116**, pp. 161 – 168.
 97. Okanla, E., Gaydecki, P., Manaf, S. and Burdekin, F. (1997). "Detecting Faults in Post tensioning Ducts by Electrical Time domain Reflectometry." *Journal of Structural Engineering*. May, pp.567–574.
 98. Oldenburger, R. and Goodson, R. (1964) "Simplification of Hydraulic Line Dynamics by the Use of Infinite Products." *Journal of Basic Engineering*, Transactions of the ASME. March, pp 1 – 10.
 99. Oppenheim, A.V. and R.W. Schaffer. (1989) *Discrete-Time Signal Processing*. Englewood.
-

-
100. Pande, L. (1982). *Engineering Applications of Plane Wave Duct Acoustics*. A dissertation submitted to Purdue University for the partial fulfilment of the degree of Doctor of Philosophy.
 101. Pejović, S., Gajić, A. and Obradović, D. (1983) "The Influence of Turbomachine Characteristic on Hydraulic Oscillations in Pipeline Systems." *4th International Conference on Pressure Surges*, September 21-23, pp. 393 – 404.
 102. Poulakis, Z., Valougeorgis, D. and Papadimitriou, C. (2003). "Leakage Detection in Water Pipe Networks using a Bayesian Probabilistic Framework." *Probabilistic Engineering Mechanics*, **18**, pp. 315 – 327.
 103. Poussart, D. and Ganguly, U. (1977). "Rapid Measurement of System Kinetics – An Instrument for Real-time Transfer Function Analysis." *Proceedings of the IEE*. **65(5)**, pp. 741-747.
 104. Pregelj, A., Drab, M. and Mozetic, M. (1997). "Leak Detection Methods and Defining the Sizes of Leaks." *The 4th International Conference of Slovenian Society for non-destructive testing, Application of contemporary non-destructive testing in engineering*, 24-25 April, Ljubljana, Slovenia.
 105. Pudar, R. and Liggett, J.A. (1992). "Leaks in Pipe Networks." *Journal of Hydraulic Engineering*, ASCE. **118(7)**, pp. 1031 – 1046.
 106. Qunli, W. and Fricke, F. (1989). "Estimation of Blockage Dimensions in a Duct using Measured Eigenfrequency Shifts." *Journal of Sound and Vibration*. **133(2)**, pp 289-301.
 107. Qunli, W. and Fricke, F. (1991). "Determination of Blockage Locations and Cross-sectional Area in a Duct by Eigenfrequency Shifts." *Journal of the Acoustical Society of America*. **87(1)**, pp. 67 – 75.
 108. Said, R., AlShawawreh, N. and Mohamed, A. (2001). "A TDR System for Subsurface Pollutants Detection (II): Application and Analysis. *Second International Symposium and Workshop on Time domain Reflectometry for the Detection of Liquid Spills*.
Online proceedings – <http://www.iti.northwestern.edu/tdr/tdr2001/proceedings>
 109. Schoukens, J., Guillaume, P. and Pintelon, R. (1993). "Design of Broadband Excitation Signals." *Perturbation Signals for System Identification*, Prentice Hall, pp. 126 – 160.
 110. Schroeder, M. R. (1967). "Determination of the Geometry of the Human Vocal Tract by Acoustic Measurements." *The Journal of the Acoustical Society of America*. **41(4)**, Part 2. pp. 1002 – 1010.
 111. Scott, D. (1999a). "DOT Mandates API Document for Leak Detection." *Oil & Gas Journal*, **97(2)**, pp. 51 – 54.
 112. Scott, D. (1999b). "PC-Based SCADA Installed on Russian Crude-Oil System." *Oil & Gas Journal*, **97(2)**, pp. 56 – 57.
 113. Sharp, D. (1996). *Acoustic Pulse Reflectometry for the Measurement of Musical Wind Instruments*. Dissertation submitted to the University of Edinburgh for the partial fulfilment of the degree of Doctor of Philosophy.
 114. Silva, R., Buiatta, C., Cruz, S. and Pereira, J. (1996). "Pressure Wave Behaviour and Leak Detection in Pipelines". *Computers Chem. Engn.* **20**, pp. S491 – S496.
 115. Simpson, A.R., Vítkovský, J. and Lambert, M. (2000). "Transients for Calibration of Pipe Roughnesses using Genetic Algorithms." *8th International Conference on Pressure Surges*, The Hague, Netherlands.
 116. Smith, J. and Wolfe, J. (2001). "Tone Holes and Cross Fingering in Wood Wind Instruments." *Proceedings of the 17th International Congress on Acoustics*, Rome, 2 – 7 September, Session 8.09, pp. 14 – 15.
-

-
117. Smith, L., Fields, K, Chen, A. and Tafuri, A. (2000). *Options for Leak and Break Detection and Repair for Drinking Water Systems*. Battelle Press, Columbia, Ohio, US.
 118. Starck, J., Pantin, E. and Murtagh (2002). "Deconvolution in astronomy: A review." *Publications of the astronomical society of the pacific.* **114** (Oct) pp. 1051 – 1069.
 119. Stephens, M.L., Lambert M.F., Simpson A.R., Vítkovský, J.P. and Nixon J. (2004b) "Field Tests for Leakage, Air Pocket and Discrete Blockage Detection Using Inverse Transient Analysis in Water Distribution Pipes", *6th Annual Symposium on Water Distribution Systems Analysis*, EWRI Water Congress, Salt Lake City, USA.
 120. Stephens, M.L., Vítkovský, J.P., Lambert, M.F., Simpson, A.R., Karney, B. and Nixon, J. (2004a). "Transient Analysis to Assess Valve Status and Topology in Pipe Networks." *The Practical Application of Surge Analysis for Design and Operation, 9th International conference on pressure surges*. Chester, UK, 24 – 26 March, 2004. pp. 211 – 224.
 121. Stoianov, I., Karney, B., Covas, D., Maksimovic, C. and Graham, N. (2002). "Wavelet Processing of Transient Signals for Pipeline Leak Location and Quantification." *1st Annual Environmental & Water Resources Systems Analysis Symposium in conjunction with ASCE Environmental & Water Resources Institute Annual Conference*, Roanoke, Virginia, USA.
 122. Streeter, V.L. and Wylie, E.B. (1983). *Fluid Mechanics – Metric Edition*. McGraw Hill, Singapore.
 123. Suo, L. and Wylie, E.B. (1989). "Impulse Response Method for Frequency Dependent Pipeline Transients." *Journal of Fluids Engineering*, ASME. **111**(12), pp. 478 – 483.
 124. Suo, L., Wylie, E.B. (1990). "Hydraulic Transients in Rock Bored Tunnels." *Journal of Hydraulic Engineering*. **116**(2), pp. 196 – 210.
 125. Swamee, P.K. and Jain, A.K. (1976). "Explicit Equations for Pipe-Flow Problems." *Journal of the Hydraulics Division*, ASCE, 102(HY5), 657-664.
 126. Svingen, B. (1996). *Fluid Structure Interaction in Piping Systems*. Dissertation submitted to the Faculty of Mechanical Engineering. Norway, The Norwegian University of Science and Technology.
 127. Tafuri, A. (2000). "Locating Leaks with Acoustic Technology." *Journal of AWWA*. **92**(7), pp. 57 – 66.
 128. Tan, A. and Godfrey, K. (2001). "The Generation of Binary and Near Binary Pseudo Random Signals: An Overview." *IEEE Instrumentation and Measurement technology Conference*. Budapest, Hungary, May 21 – 23, 2001. pp. 766 – 771
 129. Tijsseling, A.S. and Lavooij, C.S. (1990). "Waterhammer with Fluid-Structure Interaction." *Applied Scientific Research*. **47**, pp.273 – 285.
 130. Trikha, A.K. (1975). "An Efficient Method for Simulating Frequency-Dependent Friction in Transient Liquid Flow." *Journal of Fluids Engineering*, Transactions of the ASME. **97**, pp.97– 105.
 131. Tsang, S., Benson, M. and Granberg, R. (1985). "The Open and Blocked Distributed Air Transmission Lines By The Fast Fourier Transform Method." *Journal Of Dynamic Systems, Measurement and Control*. **107**, September, pp. 213 – 219.
 132. Vardy, A. and Brown, J. (1995). "Transient, Turbulent, Smooth Pipe Friction." *Journal of Hydraulic Research*, IAHR. **33**(4), pp. 435 – 456.
-

-
133. Vardy, A. and Hwang, K. (1991). "A Characteristic Model of Transient Friction in Pipes," *Journal of Hydraulic Research*, IAHR. **29**(5), pp. 669 – 684.
134. Vítkovský J.P., Simpson A.R. and Lambert M.F. (2000). "Transients for Calibration of Pipe Roughnesses using Genetic Algorithms". *Journal of Water Resources Planning and Management*, ASCE. **126** (4), pp 262 – 265.
135. Vítkovský, J.P. and Simpson, A.R. (1997). *Calibration and Leak Detection in Pipe Networks Using Inverse Transient Analysis and Genetic Algorithms*, Research Report No. R157, August, Department of Civil Engineering, University of Adelaide, Australia.
136. Vítkovský, J.P. (2001). *Inverse Analysis and Modelling of Unsteady Pipe Flow: Theory, Applications and Experimental Verification*. PhD dissertation, March, Department of Civil & Environmental Engineering, University of Adelaide, Australia.
137. Vítkovský, J.P., Simpson, A.R. and Lambert, M.F. (1999), "Leak Detection and Calibration of Water Distribution System Using Transient and Genetic Algorithms." *Water Distribution System Conference*, Division of Water Resource Planning and Management, ASCE, Tempe, Arizona, 7 – 9 June.
138. Vítkovský, J.P., Lee, P.J., Stephens, M.L., Lambert, M.F., Simpson, A.R. and Liggett, J.A. (2003a). "Leak and Blockage Detection in Pipelines via an Impulse Response Method." *Pumps, Electromechanical Devices and Systems Applied to Urban Water Management*, Volume I, E. Cabrera and E. Cabrera Jr. (eds), 22-25 April, Valencia, Spain, 423-430.
139. Vítkovský, J.P., Bergant, A., Simpson, A.R. and Lambert, M.F. (2003b). "Steady Oscillatory Flow Solution including Unsteady Friction." *International Conference on Pumps, Electromechanical Devices and Systems Applied to Urban Water Management*, IAHR and IHR, Valencia, Spain, April 22 – 25, 2003.
140. Vítkovský, J.P., Simpson, A.R., Lambert, M.F. and Wang, X.J. (2001). "An Experimental Verification of the Inverse Transient Technique." *6th Conference on Hydraulics in Civil Engineering*, I.E.Aust., 28 – 30 November, Hobart, Australia, pp. 373 – 380.
141. Wang, X.J. (2002). *Leakage and Blockage Detection in Pipelines and Pipe Network Systems Using Fluid Transients*. PhD dissertation, August, Department of Civil & Environmental Engineering, University of Adelaide, Australia.
142. Wang, X.J., Lambert, M.F., Simpson, A.R., Liggett, J.A. and Vítkovský, J.P. (2002). "Leak Detection in Pipeline Systems Using the Damping of Fluid Transients." *Journal of Hydraulic Engineering*, ASCE. **128**(7), pp. 697 – 711.
143. Watanabe, K. and Himmelblau, D. (1986). "Detection and Location of a Leak in a Gas-transport Pipeline by a New Acoustic Method." *AIChE Journal*. **32**(10), pp. 1690 – 1701.
144. Watanabe, K. and Koyama, H. (1990). "Location and Estimation of a Pipeline Leak." *Electrical Engineering in Japan*. **110**(7), pp. 92 – 100.
145. Wylie, E.B. and Streeter, V.L. (1993). *Fluid Transients in Systems*. Prentice Hall, Englewood Cliffs, New Jersey, USA.
146. Wylie, E.B. (1997). "Frictional Effect in Unsteady Turbulent Pipe Flows," *Appl. Mech. Rev.* **11**, Part 2, pp. S241 – S244.
147. Young, R.K. (1995). *Wavelet Theory and Its Applications*. Kluwer Academic Publishers, 4th edition.
148. Zhang, L., Tijsseling, A. and Vardy, A. (1995). "Frequency Response Analysis in Internal Flow." *Journal of Hydrodynamics*, Ser. B., 3(1995), pp. 39 – 49.
-

-
149. Zielke, W. (1968). "Frequency-dependent Friction in Transient Pipe Flow." *Journal of Basic Engineering*, ASME. **90**, pp. 109 – 115.
 150. Zielke, W. and Hack, H. (1972). "Resonance Frequencies and Associated Mode Shapes of Pressurised Piping Systems." *International Conference on Pressure Surges*, 6th – 8th September, Kent, Canterbury, England. pp. G1 – 1 to G1 – 13.
 151. Zielke, W. and Rösl, G. (1971). "Resonance in Pressurized Piping Systems – Discussion." *Journal of the Hydraulics Division*, ASCE. **97**(HY7), pp. 1141 – 1146.
 152. Zielke, W., Wylie, E.B. and Keller, R.B. (1969). "Forced and Self-excited Oscillations in Propellant Lines." *Journal of Basic Engineering*. (12), pp. 671 – 677.

APPENDIX A – FORMULATION OF THE TRANSFER MATRIX FOR A TWO-LEAK PIPE SEGMENT

The transfer matrix, U , of a pipeline relates the head, h , and discharge, q , between the upstream (n) and downstream ($n + 1$) of a section at a particular frequency,

$$\begin{bmatrix} q \\ h \\ 1 \end{bmatrix}^{n+1} = \begin{bmatrix} U_{11} & U_{12} & 0 \\ U_{21} & U_{22} & 0 \\ 0 & 0 & 1 \end{bmatrix} \begin{bmatrix} q \\ h \\ 1 \end{bmatrix}^n \quad (\text{A-1})$$

where U_{ij} denotes the i^{th} row and j^{th} column entry to the transfer matrix of a pipe, U . The transfer matrix for a section containing two leaks (Figure A-1) is derived as follows.

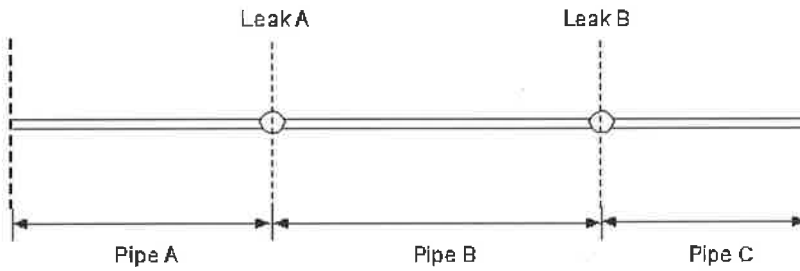


Figure A-1– Pipe section under consideration.

The unit matrix for a pipe segments is

$$\begin{bmatrix} P_{k_{11}} & P_{k_{12}} & 0 \\ P_{k_{21}} & P_{k_{22}} & 0 \\ 0 & 0 & 1 \end{bmatrix} \quad (\text{A-2})$$

where $P_{k_{mn}}$ is the entry (m, n) in the unit matrix of the k^{th} pipe section. Similarly, the unit matrix for a leak is given as

$$\begin{bmatrix} 1 & L_{k_{12}} & L_{k_{13}} \\ 0 & 1 & 0 \\ 0 & 0 & 1 \end{bmatrix} \quad (\text{A-3})$$

where $L_{k_{mn}}$ is the entry (m, n) in the unit matrix of the k^{th} leak. To form the overall transfer matrix of the pipe section, these individual matrices are multiplied together starting from the downstream end. The result of multiplying the unit matrix of pipe C [Eq. (A-2)] with the unit matrix of leak B [Eq. (A-3)] is

$$[P_C][L_B] = \begin{bmatrix} P_{C11} & P_{C11}L_{B12} + P_{C12} & P_{C11}L_{B13} \\ P_{C21} & P_{C12}L_{B12} + P_{C22} & P_{C21}L_{B13} \\ 0 & 0 & 1 \end{bmatrix} \quad (\text{A-4})$$

Similarly, the multiplication of pipe matrix B to leak matrix A is

$$[P_B][L_A] = \begin{bmatrix} P_{B11} & P_{B11}L_{A12} + P_{B12} & P_{B11}L_{A13} \\ P_{B21} & P_{B12}L_{A12} + P_{B22} & P_{B21}L_{A13} \\ 0 & 0 & 1 \end{bmatrix} \quad (\text{A-5})$$

The multiplication of Eq. (A-4) to (A-5) and subsequently to the matrix of Pipe A give the following entries in the overall transfer matrix of the system:

$U_{11} = P_{A11} [P_{C11}P_{B11} + P_{B21}(P_{C11}L_{B12} + P_{C12})] + P_{A21} [P_{C11}(P_{B11}L_{A12} + P_{B12}) + (P_{C11}L_{B12} + P_{C12})(L_{A12}P_{B21} + P_{B22})]$	(A-6)
$U_{12} = P_{A12} [P_{C11}P_{B11} + P_{B21}(P_{C11}L_{B12} + P_{C12})] + P_{A22} [P_{C11}(P_{B11}L_{A12} + P_{B12}) + (P_{C11}L_{B12} + P_{C12})(L_{A12}P_{B21} + P_{B22})]$	(A-7)
$U_{13} = P_{C11}(P_{B11}L_{A13}) + L_{A13}P_{B21}(P_{C11}L_{B12} + P_{C12}) + P_{C11}L_{B13}$	(A-8)
$U_{21} = P_{A11} [P_{C21}P_{B11} + P_{B21}(L_{B12}P_{C21} + P_{C22})] + P_{A21} [P_{C21}(P_{B11}L_{A12} + P_{B12}) + (L_{A12}P_{B21} + P_{B22})(L_{B12}P_{C21} + P_{C22})]$	(A-9)
$U_{22} = P_{A12} [P_{C21}P_{B11} + P_{B21}(L_{B12}P_{C21} + P_{C22})] + P_{A22} [P_{C21}(P_{B11}L_{A12} + P_{B12}) + (L_{A12}P_{B21} + P_{B22})(L_{B12}P_{C21} + P_{C22})]$	(A-10)
$U_{23} = P_{C21}(P_{B11}L_{A13}) + (L_{B12}P_{C21} + P_{C22})(L_{A13}P_{B21}) + L_{B13}P_{C21}$	(A-11)

These entries of the system transfer matrix, U , are used in the determination of the leak-induced modification on the peaks of the FRF in Chapter 6.